MAGMATIC AND FLUID PROCESSES IN THE UPPER MANTLE: A STUDY OF THE BAY OF ISLANDS OPHIOLITE COMPLEX, NEWFOUNDLAND

VOLUME I: TEXT
VOLUME II: TABLES AND FIGURES

STEPHEN JOHN EDWARDS, B.Sc.

FRONTISPIECE

Dawn breaks over base camp (top) and preparing for take off (bottom).

ABSTRACT

An extremely heterogeneous section of upper mantle exposed over 2 km^2 in the Springers Hill area of the Lewis Hills Massif, Bay of Islands Ophiolite Complex, consists of two distinct associations: low-Al peridotites and pyroxenites (LALPP), and high-Al peridotites, pyroxenites and gabbros (HALPPG). These represent the processes of magma and fluid generation, migration and evolution in the mantle wedge of a subduction zone.

The LALPP have Cr-spinel of Cr# = 47-90, Mg# = 23-65, and formed in the order of harzburgite--orthopyroxenite (and associated dunite and chromitite)--clinopyroxenite (and associated dunite, chromitite and websterite). Harzburgite is a refractory residue from partial melting and complete removal of low-Ti tholeiitic magma. This harzburgite has straight, positively sloping chondrite-normalized REE patterns and Pd/Ir < 1. Dykes of orthopyroxenite have U-shaped chondrite-normalized REE patterns and very high Pd/Ir ratios, and formed from hydrous, As-saturated magma of boninitic affinity, which previously had fractionated significant quantities of Cr-spinel and relatively minor olivine. By mechanical mixing or magmatic impregnation, a component of orthopyroxenite was added to some harzburgites; these harzburgites have U-shaped chondrite-normalized REE patterns and Pd/Ir > 1. Dykes of clinopyroxenite formed from LREE-depleted, high Pd/Ir, S-saturated, low-Ti tholeiitic magma. The LALPP formed at P ≤ 7-8 kbar in upwelling asthenosphere

(T = 1300 ± 100°C) below a zone of crustal accretion in a supra-subduction zone environment.

The HALPPG contain spinel of approximately Cr# = 30, Mg# = 65, and comprise dunite, wehrlite, olivine clinopyroxenite, gabbro and amphibole peridotite. The HALPPG formed in the lithosphere (T = 900 ± 100°C) at P = 5-9 kbar by combined assimilation and crystal fractionation, which involved fluid-bearing magma and LALPP. The replacement of LALPP by HALPPG involved dissolution of ortho- and clinopyroxene, precipitation of clinopyroxene, plagioclase, Ca-amphibole and phlogopite, and recrystallization of olivine and spinel. In minerals and whole-rock samples of HALPPG, the Mg# is largely controlled by the LALPP protolith, whereas concentrations of Ti, Al, Ca, Na, K and REE are controlled by the magma or fluid.

The magma parental to the HALPPG was fluid-bearing, LREE-depleted, Sr-rich and SiO_2-undersaturated, and formed by partial melting of amphibolitized oceanic crust during intra-oceanic thrusting and obduction of the Bay of Islands Ophiolite Complex. The fluid component of this magma became LREE- and Eu-enriched and SiO_2-saturated by fractionation of Ca-amphibole and reaction with LALPP. As such, this suggests a link between fluids within metamorphic soles of ophiolites, metasomatized mantle peridotites and pyroxenites, and forearc magmatic and fluid processes leading to the formation of wehrlitic bodies and high-MgO, SiO_2-saturated magmas or fluids of boninitic affinity.

ACKNOWLEDGEMENTS

It gives me great pleasure to thank John Malpas, my supervisor, for introducing me to Newfoundland and for his friendship, hospitality and support. Tom Calon and Brian Fryer are thanked for acting as members of my supervisory committee.

Sherry Dunsworth (Memorial) and Günter Suhr (Memorial) provided an excellent introduction to the mantle sequence of the Bay of Islands Ophiolite Complex, and John Clarke, Michael Edwards and Jeff Saunders proved to be very able and entertaining field assistants. Gloria and Derek Mercer and Viking Helicopters (Newfoundland) provided excellent logistical support.

The author greatly benefited from discussions with Peter Cawood, George Jenner and Mark Wilson of Memorial, and numerous participants at the meetings: Magmatism in the Ocean Basins (England), Troodos 87 - Ophiolites and Oceanic Lithosphere (Cyprus), Ophiolite Genesis and Evolution of Oceanic Lithosphere (Oman), and Orogenic Lherzolites and Mantle Processes (France). Roger Mason (Memorial), Peter Nixon (Leeds) and John Spray (New Brunswick) are thanked for their thorough and constructive review of this thesis. A special thank you to Günter Suhr for his friendship and many discussions concerning mantle petrology.

Gert Andrews, Pat Browne, Daryl Clarke, Cecilia Edwards, Roberta Ellis Hayes, Carolyn Emerson, Nancy Fagan, Gerry Ford, Bill Gosse, Dave Healey,

Pat Horan, Simon Jackson, Pam King, Teresa Lannon, Henry Longerich, Dave MacNeil, Wilf Marsh, Maureen Moore, Annie Reid, Rick Soper, Gerry Starkes, Foster Thornhill, Geoff Veinott and Lloyd Warford all greatly assisted with technical and administrative aspects of this thesis, and I thank them all. Gordon Brown and Bob MacKay greatly assisted with the acquisition of mineral analyses at Dalhousie University. Geoff Dawe, Chris Finch, Peter Haring and Hank Wagenbauer are thanked for providing analytical facilities at the Department of Mines and Energy, Newfoundland. I express my gratitude to Lisa Pope and Darryl Williams, without whose many hours of drafting, colouring, cutting and pasting, this thesis would still be in the making.

Thanks to Alasdaire and Lisa and my fellow graduate students, especially Adam, Bill, David R., David v. E., Don, Ewan, Gee Ung, Günter, Jeroen, Jim, Paul and Rob, for companionship and memorable times. Thanks to the members of the St. John's Rowing Club, especially the "men's fast four" and associates, for many hours of fun and pain on Quidi Vidi Lake.

To my whole family, especially Mum, Dad and Mike, for their encouragement of my education and their love and support, and for giving me such a good start in life.

Finally, to Karen, my fiancée, who with love and support, made many sacrifices whilst patiently awaiting the completion of this thesis. To her I express my deepest love and gratitude.

The author was supported by a Canadian Commonwealth Scholarship and a Memorial University Graduate Student Fellowship. Additional funds were

received from the Timothy Jefferson Field Research Fund (Geological Society of London), a Viking Helicopters (Newfoundland) Ltd. Scholarship, and a NSERC operating grant to John Malpas. Much of the field work and analytical costs were covered by DSS contract 20ST.23233-7-0402 to Tom Calon and John Malpas, as part of the 1984-1989 Canada-Newfoundland Mineral Development Agreement.

TABLE OF CONTENTS

VOLUME I: Text

FRONTISPIECE ii

ABSTRACT iii

ACKNOWLEDGEMENTS v

LIST OF TABLES xiv

LIST OF FIGURES xvi

LIST OF ABBREVIATIONS xxii

Chapter 1

INTRODUCTION

1.1 GENERAL STATEMENT 1
1.2 THE UPPER MANTLE 2
1.2.1 Samples of upper mantle 2
1.2.2 Composition of the upper mantle 3
1.2.3 Upper mantle heterogeneity 5
1.2.4 Mantle metasomatism 6
1.2.5 Magma- and fluid-peridotite interactions 8
1.2.6 Magma and fluid migration in the upper mantle 9
1.2.7 Factors affecting the composition of upper mantle peridotite 11
1.3 OPHIOLITIC AND OROGENIC PERIDOTITES 11
1.3.1 Classification and origin 11
1.3.2 Mafic and ultramafic bodies hosted by peridotite 13
1.3.3 Magma- and fluid-peridotite interactions 15
1.4 OBJECTIVES AND APPROACH 16

1.5 AREA OF STUDY 17
1.5.1 Regional geology and origin of the Bay of Islands Ophiolite Complex 17
1.5.2 The mantle section of the Bay of Islands Ophiolite Complex 19
1.5.3 The Springers Hill area of the Lewis Hills Massif 20
a Mapping and access 21
b Chemical classification of the Springers Hill area 21
1.6 FORMAT OF THE THESIS 22

Chapter 2

FIELD RELATIONS AND PETROGRAPHY

2.1 INTRODUCTION 23
2.2 OVERVIEW OF THE FIELD AREA 24
2.3 LOW-Al PERIDOTITES AND PYROXENITES 26
2.3.1 Harzburgite 26
a Field relations 26
b Petrography 27
2.3.2 Dunite 30
a Field relations 30
b Petrography 31
2.3.3 Chromitite 32
2.3.4 Type I orthopyroxenite, clinopyroxenite and websterite 33
a Field relations 33
b Petrography of type I orthopyroxenite 35
c Petrography of clinopyroxenite 36
d Petrography of websterite 37
e Petrography of dunite associated with clinopyroxenite 38
2.3.5 Type II orthopyroxenite 38
a Field relations 38
b Petrography 39
2.3.6 Amphibole dunite 40
a Field relations 40
b Petrography 41
2.3.7 Interpretation 43
2.3.8 Platinum group minerals and Fe-Ni-Cu-S phases in LALPP 46
2.4 HIGH-Al PERIDOTITES, PYROXENITES AND GABBROS, AND THE MARGINAL ZONE 48

2.4.1 HAL dunite 49
a Field relations 49
b Petrography 49
2.4.2 HAL wehrlite, olivine clinopyroxenite and gabbro 51
a Field relations 51
b Petrography 53
2.4.3 The marginal zone 54
a Field relations 54
b Petrography 55
2.4.4 Interpretation 56
2.4.5 Fe-Ni-Cu-S phases in HALPPG 59
2.5 D_2 SHEAR ZONES AND THRUST FAULTS 60
2.5.1 Possible tectonic setting 61
2.5.2 D_2 shear zones and ophiolite obduction 62
2.5.3 The importance of thrusting in the Springers Hill area 65
2.6 SUMMARY 66

Chapter 3

CHEMISTRY AND PETROGENESIS OF
LOW-ALUMINA PERIDOTITES AND PYROXENITES

3.1 INTRODUCTION 68
3.2 MINERAL CHEMISTRY 69
3.2.1 Olivine 69
3.2.2 Orthopyroxene 69
3.2.3 Clinopyroxene 70
3.2.4 Ca-amphibole 70
3.2.5 Cr-spinel 70
3.2.6 Interpretation 71
a Silicate chemistry 71
b Cr-spinel chemistry 73
3.2.7 Summary 77
3.3 WHOLE-ROCK CHEMISTRY 78
3.3.1 Major and trace elements 78
3.3.2 Rare earth elements 79
3.3.3 Platinum group elements 80
3.4 CHEMICAL EFFECTS OF SERPENTINIZATION 83
3.4.1 Major and trace elements 83
3.4.2 Rare earth elements 84

3.4.3 Platinum group elements 86
3.5 PETROGENESIS OF HARZBURGITE 86
3.5.1 CaO/Al_2O_3 ratio as an index of partial melting 86
3.5.2 Rare earth elements 88
3.5.3 Platinum group elements 91
3.5.4 Orthopyroxene in harzburgite 95
3.6 PETROGENESIS OF CHROMITITE 96
3.7 PETROGENESIS OF DUNITE 97
3.7.1 Platinum group elements 97
3.8 PETROGENESIS OF TYPE I ORTHOPYROXENITE AND CLINOPYROXENITE 99
3.8.1 Magmatic versus metasomatic origin of pyroxenites 99
3.8.2 Compositions of parental magmas 100
a Rare earth element abundances of parental magmas 101
b LREE enrichment of mantle sources of boninites 103
c La enrichment of mantle sources of low-Ti tholeiites 104
3.8.3 Melting models for the generation of boninites and low-Ti tholeiites 104
3.9 ENVIRONMENT OF FORMATION OF THE SPRINGERS HILL AREA 106
3.9.1 Spreading centre 106
3.9.2 Fracture zone 107
3.10 IMPLICATION OF THE SPRINGERS HILL AREA FOR THE ORIGIN OF THE BAY OF ISLANDS OPHIOLITE COMPLEX 109
3.11 SUMMARY 110
3.11.1 Platinum group elements 110

Chapter 4

CHEMISTRY AND PETROGENESIS OF HIGH-ALUMINA PERIDOTITES, PYROXENITES AND GABBROS

4.1 INTRODUCTION 112
4.2 CHEMISTRY 113
4.2.1 Mineral chemistry 114
4.2.2 Whole-rock major and trace element chemistry 115
4.2.3 Whole-rock rare earth element chemistry 115
4.2.4 Mineral chemistry of LALPP in contact with HALPPG 116
4.2.5 Interpretation 118

a HAL gabbro 118
b Contacts between HALPPG and LALPP 119
4.3 PETROGENESIS OF HIGH-Al PERIDOTITES, PYROXENITES AND GABBROS 120
4.3.1 Interaction between LALPP and the parent magma of HALPPG 120
a Assimilation and crystal fractionation 121
b Thermodynamics and kinetics of reactions 122
4.3.2 Possible parent magma of the HALPPG 124
4.3.3 Modelling of magma-rock interactions 125
4.4 THE PARENT MAGMA OF THE HIGH-Al PERIDOTITES, PYROXENITES AND GABBROS 128
4.4.1 Origin of the parent magma 128
4.4.2 Thermal regime for partial melting of amphibolite 130
4.5 ORIGIN OF BODIES OF WEHRLITE IN OPHIOLITES 131
4.6 SUMMARY 132

Chapter 5

COGENETIC ORIGIN FOR AMPHIBOLE DUNITE, TYPE II ORTHOPYROXENITE, HIGH-ALUMINA PERIDOTITES, PYROXENITES AND GABBROS, AND D_2 SHEAR ZONES

5.1 INTRODUCTION 134
5.2 MINERAL CHEMISTRY 136
5.2.1 Ca-amphibole 136
5.2.2 Cr-spinel 137
5.3 INTERACTION BETWEEN FLUID AND LOW-Al PERIDOTITES AND PYROXENITES 137
5.3.1 Source of fluid 137
5.3.2 Incongruent breakdown of orthopyroxene to olivine 138
5.3.3 Formation of the assemblage phlogopite-amphibole-olivine-spinel 139
5.3.4 Origin of type II orthopyroxenite 141
5.4 CONDITIONS OF PRESSURE AND TEMPERATURE 143
5.5 CHEMISTRY OF FLUID 144
5.5.1 Mineral assemblages and amphibole chemistry 145
a Fluid/rock ratio 145
b Sodium and potassium in hydrous phases 146

5.5.2 Rare earth elements 147
5.5.3 Platinum group elements 148
5.5.4 H-O-C species in fluid 149
5.6 TRANSPORT OF FLUID 150
5.7 SUMMARY 150
5.7.1 Mantle sources of boninitic magmas 152

Chapter 6

SUMMARY

6.1 CONCLUSIONS FROM THIS STUDY 154
6.1.1 Types of harzburgite 155
6.2 IMPORTANCE OF THE SPRINGERS HILL MANTLE SECTION TO MANTLE PETROLOGY 156
6.2.1 Processes in the mantle wedge of a subduction zone 157
6.2.2 Mantle heterogeneity 157
6.2.3 Mantle xenoliths 158

REFERENCES 159

Appendix 1: ANALYTICAL METHODS 199

Appendix 2: SAMPLES ANALYSED 213

Appendix 3: MINERAL ANALYSES 218

Appendix 4: WHOLE-ROCK ANALYSES 220

Appendix 5: ORTHOPYROXENE IN HARZBURGITE 221

Appendix 6: PUBLISHED MATERIAL RELEVANT TO THIS THESIS 223

LIST OF TABLES

VOLUME II: Tables and Figures

TABLE 1.1. Classification of ophiolites as harzburgite ophiolite types and lherzolite ophiolite types 3

TABLE 3.1. Major and trace element and normative compositions of orthopyroxenites in ophiolitic and orogenic mantle peridotites 74

TABLE A1.1. Accuracy and precision of analyses of minerals 89

TABLE A1.2. Accuracy and precision of analyses of major elements 90

TABLE A1.3. Accuracy and precision of analyses of trace elements 90

TABLE A1.4a. Limits of detection and blank compositions of rare earth elements 91

TABLE A1.4b. Precision of rare earth elements 91

TABLE A1.4c. Accuracy and precision of analyses of rare earth elements: BCR-1 92

TABLE A1.4d. Accuracy and precision of analyses of rare earth elements: PCC-1 92

TABLE A1.5. Accuracy and precision of analyses of platinum group elements 96

TABLE A3.1. Olivine analyses 97

TABLE A3.2. Orthopyroxene analyses 107

TABLE A3.3. Clinopyroxene analyses 112

TABLE A3.4. Amphibole analyses 118

TABLE A3.5. Plagioclase analyses 122

TABLE A3.6. Spinel analyses 124

TABLE A4.1. Major and trace element analyses 138

TABLE A4.2. Rare earth element analyses 142

TABLE A4.3. Platinum group element analyses 145

LIST OF FIGURES

VOLUME II: Tables and Figures

FIGURE 1.1. Classification of ultramafic rocks 1

FIGURE 1.2. Solubilities of H_2O and CO_2 in silicate melts and of solute (melt) in H_2O- and CO_2-fluids with variation in pressure 2

FIGURE 1.3. In-situ formation of dunite 4

FIGURE 1.4. Generalized geological map of the Humber Arm Allochthon 5

FIGURE 1.5. Geological map of the Lewis Hills Massif 6

FIGURE 1.6. Composition of olivine, clinopyroxene and spinel in peridotites and pyroxenites of the Springers Hill area 7

FIGURE 2.1. Geological map of the Springers Hill area map pocket

FIGURE 2.2. Stacked sequence of thrust slices 8

FIGURE 2.3. Type I orthopyroxenite dyke pervasively intruding harzburgite 9

FIGURE 2.4. Bands of olivine and orthopyroxene defining S_1 in harzburgite 10

FIGURE 2.5. Partially recrystallized Cr-spinel in harzburgite 11

FIGURE 2.6. Impregnated orthopyroxene in harzburgite 12

FIGURE 2.7. Olivine-orthopyroxene cluster in harzburgite 13

FIGURE 2.8. Disequilibrium texture between orthopyroxene and olivine in an olivine-orthopyroxene cluster in harzburgite 14

FIGURE 2.9. Recrystallized grain of Cr-spinel in harzburgite 15

FIGURE 2.10. Grain of Ca-amphibole enclosed in coarse granular olivine in LAL dunite 16

FIGURE 2.11. Chain texture exhibited by Cr-spinel in LAL dunite 17

FIGURE 2.12. Multiple F_1 folds in a band of chromitite 18

FIGURE 2.13. LAL clinopyroxenite dyke intruding harzburgite and the centre of a type I orthopyroxenite dyke 19

FIGURE 2.14. Cumulate texture exhibited by Cr-spinel in a dunitic zone in LAL olivine clinopyroxenite 20

FIGURE 2.15. Thin bands of Cr-spinel in LAL dunite envelope around LAL olivine clinopyroxenite 21

FIGURE 2.16. Parallel intergrowth of olivine and orthopyroxene in type I orthopyroxenite 22

FIGURE 2.17. Embayment of olivine, tremolite and cummingtonite in orthopyroxene in type I orthopyroxenite 23

FIGURE 2.18. Clinopyroxene partially replaced by tremolite in type I orthopyroxenite 24

FIGURE 2.19. Tremolite and cummingtonite replacing orthopyroxene in type I orthopyroxenite 25

FIGURE 2.20. Orthopyroxene cut by shear zones in type I orthopyroxenite 26

FIGURE 2.21. Well equilibrated coarse granular texture of clinopyroxene in LAL clinopyroxenite 27

FIGURE 2.22. Irregular grain boundary of clinopyroxene in LAL clinopyroxenite 28

FIGURE 2.23. Orthopyroxene replaced by tremolite and olivine in LAL websterite 29

FIGURE 2.24. Clinopyroxene replacing orthopyroxene, and tremolite replacing ortho- and clinopyroxene in harzburgite 30

FIGURE 2.25. Web texture exhibited by type II orthopyroxenite in LAL dunite 31

FIGURE 2.26. Vein of LAL clinopyroxenite offset by narrow D_2 shear zones filled with type II orthopyroxenite ribbon mylonite 32

FIGURE 2.27. Boudin of websterite associated with ribbon mylonite of type II orthopyroxenite in D_2 shear zone 33

FIGURE 2.28. Cr-spinel hosting inclusions in web-textured type II orthopyroxenite 34

FIGURE 2.29. Monomineralic bands of orthopyroxene, olivine and Ca-amphibole in type II orthopyroxenite ribbon mylonite 35

FIGURE 2.30. Conjugate vein of type I orthopyroxenite partially pseudomorphed by amphibole dunite 36

FIGURE 2.31. Enclaves of type I orthopyroxenite in amphibole dunite 37

FIGURE 2.32. Well equilibrated mosaic equigranular texture of olivine in amphibole dunite 38

FIGURE 2.33. Sieve texture in poikiloblastic Cr-spinel in amphibole dunite 39

FIGURE 2.34. Modal layering of Al-spinel in HAL dunite 40

FIGURE 2.35. Band of fine grained Al-spinel cutting coarse grained Al-spinel in HAL dunite 41

FIGURE 2.36. Chain texture exhibited by Al-spinel in HAL dunite 42

FIGURE 2.37. Protrusion of Al-spinel associated with clinopyroxene along the grain boundary of adjacent grains of olivine in HAL dunite 43

FIGURE 2.38. Al-spinel containing inclusions in HAL wehrlite 44

FIGURE 2.39. HAL gabbro dyke grading to HAL wehrlite in a HAL gabbro-clinopyroxene dunite association 45

FIGURE 2.40. HAL wehrlite grading to HAL dunite and cut by HAL olivine clinopyroxenite 46

FIGURE 2.41. Reduction in grain size of Al-spinel from HAL dunite to HAL wehrlite 47

FIGURE 2.42. Dunitic portion of a HAL olivine clinopyroxenite dyke cutting LAL dunite 48

FIGURE 2.43. Gradational contact between LAL clinopyroxenite and HAL olivine clinopyroxenite 49

FIGURE 2.44. Interstitial clinopyroxene in a matrix of olivine in HAL wehrlite 50

FIGURE 2.45. Poikilitic clinopyroxene containing chadacrysts of olivine in HAL olivine clinopyroxenite 51

FIGURE 2.46. Xenoliths of harzburgite and LAL and HAL dunite in HAL olivine clinopyroxenite 52

FIGURE 2.47. Irregular HAL dunite xenoliths in HAL olivine clinopyroxenite 53

FIGURE 2.48. Veins of HAL olivine clinopyroxenite at the contact between HAL dunite and harzburgite 54

FIGURE 2.49. Assemblage of HAL olivine-spinel-clinopyroxene replacing harzburgite 55

FIGURE 2.50. Partially schematic phase relations for ultramafic rocks modelled by the system H_2O-Na_2O-CaO-MgO-Al_2O_3-SiO_2 with excess H_2O and Mg_2SiO_4 56

FIGURE 3.1. Frequency distribution of Mg# of olivine in LALPP 57

FIGURE 3.2. Compositional variation of orthopyroxene in LALPP 58

FIGURE 3.3. Cr# vs. Mg# of spinel in LALPP 59

FIGURE 3.4. Cr# vs. Mg# composition fields of spinel 60

FIGURE 3.5. Chondrite-normalized rare earth element abundances of LALPP 61

FIGURE 3.6. Chondrite-normalized platinum group element abundances of LALPP 65

FIGURE 3.7. Mineral/matrix equilibrium partition coefficients of rare earth elements for olivine, orthopyroxene, clinopyroxene and amphibole 69

FIGURE 3.8. CaO/Al_2O_3 vs. Mg# of harzburgites 70

FIGURE 3.9. Chondrite-normalized platinum group element abundances of a LAL clinopyroxenite dyke and associated dunite envelope and harzburgite 72

FIGURE 3.10. Estimated chondrite-normalized rare earth element abundances of magmas in equilibrium with type I orthopyroxenite and LAL clinopyroxenite 73

FIGURE 4.1. NiO vs. Mg# of olivine in HALPPG 75

FIGURE 4.2. Compositional variation of spinel in HALPPG 76

FIGURE 4.3. Compositional variation of clinopyroxene in HALPPG 77

FIGURE 4.4. $Na_2O + K_2O$-$FeO_{(total)}$-MgO (AFM) and CaO-Al_2O_3-MgO (CAM) diagrams (weight %) of whole-rock samples of HALPPG 78

FIGURE 4.5. Chondrite-normalized rare earth element abundances of HALPPG and amphibolite dykes 79

FIGURE 4.6. CAM diagram (weight %) of orthopyroxene in harzburgite and type I orthopyroxenite adjacent to HALPPG 80

FIGURE 4.7. Compositional variation of spinel in LALPP associated with HALPPG 81

FIGURE 4.8. Compositional variation of Cr-spinel in harzburgite cut by a vein of HAL olivine clinopyroxenite 82

FIGURE 4.9. Compositional variation of clinopyroxene, olivine and spinel across the contact between LAL olivine clinopyroxenite and HAL olivine clinopyroxenite 83

FIGURE 4.10. AFM and CAM diagrams (weight %) used to model the formation of HALPPG 84

FIGURE 5.1. Compositional variation of Ca-amphibole in LALPP and HALPPG 86

FIGURE 5.2. Compositional variation exhibited by a grain of spinel in amphibole dunite 87

FIGURE 5.3. Chondrite-normalized rare earth element abundances of amphibole-bearing rock types in the Springers Hill area 88

FIGURE A1.1. Precision of chondrite-normalized rare earth element abundances 93

FIGURE A1.2. Precision and accuracy of chondrite-normalized rare earth element abundances of USGS peridotite standard PCC-1 94

FIGURE A1.3. Chondrite-normalized rare earth element abundances of blanks and limits of detection in runs 182 and 024 95

LIST OF ABBREVIATIONS

Unless defined otherwise, the following abbreviations are used throughout this thesis:

Ab	albite; molecular % = (Na/(Ca+Na+K)) x 100
AFM	Na_2O+K_2O-$FeO_{(total)}$-MgO
Amph	amphibole
An	anorthite; molecular % = (Ca/(Ca+Na+K)) x 100
Ap	apatite
bdl	below detection limit
BIOC	Bay of Islands Ophiolite Complex
C	corundum
°C	degrees Celsius
CAM	CaO-Al_2O_3-MgO
CC	Coastal Complex
cm	centimetre
CN	chondrite-normalized
COV	coefficient of variation = (SD/mean) x 100
Cpx	clinopyroxene
Cpxt	clinopyroxenite
Cr#	(Cr/(Cr+Al)) x 100
D_i	deformation of the ith episode
Di	diopside
E	east
En	enstatite; molecular % = (Mg/(Mg+Fe^{2+}+Ca)) x 100, all Fe as Fe^{2+}
F_i	fold of the ith episode of deformation
Fs	ferrosilite; molecular % = (Fe^{2+}/(Mg+Fe^{2+}+Ca)) x 100, all Fe as Fe^{2+}
g	gramme
HAL	high-alumina
HALPPG	high-alumina peridotites, pyroxenites and gabbros
HREE	heavy rare earth element(s)
Hy	hypersthene
ICP-MS	inductively coupled plasma-mass spectrometer
Il	ilmenite
kbar	kilobar

km	kilometre
kV	kilovolt
l	litre
L_i	lineation of the ith episode of deformation
LAL	low-alumina
LALPP	low-alumina peridotites and pyroxenites
LOD	limit of detection
LREE	light rare earth element(s)
m	metre
Ma	million years
Mg#	$(Mg/(Mg+Fe^{2+})) \times 100$, all Fe as Fe^{2+}
ml	millilitre
mm	millimetre
MORB	mid-ocean ridge basalt
N	north
n	number of samples, analyses etc.
nA	nanoampere
na	not analysed
nd	not detected
Ne	nepheline
Ol	olivine
Opx	orthopyroxene
OPXT I	type I orthopyroxenite
OPXT II	type II orthopyroxenite
Or	orthoclase; molecular % = $(K/(Ca+Na+K)) \times 100$
P	pressure
PGE	platinum group element(s)
PGM	platinum group mineral(s)
Phlog	phlogopite
Plag	plagioclase
ppb	parts per billion
ppm	parts per million
Px	pyroxene
REE	rare earth element(s)
S	south
S_i	foliation of the ith episode of deformation
SD	sample standard deviation (n-1)
SEM	scanning electron microscope
Sp	spinel
T	temperature
μm	micrometre

USGS	United States Geological Survey
W	west
Wo	wollastonite; molecular % = $(Ca/(Mg+Fe^{2+}+Ca)) \times 100$, all Fe as Fe^{2+}
wt.%	weight per cent

Chapter 1

INTRODUCTION

1.1 GENERAL STATEMENT

Understanding physical and chemical processes in the upper mantle is critical to our understanding of global chemical budgets and the geochemical and geodynamic evolution of the crust-mantle system. The upper mantle is a massive reaction vessel that is best considered as a series of chromatographic columns, in which magmas and fluids interact with a variety of solid phases as they migrate away from their source regions (Navon and Stolper, 1987; Bodinier et al., 1990). The mineralogy and chemical compositions of upper mantle materials are controlled by partial melting and magma- and fluid-rock interactions over a wide range of temperatures and pressures in specific tectonic environments. This thesis reports on an investigation of the processes involved in the generation, migration and evolution of magmas and fluids in the uppermost mantle.

1.2 THE UPPER MANTLE

The mantle is located between the crust and the core of the Earth. It is divided into upper and lower regions. The upper mantle extends from the crust-mantle interface (the Mohorovicic Discontinuity, or Moho) to a depth of 600-1000 km. The lower mantle occupies the region between the upper mantle and the outer core which begins at a depth of 2900 km.

The upper mantle comprises lithosphere and asthenosphere, which lie above (lower temperature) and below (higher temperature) the 1000°C isotherm, respectively (Nicolas, 1986a). The lithosphere is relatively stronger than the asthenosphere, is thought to behave in a relatively brittle fashion, and consists of the crust and uppermost mantle. The lithosphere is 100-200 km thick in continental regions, 50-70 km thick in oceanic regions, and 0 km thick at oceanic ridges where magma is erupted onto the surface of the Earth.

1.2.1 Samples of Upper Mantle

In-situ mantle beneath a crustal carapace is at present inaccessible, but fragments of upper mantle ranging in size from < 1 m^3 to > 1000 km^3 occur in the crust as:

1) Mantle xenoliths entrained during eruption of kimberlites and alkali basalts. The majority of these xenoliths consist of mineral assemblages which were stable at depths of < 150 km (Boyd and Nixon, 1975).

2) Ophiolitic and orogenic mantle material tectonically emplaced into the crust

in zones of compression.

3) Tectonically uplifted portions of lithosphere, such as St. Paul's Rocks on the transverse ridge of St. Paul's Fracture Zone in the Atlantic Ocean (Melson et al., 1972), and Zabargad Island in the Red Sea (Bonatti et al., 1983).

Each type of sample has advantages when used to examine the upper mantle. The most significant of these, is that tectonically emplaced or uplifted mantle material allows in-situ examination of lithological and structural relations and mapping of mantle heterogeneities. This is not possible for mantle xenoliths, and yet much of our present knowledge of the processes and chemical and isotopic compositions of the mantle is based on information from xenoliths.

1.2.2 Composition of the Upper Mantle

The rock nomenclature of Streckeisen (1976) is applicable to the study of ultramafic rocks of the mantle and is used throughout this thesis (Fig. 1.1). Based on mineralogical, geochemical and geophysical data as reviewed by Ringwood (1975) and Yoder (1976), the upper mantle beneath stable continental regions and oceanic basins is composed of peridotite (Fig. 1.1) or eclogite (almandine-pyrope garnet and omphacite). The need for olivine as an essential constituent of the upper mantle, suggests that the upper mantle is composed dominantly of peridotite, but this does not preclude the existence of regions of eclogite, especially where subducted oceanic crust has been transformed to eclogite (Green and Ringwood, 1968; Ringwood, 1969, 1975).

Upper mantle material is described as 'fertile', 'refractory' or 'residual', and 'depleted' or 'enriched'. Fertile, refractory and residual are terms used to describe mineralogy and major element composition. Fertile mantle is capable of generating basaltic magma during partial melting, whereas refractory mantle is not. Residual mantle has experienced partial melting. Owing to single or multiple episodes of different degrees of partial melting and extraction of basaltic magma, residual mantle covers a wide range of compositions, from that which still is capable of yielding basaltic magma on partial melting (i.e., is fertile), to that which is incapable of yielding basaltic magma during further partial melting (i.e., is refractory). Examples of fertile peridotite are pyrolite (Ringwood, 1966), Tinaquillo lherzolite (Jaques and Green, 1980), Hawaiian pyrolite (Jaques and Green, 1980), mid-ocean ridge basalt (MORB) pyrolite (Falloon and Green, 1987), and the lherzolite compositions of Maaløe and Aoki (1977) and Jagoutz et al. (1979).

In agreement with Menzies and Hawkesworth (1987a), enriched and depleted are used as simple geochemical (trace element or isotopic) descriptions without any implication for the process(es) responsible. Enriched and depleted are used relative to a defined composition, such as another sample or group of samples, or the bulk Earth.

Mineral, major and trace element, and isotopic compositions of upper mantle materials are controlled by processes of partial melting, magma- and fluid-rock interactions, and mechanical mixing. The important aspects of these processes are summarized in the following sections.

1.2.3 Upper Mantle Heterogeneity

Attention has focused on the distribution and composition of physical and chemical components in the mantle and their influence on the compositions of magmas erupted at the Earth's surface. In essence, this has been a study of Earth evolution and mantle heterogeneity based on trace element and isotopic studies of samples of crust and mantle (Schilling, 1973; Wasserburg and DePaolo, 1979; O'Nions et al., 1980; Allègre et al., 1981, 1982; Anderson, 1981; Thompson et al., 1984; Menzies and Hawkesworth, 1987b).

Owing to the compositional variation exhibited by crustal materials, mantle heterogeneities have been mapped on scales of (i) >1000 km^2 as evidenced by the evolution of the Earth's crust over the last 3800 Ma (O'Nions et al., 1980), (ii) >1000 km as exemplified by the Dupal anomaly in oceanic basalts which encircles the Earth at about 30°S (Hart, 1984), and (iii) <5 km as in the Lamont seamounts near the East Pacific Rise (Fornari et al., 1988). Ultimately, this leads to the question posed by Carlson (1988): "Is the Earth's mantle chemically stratified or are there chemically distinct regions of various sizes distributed like plums in a pudding throughout the whole mantle ?". On a global scale there is sub-oceanic mantle and sub-continental mantle, but within these regions there are relatively local variations which could result from: 1) Marble cake mantle, in which bands of subducted oceanic lithosphere are present in the convecting mantle (Allègre and Turcotte, 1986; Kellogg and Turcotte, 1986/87, 1990). Evidence for this comes from the extreme isotopic variability exhibited by pyroxenite bands in orogenic peridotites (Polvé and

Allègre, 1980; Allègre and Turcotte, 1986), and by basaltic glasses from the East Pacific Rise (Prinzhofer et al., 1989).

2) Veining of the mantle by magmas and fluids (Wood, 1979), and the consequent magma- and fluid-rock interactions, especially those involving volumes of magma or fluid which occupy <0.1 % of the mantle (McKenzie, 1989; Menzies, 1990).

A classic example of upper mantle heterogeneity has been documented in the Ronda Peridotite, Spain. These peridotites range from lherzolite to harzburgite and exhibit a wide range of whole-rock major element compositions (Frey et al., 1985). Partial melting of fertile lherzolite and extraction of MORB magma left residues of refractory harzburgite (Frey et al., 1985). However, isotopic compositions of Cr-diopside separates from these peridotites are extremely variable and are not restricted to the field of MORB (Reisberg and Zindler, 1986/87). This suggests that after partial melting, the peridotites interacted with a fluid which modified isotopic evolution (Reisberg and Zindler, 1986/87).

1.2.4 Mantle Metasomatism

The concept of mantle metasomatism is unavoidable in any study of the mantle, but before it can be assessed it is essential to define terminology. Wilshire (1987) defines metasomatism as "a process or processes whereby the mineralogy and/or chemical composition of a solid rock is altered by the introduction of chemical components from an external source; the alteration

process is commonly accompanied by loss of other components from the altered rock." Where components are introduced with the aid of intergranular fluids (including magmas), it is called infiltration metasomatism; where components are introduced without the aid of these intergranular phases, it is termed diffusion metasomatism (Korzhinskii, 1970). The terms cryptic and patent metasomatism (Dawson, 1984) and modal metasomatism (Harte, 1983) have been applied to mantle xenoliths. Patent and modal metasomatism essentially are synonymous and are recognizable through replacement textures and development of hydrous phases in the altered rock. Infiltration obviously is a dominant process. Cryptic metasomatism is recorded by trace element enrichment apparently unaccompanied by mineralogical changes; this implies the operation of diffusional processes.

There is some confusion over use of the term 'fluid'. Wyllie (1987) states: "'Fluid' is a descriptive term applicable in geological contexts to liquid (melt, magma, silicate melt with dissolved volatile components), vapour (dense gas, pneumatolytic gas, hydrothermal solution), supercritical solution, or to an undefined fluid phase. Fluid also has a more restricted meaning in phase equilibria; it is the phase that is indeterminate between liquid and vapour, where critical phenomena occur." Magma will be used in this work to imply a silicate melt that can contain crystals, rock fragments and dissolved volatile components; in the classification of Eggler (1987), this is a fluid-bearing melt (Fig. 1.2). Fluid will be used to imply a volatile component which corresponds to the melt-bearing fluids of Eggler (1987) (Fig. 1.2).

Frey and Green (1974) presented data on lherzolite xenoliths from Australian basanites that clearly demonstrated the concept of mantle metasomatism through a two component mixing model. Component A was the residue from partial melting which controlled the major mineralogy, major element composition, and abundances of compatible trace elements such as Ni, Co and heavy rare earth elements (HREE). Component B was a migrating fluid which was not genetically related to component A. It controlled the abundances of incompatible trace elements such as K, P, Th, U and light rare earth elements (LREE).

Following Frey and Green (1974) and Lloyd and Bailey (1975), mantle metasomatism became an essential process by which to explain the mineralogical, chemical and isotopic diversity of mantle peridotites and the magmas derived from them.

1.2.5 Magma- and Fluid-Peridotite Interactions

During the emplacement of intrusions of various sizes into mantle peridotites, associated reaction zones develop at the intrusion-peridotite interface. These zones are the sites of magma- and fluid-peridotite interactions, of which there are two types. The first type occurs where peridotites become enriched in Fe, Ti, Al, Na, K and incompatible trace elements (LREE) by injection of basaltic magma and/or associated fluid (Wilshire and Jackson, 1975; Stewart and Boettcher, 1977; Irving, 1980; Wilshire et al., 1980); this enrichment may result from the crystallization of new phases in the peridotite

(Wilshire, 1984). The second type is equatable with the process of zone refining (Harris, 1957), by which magma or fluid assimilates the minimum melting component of the peridotite and becomes enriched in Na, K, Ca, Al, Ti, Si, Rb, Sr, U and LREE (Green and Ringwood, 1967; Quick, 1981a). Both these interactions can occur together by the simultaneous solution and precipitation of mineral phases in the peridotite.

1.2.6 Magma and Fluid Migration in the Upper Mantle

The mode of magma and fluid migration in the upper mantle is extremely important, as it controls the extent of magma- and fluid-rock interactions and mantle metasomatism. Magmas and fluids migrate by (i) diapiric ascent, (ii) magma fracture and conduit flow, (iii) percolation, and (iv) transport along shear zones.

As a solid diapir rises in the upper mantle due to buoyancy effects (free convection of Spera (1980)) or stress induced flow (forced convection of Spera (1980)), it will partially melt by adiabatic decompression (Bottinga and Allègre, 1978). Magma will accumulate in zones where the permeability threshold of the diapir is reached and exceeded (Maaløe, 1981, 1982). Two possibilities exist at this point: (i) at depth, magma will accumulate and escape by fluid or magma assisted shear fracturing in the deforming peridotite (Weertman, 1972; Nicolas, 1986b), whereas at shallower depth this will occur by hydraulic fracturing (Shaw, 1980; Nicolas and Jackson, 1982; Nicolas, 1986b; Spera, 1987; Spence and Turcotte, 1990); (ii) magma will percolate through the

peridotite matrix by porous flow (Sleep, 1974; Turcotte and Ahern, 1978; McKenzie, 1984; Scott and Stevenson, 1984; Phipps Morgan, 1987). The abundance of veins and dykes in samples of upper mantle peridotite (Nicolas and Jackson, 1982; Nicolas, 1986b; Wilshire and Kirby, 1989), suggests that hydraulic fracture is the dominant mechanism of magma extraction in the upper mantle. Extremely refractory peridotites such as dunites, may be residues from highly efficient drainage of the magma conduit (Nicolas, 1986b). Percolation will be important where a magma cannot maintain hydraulic fracture and impregnates its host-rock (Nicolas, 1989). If ascent rates of magma are high and conduits are well defined, there will be minimal interaction between magma and host-rock.

Conditions for migration of fluid are significantly different from those of magma, because of the lower viscosity and reactive nature of fluid. If a fluid is in equilibrium with its host-rock, then it will migrate without reacting and hydraulic fracture theory can be applied in this situation (Spera, 1987). Generally, however, it would appear that fluids infiltrate their host-rock by percolation by porous flow and react with it (Spera, 1987). Large volumes of fluid may be concentrated in shear zones in the lithosphere (Beach, 1976; McCaig, 1984; Sinha et al., 1986; Kerrich and Rehrig, 1987), which then become important zones of heat and mass transport (Bickle and McKenzie, 1987). Because fluids generally have a more pervasive mode of migration than magmas, they are capable of significantly modifying the composition of their host-rock.

1.2.7 Factors Affecting the Composition of Upper Mantle Peridotite

From the previous sections it is evident that the upper mantle is a dynamic reaction vessel. Mineralogical, chemical and isotopic compositions of upper mantle peridotites and the magmatic and fluid components which they host, are controlled by processes of (i) partial melting, (ii) magma- and fluid-rock interactions, and (iii) mechanical mixing, all of which occur over a wide range of temperatures and pressures in specific tectonic environments. Only by integrating field, petrographic and geochemical studies can we begin to unravel the complexities of these processes. Hence, ophiolitic and orogenic peridotites must be primary targets of investigations of upper mantle processes.

1.3 OPHIOLITIC AND OROGENIC PERIDOTITES

1.3.1 Classification and Origin

Tectonically emplaced peridotite massifs were called alpine-type peridotites by Thayer (1960) and have been divided into two groups (Thayer, 1960; Green, 1967; Den Tex, 1969; Jackson and Thayer, 1972): the lherzolite group (known also as orogenic root zone or high temperature peridotites), and the harzburgite group (known also as ophiolitic or low temperature peridotites). By a sequence of tectonic events, both groups have been emplaced into or onto continental crust as bodies which are <15 km thick (Spray, 1989).

It is here proposed that peridotite bodies conforming to the Penrose Conference definition of an ophiolite (Anonymous, 1972), be called ophiolitic

peridotites, and those which do not, be called orogenic peridotites. In cases where bodies have not been severely dismembered, the former are associated with an oceanic crustal sequence, whereas the latter are not (Spray, 1989). This classification is by no means rigorous, but is in keeping with previous definitions and will serve its purpose in this work.

Orogenic peridotite massifs are composed of peridotites (mainly lherzolite) containing variable proportions of bands and dykes of pyroxenite and gabbro, e.g., Ronda (S. Spain), Lherz and Ariège (S. W. France), Lanzo (N. Italy) and Beni Bousera (N. Morocco). Equilibration is recorded in the garnet, spinel and plagioclase stability fields, e.g., the Ronda Peridotite (Obata, 1980). Nicolas and Jackson (1972) interpreted orogenic peridotite massifs as fragments of sub-continental mantle or deep sub-oceanic mantle. Prior to melting, many of these peridotites were fertile sources for the generation of MORB magmas, e.g., the Ronda Peridotite (Frey et al., 1985).

Ophiolitic peridotites (mostly lherzolite and harzburgite) contain variable proportions of bands and intrusions of dunite, chromitite, pyroxenite, wehrlite and gabbro. Equilibration occurred predominantly in the spinel stability field. As examples, ophiolitic peridotites occur in the Troodos Ophiolite (Cyprus), the Oman Ophiolite, and the Bay of Islands Ophiolite (Canada). There is a complete spectrum of compositions in ophiolitic peridotites which can be related to their crustal sequence. This has led to a number of classification schemes for ophiolite complexes and these are compiled in Table 1.1. Nicolas and Jackson (1972) interpreted ophiolitic peridotites as fragments of uppermost sub-oceanic

mantle. This view is held currently, but there is a debate prompted by Miyashiro (1973) concerning the exact tectonic environment which ophiolites represent, e.g., mid-ocean ridge, back-arc basin or forearc region. The mantle section of an ophiolite will be extremely sensitive to this environment, because it will record the degree of partial melting and the compositions of magmas and fluids that have traversed the mantle peridotites (Table 1.1).

1.3.2 Mafic and Ultramafic Bodies Hosted by Peridotite

Bodies of mafic and ultramafic material hosted by ophiolitic and orogenic peridotites occur as layers (called bands from here on so as to have no genetic implication), dykes, veins, lenses and pods that have been documented in all peridotites (Spray 1982, 1989). They typically are <1 m thick and parallel (concordant) or cross-cut (discordant) the high temperature tectonite fabric of their hosting peridotite. Textures where minerals are coarse grained with interlocking grain boundaries are indicative of magmatic crystallization, whereas granoblastic, mylonitic, schistose or gneissose textures are indicative of subsolidus deformation. Mineralogy is dominated by pyroxene $\pm$ olivine $\pm$ plagioclase $\pm$ spinel $\pm$ garnet $\pm$ amphibole $\pm$ mica. Mafic and ultramafic bodies in lherzolites are dominated by clinopyroxene and have a basaltic bulk composition (Loubet and Allègre, 1982; Spray, 1982, 1989). Those in harzburgite frequently are monomineralic, such as dunite, chromitite, orthopyroxenite and clinopyroxenite, and do not have a basaltic bulk composition (Reuber et al., 1985). Bodies of websterite, wehrlite and gabbro

also occur in harzburgite.

Numerous models have been proposed to explain the origin of mafic and ultramafic bodies hosted by ophiolitic and orogenic peridotites. These bodies represent:

1) Crystallized magmas that may be in-situ and primary (Boudier and Nicolas, 1972; Dickey et al., 1979; Reuber et al., 1985), or crystallized magma fractions (Moores, 1969; Malpas, 1978; Harkins et al., 1980; Quick, 1981b; Boudier and Coleman, 1981; Hopson et al., 1981; Loubet and Allègre, 1982; Reuber et al., 1982; Sinigoi et al., 1983; Gregory, 1984) that could form by gravitational crystal accumulation (Raleigh, 1965; Conquéré, 1977).

2) Material introduced downward into the mantle from the base of a magma chamber by subsidence of cumulates (Dickey, 1975) or injection of dykes (Reuber et al., 1982, 1985).

3) 'Xenocryst cumulates' produced by high temperature minerals accumulating when a peridotite undergoes >50 % partial melting (Ishiwatari, 1985a).

4) Flow layers within a crystal mush (Thayer, 1963).

5) Metasomatites (Bowen and Tuttle, 1949; Carswell et al., 1974; Loomis and Gottschalk, 1981).

6) Metamorphic differentiates produced by (i) deformation (Walcott, 1969; Moores, 1969; Loney and Himmelberg, 1976; Dick and Sinton, 1979), (ii) pressure solution creep (Dick and Sinton, 1979), or (iii) anatexis (Dick and Sinton, 1979).

7) Restites produced by the partial melting of pre-existing bands or dykes

(Shervais, 1979; Loubet and Allègre, 1982, Sinigoi et al., 1983).

8) Recycled oceanic crust (Allègre and Turcotte, 198€; Kellogg and Turcotte, 1986/87, 1990).

Any of the above may be transposed into parallel alignment with the peridotite foliation (Wilshire and Pike, 1975; Boudier, 1978; Cassard et al., 1981; Nicolas and Jackson, 1982).

1.3.3 Magma- and Fluid-Peridotite Interactions

Magma- and fluid-peridotite interactions were described in section 1.2.5. Classic examples of both types of interaction are found in ophiolitic and orogenic peridotites:

1) Clinopyroxene and feldspar crystallize from magmas impregnating harzburgites and dunites (Dick, 1977; Sinton, 1977; George, 1978; Savelyev and Savelyeva, 1979; Violette, 1980; Nicolas et al., 1980; Boudier and Coleman, 1981; Nicolas and Prinzhofer, 1983; Nicolas and Dupuy, 1984; Evans, 1985; Evans and Hawkins, 1989). This often occurs where magma is expelled into the peridotite ahead of the intrusion, because the magma or fluid can no longer hydraulically fracture the peridotite (Nicolas, 1989).

2) The other type of interaction is exemplified by the formation of dunite by in-situ reaction of pyroxene-bearing peridotite with an introduced magma or fluid (Boudier and Nicolas, 1972, 1977; Dick, 1977; Sinton, 1977; Dungan and Avé Lallemant, 1977; Leblanc et al., 1980; Quick, 1981a; Cassard et al., 1981; Nicolas and Prinzhofer, 1983; Gregory, 1984; Kelemen, 1990) (Fig. 1.3).

1.4 OBJECTIVES AND APPROACH

The following testable hypothesis forms the basis of this thesis:

Processes of partial melting and magma- and fluid-rock interaction in different tectonic environments are likely to be similar, but the compositions of residues, magmas and fluids will differ. As a magma or fluid migrates away from its source region it will attempt to equilibrate with the environment through which it passes. A fast moving magma or fluid undergoing little or no equilibration will reflect the composition of its source, whereas a magma or fluid undergoing continuous equilibration will reflect the composition of the rock with which it last equilibrated. Magmatic and fluid components in the upper mantle range from completely crystallized primary compositions to monomineralic crystal fractionates, all of which have experienced different degrees of magma- and fluid-rock interaction. The mantle is a dynamic system that experiences numerous episodes of partial melting and magma and fluid activity during continuous deformation. The most complete record of these episodes is preserved in regions of low strain. Heterogeneities are rapidly destroyed by diffusion and mechanical mixing in regions of high strain.

A test of this hypothesis requires a very practical approach which integrates field and petrographic observations with geochemical data. In this thesis the emphasis is on understanding the processes of magma and fluid generation, migration and evolution in the uppermost mantle. Special attention is paid to developing the platinum group elements (PGE) as petrogenetic

tracers.

1.5 AREA OF STUDY

The Bay of Islands Ophiolite Complex (BIOC), western Newfoundland, Canada, was selected for this study because of its excellent exposure of uppermost mantle, and convenient accessibility. Following reconnaissance work in the BIOC, the Springers Hill area of the Lewis Hills Massif was selected for a detailed study. Before discussing the geology of the latter, the geology of the BIOC is considered.

1.5.1 Regional Geology and Origin of the Bay of Islands Ophiolite Complex

The island of Newfoundland lies at the centre of the Appalachian-Caledonian Orogen. From west to east the island is divided into the Humber, Dunnage, Gander and Avalon tectonostratigraphic zones (Williams, 1979). The Humber Zone documents the opening and closing of the proto-Atlantic Ocean (Wilson, 1966). The Humber Arm Allochthon was emplaced onto the ancient continental margin of North America during the Middle Ordovician Taconian Orogeny as an assembled series of stacked thrust slices of east to west derivation (Malpas, 1976). The BIOC and the Coastal Complex (CC) are two adjacent Cambro-Ordovician ophiolite terranes that occupy the highest structural slices of the Humber Arm Allochthon (Stevens, 1970; Church and Stevens, 1970a, b, 1971; Bird and Dewey, 1970; Williams, 1971; Williams and

Malpas, 1972; Church, 1972; Malpas, 1973, 1976). Together they form a discontinuous, north-northeast trending belt of mafic-ultramafic rocks some 100 km long and 25 km wide (Fig. 1.4). From north to south the BIOC comprises the Table Mountain, North Arm Mountain, Blow Me Down Mountain and Lewis Hills massifs. There is disagreement over the definition of the CC. For Karson and Dewey (1978), Casey et al. (1983) and Karson (1984), the CC is that defined in Figure 1.4, whereas for Williams (1973) it is called the Little Port Complex and does not include the western part of the Lewis Hills Massif which belongs to the BIOC. In keeping with the terminology of Karson and Dewey (1978), Casey et al. (1983) and Karson (1984), their definition of the CC will be used throughout this work (Fig. 1.4).

Two distinctly different origins have been proposed for the BIOC and CC: (i) the BIOC formed at a major seafloor spreading centre (Casey et al., 1983, 1985), whereas the CC represents oceanic crust that has experienced a transform fault tectonic history within an oceanic fracture zone (Karson and Dewey, 1978; Karson, 1984); (ii) in contrast, Malpas et al. (1973) and Malpas (1979a) interpreted the CC as an arc assemblage, which is supported by the supra-subduction zone/back-arc basin origin proposed by Malpas (1976), Searle and Stevens (1984), Edwards (1990) and Jenner et al. (in press) for the evolution of the BIOC and CC. Age data are crucial for determining which origin is most plausible. The BIOC has been dated at 501-508 Ma (Mattinson, 1976; Jacobsen and Wasserburg, 1979) and 476-489 Ma (Dunning and Krogh, 1985; Jenner et al., in press), whereas the CC has been dated at 505-508 Ma

(Mattinson, 1975; Jenner et al., in press). Similar ages of the two complexes are likely to support origin (i), whereas origin (ii) may accommodate similar or dissimilar ages.

The metamorphic sole underlying the BIOC has been dated at 454-460 Ma (Dallmeyer and Williams, 1975; Archibald and Farrar, 1976) and forms an integral part of the ophiolite which documents dynamothermal metamorphism during transport of the ophiolite slice (Church and Stevens, 1971; Williams, 1971; Williams and Smyth, 1973; Malpas et al., 1973; Malpas, 1976, 1979b). Intra-oceanic thrusting and obduction of the BIOC is recorded by the mylonitic fabric in the sole and basal peridotites of the mantle sequence (Girardeau and Nicolas, 1981). The metamorphic sole may represent the hanging wall of a once east-dipping subduction zone, in which the BIOC occupied the forearc of the overriding plate (Casey and Dewey, 1984). According to Karson and Dewey (1978) and Casey and Dewey (1984), the fracture zone preserved in the CC was the nucleation site for the subduction zone and obduction of the BIOC.

1.5.2 The Mantle Section of the Bay of Islands Ophiolite Complex

In the mantle section of the BIOC, harzburgite is the most abundant residual peridotite and occurs with lesser amounts of lherzolite and dunite. These peridotites crop out in each massif and reach a maximum thickness of 5 km (Malpas, 1978). The occurrence of fertile lherzolite in Table Mountain (Malpas, 1978) and abundant refractory peridotites in the southern massifs,

suggests either a change in tectonic setting or degree of fertility in a given tectonic environment. According to the classification in Table 1.1, this southward trend reflects a change from the lherzolite to the harzburgite ophiolite type. This agrees with the relatively high abundances of chromitite and wehrlite in the Lewis Hills Massif (Dunsworth et al., 1986).

1.5.3 The Springers Hill Area of the Lewis Hills Massif

The Lewis Hills Massif preserves an original, subvertical contact between the BIOC and CC. This contact is marked by the Mount Barren Assemblage of the CC, which is a prominent belt of highly deformed greenschist, amphibolite and granulite facies rocks that are intruded by wehrlite-lherzolite crystal mush intrusions (Karson, 1977, 1979, 1984; Karson and Dewey, 1978; Karson et al., 1983) (Fig. 1.5). The Mount Barren Assemblage records the transform domain of the fracture zone in model (i) of section 1.5.1.

The Springers Hill area conforms to the harzburgite ophiolite type (Table 1.1), and is situated in the eastern part of the Lewis Hills Massif in the BIOC, but lies directly adjacent to the CC (Fig. 1.5). Dunsworth et al. (1986) defined an early suite of refractory harzburgite, dunite and mafic-ultramafic cumulates, and a late suite of dunite, wehrlite, clinopyroxenite and gabbro. These record a complex history of syn-kinematic multiple intrusion and ductile deformation (Dunsworth et al., 1986).

The area investigated in the present study is 2 km^2 and provides 40-50 % exposure of uppermost mantle peridotites which exhibit spectacular evidence

for magmatic and fluid activity and interaction. As such, it is the best locality in the BIOC to study the processes of magma and fluid generation, migration and evolution. The structure of the area has been extensively documented by Karson (1979), Dahl and Watkinson (1986), Dunsworth et al. (1986) and Suhr et al. (in press), which provided an excellent foundation on which to base this petrologic study.

1.5.3a Mapping and Access

The area was mapped by the author during the Summer of 1987. Mapping was undertaken at a scale of 1:4000 on enlargements of the Province of Newfoundland and Labrador Department of Forest Resources and Lands 1:12500 scale colour aerial photographs NF84020-14, -121 and -122. The Department of Energy Mines and Resources 1:50000 scale map sheet 12 B/16, Georges Lake, covers the eastern part of the Lewis Hills Massif.

There are no roads close to the field area and access by helicopter is a necessity. Camp equipment and provisions were flown in from the communities of Pasadena and Fox Island River which are easily accessible by road. The field area is barren, rugged and gently undulating, and is easily traversed on foot.

1.5.3b Chemical Classification of the Springers Hill Area

Based on mineral chemistry, the rock types in the mantle section of the Springers Hill area occupy two compositionally distinct fields (Fig. 1.6). Olivine

and clinopyroxene plot in two fields, but there is some degree of overlap. Spinels define two well separated fields and are used to classify the rock types as low-Al peridotites and pyroxenites (LALPP), and high-Al peridotites, pyroxenites and gabbros (HALPPG). The classification of rock types of the Springers Hill area as LALPP and HALPPG is similar to those mapped by Dunsworth et al. (1986) as early suite and late suite, respectively.

1.6 FORMAT OF THE THESIS

The subsequent chapters of this thesis are arranged in such a way that after description and interpretation of the field relations and petrography in Chapter 2, each chapter is a study which can stand alone. Chapters 3 and 4 are concerned with the chemistry and petrogenesis of LALPP and HALPPG, respectively. Chapter 5 examines the physical and chemical interactions of fluid in mantle lithosphere, and Chapter 6 is a summary of the thesis which emphasizes the importance of the Springers Hill area in studies of the upper mantle.

Chapter 2

FIELD RELATIONS AND PETROGRAPHY

2.1 INTRODUCTION

This chapter describes the rock types found in the Springers Hill area and the deformation which they record. Emphasis is placed on the spatial relations of rock types with respect to one another and to domains of deformation. Particular attention is paid to features which document interaction between low-Al peridotites and pyroxenites (LALPP) and high-Al peridotites, pyroxenites and gabbros (HALPPG).

Petrographic descriptions are broad owing to wide variations in modal composition within a given rock type, and between certain rock types. Detailed descriptions are reserved for features particularly relevant to this study. The terminology adopted for textures arising from deformation and recrystallization follows that of Mercier and Nicolas (1975), except that coarse granular (Boullier and Nicolas, 1975) is used as a purely descriptive term in place of protogranular. Terminology of cumulate textures is based on Wager et al. (1960). Recognition of textures frequently is hampered by the development of serpentine, bastite, uralite, chlorite and other minor phases arising from low temperature alteration. Thin sections were made from samples cut

perpendicular to their foliation and parallel to their lineation where lineation could be defined.

2.2 OVERVIEW OF THE FIELD AREA

As previously defined by Dunsworth et al. (1986), the Springers Hill area comprises rocks of the mantle and crust. The mantle sequence is divisible into LALPP, HALPPG, and a marginal zone which in places separates the two (Fig. 2.1 in map pocket). The LALPP are harzburgite, dunite, chromitite, orthopyroxenite, clinopyroxenite, amphibole dunite and minor websterite, whereas the HALPPG are dunite, wehrlite, olivine clinopyroxenite, gabbro and amphibole peridotite. The marginal zone contains all these rock types. The geological map (Fig. 2.1) illustrates that the uppermost mantle in the Springers Hill area is extremely heterogeneous with respect to the distribution of rock types and deformation. The crustal sequence was not mapped or sampled in any detail in this study, and its relation to the mantle sequence is not known. Hence, the crustal rocks are uncorrelated, but consist of wehrlite and gabbro which host amphibolite dykes (Fig. 2.1).

Two episodes of deformation have affected the area, and these are thoroughly documented by Dahl and Watkinson (1986), Dunsworth et al. (1986) and Suhr et al. (in press). These episodes are denoted D_1 and D_2, and are recorded by high temperature S_1 or L_1-S_1 and $L_2 \geq S_2$ tectonite fabrics, respectively. D_1 is preserved only in LALPP along the southern portion of the

mapped area, where S_1 trends N-S to NE-SW and has a vertical to steep W to NW dip. Mylonitic ductile simple shear zones that record D_2 are ≤ 700 m wide and occur in all rock types throughout the area. Along the western portion of the mapped area, S_2 trends NNE-SSW to NE-SW and has a shallow WNW to NW dip; lineations are N to NNE and shallow plunging. Along the southern portion of the mapped area, S_2 is E-W with a shallow N dip. The variation in orientation of S_2 in the northern part of the mapped area was produced by doming of this region during formation of the HALPPG (Dunsworth et al., 1986). Faulting appears to correlate with D_2 because of high temperature shear displacement along fault surfaces. The thrust faults at the northern extent of the mapped area are completely hosted within D_2 shear zones and thrust surfaces lie parallel to the plane of S_2. Multiple thrusting has juxtaposed slices of LALPP and uncorrelated wehrlite and gabbro, which has produced an interleaved stack of slices (Fig. 2.2).

To understand the mantle section of the Springers Hill area, it is imperative that magmatic and fluid activity and deformation are considered together, because deformation continually modifies primary magmatic and fluid features and relations, and magmas and fluids assist recrystallization and deformation. The relative time of formation of rock types is summarized in Figure 2.1.

2.3 LOW-Al PERIDOTITES AND PYROXENITES

Within the LALPP generally there is a west to east distribution of the rock types, which results in a regional banding parallel to the dominant tectonite fabric (Fig. 2.1). The west is dominated by harzburgite and dunite and their amphibole-bearing equivalents. On moving east, harzburgite, dunite, orthopyroxenite (OPXT I, see section 2.3.4a) and clinopyroxenite give way to harzburgite, dunite and clinopyroxenite. Harzburgite almost always is the host of OPXT I, whereas dunite usually hosts clinopyroxenite. Consequently, on moving from west to east, the ratios of harzburgite/dunite and OPXT I/clinopyroxenite both decrease. Because concentrations of chromitite correlate with abundances of dunite and clinopyroxenite, chromitite is more abundant in the east than in the west, and culminates in the Springers Hill chromitite showing. Dunites, chromitites and clinopyroxenites in the southeastern part of the mapped area often are displaced along shear zones. Folded structures have developed which were attributed to shear folding by Dahl and Watkinson (1986). These features correlate with the western limb of a synform defined by Dunsworth et al. (1986).

2.3.1 Harzburgite

2.3.1a Field Relations

Harzburgite apparently is the oldest rock type preserved in the Springers Hill area. Large volumes of pure harzburgite are rare due to the abundance of

intrusive phases and local gradation into dunite. Porphyroclasts of orthopyroxene define S_1 and S_2, and these fabrics are enhanced by concordant and subconcordant mm- to m-wide veins and dykes and their boudinaged equivalents of dunite, OPXT I and clinopyroxenite. Veins and dykes may be isoclinally folded, especially in D_2 shear zones.

Harzburgite has a modal composition of 50-90 % olivine, 10-50 % orthopyroxene, < 2 % Cr-spinel, frequent, but modally insignificant amphibole, and rare clinopyroxene. The olivine/orthopyroxene ratio of harzburgite is extremely variable. Where harzburgite grades into dunite, there is a progressive decrease in the concentration of orthopyroxene as the dunite is approached. A high concentration of orthopyroxene correlates with the presence of OPXT I, and manifests itself as (i) individual grains and veins associated with the margins or terminations of massive dykes of OPXT I (Fig. 2.3), or (ii) stretched, boudinaged and highly disaggregated veins of OPXT I. A screen of harzburgite may separate OPXT I from adjacent dunite. These relations suggest that a significant percentage of the modal orthopyroxene in harzburgite may have been derived from OPXT I.

2.3.1b Petrography

The petrographic description of harzburgite is restricted to those samples recording the D_1 deformation. The D_1 event is recorded by porphyroclasts (≤ 5 mm) and neoblasts of orthopyroxene distributed unevenly throughout a matrix of olivine. This heterogeneity can result in alternating bands of orthopyroxenite

and dunite (Fig. 2.4). Olivine is coarse granular ($\leq$10 mm) in dunite, but is much finer grained in the presence of orthopyroxene, where polygonized grains of olivine ($\leq$0.1 mm) define a mosaic equigranular texture. Olivine interstitial to orthopyroxene in aggregates of orthopyroxene is coarser grained ($\leq$0.5 mm) and embays orthopyroxene. Grain boundaries of olivine and orthopyroxene usually are well equilibrated (curvilinear to straight grain boundaries, well equilibrated triple junctions), but bent and kinked substructures occur in orthopyroxene porphyroclasts and neoblasts and coarse granular olivine. Orthopyroxene rarely has exsolutions of clinopyroxene, but contains round and oval inclusions of olivine and equant to oval inclusions of spinel. Inclusions and trails of inclusions of spinel and unidentified opaque, transparent and translucent phases are more common in finer grained olivine than in orthopyroxene and coarse granular olivine. The silicate portion of harzburgite is 40-70 % altered depending on the modal abundance of olivine.

Cr-spinel is most abundant in samples richest in orthopyroxene. Cr-spinel most commonly is found in orthopyroxenes or at the grain boundaries of orthopyroxenes, but also occurs at the grain boundaries of coarse granular olivines. The grain size of Cr-spinel exhibits a bimodal distribution occurring as large grains ($\leq$1 mm) containing inclusions of olivine, serpentine and orthopyroxene, and as minute grains disseminated throughout a sample. Porphyroclastic and pull-apart textures are dominant, but their less deformed and recrystallized equivalents do occur (Fig. 2.5). The foliation defined by Cr-spinel either is concordant or discordant with respect to S_1 defined by

orthopyroxene (Fig. 2.4).

A relatively late generation of orthopyroxene manifests itself as delicate, interstitial grains ($\leq$ 1.5 mm). This orthopyroxene is most obvious where it is oblique to banding in coarse granular olivine (Fig. 2.6). In areas of low strain, the interstitial texture is preserved, but in areas of higher strain, the texture is obliterated and the orthopyroxene inherits a porphyroclastic texture. The orthopyroxene exhibits partial replacement by olivine (Fig. 2.6).

A very distinct feature in many harzburgites is the occurrence of olivine-orthopyroxene clusters hosted in coarse granular olivine (Fig. 2.7). The clusters contain remnants of porphyroclasts and aggregates of porphyroclasts of orthopyroxene in a matrix of mosaic equigranular olivine. Spinel is a minor phase in these clusters; it occurs as minute blebs and vermicular grains in mosaic equigranular olivine, and along the contact between olivine and orthopyroxene (Fig. 2.8). The highly embayed grain boundaries of orthopyroxene in contact with olivine, and the optical continuity of islands of orthopyroxene in olivine, demonstrate that orthopyroxene has been replaced by olivine with the production of minor spinel (Fig. 2.8). In extreme cases, zones of mosaic equigranular olivine ($\leq$7 mm) exist which do not contain orthopyroxene. The irregular morphology of orthopyroxene, olivine and spinel, indicates disequilibrium with no overprint of deformation or recrystallization associated with D_1. Olivine-orthopyroxene clusters most commonly are encountered in harzburgites adjacent to HALPPG.

Ca-amphibole occurs in association with orthopyroxene and Cr-spinel in

many harzburgites. It commonly is encountered in samples with olivine-orthopyroxene clusters, but may or may not be associated with the cluster itself. Cr-spinel associated with Ca-amphibole often is equant to sub-equant, has grain boundaries embayed by Ca-amphibole, and contains inclusions of olivine, serpentine, Al-orthopyroxene, clinopyroxene, Ca-amphibole, phlogopite, magnetite and magnesioferrite (Fig. 2.9). This Cr-spinel recrystallized in the presence of Ca-amphibole after the D_1 event.

2.3.2 Dunite

2.3.2a Field Relations

The complex nature and 50-98 % serpentinization of dunites makes it difficult to correlate them. Dunites dominantly occur within harzburgite and bordering chromitite and clinopyroxenite. Their association with chromitite and clinopyroxenite is described in sections 2.3.3 and 2.3.4e, respectively.

Dunites have a modal composition of olivine (85-98 %), Cr-spinel (2-15 %) and minor pyroxene and Ca-amphibole. Morphologically, dunites occur as pods up to 400 m wide, veins and dykes. These occurrences possess both sharp (restricted mainly to veins and dykes) and ragged (restricted mainly to pods) contacts with harzburgite. Dykes and veins rarely are tabular for more than several metres, and are concordant and discordant with respect to the orthopyroxene S_1 fabric in harzburgite. Dunites that have ragged contacts with harzburgite, in some places contain fragments of harzburgite. The concordance of the foliation between harzburgite fragments and harzburgite hosting the

dunite, suggests in-situ replacement of harzburgite by dunite. These dunites contain a few isolated grains of orthopyroxene and a concentration and distribution of Cr-spinel similar to that of the adjacent harzburgite. In certain cases, the margin of a dunite may exhibit the aforementioned features, but as the centre of the dunite is approached, (i) the proportion of orthopyroxene decreases to < 2 modal %, (ii) the concentration of Cr-spinel increases, and (iii) a Cr-spinel banding may develop.

Based on the features observed in the core regions of dunite veins and dykes, two generations of dunite have been defined. The earliest contains minor orthopyroxene and is rich in Cr-spinel. The Cr-spinel is disseminated throughout the dunite matrix, but may concentrate in homogeneous and layer-like bands in the centre of the dunite (see section 2.3.3). The later generation is devoid of orthopyroxene and contains disseminated Cr-spinel at < 1 modal %. The latter may offset the former where the two intersect. This two stage formation of dunite is consistent with the observation of Suhr and Calon (1987), that the Springers Hill chromitite is cut by Cr-spinel-poor dunite.

2.3.2b Petrography

Dunites have coarse granular olivines ($\leq$ 18 mm) with well developed kinked substructures. In the absence of neoblasts and a well developed porphyroclastic texture, grain boundaries are curvilinear and smoothly interlocking. Spinel, sulphide and unidentified inclusions occur in coarse granular grains and are concentrated around Ca-amphibole enclosed in olivine

(Fig. 2.10).

Cr-spinel (≤ 4 mm) is restricted mainly to the grain boundaries of olivines, but small ovoid grains occur in olivine. The abundance and grain size of Cr-spinel approximately is inversely proportional to the grain size of olivine. Cr-spinel exists as equant, ovoid, round, lobate, cuspate and porphyroclastic grains, and granulated margins are common. Inclusions of olivine and serpentine are restricted mostly to those Cr-spinels exhibiting the most deformation and recrystallization. Olivine and Cr-spinel define the same foliation. Clinopyroxene associated with Cr-spinel has been documented in a concordant dunite which possesses a spinel chain texture (Jackson, 1961) (Fig. 2.11).

2.3.3 Chromitite

Chromitites range from massive true chromitites (95 modal % Cr-spinel) with well developed margins, to dunites rich in Cr-spinel (≥ 30 modal % Cr-spinel) where the Cr-spinel is disseminated and a faint banding is developed. Mineral graded layering may develop in the latter (Fig. 2.12). The extremes may occur together. Cr-spinel exists as equant, lobate and cuspate grains and their porphyroclastic equivalents. Cr-spinels with granulated margins occur where D_2 shear zones cut chromitite. Pull-apart fractures are filled with chlorite or serpentine. Olivine interstitial to Cr-spinel is partially to completely serpentinized. Inclusions in Cr-spinel are chlorite.

Chromitites are always enclosed in an envelope of dunite. Morphologies

and textures of the composite chromitite-dunite body are the same as those described for dunite, except that lenses, boudins and schlieren of chromitite also are present. Dunite envelopes are ≤4 m wide on either side of chromitite. These envelopes contain traces of pyroxene and the widest envelopes retain bands of harzburgite that trend parallel to the chromitite. Two types of small chromitite body are present within dunite envelopes. The first is very angular, is <10 cm wide, and appears to be xenolithic. The second is elongate or pod-like, possesses smoothly curved margins, measures up to 80 x 15 cm, and exhibits simple zonation (>95 modal % Cr-spinel at the rim, >50 modal % olivine and <50 modal % Cr-spinel in the core).

2.3.4 Type I Orthopyroxenite, Clinopyroxenite and Websterite

2.3.4a Field Relations

Websterites were not identified in the field and were mapped as clinopyroxenite. They are a minor component of clinopyroxenite. Two types of orthopyroxenite have been identified, and are described separately as Type I (OPXT I) and Type II (OPXT II) in accordance with Suhr and Calon (1987) and Suhr et al. (in press). Type II orthopyroxenites are described in section 2.3.5.

Type I orthopyroxenites (≤95 modal % orthopyroxene) and clinopyroxenites (≤99 modal % clinopyroxene) occur as veins and dykes and their boudinaged equivalents. Grain size typically is coarse to pegmatitic (≤40 mm). Recrystallization of dyke margins and veins correlates with D_1, whereas extensive mylonitization of veins and dykes is attributed to D_2. No chilled

margins have been identified. Clinopyroxenites consistently cross-cut OPXT I and are more discordant with respect to S_1 than are OPXT I (Fig. 2.13).

The olivine content of pyroxenites varies along and across strike, and many bodies exhibit features akin to lit-par-lit injection. Lensoid patches of harzburgite and wehrlite occur in OPXT I and clinopyroxenite, respectively. Patches of dunite in OPXT I usually are richer in Cr-spinel than those in clinopyroxenite. These dunite patches have cumulate texture (Fig. 2.14). Elongate bodies of host-rock occur in pyroxenite dykes where the dykes branch into numerous subparallel veins or narrower dykes. These branches may coalesce along strike to re-form a massive dyke.

The consistent association of OPXT I with harzburgite has been described in section 2.3.1a. Clinopyroxenites are hosted by harzburgite (Fig. 2.13), or are enclosed in an envelope of dunite which separates them from harzburgite (Fig. 2.15). The former is more common for true clinopyroxenites, whereas the latter dominates for olivine clinopyroxenites. The width of the dunite envelope is unrelated to the width of the clinopyroxenite (± olivine) it encloses. The dunite need not be continuous along strike, especially where there are variations in the olivine/clinopyroxene ratio of the clinopyroxenite and in the degree of strain at the dyke margin. Bands of Cr-spinel in dunite are parallel to clinopyroxenite (Fig. 2.15). A mm-wide band of chromitite often defines the contact between clinopyroxenite and dunite. True clinopyroxenites are more common in the west of the mapped area, which explains why there is no dunite envelope around clinopyroxenites cutting OPXT I (Fig. 2.13). In

the east of the mapped area, olivine clinopyroxenites are more common than clinopyroxenites.

2.3.4b Petrography of Type I Orthopyroxenite

Orthopyroxene, olivine, Cr-spinel and amphibole occur in all OPXT I. Clinopyroxene is a rare phase in some samples. The oldest texture is well equilibrated and coarse granular. Grain boundaries between adjacent grains of orthopyroxene are smoothly undulating or serrated with consertal intergrowth. Exsolutions of clinopyroxene have not been identified positively in orthopyroxene, but acicular grains of amphibole commonly are parallel to the cleavage of orthopyroxene. Olivine, Cr-spinel, clinopyroxene and amphibole occur as inclusions in orthopyroxene and interstitial to orthopyroxene. Cr-spinel (≤ 1 mm) is equant to rectangular and oval, and generally is coarser grained where it is interstitial to orthopyroxene, than where it is enclosed in orthopyroxene. Cr-spinel is everywhere associated with Ca-amphibole, which suggests that fluid was intimately involved in the formation of Cr-spinel. Olivine embays orthopyroxene in a manner characteristic of parallel growth of these two phases (Figs. 2.16 and 2.17). Clinopyroxene has poorly equilibrated grain boundaries where it replaces orthopyroxene. Amphibole occurs as tabular, acicular and bleb-like grains associated with all other mineral phases. Tremolite replaces clinopyroxene (Fig. 2.18) and tremolite and cummingtonite replace orthopyroxene (Fig. 2.19). Symplectitic growths of spinel are common in amphibole and may define a previous feature such as a pyroxene that

amphibole has replaced. Tabular grains of amphibole of the anthophyllite-gedrite series have been identified in association with orthopyroxene.

Deformation results in porphyroclastic and equigranular (mylonitic) equivalents of the features described above. Amphibole always is found in zones of deformation. Deformation primarily nucleates at inclusions of olivine and Cr-spinel in orthopyroxene, or where olivine embays orthopyroxene. Kink band boundaries are smooth to serrated and neoblasts develop at the intersection of numerous kink band boundaries. Clinoenstatite has once been identified defining a kink band. Grains of orthopyroxene are cut by shear zones that are filled with variably equilibrated, fine grains of orthopyroxene, olivine and amphibole (Fig. 2.20). Silicates have recrystallized to enclose granulated trails of Cr-spinel in zones of high strain. Pull-apart of orthopyroxene is recorded in veins of OPXT I. Tremolite and cummingtonite are in places deformed, and in others undeformed, as a consequence of the heterogeneous distribution of strain in OPXT I during their growth. Serpentinization and uralitization of OPXT I post-dates deformation and the formation of tremolite and cummingtonite.

2.3.4c Petrography of Clinopyroxenite

Orthopyroxene, olivine, Cr-spinel and Ca-amphibole occur in clinopyroxenite. Where these phases are minor, clinopyroxene is extremely well equilibrated and coarse granular (Fig. 2.21). Grain boundaries may be less equilibrated in the presence of other phases (Fig. 2.22). Clinopyroxene often

has a dusted appearance due to exsolutions of orthopyroxene(?) and spinel. Grains of Cr-spinel are equant throughout a sample, but are coarser where they are interstitial to clinopyroxene than where they occur in clinopyroxene. Olivine occurs rarely as embayments or inclusions in clinopyroxene. Ca-amphibole is a rare phase restricted mainly to regions interstitial to clinopyroxene.

Recrystallization of clinopyroxene is recorded by grain boundary migration, and possibly by linear trails of spinel grains which traverse several adjacent grains of clinopyroxene that have different orientations. Clinopyroxenites record less deformation than OPXT I. Clinopyroxene has ragged grain boundaries and substructures where porphyroclastic textures develop.

2.3.4d Petrography of Websterite

Orthopyroxene ($\leq$ 5 modal %) is present in most samples of clinopyroxenite, but localized zones of websterite occur where orthopyroxene is more abundant. Websterite that formed by the mutual exsolution of ortho- and clinopyroxene is relatively rare, and is included in the definition of clinopyroxenite from here on. The term 'websterite' is applied to a pyroxenite which is a composite assemblage of clinopyroxenite and xenocrysts of orthopyroxene. Websterites are most common where clinopyroxenites cross-cut OPXT I. Orthopyroxene xenocrysts record greater deformation than clinopyroxene, and have ragged grain boundaries. Orthopyroxene xenocrysts may be totally inert in the presence of clinopyroxene, or partially replaced by

clinopyroxene or Ca-amphibole and olivine (Fig. 2.23). This olivine often contains an interconnected network of unidentified symplectitic inclusions, which may be indicative of the presence of fluid. Orthopyroxene xenocrysts in websterite contain less amphibole than orthopyroxene in OPXT I.

2.3.4e Petrography of Dunite Associated with Clinopyroxenite

Olivine and Cr-spinel have textures as described for dunite in section 2.3.2b. Two types of dunite are definable according to the presence or absence of pyroxene and Ca-amphibole. Dunites with well developed banding of Cr-spinel are completely devoid of pyroxene and Ca-amphibole, whereas dunites with no banding usually contain orthopyroxene, clinopyroxene and/or Ca-amphibole.

Orthopyroxene is porphyroclastic, whereas clinopyroxene and Ca-amphibole are undeformed and interstitial with respect to their hosting phases. Harzburgites adjacent to these dunites may contain clinopyroxene replacing orthopyroxene, and Ca-amphibole replacing ortho- and clinopyroxene (Fig. 2.24).

2.3.5 Type II Orthopyroxenite

2.3.5a Field Relations

Dunite is the dominant host of OPXT II. There exist two end-member morphologies with a continuous spectrum between the two. Web textures occur where ribbon-like veins of OPXT II grade into an intricate network of

web-like veins that resemble stockwork veining (Fig. 2.25). Web textures of OPXT II have been observed in dunite at the contact between harzburgite and dunite. Ribbon mylonites develop in regions of high strain. They exist as mm-wide ribbon-like veins in shear zones (Fig. 2.26). Type II orthopyroxenites generally are discordant with S_1, but are found commonly in D_2 shear zones (hence the mylonitic fabric) and parallel S_2. Bodies of OPXT I are cut by ribbon mylonites.

Perhaps the most significant relationship exhibited by OPXT II is their frequent occurrence in or adjacent to zones containing HALPPG and/or amphibole dunite, i.e., in the marginal zone and D_2 shear zones.

A relatively rare occurrence of websterite is found in association with OPXT II. It occurs as <20 mm wide veins which consist of alternating zones of orthopyroxenite and clinopyroxenite along their length (Fig. 2.27). Lherzolites are produced where these websterites become highly strained and mixed with their harzburgite or dunite matrix in D_2 shear zones.

2.3.5b Petrography

The modal composition of the bulk sample (dunite matrix and OPXT II) is harzburgite with at least 3-10 modal % Ca-amphibole. Type II orthopyroxenites contain 85-98 modal % orthopyroxene and 2-15 modal % olivine, Ca-amphibole and minor Cr-spinel.

In samples with web texture, olivine is coarse granular (≤ 25 mm) in dunitic regions, but is ≤ 0.5 mm in association with orthopyroxene.

Orthopyroxene ($\leq$3.5 mm) is restricted to veins of anastomosing OPXT II that are intergranular with respect to coarse granular olivine. In rare cases, these veins cut grains of olivine. Orthopyroxene exhibits straight to undulatory extinction. It is embayed by fine grained olivine and contains inclusions of olivine. Ca-amphibole ($\leq$0.5 mm) is found with orthopyroxene only, and Cr-spinel ($\leq$1.2 mm) is almost always associated with orthopyroxene. Cr-spinel is equant to porphyroclastic and bears inclusions of serpentine, clinopyroxene, orthopyroxene, Ca-amphibole, Cr-cummingtonite, chlorite, sulphide (pentlandite) and magnetite (Fig. 2.28).

Ribbon mylonites are composed of bands ($\leq$10 mm wide) of OPXT II, dunite and Ca-amphibole (Fig. 2.29). The texture is mosaic equigranular for olivine and orthopyroxene, but orthopyroxene is coarser than olivine. Grain boundaries generally are well equilibrated. Porphyroclasts of orthopyroxene ($\leq$1 mm) and olivine ($\leq$3 mm) are rare. Porphyroclasts of orthopyroxene contain inclusions of olivine. Grains of Cr-spinel ($\leq$1 mm) are equant to sub-equant and contain inclusions of olivine, serpentine, magnetite, chlorite and amphibole. Bands of Ca-amphibole are restricted to dunitic zones, but disseminated Ca-amphibole occurs in bands of OPXT II and dunite. Ca-amphibole is contemporaneous with the formation of banding during D_2.

2.3.6 Amphibole Dunite

2.3.6a Field Relations

Amphibole dunite is a collective name for compositions that include

dunite with ≤5 modal % Ca-amphibole, and assemblages of Ca-amphibole + orthopyroxene + olivine ± chlorite which contain ≤20 modal % Ca-amphibole. Cr-spinel is always present. Amphibole dunites are encountered throughout the mapped area as discontinuous sub-metre- and metre-size bodies associated with all pyroxene-bearing LALPP, especially those in the marginal zone and D_2 shear zones. In the latter, the foliation of Ca-amphibole defines S_2. In the marginal zone, amphibole dunite often separates LALPP from HALPPG. Amphibole in amphibole dunite preserves S_1 defined by orthopyroxene in adjacent harzburgite, despite the amphibole post-dating D_1. In a similar manner, amphibole dunite may pseudomorph veins and dykes of OPXT I and clinopyroxenite (Fig. 2.30). Amphibole is most abundant where amphibole dunites are in contact with OPXT I or clinopyroxenite. In extreme cases, enclaves of these pyroxenites reside in amphibole dunite and the latter separate the former from dunite (Fig. 2.31). Undeformed amphibole may exhibit poikilitic texture.

2.3.6b Petrography

Amphibole dunites with equigranular texture are restricted to the D_2 harzburgite-dunite mylonite underlying the mylonites of uncorrelated wehrlite and gabbro in the northern part of the mapped area. Modal mineralogy is olivine (≥93 %), Cr-spinel (≤2 %) and Ca-amphibole (≤5 %). Textures of olivine range from porphyroclastic and tabular equigranular to mosaic equigranular. The latter (grain size ≤1 mm) dominates and is well equilibrated

with a weak lattice fabric (Fig. 2.32). The coarsest grains of olivine and Cr-spinel are restricted to those samples richest in Ca-amphibole. Ca-amphibole (≤1.2 mm) and Cr-spinel (≤2 mm) are commonly associated; they may exhibit a sigmoidal pattern, with Ca-amphibole in the pressure shadow of Cr-spinel. The preferred orientation of amphibole and spinel is parallel to the foliation defined by olivine. Cr-spinel is porphyroclastic to poikiloblastic, and in extreme cases, preserves a sieve texture with inclusions of olivine, serpentine, Ca-amphibole and phlogopite. These inclusions exhibit a change both in morphology and composition from core to rim of the Cr-spinel (Fig. 2.33). As in harzburgite (Fig. 2.9), the grain boundary of Cr-spinel in contact with Ca-amphibole is highly embayed.

Amphibole dunite at the margin of OPXT I exhibits a progressive evolution. As the concentration of Ca-amphibole increases above that normally associated with OPXT I, orthopyroxene is replaced by Ca-amphibole and olivine, and OPXT I grades through an intermediate composition of harzburgite, into amphibole dunite. A discontinuous seam of Cr-spinel separates harzburgite from dunite. The grain size of olivine increases with its modal abundance, and reaches 20 mm. In extreme cases of replacement of OPXT I by amphibole dunite, olivine is cut by veins of Ca-amphibole and chlorite, and Ca-amphibole is replaced by chlorite. Magnetite rims occur around most grains of chlorite and some grains of Cr-spinel.

2.3.7 Interpretation

The S_1 fabric and coarse textures of harzburgite are indicative of asthenospheric deformation dominated by plastic flow at 1200-1300°C (Mercier and Nicolas, 1975). Dykes and veins of dunite (± chromitite), OPXT I and clinopyroxenite are concordant to subconcordant with respect to S_1. As such, they were transposed into the mantle flow plane to different degrees according to (i) their relative time of formation, (ii) their original orientation with respect to the flow plane, and (iii) the intensity of strain (Nicolas and Jackson, 1982). The strain recorded by a dyke need not correlate with its relative age of formation, as strain partitioning is heterogeneous. Because veins and dykes of dunite, OPXT I and clinopyroxenite intrude harzburgite and were transposed into parallelism with S_1 under asthenospheric conditions, they may represent a major feeder system for overlying accreting crust.

Harzburgite records three stages in its evolution:

1) The earliest event is recorded by the irregular morphology of Cr-spinel (Fig. 2.5), which suggests progressive melting-out of pyroxene (especially clinopyroxene) and crystallization-recrystallization of Cr-spinel (Leblanc et al., 1980).

2) A component of orthopyroxene from OPXT I was then introduced into harzburgite by mechanical mixing of veins and narrow dykes, or by magma impregnation. These early events (1 and 2) occurred in the asthenosphere (D_1).

3) The latest event post-dates D_1, and is recorded by olivine-orthopyroxene clusters with or without associated Ca-amphibole and recrystallized grains of

olivine and Cr-spinel. Olivine is well recovered to coarse grains in areas of dunite where no other minerals were present to impede growth. Coarse grains derive from finer deformed grains by recrystallization (Harte et al., 1973). Such recrystallization requires active migration of grain boundaries at 1300°C in the presence of magma, or 1000°C in the presence of hydrous fluid (Nicolas, 1986a). Olivine in areas of dunite probably recrystallized in the presence of fluid, whilst orthopyroxene underwent incongruent breakdown (Bowen and Tuttle, 1949) to olivine and spinel in olivine-orthopyroxene clusters. Olivine in the clusters did not recrystallize. Fluid did not affect harzburgite homogeneously, and reactions occurred in-situ and at a grain by grain scale.

Dunites in the uppermost mantle of ophiolites either are magmatic (O'Hara, 1968; Jackson et al., 1975; Malpas, 1978; Elthon et al., 1982; Komor et al., 1985; Furnes et al., 1988), or are the product of reaction of harzburgite or lherzolite with a magma or fluid, thus being residual (section 1.3.3). Features documented in LAL dunites suggest both magmatic and residual origins. Bands and layers of Cr-spinel in dunite suggest a magmatic origin. Textures of coarse granular olivines associated with chains of Cr-spinel are identical to those of olivine cumulates (Jackson, 1961). A gradational contact with harzburgite, where fragments of harzburgite may be enclosed in dunite, suggests formation by reaction. These dunites often contain porphyroclasts of orthopyroxene, and are frequently impregnated by clinopyroxene and Ca-amphibole. Dunites may exhibit magmatic features in their interiors and residual features at their margins, as often observed in dunite

surrounding clinopyroxenite. The textural evolution of olivine and Cr-spinel, from coarse granular olivine and lobate-cuspate Cr-spinel to their porphyroclastic equivalents, results from progressive recrystallization during plastic flow (Mercier and Nicolas, 1975). Mosaic equigranular texture is characteristic of amphibole dunites which are considered in Chapter 5.

The sequence of dyke intrusion is dunite (± chromitite)--OPXT I--clinopyroxenite (± dunite), but nowhere has any gradation of one rock type into another been observed along strike. However, many olivine clinopyroxenites have a Cr-spinel dunite envelope, whereas clinopyroxenites generally do not. From this it is assumed that clinopyroxenite (± olivine) and its associated dunite are comagmatic. Clinopyroxenite bands in olivine clinopyroxenites represent relatively evolved fractionates from the magma. Type I orthopyroxenites are not related to this sequence, but Dahl and Watkinson (1986) have documented orthopyroxene in dunitic dykes and veins near the main Springers Hill chromitite. Consequently, it would appear that the OPXT I event is olivine--orthopyroxene, which is post-dated by a separate event of olivine (± Cr-spinel)--clinopyroxenite. Further evidence that OPXT I and clinopyroxenite record separate events, is that OPXT I contains relatively abundant amphibole, whereas clinopyroxenites do not. This amphibole is not cogenetic with that in amphibole dunite.

Clinopyroxenites contain xenocrysts of orthopyroxene from OPXT I. The deformation recorded by the xenocrysts pre-dates the crystallization of clinopyroxenite. Incorporation of xenoliths of OPXT I into the magma from

which clinopyroxenite precipitated, would locally have increased the volatile content of the magma. This is additional evidence for OPXT I forming before clinopyroxenite.

Clinopyroxenites and OPXT I preserve textures identical to adcumulates and mesocumulates. Apparently undeformed interiors of massive dykes of pyroxenite should record relatively primary features, because it is extremely difficult for pyroxene to recrystallize or flow under normal mantle conditions when isolated in a much weaker olivine-rich matrix (Mercier, 1985). However, OPXT I crystallized in the presence of fluid which would have aided recrystallization, especially as the solidus of amphibole is lower than that of olivine and orthopyroxene. This, and evidence of grain boundary migration in clinopyroxenites, suggests that primary magmatic textures of pyroxenites may have been modified or obliterated during recrystallization in the asthenosphere.

Interpretation of amphibole dunite and OPXT II is reserved for Chapter 5.

2.3.8 Platinum Group Minerals and Fe-Ni-Cu-S Phases in LALPP

Extensive documentation of platinum group minerals (PGM) and Fe-Ni-Cu-S phases in LALPP is given by Edwards (1990), and only a summary of this work is presented here. Platinum group minerals occur as: (i) Os-bearing laurite (RuS_2) in unaltered Cr-spinel in chromitite (two samples); (ii) trails of inclusions of arsenides of Pt and Pd in unaltered orthopyroxene in OPXT I (one sample); (iii) an assemblage of Pt-Pd-Fe-Co-Ni-Cu-As phases in unaltered clinopyroxene

in websterite (one sample). These PGM formed with their hosting silicate or Cr-spinel and are primary and in-situ.

Harzburgites, dunites and OPXT I contain minute wisps and flecks of undeformed Fe-Ni-Cu-S phases which were derived from silicates during serpentinization. Chromitites very rarely contain Fe-Ni-Cu-S phases associated with laurite, and these are primary in origin. In clinopyroxenites and websterites, Fe-Ni-Cu-S phases form grains <0.15 mm in diameter. Nickel-rich pentlandite and native Cu, and minor associated Cu sulphide, are the most common phases found, both within clinopyroxene and at clinopyroxene grain boundaries. Native Cu has exsolved from pentlandite and locally has been mobilized during serpentinization. Before crystallization, exsolution and serpentinization, the sulphide formed immiscible Cu-bearing, Ni-rich pentlandite globules in silicate magma. Such a sulphide component was derived from a mantle source which previously had experienced partial melting and removal of Fe and S (Garuti et al., 1984). Harzburgites, dunites and OPXT I adjacent to clinopyroxenites, in some places contain minor Fe-Ni-Cu-S phases derived from the latter.

Fe-Ni-Cu-S phases are rare to absent in amphibole dunite and OPXT II. Where they occur in the silicate matrix, they are most commonly associated with Ca-amphibole and have been variably affected by serpentinization. Sulphides occur in orthopyroxene and Cr-spinel in OPXT II with web texture (Fig. 2.28).

2.4 HIGH-Al PERIDOTITES, PYROXENITES AND GABBROS, AND THE MARGINAL ZONE

The main body of HALPPG crops out in the centre of the mapped area and extends eastward (Fig. 2.1). Upward from the lowest ground, spinel dunite progressively grades into clinopyroxene dunite, wehrlite, olivine clinopyroxenite and gabbro; all contacts are gradational. The main body truncates lithological domains and S_1 defined by LALPP. However, in undeformed HALPPG, dykes and the foliation defined by clinopyroxene have a very similar trend to dykes and S_1 of LALPP. The trend of S_2 in HALPPG is consistent with that in the adjacent LALPP. Faulted contacts apart, the contact between HALPPG and LALPP is marked by the marginal zone, except along the southern contact where HAL dunites are in direct contact with LALPP over a distance of 340 m. The chromitite-rich zone in the LALPP appears to continue into the HAL dunites across this contact (Fig. 2.1). This suggests that the chromitite bodies in the HAL dunites are xenolithic, as suggested by Dunsworth et al. (1986), and implies that a marginal zone exists along the contact.

Localized bodies of HALPPG crop out in LALPP. The most prominent is in the southeastern corner of the mapped area. These bodies exhibit the features found in the main body.

2.4.1 HAL Dunite

2.4.1a Field Relations

Dunites are composed of ≥85 modal % olivine, ≤15 modal % Al-spinel and <2 modal % clinopyroxene and Ca-amphibole. Volumetrically they are the most abundant rock type exposed in the HALPPG. Al-spinel is disseminated, but banding and modal layering occur on a mm-cm scale (Figs. 2.34 and 2.35). Some layers appear overturned. Banding and layering are oriented approximately north-south or east-west. The former orientation is concordant with the trend of dykes of olivine clinopyroxenite and gabbro, and the foliation defined by clinopyroxene in wehrlite.

Three types of Al-spinel are found in dunite. Spinel-rich bands (cm-wide) cross-cut disseminated spinel (Fig. 2.35), and chromitite bands (<20 mm wide) cross-cut spinel-rich bands. Lenses and angular pods (<1 m long) of chromitite occur in all HALPPG; these are the chromitite xenoliths of Dunsworth et al. (1986).

Bands of Al-spinel in places define the contact between spinel dunite and spinel wehrlite. In contrast, the foliation defined by clinopyroxene in wehrlite may cross-cut spinel banding at a high angle.

2.4.1b Petrography

The features described here have not been affected by D_2. Olivine (≤10 mm) commonly is coarse granular with well equilibrated to lobate, cuspate interlocking grain boundaries. Kink bands and deformation lamellae are

common. Olivines have been observed having grown through one another. Ti-spinel and Ti-Cr-magnetite occur as inclusions. Mosaic equigranular olivine is very rare.

Clinopyroxene and Ca-amphibole are interstitial to olivine and Al-spinel. Veins of clinopyroxene and Ca-amphibole occur within coarse granular grains of olivine associated with mosaic equigranular olivine. The veins may define original grain boundaries of olivine which have been destroyed during recrystallization of olivine to coarser grains.

Al-spinel (≤ 8 mm) is equant to lobate-cuspate. It is disseminated throughout the olivine matrix with a preference for grain boundaries of olivine rather than grain interiors; grain size is similar in both environments. Chains of Al-spinel frequently occur parallel and perpendicular to layering defined by Al-spinel in layered dunite (Fig. 2.36). Sharp contacts are preserved between zones of coarse and fine grained Al-spinel. Al-spinel may protrude along grain boundaries of adjacent olivines, where the grain boundary is filled with clinopyroxene (Fig. 2.37). Porphyroclasts are rare.

One case has been documented of a band of Al-spinel hosted by wehrlite in dunite. The band has a higher concentration of Al-spinel and sulphide than its host, in which Al-spinel is finer grained. Inclusions in Al-spinel in the host usually are single round grains of olivine, whereas those in Al-spinel of the band are abundant and comprise olivine or serpentine, chlorite (clinochlore), ilmenite, pargasite, tremolite, phlogopite, Ca-plagioclase and orthopyroxene (Fig. 2.38).

2.4.2 HAL Wehrlite, Olivine Clinopyroxenite and Gabbro

2.4.2a Field Relations

Modal compositions are not defined for the rock types bearing clinopyroxene, because proportions of constituent minerals are so highly variable. This arises because of multiple generations of a complete spectrum of compositions, which may grade from clinopyroxene dunite to gabbro over a distance of <1 m to >10 m. The complete spectrum is observed along strike of gabbro dykes and normal to these dykes. The complete gradational sequence hosted by dunite is anorthositic gabbro (core)--olivine gabbro--plagioclase, olivine clinopyroxenite--olivine clinopyroxenite--wehrlite--clinopyroxene dunite (Fig. 2.39), which suggests a crystallization sequence of olivine--clinopyroxene--plagioclase. The grain size of clinopyroxene decreases from pegmatitic in gabbro and olivine clinopyroxenite, to medium-coarse in wehrlite and clinopyroxene dunite. The orientation of the foliation defined by clinopyroxene in wehrlite and clinopyroxene dunite is concordant with the strike of dykes of gabbro and olivine clinopyroxenite. It is rare to find the complete gradational sequence because dyke interiors concentrate strain and much of the sequence may be sheared out (Fig. 2.39). Also, multiple injection of these dykes causes overprinting of one sequence by another, and foliations and dyke orientations may cross-cut one another. Discontinuous cm- to m-wide bands and irregular zones of dunite separate sequences where the sequences do not overlap. The contacts between this dunite and wehrlite or olivine clinopyroxenite are both gradational and sharp (Fig. 2.40). Grains of Al-spinel

in the dunite generally are coarser and more abundant than those in adjacent wehrlite (Fig. 2.41). Gabbros outside of the composite dunite-gabbro sequences, occur as isolated, discrete (<1 m wide) dykes with sharp margins against their host-rock.

Unlike the gradational dyke contacts described above, there exist essentially plagioclase-free olivine clinopyroxenite dykes with well defined margins. These dykes are <1 m wide and have a margin of pegmatitic clinopyroxenite and a core of coarse grained olivine clinopyroxenite, wehrlite or dunite. The pegmatitic margin in some places is developed on one side of the dyke only. Along strike, non-poikilitic olivine clinopyroxenite (clinopyroxene ≤12 cm) often grades into poikilitic olivine clinopyroxenite (clinopyroxene ≤5 cm), wehrlite with interstitial clinopyroxene (<1 cm), and finally dunite. These dykes often contain bands of Al-spinel at their margin with dunite. Olivine clinopyroxenite dykes of this nature are relatively abundant in the marginal zone and traversing LALPP outside of the marginal zone (Fig. 2.42). They are most voluminous where they grade into LAL clinopyroxenites in the marginal zone (Fig. 2.43). Associated with these dykes, are amphibole peridotites which crop out as dykes (<1 m wide) in LALPP and the marginal zone. These dykes have olivine (≥55 modal %) and Ti-amphibole (≤45 modal %).

The central regions of some dykes exhibit an intense L≥S fabric which is attributed to D_2. The orientation of the fabric and dyke are the same. D_2 is preserved in the form of shear zones in the northern extent of the HALPPG.

2.4.2b Petrography

The features described here have not been affected by D_2. Textures are gradational in parallel with progressive evolution of modal compositions from wehrlite to gabbro. The crystallization sequence in gabbro is olivine--plagioclase--clinopyroxene, which is a reversal of the order of crystallization of plagioclase and clinopyroxene that is predicted from field relations. This is an important point and is dealt with in Chapter 4.

Olivine in wehrlite is similar to that in dunite. Clinopyroxene is interstitial to olivine in wehrlite, but develops into more massive crystals exhibiting broad twins as its modal abundance increases (Figs. 2.44 and 2.45). Clinopyroxene embays olivine and may dissect a large grain of olivine into a number of islands that are optically continuous. Rarely, isolated veinlets and negative crystals of clinopyroxene occur in olivine. Al-spinel is equant and decreases in abundance and grain size with increase in abundance of clinopyroxene and plagioclase. Al-spinel is rare to absent in gabbro. Plagioclase is present in most cases, but is less abundant with respect to clinopyroxene. The morphology of plagioclase, or its altered equivalent of hydrogrossular garnet, is similar to that of clinopyroxene. Clinopyroxene or a Ca-amphibole-spinel symplectite separates Al-spinel from plagioclase. Plagioclase always is separated from olivine by an inner symplectitic intergrowth of Ca-amphibole and spinel, and an outer rim of orthopyroxene. Ca-amphibole mimics the morphology of clinopyroxene and plagioclase, except where it occurs as rare veins with magnetite. Ca-amphibole may partially replace clinopyroxene. Brown Ti-amphibole occurs as interstitial

grains associated with olivine and also enclosed within or rimming clinopyroxene. Phlogopite occurs with Ti-amphibole and as inclusions in Al-spinel. Sphene has been identified in Al-spinel in olivine clinopyroxenite. Ti-amphibole partially replaces olivine in amphibole peridotite.

There is little sign of deformation outside of D_2 shear zones. That which is present, is recorded by undulatory extinction, deformation lamellae and kink bands in olivine. Porphyroclastic textures are poorly developed in other phases.

2.4.3 The Marginal Zone

2.4.3a Field Relations

The marginal zone is ≤ 160 m wide and contains all LALPP and HALPPG. Consequently, this zone is extremely complex and preserves essentially all the features documented so far. The striking feature of the marginal zone is the local abundance of spectacular xenoliths of harzburgite, LAL and HAL dunite, and minor chromitite in HAL wehrlites and HAL olivine clinopyroxenites. Two types of xenolith are found: (i) xenoliths with straight edges and angular or rounded corners, and (ii) xenoliths with extremely irregular margins that are diffuse (Fig. 2.46). Features of both types can be found in an individual xer. [illegible] This situation arises commonly where a rim (<2 cm wide) of Al-spinel and/or clinopyroxene is discontinuous around a xenolith of LAL or HAL dunite. Where the rim is present, the xenolith margin is sharp, but where the rim is absent, the margin is very diffuse due to clinopyroxene impregnation (Fig. 2.47). Trails of Cr-spinel in harzburgite xenoliths in some places are traceable

into their enclosing HAL wehrlite or HAL olivine clinopyroxenite.

Dykes and anastomosing veins of dunite, wehrlite, olivine clinopyroxenite and amphibole peridotite of HALPPG which traverse LALPP, exhibit features similar to those documented for xenoliths. The development of HAL olivine clinopyroxenite is governed by the composition of the LALPP encountered. It develops where harzburgite is intersected (Figs. 2.48 and 2.49), but is discontinuous or absent adjacent to LAL dunite (Figs. 2.42 and 2.43). Dyke margins may be diffuse adjacent to LAL dunite, but sharp adjacent to harzburgite. Most dykes of HAL olivine clinopyroxenite and HAL amphibole peridotite have a zone of HAL or LAL dunite separating them from LALPP. The same feature is observed for dyke-like LAL amphibole dunites (Fig. 2.30).

2.4.3b Petrography

Xenoliths of harzburgite and LAL dunite contain variable proportions of impregnated HAL clinopyroxene, and olivine-orthopyroxene clusters at different stages of development. Narrow zones (mm- to cm-wide) of HAL dunite which separate harzburgite (with olivine-orthopyroxene clusters) from HAL olivine clinopyroxenite dykes, contain minor HAL clinopyroxene and abundant Al-spinel. LAL dunites defining this zone, contain minor HAL clinopyroxene, and Cr-spinel in no greater abundance than that in the adjacent harzburgite. In any of these situations, Cr-spinel contained within HAL clinopyroxene frequently is skeletal.

Type I orthopyroxenite in contact with HAL wehrlite or HAL olivine

clinopyroxenite either is replaced by clinopyroxene, olivine and minor spinel, or is replaced by Ca-amphibole and olivine to amphibole dunite. Type I orthopyroxenite in contact with HAL amphibole peridotite is replaced by harzburgite.

Inclusions of ilmenite rimmed by perovskite occur in spinel in a chromitite xenolith in HAL dunite.

2.4.4 Interpretation

The temperature and pressure of equilibration of HALPPG can be estimated from mineral assemblages and textures. The close spatial association of Al-spinel and plagioclase, with plagioclase occasionally rimming Al-spinel, demonstrates that the HALPPG equilibrated at or below the spinel-plagioclase boundary. Under hydrous conditions, maximum temperatures and pressures are 875°C, 6 kbar to 1050°C, 9 kbar according to the phase relations for ultramafic rocks modelled by Jenkins (1983) for the system H_2O-Na_2O-CaO-MgO-Al_2O_3-SiO_2 (Fig. 2.50). Corona textures in HALPPG are (i) orthopyroxene between olivine and plagioclase in gabbro, and (ii) symplectites of amphibole-spinel and rare clinopyroxene-spinel around plagioclase in contact with olivine in wehrlite. These coronas may correspond to the Seiland subfacies of the spinel lherzolite facies as defined by O'Hara (1967). The low pressure side of this subfacies is bounded by reaction R2.1:

[R2.1] Plag + Ol = = Al-Px + Sp

Experimental studies in the system pure anorthite-forsterite ($\pm H_2O$) yield

pressures of 8 kbar at 1100-1300°C (Kushiro and Yoder, 1966) and 7 kbar at 900°C (Yoder, 1967) for this reaction. At 800°C the pressure can be reduced to 6 kbar (Herzberg, 1978) or 5 kbar (Obata, 1976). These conditions restrict the formation of HALPPG and D_2 shear zones to a high pressure environment within the lithosphere. This in turn, requires that LALPP were part of the lithosphere by this time.

All HALPPG are intimately associated through gradational contacts and textures. These features are characteristic of cumulates and rocks impregnated by magma. Nicolas (1989) states that fabric studies of olivine are necessary to distinguish between true cumulates and impregnated mantle rocks. Fabric studies have not been undertaken in this study, but mineral and whole-rock chemical criteria will be used to assess the possible origins of the HALPPG, which are:

1) If a magmatic origin is assumed, then HAL dunites are adcumulates that have experienced very efficient removal of intercumulus material. During compaction of the cumulate pile, Al-spinel was jostled into vertical and horizontal alignment along channels accessed by migrating postcumulus material in a manner similar to that proposed by Irvine (1980) for the Muskox Intrusion, Canada. Postcumulus growth of Al-spinel resulted in grains joined by bridges of Al-spinel and sulphide, and protrusions of Al-spinel along olivine grain boundaries occupied by clinopyroxene. Also consistent with Irvine's model, is that maximum compaction of the cumulate pile occurred in zones where crystals are aligned. It is in these zones that extreme adcumulate

textures develop, and weak substructures develop in olivine due to compaction. The postcumulus material concentrated progressively in zones of wehrlite, olivine clinopyroxenite and gabbro. Cross-cutting relations demonstrate that expulsion of postcumulus material was not a single stage event. It is possible that postcumulus material impregnated its host-rock as it migrated away from the zone of maximum compaction of cumulate crystals. In this model, the marginal zone represents a zone of reaction surrounding a large igneous intrusion. A simple model of fractional crystallization may be used to estimate the composition of the parental magma. A variation of the magmatic model would involve gabbroic or more evolved magma impregnating HAL dunite and precipitating clinopyroxene. This also would explain the concentric zonation of decreasing clinopyroxene and absence of plagioclase away from a gabbroic dyke.

2) If a metasomatic origin is assumed, then the marginal zone represents the extent of a metasomatic front which passed through LALPP and metasomatized them to HALPPG. Within the main body of HALPPG, all evidence of LALPP has been obliterated by dissolution and diffusion. Reaction would have been most extensive in regions containing clinopyroxene and plagioclase. Gabbros may represent extreme reaction, or conduits through which passed the magma or fluid responsible for metasomatism. Estimation of the parental magma or fluid may require complicated modelling of combined assimilation and fractional crystallization (Bowen, 1928; Taylor, 1980; DePaolo, 1981).

Evidently, any model for the origin of HALPPG must consider the features

observed in zones of interaction of HALPPG and LALPP. The most important of these are here summarized. Pyroxene in harzburgite, OPXT I and LAL clinopyroxenite has been replaced by Ca-amphibole, olivine and minor spinel. Concentrations of chromitite and distributions of Cr-spinel in harzburgite are traceable into HAL dunites and HAL wehrlites in much the same way as sedimentary structures are preserved in granites produced by granitization (see review by Hatch et al. (1972)). Contacts between HALPPG and LALPP commonly are defined by HAL olivine clinopyroxenite and/or Al-spinel, which likely represent reaction fronts. In the absence of these reaction fronts, contacts are diffuse and LALPP are pervaded by HAL clinopyroxene. All these features suggest replacement reactions involving LALPP and magma or fluid related to HALPPG. Reactions occurred mostly in-situ. The close spatial association of some xenoliths of LAL dunite, harzburgite and mylonitic harzburgite prohibits an in-situ origin for these xenoliths. Interactions between LALPP and magma and fluid related to HALPPG are considered in chapter 4 and 5.

2.4.5 Fe-Ni-Cu-S Phases in HALPPG

Fe-Ni-Cu-S phases occur as <0.5 mm grains, which rarely exceed 1 modal % and occur nearly always with clinopyroxene. Outside of D_2 shear zones, Fe-Ni-Cu-S phases are undeformed. Pentlandite is the most primitive sulphide and volumetrically is most abundant. Pyrrhotite which pre-dates serpentinization, increases in abundance with increasing modal proportion of

plagioclase. In gabbros, pyrrhotite occurs with unaltered heazlewoodite. Harzburgites, LAL dunites and OPXT I adjacent to HALPPG, in some places contain minor Fe-Ni-Cu-S phases derived from the latter.

During serpentinization, sulphides were altered to an assemblage of awaruite, wairauite, native Cu, digenite, chalcopyrite, pyrrhotite (believed to be mackinawite), magnetite, pentlandite, and possible goethite and cuprite. Such an assemblage is characteristic of ultramafic rocks serpentinized by extremely reducing fluids (Eckstrand, 1975; Moody, 1976).

The morphology of pentlandite and pyrrhotite and their serpentinized equivalents, and their common association with clinopyroxene, is very similar to that of Fe-Ni-Cu-S phases in upper mantle peridotites of Table and Blow Me Down mountains of the BIOC (Lorand, 1987), and the Oman Ophiolite (Lorand, 1988). In these localities, Fe-Ni-Cu-S phases are of metasomatic origin, having precipitated from S-saturated basaltic magmas which became trapped as they percolated through dunite at the top of a mantle diapir (Lorand, 1987, 1988). The origin of Fe-Ni-Cu-S phases is intimately associated with the formation of clinopyroxene in HALPPG, which is discussed in Chapter 4.

2.5 D_2 SHEAR ZONES AND THRUST FAULTS

The contemporaneity of HALPPG, LAL amphibole dunites, OPXT II, and D_2 shear zones and thrust faults, is evidence of magmatic and fluid activity associated with a significant tectonic event. Constraining the nature and origin

of D_2 is essential to understand the tectonic environment within which HALPPG formed.

The abundance of LAL dunite and chromitite in the Springers Hill area suggests that this section of mantle was situated just below the petrologic Moho (Malpas, 1973) during formation of the HALPPG. The normal ophiolite sequence of harzburgite grading upward into olivine-pyroxene-plagioclase cumulates was disrupted by ductile shearing and thrusting of the D_2 event. This event removed evidence of the petrologic Moho, as partially amphibolitized, uncorrelated wehrlite and gabbro mylonites were thrust against mylonitic LALPP. Thrust-bound lenses of uncorrelated wehrlite and gabbro mylonites occur in mylonitic LALPP (Fig. 2.2). Obviously there has been significant tectonic disruption, which resulted in the removal of at least several hundred metres of uppermost mantle and lower crustal cumulates.

2.5.1 Possible Tectonic Setting

The models of Girardeau and Nicolas (1981), Nicolas and Violette (1982), Casey et al. (1983), Nicolas and Rabinowicz (1984), Dunsworth et al. (1986) and Calon et al. (1988), suggest that D_2 shear zones may relate to subhorizontal flow directed away from a ridge axis. Several features are inconsistent with this interpretation: (i) D_2 mylonites and amphibole-bearing LALPP mylonites are atypical of ophiolites, c.f., the Oman Ophiolite (Christiansen, 1985); (ii) high pressures (5-9 kbar) recorded by HALPPG are far too deep for HALPPG to have formed just below normal oceanic crust; (iii) in

a spreading environment, fabrics of D_2 should be contemporaneous and gradational with those of D_1, but clearly they are not in the Springers Hill area.

Many of the features in D_2 shear zones and HALPPG are similar to those of the Ingalls Complex, Washington, which is a fracture zone ophiolite that has widespread amphibole-rich mylonites in imbricate thrust slices of ultramafic rocks (Miller and Mogk, 1987; Miller, 1988). Based on evidence from the St. Paul's Rocks (Melson et al., 1972), Miller and Mogk (1987) suggested that mylonitic amphibole peridotites are an important component of oceanic transform-fracture zones. D_2 shear zones and HALPPG may be explained in this way if the Mount Barren Assemblage represents a fracture zone (Karson and Dewey, 1978), but this explanation cannot account for the high pressures recorded by HALPPG, as oceanic crust is thin at fracture zones (Fox et al., 1980).

Karson (1979) proposed that WSW to ENE shear zones in the Lewis Hills Massif (Fig. 1.5) were tear faults that developed and evolved during early obduction of the BIOC and CC. D_2 shear zones correspond with these zones and, therefore, may relate to obduction. This possibility is considered below.

2.5.2 D_2 Shear Zones and Ophiolite Obduction

There are striking similarities in rock type, metamorphic grade and structural style between D_2 shear zones and the Mount Barren Assemblage (Dunsworth et al., 1986), and between these and the basal peridotite mylonites and metamorphic sole of the BIOC as documented by Malpas (1979b), McCaig

(1983) and P. Cawood and G. Suhr (pers. comm., 1990). The Mount Barren Assemblage grades from granulite to amphibolite and greenschist facies mylonites over a distance of several kilometres on moving away from the BIOC (Fig. 1.5). The same change is true in the metamorphic sole over a distance of several hundred metres (Malpas, 1979b).

A noticeable difference between the Mount Barren Assemblage and metamorphic sole, is the abundance of syn- to post-kinematic intrusions of feldspathic wehrlite and lherzolite, diabase and plagiogranite in the former (Karson, 1984). These intrusions are lacking in the metamorphic sole of the BIOC, but plagiogranites produced by anatexis of amphibolites during obduction are relatively common in some other ophiolites, e.g., Oman (Searle and Malpas, 1980, 1982; Boudier et al., 1988), the Lizard, England (Malpas and Langdon, 1987), and Karmoy, Norway (Pedersen and Malpas, 1984).

Despite similarities between the metamorphic sole of the BIOC and the Mount Barren Assemblage of the CC, very different origins have been proposed. The basal peridotite mylonites and metamorphic sole of the BIOC record intra-oceanic thrusting and obduction of the ophiolite (Williams and Smyth, 1973; Malpas, 1979b; Girardeau and Nicolas, 1981; McCaig, 1983). The Mount Barren Assemblage records the transform domain of a ridge-transform-fracture zone system (Karson and Dewey, 1978). Massive hydration of the crust and upper mantle along the fracture zone resulted in the formation of amphibolite and serpentinite (Karson et al., 1983). Consequently, it would appear that the Mount Barren Assemblage and metamorphic sole developed in

distinctly different tectonic environments. In fact, this may not be so, because the model of Karson and Dewey (1978) has the site of obduction of the BIOC at the transform-fracture zone. With the intensity of deformation during the obduction process, the original features of the Mount Barren Assemblage are likely to have been obliterated.

A new interpretation of the Mount Barren Assemblage is suggested here, which has it as a thick sequence of metamorphic sole. This interpretation explains the similarity between shear zones and thrust faults in the Springers Hill area, the Mount Barren Assemblage, and the metamorphic sole. In particular, it explains the generally consistent north, shallow plunging lineations in shear zones in the Springers Hill area, Mount Barren Assemblage, and harzburgites and metamorphic sole at the base of the Lewis Hills Massif (data from Karson (1979) and Dunsworth et al. (1986)), which may correlate with northward thrusting during obduction of the BIOC (Girardeau, 1982). The original morphology and origin of the Mount Barren Assemblage is open to question, but indeed it may once have been part of a transform-fracture zone.

Casey and Dewey (1984) proposed that the metamorphic sole of the BIOC represents the hanging wall of a once east-dipping subduction zone, in which the BIOC occupied the forearc of the overriding plate. An evaluation of this tectonic situation is not possible here, but if it were so, the Mount Barren Assemblage would represent a thick metamorphic sole accreted to the leading edge of the forearc region of the overriding plate.

2.5.3 The Importance of Thrusting in the Springers Hill Area

The HALPPG formed at the very top of the mantle, and the high pressures of 5-9 kbar which they record must be accounted for in the crust. The minimum pressure of 5 kbar requires 15 km of crust above the HALPPG. There are at least four possible explanations of these high pressures:

1) The assemblages of minerals from which the pressures are estimated are metastable, and actually they formed at pressures of 2-3 kbar, which is expected for the thickness of normal oceanic crust. This possibility cannot be evaluated.

2) McCaig (1983) used the model of Nicolas and Le Pichon (1980) to explain high pressures in the metamorphic sole of Table Mountain, by detachment of the BIOC from below a subduction zone. This mechanism cannot be evaluated at present.

3) Similar pressures as those in HALPPG occur in granulite facies metacumulates of the Yakuno Ophiolite, Japan, where they record thick oceanic crust like that beneath the Black Sea (Ishiwatari, 1985b). There is no evidence for such thick crust in the BIOC, but D_2 shearing and thrusting may have transported HALPPG and LALPP from a higher pressure environment.

4) Tectonic thickening by stacking of thrust slices. The interleaved stack of thrust slices of uncorrelated wehrlite and gabbro and LALPP attest to the importance of thrusting in the Springers Hill area. However, there are several problems with this explanation: (i) the overall effect of thrusting in the area was the removal of material; (ii) if the crustal sequence originally was 5 km thick,

thrusting would have to add a further thickness of 10-22 km; (iii) pressures in the crustal sequence permit little, if any, tectonic thickening.

At this time it is not possible to say which explanation is most plausible. Clearly this is a problem which requires further investigation.

2.6 SUMMARY

Harzburgite is a refractory residue from extensive partial melting and complete extraction of magma, as attested by its total lack of clinopyroxene other than that resulting from impregnation. Dunite, chromitite, OPXT I and clinopyroxenite of the LALPP intruded harzburgite under asthenospheric conditions (D_1, T = 1200-1300°C) below a region of crustal accretion. A component of the dunite is residual by replacement of harzburgite. Harzburgite has a component of OPXT I that was introduced by impregnation or mechanical mixing. Type I orthopyroxenites were derived from hydrous, As-saturated magma which fractionated olivine (± Cr-spinel) and orthopyroxene, whereas clinopyroxenites were derived from relatively anhydrous, S-saturated magma which fractionated olivine, Cr-spinel and clinopyroxene. Clearly these magmas are not comagmatic.

Dunite, wehrlite, olivine clinopyroxenite and gabbro constitute the HALPPG, which are essentially devoid of orthopyroxene. They formed in the uppermost mantle lithosphere at abnormally high pressure, by magmatic crystallization, or magma or fluid metasomatism. Olivine, clinopyroxene and Al-

spinel formed as reaction fronts at the interface between HALPPG and LALPP.

D_2 shear zones and thrust faults, HALPPG, and amphibole dunite and OPXT II of LALPP, are contemporaneous with intra-oceanic thrusting and obduction of the BIOC and formation of the metamorphic sole. The Mount Barren Assemblage in the Lewis Hills Massif represents an unusually thick sequence of metamorphic sole, which was accreted to the leading edge of the BIOC as it was obducted in a northerly direction.

Chapter 3

CHEMISTRY AND PETROGENESIS OF LOW-ALUMINA PERIDOTITES AND PYROXENITES

3.1 INTRODUCTION

The aim of this chapter is to characterize the chemistry of LALPP, and use it in combination with field relations and petrography (Chapter 2) to determine the petrogenesis of LALPP. Data for amphibole dunite and OPXT II are presented, but they are not discussed until Chapter 5. Chemical analyses of LALPP at LALPP-HALPPG contacts and in LALPP-HALPPG reaction zones are not considered in this chapter. They are dealt with in chapters 4 and 5.

A major aim of this thesis has been to develop a method to analyse the rare earth elements, La-Lu (REE), at sub-ppm concentrations by inductively coupled plasma-mass spectrometry. The analysis of REE in LALPP caused many problems owing to extremely low absolute concentrations of REE. Sample preparation procedures, and precision and accuracy of the analyses, are discussed in Appendix 1, which should be read before assessing the significance of REE data presented in this chapter.

Analytical methods are described in Appendix 1, and mineral and whole-rock chemical analyses of LALPP are presented in appendices 3 and 4, respectively.

3.2 MINERAL CHEMISTRY

Unless stated otherwise, the compositions reported below are for analyses of cores of grains.

3.2.1 Olivine

The composition of olivine in LALPP is summarized in Figure 3.1, which illustrates that the Mg# of olivine generally occupies the compositional range 88.3-91.9, but extends to 85.7 and 92.7. Olivine has the highest Mg# in harzburgite, dunite, amphibole dunite, OPXT I veins, OPXT II, and dunite associated with clinopyroxenite, whereas olivine in OPXT I dykes, websterite and clinopyroxenite has a slightly lower Mg#. The Mg# of olivine associated with Cr-spinel is high; olivine of Mg# = 92.7 occurs in Cr-spinel in OPXT I, and the Mg# of olivine increases from 89.9 to 91.9 over 6 mm on passing from dunite into a band of chromitite in a dunite envelope around clinopyroxenite. Olivine of Mg# = 85.7 in websterite sample L288 is anomalous and may correlate with olivine in HALPPG.

The NiO content of olivine is 0.08-0.73 wt.%, but the majority of analyses cluster about 0.40-0.50 wt.%.

3.2.2 Orthopyroxene

Orthopyroxene in all LALPP has very low concentrations of TiO_2 ($\leq$0.08 wt.%) and Al_2O_3 ($\leq$1.40 wt.%), and high Mg#. The Mg# ranges from 88.6 in

clinopyroxenite to 92.2 in harzburgite, and exhibits the same trend as olivine (Fig. 3.2). Orthopyroxene in harzburgite exhibits wide variation in CaO (0.26-1.73 wt.%) and Al_2O_3 (0.32-1.40 wt.%) for a narrow range of Mg# (91.1-92.2). Variation in CaO may be attributed to extremely fine lamellae of clinopyroxene parallel to the cleavage of orthopyroxene. Analyses of dykes of OPXT I and clinopyroxenite are limited, but they exhibit a slight FeO enrichment trend as CaO and Al_2O_3 increase.

3.2.3 Clinopyroxene

Clinopyroxene in all LALPP is diopside having extremely depleted chemistry of CaO = 23-26 wt.%, $TiO_2 \leq 0.07$ wt.%, $Al_2O_3 < 1.0$ wt.% and $Fs \leq 4.0$. Clinopyroxene in harzburgite, dunite and OPXT I has Mg# = 94.3-95.3, whereas in websterite Mg# = 94.3 and in clinopyroxenite Mg# = 92.5-94.3, which is the same trend as for olivine and orthopyroxene.

3.2.4 Ca-Amphibole

Ca-amphibole exhibits a continuous compositional range from tremolite to pargasite. The chemistry of Ca-amphibole is dealt with in Chapter 5.

3.2.5 Cr-Spinel

Cr-spinel exhibits the widest variability in composition of all the mineral phases in LALPP. It occupies the compositional range of Cr# = 47-90, Mg# = 23-65 (Fig. 3.3). Cr-spinels exhibit a relatively uniform change in

composition from low Cr#, high Mg# in chromitites, changing through harzburgites, dunites and amphibole dunites, to high Cr#, low Mg# in pyroxenites. The widest variation is exhibited by amphibole dunite (Cr# = 55-89, Mg# = 37-61). A bimodal distribution occurs in harzburgite, where grains of Cr-spinel associated with Ca-amphibole have lower Cr# than those associated with olivine and orthopyroxene. As observed for silicates, OPXT II and the vein of OPXT I plot in the field of harzburgite. Dunites overlap with OPXT I and clinopyroxenite. Websterites, and clinopyroxenites containing xenoliths of OPXT I, have lower Cr# than OPXT I and clinopyroxenite.

3.2.6 Interpretation

3.2.6a Silicate Chemistry

Harzburgites have olivine and orthopyroxene that are similar in composition to these phases in (i) harzburgites of the Lewis Hills Massif (Smith and Elthon, 1988), the whole BIOC (Malpas, 1978), and the White Hills Peridotite, Newfoundland (Talkington, 1981), and (ii) abyssal peridotites (Prinz et al., 1976; Hamlyn and Bonatti, 1980; Shibata and Thompson, 1986). As such, they represent residues from extensive partial melting (approximately 23 %) of fertile lherzolite and efficient extraction of magma (Malpas, 1978).

Nicolas (1989) suggested that magmatic dunites should have olivines with Mg# that are less than or equal to those in adjacent harzburgite, whereas residual dunites should have olivines with Mg# that are greater than or equal to those in adjacent harzburgite. The trend of olivine in LAL dunite is to lower

Mg#, but limited data do not permit a conclusive statement.

The highly magnesian and depleted chemistry of silicates in OPXT I, clinopyroxenite and websterite, is unusual for pyroxenite dykes and crustal cumulates of the BIOC, which generally are richer in Al_2O_3 (Elthon et al., 1982; Komor et al., 1985; Smith and Elthon, 1988). Elthon et al. (1982) explained the depleted chemistry and absence of plagioclase in pyroxenites, by high pressure (P > 10 kbar) polybaric crystal fractionation of primary MORB magmas beneath a mid-ocean spreading centre. However, large volumes of orthopyroxenite were not documented by Elthon et al. (1982), who suggested that orthopyroxenite would be related to boninitic magmatism.

Pyroxenite bodies in several localities have been attributed to arc magmatism. Jan and Windley (1990) proposed that the highly depleted mineral chemistry of pyroxenite bodies in the Jijal Complex, Pakistan, correlates with high pressure (P>8 kbar) crystallization of arc-related magmas. Orthopyroxenite dykes cutting mantle harzburgite in the Papuan Ultramafic Belt contain orthopyroxene with Mg# = 89.4, Al_2O_3 < 0.09 wt.% and CaO = 0.14 wt.% (Jaques and Chappell, 1980). These orthopyroxenites are related to tonalites, which represent the early stages of island arc magmatism immediately prior to emplacement of the Papuan Ultramafic Belt (Jaques and Chappell, 1980). Pyroxenites associated with chromite in the White Hills Peridotite, Newfoundland, have highly depleted mineral chemistry, and crystallized from a second-stage magma of magnesian quartz tholeiite (Duncan and Green, 1980) at P<8 kbar (Talkington, 1981). Similar silicate mineral

chemistry is found in boninitic lavas (Crawford, 1980; Crawford et al., 1989; Coish, 1989; Falloon et al., 1989). Silicate mineral assemblages and chemistry in LAL OPXT I, clinopyroxenite and websterite, are very similar to those in the aforementioned occurrences, and suggest that these LAL pyroxenites correlate with high-SiO_2, high-MgO arc-related magmas.

3.2.6b Cr-Spinel Chemistry

The considerable solid solution exhibited by spinel makes it a very useful monitor of magma composition and the extent of partial melting recorded by a peridotite residue. Spinel also is sensitive to subsolidus reequilibration and alteration, and these effects must be determined prior to using spinel chemistry as a petrogenetic indicator.

i) Alteration. Serpentinization has affected all LALPP, and serpentinization is often most severe around grains of Cr-spinel, which is why olivine in chromitite generally is completely serpentinized. Cr-spinel may be altered to magnetite and ferrichromite at grain margins and along internal fractures. Alteration and metamorphism increase Cr# and decrease Mg# relative to the unaltered parent grain (Frost, 1975; Bliss and MacLean, 1975; Lipin, 1984; Jan and Windley, 1990). Analyses of Cr-spinels in LALPP are from cores of grains which are unfractured and exhibit no optical evidence of alteration. It is assumed that the analyses record little evidence of alteration, which is supported by the increase in Cr# and decrease in Mg# of LALPP exhibiting progressively less alteration, i.e., chromitite, dunite and harzburgite

are significantly more altered than pyroxenite.

ii) Subsolidus reequilibration. Mg = $=Fe^{2+}$ and Cr = = Al substitutions control the chemistry of spinel. Subsolidus Mg = $=Fe^{2+}$ exchange between spinel and silicate lowers the Mg# of spinel (Irvine, 1967; Dick and Bullen, 1984; Jan and Windley, 1990). The lower Mg# of accessory Cr-spinel in dunite and harzburgite relative to chromitite (Fig. 3.3), probably is the result of subsolidus reequilibration. Two major reactions affect the Cr# of spinel: (i) transfer of Cr from spinel to pyroxene (Irvine, 1967; Komor et al. 1985), and (ii) transfer of Al from spinel to plagioclase (Irvine, 1967; Henderson, 1975). Plagioclase is not present in LALPP and is not involved in reequilibration. The Cr# of Cr-spinel in pyroxenite, especially clinopyroxenite, may be lower than its original value due to subsolidus reequilibration.

iii) Chromitite. Cr-spinel in chromitites from the Springers Hill area lies within the field of podiform chromitites of ophiolites, and overlaps with chromitites from stratiform intrusions (Figs. 3.3 and 3.4). The wide range of Cr# and narrow range of Mg# are typical of podiform chromitite deposits (Thayer, 1964). The low TiO_2 content (0.12-0.23 wt.%) of Cr-spinel in Springers Hill chromitites is characteristic of podiform deposits (Dickey, 1975).

In ophiolite mantle sequences, Al-rich and Cr-rich chromitites occur at the harzburgite-dunite and iherzolite-harzburgite transitions, respectively (Leblanc and Violette, 1983). The Cr-rich chromitites precipitated from Cr-rich magmas that were produced by the complete melting-out of Cr-diopside (Leblanc and Violette, 1983). The Al-rich chromitites have a genetic relation with Al-rich

magmas that were parental to crustal cumulates (Thayer, 1969; Golding and Johnson, 1971). Such a correlation does not hold for the Springers Hill area, as all chromitites are hosted in dunite associated with harzburgite. Subsolidus reequilibration or reaction may be responsible for the observed variation in composition, as one traverse of a Cr-spinel grain in sample L289 shows a core of Mg# = 65, Cr# = 47 and a rim of Mg# = 58, Cr# = 61, i.e., a large variation in Cr# for a relatively small change in Mg#.

iv) Accessory Cr-spinel. The Mg# of accessory Cr-spinel appears more susceptible than Cr# to change with alteration, metamorphism and subsolidus reequilibration. The Cr# is here considered more representative as a petrogenetic tracer than Mg#. Apart from several Cr-spinel grains associated with Ca-amphibole in harzburgite and amphibole peridotite, all Cr-spinels analysed have Cr# > 60. According to Dick and Bullen (1984), Cr# > 60 are indicative of arc environments.

Harzburgites lie in the high Cr# field of harzburgites from the BIOC, but at higher Cr# than harzburgites previously analysed from the Lewis Hills Massif (Figs. 3.3 and 3.4). Using the argument of Dick and Fisher (1984), the low content of CaO and Al_2O_3 in orthopyroxene, and high Cr# of Cr-spinel, indicate that partial melting occurred well into the three phase field of olivine-orthopyroxene-spinel-magma. This is in total agreement with the petrographic evidence that harzburgite is devoid of clinopyroxene. If the precursor to harzburgite approximated the composition of Tinaquillo lherzolite, then, under anhydrous conditions, 12-15 % magma could have been extracted from the

lherzolite before clinopyroxene in the residue was exhausted (Jaques and Green, 1980). Cr-spinel in harzburgite of the Springers Hill area is similar to that in harzburgite of the Miyamori Ophiolite Complex, Japan (Figs. 3.3 and 3.4), which represents residual mantle of an island arc (Ozawa, 1988).

Dunites, OPXT I, clinopyroxenites and websterites lie in the field of stratiform intrusions (Figs. 3.3 and 3.4). Dunites lie in the field of peridotites of the BIOC and Miyamori Ophiolite Complex (Figs. 3.3 and 3.4). Type I orthopyroxenites, clinopyroxenites and websterites have Cr#(Sp) similar to those of low-alumina orthopyroxenites of the White Hills Peridotite, olivine clinopyroxenites of the Miyamori Ophiolite Complex, boninites, and basaltic komatiites (Figs. 3.3 and 3.4). Dunites, OPXT I and clinopyroxenites do not exhibit the fractionation trend of decreasing Mg# and Cr# that is observed in stratiform intrusions (Figs. 3.3 and 3.4). This is expected as OPXT I and clinopyroxenite (and their associated dunites) are not comagmatic. Type I orthopyroxenites and clinopyroxenites precipitated from different magmas which had fractionated olivine (± Cr-spinel), and yet they have very high Cr#(Sp), which may have been even higher prior to subsolidus reequilibration. High Cr#(Sp) and lack of fractionation recorded by Cr#(Sp) was explained by Irvine (1976) and Dick and Bullen (1984) in terms of Cr-spinel precipitating from a magma with high molecular Si/Al. Pyroxenites (and their associated dunites and chromitites), therefore, precipitated from magmas with high SiO_2 and low Al_2O_3, which is in total agreement with silicate mineral chemistry. These magmas are diagnostic of an arc environment (Dick and Bullen, 1984).

3.2.7 Summary

Mineral chemistry, field relations and petrography of LALPP demonstrate that harzburgite, dunite, OPXT I and clinopyroxenite are not cogenetic, except perhaps for dunites associated with their respective pyroxenites. Prior to intrusion of magmas from which dunite, chromitite and pyroxenite precipitated, harzburgites had experienced melting well into the three phase field of olivine-orthopyroxene-spinel-magma. Following the argument of Dick and Bullen (1984), this melting would have occurred in an arc environment. Clinopyroxenites and OPXT I (and their associated dunites and chromitites) precipitated from magmas with high MgO and SiO_2 and low Al_2O_3. These magmas are present in arc environments (Dick and Bullen, 1984), and the pyroxenites could not have formed by high pressure (P>10 kbar) polybaric crystal fractionation of a basaltic magma parental to MORB, as proposed by Elthon et al. (1982) for cumulates in North Arm Mountain.

The mineral chemistry of OPXT II and veins of OPXT I indicates that they are in equilibrium with harzburgite. Veins of OPXT I equilibrated with harzburgite by subsolidus reequilibration. The harzburgitic composition of OPXT II is considered in Chapter 5.

3.3 WHOLE-ROCK CHEMISTRY

3.3.1 Major and Trace Elements

Major elements and Sc, V, Cr and Ni reflect the modal mineralogy and mineral chemistry of LALPP. Extremely low concentrations of TiO_2 (<0.02 wt.%), Rb (≤1 ppm), Y (≤2 ppm) and Zr (≤2 ppm) are consistent with the depleted mineral chemistry of LALPP. Concentrations of Sr range from ≤0.8 ppm to 64 ppm, and these values will be considered in the next section on rare earth elements. Native Cu and minor associated Cu sulphide account for 125-313 ppm Cu in clinopyroxenite.

Whole-rock Mg# is equivalent to that of Mg#(Ol) for harzburgites, dunites, amphibole dunites and OPXT II, which have olivine as the dominant phase. Whole-rock Mg# is noticeably higher than Mg#(Ol) for OPXT I, clinopyroxenite and websterite, which have pyroxene as the dominant phase and Mg#(Px) > Mg#(Ol). Whole-rock Cr# are lower than those of Cr-spinel for all LALPP because Cr-spinel is an accessory phase. Whole-rock Cr# of dunite approach those of Cr-spinel because pyroxene and amphibole are minor phases or absent. In all other rock types, the modal abundances of pyroxene and amphibole are significantly higher than in dunite and Cr#(whole-rock) is approximately half that of Cr#(Sp) because of the low Cr# of pyroxene and amphibole.

3.3.2 Rare Earth Elements

Absolute concentrations and specific ratios of REE in LALPP are not used because of uncertainty of the quality of the REE data (Appendix 1). Despite this, chondrite-normalized REE (CNREE) patterns of LALPP are assumed to closely approximate the true patterns of LALPP, because CNREE patterns of standard PCC-1 determined in this study are very similar to those determined in other studies (Appendix 1).

All CNREE patterns of LALPP lie in the range 0.001-1.0 x chondrite (Fig. 3.5). The lowest abundances of REE occur in harzburgite, dunite, amphibole dunite, OPXT I and OPXT II, whereas the highest abundances occur in clinopyroxenite and websterite. Flat to positively sloping CNREE patterns occur in harzburgite (sample L225) and dunite (samples L246 and L262), which are composed of olivine, Cr-spinel and orthopyroxene (harzburgite only). Harzburgite sample L225 records the earliest documented partial melting event and apparently does not contain introduced OPXT I, clinopyroxene or Ca-amphibole. Harzburgite containing OPXT I (sample L106) has a U-shaped CNREE pattern very similar to those of OPXT I. Type I orthopyroxenites have negative Eu anomalies. Harzburgite containing Ca-amphibole (sample L103) has a positive Eu anomaly and U-shaped CNREE pattern similar to amphibole dunites. Type II orthopyroxenites have U-shaped CNREE patterns similar to OPXT I, harzburgite containing OPXT I, and amphibole dunite. Dunites (samples L216 and L217) enveloping clinopyroxenite contain orthopyroxene (both samples), clinopyroxene (sample L216) and Ca-amphibole (sample L216),

and have CNREE patterns similar to the LREE-depleted patterns of clinopyroxenites. Websterites are composite pyroxenites of OPXT I and clinopyroxenite and have flatter CNREE patterns than clinopyroxenite, which may be explained by the LREE-enriched patterns of OPXT I.

Concentrations of Sr correlate well with the CNREE patterns of LALPP. Consistent values occur in amphibole dunite (2-13 ppm Sr) and amphibole-bearing harzburgite (8 ppm Sr), which have U-shaped CNREE patterns with positive Eu anomalies. Type I orthopyroxenites and clinopyroxenite have 2-6 ppm and 2-19 ppm Sr, respectively; these concentrations cannot account for 53-64 ppm Sr in websterite. Concentrations of Sr in harzburgite and dunite are $\leq$0.8-15 ppm.

3.3.3 Platinum Group Elements

Harzburgites have flat chondrite-normalized platinum group element (CNPGE) patterns at approximately 0.01 x chondrite (Fig. 3.6a). Ratios of Pd/Ir are 0.6-1.7. The lowest value occurs in sample L225, which records the earliest documented partial melting event, whereas the highest value occurs in harzburgite sample L106, which has been impregnated by OPXT I. Sample L218 is from harzburgite adjacent to dunite enveloping clinopyroxenite, and it contains clinopyroxene and Ca-amphibole, and has Pd/Ir = 1.2.

Chromitites have remarkably uniform CNPGE patterns despite the wide range of composition of Cr-spinel in these samples (Fig. 3.6b). The V-shaped Os-Ir-Ru patterns support the occurrence of Os-bearing laurite in these samples.

The CNPGE pattern of a xenolith of chromitite in HAL olivine clinopyroxenite is indistinguishable from the other chromitites, except for Pd. Osmium-bearing laurite occurs in the xenolith. All samples have characteristic CNPGE patterns typical of ophiolites (e.g., Page et al., 1982, 1983; Page and Talkington, 1984), but exhibit a positive slope from Pt to Pd, which is a characteristic feature of Newfoundland ophiolites (Page and Talkington, 1984).

The dunites that have been analysed for PGE are all associated with clinopyroxenite. The samples that have CNPGE patterns similar to chromitite (Fig. 3.6c), either contain minor orthopyroxene and clinopyroxene (sample L254), or they are devoid of these phases (sample L054). Those samples with very different patterns (Fig. 3.6d) contain orthopyroxene (samples L216 and L217), clinopyroxene (sample L216) and Ca-amphibole (sample L216). Similar CNPGE patterns and Pd/Ir ratios of chromitites and dunites (Figs. 3.6b and 3.6c), suggest that the Cr-spinel component of these dunites controls their abundances of PGE, although no platinum group minerals (PGM) or base metal phases have been identified. This is supported by the highest abundances of PGE in the dunite richest in Cr-spinel (sample L054). Consequently, a similar origin is suspected for the chromitites and these dunites. The low Os/Ru value of the highly serpentinized dunite (sample L054) may argue for the presence of Os-poor to Os-free laurite in this sample. Osmium-free laurite has been observed in serpentine and chlorite interstitial to chromite grains in chromite-rich samples from the Shetland Ophiolite (Tarkian and Prichard, 1987). Dunites in Figure 3.6d contain minor base metal sulphide and native Cu associated with

clinopyroxene and Ca-amphibole. These dunites have relatively high Pd/Ir ratios and a somewhat positive slope from Os to Pd.

Type I orthopyroxenites have Pd/Ir = 32-470 and CNPGE patterns which approximate a mirror image of the patterns for chromitite (Fig. 3.6e). The CNPGE patterns of OPXT I support the occurrence of Pt- and Pd-arsenide grains in orthopyroxene. Websterite has Pd/Ir = 120 and a CNPGE pattern similar to that of OPXT I (Fig. 3.6f). The pattern is consistent with the occurrence of Pt and Pd phases in clinopyroxene. Clinopyroxenites have Pd/Ir > 44-1040 and highly variable CNPGE patterns (Fig. 3.6f). Clinopyroxenites without a dunite envelope, have CNPGE patterns somewhat similar to OPXT I, whereas those with a dunite envelope, exhibit extreme depletion of Ru and negative slopes from Os to Ir. Both types of clinopyroxenite contain abundant primary native Cu and base metal sulphides, but PGM have not been identified.

The CNPGE patterns of OPXT II are very different from those of OPXT I, and are more like those of harzburgite and chromitite (Fig. 3.6g). Their Pd/Ir ratios are equivalent to those of harzburgite. The anomalous enrichment of Ru in the web-textured OPXT II could be inherited from Cr-spinel, as Legendre (1982) reports chromitites with extreme enrichment in Ru from ophiolites of Oman and Cyprus. Alternatively, the high concentration of Ru could represent contamination from HCl during sample preparation (Jackson et al., 1990). The latter is favoured because a sample previously analysed and reanalysed with sample L271 shows no change in abundances of PGE, except for extreme enrichment in Ru. The sulphide content of OPXT II may influence their CNPGE

patterns. No sulphide is observed in the ribbon mylonite which has a harzburgitic CNPGE pattern. Harzburgites do not contain sulphide that predates serpentinization. Sulphide occurs in the web-textured OPXT II which has a chromititic CNPGE pattern.

Only amphibole dunites associated with OPXT I have been analysed for PGE. Their CNPGE patterns exhibit remarkable similarity with those of OPXT I (Fig. 3.6h). Ratios of Pd/Ir in amphibole dunite are lower than those of OPXT I. Platinum group minerals have not been identified in these samples and sulphide is absent, except for rare altered sulphide or native Cu in amphibole-rich areas.

3.4 CHEMICAL EFFECTS OF SERPENTINIZATION

In order to use whole-rock concentrations of major and trace elements, REE and PGE as petrogenetic tracers, the effects of alteration must be known. The silicate portion of LALPP is always serpentinized. Serpentinization is most severe in areas rich in olivine and the silicate portion of some dunites is 100 % serpentinized. An extensive discussion of the effects of serpentinization is beyond the scope of this thesis, but the most important points are considered below.

3.4.1 Major and Trace Elements

Under conditions of non-constant volume, serpentinization is an

isochemical process except for the introduction of H_2O and loss of Ca (Coleman and Keith, 1971; Eckstrand, 1975). Frey et al. (1985) report no change in major element abundances for serpentinized peridotites of Ronda ($\leq$31 % serpentinization). Concentrations of Si, Mg, Fe, Cr, Al and Ni in Archean dunites of Western Australia are unaffected by serpentinization (Donaldson, 1981). Concentrations of Fe, Ni and Cu are redistributed during serpentinization, but are unaffected at the scale of a whole-rock sample (Shiga, 1987; Edwards, 1990). Peridotite samples in the Springers Hill area have Mg#(whole-rock) = Mg#(Ol), which demonstrates that Mg#(whole-rock) is unaffected by serpentinization. Pyroxenite samples are much less serpentinized than peridotite samples.

For the purpose of this thesis, it is adequate to assume that serpentinization in the Springers Hill area had relatively little influence on abundances of major and trace elements, except for the introduction of H_2O.

3.4.2 Rare Earth Elements

There is no clear consensus as to the mobility of REE during serpentinization. It has been argued that hydrous alteration can result in either a subparallel shift downward of CNREE patterns, or development of negative Ce anomalies with preferential loss of LREE (Ottonello et al., 1979). Frey (1969) also predicted that LREE are removed during serpentinization. Mobility of Eu^{2+} during serpentinization (Sun and Nesbitt, 1978) may account for positive Eu anomalies in peridotites lacking plagioclase (Frey, 1984). On the

other hand, there is strong evidence to argue that concentrations of REE are unaffected by serpentinization. Michard (1989) suggested that because hydrothermal fluids have low concentrations of REE, hydrothermal activity is not expected to change REE abundances of a rock unless water/rock ratios are extremely high. In agreement with this argument, Frey (1984) presented data for serpentinites which appear to preserve the original CNREE patterns of their ultramafic protoliths. Further agreement comes from the harzburgites and dunites of the New Caledonia Ophiolite, where there is no correlation between the degree of serpentinization ($\leq$40 %) and LREE enrichment (Prinzhofer and Allègre, 1985). Frey (1984) made a similar observation for the peridotites of Ronda that were $\leq$30 % serpentinized.

In the Springers Hill area, serpentine and associated alteration products occur mostly in areas rich in olivine. Pyroxene and amphibole generally are unaltered to partially altered. Because partition coefficients of REE are so much greater for pyroxene and amphibole than olivine (Fig. 3.7), and because pyroxene and amphibole control CNREE patterns of peridotites (Stosch and Seck, 1980), the removal of REE from olivine will have little effect on CNREE patterns of whole-rock samples. This appears to be the situation in the Springers Hill area, especially as all CNREE patterns of LALPP are adequately explained by their mineralogy which pre-dates serpentinization. Consequently, CNREE patterns of whole-rock samples of LALPP reflect processes pre-dating serpentinization of the Springers Hill area.

3.4.3 Platinum Group Elements

Platinum group elements generally are immobile during serpentinization (Keays and Davison, 1976; Groves and Keays, 1979; Oshin and Crocket, 1982; Prichard and Tarkian, 1988; Edwards, 1990), and concentrations of PGE in whole-rock samples of LALPP reflect processes pre-dating serpentinization of the Springers Hill area. This is well supported by the similarity of CNPGE patterns of dunite (sample L254) and extensively serpentinized Cr-spinel-rich dunite (sample L054) (Fig. 3.6c). The mineralogy of PGM in LALPP is primary and related to fractionation of immiscible As-S-rich liquids in the early stages of crystal fractionation (see sections 2.3.8 and 2.6).

3.5 PETROGENESIS OF HARZBURGITE

3.5.1 CaO/Al_2O_3 Ratio as an Index of Partial Melting

Harzburgites have experienced melting well into the three phase field olivine-orthopyroxene-spinel-magma. Klein and Langmuir (1987) stated that melting-out of clinopyroxene from lherzolite to produce harzburgite, causes an increase in CaO/Al_2O_3 ratio of the whole-rock until clinopyroxene is exhausted; as melting continues, the CaO/Al_2O_3 ratio decreases. Extremely refractory harzburgites in the Papuan Ultramafic Belt (Jaques and Chappell, 1980), provide evidence that CaO/Al_2O_3 ratios drop sharply as orthopyroxene is progressively melted out of harzburgite (Fig. 3.8a). Falloon and Green (1987) demonstrated this trend in experiments of equilibrium partial melting of MORB

pyrolite at 10 kbar. Further work by Falloon et al. (1989) confirmed this trend (Fig. 3.8a).

Samples of harzburgite from the Springers Hill area record melting well beyond the melting-out of clinopyroxene. These samples should have CaO/Al_2O_3 ratios similar to, or lower than, those in lherzolites, but they have CaO/Al_2O_3 ratios which generally are higher than lherzolites (Fig. 3.8a). The lowest ratios (samples L097 and L225) correlate with harzburgites from other ophiolites, and agree with petrographic and chemical evidence that they are residues from the earliest documented episode of partial melting and efficient extraction of magma. Due to the abundance of chemical data on sample L225 relative to sample L097, the former will be used as the harzburgite end-member of partial melting and efficient extraction of magma. This sample has not been modified petrographically or chemically by subsequent processes, except for the formation of serpentine from olivine.

Harzburgites having CaO/Al_2O_3 ratios higher than that of sample L225, contain clinopyroxene and/or Ca-amphibole, or infiltrated OPXT I (Fig. 3.8a). Clinopyroxene and Ca-amphibole have high CaO/Al_2O_3 ratios. Petrographic evidence shows that 1-2 modal % of these phases in harzburgite cause the observed increase in CaO/Al_2O_3 ratio. Type I orthopyroxenite has a lower CaO/Al_2O_3 ratio than clinopyroxene or Ca-amphibole, and yet the harzburgite containing introduced OPXT I (sample L106) has the highest CaO/Al_2O_3 ratio. Figure 3.8b shows that sample L106 contains a large component of OPXT I in addition to a component of sample L225. The composition of sample L106

estimated from CaO/Al_2O_3 ratios is 58 % sample L225 and 42 % OPXT I (Appendix 5). Modal abundances of orthopyroxene are 15 % in sample L225, 90 % in OPXT I and 45 % in sample L106. Therefore, sample L106 contains an estimated 8.7 % orthopyroxene from sample L225 and 37.8 % orthopyroxene from OPXT I, which is a total of 46.5 % orthopyroxene, i.e., essentially identical to the 45 % orthopyroxene estimated visually.

The introduced component of orthopyroxene in harzburgite is not apparent from mineral chemistry, even though compositions of minerals in OPXT I are very different from those in harzburgite. The changes in mineral chemistry associated with the introduction of OPXT I into harzburgite should be accounted for by reequilibration at magmatic and subsolidus temperatures with or without the later effects of serpentinization. To determine the response of mineral chemistry to these changes is an immense task well beyond the scope of this thesis.

3.5.2 Rare Earth Elements

At the present time, the key to understanding the origin of ophiolite harzburgites lies largely in understanding their CNREE patterns. Unfortunately, the REE data acquired in this thesis limits interpretation, and modelling using the REE is not possible. The essence of the following discussion is that CNREE patterns of harzburgites of the Springers Hill area are representative of processes which pre-date serpentinization of the area.

Sample L225 has a straight, positive sloping CNREE profile from La-Lu

(Fig. 3.5a). The pattern is controlled by orthopyroxene as suggested by (i) modal mineralogy, (ii) partition coefficients of REE in orthopyroxene (Fig. 3.7), and (iii) REE analyses of orthopyroxene separates from anhydrous spinel peridotite nodules from Dreiser Weiher, Germany (Stosch and Seck, 1980). Patterns of this type are rare in ophiolites, but they have been documented in harzburgites from the New Caledonia (Nicolas and Dupuy, 1984) and Trinity (Brouxel and Lapierre, 1988) ophiolites. They also have been documented in the Ronda Peridotite (Frey et al., 1985). Schilling (1975), Menzies et al. (1977) and Frey et al. (1985) have calculated that positive sloping CNREE profiles in residues can be produced by 9-30 % partial melting of LREE-depleted lherzolite. The magmas which segregated from the Ronda peridotites were picritic (12-22 wt.% MgO) and may have been parental to MORB (Frey et al., 1985). Ronda harzburgites with CNREE patterns similar to that of sample L225 were in equilibrium with the picritic magma for 26-32 % partial melting (Frey et al., 1985). Experiments performed by Green et al. (1979) show that such picrites are multiply saturated in olivine and orthopyroxene at P = 20 kbar (60-70 km depth) and T = 1430°C. The harzburgite residue left after extraction of this picrite would contain orthopyroxene with > 5 wt.% Al_2O_3 and > 2.5 wt.% CaO, and would recrystallize to spinel lherzolite at lower pressure (Green et al., 1979).

The mineral chemistry of sample L225 is inconsistent with it being a residue from extraction of picritic magma at P = 20 kbar. Cr-spinel in sample L225 lies in the range of those analysed from the Troodos Upper Pillow Lavas

by Duncan and Green (1987). Many of these lavas are severely LREE-depleted (Kay and Senechal, 1976; Smewing and Potts, 1976), which correlates with the CNREE pattern of sample L225. Consequently, this sample could be a residue from (i) continuous melting of a lherzolite diapir (Smewing and Potts, 1976), or (ii) 5-10 % second-stage partial melting of an anhydrous, residual lherzolite diapir at P = 7-8 kbar ($\leq$ 25 km depth) and T = 1360°C, and extraction of a LREE-depleted magnesian quartz tholeiite or olivine-poor tholeiite (Duncan and Green, 1980). The latter would correlate with melting in a back-arc basin (Duncan and Green, 1987).

The majority of harzburgites in the Springers Hill area are assumed to have an initial origin similar to sample L225, but some experienced subsequent modification by the addition of OPXT I (sample L106) and Ca-amphibole (sample L103), which produced U-shaped CNREE patterns. Although these modifications occurred during separate events, they both produced significant enrichment in the LREE. If these harzburgites had undergone further melting, they would have produced high-MgO and -SiO_2 magmas with U-shaped CNREE patterns. Magmas of this type occur as boninites in arc environments (Hickey and Frey, 1982).

It has been argued on the basis of CNREE patterns of ophiolitic rocks, that harzburgites possessing U-shaped patterns are not genetically related to overlying rocks of the crustal sequence through a simple parent-daughter relationship because of the relative LREE depletion exhibited by the crustal sequence (Suen et al., 1979; Pallister and Knight, 1981; Frey, 1984).

Harzburgites of the Springers Hill area having U-shaped CNREE patterns support this view, but the positively sloping CNREE pattern of sample L225 suggests that prior to involvement of fluids and fluid-rich magmas, ophiolite harzburgites may indeed have LREE-depleted CNREE patterns and be related to the LREE-depleted component of the crustal sequence. Such a suggestion disagrees with the sequential integrated disequilibrium melting model developed by Prinzhofer and Allègre (1985), which requires that LREE-enriched residues and LREE-depleted magmas are cogenetic. Prinzhofer and Allègre (1985) developed this model from harzburgites in the New Caledonia Ophiolite which have CNREE patterns similar to that of harzburgite in the Springers Hill area which contains OPXT I. The importance of this will be discussed in section 3.5.4.

3.5.3 Platinum Group Elements

Before interpreting the PGE chemistry of harzburgites, it is necessary to understand the behaviour of PGE, base metals and sulphides in these rocks. The sulphide component of the upper mantle has a low melting point (Naldrett, 1973) and is largely involved in mantle melting (Garuti et al., 1984). This allows the abundance of Fe-Ni-Cu-S phases to be used as a depletion index, especially as their abundance correlates with the modal abundance of clinopyroxene and plagioclase in residual mantle material (Lorand, 1988). The Springers Hill harzburgites are devoid of primary Fe-Ni-Cu-S phases and residual clinopyroxene and plagioclase, which is consistent with their having experienced extensive partial melting prior to local modification by infiltrating

fluid and fluid-rich magma.

It is possible to estimate the degree of partial melting required of a mantle source to yield a harzburgite residue totally barren of sulphide (Barnes et al., 1985). Garuti et al. (1984) report an Fe-depleted, Ni- and Cu-enriched mantle sulphide component for the Baldissero and Balmuccia lherzolites of the Ivrea-Verbano mantle peridotites, western Italian Alps. These lherzolites preserve S contents of 140-320 ppm, which are representative of the S content of undepleted to partially depleted upper mantle (Garuti et al., 1984). For the Springers Hill harzburgites, it is assumed that the initial S content of the mantle source was 140-320 ppm, that partial melting occurred at a depth of <40 km (Duncan and Green, 1987), and that S solubility in basic silicate magmas is 0.19 wt.% (Wendlandt, 1982). For these parameters, 7-17 % partial melting is required to remove all of the mantle sulphide into the magma for, respectively, S concentrations between 140-320 ppm in the initial mantle source. Partial melting to produce Springers Hill harzburgites was far in excess of 17 %. These rocks contain no petrographically visible sulphide phase, apart from that resulting from serpentinization of the silicate phases. During partial melting, the dissolution of all of the mantle sulphide left no sulphide residue into which the PGE could partition. Magma has been very effectively removed from the Springers Hill harzburgites, as there is no evidence for trapped silicate or sulphide magma.

The Springers Hill harzburgites contain 23-38 ppb total PGE. Because there is no sulphide in which the PGE can exist, they must be present in either

Cr-spinel and silicate phases, or an intergranular phase. It has been postulated that refractory Cr-spinel and olivine in S-poor ultramafic rocks may act as a sink for Ir (Crocket, 1979; Naldrett et al., 1979). In addition, Mitchell and Keays (1981) predicted that high-temperature Ir alloys may exist under upper mantle P-T conditions in environments of low fS_2. Iridium in this form would remain as a residual phase during partial melting of the mantle (Mitchell and Keays, 1981). In contrast to Ir, Pd is more volatile (Arculus and Delano, 1981) and, therefore, during partial melting Pd fractionates from Ir which is left in the residue (Hertogen et al., 1980; Mitchell and Keays, 1981). Hence, highly depleted and refractory mantle peridotites have low total PGE contents, fractionated CNPGE patterns with negative slopes from Ir to Pd, and $Pd/Ir << 1$. Such patterns have been reported from the Thetford Mines Ophiolite, Quebec (Oshin and Crocket, 1982), and the Ronda Peridotite, Spain (Stockman, 1982), and calculated for the Vourinos Ophiolite Complex, Greece (Cocherie et al., 1989).

The CNPGE pattern and $Pd/Ir = 0.6$ of sample L225 is consistent with it being a residue from partial melting. However, more extreme fractionation of Pd and Ir is expected for harzburgite as refractory as sample L225. The PGE-depleted (Ir = 2.1-2.9 ppb, Pd = 0.45-0.68 ppb) Black Lake harzburgites of the Thetford Mines Ophiolite have average $Pd/Ir = 0.22$ (Oshin and Crocket, 1982), which are expected to be more typical of harzburgites that are residues from extensive partial melting and efficient extraction of magma. Despite this, sample L225 will be used as the starting composition for discussing the PGE

content of harzburgite with Pd/Ir > 1.

The CNPGE patterns and Pd/Ir = 1.2-1.7 of Springers Hill harzburgites that contain OPXT I, and Ca-amphibole and clinopyroxene derived from clinopyroxenite, are completely inconsistent with a simple residual origin. In fact, the flat PGE patterns coincide with the CNPGE data compiled by Arculus and Delano (1981) for undepleted upper mantle (Jagoutz et al., 1979; Morgan and Wandless, 1979; Morgan et al., 1980; Mitchell and Keays, 1981). The discrepancy can be explained by the introduced components. That involving a component of clinopyroxenite is of minor significance based on petrographic evidence; it will be considered with the origin of dunite in section 3.7.1. The addition of OPXT I to harzburgite is, however, significant.

The formation of sample L106 by addition of OPXT I to sample L225 has been demonstrated earlier. Using the same approach as for CaO/Al_2O_3 ratios, the proportions of OPXT I and sample L225 in sample L106 are calculated using Pd/Ir ratios (Appendix 5). Concentrations of Ir are similar for all components, whereas concentrations of Pd differ significantly, so that addition of OPXT I to harzburgite will produce large variations in concentrations of Pd at approximately constant concentrations of Ir. The composition of sample L106 estimated from Pd/Ir ratios is 98 % sample L225 and 2 % OPXT I. This clearly is inconsistent with petrographic evidence and the calculation involving CaO/Al_2O_3 ratios, which estimated 58 % sample L225 and 42 % OPXT I for sample L106. Using the OPXT I sample poorest in PGE (sample L071), the estimate becomes 81 % sample L225 and 19 % OPXT I (Appendix 5).

Significant variations are expected in the calculation using Pd/Ir ratios because these ratios in the mixing components are very different relative to CaO/Al_2O_3 ratios. Consequently, it is predicted that the component of OPXT I in sample L106 has a lower Pd/Ir ratio and total abundance of PGE than the massive dykes sampled in this study. Alternatively, Pd may have been removed from sample L106 by fluids associated with the formation of the HALPPG (section 5.5.3). Some orthopyroxene in sample L106 was converted to olivine during this late event.

3.5.4 Orthopyroxene in Harzburgite

Although extensive field and petrographic work has documented the addition of OPXT I to harzburgite by magmatic impregnation or mechanical mixing, the chemical data base is limited to several carefully selected samples. The question arises as to how significant are the orthopyroxene-addition processes in terms of modifying harzburgite compositions in mantle sequences of ophiolites. In the Springers Hill area, dykes and veins of OPXT I are abundant, and a significant proportion of the harzburgite appears to be modified. However, the area mapped in this study is only 2 km^2. There is evidence of orthopyroxene impregnation in other massifs of the BIOC (G. Suhr, pers. comm., 1990). A survey of literature data on the PGE content of harzburgites from ophiolites, reveals that many of them preserve $Pd/Ir > 1$, e.g., the Troodos Ophiolite (Becker and Agiorgitis, 1978), the Thetford Mines Ophiolite (Oshin and Crocket, 1982), and the Vourinos Ophiolite (Cocherie et

al., 1989). A similar survey reveals that harzburgites from the ophiolites of Othris, Vourinos, Troodos, Oman, New Caledonia and Bay of Islands, exhibit U-shaped CNREE patterns (Prinzhofer and Allègre, 1985; compilation of Frey (1984)). Without detailed field and petrographic studies of harzburgites from these ophiolites, it is premature to attribute elevated Pd/Ir ratios and U-shaped CNREE patterns to addition of orthopyroxenite. If such a process operated in these ophiolites, then significant modification of the trace element composition of harzburgite, with little or no evidence of this in the petrography or mineral chemistry, would appear to be the rule rather than the exception. Partial melting of these harzburgites should produce magmas of the boninitic series which have U-shaped CNREE patterns, negative Eu anomalies, and high Pd/Ir ratios.

3.6 PETROGENESIS OF CHROMITITE

Lago et al. (1982) have discussed the origin of chromite deposits in ophiolites. They concluded that chromitites represent magmatic accumulations from basaltic magmas. Field, petrographic, mineral chemical and PGE data support a similar origin for the chromitites of the Springers Hill area, which are magmatic accumulations from magmas with high molecular Si/Al ratios. This is in agreement with Roberts (1988), who proposed that extensive chromite mineralization is restricted to ophiolites with supra-subduction zone characteristics.

The CNPGE pattern of the xenolith of chromitite (sample L326) from the marginal zone of the HALPPG, and the occurrence of Os-laurite in this sample, suggests that it is a xenolith of LALPP affinity (Fig. 3.6b). This evidence disagrees with the interpretation of Bèdard (1991), that chromitites may be products of the assimilation of gabbro and pyroxenite by invading primitive magma.

3.7 PETROGENESIS OF DUNITE

The origin of dunites in ophiolites as residual versus magmatic is a topic of major discussion which is largely beyond the scope of this chapter. For a review of the problem see Nicolas (1989, pages 225-236). Field and petrographic observations presently are the best way to examine the origins of dunite in LALPP. These observations have been interpreted in section 2.3.7. The chemical data available for dunites is varied, limited, and may be affected by serpentinization, but some general statements will be made based on abundances of PGE in dunites enveloping clinopyroxenites.

3.7.1 Platinum Group Elements

The CNPGE patterns of dunites with chromititic patterns (Fig. 3.6c) are controlled by Cr-spinel, which is inferred to be magmatic based on the origin of chromitite. Whether or not olivine is magmatic is questionable because rare porphyroclasts of orthopyroxene are hosted in one sample. According to Lago

et al. (1982), residual dunite is expected to develop by the incongruent melting of orthopyroxene at the interface between harzburgite and the magma conduit in which olivine and Cr-spinel are accumulating by magmatic crystallization. Olivine and Cr-spinel in dunites having chromititic CNPGE patterns would appear to have developed by this process.

A more complicated situation is portrayed by dunites containing Ca-amphibole and relatively abundant pyroxene (Fig. 3.6d). To explain the CNPGE patterns of these dunites, they are considered with the clinopyroxenite dyke which they envelope and the harzburgite which hosts them (Fig. 3.9). Figure 3.9 shows that Pd/Ir = 1.2 in harzburgite is due to a component of clinopyroxenite. The same conclusion was reached using CaO/Al_2O_3 ratios (see section 3.5.1). Dunite (sample L217) sampled 1.5 m from this harzburgite is residual in origin as supported by (i) olivine of Mg# = 91.3, which is the same as that in harzburgite, (ii) orthopyroxene porphyroclasts, and (iii) a CNPGE pattern almost identical to harzburgite except for Pd. The elevated Pd value demonstrates that a component of clinopyroxenite is contained by sample L217, although it is not visible in the field or in thin section. This variation in Pd is testimony to the much higher degree of incompatibility of Pd relative to Pt (Peck and Keays, 1990). The dunite (sample L216) sampled 0.7 m from sample L217 has clots of Cr-spinel and a very different CNPGE pattern. The pattern is a mirror image of that of chromitite and may indicate that a significant amount of Cr-spinel had fractionated previously from the magma. However, porphyroclasts of orthopyroxene are present, which indicate that a

component of the dunite is residual. The extreme depletion of Ru in clinopyroxenite also may support the conclusion that the magma had fractionated significantly large amounts of a Ru-bearing phase (most likely laurite).

Thus, CNPGE patterns are very sensitive to the magmatic and residual components in a dunite. A better understanding of the PGE, and careful use of the data in combination with field and petrographic observations, may make these elements an important tool for solving the dunite problem.

3.8 PETROGENESIS OF TYPE I ORTHOPYROXENITE AND CLINOPYROXENITE

3.8.1 Magmatic versus Metasomatic Origin of Pyroxenites

In section 1.3.2, numerous models were outlined that can be used to explain the origin of pyroxenites. From the field and petrographic observations and geochemical evidence presented for OPXT I and clinopyroxenite, there are two plausible origins for these rocks. Either they may have crystallized directly from two distinct magmas, or they may represent the products of metasomatism of harzburgite and dunite by two distinct fluids.

Bowen and Tuttle (1949) suggested that pyroxenites are produced by the interaction of hydrous, SiO_2-saturated fluid with olivine (dunite). Pyroxenite-amphibolite bands have a hydrothermal origin in the Seiad Complex, California (Loomis and Gottschalk, 1981). These authors stated that as fluid equilibrates with peridotite, the minerals that precipitate in the bands should

have compositions similar to those in the peridotite. Orthopyroxene is the dominant pyroxene in most metasomatic bands (Carswell et al., 1974; Loomis and Gottschalk, 1981).

There are a number of difficulties in accepting this interpretation. The first is that clinopyroxenites essentially are anhydrous. Secondly, OPXT I are hydrous, but they do not contain the abundance of amphibole expected for a metasomatic origin. Thirdly, the CNPGE patterns of OPXT I may be explained by previous fractionation of a significant volume of Cr-spinel as chromitite; chromitites are magmatic in origin (section 3.6). Alternatively, field and petrographic observations and mineral chemistry of OPXT I and clinopyroxenites, are best explained by these pyroxenites having precipitated from hydrous and anhydrous magmas with high molecular Si/Al ratios which fractionated olivine, Cr-spinel and pyroxene.

3.8.2 Compositions of Parental Magmas

At least two parental magmas were required to produce OPXT I and clinopyroxenite. These magmas had high MgO, high molecular Si/Al ratios, and high Pd/Ir ratios. The high Mg# of olivine and pyroxene in the pyroxenites, suggests that the magmas from which they precipitated had undergone very little olivine fractionation before pyroxene became the dominant fractionating phase. Cr-spinel fractionated with olivine as exemplified by the strong control of Cr-spinel on CNPGE patterns of pyroxenites. Despite these similarities, there were important differences between the two magmas: OPXT I precipitated from

a hydrous magma with abundances of REE very different from the essentially anhydrous magma which precipitated clinopyroxenites.

3.8.2a Rare Earth Element Abundances of Parental Magmas

The uncertainty in the REE data of the pyroxenites does not preclude an estimation of the CNREE patterns of the magmas from which they precipitated. If all crystalline products remained in chemical equilibrium with the magma, the situation is a reversal of batch melting. This is a plausible situation in the pyroxenite dykes because crystals are unzoned (although this may be the effect of subsolidus reequilibration) and dykes internally are unfractionated. For clinopyroxenites, the latter applies to any dyke without a dunite envelope. Crystals in the dykes probably grew dominantly by an adcumulus process, whereby all interstitial magma was physically removed as a result of crystal growth. This process is in agreement with the assumption of mineral-magma equilibrium. It is assumed that the system was open and homogeneous crystal growth occurred by crystals plating to dyke walls. The composition of the magma passing through the dyke was constant because no mineralogical zonation is present.

Equation E3.1 is the Berthelot-Nernst equation and is used here to calculate the composition of the magma in equilibrium with the pyroxenite:

[E3.1] $C_L/C_s = 1/(F+D-FD)$, if $F=0$, then

$C_L = C_S/D$,

where C_L is the concentration of the element in the magma, C_s is the concentration of the element in the pyroxenite, F is the proportion of material representing trapped magma in the pyroxenite, and D is the bulk partition coefficient of the element (calculated as the product of the weight proportion of each mineral in the pyroxenite multiplied by its mineral/matrix partition coefficient (K_D)).

For the clinopyroxenites, the equation with $F=0$ provides a good estimate of the composition of the magma because there is no interstitial material representing trapped magma. For the OPXT I, the equation with $F=0$ is used, but it is questionable because amphibole is present, which may represent a component of trapped magma. In OPXT I sample L268 used for the calculation, amphibole is 5 wt.%. It is unlikely that $F=5$ wt.% because amphibole replaces clinopyroxene and orthopyroxene, i.e., $F<5$ wt.%. Because partition coefficients of clinopyroxene and amphibole are similar (Fig. 3.7), amphibole is considered in the calculation for $F=0$.

The estimated CNREE patterns of magmas in equilibrium with pyroxenites are very different (Fig. 3.10). Type I orthopyroxenite was in equilibrium with a magma with a U-shaped CNREE pattern, whereas clinopyroxenites formed from a magma with a relatively flat CNREE pattern. These patterns are

characteristic of boninites and low-Ti arc tholeiites, respectively. Locations where these two magma types are juxtaposed are the western Pacific island arcs (Hickey and Frey, 1982), the Betts Cove Ophiolite, Newfoundland (Coish et al., 1982), the Upper Pillow Lavas of the Troodos Ophiolite (McCulloch and Cameron, 1983; Cameron, 1985), and western Tasmania (Brown and Jenner, 1989). Whether boninites are produced before or after low-Ti tholeiites varies from one location to the next. In the Betts Cove Ophiolite, boninites formed before and during the formation of low-Ti tholeiites (Coish et al., 1982), which is similar to the sequence in the Springers Hill area.

3.8.2b LREE Enrichment of Mantle Sources of Boninites

The LREE enrichment of the source region of boninites is explained by invasion of a LREE-depleted harzburgite by small volumes of a LREE-enriched, Ti-depleted component (Sun and Nesbitt, 1978; Jenner, 1981; Hickey and Frey, 1982; Coish et al., 1982). This component may be from a sedimentary source, or a mantle source with recent to ancient LREE enrichment (Hickey and Frey, 1982; McCulloch and Cameron, 1983; McCulloch et al., 1983). The LREE-enriched component may be similar to that associated with ocean island basalts (Hickey and Frey, 1982). The fluid or magma which produces the LREE enrichment may crystallize as veins (Wood, 1979), or react with harzburgite and crystallize new minerals such as mica, amphibole, rutile, ilmenite and diopside (MARID) that are found in MARID suite xenoliths in kimberlites (Kramers et al., 1983). The LREE-enriched source may then experience partial

melting. Alternatively, flushing of harzburgite by fluid may trigger incongruent melting of orthopyroxene, given the experimental evidence of Kushiro (1969, 1972) and Nicholls and Ringwood (1973).

3.8.2c La Enrichment of Mantle Sources of Low-Ti Tholeiites

The analytical uncertainty in the LREE data of clinopyroxenites does not permit a conclusive statement to be made about the positive La, or negative Ce, anomaly diagnostic of this rock type. If the anomaly is not associated with contamination during sample preparation, then it would correlate with similar anomalies found in supra-subduction zone volcanics (Rautenschlein et al., 1985; Brown and Jenner, 1989) and island arc volcanics (White and Patchett, 1984), and could correlate with a sedimentary component in the mantle source (Hole et al., 1984).

3.8.3 Melting Models for the Generation of Boninites and Low-Ti Tholeiites

Smewing and Potts (1976) explained the variation in chemistry of the lava sequences in the Troodos Ophiolite by continuous partial melting of a lherzolite diapir. Cameron (1985) proposed that the Upper Pillow Lavas of Troodos were produced by incremental melting of a variably depleted and residual source region. The latter is similar to the model proposed by Hickey and Frey (1982) for production of boninites and low-Ti tholeiites in western Pacific island arcs by partial melting of a variably depleted and residual source which had been pervasively enriched in LREE. This kind of model was used by

Coish et al. (1982) to explain the lava sequence in the Betts Cove Ophiolite.

The OPXT I are very similar in composition to orthopyroxenite veins and dykes in the mantle sequences of the Pindos Ophiolite, Greece (Montigny et al., 1973), the Troodos Ophiolite (Menzies and Allen, 1974), the Papuan Ultramafic Belt (Jaques and Chappell, 1980), the White Hills Peridotite (Talkington, 1981), and the Oman Ophiolite (Lippard et al., 1986) (Table 3.1). Montigny et al. (1973), Menzies and Allen (1974) and Jaques and Chappell (1980) interpreted orthopyroxenites as the final products of partial melting of extremely residual peridotite. Talkington (1981) proposed that orthopyroxenites formed from a magma of magnesian quartz tholeiite produced by localized second-stage partial melting at $P \leq 8$ kbar of lherzolite nearly devoid of clinopyroxene (Duncan and Green, 1980). This magma crystallized significant quantities of chromitite, orthopyroxenite and websterite, in this order. The situation in the White Hills Peridotite most closely approaches that of the Springers Hill area, except that websterite is not present in the latter, and mineral compositions are more depleted in the latter with respect to the former.

Harzburgites, as exemplified by sample L225, are residues from the extraction of magnesian quartz tholeiite, which probably was LREE-depleted, low-Ti tholeiite. This residue subsequently was intruded, respectively, by OPXT I (boninite magma) and clinopyroxenite (low-Ti tholeiite magma), and their respective dunites and chromitites. The juxtaposition of these rock types, suggests that partial melting and magma intrusion occurred within a well defined vertical column of upwelling asthenosphere. The experimental work of

Duncan and Green (1987) demonstrated that all these events could have occurred through partial melting of residual lherzolite and harzburgite diapir(s) at $P \leq 7$-8 kbar (≤ 25 km) with and without the presence of hydrous fluid. These conditions agree with the supra-subduction zone environment proposed for the BIOC by Malpas (1976), Edwards (1990) and Jenner et al. (in press).

3.9 ENVIRONMENT OF FORMATION OF THE SPRINGERS HILL AREA

3.9.1 Spreading Centre

The S_1 fabric and coarse textures of harzburgite are indicative of asthenospheric deformation dominated by plastic flow at 1200-1300°C (section 2.3.7). These fabrics and textures are indicative of the low velocity zone beneath a ridge (Mercier and Nicolas, 1975), and this environment has been proposed for the Springers Hill area by Dahl and Watkinson (1986). Consequently, the Springers Hill area could represent a zone of asthenospheric upwell, extreme partial melting and magmatic activity below a spreading centre in a supra-subduction zone. Such an interpretation is consistent with the steep foliations in the mantle sections of the Troodos and Oman ophiolites, which have been ascribed to asthenospheric flow beneath a spreading centre (George, 1978; Ceuleneer et al., 1988). Also consistent with this interpretation are the occurrence of veins and dykes of pyroxenite and economic concentrations of chromitite in the residual mantle peridotites of ophiolites such as Troodos (Menzies and Allen, 1974; Greenbaum, 1977).

3.9.2 Fracture Zone

In section 1.5, the models for the origin of the BIOC were summarized. In the model of Karson and Dewey (1978), the Springers Hill area would have been situated adjacent the non-transform domain of an oceanic fracture zone. Several features in the Springers Hill area are consistent with this environment of formation:

1) Fabrics similar to those in harzburgites of the Springers Hill area have been documented in the Bogota Peninsula, New Caledonia (Prinzhofer and Nicolas, 1980), the Antalya Ophiolite, Turkey (Reuber, 1984), and the Western Limassol Forest Complex, Cyprus (Murton, 1986). In all three cases the fabric was formed in a transform fault zone.

2) Chromitite mineralization is associated with fracture zone ophiolites. One of the largest chromite deposits in the world is the Tiébaghi chromitite pod in New Caledonia. This chromitite contains Cr-spinel of 59 wt.% Cr_2O_3 and marks the lherzolite-harzburgite contact (Leblanc, 1987). The deposit is located along the Tiébaghi-Poum-Belep Fracture Zone, which represents a palaeotransform fault (Sécher, 1981).

3) Magmas having highly depleted chemistry are associated with fracture zone ophiolites. Separating the Troodos Complex from the Limassol Forest Complex in Cyprus, is the Arakapas Fault Belt, which Moores and Vine (1971) interpreted as a palaeotransform fault. Murton (1986) explained LREE-depleted or U-shaped CNREE patterns of lavas in the Arakapas Fault Belt, by partial melting of mantle material associated with a once active palaeotransform fault

zone in a supra-subduction zone environment.

Evidently, features in the LALPP of Springers Hill area can be explained by the presence of a fracture zone. If such a tectonic environment existed, then, as the CC is older than the BIOC by 14-29 Ma (Jenner et al., in press), relatively cold lithosphere ($T < 1000°C$) of the CC would be juxtaposed against relatively hot ($T = 1200\text{-}1300°C$) asthenosphere of the BIOC at the fracture zone. The lithosphere would act as a thermal and mechanical boundary to the upwelling asthenosphere (Sécher, 1981; Nicolas, 1989), and flow would be channelled parallel to the fracture zone (Vogt and Johnson, 1975). Fluids and magmas also would be channelled parallel to the fracture zone. Casey and Dewey (1984) explained the association of boninites with a fracture zone by initiation of subduction along a transform-fracture zone. In this model, underthrusting of the CC would explain arc magmatism in the overriding BIOC.

At the present time, it is not possible to make a conclusive statement about the possible involvement or influence of a fracture zone adjacent to the Springers Hill area, especially as (i) the original morphology of the Mount Barren Assemblage (which would represent the fracture zone if it existed) is open to question (section 2.5.2), and (ii) the fabrics, textures and chemistry of LALPP (excluding amphibole dunites and OPXT II) are adequately explained by a spreading centre in a supra-subduction environment. However, Suhr et al. (in press) suggest that the proximity of a fracture zone explains many features in the Springers Hill area. Once again, this aspect requires further investigation.

3.10 IMPLICATION OF THE SPRINGERS HILL AREA FOR THE ORIGIN OF THE BAY OF ISLANDS OPHIOLITE COMPLEX

The mapped area is 2 km^2 and is anomalous with respect to the rest of the Lewis Hills Massif and BIOC. Nowhere else in the BIOC has such an abundance of pyroxenite and chromitite bodies been documented. Comparison of mineral chemistry of harzburgites and LAL pyroxenites with the data of Malpas and Strong (1975) and Smith and Elthon (1988), demonstrates that the Springers Hill area may represent the most residual and depleted section of mantle in the BIOC. This would agree with the proposed idea that the Springers Hill area is located in a zone of extreme partial melting and magmatic activity. The mineralogical and chemical signatures of harzburgite, OPXT I and clinopyroxenite reflect a supra-subduction zone environment, which may or may not be recorded in the rest of the BIOC. Jenner et al. (in press) propose that the whole BIOC has this signature.

The mineralogy and chemistry of cumulates in North Arm Mountain need not be explained by high pressure ($P > 10$ kbar) polybaric crystallization of a MORB parent (Elthon et al., 1982), if these cumulates crystallized from magmas of arc tholeiite composition. It is important to mention that MORB-like chemistry is to be expected in a supra-subduction zone environment. The arc may be built on MORB basement and MORB-type magmatism is to be expected as an arc evolves (Crawford et al., 1981).

3.11 SUMMARY

Three partial melting events are recorded by LALPP (excluding amphibole dunite and OPXT II). All occurred at $P \leq 7$-8 kbar under anhydrous or hydrous conditions. Harzburgite was the residue from melting and extraction of low-Ti tholeiite. These harzburgites then were intruded by boninitic magmas which fractionated hydrous OPXT I (± dunite and chromitite). Subsequently, low-Ti tholeiitic magmatism returned with the formation of anhydrous clinopyroxenite (± dunite and chromitite). This sequence of intrusion, and the extremely depleted nature of all components involved, is predicted for a supra-subduction zone setting of the Springers Hill area. The steep foliation of orthopyroxene in harzburgite, and the parallel to subparallel alignment of veins and dykes of dunite and pyroxenite to this foliation, was produced as asthenosphere flowed up below a zone of crustal accretion.

Harzburgites with slightly LREE-depleted CNREE patterns are refractory residues from the removal of low-Ti tholeiitic magma. Addition of a component of OPXT I or Ca-amphibole to some of these harzburgites has produced U-shaped CNREE patterns. These modified harzburgites are a potential source of boninitic magma.

3.11.1 Platinum Group Elements

The PGE are essentially immobile during serpentinization. Ratios of Pd/Ir used in conjunction with CNPGE diagrams are a very powerful tool for

understanding the petrogenesis of highly depleted ultramafic rocks where other more conventional trace elements fail. Further development of the PGE as petrogenetic tracers, particularly with the Re-Os isotopic pair, should be pursued in the future. Although ophiolites have not yet yielded economic concentrations of PGE, it is possible that pyroxenites which fractionated from arc-related magmas may be of economic interest.

Chapter 4

CHEMISTRY AND PETROGENESIS OF HIGH-ALUMINA PERIDOTITES, PYROXENITES AND GABBROS

4.1 INTRODUCTION

Bodies of wehrlite are diagnostic of the harzburgite ophiolite type (Table 1.1), and the occurrence of HALPPG in the Springers Hill area is in keeping with this classification. However, the HALPPG are different from wehrlite crystal mush intrusions in other ophiolites, as these intrusions contain orthopyroxene and either are never found in harzburgite (Benn and Laurent, 1987; Benn et al., 1988; Juteau et al., 1988), or have sharp intrusive contacts with harzburgite (Murton, 1986). The observation that the HALPPG post-date asthenospheric deformation, is inconsistent with the model of Benn and Laurent (1987) and Benn et al. (1988), who proposed that wehrlite intrusions are a normal product of magmatic activity at a fast spreading centre. One feature that is common to the HALPPG and most wehrlite intrusions is that olivine may be a cumulus phase or a xenocryst from the mantle. The difficulty in distinguishing between these two origins of olivine arises because adcumulate and heteradcumulate textures may be produced by the corrosion and recrystallization of olivine and spinel xenocrysts during crystallization of clinopyroxene and plagioclase as

poikilitic grains (Violette, 1980; Nicolas and Prinzhofer, 1983; Donaldson, 1985).

According to Figure 1.5, the HALPPG do not correlate with the wehrlite-lherzolite crystal mush intrusions in the Mount Barren Assemblage of the CC. These intrusions contain orthopyroxene, but otherwise possess many features which are similar to the HALPPG (Karson et al., 1983).

The aim of this chapter is to examine the processes involved in the formation of the HALPPG. As discussed in section 2.5, the contemporaneity of HALPPG, amphibole dunites and OPXT II of LALPP, and D_2 shear zones and thrust faults, is evidence of magmatic and fluid activity in the lithosphere during intra-oceanic thrusting and obduction of the BIOC. The magmatic activity is the focus of this chapter, whilst the fluid activity associated with the formation of the HALPPG is the subject of Chapter 5.

4.2 CHEMISTRY

Analytical methods are described in Appendix 1; mineral analyses of HALPPG and LALPP-HALPPG contacts and reaction zones are presented in Appendix 3, and whole-rock analyses of HALPPG are presented in Appendix 4. The effects of alteration and subsolidus reequilibration on mineral and whole-rock chemical analyses have been discussed in Chapter 3.

4.2.1 Mineral Chemistry

Unless stated otherwise, the compositions reported below are for analyses of cores of grains.

Olivine has a composition of Mg# = 80.2-90.4 and NiO = 0.10-0.40 wt.%, and has fairly constant values of NiO with decreasing Mg# (Fig. 4.1). Within-sample variations are limited, except in gabbros where the Mg# of olivine varies by as much as 1.7.

Al-spinel ranges from approximately Cr# = 30, Mg# = 65 in dunites and wehrlites, to Cr# = 78, Mg# = 22 in amphibole peridotite (Fig. 4.2). This wide variation also is exhibited by TiO_2 (Fig. 4.2). For a given Mg#, Al-spinel in dunite has a higher Cr# than Al-spinel in wehrlite. Within-sample and within-grain variations are present, but these have not been studied systematically.

Clinopyroxene is high-Ca diopside and occupies the compositional range En = 43.5-48.6, Fs = 3.2-8.0, Wo = 45.1-52.3 (with the exception of sample L115). Iron enrichment is very limited through the compositional range from dunite to gabbro. Variation diagrams are plotted in Figure 4.3. There is a clear positive correlation between Mg# and CaO, whereas the converse is true of Mg# and Al_2O_3. Concentrations of Na_2O, TiO_2 and Cr_2O_3 exhibit no systematic change with Mg#. The Mg# of clinopyroxene is significantly higher than that of olivine with which it is associated. The composition of clinopyroxene varies to different degrees within a given sample.

Plagioclase has been analysed only in gabbroic parts of HALPPG. Plagioclase is labradorite (An = 66.7, Ab = 33.3) to bytownite (An = 75.5,

Ab = 24.5) and essentially is devoid of K_2O.

Ca-amphibole is pargasitic and its chemistry is described and discussed in Chapter 5.

4.2.2 Whole-Rock Major and Trace Element Chemistry

The CaO-Al_2O_3-MgO (CAM) diagram reflects the modal mineralogy of HALPPG, in that the progressive increases in abundances of clinopyroxene and then plagioclase produce enrichment in CaO and then Al_2O_3 (Fig. 4.4). A surprising feature of the $Na_2O + K_2O$-FeO(t)-MgO (AFM) diagram is that gabbros do not show any enrichment in FeO with increase in their proportion of alkalies (Fig. 4.4). The enrichment in alkalies essentially is caused by Na_2O, which supports the evidence from mineral chemistry that minerals in HALPPG essentially are devoid of K_2O, except for rare phlogopite. In the CAM and AFM diagrams there is little evidence of olivine control on the compositional evolution of the HALPPG.

Variations in trace element concentrations correlate with modal mineralogy. Nickel and Cr decrease with decreasing modal abundance of olivine and Al-spinel, respectively. Scandium and V increase with increasing modal abundance of clinopyroxene, and Sr increases with increasing modal abundance of plagioclase. Zirconium is concentrated in gabbro.

4.2.3 Whole-Rock Rare Earth Element Chemistry

Appendix 1 should be read before assessing the significance of REE data

presented in this section. However, because absolute concentrations of REE in HALPPG are so much greater than those in LALPP, analyses of the former are more reliable than those of the latter.

The CNREE patterns of HALPPG all exhibit LREE depletion with the exception of dunite (Fig. 4.5). The evolution of CNREE patterns from dunite to olivine clinopyroxenite is simply explained in terms of an increase in the ratio of clinopyroxene/olivine. The shape of the CNREE pattern of the amphibole peridotite is indistinguishable from those of wehrlite and olivine clinopyroxenite. The CNREE patterns of gabbros are controlled by clinopyroxene and plagioclase, and this control is in agreement with concentrations of REE in plagioclase and clinopyroxene mineral separates from cumulate gabbros of the Oman Ophiolite (Pallister and Knight, 1981). The CNREE patterns of amphibolite dykes are discussed in section 4.3.

4.2.4 Mineral Chemistry of LALPP in Contact with HALPPG

The mineral chemistry of phases in LALPP in contact with HALPPG have been examined at a scale of <40 mm unless otherwise indicated. Olivine, orthopyroxene, clinopyroxene and Cr-spinel in LALPP all exhibit significant changes in composition adjacent to HALPPG.

The Mg# of olivine in harzburgite (Mg# = 90.9-91.9) decreases to Mg# = 89.0-90.2 adjacent to HALPPG (Mg# = 80.2-90.4). Harzburgite rarely is in contact with HALPPG as the boundary is marked by a 7-12 mm wide zone of dunite which has olivine of Mg# = 85.3-88.5. Olivine in dykes of OPXT I has

Mg# = 89.6-90.9, but adjacent to HALPPG this decreases to 89.3. Similarly, where OPXT I has been converted to an olivine orthopyroxenite-harzburgite assemblage adjacent to a dyke of HAL amphibole peridotite, olivine in the assemblage has Mg# = 86.9.

Orthopyroxene in harzburgite and OPXT I adjacent to HALPPG exhibits enrichment in CaO and Al_2O_3 (Fig. 4.6), in addition to FeO, relative to the unaffected protolith. Orthopyroxene in xenoliths of harzburgite record the greatest change. The Mg# of orthopyroxene adjacent to HALPPG is always lower than that not associated with HALPPG.

The composition of Cr-spinel straddles the gap between LALPP and HALPPG (Fig. 4.7). Where amphibole dunite replaces OPXT I, spinel exhibits a decrease in Cr# and increase in Mg#, much the same as observed for Cr-spinel associated with Ca-amphibole in harzburgite (Figs. 3.3 and 4.7). Concentrations of TiO_2 are highly variable, often higher than those in HALPPG, and almost always are higher than those in precursor LALPP (Fig. 4.7). Cr-spinels in harzburgite intruded by HAL olivine clinopyroxenite exhibit smooth and symmetrical increases in concentrations of V_2O_3 and TiO_2, which peak in the HAL olivine clinopyroxenite, but show less regular patterns for Mg# and Cr# (Fig. 4.8).

Only one case has been studied of LAL olivine clinopyroxenite in contact with HAL olivine clinopyroxenite. On passing from LAL olivine clinopyroxenite into HAL olivine clinopyroxenite, (i) the Mg# of olivine remains approximately constant, (ii) the Mg# of clinopyroxene decreases, (iii) the concentrations of

Al_2O_3 and TiO_2 in clinopyroxene increase, (iv) the Cr# of spinel decreases, and (v) the Mg# of spinel increases (Fig. 4.9).

4.2.5 Interpretation

4.2.5a HAL Gabbro

No clear fractionation trend is apparent for the HALPPG. The HAL gabbros do not represent magma compositions because of their (i) high whole-rock Mg#, (ii) high Mg# of olivine, and (iii) positive Eu anomaly which is supportive of textural evidence for the accumulation of plagioclase. Using sample L294 as an example, the anorthite content (An = 69) of plagioclase is much lower than predicted for olivine of Mg# = 83 with which it coexists. As a comparison, leucogabbros in North Arm Mountain with olivine of Mg# = 76-88 have plagioclase of An = 78-88 (Komor et al., 1987). This association of high MgO in olivine and relatively high Na_2O in plagioclase is portrayed in the AFM diagram by the lack of FeO enrichment with increasing proportion of Na_2O (Fig. 4.4). Consequently, the HALPPG do not exhibit a tholeiitic or calc-alkaline trend, but a trend where enrichment in FeO is suppressed below that of the normal calc-alkaline trend. This trend may be explained by combined assimilation and crystal fractionation. The effect of assimilation of rocks rich in MgO by a fractionating magma, is to produce a less FeO-enriched, more alkaline derivative magma than would be produced by crystal fractionation alone (Kelemen, 1986). Such a process is believed to have operated during formation of the HALPPG and is considered in section 4.3.

Another striking feature of the HAL gabbros is their high concentration of Sr (320-860 ppm). These high values and associated positive Eu anomalies (Fig. 4.5), attest to the precipitation of plagioclase. Gabbros in the BIOC have significantly lower concentrations of Sr (60-290 ppm) (Malpas, 1976; Komor et al., 1987; Komor and Elthon, 1990), as do gabbros from the Oman Ophiolite (70-200 ppm) (Lippard et al., 1986). Such high concentrations of Sr in HAL gabbros indicate that plagioclase could not have been retained in the magma source during melting, unless concentrations of Sr in the source were extremely high. Alternatively, the magma from which HAL gabbro precipitated could have been contaminated by seawater or continental material.

4.2.5b Contacts between HALPPG and LALPP

Chemical differences between LALPP and HALPPG confirm field and petrographic observations that these two associations are not cogenetic. This especially is supported by steep chemical and mineralogical gradients at the contact between LALPP and HALPPG, which imply extreme disequilibrium and limited reequilibration, i.e., the contact represents a reaction front which has not been smoothed by subsolidus reequilibration. The mechanisms by which LALPP are modified are (i) by the interaction of magma and fluid as evidenced by the presence of HAL clinopyroxene and Ca-amphibole in LALPP, and (ii) by diffusion according to the criteria of McCaig and Knipe (1990), as evidenced by smooth compositional variations and symmetrical profiles in Figure 4.8.

Mineral chemistry described in section 4.2.4, demonstrates that in the

immediate vicinity of HALPPG, LALPP experience a depletion in Si, especially by the incongruent breakdown of orthopyroxene to olivine and spinel, and an enrichment in Ti, Al, Ca and Fe. In many cases, Cr-spinel experiences Mg = =Fe exchange favouring Mg in the spinel structure, in order to accommodate the increase in Al_2O_3 as Cr-spinel evolves toward $MgAl_2O_4$ by Cr = =Al exchange. By these exchange reactions, Cr-spinel in LALPP is converted to Al-spinel in HALPPG. All these compositional changes are very similar to those reported by Evans (1985) for the Zambales Ophiolite, Philippines, where peridotites have reacted with mafic material impregnated from mafic dykes.

4.3 PETROGENESIS OF HIGH-Al PERIDOTITES, PYROXENITES AND GABBROS

4.3.1 Interaction between LALPP and the Parent Magma of HALPPG

Evidence that reaction has occurred between LALPP and the parent magma and associated fluid of HALPPG is supported by (i) reaction zones at the contact between HALPPG and LALPP, (ii) mineral compositions in this zone that bridge the compositional gap between LALPP and HALPPG, (iii) impregnations of HAL clinopyroxene and Ca-amphibole in LALPP, (iv) the lack of FeO enrichment exhibited by HALPPG, and (v) HAL gabbros having plagioclase with a lower content of anorthite than predicted from the Mg# of coexisting olivine.

4.3.1a Assimilation and Crystal Fractionation

Several reactions best summarize the evidence for reaction of magma and its associated fluid with LALPP:

[R4.1] Mg-Ol + Opx + Cpx + Cr-Sp + Fluid = =

Ol (lower Mg#) + Cr-Al-Sp + Ca-Amph + Phlog + Si-Fluid

[R4.2] Mg-Ol + Opx + Cpx + Cr-Sp + Magma = =

Ol (lower Mg#) + Al-Sp + Cpx {assemblage A}

[R4.3] {A} + Magma = =

Ol (even lower Mg#) + Al-Sp + Cpx + Plag {assemblage B}

[R4.4] {B} + Magma = = Cpx + Plag

At low pressure, fluid exsolves from magma (Burnham, 1979) and a fluid front advances ahead of the magmatic front. In so doing, it would convert pyroxene-bearing LALPP to pyroxene-poor LALPP or dunite with affinities to HAL dunite (reaction R4.1).

Reactions R4.2 to R4.4 describe the evolution of the HALPPG in terms of magma/rock ratio. In the gabbros, magma/rock ratios are highest and plagioclase crystallizes before clinopyroxene. As the magma/rock ratio decreases, dyke-like intrusions grade into impregnations along olivine grain boundaries. This is observed as gabbro dykes grade into HAL dunites by the progressive decrease in modal abundance of plagioclase and then clinopyroxene. Hence, clinopyroxene in wehrlite represents the complete reaction of magma with olivine. These relations explain the crystallization sequence of plagioclase before clinopyroxene in gabbros, and the appearance

of clinopyroxene before plagioclase in wehrlites as the proportion of impregnated material in the olivine matrix decreases. In terms of field relations, the highest magma/rock ratios are recorded in the northern extent of the HALPPG, where dunite is absent and gabbro, olivine clinopyroxenite and wehrlite are most abundant.

4.3.1b Thermodynamics and Kinetics of Reactions

Much of the discussion in this section is based on the work of Kelemen (1986) and Kelemen and Ghiorso (1986).

Reaction between LALPP and fluid-bearing magma parental to HALPPG was possible only if the temperature of LALPP was high enough to permit reaction. Temperatures estimated from assemblages of hydrous phases in amphibole dunite and OPXT II of LALPP are 750-1050°C (section 5.4), which approximate the temperature of the lithosphere at the time of formation of HALPPG. The addition of magma to the lithosphere would locally have raised the ambient temperature at sites of reaction, and the reactions themselves may liberate heat. Consequently, it is considered that the temperature of LALPP was high enough to permit reaction.

Thermodynamic modelling by Kelemen and Ghiorso (1986) shows that isothermal assimilation of olivine-rich rocks in hydrous dioritic magma is spontaneous and exothermic because reactions involve large negative changes in enthalpy, volume and free energy of the magma-rock system. This system may approximate the LALPP-magma system; a negative volume change during

reaction of magma with LALPP may have produced fracturing concordant with S_1 in LALPP, as evidenced by the concordance of dykes and foliations of HALPPG with dykes and S_1 of LALPP. However, upward doming of the wide D_2 shear zone around the northern part of the mapped area during the formation of the HALPPG, demonstrates that the overall volume change during the formation of the HALPPG was positive. This results because not all the fluid-bearing magma reacted, and the volume of unreacted magma exceeded the negative volume change produced by reaction.

Where fracturing could not be sustained, magma was injected along grain boundaries of olivine in a manner demonstrated experimentally by Stolper (1980) and Watson (1982). Viscosity influences the kinetics of infiltration and is related to the surface energy difference which determines the equilibrium wetting angle in a given system (Bulau and Waff, 1979; McKenzie, 1984). The ability of silicate magma to infiltrate is greatly enhanced by H_2O, which depolymerizes the molten silicate phase and lowers the viscosity of the magma (Burnham, 1979). H_2O also is important in diffusion of magmatic components into wall-rocks, as diffusion is significantly enhanced in the presence of H_2O (Walther and Wood, 1984). Infiltration and diffusion both have been important in producing HALPPG from LALPP (section 4.2.5b).

High activities of H_2O and alkalies in the magma would cause dissolution of pyroxene and greatly expand the olivine stability field (Kushiro, 1975). Ca-amphibole and phlogopite attest to the presence of H_2O and alkalies in the magma, but the formation of clinopyroxene from magma reacting with olivine

suggests that activities of H_2O and alkalies were low enough to permit stability of clinopyroxene. Amphibole dunite and OPXT II in LALPP are evidence that the activities of H_2O and alkalies in HALPPG were kept low by the release of these components into LALPP.

At the present time, it is difficult to distinguish between rocks precipitated entirely from the magma and those which have been recrystallized and reacted in the presence of magma. Even cumulate textures and chemistry of Al-spinel and olivine in the HALPPG are probably the product of in-situ recrystallization of Cr-spinel and Mg-rich olivine of LALPP parentage in the presence of the magma and its associated fluid.

4.3.2 Possible Parent Magma of the HALPPG

It has been previously stated that the HAL gabbros do not represent the composition of the parent magma of the HALPPG. The compositions of HAL gabbros, olivine clinopyroxenites and wehrlites do, however, reflect the composition of the parental magma. They require that the magma was fluid-bearing, LREE-depleted, Sr-enriched, and was capable of precipitating plagioclase before clinopyroxene.

In the upper thrust slice in the northern part of the mapped area there are brown amphibolite dykes < 1 m wide, which intrude uncorrelated wehrlite and gabbro. These dykes have sharp contacts with their host and exhibit variable deformation. Three samples have been examined: SD194, SD380 (kindly donated by S. Dunsworth) and L341. Mineralogically they consist of

plagioclase, Ti-ferroan pargasite, clinopyroxene and minor opaques. Plagioclase and pargasite are most abundant and the latter may reach 60 modal %. Clinopyroxene contains abundant inclusions of pargasite. Orthopyroxene and olivine have not been found. The amphibolite dykes have CNREE patterns very similar to those of HALPPG (Fig. 4.5).

The amphibolite dykes have relatively low SiO_2, low P_2O_5, high CaO and high Mg#, which correlate them with diabase dykes of the Lewis Hills Depleted Suite of Casey et al. (1985) and Elthon et al. (1986). Petrographic and REE data are unavailable for the diabase dykes, but they are high in Sr (117-649 ppm) (Elthon et al., 1986). All samples studied by Elthon et al. (1986) in the vicinity of the Springers Hill area belong to the Lewis Hills Depleted Suite. The diabase dykes of the Lewis Hills Depleted Suite are syn- to post-kinematic with respect to deformation in the Mount Barren Assemblage (Casey et al., 1985). These dykes often strike ENE (Casey et al., 1985), which is approximately consistent with the orientation of HAL dykes of gabbro and olivine clinopyroxenite. Consequently, there may be a genetic link between diabase dykes of the Lewis Hills Depleted Suite, amphibolite dykes in the uncorrelated wehrlite and gabbro, and the HALPPG.

4.3.3 Modelling of Magma-Rock Interactions

In order to determine whether the diabase dykes of the Lewis Hills Depleted Suite and amphibolite dykes represent the parent magma of the HALPPG, it is convenient to model magma-rock interactions on AFM and CAM

diagrams (Fig. 4.10). This modelling is at best semi-quantitative. As will be expounded in section 4.4, it is reasonable to assume that dykes having sharp contacts with their hosting metamorphosed mafic rocks are close to their source region and record little if any crystal fractionation or assimilation. This is supported by the high Mg# of amphibolite dykes (Mg# = 65-71) and diabase dykes (Mg# = 56-77 (Elthon et al., 1986)), which may be controlled by ferroan pargasite (Mg# = 68) in the case of amphibolite dykes.

The FeO enrichment trend followed by the diabase dykes is assumed to represent crystal fractionation alone (Fig. 4.10a). Based on field, petrographic and chemical evidence, reaction of the magma of these dykes and amphibolite dykes with LAL harzburgite, dunite, OPXT I and clinopyroxenite will generate HAL wehrlite, olivine clinopyroxenite and clinopyroxenite. HAL gabbros do not represent complete reaction of the magma with LALPP; their Mg# is controlled by reaction which produced clinopyroxene and perhaps olivine, whereas their relative proportions of alkalies reflect the compositional evolution of the magma (Fig. 4.10a). The AFM diagram demonstrates that following reaction, the resultant magma will have a higher Mg# than predicted from its proportion of alkalies, i.e., plagioclase with a relatively low anorthite content can coexist with olivine with a relatively high Mg#, as is observed in the HAL gabbros.

The CAM diagram (Fig. 4.10b) is more sensitive of the reactive system magma-LALPP, because it considers proportions of element oxides that are more sensitive of the system than the AFM diagram. The triangle HC-MA-LO in Figure 4.10b represents the three component system of 100 % unreacted

olivine and orthopyroxene in LAL dunite, harzburgite and OPXT I (LO), 100 % HAL clinopyroxenite produced by 100 % reaction of magma with LO (HC), and 100 % magma not having experienced any reaction with LO (MA). LAL clinopyroxenite is a minor reactant relative to LAL olivine and orthopyroxene, and is not considered for simplicity. Most of the whole-rock compositions of HALPPG are restricted to the triangle HC-MA-LO, which supports the field and petrographic evidence that they are composite rocks containing variable proportions of the end-members HC, MA and LO. The relative proportions of these end-members in a sample, as estimated from the triangle HC-MA-LO, agree well with the modal abundances of minerals in the sample. Problems arise with the HAL gabbros because the proportion of unreacted magma (MA) is overestimated due to the accumulation of large amounts of plagioclase, which drives the composition of HAL gabbro toward anorthosite (indicated by P in Figure 4.10b). Despite this problem, CaO/Al_2O_3 ratios of HAL gabbros (0.70-0.80, average 0.74) are similar to those in dykes of amphibolite (0.70-0.76, average 0.73) and diabase (0.46-0.98, average 0.73). Consequently, the magma controls this ratio in HAL gabbros.

In summary, CaO/Al_2O_3 ratios and relative proportions of alkalies in HAL gabbros reflect the composition of the magma, whereas their Mg# is controlled by olivine and clinopyroxene produced by reaction of magma with olivine and orthopyroxene in LAL dunite, harzburgite and OPXT I. Olivine in HAL gabbro may represent incompletely reacted xenocrysts, which have reequilibrated to a lower Mg# by interaction with the magma. Alternatively, olivine may have

formed by chemical stoping (Watson, 1982), whereby chemical solution of olivine is accompanied by simultaneous precipitation of olivine in the magma reservoir (represented by HAL gabbro). In a magma which does not have olivine on the liquidus, as appears to be the case for the amphibolite dykes, the process of chemical stoping enables olivine to appear as a liquidus phase by driving the magma into the olivine stability field. Considering all the evidence presented in this section, magmas represented by the diabase dykes of the Lewis Hills Depleted Suite and amphibolite dykes are capable of reacting with LALPP to produce HALPPG.

4.4 THE PARENT MAGMA OF THE HIGH-Al PERIDOTITES, PYROXENITES AND GABBROS

4.4.1 Origin of the Parent Magma

Diabase dykes of the Lewis Hills Depleted Suite were not derived from magmas produced by partial melting of the mantle because they are not saturated with respect to orthopyroxene (Elthon et al., 1986). Diabase dykes (and amphibolite dykes) are significantly different in composition from MORB, island arc tholeiites, calc-alkaline basalts and within-plate basalts (Casey et al., 1985). In order to explain the unusual chemistry of SiO_2 undersaturation and low concentrations of incompatible trace elements of diabase dykes, Elthon et al. (1986) proposed that these dykes formed from magmas derived by partial melting of gabbroic and troctolitic cumulates at 2-3 kbar within a fracture zone.

This partial melting occurred under dominantly anhydrous conditions in order to produce SiO_2-undersaturated magmas (Elthon et al., 1986). There are three major problems with this model:

1) Fracture zones are sites of fluid circulation at temperatures as high as 900°C (Kimball et al., 1985), where fluid and stress induce ductile deformation and equilibrium recrystallization of gabbro under amphibolite facies conditions (Honnorez et al., 1984). Under these conditions it is unlikely that partial melting of gabbroic and troctolitic rocks could have occurred under anhydrous conditions.

2) Amphibolite dykes are syn-kinematic with respect to deformation in D_2 shear zones (section 2.2), and diabase dykes of the Lewis Hills Depleted Suite are syn- to post-kinematic with respect to deformation in the Mount Barren Assemblage (Karson, 1984). This deformation is attributed to intra-oceanic thrusting and obduction of the BIOC and is unlikely to record deformation in a fracture zone (section 2.5).

3) The HALPPG equilibrated at pressures of 5-9 kbar (section 2.4.4).

Evidently, it is necessary to have a period of magmatism and associated fluid activity during intra-oceanic thrusting and obduction of the BIOC. The composition of amphibolite dykes indicates that amphibolite in the metamorphic sole and Mount Barren Assemblage may have been the source of this magma. Melting under hydrous conditions is documented in amphibolites of the Mount Barren Assemblage, where net veins and massive bodies of plagiogranite are associated with granulite facies mafic gneiss, which is the residue of partial

melting and magma extraction (Karson, 1984).

Plagiogranites produced by partial melting of amphibolite are enriched in SiO_2 relative to Al_2O_3, depleted in Sr, and enriched in LREE and Eu, because of preferential melting-out of plagioclase and stabilization of amphibole and Ca-plagioclase in the amphibolite residue (Helz, 1973, 1976; Pedersen and Malpas, 1984). These plagiogranite magmas are unsuitable as parents to the HALPPG. However, continued melting of amphibolite beyond the point required for the production of plagiogranite, or second-stage melting of the amphibolite residue from which plagiogranitic magma had been extracted, will generate magma approaching the composition of amphibolite. This magma will be fluid-bearing, SiO_2-undersaturated, LREE-depleted, and have a flat to positive Eu anomaly. Such a composition is identical to the amphibolite dykes. High concentrations of Sr in HAL gabbros attest to the melting of plagioclase and involvement of seawater.

4.4.2 Thermal Regime for Partial Melting of Amphibolite

Partial melting of amphibolite to produce magma saturated with plagioclase before amphibole requires $T > 925°C$ and $P(H_2O) > 2$ kbar (Yoder and Tilley, 1962). Several sources of heat may produce these temperatures in amphibolite:

1) Wehrlite-lherzolite crystal mush intrusions in the Mount Barren Assemblage (Figure 1.5). Many diabase dykes of the Lewis Hills Depleted Suite are spatially associated with these intrusions (Elthon et al., 1986).

2) Subduction of a dying spreading centre (Boudier et al., 1988; Ernewein et al., 1988).

3) Juxtaposition of hot obducted lithosphere (T = 1000°C) against subducted lithosphere (Malpas, 1979b; Boudier et al., 1988).

4) Frictional heating during obduction (Malpas, 1979b; Pavlis, 1986).

5) Thickening of the lithosphere (England and Thompson, 1984).

These sources of heat constrain distinct tectonic environments. The question is how does all the syn- to post-kinematic magmatism recorded by diabase dykes of the Lewis Hills Depleted Suite, amphibolite dykes, plagiogranites, wehrlite-lherzolite crystal mush intrusions, and HALPPG relate to a tectonic environment. This question is addressed in section 4.5.

4.5 ORIGIN OF BODIES OF WEHRLITE IN OPHIOLITES

Field and petrographic evidence suggests that the HALPPG are quite different from wehrlite crystal mush intrusions in ophiolites (section 4.1). This difference is borne out by mineral and whole-rock chemistry in the Oman Ophiolite, where gabbros associated with wehrlite exhibit FeO enrichment and have 50-180 ppm Sr (Lippard et al., 1986), and wehrlites have spinel of Cr# = 50-70, Mg# = 5-70 and plagioclase of An = 73-95 (Ernewein et al., 1988). Despite these differences, wehrlite crystal mush intrusions in the Oman Ophiolite may indicate a genetic link with the environment of formation of the HALPPG, as they are contemporaneous with magmatism at a ridge during intra-

oceanic thrusting and obduction of the ophiolite (Boudier et al., 1988; Ernewein et al., 1988; Juteau et al., 1988). Picritic to ankaramitic dykes which are cogenetic with these wehrlites (Ernewein et al., 1988; Juteau et al., 1988), correlate with the Lasail Lava Unit and the Alley and Clinopyroxene-phyric lava units, which record an arc seamount environment and a rifting event in a supra-subduction zone, respectively (Alabaster et al., 1982).

In conclusion, although the HALPPG appear quite unique, these and wehrlite crystal mush intrusions suggest a link between fluids within metamorphic soles derived from oceanic crust, metasomatized mantle peridotites, and forearc igneous processes leading to the formation of wehrlite. To test for this link, age determinations of all components involved are crucial.

4.6 SUMMARY

The HALPPG do not represent crystal mush intrusions, but an extensive zone of lithospheric mantle metasomatized during obduction of the BIOC. Fluid-bearing, SiO_2-undersaturated, LREE-depleted, Sr-rich magmas were produced by partial melting of dominantly amphibole and plagioclase in amphibolite. These magmas reacted with LAL dunite, harzburgite, OPXT I and clinopyroxenite to produce HALPPG. A situation of this type suggests a link between fluids within metamorphic soles derived from oceanic crust, metasomatized mantle peridotites, and forearc igneous processes leading to the formation of wehrlite.

Reactions which produced the HALPPG involved a fluid front preceding a magmatic front. The clinopyroxene content of the reaction product is proportional to the extent of reaction, which in turn is proportional to the magma/rock ratio. Increasing modal abundances of clinopyroxene and then plagioclase reflect an increasing magma/rock ratio. Unreacted magma is represented by plagioclase, which is cumulus in HAL gabbros, and minor Ca-amphibole. The Mg# of HAL gabbros is controlled largely by the Mg# of the LALPP with which the magma reacted. CaO/Al_2O_3 ratios and relative proportions of alkalies in HAL gabbros essentially were unaffected by reaction and reflect the composition of the original magma and the compositional evolution of the magma. Through reaction with LALPP, the magma evolved toward SiO_2 saturation, as the precipitating ferromagnesian mineral changed from Ca-amphibole (amphibolite dyke) to clinopyroxene (HAL gabbro dyke).

Evidently, the chemical and mineralogical composition of a magma may change significantly during magma-rock interactions, to the point where it is difficult to define the original composition of the magma. For example, a magma which does not have olivine on the liquidus, may react with an olivine-bearing solid by chemical stoping (Watson, 1982) to the point where olivine appears on the liquidus. Such possibilities must be considered when modelling magma evolution.

Chapter 5

COGENETIC ORIGIN FOR AMPHIBOLE DUNITE, TYPE II ORTHOPYROXENITE, HIGH-ALUMINA PERIDOTITES, PYROXENITES AND GABBROS, AND D_2 SHEAR ZONES

5.1 INTRODUCTION

A knowledge of the physical and chemical behaviour of fluids is central to our understanding of the upper mantle. Fluids have a tremendous influence on the physics and chemistry of mineral stability, heat and mass transport, melting, and processes of deformation and recrystallization. Much attention in mantle petrology focuses on the influence of fluids in the development of petrographic features and chemical variations in mantle samples. In recent years, this has culminated in compilations devoted solely to this topic, especially mantle metasomatism (Menzies and Hawkesworth, 1987a; Morris and Pasteris, 1987; Nixon, 1987). Despite this interest, a hitherto poorly documented aspect of mantle petrology is the role of fluids in ophiolite mantle sequences. Perhaps a reason for this is that magmas associated with ophiolites often are considered anhydrous. With the occurrence of boninites and hydrous

wehrlites in ophiolite sequences, there is a need to consider fluid activity.

This chapter attempts to place some constraints on fluid processes in ophiolitic upper mantle, by investigating amphibole-bearing harzburgite, amphibole dunite, OPXT II, HALPPG, and D_2 shear zones in the Springers Hill area. The field, petrographic and chemical features of these have been documented in chapters 2, 3 and 4, and should be referred to if necessary. Certain points are crucial and must be emphasized:

1) The HALPPG formed by reaction of fluid-bearing magma with LALPP under lithospheric conditions. Amphibole in LALPP is concentrated at the contact of LALPP with HALPPG. Amphibole dunite and OPXT II are often rooted in the marginal zone of HALPPG and are most abundant in D_2 shear zones which are contemporaneous with HALPPG.

2) Olivine-orthopyroxene clusters in harzburgite were produced by the incongruent breakdown of orthopyroxene to olivine and minor spinel in the presence of fluid (Figs. 2.7 and 2.8). In amphibole-bearing harzburgite and amphibole dunite, grains of Cr-spinel which recrystallized in the presence of fluid are associated with Ca-arnphibole and phlogopite (Figs. 2.9 and 2.33). Some olivine in LAL dunite recrystallized to coarse grains in the presence of fluid (Fig. 2.10).

3) The mineral and whole-rock chemistry of OPXT II is very similar to that of harzburgite. The bulk modal composition of web-textured OPXT II and its dunite matrix is harzburgite.

As already stated in section 2.5 and Chapter 4, these points emphasize

that OPXT II, HALPPG, D_2 shear zones and amphibole in dunite and harzburgite are contemporaneous. They all relate to magmatic and fluid activity during intra-oceanic thrusting and obduction of the BIOC.

5.2 MINERAL CHEMISTRY

5.2.1 Ca-Amphibole

Ca-amphibole exhibits a continuum of compositions from tremolitic to pargasitic end-members as Na+K (formula units) increases and Si (formula units) decreases (Fig. 5.1a). Ca-amphibole in harzburgite and OPXT II generally is tremolitic, whereas amphibole dunite contains edenite-pargasite amphibole. Ca-amphiboles in HALPPG contain a large component of pargasite, and overlap with the compositions of Ca-amphibole in amphibole dunite and OPXT II. Ca-amphibole in harzburgite, amphibole dunite and OPXT II exhibits a relatively narrow range of Mg#, but wide range of Na + K (formula units); Ca-amphibole in HALPPG exhibits the opposite trend (Fig. 5.1b). The Mg# of Ca-amphibole is always higher than that of olivine and orthopyroxene with which it is associated. An exception occurs in the web-textured OPXT II sample L271, where the Mg# of olivine is greater than that of Ca-amphibole. Concentrations of TiO_2 in Ca-amphibole (Fig. 5.1c) are 0.04-0.14 wt.% in harzburgite and OPXT II, with the exception of 1.4 wt.% TiO_2 in the web-textured OPXT II sample L271. In amphibole dunites, TiO_2=0.07-0.58 wt.%. Ca-amphibole in the HALPPG has TiO_2=0.01-3.1 wt.%. Ca-amphibole exhibits within-sample

variation of all elements.

5.2.2 Cr-Spinel

Cr-spinel exhibits significant within-grain and within-sample variation, but certain trends have been identified. In harzburgite, Cr-spinel has a lower Cr# where it is associated with Ca-amphibole than where it is not (Fig. 3.3a). A detailed study of a grain of Cr-spinel associated with Ca-amphibole in harzburgite sample L173, reveals little within-grain variation (Fig. 2.9). Within the same sample, grains of Cr-spinel associated with Ca-amphibole cover a wide compositional range of Cr# = 59-71, Mg# = 44-54. A wide range of compositions occur in amphibole dunite (Fig. 3.3b), and extreme within-grain variation is preserved in some samples (Fig. 5.2). Cr-spinel in OPXT II is very similar to that in harzburgite (Fig. 3.3).

5.3 INTERACTION BETWEEN FLUID AND LOW-Al PERIDOTITES AND PYROXENITES

5.3.1 Source of Fluid

The contemporaneity of rock types and deformation (D_2) associated with fluid, necessitates a common source of fluid and a well defined period of flux of fluid. Several features support a source of fluid in, or associated with, HALPPG: (i) the occurrence of Ca-amphibole and phlogopite in LALPP and HALPPG, (ii) the continuous chemical evolution of Ca-amphibole between

LALPP and HALPPG, (iii) the rooting of some amphibole dunites and OPXT II in the marginal zone of HALPPG, (iv) the syn-kinematic formation of HALPPG with D_2, and (v) the common occurrence of amphibole dunite and OPXT II in D_2 shear zones.

5.3.2 Incongruent Breakdown of Orthopyroxene to Olivine

Bowen and Tuttle (1949) showed that orthopyroxene transforms to olivine in the presence of H_2O-fluid. This concept has since been applied to the formation of dunite bodies by the metasomatic transformation of harzburgite in the Canyon Mountain Ophiolite, northeast Oregon (Dungan and Avé Lallemant, 1977). Many of the features described by Dungan and Avé Lallemant (1977) are found in the Springers Hill area, such as the replacement of orthopyroxene by amphibole, and the abundance of amphibole dunite at the contact between dunite and OPXT I.

Olivine-orthopyroxene clusters in harzburgite formed at the same time as amphibole dunite and OPXT II; all formed in the presence of fluid. The clusters are poorly equilibrated and represent the incongruent breakdown of porphyroclasts and neoblasts of orthopyroxene to olivine and minor spinel. Breakdown occurred locally, in-situ, and at a grain by grain scale, depending on the presence of fluid. Grains of orthopyroxene at different stages of breakdown, attest to heterogeneous distribution of fluid in harzburgite. The conversion of orthopyroxene to olivine or Ca-amphibole appears isovolumetric. Silica is liberated by the conversion of orthopyroxene to olivine (Nakamura and

Kushiro, 1974); the consequence of this is addressed in section 5.3.4.

5.3.3 Formation of the Assemblage Phlogopite-Amphibole-Olivine-Spinel

The assemblage phlogopite-amphibole-olivine-spinel is found in LALPP and HALPPG. Phlogopite and amphibole are important constituents of many mantle xenoliths in kimberlites and alkali basalts, but they are rare in orogenic and ophiolitic peridotites. In both occurrences, spinel and hydrous phases are associated, but two different modes of formation are postulated:

1) In the orogenic and ophiolitic peridotites, the hydrous phases usually are associated with chromite in podiform chromitites. Inclusions of olivine, ortho- and clinopyroxene, edenite-pargasite amphibole, phlogopite and plagioclase occur in chromite (Johan et al., 1983; Talkington et al., 1984; Augé, 1987; Leblanc, 1987; Leblanc and Temagoult, 1989; Bacuta et al., 1990). An extensive discussion of the origin of these inclusions is inappropriate here. It is sufficient to say that the silicate inclusions in chromite are believed to be magmatic phases crystallized at high temperature with their chromite host (Talkington et al., 1984; Augé, 1987; Bacuta et al., 1990).

2) Based on textural criteria from xenoliths sampled by kimberlites, spinel and hydrous phases often are associated as a result of metasomatic reaction. Phlogopite frequently is observed replacing orthopyroxene (Kushiro and Aoki, 1968; Dawson, 1987; Hatton and Gurney, 1987; Erlank et al., 1987), and garnet and clinopyroxene (Hatton and Gurney, 1987; Erlank et al., 1987). Phlogopite forms more easily from orthopyroxene than clinopyroxene or garnet,

as the latter minerals possess substantial amounts of Ca which cannot be accommodated in the structure of phlogopite (Hatton and Gurney, 1987). Of course, Ca is involved in the formation of amphibole. Spinel, as a reaction product, is an essential constituent where phlogopite replaces garnet, olivine, and ortho- and clinopyroxene; the amount of Cr-spinel in phlogopite-bearing garnet peridotites is indicative of the amount of garnet replaced (Erlank et al., 1987). In metasomatic reactions, amphibole appears generally after phlogopite, but in rare cases, pargasite and edenite accompany replacement of garnet by phlogopite (Erlank et al., 1987).

The textural relations of the assemblage phlogopite-amphibole-olivine-spinel (Figs. 2.9 and 2.33), and the occurrence of such an assemblage in harzburgite, which is a refractory residue from partial melting and complete removal of magma, disagree with a magmatic origin. A metasomatic origin for phlogopite and amphibole is more likely, but garnet and clinopyroxene were not present as reactants, and orthopyroxene was low in Al_2O_3. Cr-spinel could have supplied Mg and Al needed for the production of phlogopite and edenite-pargasite amphibole. Cr-spinel was present in the rock prior to metasomatism, and would have also been produced by the incongruent breakdown of orthopyroxene to olivine. The involvement of Cr-spinel in reaction is supported by its variable Cr# and Mg# in amphibole dunite, and its textural disequilibrium with respect to phlogopite and Ca-amphibole.

The formation of olivine-amphibole-spinel symplectitic intergrowths (Fig. 2.33) can be accounted for by reaction R5.1 (Jenkins, 1983; Schneider and

Eggler, 1986; Piccardo et al., 1988):

[R5.1] Opx + Cpx + Sp + Fluid = = Ol + Amph

The reaction involves clinopyroxene. With the exception of LAL clinopyroxenite, which appears to be a relatively minor reactant, protoliths for the metasomatites did not contain significant clinopyroxene or Ca. However, significant quantities of Ca were contained in the fluid-bearing magma which was parental to the HALPPG.

In summary, Ca-amphibole and phlogopite could not have been produced from LALPP simply by the addition of H_2O, although Mg and Al could have been supplied by orthopyroxene and Cr-spinel. Mineral chemistry of hydrous phases suggests that at the site of formation of Ca-amphibole and phlogopite the fluid contained appreciable concentrations of Ca, Na, K, Ti, Al and H_2O. The breakdown of orthopyroxene during reaction liberated Si into the fluid.

5.3.4 Origin of Type II Orthopyroxenite

Field relations, petrography, and mineral and whole-rock chemistry are supportive of a non-cogenetic origin for OPXT II and OPXT I, but a cogenetic origin for OPXT II, amphibole dunite and HALPPG. The fluid-bearing magma parental to the HALPPG had alkaline affinities (Chapter 4). The fluid exsolved from this magma, or liberated during the reaction of this magma with LALPP, was SiO_2-undersaturated. This fluid reacted with Cr-spinel and LAL pyroxene, and Si was liberated. Reaction continued until the fluid equilibrated with LAL pyroxene, i.e., until the fluid was saturated with Si. At this point, the fluid was

in equilibrium with harzburgite, OPXT I and LAL clinopyroxenite, but in disequilibrium with dunite. Consequently, as the Si-saturated fluid passed from harzburgite, OPXT I or LAL clinopyroxenite into dunite, it reacted with olivine to form pyroxene (reaction R5.2):

[R5.2] Ol + Si-saturated Fluid = = Px + Si-undersaturated Fluid

Fluid in equilibrium with harzburgite and OPXT I reacted to form OPXT II. Clinopyroxenite in websteritic veins associated with OPXT II, indicate that the fluid was in equilibrium with LAL clinopyroxenite. The scarcity of clinopyroxene associated with OPXT II, agrees with the field evidence that LAL clinopyroxenite was a relatively minor reactant with respect to harzburgite and OPXT I. Such an origin for OPXT II is similar to the hydrothermal production of pyroxene according to Bowen and Tuttle (1949). In keeping with their model, OPXT II does not extend into the HALPPG, which are the source of fluid.

Similar fluid-rock interactions have been documented in other localities. A classic example are the pyroxenite-amphibolite layers in the Seiad Complex, California, which have a hydrothermal origin (Loomis and Gottschalk, 1981). These authors stated that as a fluid equilibrates with peridotite, the hydrothermal pyroxenes that precipitate will be similar in composition to those in the peridotite. The OPXT II have the modal composition of harzburgite, when considered as a bulk sample with their dunite host, and have mineral chemistry and CNPGE patterns similar to harzburgite. These features are proof that OPXT II precipitated from fluid that was in equilibrium with harzburgite.

5.4 CONDITIONS OF PRESSURE AND TEMPERATURE

Before examining the compositional evolution of the fluid from which hydrous phases precipitated (section 5.5), it is necessary to define T, P conditions because the composition of Ca-amphibole varies with T and P (Jenkins, 1983). Fluids are associated with HALPPG, which record maximum T, P conditions of equilibration of 875-1050°C, 5-9 kbar (section 2.4.4). The assemblages of minerals in amphibole-bearing harzburgite, amphibole dunite and OPXT II span the T, P range of 750°C, 5 kbar, for the breakdown of chlorite (Zen, 1972), to 1050°C, 6 kbar for the upper limits of stability of pargasite and phlogopite (Holloway, 1973; Westrich and Holloway, 1981; Montana and Brearley, 1989). The upper limit of stability of Al-tremolite is 870°C, 6 kbar (Jenkins, 1983). LAL dunites and amphibole dunites that are unaffected by D_2, may preserve coarse granular olivines containing inclusions of Ca-amphibole. This is evidence of growth of olivine in the presence of fluid at temperatures of about 1000°C (section 2.3.7).

The wide range of temperature has important consequences for the stability of hydrous phases: (i) phlogopite and pargasite formed at about 1000°C by reaction of a fluid that caused recrystallization of olivine to coarse grains in areas not experiencing D_2; (ii) tremolite and pargasite formed a continuous series of solid solution at about 850°C (Oba, 1980), which suggests that phlogopite and coarse grains of olivine formed at this lower temperature in the presence of fluid.

Although the intrusion of fluid-bearing magma may have caused local heating, fluids are important transporters of heat (Bickle and McKenzie, 1987) and should have carried heat into LALPP. A fairly constant thermal regime, therefore, is likely for the formation of hydrous phases. This is supported by the occurrence of tremolitic and edenitic amphibole in the same sample, with no overgrowth of one on the other. Consequently, Ca-amphibole and phlogopite formed at approximately 900°C, and compositional variations between tremolite and pargasite end-members are due to solid solution. This is corroborated by Dahl and Watkinson (1986), who estimated $T \leq 900°C$ for D_2 shear zones in the Springers Hill area.

5.5 CHEMISTRY OF FLUID

In Chapter 4 it was demonstrated that HALPPG formed by the interaction of fluid-bearing magma with LALPP. This magma is arguably represented by amphibolite dykes located in the uncorrelated wehrlite and gabbro in and adjacent to the Springers Hill area. In keeping with this, the compositions of these dykes will be used as an approximation of the ultimate source of the fluid which reacted with LALPP. In the amphibolite dyke sample L341, Ca-amphibole is ferroan pargasite of Mg# = 68 and has 3.3 wt.% TiO_2.

5.5.1 Mineral Assemblages and Amphibole Chemistry

5.5.1a Fluid/Rock Ratio

Two reactions govern the assemblages of minerals arising from metasomatism. The first involves the disappearance of orthopyroxene and formation of amphibole (sections 5.3.2 and 5.3.3), whereas the second involves the formation of orthopyroxene as OPXT II (section 5.3.4). The former is considered here.

With increasing metasomatism, the assemblages of minerals change in the sequence: olivine-orthopyroxene-spinel (unmetasomatized harzburgite and OPXT I)--olivine-orthopyroxene-spinel-tremolite--olivine-spinel-edenite-phlogopite (amphibole dunite)--olivine-spinel-clinopyroxene-plagioclase-pargasite-phlogopite (HALPPG). Largely, this sequence correlates with the fluid/rock ratio as estimated from the abundances of orthopyroxene and Ca-amphibole. Ca-amphibole exhibits enrichment in Ti, Al, Fe, Na and K, and depletion in Si and Mg, as fluid/rock ratio increases, i.e, as the occurrence of Ca-amphibole changes from rare, dominantly interstitial grains in harzburgite, to more abundant and occasionally poikilitic grains in HALPPG. These trends correlate with progressively larger volumes of fluid (Best, 1974), and have the effect of increasing the apparent metamorphic grade of amphibole (Jenkins, 1983), because of the solid solution series between tremolite and pargasite (Oba, 1980). Hydrating the assemblage olivine-orthopyroxene-spinel is retrogressive, which is the opposite of what the chemistry of Ca-amphibole indicates. This apparent contradiction is explained by looking at small volumes of fluid. Within

a given sample of harzburgite, Al-tremolite replaces orthopyroxene, whereas edenitic amphibole and phlogopite occur in textural disequilibrium with spinel. This suggests that the Al required in metasomatic reactions was provided dominantly by the phase being replaced, and does not relate to the volume of fluid involved when the volume is relatively small. When fluid volumes are large, as indicated by extensive metasomatism, the chemistry of amphibole correlates with the volume of fluid (Best, 1974).

5.5.1b Sodium and Potassium in Hydrous Phases

Ratios of Na/K of the fluid change through fractionation and reaction. A feature of this is the zonal distribution of hydrous phases in grains of Cr-spinel, where phlogopite occurs in the core and Ca-amphibole at the rim (Figs. 2.9 and 2.33). On a much larger scale, Arai (1986) attributed decreasing phlogopite/amphibole ratios in upper mantle peridotites to fractionation of rising metasomatic fluids. Similarly, K/(K+Na) ratios of phlogopites in the Horoman Peridotite Complex, Japan, reflect this fractionation (Arai and Takahashi, 1989).

The variation of Na+K (formula units) and Mg# of Ca-amphibole (Fig. 5.1b), demonstrates that Na+K in HALPPG is controlled by that of the parent magma (pargasite in amphibolite dykes has Na+K=0.874 formula units), whereas Mg# is controlled largely by the Mg# of LALPP which HALPPG replaced. The same conclusion was reached in Chapter 4, where the Mg# of olivine in HAL gabbros was higher than expected for the alkali content of

coexisting plagioclase. Consequently, reaction of magma and fluid with LALPP has a much greater influence on the composition of ferromagnesian minerals formed in HALPPG, than does simple fractionation. The alkali content of these minerals is controlled by that of the parent magma or fluid. Because Ca-amphibole is a ferromagnesian mineral with a relatively high concentration of Na_2O, it records the alkali content of the fluid from which it precipitated, but its Mg# is controlled by that of LALPP. As such, the composition of Ca-amphibole is a very powerful tool for monitoring the extent of reaction (Mg#) and fractionation (Na + K) of magma or fluid.

5.5.2 Rare Earth Elements

The CNREE patterns of amphibolite dykes and HAL amphibole peridotite are LREE-depleted, whereas those of LAL amphibole dunite, OPXT II and amphibole-bearing harzburgite are U-shaped, but overall more depleted (Fig. 5.3). These patterns are controlled by Ca-amphibole, as it has the highest mineral/matrix partition coefficients for REE of any phase in these rock types (Fig. 3.7; see Arth and Barker (1976) for comparison of partition coefficients of hornblende and plagioclase). Consequently, the CNREE patterns in Figure 5.3 trace the evolution of fluid by assimilation of LALPP and fractionation of Ca-amphibole. With progressive evolution, the fluid evolves from SiO_2-undersaturated and LREE-depleted (amphibolite dykes and HAL amphibole peridotite), to SiO_2-undersaturated and LREE- and Eu-enriched (amphibole-bearing harzburgite and amphibole dunite), and SiO_2-saturated and LREE- and

Eu-enriched (OPXT II). This is much the same origin as for LREE and Eu enrichment in trondhjemitic-tonalitic magmas (Arth and Barker, 1976). The negative Eu anomaly of the web-textured OPXT II must be treated with caution, as Pr-Tb values are affected by the blank and fall below the limit of detection.

5.5.3 Platinum Group Elements

Data are not available for the PGE content of the fluid. The CNPGE patterns of harzburgite, chromitite and OPXT II are similar (Figs. 3.6a, b and g, respectively), which suggests that the fluid from which OPXT II precipitated was in equilibrium with harzburgite and Cr-spinel. This is in total agreement with mineral chemistry.

The CNPGE patterns of amphibole dunite (Fig. 3.6h) reflect the pattern of their protolith, i.e., OPXT I (Fig. 3.6e). During metasomatism, concentrations of Os, Ir, Ru and Rh in the whole-rock were unaffected, whereas Pt and Pd were removed. The greatest loss of Pt and Pd is recorded for the most extensively metasomatized sample, where minor orthopyroxene remains from OPXT I. This fractionation of the PGE may be produced by high temperature, Cl-bearing, supercritical fluids (Mitchell and Keays, 1981; Keays et al., 1982; Ballhaus and Stumpfl, 1986; Boudreau et al., 1986; Wood, 1987). An important conclusion is that the concentrations of Os, Ir, Ru and Rh can be used as a fingerprint of the rock type which existed prior to metasomatism, whereas the REE reflect the composition of the fluid that caused metasomatism. This property of the PGE should be a very powerful tool in

defining the composition of a rock type prior to metasomatism, where there is little or no record remaining of that rock type.

5.5.4 H-O-C Species in Fluid

Fluid inclusions in olivine of the mantle are typically found to be of CO_2 (Roedder, 1965). Inclusions in olivine in the Springers Hill area have not been investigated and their composition is unknown. However, the absence of carbonate in metasomatic assemblages in the area, suggests that $H_2O/(H_2O + CO_2)$ of the fluid was high. The ability of the fluid to dissolve SiO_2 supports this, as there is a marked increase in the solubility of SiO_2 in H_2O-fluid relative to H_2O-CO_2--fluid (Walther and Orville, 1983). The CNPGE patterns of amphibole dunites, suggest that Cl was present in the fluid. Consequently, the fluid appears to have been H_2O-rich and Cl-bearing. The ultimate provenance of such a fluid could be seawater, which is consistent with the origin of the fluid-bearing magma of the HALPPG, by partial melting of oceanic crust that had been altered to amphibolite by seawater interaction. In support of this, Peacock (1990) estimated that hydrothermally altered oceanic basalts and gabbros contain 1-2 wt.% H_2O and 0.1 wt.% CO_2 bound in minerals.

5.6 TRANSPORT OF FLUID

Magmatic and fluid activity associated with the formation of HALPPG is contemporaneous with the D_2 event, which is attributed to deformation during obduction of the BIOC (section 2.5). Fluid migrated by two distinct processes: (i) by migration along grain boundaries as evidenced by interstitial Ca-amphibole; (ii) by flow along shear zones. The latter is by far the most important mechanism of fluid transport, and attests to the importance of D_2 shear zones in focusing fluid flow during obduction of the BIOC. Consequently, metasomatism is most prevalent in shear zones. Shear zones probably nucleated in zones of high pore fluid pressure, as evidenced by the rooting of OPXT II ribbon mylonites in the marginal zone of HALPPG. The olivine-orthopyroxene-amphibole banding developed in ribbon mylonites may not represent metamorphic differentiation, but lit-par-lit injection along shear zones of fluids at different stages of their evolution.

5.7 SUMMARY

The kinetics and mode of fluid migration will govern the type and extent of reaction between fluid and wall-rock. A fluid unable to equilibrate with the environment through which it migrates, will reflect the composition of its source; a fluid experiencing continuous equilibration with its wall-rock, will reflect the composition of the rock with which it last equilibrated.

The compositions of hydrous phases produced by metasomatic reactions involving small volumes of fluid, strongly reflect the composition of the solid phase(s) involved in reaction. For example, in a given sample, Al-tremolite was produced by fluid reacting with orthopyroxene, and edenitic-pargasitic amphibole and phlogopite were produced by reaction of fluid with Cr-spinel. This reflects the microscopic scale. As the volume of fluid increases, so the compositions of precipitated hydrous phases reflect more the composition of the fluid; hydrous phases will also reflect variations in the bulk composition of the protolith. This reflects the megascopic scale.

Caution must be exercised when using modal proportions of hydrous phases to estimate fluid/rock ratios. Consider a fixed volume of fluid fluxing a fixed volume of rock in which olivine remains a stable phase, and let the volume of fluid be in excess of that required to completely replace orthopyroxene in harzburgite and orthopyroxenite by amphibole. The metasomatite produced from orthopyroxenite will have a higher modal abundance of amphibole and will appear to record a higher fluid/rock ratio than the metasomatite produced from harzburgite, and yet both protoliths experienced the same fluid/rock ratio. Consequently, modal proportions of hydrous phases can be used as an indication of fluid/rock ratio, provided that similar protoliths are considered. Fluid/rock ratios can be estimated when different protoliths are involved, by using Os, Ir, Ru and Rh as a fingerprint of the protoliths, as these PGE appear essentially immobile during metasomatic reactions. H_2O-fluid does not appear to carry significant concentrations of PGE,

especially Os, Ir, Ru and Rh, at 800-900°C, and is unlikely to add these PGE to metasomatites during metasomatism.

5.7.1 Mantle Sources of Boninitic Magmas

The formation of olivine-orthopyroxene-spinel-amphibole assemblages with U-shaped CNREE patterns and positive Eu anomalies could be an important mechanism by which to generate the mantle source of boninites. Boninites derived from such a source would have positive Eu anomalies, which is in contrast to those that would be produced by partial melting of harzburgites containing a component of OPXT I, which have negative Eu anomalies (section 3.5.4).

Fluids from which OPXT II formed were boninitic, in that they had a high Mg#, were SiO_2-saturated, and had U-shaped CNREE patterns. These fluids were in equilibrium with Cr-spinel and harzburgite, which is a requirement of boninite genesis. Some OPXT II ribbon mylonites are 1-2 m wide, which suggests that large volumes of boninitic fluid may have been transported away from the Springers Hill area via shear zones during the formation of HALPPG. If this were the case, then although HALPPG and wehrlite bodies in other ophiolites do not have compositions anywhere approaching those of boninites, they may be an essential source of fluid and heat for the generation of high-MgO, SiO_2-saturated magmas or fluids. Once again, this emphasizes the importance of fluids within metamorphic soles derived from oceanic crust, metasomatized mantle peridotites and pyroxenites, and forearc magmatic and

fluid processes leading to the formation of wehrlites and high-MgO, SiO_2-saturated magmas or fluids (section 4.5). Plagiogranites with U-shaped CNREE patterns may be the evolved component of the boninitic fluid. Some plagiogranites in the Mount Barren Assemblage may represent this component, but a genetic link cannot be made without a detailed study of the bodies.

Chapter 6

SUMMARY

6.1 CONCLUSIONS FROM THIS STUDY

Integrated field, petrographic and chemical studies of veins and dykes in ophiolite mantle peridotites can be used to construct a sequence of magmatic events in much the same way as can be done for the extrusive sequences of ophiolites. Modelling is required to determine the origin of mineral and chemical compositions of extrusive sequences, whereas studies in the mantle allow first-hand definition of the processes by which these compositions arise.

The Springers Hill area of the Lewis Hills Massif, BIOC, is a section of extremely heterogeneous ophiolitic upper mantle which developed in a supra-subduction zone environment. Harzburgite, dunite, chromitite, OPXT I and clinopyroxenite of LALPP, formed at pressures of $\leq$7-8 kbar during upwelling of asthenosphere below a zone of crustal accretion. Harzburgite formed as a refractory residue from partial melting and complete removal of low-Ti tholeiitic magma. Harzburgite was intruded by hydrous boninitic dykes which fractionated OPXT I (and associated dunite and chromitite), and these were intruded by dykes of anhydrous low-Ti tholeiite which fractionated clinopyroxenite (and associated dunite and chromitite). This sequence was

metasomatized at 5-9 kbar in the lithosphere, by fluid-bearing magmas that were produced by partial melting of underthrust amphibolitized oceanic crust during intra-oceanic thrusting and obduction of the BIOC. The metasomatites are HALPPG, and amphibole dunites and OPXT II of LALPP. These document a link between amphiboiite and granulite facies oceanic crust in metamorphic soles of ophiolites, metasomatized mantle peridotites, and forearc igneous processes leading to the formation of wehrlitic bodies.

6.1.1 Types of Harzburgite

Harzburgites that are products of extreme partial melting and complete magma extraction should have positive sloping CNREE patterns, relatively low CaO/Al_2O_3 ratios, and $Pd/Ir << 1$. There are several ways of producing U-shaped CNREE patterns in harzburgites:

1) By impregnation of boninitic magma, or by mechanical mixing of orthopyroxenite precipitated from boninitic magma. These harzburgites have CaO/Al_2O_3 ratios higher than expected, $Pd/Ir > 1$, and may have negative Eu anomalies. Harzburgites with these characteristics may also form from dunites.

2) By introducing minor Ca-amphibole which precipitates from SiO_2-undersaturated fluid that previously fractionated hornblende. These harzburgites have CaO/Al_2O_3 ratios higher than expected, Pd/Ir ratios similar to those of the harzburgite prior to introduction of fluid, positive Eu anomalies, and orthopyroxene partially replaced by olivine and Ca-amphibole.

3) By formation of orthopyroxene by reaction of dunite with SiO_2-saturated fluid

that had previously fractionated hornblende. These harzburgites have the chemical characteristics of the olivine-orthopyroxene assemblage with which the fluid was in equilibrium.

If these harzburgites with U-shaped CNREE patterns are homogenized by deformation in the upper mantle, they will not exhibit textural evidence for processes (1) to (3). Formation of harzburgite in this way, may explain the absence of a simple parent-daughter relationship between crust and mantle in many ophiolites, because harzburgite is a hybrid rock with mineral chemistry and textures indistinguishable from those of a true residue. However, these harzburgites are potential sources of boninitic magmas.

6.2 IMPORTANCE OF THE SPRINGERS HILL MANTLE SECTION TO MANTLE PETROLOGY

Similar physical and chemical processes of interaction of rocks, magmas and fluids occur in all tectonic environments, but compositions differ. The results from this study are specifically pertinent to processes in ultramafic rocks at pressures <10 kbar (30 km depth) in the mantle wedge of a subduction zone, and more generally to processes in ultramafic rocks over a wide range of temperature and pressure in all tectonic environments. It is at shallow depth that fluid exsolves from magma (Burnham, 1979), and this is where significant changes will occur in fluid, magma and wall-rock compositions, as found in the Springers Hill area.

6.2.1 Processes in the Mantle Wedge of a Subduction Zone

Subduction zones are one of the most dynamic parts of the Earth and processes in them have fundamental consequences for energy and chemical budgets in the asthenosphere-lithosphere-hydrosphere system. Although the volume of magma reaching the Earth's crust is relatively small in comparison to mid-ocean ridges, the processes in subduction zones have important implications for the generation of crust in island arcs and continents. The petrogenesis of HALPPG, and LAL amphibole dunite and OPXT II is directly applicable to studies of assimilation and hybridization of peridotites by fluid-bearing mafic and felsic magmas. Thus, it is suggested that the magmatic and fluid processes associated with the formation of these HALPPG and LALPP are applicable to the deeper levels of subduction zones, which are important for production of magmas of the calc-alkaline rock series. Studies of these deep processes have concentrated on experimental phase relations (Green and Ringwood, 1968; Sekine and Wyllie, 1982b, 1983; Carroll and Wyllie, 1989), and modelling of reactions and phase relations (Sekine and Wyllie, 1982a, c; Wyllie and Sekine, 1982; Kelemen, 1986, 1990). Such studies are hampered by the lack of mantle exposure and this is why the Springers Hill area is so important for these studies.

6.2.2 Mantle Heterogeneity

Although the Springers Hill area may represent an exceptional piece of uppermost mantle because of its abundance of peridotites and pyroxenites

which formed over a period of time from distinctly different sources, it demonstrates the extreme mineral and chemical heterogeneity which may be present in the upper mantle. The heterogeneity arises from mechanical mixing, and magma and fluid intrusion, impregnation and reaction. Small volumes of magma or fluid (McKenzie, 1989; Menzies, 1990) derived from heterogeneous mantle will very effectively transfer heterogeneities to other regions of asthenosphere or lithosphere, whereas larger volumes will not, due to homogenization in the resulting magma or fluid. The latter is partly dependent on the mode of melting, as successive batches of magma produced by equilibrium modal melting will be relatively homogeneous with respect to those produced by non-modal melting.

6.2.3 Mantle Xenoliths

Several important points are applicable to the study of mantle xenoliths where there is not the advantage of a regional overview:

1) The mantle is extremely heterogeneous on a sub-km scale, and xenoliths that are derived from adjacent parts of the mantle may reflect very different environments even if they record similar pressures and temperatures.

2) Xenoliths having cumulate textures may be products of extreme textural and chemical reequilibration of non-cumulate mantle material in the presence of magma or fluid. An example of this are the dunites, wehrlites and olivine clinopyroxenites of the HALPPG.

REFERENCES

ALABASTER, T., PEARCE, J. A. & MALPAS, J. 1982. The volcanic stratigraphy and petrogenesis of the Oman Ophiolite Complex. Contributions to Mineralogy and Petrology, 81, 168-183.

ALLEGRE, C. J. & TURCOTTE, D. L. 1986. Implications of a two-component marble-cake mantle. Nature, 323, 123-127.

ALLEGRE, C. J., DUPRE, B. LAMBERT B. & RICHARD, P. 1981. The subcontinental versus suboceanic debate; I. Lead-neodymium-strontium isotopes in primary alkali basalts from a shield area; the Ahaggar volcanic suite. Earth and Planetary Science Letters, 52, 85-92.

ALLEGRE, C. J., DUPRE, B., RICHARD, P., ROUSSEAU, D. BROOKS, C. 1982. The subcontinental versus suboceanic debate; II. Nd-Sr-Pb isotopic comparison of continental tholeiites with mid-ocean ridge tholeiites, and the structure of continental lithosphere. Earth and Planetary Science Letters, 57, 25-34.

ANDERSON, D. L. 1981. Hotspots, basalts and the evolution of the mantle. Science, 213, 82-89.

ANONYMOUS. 1972. Penrose field conference on ophiolites. Geotimes, 17, 24-25.

ARAI, S. 1986. K/Na variation in phlogopite and amphibole of upper mantle peridotites due to fractionation of the metasomatizing fluids. Journal of Geology, 94, 436-444.

ARAI, S. & TAKAHASHI, N. 1989. Formation and compositional variation of phlogopites in the Horoman peridotite complex, Hokkaido, northern Japan: implications for origin and fractionation of metasomatic fluids in the upper mantle. Contributions to Mineralogy and Petrology, 101, 165-175.

ARCHIBALD, D. A. & FARRAR, E. 1976. K-Ar ages of amphibole from the Bay of Islands Ophiolite and the Little Port Complex, western Newfoundland, and their geological implications. Canadian Journal of Earth Sciences, 13, 520-529.

ARCULUS, R. J. & DELANO, J. W. 1981. Siderophile element abundances in the upper mantle: evidence for a sulfide signature and equilibrium with the core. Geochimica et Cosmochimica Acta, 45, 1331-1343.

ARTH, J. G. & BARKER, F. 1976. Rare-earth partitioning between hornblende and dacitic liquid and implications for the genesis of trondhjemitic-tonalitic magmas. Geology, 4, 534-536.

AUGE, T. 1987. Chromite deposits in the northern Oman ophiolite: mineralogical constraints. Mineralium Deposita, 22, 1-10.

BACUTA, G. C. jr., KAY, R. W., GIBBS, A. K. & LIPIN, B. R. 1990. Platinum-group element abundance and distribution in chromite deposits of the Acoje Block, Zambales Ophiolite Complex, Philippines. In: DUNN, C. E., CURTIN, G. C. & HALL, G. E. M. (eds.), Geochemistry of Platinum-Group Elements. Journal of Geochemical Exploration, 37, 113-145.

BALLHAUS, C. G. & STUMPFL, E. F. 1986. Sulfide and platinum mineralization in the Merensky Reef: evidence from hydrous silicates and fluid inclusions. Contributions to Mineralogy and Petrology, 94, 193-204.

BARNES, S.-J., NALDRETT, A. J. & GORTON, M. P. 1985. The origin and fractionation of platinum-group elements in terrestrial magmas. Chemical Geology, 53, 303-323.

BEACH, A. 1976. The interrelations of fluid transport, deformation, geochemistry and heat flow in early Proterozoic shear zones in the Lewisian Complex. Philosophical Transactions of the Royal Society of London, A280, 569-604.

BECKER, R. & AGIORGITIS, G. 1978. Iridium, osmium and palladium distribution in rocks of the Troodos Complex, Cyprus. Chemica Erde, 37, 302-306.

BEDARD, J. H. 1991. Cumulate recycling and crustal evolution in the Bay of Islands Ophiolite. Journal of Geology, 99, 225-249.

BENCE, A. E. & ALBEE, A. L. 1968. Empirical correction factors for the electron microanalysis of silicates and oxides. Journal of Geology, 76, 382-403.

BENN, K. & LAURENT, R. 1987. Intrusive suite documented in the Troodos ophiolite plutonic complex, Cyprus. Geology, 15, 821-824.

BENN, K., NICOLAS, A. & REUBER, I. 1988. Mantle-crust transition zone and origin of wehrlitic magmas: evidence from the Oman ophiolite. Tectonophysics, 151, 75-85.

BEST, M. G. 1974. Mantle-derived amphibole within inclusions in alkalic-basaltic lavas. Journal of Geophysical Research, 79, 2107-2113.

BICKLE, M. J. & McKENZIE, D. 1987. The transport of heat and matter by fluids during metamorphism. Contributions to Mineralogy and Petrology, 95, 384-392.

BIRD, J. M. & DEWEY, J. F. 1970. Lithosphere plate-continental margin tectonics and the evolution of the Appalachian orogen. Geological Society of America Bulletin, 81 1031-1060.

BLISS, N. W. & MacLEAN, W. H. 1975. The paragenesis of zoned chromite from central Manitoba. Geochimica et Cosmochimica Acta, 39, 973-990.

BODINIER, J. L., VASSEUR, G., VERNIERES, J., DUPUY, C. & FABRIES, J. 1990. Mechanisms of mantle metasomatism: geochemical evidence from the Lherz Orogenic Peridotite. Journal of Petrology, 31, 597-628.

BONATTI, E., CLOCCHIATTI, R., COLANTONI, P., GELMINI, R. MARINELLI, G., OTTONELLO, G., SANTACROSE, R., TAVIANI, M., ABDEL-MEQUID, A. A., ASSAF, H. S. & EL TAHIR, M. A. 1983. Zabargad (St. John) Island: an uplifted fragment of sub-Red Sea lithosphere. Journal of the Geological Society, London, 140, 677-690.

BOTTINGA, Y. & ALLEGRE, C. J. 1978. Partial melting under spreading ridges. Philosophical Transactions of the Royal Society of London, A288, 501-525.

BOUDIER, F. 1978. Structure and petrology of the Lanzo peridotite massif (Piedmont Alps). Geological Society of America Bulletin, 89, 1574-1591.

BOUDIER, F. & COLEMAN, R. G. 1981. Cross section through the peridotites in the Samail ophiolite, southeastern Oman. Journal of Geophysical Research, 2573-2592.

BOUDIER, F. & NICOLAS, A. 1972. Fusion partielle gabbroique dans la lherzolite de Lanzo. Schweizerische Mineralogische und Petrographische Mitteilungen, 52, 39-56.

BOUDIER, F. & NICOLAS, A. 1977. Structural controls on partial melting in the Lanzo peridotites. In: DICK, H. J. B. (ed.), Magma Genesis. Oregon Department of Geology and Mineral Industries Bulletin 96, 63-78.

BOUDIER, F. & NICOLAS, A. 1985. Harzburgite and lherzolite subtypes in ophiolitic and oceanic environments. Earth and Planetary Science Letters, 76, 84-92.

BOUDIER, F., CEULENEER, G. & NICOLAS, A. 1988. Shear zones, thrusts and related magmatism in the Oman ophiolite: initiation of thrusting of an oceanic ridge. Tectonophysics, 151, 275-296.

BOUDREAU, A. E., MATHEZ, E. A. & McCALLUM, I. S. 1986. Halogen geochemistry of the Stillwater and Bushveld complexes: evidence for transport of the platinum-group elements by Cl-rich fluids. Journal of Petrology, 27, 967-986.

BOULLIER, A. M. & NICOLAS, A. 1975. Classification of textures and fabrics of peridotites xenoliths from South Africa kimberlites, Physics and Chemistry of the Earth, 9, 97-105.

BOWEN, N. L. 1928. The Evolution of the Igneous Rocks. Princeton University Press, Princeton, 334 p.

BOWEN, N. L. & TUTTLE, O. F. 1949. The system MgO-SiO_2-H_2O. Geological Society of America Bulletin, 60, 439-460.

BOYD, F. R. & NIXON, P. H. 1975. Origins of the ultramafic nodules in kimberlites of northern Lesotho and the Monastery Mine, South Africa. Physics and Chemistry of the Earth, 9, 431-454.

BROUXEL, M. & LAPIERRE, H. 1988. Geochemical study of an early Paleozoic island-arc--back-arc basin system. Part 1: the Trinity Ophiolite (northern California). Geological Society of America Bulletin, 100, 1111-1119.

BROWN, A. V. & JENNER, G. A. 1989. Geological setting, petrology and chemistry of Cambrian boninite and low-Ti tholeiite lavas in western Tasmania. In: CRAWFORD, A. J. (ed.), Boninites and Related Rocks. Unwin Hyman, London, 232-262.

BULAU, J. R. & WAFF, H. S. 1979. Mechanical and thermodynamic constraints on fluid distribution in partial melts. Journal of Geophysical Research, 84, 6102-6108.

BURNHAM, C. W. 1979. Magmas and hydrothermal fluids. In: BARNES, H. L. (ed.), Geochemistry of Hydrothermal Ore Deposits. Wiley Interscience, New York, 71-136.

CALON, T. J., DUNSWORTH, S. D. & SUHR, G. 1988. The Bay of Islands Ophiolite. Geological Association of Canada - Mineralogical Association of Canada Field Trip Guidebook, Trip B8, 92 p.

CAMERON, W. E. 1985. Petrology and origin of primitive lavas from the Troodos ophiolite, Cyprus. Contributions to Mineralogy and Petrology, 89, 239-255.

CAMERON, W. E., NISBET, E. G. & DIETRICH, V. J. 1979. Boninites, komatiites and ophiolitic basalts. Nature, 280, 550-553.

CANIL, D., VIRGO, D. & SCARFE, C. M. 1990. Oxidation state of mantle xenoliths from British Columbia, Canada. Contributions to Mineralogy and Petrology, 104, 453-462.

CARLSON, R. W. 1988. Layer cake or plum pudding? Nature, 334, 380-381.

CARROLL, M. R. & WYLLIE, P. J. 1989. Experimental phase relations in the system tonalite-peridotite-H_2O at 15 kb; implications for assimilation and differentiation processes near the crust-mantle boundary. Journal of Petrology, 30, 1351-1382.

CARSWELL, D. A., CURTIS, C. D. & KANARIS-SOTIRIOU, R. 1974. Vein metasomatism in peridotite at Kalskaret near Tafjord, South Norway. Journal of Petrology, 15, 383-402.

CASEY, J. F. & DEWEY, J. F. 1984. Initiation of subduction zones along transform and accreting plate boundaries, triple-junction evolution, and forearc spreading centres--implications for ophiolitic geology and obduction. In: GASS, I. G., LIPPARD, S. J. & SHELTON, A. W. (eds.), Ophiolites and Oceanic Lithosphere. Geological Society of London Special Publication 13. Blackwell, Oxford, 269-290.

CASEY, J. F., ELTHON, D. L., SIROKY, F. X., KARSON, J. A. & SULLIVAN, J. 1985. Geochemical and geological evidence bearing on the origin of the Bay of Islands and Coastal Complex ophiolites of western Newfoundland. Tectonophysics, 116, 1-40.

CASEY, J. F., KARSON, J. A., ELTHON, D., ROSENCRANTZ, E. & TITUS, M. 1983. Reconstruction of the geometry of accretion during formation of the Bay of Islands Ophiolite Complex. Tectonics, 2, 509-528.

CASSARD, D., NICOLAS, A., RABINOWICZ, M., MOUTTE, M., LEBLANC, M. & PRINZHOFER, A. 1981. Structural classification of chromite pods in southern New Caledonia. Economic Geology, 76, 805-831.

CEULENEER, G., NICOLAS, A. & BOUDIER, F. 1988. Mantle flow patterns at an oceanic spreading centre: the Oman peridotites record. Tectonophysics, 151, 1-26.

CHRISTIANSEN, F. G. 1985. Deformation fabric and microstructures in ophiolitic chromitite and host ultramafics, Sultanate of Oman. Geologische Rundschau, 74, 61-76.

CHURCH, W. R. 1972. Ophiolite: its definition, origin as oceanic crust and mode of emplacement in orogenic belts with special reference to the Appalachians. In: IRVING, E. (ed.), The Ancient Oceanic Lithosphere. Earth Physics Branch Publication, Energy Mines and Resources, Ottawa, 42, 71-86.

CHURCH, W. R. & STEVENS, R. K. 1970a. Mantle peridotite and the early Palaeozoic ophiolite complexes of the Newfoundland Appalachians. University of Western Ontario, Department of Geology Contributions, Preliminary Report 175.

CHURCH, W. R. & STEVENS, R. K. 1970b. Mantle peridotites and early Palaeozoic ophiolite complexes of the Newfoundland Appalachians. International Symposium on Mechanical Properties and Processes in the Mantle, Abstracts and Program, Flagstaff, Arizona.

CHURCH, W. R. & STEVENS, R. K. 1971. Early Paleozoic ophiolite complexes of the Newfoundland Appalachians as mantle-oceanic crust sequences. Journal of Geophysical Research, 76, 1460-1466.

COCHERIE, A., AUGE, T. & MEYER, G. 1989. Geochemistry of the platinum-group elements in various types of spinels from the Vourinos ophiolitic complex, Greece. Chemical Geology, 77, 27-39.

COISH, R. A. 1989. Boninitic lavas in Appalachian ophiolites: a review. In: CRAWFORD, A. J. (ed.), Boninites and Related Rocks. Unwin Hyman, London, 264-287.

COISH, R. A., HICKEY, R. & FREY, F. A. 1982. Rare earth element geochemistry of the Betts Cove ophiolite, Newfoundland: complexities in ophiolite formation. Geochimica et Cosmochimica Acta, 46, 2117-2134.

COLEMAN, R. G. & KEITH, T. E. 1971. A chemical study of serpentinization--Burro Mountain, California. Journal of Petrology, 12, 311-328.

CONQUERE, F. 1977. Pétrologie des pyroxénites litées dans les complexes ultramafiques de l'Ariège (France) et autres gisements de lherzolite a spinelle I: compositions minéralogiques et chimiques, évolution des conditions d'équilibre des pyroxénites. Bulletin de la Societe Francaise de Mineralogie et de Cristallographie, 100, 42-80.

CRAWFORD, A. J. 1980. A clinoenstatite-bearing cumulate olivine pyroxenite from Howqua, Victoria. Contributions to Mineralogy and Petrology, 75, 353-367.

CRAWFORD, A. J., BECCALUVA, L. & SERRI, G. 1981. Tectono-magmatic evolution of the West Philippine-Mariana region and the origin of boninites. Earth and Planetary Science Letters, 54, 346-356.

CRAWFORD, A. J., FALLOON, T. J. & GREEN, D. H. 1989. Classification, petrogenesis and tectonic setting of boninites. In: CRAWFORD, A. J. (ed.), Boninites and Related Rocks. Unwin Hyman, London, 1-49.

CROCKET, J. H. 1979. Platinum group elements in mafic and ultramafic rocks: a survey. Canadian Mineralogist, 17, 391-402.

DAHL, R. & WATKINSON, D. H. 1986. Structural control of podiform chromitite in Bay of Islands Ophiolite, Springer Hill area, Newfoundland. In: Current Research, Part B, Geological Survey of Canada, Paper 86-1B, 757-766.

DALLMEYER, R. D. & WILLIAMS, H. 1975. $^{40}Ar/^{39}Ar$ ages from the Bay of Islands metamorphic aureole: their bearing on the timing of Ordovician ophiolite obduction. Canadian Journal of Earth Sciences, 12, 1685-1690.

DAWSON, J. B. 1984. Contrasting types of upper-mantle metasomatism? In: KORNPROBST, J. (ed.), Kimberlites I: The Mantle and Crust-Mantle Relationships. Elsevier, Amsterdam, 289-294.

DAWSON, J. B. 1987. Metasomatized harzburgites in kimberlite and alkaline magmas: enriched restites and 'flushed' lherzolites. In: MENZIES, M. A. & HAWKESWORTH, C. J. (eds.), Mantle Metasomatism. Academic Press, London, 125-144.

DEN TEX, E. 1969. Origin of ultramafic rocks, their tectonic setting and history: a contribution to the discussion of the paper "The origin of ultramafic and ultrabasic rocks" by P. J. Wyllie. Tectonophysics, 7, 457-488.

DePAOLO, D. J. 1981. Trace element and isotopic effects of combined wallrock assimilation and fractional crystallization. Earth and Planetary Science Letters, 53, 189-202.

De WAAL, S. A. 1975. The mineralogy, chemistry and certain aspects of reactivity of chromitite from the Bushveld Igneous Complex. South Africa National Institute for Metallurgy Report 1709, 80 p.

DICK, H. J. B. 1977. Evidence of partial melting in the Josephine peridotite. In: DICK, H. J. B. (ed.), Magma Genesis. Oregon Department of Geology and Mineral Industries Bulletin 96, 59-62.

DICK, H. J. B. & BULLEN, T. 1984. Chromian spinel as a petrogenetic indicator in abyssal and alpine-type peridotites and spatially associated lavas. Contributions to Mineralogy and Petrology, 86, 54-76.

DICK, H. J. B. & FISHER, R. L. 1984. Mineralogic studies of the residues of mantle melting: abyssal and alpine-type peridotites. In: KORNPROBST, J. (ed.), Kimberlites II: The Mantle and Crust-Mantle Relationships. Elsevier, Amsterdam, 295-308.

DICK, H. J. B. & SINTON, J. M. 1979. Compositional layering in alpine peridotites: evidence for pressure solution creep in the mantle. Journal of Geology, 87, 403-416.

DICKEY, J. S. jr. 1975. A hypothesis of origin for podiform chromite deposits. Geochimica et Cosmochimica Acta, 39, 1061-1074.

DICKEY, J. S. jr., OBATA, M. & SUEN, C. J. 1979. Chemical differentiation of the lower lithosphere as represented by the Ronda ultramafic massif, southern Spain. In: AHRENS, L. H. (ed.), Origin and Distribution of the Elements. Pergamon Press, Oxford, 587-595.

DONALDSON, C. H. 1985. The rates of dissolution of olivine, plagioclase, and quartz in a basalt melt. Mineralogical Magazine, 49, 683-693.

DONALDSON, M. J. 1981. Redistribution of ore elements during serpentinization and talc-carbonate alteration of some Archean dunites, Western Australia. Economic Geology, 76, 1698-1713.

DUNCAN, R. A. & GREEN, D. H. 1980. Role of multistage melting in the formation of oceanic crust. Geology, 8, 22-26.

DUNCAN, R. A. & GREEN, D. H. 1987. The genesis of refractory melts in the formation of oceanic crust. Contributions to Mineralogy and Petrology, 96, 326-342.

DUNGAN, M. A. & AVE LALLEMANT, H. G. 1977. Formation of small dunite bodies by metasomatic transformation of harzburgite in the Canyon Mountain Ophiolite, northeast Oregon. In: DICK, H. J. B. (ed.), Magma Genesis. Oregon Department of Geology and Mineral Industries Bulletin 96, 109-128.

DUNNING, G. R. & KROGH, T. E. 1985. Geochronology of ophiolites of the Newfoundland Appalachians. Canadian Journal of Earth Sciences, 22, 1659-1670.

DUNSWORTH, S., CALON, T. & MALPAS, J. 1986. Structural and magmatic controls on the internal geometry of the plutonic complex and its chromite occurrences in the Bay of Islands Ophiolite, Newfoundland. Geological Survey of Canada Current Research, Part A, Paper 86-1B, 471-482.

ECKSTRAND, O. R. 1975. The Dumont Serpentinite: a model for control of nickeliferous opaque mineral assemblages by alteration reactions in ultramafic rocks. Economic Geology, 70, 183-201.

EDWARDS, S. J. 1990. Harzburgites and refractory melts in the Lewis Hills Massif, Bay of Islands Ophiolite Complex: the base-metals and precious-metals story. Canadian Mineralogist, 28, 537-552.

EGGLER, D. H. 1987. Solubility of major and trace elements in mantle metasomatic fluids: experimental constraints. In: MENZIES, M. A. & HAWKESWORTH, C. J. (eds.), Mantle Metasomatism. Academic Press, London, 21-41.

ELTHON, D., CASEY, J. F. & KOMOR, S. 1982. Mineral chemistry of ultramafic cumulates from the North Arm Mountain Massif of the Bay of Islands Ophiolite: implication for high pressure fractionation of oceanic basalts. Journal of Geophysical Research, 87, 8717-8734.

ELTHON, D., KARSON, J. A., CASEY, J. F., SULLIVAN, J. & SIROKY, F. X. 1986. Geochemistry of diabase dikes from the Lewis Hills Massif, Bay of Islands ophiolite: evidence for partial melting of oceanic crust in transform faults. Earth and Planetary Science Letters, 78, 89-103.

ENGLAND, P. C. & THOMPSON, A. B. 1984. Pressure-temperature-time paths of regional metamorphism I. Heat transfer during the evolution of regions of thickened continental crust. Journal of Petrology, 25, 894-928.

ERLANK, A. J., WATERS, F. G., HAWKESWORTH, C. J., HAGGERTY, S. E., ALLSOPP, H. L., RICKARD, R. S. & MENZIES, M. 1987. Evidence for mantle metasomatism in peridotite nodules from the Kimberley pipes, South Africa. In: MENZIES, M. A. & HAWKESWORTH, C. J. (eds.), Mantle Metasomatism. Academic Press, London, 221-311.

ERNEWEIN, M., PFLUMIO, C. & WHITECHURCH, H. 1988. The death of an accretion zone as evidenced by the magmatic history of the Sumail ophiolite (Oman). Tectonophysics, 151, 247-274.

EVANS, C. A. 1985. Magmatic 'metasomatism' in peridotites from the Zambales ophiolite. Geology, 13, 166-169.

EVANS, C. & HAWKINS, J. W. jr. 1989. Compositional heterogeneities in upper mantle peridotites from the Zambales Range Ophiolite, Luzon, Philippines. Tectonophysics, 168, 23-41.

FALLOON, T. J. & GREEN, D. H. 1987. Anhydrous partial melting of MORB pyrolite and other peridotite compositions at 10 kbar: implications for the origin of primitive MORB glasses. Mineralogy and Petrology, 37, 181-219.

FALLOON, T. J., GREEN, D. H. & McCULLOCH, M. T. 1989. Petrogenesis of high-Mg and associated lavas from the north Tonga Trench. In: CRAWFORD, A. J. (ed.), Boninites and Related Rocks. Unwin Hyman, London, 357-395.

FORNARI, D. J., PERFIT, M. R., ALLAN, J. F. & BATIZA, R. 1988. Small-scale heterogeneities in depleted mantle sources: near-ridge seamount lava geochemistry and implications for mid-ocean-ridge magmatic processes. Nature, 331, 511-513.

FOX, P. J., DETRICK, R. S. & PURDY, G. M. 1980. Evidence for crustal thinning near fracture zones: implications for ophiolites. In: PANAYIOTOU, A. (ed.), Ophiolites, Proceedings of the International Ophiolite Symposium, Cyprus, 1979. Geological Survey Department, Nicosia, Cyprus, 161-168.

FREY, F. A. 1969. Rare earth abundances in a high-temperature peridotite intrusion. Geochimica et Cosmochimica Acta, 33, 1429-1447.

FREY, F. A. 1984. Rare earth element abundances in upper mantle rocks. In: HENDERSON, P. (ed.), Rare Earth Element Geochemistry. Elsevier, Amsterdam, 153-203.

FREY, F. A. & GREEN, D. H. 1974. The mineralogy, geochemistry and origin of lherzolite inclusions in Victorian basanites. Geochimica et Cosmochimica Acta, 38, 1023-1059.

FREY, F. A., SUEN, C. J. & STOCKMAN, H. W. 1985. The Ronda high temperature peridotite: geochemistry and petrogenesis. Geochimica et Cosmochimica Acta, 49, 2469-2491.

FROST, B. R. 1975. Contact metamorphism of serpentinite, chloritic blackwall and rodingite at Paddy-Go-Easy Pass, Central Cascades, Washington. Journal of Petrology, 16, 272-313.

FURNES, H., PEDERSEN, R. B. & STILLMANN, C. J. 1988. The Leka Ophiolite Complex, central Norwegian Caledonides: field characteristics and geotectonic significance. Journal of the Geological Society, London, 145, 401-412.

GARUTI, G., GORGONI, C. & SIGHINOLFI, G. P. 1984. Sulfide mineralogy and chalcophile and siderophile element abundances in the Ivrea-Verbano mantle peridotites (Western Italian Alps). Earth and Planetary Science Letters, 70, 69-87.

GEORGE, R. P. jr. 1978. Structural petrology of the Olympus ultramafic complex in the Troodos ophiolite, Cyprus. Geological Society of America Bulletin, 89, 845-865.

GIRARDEAU, J. 1982. Tectonic structures related to thrusting of ophiolitic complexes: the White Hills Peridotite, Newfoundland. Canadian Journal of Earth Sciences, 19, 709-722.

GIRARDEAU, J. & NICOLAS, A. 1981. The structure of two ophiolite massifs, Bay-of-Islands, Newfoundland: a model for the oceanic crust and upper mantle. Tectonophysics, 77, 1-34.

GOLDING, H. G. & JOHNSON, K. R. 1971. Variation in gross chemical composition and related physical properties of podiform chromite in the Coolac district, N. S. W., Australia. Economic Geology, 66, 1017-1027.

GOVINDARAJU, K. 1989. 1989 Compilation of working values and sample description for 272 geostandards. Geostandards Newsletter, 13, Special Issue, 1-113.

GREEN, D. H. 1967. High-temperature peridotite intrusions. In: WYLLIE, P. J. (ed.), Ultramafic and Related Rocks. Wiley, New York, 212-222.

GREEN, D. H. & RINGWOOD, A. E. 1967. The genesis of basaltic magmas. Contributions to Mineralogy and Petrology, 15, 103-190.

GREEN, D. H., HIBBERSON, W. O. & JAQUES, A. L. 1979. Petrogenesis of mid-ocean ridge basalts. In: McELHINNY, M. W. (ed.), The Earth: Its Origin, Structure and Evolution. Academic Press, London, 265-299.

GREEN, T. H. & RINGWOOD, A. E. 1968. Genesis of the calc-alkaline igneous rock suite. Contributions to Mineralogy and Petrology, 18, 105-162.

GREENBAUM, D. 1977. The chromitiferous rocks of the Troodos Ophiolite Complex, Cyprus. Economic Geology, 72, 1175-1194.

GREGORY, R. T. 1984. Melt percolation beneath a spreading ridge: evidence from the Semail peridotite, Oman. In: GASS, I. G., LIPPARD, S. J. & SHELTON, A. W. (eds.), Ophiolites and Oceanic Lithosphere. Geological Society of London Special Publication 13. Blackwell, Oxford, 55-62.

GROVES, D. I. & KEAYS, R. R. 1979. Mobilization of ore-forming elements during alteration of dunites, Mt. Keith-Betheno, Western Australia. Canadian Mineralogist, 17, 373-389.

HAMLYN, P. R. & BONATTI, E. 1980. Petrology of mantle-derived ultramafics from the Owen fracture zone, northwest Indian Ocean: implications for the nature of the oceanic mantle. Earth and Planetary Science Letters, 48, 65-79.

HARKINS, M. E., GREEN, H. W. II. & MOORES, E. H. 1980. Multiple intrusive events documented from the Vourinos ophiolite complex, northern Greece. American Journal of Science, 280-A, 284-295.

HARRIS, P. G. 1957. Zone refining and the origin of potassic basalts. Geochimica et Cosmochimica Acta, 12, 195-208.

HART, S. R. 1984. A large-scale isotope anomaly in the Southern Hemisphere mantle. Nature, 309, 753-757.

HARTE, B. 1983. Mantle peridotites and processes; the kimberlite sample. In: HAWKESWORTH, C. J. & NORRY, M. J. (eds.), Continental Basalts and Mantle Xenoliths. Shiva Publishing, Norwich, 46-91.

HARTE, B., COX, K. G. & GURNEY, J. J. 1973. Petrography and geological history of upper-mantle xenoliths from the Matsoku kimberlite. First International Kimberlite Conference, Extended Abstracts, 155-158.

HATCH, F. H., WELLS, A. K. & WELLS, M. K. 1972. Petrology of the Igneous Rocks. Thomas Murby & Co., George Allen & Unwin, London, 551 p.

HATTON, C. J. & GURNEY, J. J. 1987. Roberts Victor eclogites and their relation to the mantle. In: NIXON, P. H. (ed.), Mantle Xenoliths. Wiley, Chichester, 453-463.

HELZ, R. T. 1973. Phase relations of basalts in their melting range at P $H_2O = 5$ kb as a function of oxygen fugacity: part I. Mafic phases. Journal of Petrology, 14, 249-302.

HELZ, R. T. 1976. Phase relations of basalts in their melting ranges at P $H_2O = 5$ kb: part II. Melt compositions. Journal of Petrology, 17, 139-193.

HENDERSON, P. 1975. Reaction trends shown by chrome-spinels of the Rhum layered intrusion. Geochimica et Cosmochimica Acta, 39, 1035-1044.

HERTOGEN, J., JANSSENS, M.-J. & PALME, H. 1980. Trace elements in ocean ridge basalt glasses: implications for fractionation during mantle evolution and petrogenesis. Geochimica et Cosmochimica Acta, 44, 2125-2143.

HERZBERG, C. T. 1978. Pyroxene geothermometry and geobarometry: experimental and thermodynamic evaluation of some subsolidus phase relations involving pyroxenes in the system CaO-MgO-Al_2O_3-SiO_2. Geochimica et Cosmochimica Acta, 42, 945-957.

HICKEY, R. L. & FREY, F. A. 1982. Geochemical characteristics of boninite series volcanics: implications for their source. Geochimica et Cosmochimica Acta, 46, 2099-2115.

HICKSON, C. J. & JURAS, S. J. 1986. Sample contamination by grinding. Canadian Mineralogist, 24, 585-589.

HOLE, M. J., SAUNDERS, A. D., MARRINER, G. F. & TARNEY, J. 1984. Subduction of pelagic sediments: implications for the origin of Ce-anomalous basalts from the Mariana Islands. Journal of the Geological Society, London, 141, 453-472.

HOLLOWAY, J. R. 1973. The system pargasite-H_2O-CO_2: a model for melting of a hydrous mineral with a mixed-volatile fluid I. Experimental results to 8 kbar. Geochimica et Cosmochimica Acta, 37, 651-666.

HONNOREZ, J., MEVEL, C. & MONTIGNY, R. 1984. Occurrence and significance of gneissic amphibolites in the Vema fracture zone, equatorial Mid-Atlantic Ridge. In: GASS, I. G., LIPPARD, S. J. & SHELTON, A. W. (eds.), Ophiolites and Oceanic Lithosphere. Geological Society of London Special Publication 13. Blackwell, Oxford, 121-130.

HOPSON, C. A., COLEMAN, R. G., GREGORY, R. T., PALLISTER, J. S. & BAILEY, E. H. 1981. Geologic section through the Samail ophiolite and associated rocks along a Muscat-Ibra transect. Journal of Geophysical Research,86, 2527-2544.

IRVINE, T. N. 1967. Chromium spinel as a petrogenetic indicator. Part 2, petrologic applications. Canadian Journal of Earth Sciences, 4, 71-103.

IRVINE, T. N. 1976. Chromite crystallization in the join Mg_2SiO_4-$CaMgSi_2O_6$-$CaAl_2Si_2O_8$-$MgCr_2O_4$-SiO_2. Carnegie Institution of Washington Year Book 76, 465-472.

IRVINE, T. N. 1980. Magmatic infiltration metasomatism, double-diffusive fractional crystallization, and adcumulus growth in the Muskox Intrusion and other layered intrusions. In: HARGRAVES, R. B. (ed.), Physics of Magmatic Processes. Princeton University Press, Princeton, 325-383.

IRVING, A. J. 1980. Petrology and geochemistry of composite ultramafic xenoliths in alkalic basalts and implications for magmatic processes within the mantle. American Journal of Science, 280-A, 389-426.

IRVING, A. J. & FREY, F. A. 1984. Trace element abundances in megacrysts and their host basalts: constraints on partition coefficients and megacryst genesis. Geochimica et Cosmochimica Acta, 48, 1201-1221.

ISHIWATARI, A. 1985a. Igneous petrogenesis of the Yakuno Ophiolite (Japan) in the context of the diversity of ophiolites. Contributions to Mineralogy and Petrology, 89, 155-167.

ISHIWATARI, A. 1985b. Granulite-facies metacumulates of the Yakuno Ophiolite, Japan: evidence for unusually thick oceanic crust. Journal of Petrology, 26, 1-30.

JACKSON, E. D. 1961. Primary textures and mineral associations in the ultramafic zone of the Stillwater Complex, Montana. United States Geological Survey Professional Paper 358, 100 p.

JACKSON, E. D. 1969. Chemical variation in coexisting chromite and olivine in chromitite zones of the Stillwater Complex. Economic Geology Monographs, 4, 61-75.

JACKSON, E. D. & THAYER, T. P. 1972. Some criteria for distinguishing between stratiform, concentric and alpine peridotite-gabbro complexes. 24th International Geological Congress, Section 2, 289-296.

JACKSON, E. D., GREEN, H. W. & MOORES, E. M. 1975. The Vourinos ophiolite, Greece: cyclic units of lineated cumulates overlying harzburgite tectonite. Geological Society of America Bulletin, 86, 390-398.

JACKSON, S. E., FRYER, B. J., GOSSE, W., HEALEY, D. C., LONGERICH, H. P. & STRONG, D. F. 1990. Determination of the precious metals in geological materials by inductively coupled plasma-mass spectrometry (ICP-MS) with nickel sulphide fire assay collection and tellurium coprecipitation. Chemical Geology, 83, 119-132.

JACOBSEN, S. B. & WASSERBURG, G. J. 1979. Nd and Sr isotopic study of the Bay of Islands Ophiolite Complex and the evolution of the source of midocean ridge basalts. Journal of Geophysical Research, 84, 7429-7445.

JAGOUTZ, E., PALME, H., BADDENHAUSEN, H., BLUM, K., CENDALES, M., DREIBUS, G., SPETTEL, B., LORENZ, V. & WANKE, H. 1979. The abundances of major, minor and trace elements in the earth's mantle as derived from primitive ultramafic nodules. Proceedings of the 10th Lunar and Planetary Science Conference, 2031-2050.

JAN, M. Q. & WINDLEY, B. F. 1990. Chromian spinel-silicate chemistry in ultramafic rocks of the Jijal Complex, northwest Pakistan. Journal of Petrology, 31, 667-715.

JAQUES, A. L. & CHAPPELL, B. W. 1980. Petrology and trace element geochemistry of the Papuan Ultramafic Belt. Contributions to Mineralogy and Petrology, 75, 55-70.

JAQUES, A. L. & GREEN, D. H. 1980. Anhydrous melting of peridotite at 0-15 kb pressure and the genesis of tholeiitic basalts. Contributions to Mineralogy and Petrology, 73, 287-310.

JENKINS, D. M. 1983. Stability and composition relations of calcic amphiboles in ultramafic rocks. Contributions to Mineralogy and Petrology, 83, 375-384.

JENNER, G. A. 1981. Geochemistry of high-Mg andesites from Cape Vogel, northern Papua New Guinea. Chemical Geology, 33, 307-332.

JENNER, G. A., DUNNING, G. R., MALPAS, J., BROWN, M. & BRACE, T. (in press). Bay of Islands and Little Port complexes, revisited: age, geochemical and isotopic evidence confirm supra-subduction zone origin. Canadian Journal of Earth Sciences.

JOHAN, Z., DUNLOP, H., Le BEL, L., ROBERT, J. L. & VOLFINGER, M. 1983. Origin of chromite deposits in ophiolite complexes: evidence for a volatile and sodium-rich reducing fluid phase. Fortschritte der Mineralogie, 61, 105-107.

JUTEAU, T., ERNEWEIN, M. REUBER, I., WHITECHURCH, H. & DAHL, R. 1988. Duality of magmatism in the plutonic sequence of the Sumail Nappe, Oman. Tectonophysics, 151, 107-135.

KARSON, J. A. 1977. The geology of the northern Lewis Hills, western Newfoundland. Unpublished Ph.D. thesis, State University of New York at Albany, 474 p.

KARSON, J. A. 1979. Geology of the Lewis Hills Massif, western Newfoundland. Geological Survey of Canada, Open File Map and Report 628, 21 p.

KARSON, J. A. 1984. Variations in structure and petrology in the Coastal Complex, Newfoundland: anatomy of an oceanic fracture zone. In: GASS, I. G., LIPPARD, S. J. & SHELTON, A. W. (eds.), Ophiolites and Oceanic Lithosphere. Geological Society of London Special Publication 13. Blackwell, Oxford, 131-144.

KARSON, J. A. & DEWEY, J. F. 1978. Coastal Complex, western Newfoundland: an Early Ordovician oceanic fracture zone. Geological Society of America Bulletin, 89, 1037-1049.

KARSON, J. A., ELTHON, D. L. & DeLONG, S. E. 1983. Ultramafic intrusions in the Lewis Hills Massif, Bay of Islands Ophiolite Complex, Newfoundland: implications for igneous processes at oceanic fracture zones. Geological Society of America Bulletin, 94, 15-29.

KAY, R. W. & SENECHAL, R. G. 1976. The rare earth geochemistry of the Troodos Ophiolite Complex. Journal of Geophysical Research, 81, 964-970.

KEAYS, R. R. & DAVISON, R. M. 1976. Palladium, iridium and gold in the ores and host rocks of nickel sulfide deposits in Western Australia. Economic Geology, 71, 1214-1228.

KEAYS, R. R., NICKEL, D. H., GROVES, D. I. & MacGOLDRICK, P. J. 1982. Iridium and palladium as discriminants of volcanic-exhalative, hydrothermal, and magmatic nickel sulfide mineralizations. Economic Geology, 77, 1535-1547.

KELEMEN, P. B. 1986. Assimilation of ultramafic rock in subduction-related magmatic arcs. Journal of Geology, 94, 829-843.

KELEMEN, P. B. 1990. Reaction between ultramafic rock and fractionating basaltic magma I. Phase relations, the origin of calc-alkaline magma series, and the formation of discordant dunite. Journal of Petrology, 31, 51-98.

KELEMEN, P. B. & GHIORSO, M. S. 1986. Assimilation of peridotite in zoned calc-alkaline plutonic complexes: evidence from the Big Jim complex, Washington Cascades. Contributions to Mineralogy and Petrology, 94, 12-28.

KELLOGG, L. H. & TURCOTTE, D. L. 1986/87. Homogenization of the mantle by convective mixing and diffusion. Earth and Planetary Science Letters, 81, 371-378.

KELLOGG, L. H. & TURCOTTE, D. L. 1990. Mixing and the distribution of heterogeneities in a chaotically convecting mantle. Journal of Geophysical Research, 95, 421-432.

KERRICH, R. & REHRIG, W. 1987. Fluid motion associated with Tertiary mylonitization and detachment faulting: $^{18}O/^{16}O$ evidence from the Picacho metamorphic core complex, Arizona. Geology, 15, 58-62.

KIMBALL, K. L., SPEAR, F. S. & DICK, H. J. B. 1985. High temperature alteration of Abyssal ultramafics from the Islas Orcadas Fracture Zone, South Atlantic. Contributions to Mineralogy and Petrology, 91, 307-320.

KLEIN, E. M. & LANGMUIR, C. H. 1987. Global correlations of ocean ridge basalt chemistry with axial depth and crustal thickness. Journal of Geophysical Research, 92, 8089-8115.

KOMOR, S. C. & ELTHON, D. 1990. Formation of anorthosite-gabbro rhythmic phase layering: an example at North Arm Mountain, Bay of Islands Ophiolite. Journal of Petrology, 31, 1-50.

KOMOR, S. C., ELTHON, D. & CASEY, J. F. 1985. Mineralogic variation in a layered ultramafic cumulate sequence at the North Arm Mountain Massif, Bay of Islands Ophiolite, Newfoundland. Journal of Geophysical Research, 90, 7705-7736.

KOMOR, S. C., ELTHON, D. & CASEY, J. F. 1987. Petrology of a leucogabbroic interval within basal layered gabbros at North Arm Mountain, Bay of Islands ophiolite. Contributions to Mineralogy and Petrology, 95, 278-300.

KORZHINSKII, D. S. 1970. Theory of Metasomatic Zoning. Clarendon Press, Oxford, 162 p. (Translated by J. Agrell).

KRAMERS, J. D., RODDICK, J. C. M. & DAWSON, J. B. 1983. Trace element and isotope studies on veined, metasomatic and 'MARID' xenoliths from Bultfontein, South Africa. Earth and Planetary Science Letters, 65, 90-106.

KUSHIRO, I. 1969. The system forsterite-diopside-silica with and without water at high pressure. American Journal of Science, 267-A, 269-294.

KUSHIRO, I. 1972. Effect of water on the composition of magmas formed at high pressures. Journal of Petrology, 13, 311-334.

KUSHIRO, I. 1975. On the nature of silicate melt and its significance in magma genesis: regularities in the shift of the liquidus boundaries involving olivine, pyroxene, and silica minerals. American Journal of Science, 275, 411-431.

KUSHIRO, I. & AOKI, K. 1968. Origin of some eclogite inclusions in kimberlite. American Mineralogist, 53, 1347-1367.

KUSHIRO, I. & YODER, J. S. jr. 1966. Anorthite-forsterite and anorthite-enstatite reactions and their bearing on the basalt-eclogite transformation. Journal of Petrology, 7, 337-362.

LAGO, B. L., RABINOWICZ, M., & NICOLAS, A. 1982. Podiform chromite ore bodies: a genetic model. Journal of Petrology, 23, 103-125.

LEBLANC, M. 1987. Chromite in oceanic arc environments: New Caledonia. In: STOWE, C. W. (ed.), Evolution of Chromium Ore Fields. Van Nostrand Reinhold, New York, 265-296.

LEBLANC, M. & TEMAGOULT, A. 1989. Chromite pods in a lherzolite massif (Collo, Algeria): evidence of oceanic-type mantle rocks along the West Mediterranean Alpine Belt. Lithos, 23, 153-162.

LEBLANC, M. & VIOLETTE, J.-F. 1983. Distribution of aluminum-rich and chromium-rich chromite pods in ophiolite peridotites. Economic Geology, 78, 293-301.

LEBLANC, M., DUPUY, C., CASSARD, D., MOUTTE, J., NICOLAS, A., PRINZHOFER, A., RABINOWICZ, M. & ROUTHIER, P. 1980. Essai sur la génèse des corps podiformes de chromite dans les peridotites ophiolitiques: étude des chromites de Nouvelle Calédonie et comparaison avec celles de Méditerranée orientale. In: PANAYIOTOU, A. (ed.), Ophiolites, Proceedings of the International Ophiolite Symposium, Cyprus, 1979. Geological Survey Department, Nicosia, Cyprus, 691-701.

LEGENDRE, O. 1982. Minéralogie et géochimie des platinoides dans les chromitites ophiolitiques--Comparaison avec d'autres types de concentrations en platinoides. Thèse, Université de Paris VI, 171 p.

LIPIN, B. R. 1984. Chromite from the Blue Ridge Province of North Carolina. American Journal of Science, 284, 507-529.

LIPPARD, S. J., SHELTON, A. W. & GASS, I. G. 1986. The Ophiolite of Northern Oman. Geological Society of London Memoir 11, 178 p.

LLOYD, F. E. & BAILEY, D. K. 1975. Light element metasomatism of the continental mantle: the evidence and the consequences. Physics and Chemistry of the Earth, 9, 389-416.

LONEY, R. A. & HIMMELBERG, G. F. 1976. Structure of the Vulcan Peak alpine-type peridotite, southwestern Oregon. Geological Society of America Bulletin, 87, 259-274.

LOOMIS, T. P. & GOTTSCHALK, R. R. 1981. Hydrothermal origin of mafic layers in Alpine-type peridotites: evidence from the Seiad Ultramafic Complex, California, U. S. A. Contributions to Mineralogy and Petrology, 76, 1-11.

LORAND, J. P. 1987. Cu-Fe-Ni-S mineral assemblages in upper-mantle peridotites from the Table Mountain and Blow-Me-Down Mountain ophiolite massifs (Bay of Islands area, Newfoundland): their relationships with fluids and silicate melts. Lithos, 20, 59-76.

LORAND, J. P. 1988. Fe-Ni-Cu sulfides in tectonite peridotites from the Maqsad District, Sumail Ophiolite, southern Oman: implications for the origin of the sulfide component in the oceanic upper mantle. Tectonophysics, 151, 57-73.

LOUBET, M. & ALLEGRE, C. J. 1982. Trace elements in orogenic lherzolites reveal the complex history of the upper mantle. Nature, 298, 809-814.

MAALØE, S. 1981. Magma accumulation in the ascending mantle. Journal of the Geological Society, London, 138, 223-236.

MAALØE, S. 1982. Geochemical aspects of permeability controlled partial melting and fractional crystallization. Geochimica et Cosmochimica Acta, 46, 43-57.

MAALØE, S. & AOKI, K. 1977. The major element composition of the upper mantle estimated from the composition of lherzolites. Contributions to Mineralogy and Petrology, 63, 161-173.

MALPAS, J. 1973. A restored section of oceanic crust and mantle in western Newfoundland. Geological Society of America 8th Annual Meeting, Northeastern Section, Abstracts with Programs, 5, 192.

MALPAS, J. 1976. The petrology and petrogenesis of the Bay of Islands ophiolite suite, western Newfoundland. Unpublished Ph.D. thesis, Memorial University of Newfoundland, 431 p.

MALPAS, J. 1978. Magma generation in the upper mantle, field evidence from ophiolite suites, and application to the generation of oceanic lithosphere. Philosophical Transactions of the Royal Society of London, A288, 527-546.

MALPAS, J. 1979a. Two contrasting trondhjemite associations from transported ophiolites in western Newfoundland: initial report. In BARKER, F. (ed.), Trondhjemites, Dacites, and Related Rocks. Elsevier, Amsterdam, 465-487.

MALPAS, J. 1979b. The dynamothermal aureole of the Bay of Islands ophiolite suite. Canadian Journal of Earth Sciences, 16, 2086-2101.

MALPAS, J. & LANGDON, G. S. 1987. The Kennack Gneisses of the Lizard Complex, Cornwall, England: partial melts produced during ophiolite emplacement. Canadian Journal of Earth Sciences, 24, 1966-1974.

MALPAS, J. & STRONG, D. F. 1975. A comparison of chrome-spinels in ophiolites and mantle diapirs of Newfoundland. Geochimica et Cosmochimica Acta, 39, 1045-1060.

MALPAS, J., STEVENS, R. K. & STRONG, D. F. 1973. Amphibole associated with Newfoundland ophiolite: its classification and tectonic significance. Geology, 1, 45-47.

MATTINSON, J. M. 1975. Early Paleozoic ophiolite complexes of Newfoundland: isotopic ages of zircons. Geology, 3, 181-183.

MATTINSON, J. M. 1976. Ages of zircons from the Bay of Islands Ophiolite Complex, western Newfoundland. Geology, 4, 393-394.

McADAM, R. C., SUTARNO & MOLOUGHNEY, P. E. 1973. Noble-metals-bearing sulphide concentrate PTC: its characterization and preparation for use as a standard reference material. Department of Energy, Mines and Resources, Ottawa Mines Branch, Technical Bulletin TB 176, 26 p.

McCAIG, A. M. 1983. P-T conditions during emplacement of the Bay of Islands Ophiolite Complex. Earth and Planetary Science Letters, 63, 459-473.

McCAIG, A. M. 1984. Fluid-rock interaction in some shear zones from the Central Pyrenees. Journal of Metamorphic Geology, 2, 129-141.

McCAIG, A. M. & KNIPE, R. J. 1990. Mass-transport mechanisms in deforming rocks: recognition using microstructural and microchemical criteria. Geology, 18, 824-827.

McCULLOCH, M. T. & CAMERON, W. E. 1983. Nd-Sr isotopic study of primitive lavas from the Troodos Ophiolite, Cyprus: evidence for a subduction-related setting. Geology, 11, 727-731.

McCULLOCH, M. T., JAQUES, A. L., NELSON, D. R. & LEWIS, J. D. 1983. Nd and Sr isotopes in kimberlites and lamproites from Western Australia: an enriched mantle origin. Nature, 302, 400-403.

McGUIRE, A. V., DYAR, M. D. & WARD, K. A. 1989. Neglected Fe^{3+}/Fe^{2+} ratios - a study of Fe^{3+} content of megacrysts from alkali basalts. Geology, 17, 687-690.

McKENZIE, D. P. 1984. The generation and compaction of partially molten rock. Journal of Petrology, 25, 713-765.

McKENZIE, D. 1989. Some remarks on the movement of small melt fractions in the mantle. Earth and Planetary Science Letters, 95, 53-72.

MELSON, W. G., HART, S. R. & THOMPSON, G. 1972. St. Paul's Rocks, Equatorial Atlantic: petrogenesis, radiometric ages, implications on sea-floor spreading. Geological Society of America Memoir 132, 241-272.

MENZIES, M. 1990. Effects of small volume melts. Nature, 343, 312-313.

MENZIES, M. & ALLEN, C. 1974. Plagioclase lherzolite-residual mantle relationships within two eastern Mediterranean ophiolites. Contributions to Mineralogy and Petrology, 45, 197-213.

MENZIES, M. A. & HAWKESWORTH, C. J. (eds.) 1987a. Mantle Metasomatism. Academic Press, London, 472 p.

MENZIES, M. & HAWKESWORTH, C. J. 1987b. Upper mantle processes and composition. In: NIXON, P. H. (ed.), Mantle Xenoliths. Wiley, Chichester, 725-738.

MENZIES, M., BLANCHARD, D., BRANNON, J. & KOROTEV, R. 1977. Rare earth geochemistry of fused ophiolitic and alpine lherzolites. Contributions to Mineralogy and Petrology, 64, 53-74.

MERCIER, J.-C. 1985. Olivines and pyroxenes. In: WENK, H. R. (ed.), Preferred Orientation in Deformed Metals and Rocks. Academic Press, 407-423.

MERCIER, J.-C. C. & NICOLAS, A. 1975. Textures and fabrics of upper-mantle peridotites as illustrated by xenoliths from basalts. Journal of Petrology, 16, 454-487.

MICHARD, A. 1989. Rare earth element systematics in hydrothermal fluids. Geochimica et Cosmochimica Acta, 53, 745-750.

MILLER, R. B. 1988. Fluid flow, metasomatism and amphibole deformation in an imbricated ophiolite, North Cascades, Washington. Journal of Structural Geology, 10, 283-296.

MILLER, R. B. & MOGK, D. W. 1987. Ultramafic rocks of a fracture-zone ophiolite, North Cascades, Washington. Tectonophysics, 142, 261-289.

MITCHELL, R. H. & KEAYS, R. R. 1981. Abundance and distribution of gold, palladium and iridium in some spinel and garnet lherzolites: implications for the nature and origin of precious metal-rich intergranular components in the upper mantle. Geochimica et Cosmochimica Acta, 45, 2425-2442.

MIYASHIRO, A. 1973. The Troodos Complex was probably formed in an island arc. Earth and Planetary Science Letters, 19, 218-224.

MONTANA, A. & BREARLEY, M. 1989. An appraisal of the stability of phlogopite in the crust and in the mantle. American Mineralogist, 74, 1-4.

MONTIGNY, R., BOUGAULT, H., BOTTINGA, Y. & ALLEGRE, C. J. 1973. Trace element geochemistry and genesis of the Pindos ophiolite suite. Geochimica et Cosmochimica Acta, 37, 2135-2147.

MOODY, J. B. 1976. Serpentinization: a review. Lithos, 9, 125-138.

MOORES, E. M. 1969. Petrology and structure of the Vourinos ophiolitic complex, northern Greece. Geological Society of America Special Paper 118, 74 p.

MOORES, E. M. & VINE, F. J. 1971. The Troodos Massif, Cyprus and other ophiolites as oceanic crust: evaluation and implications. Philosophical Transactions of the Royal Society of London, A268, 443-466.

MORGAN, J. W. & WANDLESS, G. A. 1979. Terrestrial upper mantle: siderophile and volatile trace element abundances. Proceedings of the 10th Lunar and Planetary Science Conference, 855-857.

MORGAN, J. W., WANDLESS, G. A., PETRIE, R. K. & IRVING, A. J. 1980. Earth's upper mantle: volatile element distribution and origin of siderophile element content. Proceedings of the 11th Lunar and Planetary Science Conference, 740-742.

MORRIS, E. M. & PASTERIS, J. D. (eds.) 1987. Mantle Metasomatism and Alkaline Magmatism. Geological Society of America Special Paper 215, 383 p.

MURTON, B. J. 1986. Anomalous oceanic lithosphere formed in a leaky transform fault: evidence from the Western Limassol Forest Complex, Cyprus. Journal of the Geological Society, London, 143, 845-854.

NAKAMURA, Y. & KUSHIRO, I. 1974. Composition of the gas phase in Mg_2SiO_4-SiO_2-H_2O at 15 kbar. Carnegie Institution of Washington Year Book 73, 255-258.

NALDRETT, A. J. 1973. Nickel sulfide deposits - their classification and genesis with special emphasis on deposits of volcanic association. Canadian Institute of Mining and Metallurgy Transactions, 76, 183-201.

NALDRETT, A. J. & DUKE, J. M. 1980. Platinum metals in magmatic sulphide ores. Science, 208, 1417-1424.

NALDRETT, A. J., HOFFMAN, E. L., GREEN, A. H., CHEN-LIN CHOU & NALDRETT, S. R. 1979. The composition of Ni-sulfide ores, with particular reference to their content of PGE and Au. Canadian Mineralogist, 17, 403-415.

NAVON, O. & STOLPER, E. 1987. Geochemical consequences of melt percolation: the upper mantle as a chromatographic column. Journal of Geology, 95, 285-307.

NICHOLLS, I. A. & RINGWOOD, A. E. 1973. Effect of water on olivine stability in tholeiites and the production of silica-saturated magmas in the island-arc environment. Journal of Geology, 81, 285-300.

NICOLAS, A. 1986a. Structure and petrology of peridotites: clues to their geodynamic environment. Reviews of Geophysics, 24, 875-895.

NICOLAS, A. 1986b. A melt extraction model based on structural studies in mantle peridotites. Journal of Petrology, 27, 999-1022.

NICOLAS, A. 1989. Structures of Ophiolites and Dynamics of Oceanic Lithosphere. Kluwer Academic Publishers, Dordrecht, 367 p.

NICOLAS, A. & DUPUY, C. 1984. Origin of ophiolitic and oceanic lherzolites. Tectonophysics, 110, 177-187.

NICOLAS, A. & JACKSON, E. D. 1972. Répartition en deux provinces des peridotites des chaines alpines longent la Méditerranée: implications géotectonique. Bulletin Suisse Mineralogische und Petrographische, 52, 479-495.

NICOLAS, A. & JACKSON, M. 1982. High temperature dikes in peridotites: origin by hydraulic fracturing. Journal of Petrology, 23, 568-582.

NICOLAS, A. & Le PICHON, X. 1980. Thrusting of young lithosphere in subduction zones with special reference to structures in ophiolitic peridotites. Earth and Planetary Science Letters, 46, 397-406.

NICOLAS, A. & PRINZHOFER, A. 1983. Cumulative or residual origin for the transition zone in ophiolites: structural evidence. Journal of Petrology, 24, 188-206.

NICOLAS, A. & RABINOWICZ, M. 1984. Mantle flow pattern at oceanic spreading centres: relation with ophiolitic and oceanic structures. In: GASS, I. G., LIPPARD, S. J. & SHELTON, A. W. (eds.), Ophiolites and Oceanic Lithosphere. Geological Society of London Special Publication 13. Blackwell, Oxford, 147-151.

NICOLAS, A. & VIOLETTE, J.-F. 1982. Mantle flow at oceanic spreading centres: models derived from ophiolites. Tectonophysics, 81, 319-339.

NICOLAS, A., BOUDIER, F. & BOUCHEZ, J.-L. 1980. Interpretation of peridotite structures from ophiolitic and oceanic environments. American Journal of Science, 280-A, 192-210.

NIXON, P. H. (ed.). 1987. Mantle Xenoliths. Wiley, Chichester, 844 p.

OBA, T. 1980. Phase relations in the tremolite-pargasite join. Contributions to Mineralogy and Petrology, 71, 247-256.

OBATA, M. 1976. The solubility of Al_2O_3 in orthopyroxene in spinel and plagioclase peridotites and spinel pyroxenite. American Mineralogist, 61, 804-816.

OBATA, M. 1980. The Ronda Peridotite: garnet-, spinel-, and plagioclase-lherzolite facies and the P-T trajectories of a high-temperature mantle intrusion. Journal of Petrology, 21, 533-572.

O'HARA, M. J. 1967. Mineral facies in ultrabasic rocks. In: WYLLIE, P. J. (ed.), Ultramafic and Related Rocks. Wiley, New York, 7-18.

O'HARA, M. J. 1968. Are ocean floor basalts primary magma? Nature, 220, 683-686.

O'NIONS, R. K., EVENSEN, N. M. & HAMILTON, P. J. 1980. Differentiation and evolution of the mantle. Philosophical Transactions of the Royal Society of London, A297, 479-493.

OSBORNE, M. D., FLEET, M. E. & BANCROFT, G. M. 1981. Fe^{2+}-Fe^{3+} ordering in chromite and Cr-bearing spinels. Contributions to Mineralogy and Petrology, 77, 251-255.

OSHIN, I. O. & CROCKET, J. H. 1982. Noble metals in Thetford Mines ophiolites, Quebec, Canada. Part I: distribution of gold, iridium, platinum, and palladium in the ultramafic and gabbroic rocks. Economic Geology, 77, 1556-1570.

OTTONELLO, G., PICCARDO, G. B. & ERNST, W. G. 1979. Petrogenesis of some Ligurian peridotites - II. Rare earth element chemistry. Geochimica et Cosmochimica Acta, 43, 1273-1284.

OZAWA, K. 1988. Ultramafic tectonite of the Miyamori ophiolitic complex in the Kitakami Mountains, Northeast Japan: hydrous upper mantle in an island arc. Contributions to Mineralogy and Petrology, 99, 159-175.

PAGE, N. J. & TALKINGTON, R. W. 1984. Palladium, platinum, rhodium, ruthenium and iridium in peridotites and chromitites from the ophiolite complexes in Newfoundland. Canadian Mineralogist, 22, 137-149.

PAGE, N. J., ARUSCAVAGE, P. J. & HAFFTY, J. 1983. Platinum-group elements in rocks from the Voikar-Syninsky Ophiolite Complex, Polar Urals, U. S. S. R. Mineralium Deposita, 18, 443-455.

PAGE, N. J., CASSARD, D. & HAFFTY, J. 1982. Palladium, platinum, rhodium, ruthenium, and iridium in chromitites from the Massif du Sud and Tiébaghi Massif, New Caledonia. Economic Geology, 77, 1571-1577.

PALLISTER, J. S. & KNIGHT, R. J. 1981. Rare-earth element geochemistry of the Samail Ophiolite near Ibra, Oman. Journal of Geophysical Research, 86, 2673-2697.

PAVLIS, T. L. 1986. The role of strain heating in the evolution of megathrusts. Journal of Geophysical Research, 91, 12407-12422.

PEACOCK, S. M. 1990. Fluid processes in subduction zones. Science, 248, 329-337.

PEARCE, J. A., LIPPARD, S. J. & ROBERTS, S. 1984. Characteristics and tectonic significance of supra-subduction zone ophiolites. In: KOKELAAR, B. P. & HOWELLS, M. F. (eds.), Marginal Basin Geology. Geological Society of London Special Publication 16. Blackwell, Oxford, 77-94.

PEARSON, D. G. 1989. The petrogenesis of pyroxenites containing octahedral graphite and associated mafic and ultramafic rocks of the Beni Bousera Peridotite Massif, N. Morocco. Unpublished Ph.D. thesis, University of Leeds, 413 p.

PECK, D. C. & KEAYS, R. R. 1990. Insights into the behaviour of precious metals in primitive, S-undersaturated magmas: evidence from the Heazlewood River Complex, Tasmania. Canadian Mineralogist, 28, 553-577.

PEDERSEN, R. B. & MALPAS, J. 1984. The origin of oceanic plagiogranites from the Karmoy ophiolite, Western Norway. Contributions to Mineralogy and Petrology, 88, 36-52.

PHIPPS MORGAN, J. 1987. Melt migration beneath mid-ocean spreading centers. Geophysical Research Letters, 14, 1238-1241.

PICCARDO, G. B., MESSIGA, B. & VANNUCCI, R. 1988. The Zabargad peridotite-pyroxenite association: petrological constraints on its evolution. Tectonophysics, 150, 135-162.

POLVE, M. & ALLEGRE, C. J. 1980. Orogenic lherzolite complexes studied by ^{87}Rb-^{87}Sr: a clue to understand the mantle convection processes? Earth and Planetary Science Letters, 51, 71-93.

PRICHARD, H. M. & TARKIAN, M. 1988. Platinum and palladium minerals from two PGE-rich localities in the Shetland Ophiolite Complex. Canadian Mineralogist, 26, 979-990.

PRINZ, M., KEIL, K., GREEN, J. A., REID, A. M., BONATTI, E. & HONNOREZ, J. 1976. Ultramafic and mafic dredge samples from the equatorial mid-Atlantic ridge and fracture zones. Journal of Geophysical Research, 81, 4087-4103.

PRINZHOFER, A. & ALLEGRE, C. J. 1985. Residual peridotites and the mechanisms of partial melting. Earth and Planetary Science Letters, 74, 251-265.

PRINZHOFER, A. & NICOLAS, A. 1980. The Bogota Peninsula, New Caledonia: a possible oceanic transform fault. Journal of Geology, 88, 387-398.

PRINZHOFER, A., LEWIN, E. & ALLEGRE, C. J. 1989. Stochastic melting of the marble cake mantle: evidence from local study of the East Pacific Rise at 12°50'N. Earth and Planetary Science Letters, 92, 189-206.

QUICK, J. E. 1981a. The origin and significance of large, tabular dunite bodies in the Trinity Peridotite, northern California. Contributions to Mineralogy and Petrology, 78, 413-422.

QUICK, J. E. 1981b. Petrology and petrogenesis of the Trinity Peridotite, an upper mantle diapir in the eastern Klamath Mountains, northern California. Journal of Geophysical Research, 86, 11837-11863.

RALEIGH, C. B. 1965. Structure and petrology of an alpine peridotite on Cypress Island, Washington, U. S. A. Contributions to Mineralogy and Petrology, 11, 719-741.

RAUTENSCHLEIN, M., JENNER, G. A., HERTOGEN, J., HOFMANN, A. W., KERRICH, R., SCHMINCKE, H.-U. & WHITE, W. M. 1985. Isotopic and trace element composition of volcanic glasses from the Akaki Canyon, Cyprus: implications for the origin of the Troodos Ophiolite. Earth and Planetary Science Letters, 75, 369-383.

REISBERG, L. & ZINDLER, A. 1986/87. Extreme isotopic variations in the upper mantle: evidence from Ronda. Earth and Planetary Science Letters, 81, 29-45.

REUBER, I. 1984. Mylonitic ductile shear zones within tectonites and cumulates as evidence for an oceanic transform fault in the Antalya ophiolite, S. W. Turkey. In: DIXON, J. E. & ROBERTSON, A. H. F. (eds.), The Geological Evolution of the Eastern Mediterranean. Geological Society of London Special Publication 17. Blackwell, Oxford, 319-334.

REUBER, I., WHITECHURCH, H. & CARON, J. M. 1982. Setting of gabbroic dykelets in an ophiolitic complex by hydraulic fracturing. Nature, 296, 141-143.

REUBER, I., WHITECHURCH, H. & JUTEAU, Th. 1985. Successive generations of coarse grained dikelets in the ophiolite complex of Antalya, Turkey: products of partial fusion and residual liquids. Ofioliti, 10, 35-62.

RINGWOOD, A. E. 1966. The chemical composition and origin of the Earth. In: HURLEY, P. (ed.), Advances in Earth Science. Massachusetts Institute of Technology Press, Cambridge, 287-356.

RINGWOOD, A. E. 1969. Composition and evolution of the upper mantle. In: The Earth's Crust and Upper Mantle. American Geophysical Union Geophysical Monograph 13, 1-17.

RINGWOOD, A. E. 1975. Composition and Petrology of the Earth's Mantle. McGraw Hill, 618 p.

ROBERTS, S. 1988. Ophiolitic chromitite formation: a marginal basin phenomenon? Economic Geology, 83, 1034-1036.

ROEDDER, E. 1965. Liquid CO_2 inclusions in olivine bearing nodules and phenocrysts from basalts. American Mineralogist, 50, 1746-1782.

SAVELYEV, A. A. & SAVELYEVA, G. N. 1979. Ophiolites of the Voykar Massif (Polar Urals). In: MALPAS, J. & TALKINGTON, R. W. (eds.), Ophiolites of the Canadian Applachians and Soviet Urals. Memorial University of Newfoundland, Department of Geology, Report No. 8, Contribution to I. G. C. P. Project 39, 127-140.

SCHILLING, J. G. 1973. Iceland mantle plume: geochemical evidence along the Rekjanes Ridge. Nature, 242, 565-571.

SCHILLING, J. G. 1975. Rare earth variations across normal segments of the Rekjanes ridge 60-53°N, Mid Atlantic ridge 29°S and East Pacific ridge 2-19°S and evidence of the composition of the underlying low velocity layer. Journal of Geophysical Research, 80, 1459-1473.

SCHNEIDER, M. E. & EGGLER, D. H. 1986. Fluids in equilibrium with peridotite minerals: implications for mantle metasomatism. Geochimica et Cosmochimica Acta, 50, 711-724.

SCOTT, D. R. & STEVENSON, D. J. 1984. Magma solitons. Geophysical Research Letters, 11, 1161-1164.

SEARLE, M. P. & MALPAS, J. 1980. Structure and metamorphism of rocks beneath the Semail ophiolite of Oman and their significance in ophiolite obduction. Transactions of the Royal Society of Edinburgh: Earth Sciences, 71, 247-262.

SEARLE, M. P. & MALPAS, J. 1982. Petrochemistry and origin of sub-ophiolitic metamorphic and related rocks in the Oman Mountains. Journal of the Geological Society, London, 139, 235-248.

SEARLE, M. P. & STEVENS, R. K. 1984. Obduction processes in ancient, modern and future ophiolites. In: GASS, I. G., LIPPARD, S. J. & SHELTON, A. W. (eds.), Ophiolites and Oceanic Lithosphere. Geological Society of London Special Publication 13. Blackwell, Oxford, 303-319.

SECHER, D. 1981. Les lherzolites ophiolitiques de Nouvelle Calédonie et leurs gisements de chromite-Déformation de la chromite. Thèse Doc. 3° cycle, Université de Nantes, 247 p.

SEKINE, T. & WYLLIE, P. J. 1982a. Phase relationships in the system $KAlSiO_4$-Mg_2SiO_4-SiO_2-H_2O as a model for hybridization between hydrous siliceous melts and peridotite. Contributions to Mineralogy and Petrology, 79, 368-374.

SEKINE, T. & WYLLIE, P. J. 1982b. The system granite-peridotite-H_2O at 30 kbar, with applications to hybridization in subduction zone magmatism. Contributions to Mineralogy and Petrology, 81, 190-202.

SEKINE, T. & WYLLIE, P. J. 1982c. Synthetic systems for modeling hybridization between hydrous siliceous magmas and peridotite in subduction zones. Journal of Geology, 90, 734-741.

SEKINE, T. & WYLLIE, P. J. 1983. Experimental simulation of mantle hybridization in subduction zones. Journal of Geology, 91, 511-528.

SERRI, G. 1981. The petrochemistry of ophiolite gabbroic complexes: a key for the classification of ophiolites into low-Ti and high-Ti types. Earth and Planetary Science Letters, 52, 203-212.

SHAW, H. R. 1980. The fracture mechanisms of magma transport from the mantle to the surface. In: HARGRAVES, R. B. (ed.), Physics of Magmatic Processes. Princeton University Press, Princeton, 201-264.

SHERVAIS, J. W. 1979. Ultramafic and mafic layers in the alpine type lherzolite massif at Balmuccia (Italy). Memoire di Scienze Geologiche, Padova, 33, 135-145.

SHIBATA, T. & THOMPSON, G. 1986. Peridotites from the Mid-Atlantic Ridge at 43°N and their petrogenetic relation to abyssal tholeiites. Contributions to Mineralogy and Petrology, 93, 144-159.

SHIGA, Y. 1987. Behaviour of iron, nickel, cobalt and sulfur during serpentinization, with reference to the Ha 'achine ultramafic rocks of the Kamaishi Mining District, Northeastern Japan. Canadian Mineralogist, 25, 611-624.

SINHA, A. K., HEWITT, D. A. & RIMSTIDT, J. D. 1986. Fluid interaction and element mobility in the development of ultramylonites. Geology, 14, 883-886.

SINIGOI, S., COMIN-CHIARAMONTI, P., DEMARCHI, G. & SIENA, F. 1983. Differentiation of partial melts in the mantle: evidence from the Balmuccia Peridotite, Italy. Contributions to Mineralogy and Petrology, 82, 351-359.

SINTON, J. 1977. Equilibration history of the basal alpine-type peridotite, Red Mountain, New Zealand. Journal of Petrology, 18, 216-246.

SLEEP, N. H. 1974. Segregation of magma from a mostly crystalline mush. Geological Society of America Bulletin, 85, 1225-1232.

SMEWING, J. D. & POTTS, P. J. 1976. Rare earth abundances in basalts and metabasalts from the Troodos Massif, Cyprus. Contributions to Mineralogy and Petrology, 57, 245-258.

SMITH, C. H. 1958. Bay of Islands Igneous Complex, Western Newfoundland. Geological Survey of Canada Memoir 290, 132 p.

SMITH, S. E. & ELTHON, D. 1988. Mineral compositions of plutonic rocks from the Lewis Hills Massif, Bay of Islands Ophiolite. Journal of Geophysical Research, 93, 3450-3468.

SPENCE, D. A. & TURCOTTE, D. L. 1990. Buoyancy-driven magma fracture: a mechanism for ascent through the lithosphere and the emplacement of diamonds. Journal of Geophysical Research, 95, 5133-5139.

SPERA, F. J. 1980. Aspects of magma transport. In: HARGRAVES, R. B. (ed.), Physics of Magmatic Processes. Princeton University Press, Princeton, 265-323.

SPERA, F. J. 1987. Dynamics of translithospheric migration of metasomatic fluid and alkaline magma. In: MENZIES, M. A. & HAWKESWORTH, C. J. (eds.), Mantle Metasomatism. Academic Press, London, 1-20.

SPRAY, J. G. 1982. Mafic segregations in ophiolite mantle sequences. Nature, 299, 524-528.

SPRAY, J. G. 1989. Upper mantle segregation processes: evidence from alpine-type peridotites. In: SAUNDERS, A. D. & NORRY, M. J. (eds.), Magmatism in the Ocean Basins. Geological Society of London Special Publication 42. Blackwell, Oxford, 29-40.

STEVENS, R. K. 1970. Cambro-Ordovician flysch sedimentation and tectonics in west Newfoundland and their possible bearing on a proto-Atlantic Ocean. Geological Association of Canada Special Paper 7, 165-177.

STEWART, D. C. & BOETTCHER, A. L. 1977. Chemical gradients in mantle xenoliths. Geological Society of America, Abstracts with Programs, 9, 1191-1192.

STOCKMAN, H. W. 1982. Noble metals in the Ronda and Josephine peridotites. Unpublished Ph.D. thesis, Massachusetts Institute of Technology, 180 p.

STOLPER, E. 1980. A phase diagram for mid-ocean ridge basalts: preliminary results and implications for petrogenesis. Contributions to Mineralogy and Petrology, 74, 13-27.

STOSCH, H.-G. 1982. Rare earth element partitioning between minerals from anhydrous spinel peridotite xenoliths. Geochimica et Cosmochimica Acta, 46, 793-811.

STOSCH, H.-G. & SECK, H. A. 1980. Geochemistry and mineralogy of two spinel peridotite suites from Dreiser Weiher, West Germany. Geochimica et Cosmochimica Acta, 44, 457-470.

STRECKEISEN, A. 1976. To each plutonic rock its proper name. Earth Science Reviews, 12, 1-33.

SUEN, C. J., FREY, F. A. & MALPAS, J. 1979. Bay of Islands ophiolite suite, Newfoundland: petrologic and geochemical characteristics with emphasis on rare earth element geochemistry. Earth and Planetary Science Letters, 45, 337-348.

SUHR, G. & CALON, T. 1987. A structural and microstructural study of mantle tectonites in the Springers Hill area (Bay of Islands Ophiolite, Newfoundland). Geological Survey of Canada, unpublished report.

SUHR, G., CALON, T. & DUNSWORTH, S. M. (in press). Origin of complex upper mantle structures in the Southern Lewis Hills (Bay of Islands Ophiolite, Newfoundland). Canadian Journal of Earth Sciences.

SUN, S.-S. & NESBITT, R. W. 1978. Petrogenesis of Archean ultrabasic and basic volcanics: evidence from rare earth elements. Contributions to Mineralogy and Petrology, 65, 301-325.

TALKINGTON, R. W. 1981. The geology, petrology and petrogenesis of the White Hills Peridotite, St. Anthony Complex, northwestern Newfoundland. Unpublished Ph.D. thesis, Memorial University of Newfoundland, 292 p. plus appendices.

TALKINGTON, R. W. & MALPAS, J. 1984. The formation of spinel phases of the White Hills Peridotite, St. Anthony Complex, Newfoundland. Neues Jahrbuch fur Mineralogie. Abhandlungen, 149, 65-90.

TALKINGTON, R. W., WATKINSON, D. H., WHITTAKER, P. J. & JONES, P. C. 1984. Platinum-group minerals and other solid inclusions in chromite of ophiolitic complexes: occurrence and petrological significance. Tschermaks Mineralogische und Petrografische Mitteilungen, 32, 285-301.

TARKIAN, M. & PRICHARD, H. M. 1987. Irarsite-hollingworthite solid-solution series and other associated Ru-, Os-, Ir-, and Rh-bearing PGM's from the Shetland Ophiolite Complex. Mineralium Deposita, 22, 178-184.

TAYLOR, H. P. jr. 1980. The effects of assimilation of country rocks by magmas on $^{18}O/^{16}O$ and $^{87}Sr/^{86}Sr$ systematics in igneous rocks. Earth and Planetary Science Letters, 47, 243-254.

THAYER, T. P. 1960. Some critical differences between alpine-type and stratiform peridotite-gabbro complexes. 21st International Geological Congress, Copenhagen 13, 247-259.

THAYER, T. P. 1963. Flow layering in alpine peridotite-gabbro complexes. Mineralogical Society of America Special Paper 1, 55-61.

THAYER, T. P. 1964. Principal features and origin of podiform chromite deposits, and some observations on the Guleman-Soridag district, Turkey. Economic Geology, 59, 1497-1524.

THAYER, T. P. 1969. Gravity differentiation and magmatic re-emplacement of podiform chromite deposits. Economic Geology Monographs, 4, 132-146.

THOMPSON, R. N., MORRISON, M. A., HENDRY, G. L. & PARRY, S. J. 1984. An assessment of the relative roles of crust and mantle in magma genesis: an elemental approach. Philosophical Transactions of the Royal Society of London, A310, 541-590.

TURCOTTE, D. L. & AHERN, J. L. 1978. A porous flow model for magma migration in the asthenosphere. Journal of Geophysical Research, 83, 767-772.

VIOLETTE, J.-F. 1980. Structure des ophiolites des Philippines (Zambales et Palawan) et de Chypre. Ecoulement asthénosphérique sous les zones d'expansion océaniques. Thèse Doc. 3° cycle, Université de Nantes, 152 p.

VOGT, P. R. & JOHNSON, G. L. 1975. Transform faults and longitudinal flow below the midocean ridge. Journal of Geophysical Research, 80, 1399-1428.

WAGER, L. R., BROWN, G. M. & WADSWORTH, W. J. 1960. Types of igneous cumulates. Journal of Petrology, 1, 73-85.

WAKITA, H., REY, P. & SCHMITT, R. A. 1971. Abundances of the 14 rare-earth elements and 12 other trace-elements in Apollo 12 samples: five igneous and one breccia rocks and four soils. Proceedings of the 2nd Lunar Science Conference, 1319-1329.

WALCOTT, R. I. 1969. Geology of the Red Hill Complex, New Zealand. Transactions of the Royal Society of New Zealand, Earth Sciences, 7, 57-88.

WALTHER, J. V. & ORVILLE, P. M. 1983. The extraction-quench technique for determination of the thermodynamic properties of solute complexes: application to quartz solubility in fluid mixtures. American Mineralogist, 68, 731-741.

WALTHER, J. V. & WOOD, B. J. 1984. Rate and mechanism in prograde metamorphism. Contributions to Mineralogy and Petrology, 88, 246-259.

WASSERBURG, G. J. & DePAOLO, D. J. 1979. Models of earth structure inferred from neodymium and strontium isotopic abundances. Proceedings of the National Academy of Sciences, 76, 3594-3598.

WATSON, E. B. 1982. Melt infiltration and magma evolution. Geology, 10, 236-240.

WEERTMAN, J. 1972. Coalescence of magma pockets into large pools in the upper mantle. Geological Society of America Bulletin, 83, 3531-3632.

WENDLANDT, R. F. 1982. Sulfide saturation of basalt and andesite melts at high pressures and temperatures. American Mineralogist, 67, 877-885.

WESTRICH. H. R. & HOLLOWAY, J. R. 1981. Experimental dehydration of pargasite and calculation of its entropy and Gibbs energy. American Journal of Science, 281, 922-934.

WHITE, W. M. & PATCHETT, J. 1984. Hf-Nd-Sr and incompatible element abundances in island arcs: implications for magma origins and crust-mantle evolution. Earth and Planetary Science Letters, 67, 167-185.

WILLIAMS, H. 1971. Mafic-ultramafic complexes in western Newfoundland Appalachians and the evidence for their transportation: a review and interim report. In: A Newfoundland Decade, Geological Association of Canada Proceedings, 24, 9-25.

WILLIAMS, H. 1973. Bay of Islands map-area, Newfoundland. Geological Survey of Canada Paper 72-34.

WILLIAMS, H. 1979. Appalachian Orogen in Canada. Canadian Journal of Earth Sciences, Tuzo Wilson Volume, 16, 792-807.

WILLIAMS, H. & CAWOOD, P. A. 1989. Geology, Humber Arm Allochthon, Newfoundland. Geological Survey of Canada, Map 1678A, scale 1:250000.

WILLIAMS, H. & MALPAS, J. 1972. Sheeted dikes and brecciated dike rocks within transported igneous complexes, Bay of Islands, western Newfoundland. Canadian Journal of Earth Sciences, 9, 1216-1229.

WILLIAMS, H. & SMYTH, W. R. 1973. Metamorphic aureoles beneath ophiolite suites and Alpine peridotites: tectonic implications with west Newfoundland examples. American Journal of Science, 273, 594-621.

WILSHIRE, H. G. 1984. Mantle metasomatism: the REE story. Geology, 12, 395-398.

WILSHIRE, H. G. 1987. A model of mantle metasomatism. In: MORRIS, E. M. & PASTERIS, J. D. (eds.), Mantle Metasomatism and Alkaline Magmatism. Geological Society of America Special Paper 215, 47-60.

WILSHIRE, H. G. & JACKSON, E. D. 1975. Problems in determining mantle geotherms from pyroxene compositions of ultramafic rocks. Journal of Geology, 83, 313-329.

WILSHIRE, H. G. & KIRBY, S. H. 1989. Dikes, joints, and faults in the upper mantle. Tectonophysics, 161, 23-31.

WILSHIRE, H. G. & PIKE, J. E. N. 1975. Upper-mantle diapirism: evidence from analogous features in alpine peridotite and ultramafic inclusions in basalt. Geology, 3, 467-470.

WILSHIRE, H. G., PIKE, J. E. N., MEYER, C. E. & SCHWARZMAN, E. C. 1980. Amphibole-rich veins in lherzolite xenoliths, Dish Hill and Deadman Lake, California. American Journal of Science, 280-A, 576-593.

WILSON, G. D. 1955. A new method for the determination of ferrous iron in rocks and minerals. Bulletin of the Geological Survey of Great Britain, 9, 56-58.

WILSON, J. T. 1966. Did the Atlantic close and then re-open? Nature, 211, 676-681.

WOOD, B. J. & VIRGO, D. 1989. Upper mantle oxidation state: ferric iron contents of lherzolite spinels by ^{57}Fe Mössbauer spectroscopy and resultant oxygen fugacities. Geochimica et Cosmochimica Acta, 53, 1277-1291.

WOOD, D. A. 1979. A variably veined suboceanic upper mantle - genetic significance for mid-ocean ridge basalts from geochemical evidence. Geology, 7, 499-503.

WOOD, S. A. 1987. Thermodynamic calculations of the volatility of the platinum group elements (PGE): the PGE contents of fluids at magmatic temperatures. Geochimica et Cosmochimica Acta, 51, 3040-3050.

WYLLIE, P. J. 1987. Metasomatism and fluid generation in mantle xenoliths. In: NIXON, P. H. (ed.), Mantle Xenoliths. Wiley, Chichester, 609-621.

WYLLIE, P. J. & SEKINE, T. 1982. The formation of mantle phlogopite in subduction zone hybridization. Contributions to Mineralogy and Petrology, 79, 375-380.

YODER, H. S. jr. 1967. Spilites and serpentinites. Carnegie Institution of Washington Year Book 65, 269-279.

YODER, H. S. jr. 1976. Generation of Basaltic Magma. National Academy of Sciences, Washington, D.C., 265 p.

YODER, H. S. jr. & TILLEY, C. E. 1962. Origin of basaltic magmas: an experimental study of natural and synthetic rock systems. Journal of Petrology, 3, 342-532.

ZEN, E-an. 1972. Gibbs free energy, enthalpy, and entropy of the rock-forming minerals: calculations, discrepancies, implications. American Mineralogist, 57, 524-553.

Appendix 1

ANALYTICAL METHODS

A1.1 MINERAL ANALYSES

Silicate minerals were analysed at Dalhousie University using a JEOL 733 automated electron microprobe. Spinels were analysed at Memorial University using a JEOL JXA-50A automated electron microprobe. Both machines utilize wavelength dispersive spectrometers.

Operating conditions for the JEOL 733 electron microprobe were 15 kV accelerating voltage, 5 nA beam current, 10 μm diameter electron beam, and 40 seconds counting time for each element. Data was reduced with a Tracor Northern data processor using ZAF matrix correction. Only one calibration was required for all silicates analysed, which was based on natural mineral standards and Cr metal.

Operating conditions for the JEOL JXA-50A electron microprobe were 15 kV accelerating voltage, 22 nA beam current, 10 μm diameter electron beam, and 30 seconds counting time or 60000 counts for each element. Alpha corrections (Bence and Albee, 1968) were used in data reduction. Two calibrations were required because of the compositional variation of spinel in LALPP (high Cr#) and HALPPG (low Cr#); these were based on spinel standards

53IN8 (12.82 wt.% Al_2O_3, 49.31 wt.% Cr_2O_3) and SPIN-B (59.40 wt.% Al_2O_3, 8.05 wt.% Cr_2O_3), respectively, and other natural mineral standards and metals.

Accuracy and precision are reported in Table A1.1. Precision, measured as the coefficient of variation (COV), generally is < 6 %. The high COV of NiO and Cr_2O_3 in silicate standards, would appear to result from heterogeneity associated with the standard. Analyses of apparently homogeneous silicates in samples, give COV < 6 % for both these oxides. Two tests were undertaken to examine the poor accuracy of Cr_2O_3 indicated by analyses of the Cr-diopside standard: (i) the spinel standard 53IN8 at Dalhousie University was analysed using the same calibration as for Cr-diopside, and results were within ± 2 % of the accepted value; (ii) several grains of clinopyroxene in samples of LALPP were reanalysed at Memorial University, and excellent agreement was obtained. Hence, values of Cr_2O_3 appear both accurate and precise.

A1.2 WHOLE-ROCK MAJOR ELEMENT ANALYSES

A1.2.1 Preparation of Rock Powder

Samples selected for whole-rock analyses were trimmed to remove weathered surfaces, and broken into chips (< 10 mm diameter) using a steel jaw crusher. Chips were washed, dried, and ground in an agate puck mill for at least 6 minutes until a fine powder was obtained. This powder was used for all whole-rock analyses. The use of agate for grinding should not produce

measurable contamination (Hickson and Juras, 1986).

A1.2.2 Samples Analysed at Memorial University

Major element analyses were obtained by atomic absorption spectrophotometry using a Perkin-Elmer digitized spectrophotometer at Memorial University. Samples were prepared for analysis using the following procedure. Add 5 ml concentrated HF to 0.1000 g of rock powder in a digestion flask. Tightly cover and heat for 30 minutes on a steam bath (residue should be white). Remove from heat, cool, and add exactly 50 ml saturated boric acid solution. Place back on steam bath until solution is clear. Remove, cool, add exactly 145 ml distilled H_2O, cover and shake. This solution is treated with lanthanum oxide solution for the determination of CaO and MgO. FeO was determined by dissolving rock powder in HF and ammonium metavanadate, adding ferrous ammonium sulphate, and titrating the solution against potassium dichromate (Wilson, 1955); Fe_2O_3 = Fe_2O_3(total) - (1.1114 x FeO). P_2O_5 was determined by calorimetry. Loss on ignition (LOI) was determined after heating a known amount of rock powder at about 1000°C for 2-3 hours. Accuracy and precision are given in Table A1.2. Values of 0.42 wt.% Al_2O_3 were obtained for USGS peridotite standard PCC-1 by this method, which are much lower than the accepted value of 0.67 wt.% from Govindaraju (1989). This low yield of Al_2O_3 resulted from incomplete dissolution of spinel, even when the rock powder was treated with aqua regia.

A1.2.3 Samples Analysed at the Department of Mines and Energy

In order to determine Al_2O_3, samples were analysed by atomic absorption spectrophotometry at the Mineral Development Division of the Department of Mines and Energy, Government of Newfoundland and Labrador. Samples were prepared using the following procedure. Place rock powder (0.1000 g) in a graphite crucible and mix with 0.5 g $LiBO_2$. Fuse mixture for 1 hour at 1000°C and transfer to a digestion bottle containing 25 ml 4 % HCl and 5 ml concentrated HF. Place bottle in steam bath at 90°C for 1.5 hours, remove, add 50 ml saturated boric acid solution, and return to steam bath for a further 1.5 hours. Cool and make up to volume.

Values of Al_2O_3 are very accurate and precise (Table A1.2). Standard PCC-1 was analysed by both methods and excellent agreement was obtained for all oxides except Al_2O_3. Consequently, the incomplete dissolution of spinel has relatively little effect on concentrations of major element oxides except Al_2O_3.

A1.3 WHOLE-ROCK TRACE ELEMENT ANALYSES

Trace element analyses were obtained on pellets of pressed powdered sample (10 g sample, 1.45 g Bakelite brand phenolic resin binder) using a Philips PW1450 X-ray fluorescence spectrometer at Memorial University. TiO_2, Sc, V, Cr, Ni, Cu and Zn were determined using the TRACE2 program, whilst Rb, Sr, Y and Zr were determined using the TRACE4 program.

Accuracy and precision are given in Table A1.3. Problems exist with the determination of Cu, as there are Cu-bearing components in the Philips machine. For this reason, Cu values are reported solely for the purpose of comparing Cu-rich and -poor samples, and the data are not considered quantitative.

A1.4 WHOLE-ROCK RARE EARTH ELEMENT ANALYSES

A1.4.1 Sample Preparation

The REE were analysed using the SCIEX ELAN inductively coupled plasma-mass spectrometer (ICP-MS) at Memorial University. Sample solutions of peridotite, pyroxenite and gabbro were prepared by dissolution of rock powders in a clean laboratory. Several dissolution procedures were used. The procedure adopted depended on the predicted concentrations of REE in a sample, which was based on mineral analyses and whole-rock major and trace element analyses. FEP teflon beakers and double-distilled reagents were used for all procedures. Dissolutions for procedures 1, 2 and 3 were carried out in teflon beakers on a hot plate at low heat. Samples were covered at all stages during the dissolution procedure, except during evaporation. Sample solutions were always evaporated slowly over a period of 2-3 days. The quartz and pyrex columns used for cation exchange were packed with CG120 Amberlite (200 mesh) cation exchange resin. The resin was in the chloride or nitrate form for HCl or HNO_3 separation of the REE, respectively. All sample solutions

analysed by ICP-MS were calibrated by standard addition, which involved splitting the sample solution. The first split was composed of sample solution (9 g) and 0.2 N HNO_3 (1 g); the second split was composed of sample solution (9 g) and mixed spike solution (1 g).

A1.4.1a Procedure 1 (ICP-MS Runs 116 and 153)

This procedure was adopted for the most depleted samples. To the rock powder (1.00000 ± 0.1 g) add several drops of 6.0 N HCl to test for the presence of carbonate, then dissolve in a mixture of ≤3 ml 8.0 N HNO_3, 10 ml HF and 2-3 ml $HClO_4$, and evaporate. Add 1-2 ml HF and 2-3 ml 8.0 N HNO_3, and evaporate. Dissolve residue in 2 ml 8.0 N HNO_3, evaporate and repeat. Dissolve residue in ≤5 ml 2.5 N HCl and filter onto a quartz column whilst rinsing with ≤3 ml 2.5 N HCl. Flush the column with 20 ml 2.5 N HCl and discard filtrate. Refill column with 100 ml 6.0 N HCl, collect filtrate and evaporate. Take up residue in a minimum amount of 8.0 N HNO_3 and evaporate. Dissolve residue in 0.2 N HNO_3 and make sample solution up to 20.0 ± 0.1 g with 0.2 N HNO_3. The approximate concentration of sample in solution is 50 g/l.

During dissolution of the rock powder, a poorly soluble gel-like material formed; this may have been a fluoride complex. With continued acid digestion and evaporation the gel dissolved. Opaque grains and a rare transparent gel remained as residues in the filter paper during loading of the sample solution onto the column. The effect of these residua on the concentrations of REE in

the final sample solution is presently unknown. The dominant residue was spinel, which is unlikely to have affected whole-rock concentrations of REE, as it has the lowest concentrations of REE of minerals found in ultramafic rocks (Stosch, 1982). However, spinel does contain silicate inclusions which may contain significant concentrations of REE. It is assumed that because rock samples were crushed and ground to a very fine powder, the majority of inclusions were dissolved. The incomplete dissolution of spinel will affect the computed absolute concentrations of REE in a sample, as the actual weight of sample dissolved is less than that weighed initially, which is the weight used in computation.

A1.4.1b Procedure 2 (ICP-MS Run 240)

Procedure 2 (D. Scott, pers. comm., 1989) was used for samples similar in composition to those prepared by procedure 1. To the rock powder (0.5 g) add 3 ml HF and 4 ml 8.0 N HNO_3, and evaporate. Add 4 ml 8.0 N HNO_3 and 4 ml 6.0 N HCl, and evaporate. Add 4 ml 8.0 N HNO_3, dry and repeat. Dissolve residue in 5 ml 1.5 N HNO_3, filter with washing, and evaporate. Dissolve residue in 2 ml 1.5 N HNO_3, load onto a quartz column, flush with 45 ml 1.5 N HNO_3, discard filtrate, flush with 23 ml 8.0 N HNO_3, collect filtrate and evaporate. Dissolve residue in 2 ml 2.5 N HCl, load onto a quartz column, flush with 5 ml 2.5 N HCl, discard filtrate, flush with 25 ml 6.0 N HCl, collect filtrate, evaporate, take up residue in a minimum amount of 0.2 N HNO_3, and make sample solution up to 50 g with 0.2 N HNO_3. The approximate

concentration of sample in solution is 10 g/l.

A1.4.1c Procedure 3 (ICP-MS Run 182)

Procedure 3 (P. Moore, pers. comm., 1989) was adopted for samples relatively enriched in REE. Dissolve the rock powder (0.2 g) in HF, 6.0 N HCl and $HCLO_4$ (2 ml, 3 ml and 1 drop, respectively), evaporate, add 6.0 N HCl, evaporate, and dissolve residue in 5-8 ml 2.5 N HCl. Filter onto a pyrex column and rinse filter paper with 2.5 N HCl. Flush the column with 20 ml 2.5 N HCl, discard filtrate, flush column with 120 ml 6.0 N HCl, retain filtrate, and evaporate. Repeat the column procedure to clean up the sample. Add and evaporate 10 ml 8.0 N HNO_3, dissolve residue in 0.2 N HNO_3, and make sample solution up to 20 g with 0.2 N HNO_3. The approximate concentration of the sample in solution is 10 g/l.

A1.4.1d Procedure 4 (ICP-MS Run 024)

This procedure was used for samples richest in REE, and as a comparison for samples whose concentrations of REE were determined using procedures 1, 2 and 3. Mix rock powder (0.2 g) and Na_2O_2 (0.8 g) in a 30 ml Ni crucible, place in an oven for 1 hour at 480-490°C, remove and allow to cool for 15 minutes. Very slowly add H_2O until effervescence ceases. Wash cake and solution into a teflon centrifuge tube. Centrifuge for 10 minutes at high speed, decant and discard liquid, add $\leq$5 ml H_2O, stir with a teflon rod, and repeat. Centrifuge for 10 minutes, decant and discard liquid, pour sinter and cake into

a 125 ml teflon bottle, add 2.0 ml 8.0 N HNO_3 and shake vigorously. Rinse Ni crucible with 0.5 ml 8.0 N HNO_3 and add washings to the bottle. Stir sample solution with a teflon rod and filter if sample solution contains residue. Make up to 90.0 g with H_2O. The approximate concentration of sample in solution is 2 g/l.

A1.4.2 Limits of Detection (LOD)

Limits of detection (Table A1.4a) are $\leq$0.01 x chondrite (runs 116 and 153), $\leq$0.02 x chondrite (run 240), $\leq$0.05 x chondrite (run 182) and $\leq$0.4 x chondrite (run 024).

A1.4.3 Blank

Blank solutions were prepared in exactly the same way as sample solutions, except that no 'sample' was used. The composition of the blank generally lies at or below the LOD for runs 116, 153, 240 and 024, but significantly above the LOD for run 182 (Table A1.4a). The influence of the blank on sample data is discussed below.

A1.4.4 Precision

Based on duplicate analyses of samples in a given run, the COV is 7-40 % for runs 116, 153 and 240, and 2-4 % for runs 024 and 182 (Table 1.4b). Within a given run, precision of CNREE patterns is good (Fig. A1.1).

The COV for USGS basalt standard BCR-1, for one determination in each

of runs 182 and 024, ranges from 0.1 % (Yb) to 6 % (La and Ce) (Table A1.4c). The precision of CNREE patterns of a given sample analysed in both these runs is good, except for concentrations of La below chondrite (Fig. A1.1). The COV for PCC-1, for one determination in each of runs 116, 153 and 240, ranges from 4 % (La) to 64 % (Tb) (Table A1.4d). These values are reflected in the CNREE patterns of PCC-1 (Fig. A1.2), and suggest that HREE are more susceptible to sample preparation procedure and operating conditions of the ICP-MS, than are LREE.

A1.4.5 Accuracy

Standards BCR-1 and PCC-1 were analysed to determine the accuracy of the sample preparation procedures and the subsequent analyses. The results for BCR-1 indicate that although yields of REE are somewhat lower than accepted, CNREE patterns will be consistent with the accepted pattern (Table A1.4c). Run 024 is more accurate than run 182 at the REE concentrations found in BCR-1.

The accuracy of concentrations of REE in PCC-1 are difficult to ascertain, as the concentrations of REE in this standard are not known to better than ± 10 % (Frey, 1984). The best way to examine the quality of the data is on CNREE diagrams. The CNREE patterns of PCC-1 determined in runs 116, 153 and 240, consistently exhibit U-shaped patterns, but analyses from these runs lie at the lower end of, or out of, the range of REE values published for PCC-1 (Table A1.4d; Fig. A1.2). High La values in PCC-1 result from laboratory

contamination. The CNREE patterns arising from this study have a shallower U-shape than those published. The problem of yield is most prevalent for Tm, Yb and Lu, especially in runs 116 and 153, but loss of HREE may occur over the range Ho-Lu. In order to test for HREE loss in samples analysed in runs 116, 153 and 240, PCC-1 and some of these samples were analysed using procedure 4 and run 024. Ytterbium values obtained in run 024 are as much as 2-3 times higher than Yb values obtained in runs 116, 153 and 240. Extrapolation of the slope Ho-Er on CNREE diagrams, predicts Yb and Lu values in close agreement with those determined in run 024. With the exception of PCC-1, this generally also applies for CNREE patterns of samples for extrapolation of the slope Gd-Dy. The slope Gd-Dy is more reliable than the slope Ho-Er, due to the possible loss of HREE over the range Ho-Lu. Hence, in cases where Tm, Yb and Lu deviate significantly from the trend defined by the slope Gd-Dy (and Ho-Er), it is likely that there has been a major loss of Tm, Yb and Lu. The CNREE patterns of samples where this is observed are treated with caution, as Tm-Lu have been selectively lost with respect to the other REE. Ytterbium and Lu values from run 240 are probably more representative of true values than are those obtained from runs 116 and 153.

The description and discussion of CNREE patterns in chapters 3, 4 and 5 are based on uncorrected patterns, bearing in mind the HREE trend defined by the slope Gd-Dy. Unfortunately, it was not possible to check LREE values, as procedure 4 and run 024 are not sensitive enough for these elements at low concentrations. However, LREE trends of CNREE patterns generally are smooth

and any breaks in the pattern are explained in terms of the mineralogy of a sample. Consequently, it is not possible to predict the relative loss of individual REE throughout the series, and the data cannot be corrected. In summary, despite the apparent overall loss of the REE and the lower yield of Tm, Yb and Lu with respect to all other REE, the values obtained for REE in runs 116, 153 and 240 are representative of concentrations of REE in a given sample.

A1.4.6 Influence of the Blank Composition on Sample Data

As previously mentioned, the concentrations of REE in the blank are significantly above the LOD in run 182 (Fig. A1.3). The concentrations of La and Ce in the blank for run 024 are also well above the LOD (Fig. A1.3). The blanks are enriched in LREE relative to HREE. In order to test for a blank signature in a sample, REE data are compared for blank and sample. The LAL clinopyroxenite sample L213 is used as an example; comparison of Figures A1.1 and A1.3 for run 182, shows that La, Ce and Pr lie at or below the composition of the blank, and that the Ce anomalies are inconsistent. Likewise for run 024, La and Ce lie at or below the blank composition, and the trends of the La-Ce slopes in the blank and sample oppose one another. There is obvious inconsistency between CNLREE patterns of sample and blank, and the occurrence of samples with LREE abundances less than those of their associated blank. Even the disagreement between the sample data for La, Ce and Pr from runs 182 and 024 cannot be explained by the abundances of REE in the blanks.

Unlike the procedure used to analyse the PGE (see section A1.5), no 'sample' was used in preparation of blanks for REE analysis. The problem with the REE blank is that solution chemistry throughout a given procedure will likely be different when a sample is present compared to when it is not. Therefore, the blank may not be representative of the blank associated with a sample. This manifests itself in situations where concentrations of REE in a sample fall below those of their blank, and where samples have CNREE patterns which are inconsistent with those of their blank. In this situation it becomes meaningless to subtract the composition of the blank from the sample data, because it is not possible to quantify the component of the blank in the sample data. Consequently, REE data for samples from the Springers Hill area have not been corrected for the blank. Sample analyses where the blank is thought to interfere are indicated in parentheses in Table A4.2.

At this time it is difficult to assess the involvement of the blank in samples analysed in runs 116, 153 and 240. However, in Table A4.2, values from these runs which lie at or below the LOD, or appear to contain a component of the blank, are placed in parentheses. These analyses are plotted in CNREE diagrams, as they are consistent with the overall CNREE pattern of a sample (see chapters 3, 4 and 5).

A1.5 WHOLE-ROCK PLATINUM GROUP ELEMENT ANALYSES

The PGE were analysed using the SCIEX ELAN ICP-MS at Memorial University. Samples were prepared by fusing a mixture of rock powder (15.0 g), Ni carbonyl (9.6 g), S (6.0 g), Na_2CO_3 (18.0 g), $Na_2B_4O_7$ (36.0 g) and SiO_2 (15.0 g) in a clay crucible at 1000°C for 1.25 hours to produce a NiS button. This button was dissolved in HCl and the PGE were collected by Te precipitation (Jackson et al., 1990). Blanks were prepared in the same way as samples, except that an additional 15.0 g of SiO_2 was used in place of rock powder.

Accuracy and precision of PGE analyses vary widely, but are good for Pd and Ir (Table A1.5). The average blank composition has been subtracted from all sample analyses (Appendix 4), in order to remove the effects of contamination from samples having low concentrations of PGE. Prior to correction, samples low in Pd and Ir exhibited Pd/Ir ratios biased by the blank component. Some corrected values lie at or below the LOD, but these are still considered because they were above the LOD before correction.

Appendix 2

SAMPLES ANALYSED

A2.1 GENERAL STATEMENT

All samples contain spinel, with the exception of some HAL olivine clinopyroxenites and gabbros. Abbreviations are in parentheses.

A2.2 LOW-Al PERIDOTITES AND PYROXENITES (LALPP)

SJE-L097	Harzburgite (H).
SJE-L103	Harzburgite containing Ca-amphibole (H).
SJE-L106	Harzburgite containing an introduced component of type I orthopyroxenite (H).
SJE-L157	Harzburgite (H).
SJE-L173	Harzburgite containing Ca-amphibole and phlogopite (H).
SJE-L218	Harzburgite containing clinopyroxene and Ca-amphibole (H); 2.4 m from clinopyroxenite (L211-L214).
SJE-L225	Harzburgite (H).
SJE-L263	Harzburgite (H).
SJE-L264	Harzburgite (H).
SJE-L153	Harzburgite (H) cut by vein of type I orthopyroxenite (OI).
SJE-L193	Harzburgite (H)-dunite (D) contact.
SJE-L226	Harzburgite band (H) in dunite (D).
SJE-L336	Harzburgite (H)-amphibole dunite (AD) contact.
SJE-L143	Spinel-rich dunite (D).
SJE-L162	Spinel-rich dunite (D).

SJE-L254 Dunite containing orthopyroxene and clinopyroxene (D) from dunite envelope around clinopyroxenite (C).
SJE-L262 Dunite containing Ca-amphibole (D).

SJE-L050 Spinel-rich dunite envelope (D) around clinopyroxenite (C).
SJE-L053 Spinel-rich dunite (D)-olivine clinopyroxenite (C) contact.
SJE-L054 Extensively serpentinized spinel-rich dunite from dunite envelope (D) around clinopyroxenite (C).
SJE-L055 Spinel-rich dunite (D)-olivine clinopyroxenite (C) contact.
SJE-L176 Spinel-rich dunite (D) in type I orthopyroxenite (OI).
SJE-L199 Spinel-rich dunite (D) in clinopyroxenite (C).
SJE-L216 Spinel-rich dunite containing orthopyroxene, clinopyroxene and Ca-amphibole (D); 0.2 m from clinopyroxenite (L211-L214).
SJE-L217 Dunite containing orthopyroxene (D); 0.9 m from clinopyroxenite (L211-L214).
SJE-L246 Dunite envelope (D) around chromitite (CR); 0.4 m from massive chromitite (L244 and L245).

SJE-L130 Chromitite vein (CR).
SJE-L161 Chromitite schlieren (CR).
SJE-L203 Massive chromitite from Springers Hill chromite showing (CR).
SJE-L244 Massive chromitite (CR).
SJE-L245 Massive chromitite (CR).
SJE-L289 Massive chromitite (CR).

SJE-L125 Amphibole dunite (AD).
SJE-L129 Amphibole dunite (AD).
SJE-L132 Amphibole dunite (AD).
SJE-L140 Amphibole dunite (AD).
SJE-L148 Amphibole dunite (AD).
SJE-L172 Amphibole dunite (AD).
SJE-L200 Amphibole dunite (AD).
SJE-L265 Amphibole dunite (AD) replacing type I orthopyroxenite (OI).
SJE-L266 Amphibole dunite (AD) replacing type I orthopyroxenite (OI).
SJE-L275 Amphibole dunite (AD) replacing type I orthopyroxenite (OI).

SJE-L066 Type I orthopyroxenite (OI).
SJE-L067 Type I orthopyroxenite (OI).
SJE-L068 Type I orthopyroxenite (OI).
SJE-L071 Type I orthopyroxenite (OI).
SJE-L073 Type I orthopyroxenite mylonite from dyke margin (OI).

SJE-L267 Type I orthopyroxenite (OI).
SJE-L268 Type I orthopyroxenite (OI).
SJE-L286 Type I orthopyroxenite (OI).

SJE-L271 Type II orthopyroxenite (OII); web texture in olivine matrix.
SJE-L351 Type II orthopyroxenite (OII); ribbon mylonite.

SJE-L004 Olivine clinopyroxenite (C).
SJE-L012 Olivine clinopyroxenite (C).
SJE-L026 Clinopyroxenite and olivine clinopyroxenite (C).
SJE-L211 Clinopyroxenite (C).
SJE-L212 Clinopyroxenite (C).
SJE-L213 Clinopyroxenite (C).
SJE-L214 Olivine clinopyroxenite containing shear bands (C).
SJE-L231 Olivine clinopyroxenite (C).
SJE-L293 Clinopyroxenite (C).

SJE-L069 Websterite (WB); orthopyroxenes are xenocrysts.
SJE-L283 Websterite (WB); orthopyroxenes are xenocrysts.
SJE-L288 Websterite (WB); orthopyroxenes are xenocrysts.
SJE-L290 Websterite containing mutual exsolution intergrowths of clinopyroxene and orthopyroxene (included in definition of clinopyroxenite (C)).

SJE-L201 Wehrlite (W).

A2.3 HIGH-Al PERIDOTITES, PYROXENITES AND GABBROS (HALPPG)

SJE-L107 Dunite (D).
SJE-L108 Dunite (D).
SJE-L229 Spinel-rich dunite (D).
SJE-L298 Dunite (D).
SJE-L299 Spinel-rich dunite (D).
SJE-L302 Spinel-rich dunite (D).
SJE-L305 Clinopyroxene, plagioclase dunite (D).
SJE-L324 Dunite (D).
SJE-L350 Layered dunite (D).

SJE-L093 Wehrlite (W).
SJE-L109 Plagioclase wehrlite (W).
SJE-L114 Wehrlite containing Ca-amphibole (W).
SJE-L301 Spinel-rich wehrlite containing plagioclase and Ca amphibole (W).
SJE-L307 Wehrlite (W).
SJE-L316 Plagioclase wehrlite (W).
SJE-L317 Wehrlite (W).
SJE-L331 Plagioclase wehrlite (W).

SJE-L310 Plagioclase wehrlite (W)-olivine clinopyroxenite (C) contact.
SJE-L315 Wehrlite (W)-clinopyroxenite (C) contact.

SJE-L186 Olivine clinopyroxenite (C).
SJE-L241 Olivine clinopyroxenite (C).
SJE-L296 Olivine clinopyroxenite (C).
SJE-L297 Olivine clinopyroxenite (C).
SJE-L303 Plagioclase, olivine clinopyroxenite (C).
SJE-L312 Plagioclase, olivine clinopyroxenite (C).
SJE-L349 Olivine clinopyroxenite (C).

SJE-L309 Interbanded wehrlite and gabbro in dyke (WG).
SJE-L314 Interbanded wehrlite and gabbro in dyke (WG).

SJE-L090 Gabbro (G).
SJE-L294 Olivine gabbro mylonite (G).
SJE-L295 Clinopyroxene troctolite (G).
SJE-L313 Gabbro (G).

SJE-L273 Amphibole peridotite (AP).

A2.4 LALPP-HALPPG CONTACT RELATIONS AND REACTIONS ZONES

SJE-L115 Harzburgite (H) cut by vein of HAL olivine clinopyroxenite (C).
SJE-L177 Harzburgite (H) cut by vein of HAL clinopyroxenite (C).
SJE-L221 Harzburgite (H)-HAL clinopyroxene dunite (D) contact.
SJE-L274 Harzburgite mylonite (H) and type I orthopyroxenite (OI) cut by HAL amphibole peridotite (AP).
SJE-L327 Harzburgite xenolith (H-X) in HAL olivine clinopyroxenite (C).
SJE-L328 Harzburgite xenolith (H-X) in HAL olivine clinopyroxenite (C).

SJE-L329 Dunite xenolith (D-X) in HAL olivine clinopyroxenite (C).
SJE-L330 Dunite xenolith (D-X) in HAL olivine clinopyroxenite (C).

SJE-L326 Chromitite xenolith (CR-X) in HAL olivine clinopyroxenite (C).

SJE-L333 Type I orthopyroxenite (OI)-HAL Ca-amphibole wehrlite (W) contact, with development of amphibole dunite (AP).
SJE-L348 Type I orthopyroxenite (OI)-HAL dunite (D) contact, with development of clinopyroxene (C).

SJE-L234 Olivine clinopyroxenite reaction front (C) 20 m from L231 and 20 m from L241.
SJE-L236 Olivine clinopyroxenite reaction front (C) 20 m from L231 and 20 m from L241.

A2.5 UNCORRELATED (UC)

SJE-L341 Amphibolite dyke (AMPT).
SD194 Amphibolite dyke (AMPT).
SD380 Amphibolite dyke (AMPT).

Appendix 3

MINERAL ANALYSES

A3.1 GENERAL STATEMENT

Mineral analyses of olivine, orthopyroxene, clinopyroxene, amphibole, plagioclase and spinel are presented in Tables A3.1 to A3.6, respectively. Analyses are tabulated in the sequence of LALPP, HALPPG, LALPP-HALPPG contact relations and reaction zones, and uncorrelated samples (see Appendix 2 for sample listing and abbreviations). 'Location' is the spot number and mineral analysed in a sample. With the exception of several very small grains, all analyses in Tables A3.1 to A3.6 are the average of 2-3 adjacent points in a mineral grain.

A3.2 CHEMICAL CLASSIFICATION OF THE SPRINGERS HILL AREA

The classification of samples as LALPP or HALPPG is based on spinels with high or low Cr#, respectively. This classification does not hold strictly for LALPP-HALPPG contact relations and reaction zones, because Cr-spinel may occur in HALPPG, and Al-spinel may occur in LALPP. In these situations, classification as LALPP or HALPPG is based on (i) the presence or absence of

orthopyroxene, (ii) deformation features, and (iii) chemistry of silicate minerals. No record in 'type' in Tables A3.1 to A3.6, indicates that it is not possible to assign to LALPF or HALPPG in this case.

A3.3 SPINEL ANALYSES

Sp* in 'location' for harzburgite in Table A3.6, indicates spinel is associated with Ca-amphibole ± phlogopite.

A3.3.1 Calculation of Fe^{3+} in Spinel

Calculated Fe^{3+} values from electron microprobe analyses of spinels are comparable to Fe^{3+} values determined by wet chemical techniques and Mössbauer spectroscopy (Osborne et al., 1981; McGuire et al., 1989; Wood and Virgo, 1989). Consequently, in Table A3.6, Fe^{3+} values of spinels are calculated from electron microprobe analyses, assuming charge balance and perfect stoichiometry of cations to O^{2-} in the ratio of 24:32 for the ideal spinel structure $A_8B_{16}O_{32}$. Cations (A and B) are not assigned to sites of tetrahedral or octahedral coordination because the degree of inversion of the spinel structure is not known.

Redox ratios calculated from electron microprobe analyses, with the assumption of ideal stoichiometry, tend to overestimate Fe^{3+} values (Osborne et al., 1981; Canil et al., 1990), but this is not too significant (Osborne et al., 1981).

Appendix 4

WHOLE-ROCK ANALYSES

Major and trace element analyses in wt.% and ppm, respectively, are tabulated in Table A4.1. Values of Cu are not quantitative.

Rare earth element analyses in ppb are tabulated in Table A4.2. Values in parentheses either are at or below the LOD, or appear to contain a component of the blank. Yb* and Lu* are values of Yb and Lu in extremely REE-depleted samples that were determined by procedure 4 and run 024. The chondrite values used for normalization are those of Wakita et al. (1971): 340 ppb La, 910 ppb Ce, 121 ppb Pr, 640 ppb Nd, 195 ppb Sm, 73 ppb Eu, 260 ppb Gd, 47 ppb Tb, 300 ppb Dy, 78 ppb Ho, 200 ppb Er, 32 ppb Tm, 220 ppb Yb and 34 ppb Lu.

Platinum group element analyses in ppb are tabulated in Table A4.3. The composition of the average blank has been subtracted from all analyses. The composition of this blank is: bdl Ru, 0.05 ppb Rh, 0.92 ppb Pd, 0.15 ppb Re, bdl Os, 0.03 ppb Ir and 0.33 ppb Pt. The chondrite values used for normalization are those compiled by Naldrett and Duke (1980): 690 ppb Ru, 200 ppb Rh, 545 ppb Pd, 514 ppb Os, 540 ppb Ir and 1020 ppb Pt.

Refer to Appendix 2 for sample listing and abbreviations.

Appendix 5

ORTHOPYROXENE IN HARZBURGITE

In Chapter 3, evidence was presented which suggested that some harzburgites contain an introduced component of OPXT I. In this appendix, the proportion of introduced OPXT I is estimated from values of CaO, Al_2O_3 and CaO/Al_2O_3 (Table A4.1), and Pd, Ir and Pd/Ir (Table A4.3). All values used in calculations have been recalculated to 100 wt.% on an anhydrous basis with all iron oxide as FeO. Sample L225 is a harzburgite residue from partial melting and complete removal of magma, whereas harzburgite sample L106 contains a component of OPXT I. Samples L225 and L106 have 15 and 45 modal % orthopyroxene, respectively. The proportions of residual harzburgite (represented by sample L225) and introduced OPXT I in sample L106 are estimated by simultaneous solution of equations of the form:

$xL225 + yOPXT = L106.$

(i) CaO and Al_2O_3

CaO $\quad 0.30x + 1.67y = 0.90$

Al_2O_3 $\quad 0.21x + 0.66y = 0.41$

Solving gives $x = 0.59397$ and $y = 0.43222$, but $x + y = 100$ % and $x = 57.9$ % and $y = 42.1$ %. Therefore, the composition of L106 is 58 % L225 and 42

% average OPXT I.

(ii) Pd and Ir

Pd $1.90x + 182.2y = 9.23$

Ir $3.22x + 3.57y = 5.38$

Solving gives $x = 1.63353$ and $y = 0.03362$, and therefore, the composition of L106 is 98 % L225 and 2 % average OPXT I.

(iii) Pd and Ir using OPXT I sample L071

Pd $1.90x + 16.6y = 9.23$

Ir $3.22x + 0.46y = 5.38$

Solving gives $x = 1.61783$ and $y = 0.37085$, and therefore, the composition of L106 is 81 % L225 and 19 % L071 (OPXT I).

Appendix 6

PUBLISHED MATERIAL RELEVANT TO THIS THESIS

Canadian Mineralogist
Vol. 28, pp. 537-552 (1990)

HARZBURGITES AND REFRACTORY MELTS IN THE LEWIS HILLS MASSIF, BAY OF ISLANDS OPHIOLITE COMPLEX: THE BASE-METALS AND PRECIOUS-METALS STORY

STEPHEN J. EDWARDS

Centre for Earth Resources Research, Department of Earth Sciences, Memorial University of Newfoundland, St. John's, Newfoundland A1B 3X5

ABSTRACT

The immobility of the platinum-group elements (*PGE*) during serpentinization enables these elements to provide important information on the history of ophiolite mantle. In the Springers Hill area, Lewis Hills Massif, Bay of Islands Ophiolite Complex, Newfoundland, a residuum of harzburgite and minor dunite is intruded successively by a suite of dunite ± chromite, orthopyroxenite and clinopyroxenite veins and dykes. These intrusive bodies represent crystal fractionates rather than liquid compositions. The fractionation sequence is typical of refractory melts such as boninites. Platinum-group minerals (*PGM*) and chondrite-normalized *PGE* patterns show that as the melt evolves, solid grains of Os-bearing laurite become entrapped in chromite, whereas solid Pt-Pd arsenide phases are incorporated in pyroxene. Consequently, the Pd-Ir value of the melt increases with progressive crystal fractionation, as the immiscible liquid phase changes from S-saturated to As-saturated. Harzburgites of residual origin have Pd Ir $<<1$. The Springers Hill harzburgites are *PGE*-enriched (Pd Ir 1.2–1.7), but otherwise possess residual characteristics arising from a minimum of 17% partial melting. Partial melting would have partitioned all sulfide in the source into the melt. Melt extraction was highly efficient, and no sulfide or silicate melt remained in the Springers Hill harzburgites. Therefore, *PGE* in the Springers Hill harzburgites are not present in sulfides. Field and petrographic evidence shows that enrichment of the *PGE* in Springers Hill harzburgites resulted from addition of an early-suite orthopyroxenite component (average Pd Ir 51). Orthopyroxene addition occurred by melt impregnation or mechanical mixing.

Keywords: Bay of Islands ophiolite, Newfoundland, harzburgite, dunite, chromite, pyroxenite, melt impregnation, platinum-group elements, base-metal sulfides

SOMMAIRE

L'immobilité des éléments du groupe du platine (*EGP*) pendant la serpentinisation permet l'utilisation de ces éléments pour déduire de l'information utile concernant le manteau à la base des ophiolites. Dans la région de Springers Hill, dans le massif de Lewis Hills de l'ophiolite de Bay of Islands, à Terre-Neuve, un résidu de harzburgite et de dunite accessoire est recoupé successivement par une suite de dunite ± chromite, orthopyroxénite et clinopyroxénite en veines et en filons. Ce cortège de roches intrusives comagmatiques représenterait des produits d'un fractionnement de cristaux plutôt que des compositions de liquides. La séquence de fractionnement est typique de celle suivant un magma résiduel, comme un magma boninitique. Les minéraux des *EGP* et les teneurs de ces éléments normalisées par rapport à une chondrite, montrent à mesure que le magma évoluait, des cristaux de laurite tenant de l'osmium ont été englobés par la chromite, tandis que les arséniures de Pt et de Pd ont été incorporés dans le pyroxène. Par conséquent, la valeur Pd-Ir du magma augmentait à mesure que progressait le fractionnement et que la phase liquide immiscible devenait saturée en As plutôt qu'en S. Dans les harzburgites résiduelles le rapport Pd Ir est beaucoup plus faible que 1. Les harzburgites de Springers Hill sont enrichies en *EGP* (1.2 < Pd Ir < 1.7), mais sont autrement typiquement résiduelles, ayant résulté d'un minimum de 17% de fusion partielle. Cette étape de fusion aurait causé tout sulfure disponible à la source à favoriser la phase liquide. L'extraction du liquide fondu aurait été très efficace, de telle sorte que ni liquide sulfuré, ni liquide silicaté ne restait dans la harzburgite. C'est donc dire que dans la harzburgite de Springers Hill, les *EGP* ne sont pas situés dans les sulfures. A la lumière des relations de terrain et de la pétrographie, l'enrichissement des *EGP* semble avoir accompagné l'addition d'une composante orthopyroxénitique, partie d'une suite précoce, qui avait, en moyenne, un rapport Pd Ir de 51. Cette fraction d'orthopyroxénite s'est ajoutée soit par imprégnation d'un liquide, soit par mélange mécanique.

(Traduit par la Rédaction)

Mots clés: ophiolite de Bay of Islands, Terre Neuve, harzburgite, dunite, chromite, pyroxénite, imprégnation d'un liquide, éléments du groupe du platine, sulfures des métaux de base

INTRODUCTION

It is now well established that stratiform complexes such as those of the Bushveld, Great Dyke and Stillwater are important hosts for the platinum-group elements (*PGE*); on the other hand, economic concentrations of these elements have yet to be found in ophiolite complexes, in spite of their close similarity to stratiform complexes. To date, there have been very few complete studies of the base- and precious-metal concentrations in an ophiolite section. Oshin & Crocket (1982, 1986) carried out the most thorough investigation, and focused on the ultramafic, gabbroic and volcanosedimentary sections of the Thetford Mines Ophiolite, Quebec.

This paper combines field, petrographic, and base- and precious-metal data in order to explain the occurrence and origin of base and precious metals in residual and magmatic lithologies of the Springers Hill area, Lewis Hills Massif, Bay of Islands Ophiolite Complex (BIOC), western Newfoundland. Emphasis is placed upon trends of magmatic fractionation defined by the *PGE*, and the use of these elements to document modifications to pyroxenite and peridotite mineralogy and chemistry.

Geological Setting and Field Relationships

On the western coast of Newfoundland, the Humber Arm Allochthon (Williams & Cawood 1989) of the Humber Zone (Williams 1979) preserves two ophiolite terranes: the BIOC and the Coastal Complex (CC). These adjacent terranes form an approximately north–south-trending zone some 100 km long and 25 km wide (Fig. 1). The CC lies to the west of the BIOC. The BIOC comprises four ophiolite massifs that, from north to south, crop out as the Table Mountain, North Arm Mountain, Blow Me Down Mountain and Lewis Hills massifs, respectively. The Lewis Hills is unique in that it preserves an original, subvertical contact between the CC to the west and BIOC to the east (Karson 1977, 1979, Karson & Dewey 1978). The BIOC formed at a spreading center (Casey *et al.* 1983, 1985), whereas the CC represents oceanic crust that has experienced a transform-

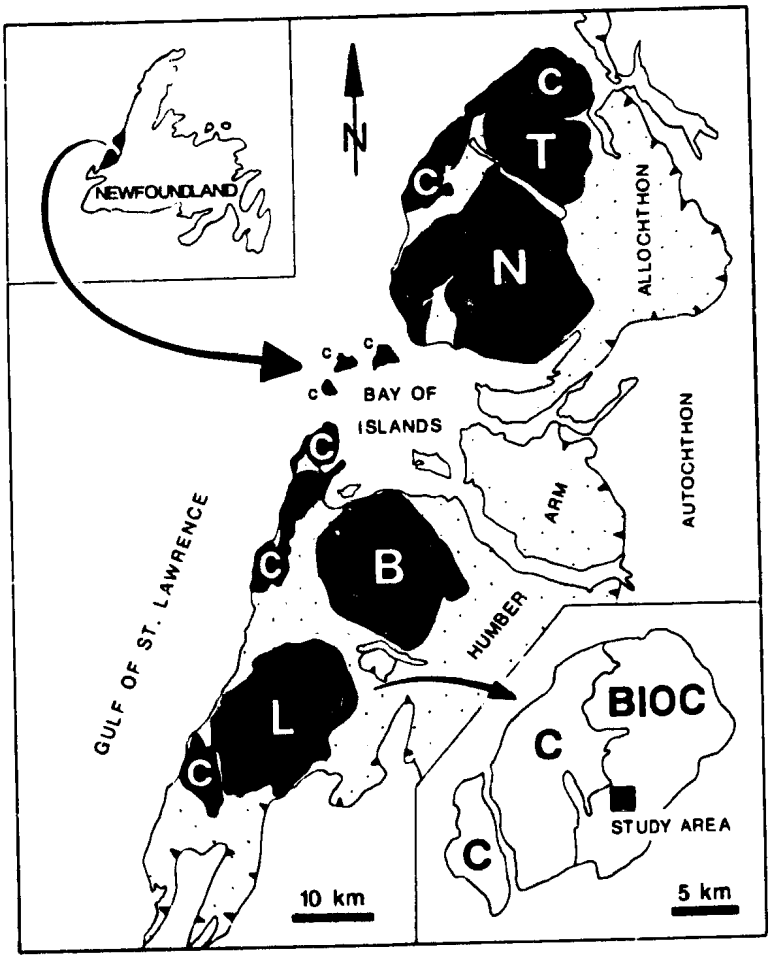

FIG. 1. Generalized geological map of the Humber Arm Allochthon (Williams & Cawood 1989). Geology of the Lewis Hills Massif is taken from Karson (1979). BIOC: Bay of Islands Ophiolite Complex, T: Table Mountain, N: North Arm Mountain, B: Blow Me Down Mountain, and L: Lewis Hills Massif; C stands for the Coastal Complex.

fault tectonic history within an oceanic fracture-zone (Karson & Dewey 1978, Karson 1984).

The Springers Hill area is located in the southern part of the Lewis Hills Massif, within the BIOC (Fig. 1). The area has been studied by Karson (1979), Dahl & Watkinson (1986), Dunsworth *et al.* (1986), Suhr & Calon (1987) and Edwards (1988a). Two magmatic suites are hosted within a harzburgite–dunite residuum (Edwards 1988a, b). The early suite is defined by successive intrusions of variably deformed dunite (with or without chromitite), orthopyroxenite and clinopyroxenite, as millimeter- to meter-wide veins and dykes lying parallel and subparallel to the plane of mantle flow defined by the tectonite fabric of the residuum. The order of crystallization among silicate minerals mimics the sequence of crystallization of melts derived from highly refractory mantle sources. The later suite is relatively undeformed, cropping out as a kilometer-sized body of dunite, wehrlite, clinopyroxenite and gabbro. The margin of the late suite cross-cuts the foliation defined by the residual tectonites and early-suite veins and dykes. This margin contains xenoliths of residuum and early-suite lithologies. The abundance of early-suite veins and dykes and the presence of the massive, late-suite intrusive body are unique to the Springers Hill area. In no other part of the BIOC has such a concentration of varied intrusive phases been observed in the mantle sequence. The late suite is not considered in this study; attention will focus on the origin and evolution of the residuum and early-suite lithologies.

The residual nature of the harzburgite is supported by the absence of clinopyroxene, presence of chromite, occurrence of porphyroclastic orthopyroxene with margins corroded to olivine, and occurrence of minor residual dunite. The latter is produced either by 35–45% partial melting of pyrolite (Jaques & Green 1980), or by reaction of peridotite with an introduced fluid, resulting in incongruent melting of orthopyroxene (*e.g.*, Dick 1977). In the Springers Hill area, residual dunites contain isolated grains of orthopyroxene and a chromite foliation and concentration similar to those in the adjacent harzburgite (Edwards 1987, 1988a). As the modal abundance of orthopyroxene decreases, harzburgite grades into residual dunite. Residual dunites are most easily recognized where they cross-cut the foliation of the harzburgite; remnants of the foliation they cross-cut are preserved. Massive bodies of pure harzburgite are rare owing to the presence of abundant early-suite veins and dykes.

Magmatic dunites are generally dyke-like in appearance, preserve a higher concentration of chromite than their harzburgite host, and parallel or cross-cut the harzburgite foliation. The margins of some magmatic dunites have residual characteristics. Chromitite bodies are always hosted in a dunite envelope.

The orthopyroxenite and clinopyroxenite bodies occur as coarse-grained to pegmatitic veins and dykes and their boudinaged equivalents. Both types of pyroxenite preserve magmatic textures such as olivine–pyroxene parallel growth, adcumulus texture and consertal intergrowth texture. The pyroxenites rarely occur together, and it is very rare for clinopyroxenite to intrude orthopyroxenite. Orthopyroxenites are hosted by harzburgite, whereas clinopyroxenites are usually hosted by dunite. Consequently, the pyroxenites and their associated host rocks define domains, which can be several hundred meters in width.

The orthopyroxene content of harzburgite is highly variable and ranges from < 10 modal % (orthopyroxene dunite) to < 90 modal % (olivine orthopyroxenite). However, the majority of harzburgites have an intermediate composition, *i.e.*, between 10 and 50 modal % orthopyroxene. The low end of this range is associated with dunite, whereas elevated orthopyroxene contents almost always occur in the vicinity of orthopyroxenite veins and dykes.

Two types of harzburgite have been defined on the basis of field and petrographic observations. The first type is residual, and has characteristics of a residue, as already described. The other type is residual harzburgite, or in rare cases, residual or magmatic dunite, with an overprint of up to 20 modal % orthopyroxene derived from the early-suite orthopyroxenites. The addition of orthopyroxene to harzburgite occurs either by mechanical mixing or melt impregnation. The former case arises by partial to complete tectonic disaggregation of orthopyroxenite veins and narrow dykes (< 1 m) in harzburgite during progressive flow of mantle. The distribution of orthopyroxene in the resulting harzburgite is partly to completely homogenized, and orthopyroxene has a porphyroclastic texture. Melt impregnation occurs where orthopyroxenite veins and dykes become diffuse. The diffuse bodies occur in zones where melt could no longer hydraulically fracture the host rock to form dykes. Petrographically, the impregnations of undeformed orthopyroxene are present as delicate, interstitial grains, whereas impregnations of deformed orthopyroxene also exhibit a porphyroclastic texture. Nicolas & Prinzhofer (1983) and Nicolas & Dupuy (1984) have used melt impregnation to explain the enrichment of clinopyroxene and feldspar in harzburgite and dunite to yield lherzolite, wehrlite and troctolite.

Petrography

Polished thin sections were examined in detail using transmitted- and reflected-light microscopy in order to determine the nature and occurrence of base and precious-metal sulfides, arsenides, alloys and

native metals. A Hitachi S-570 scanning electron microscope was used to identify mineral grains and obtain semiquantitative analyses where appropriate. The distribution of base-metal phases and *PGM* is heterogeneous at the scale of a thin section.

Platinum-group minerals (PGM)

Discrete *PGM* have been identified in only three samples belonging to the early suite: a chromitite (L245), a pegmatitic orthopyroxenite dyke (L068), and a clinopyroxenite dyke that intrudes an orthopyroxenite dyke (L283).

A single grain of Os-bearing laurite (RuS_2) has been found in the chromitite sample. The grain is located within unaltered chromite, in association with native Cu and a Ca-Mg-Al silicate (Fig. 2A). Os-bearing laurite is commonly found in chromitite from ophiolites (Talkington *et al.* 1984).

The orthopyroxenite sample preserves a trail of Pt- and Pd-arsenide mineral grains at the margin of a pegmatitic orthopyroxene grain that is in contact with Ca-amphibole (Fig. 2B). Of the seven grains in Figure 2B, six are Pd-arsenide and one is Pt-arsenide. The Pd/As value is lower in the Pd-arsenide associated with the Pt-arsenide than in any other grain of Pd-arsenide. Low concentrations of Fe and Ni occur in Pd-arsenide.

In the clinopyroxenite sample, a single, hexagonal, composite grain of *PGM* occurs fully enclosed within the margin of a clinopyroxene grain (Fig. 3). Phases present in the composite grain are native Pt, native Cu, Pd-Cu and minor Pt-Cu alloys, and Pt-Pd arsenide phases with or without Fe, Co and Ni. The Pt-Cu alloy probably is hongshiite (PtCu), which has only been described from Hung, China (Peng *et al.* 1978) and the Shetland Ophiolite (Prichard & Tarkian 1988). The Pd-Cu alloy identified in the Springers Hill area may be a new mineral.

Sulfides, alloys and native metals

In harzburgite, residual dunite, and dunite, chromitite and orthopyroxenite of the early suite, rare base-metal phases occur as minute wisps, flecks and grains in serpentine. Grains are commonly too small to be identified positively. Awaruite (Ni-Fe alloy) and magnetite are the most common phases identified. In some harzburgites, wüstite has altered to magnetite and native Fe. Pentlandite, heazlewoodite (Ni_3S_2), awaruite and millerite (NiS) occur in some dunites. Copper sulfides and native Cu are found in orthopyroxene, parallel to the cleavage and in fractures, respectively. All the base-metal phases are believed to be of secondary origin, related to serpentinization. In the harzburgite-dunite tectonite,

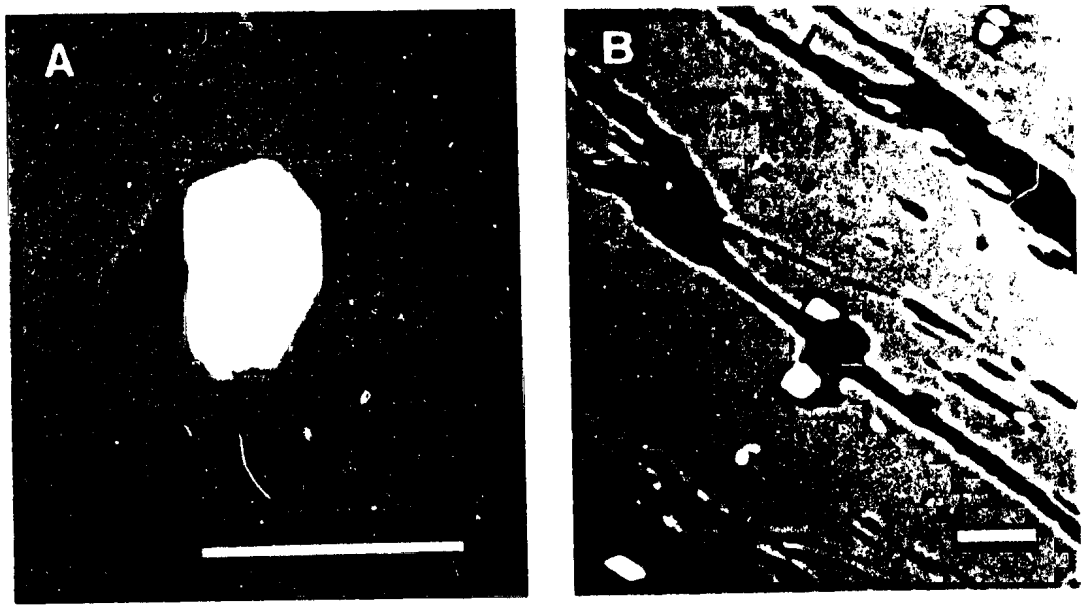

FIG. 2. Scanning electron photomicrographs. (A) Euhedral Os-bearing laurite (white), euhedral Ca-Mg-Al silicate (black), and tongue of native Cu in a grain of unaltered chromite (grey). Early-suite chromitite, L245. (B) Trail of euhedral Pt- and Pd-arsenide grains (white) in unaltered orthopyroxene (grey). The trail of arsenide grains is perpendicular to the cleavage in orthopyroxene, which is partly altered (dark grey). Early-suite orthopyroxenite, L068. Scale bar 10 μm in both cases.

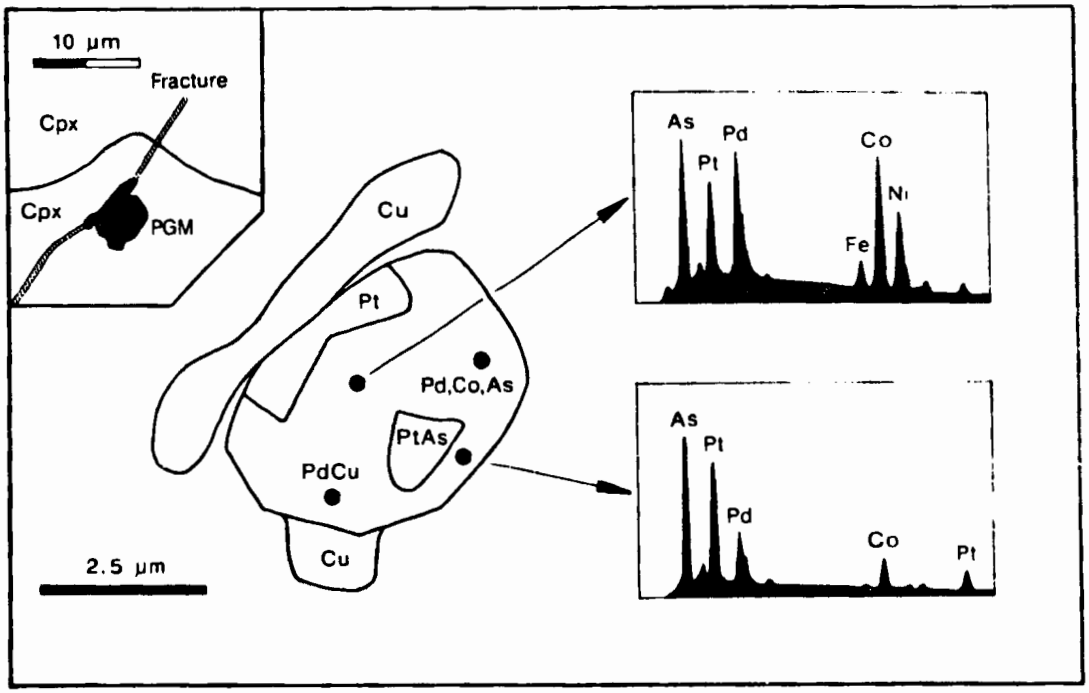

FIG. 3. Line drawing of a scanning electron photomicrograph that illustrates the composite nature of a *PGM* grain hosted by clinopyroxene. Early-suite clinopyroxenite, 1283.

magnetite and Fe-Ni-Cu-S phases are undeformed and show no evidence of recrystallization, which supports their late origin.

In clinopyroxenite of the early suite, Fe-Ni-Cu-S phases form grains < 0.15 mm in diameter, and are more abundant in the early-suite clinopyroxenites than in any other lithology of the early suite. Moreover, within meter-wide dykes of clinopyroxenite, which contain variable amounts of olivine, the Fe-Ni-Cu-S phases occur ubiquitously, but not exclusively, in clinopyroxene-rich areas. Hence, the distribution of Fe-Ni-Cu-S phases is heterogeneous and suggestive of localized zones of S saturation in clinopyroxene-rich areas.

Pentlandite and native Cu with minor associated Cu sulfide are the most common phases found, both within clinopyroxene and at clinopyroxene-clinopyroxene grain boundaries. These base-metal phases may or may not be associated with chromite and amphibole. Pentlandite and native Cu commonly exhibit a symplectitic texture (Fig. 4), which probably resulted from the exsolution of native Cu from pentlandite and its subsequent migration to the margin of the grain. In places, pentlandite fragments are wholly enclosed in native Cu. Discrete ovoid grains of native Cu occur in unaltered, unfractured clinopyroxene grains.

The occurrence of pentlandite and native Cu as inclusions in clinopyroxene, and at grain boundaries of clinopyroxene, is best explained in terms of immiscible globules of liquid forming at or near the surface of growing crystals of clinopyroxene. Some globules became entrapped, whereas others were pushed ahead of the crystallization front (Peterson & Francis 1977, Sharkov 1983, Andersen *et al.* 1987). This would also explain why the majority of inclusions in the Springers Hill samples are hosted in the margin of clinopyroxene crystals. Alternatively, native Cu could have exsolved from clinopyroxene, especially in cases where native Cu occurs as irregular blebs parallel to the cleavage in grains of unaltered clinopyroxene.

During late-stage alteration, Cu was mobile, and was removed from pentlandite. Other reactions include the formation of awaruite at the contact between pentlandite and native Cu, the replacement of pentlandite by magnetite, and the formation of cuprite where native Cu is oxidized in the presence of magnetite.

Cobalt-bearing awaruite or a composite awaruite–wairauite (Co-Fe alloy) grain has been identified at the silicate-chromite contact of a silicate inclusion in a chromite grain hosted by clinopyroxene.

Semiquantitative analyses of pentlandite and

awaruite show that they are Ni-rich. The absence of olivine in the vicinity of the assemblage pentlandite + awaruite may explain the elevated Ni/Fe value.

Whole-Rock Base-Metal and Precious-Metal Chemistry

Analytical techniques

Eighteen whole-rock samples were analyzed for *PGE* and Au using the SCIEX ELAN inductively coupled plasma - mass spectrometer (ICP-MS) at Memorial University. Nickel and Cu concentrations were determined by X-ray fluorescence (XRF) in fourteen whole-rock samples using the Philips PW1450 instrument at Memorial University. Large samples were powdered in order to minimize sampling error arising from grain size and mineral distribution.

Pellets of pressed powdered sample (10 g sample, 1.45 g Bakelite brand phenolic resin binder) were analyzed on the XRF. Based on standards, Cu values are considered to be consistently much lower than true values. Consequently, Cu values are reported solely for the purpose of comparing Cu-rich and Cu-poor samples, and the data are not used quantitatively. Standards demonstrate that Ni values are precise and accurate (Table 1).

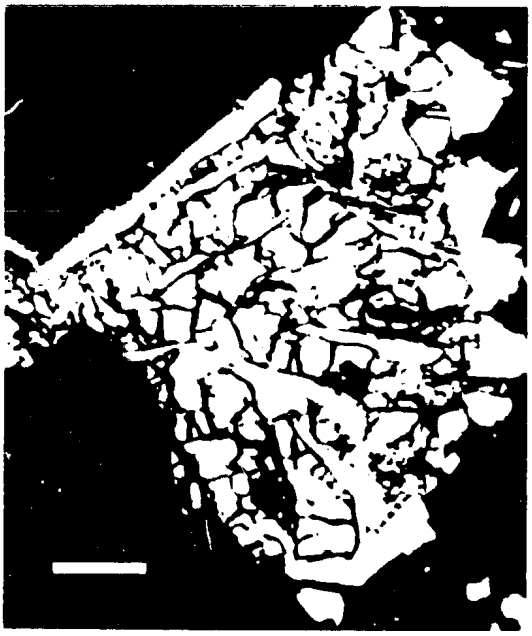

FIG. 4. Scanning electron photomicrograph of vermiform exsolution blebs of native Cu (white) in Ni-rich pentlandite (grey) hosted by clinopyroxene (black). Early-suite clinopyroxenite, I 214. Scale bar 20 μm.

Samples run on the ICP–MS were prepared by fusing a mixture of rock (15.0 g), Ni carbonyl (9.6 g), S (6.0 g), Na_2CO_3 (18.0 g), $Na_2B_4O_7$ (36.0 g) and SiO_2 (15.0 g) to produce a NiS button. This button was then dissolved in HCl, and the *PGE* and Au were collected by Te precipitation (Jackson *et al.* 1988). Detection limits are at or below 0.3 ppb (Table 1). The precision and accuracy of the Au and *PGE* analyses vary widely, but Pd and Ir both exhibit good precision and accuracy (Table 1). The average blank composition (Table 2) has been subtracted from all Springers Hill data in order to remove the effects of contamination from samples yielding low elemental concentrations. Prior to correction, samples low in Pd and Ir exhibited Pd/Ir values biased by the blank component. Some corrected values lie at or below the detection limit (Tables 1, 2). These values are still considered because they were above the detection limit before correction.

Whole-rock chemistry

Nickel, Cu and *PGE* values (Table 2) support the petrographic evidence for the presence of pentlandite, awaruite, native Cu and *PGM*. Based on all of the analyses, only the early-suite orthopyroxenites consistently show significant enrichment in *PGE*. Gold exhibits an affinity for clinopyroxenites. The highest Au values are restricted to those samples with high Cu values.

Origin of the Base- and Precious Metals

Prior to an interpretation of the base- and precious-metal data, it is first necessary to determine whether the measured values reflect primary or secondary processes. The distribution of the elements may reflect conditions during initial crystallization of the melt, subsequent subsolidus re-equilibration, and later low-temperature alteration related to serpentinization.

Primary grains of base- and precious-metal minerals

It is assumed that grains of base- and precious-metal minerals enclosed in unaltered and unfractured chromite and silicate grains are primary because subsolidus reactions occurred as a closed system (Lorand 1987a). Phases interstitial to chromite and silicate grains have clearly reacted with serpentinizing fluids.

The laurite - native Cu - silicate assemblage in chromite (Fig. 2A) is primary and *in situ*. The euhedral nature of the laurite and silicate grains indicates that they were incorporated into chromite as solid grains during chromite growth. Johan & Le Bel (1978), Constantinides *et al.* (1980), Prichard *et al.* (1981), Stockman (1982) and Talkington *et al.* (1983) also have found that euhedral grains of *PGM* are

TABLE 1 PRECISION AND ACCURACY OF ANALYTICAL METHODS

Standard	Element	n	DL	Precision	Mean	MUN	Ref
PCC-1	Ni	19	7	1 1	2291	-	2400
PTC-1	Au	4	0 14	23 2	551	461	650
PTC-1	Ru	4	0 08	14 2	436	440	650
PTC-1	Rh	4	0 02	3 1	605	609	620
PTC-1	Pd	4	0 13	5 8	11354	11405	12700
PTC-1	Re	4	0 04	18 2	67	67	-
PTC-1	Os	4	0 31	32 8	160	192	240
PTC-1	Ir	4	0 01	7 5	171	164	170
PTC-1	Pt	4	0 05	18.4	2583	2699	3000
	Pd/Ir				66 4	69.5	74 7

Concentrations in ppm for Ni and ppb for Au and PGE n = number of analyses of the standard DL = detection limit Precision (as %) reported as the coefficient of variation MUN are the Memorial University reported values for PTC-1 Ref are accepted standard values: Ni (Abbey 1983), Au and PGE (McAdam et al 1973).

The origin of As in *PGM* is equivocal, and the origin of the Pt-Pd arsenide phases is reserved for the following section on alteration.

The primary composition of the base metal sulfide in the early-suite clinopyroxenites is most likely approximated by grains of pentlandite that host exsolution blebs of native Cu (Fig. 4). If subsolidus re-equilibration of such grains was isochemical, the bulk composition of the original sulfide phase was that of a Cu-bearing, Ni-rich pentlandite. Such a sulfide phase is likely derived from a mantle source that had previously undergone partial melting, which decreased the Fe and S content of the mantle sulfide component (Garuti *et al.* 1984).

TABLE 2. Ni, Cu, Au AND PGE CONTENT OF SPRINGERS HILL AREA LITHOLOGIES

		ppm		ppb									
Sample	Lithology	Ni	Cu	Au	Ru	Rh	Pd	Re	Os	Ir	Pt	Sum PGE	Pd/Ir
L106	Harz	1908	bdl	0.14	8.75	1.53	8.16	0.39	4.61	4.76	9.54	37.74	1.71
L218	Harz	1992	bdl	0.32	7.23	1.84	3.87	0.05	3.16	3.13	5.19	24.47	1.24
L054	ES Serp	na	na	0.09	20.98	3.59	2.67	0.00	4.04	9.60	1.13	42.01	0.28
L254	ES Dn	2186	bdl	0.38	3.56	0 44	0.71	bdl	1.90	2.00	0.20	8.81	0.36
L203	ES Chrm	na	na	0.14	50.66	4.62	2.79	0.06	14.61	15.05	1.58	89.37	0.19
L244	ES Chrm	na	na	4.57	50.41	2.83	0.00	0.00	22.41	11.91	2.13	89.69	-
L289	ES Chrm	na	na	0.12	25.60	2.35	5.31	0.00	13.31	6.05	2.13	54.75	0.88
L068	ES Opxt	721	bdl	0.59	0.13	0.48	170.38	0.00	0.14	0.36	170.85	342.34	473.28
L071	ES Opxt	775	bdl	0.94	0.19	1.60	15.92	16.43	bdl	0.44	14.58	49.16	36.18
L267	ES Opxt	711	bdl	0.50	0.56	10.12	104.74	0.30	1.29	3.32	141.70	262.03	31.55
L268	ES Opxt	703	bdl	0.63	2.02	30.92	405.68	0.00	2.79	9.51	517.20	968.12	42.66
	Av Opxt	728	bdl	0.66	0.73	10.78	174.18	4.18	1.06	3.41	211.08	405.41	51.08
L026	ES Cpxt	744	313	29.23	0.17	0.74	67.98	0.00	0.26	0.31	61.24	130.70	219.29
L211	ES Cpxt	948	176	28.81	bdl	0.31	10.38	0.94	0.13	0.01	3.47	15.24	1038.00
L212	ES Cpxt	794	132	21.11	bdl	0.13	0.44	0.54	0.63	bdl	0.18	1.92	
L213	ES Cpxt	558	bdl	2.13	bdl	0.13	3.83	1.05	0.53	0.03	0.77	6.34	127.67
L214	ES Cpxt	1354	125	16.34	bdl	0.03	6.05	13.28	bdl	0.07	1.00	20.43	86.43
L283	ES Cpxt	745	bdl	7.94	0.23	3.73	193.71	0.05	0.35	1.62	520.53	720.22	119.57
L293	ES Cpxt	560	bdl	0.13	0.16	0.08	10.16	0.00	0.05	0.06	3.41	13.92	169.33
	Blank			0.56	bdl	0.05	0.92	0.15	bdl	0.03	0.33	1.48	30.67

Au and PGE values are reported as the original values minus the reagent blank composition. bdl = below detection limit; na = not analyzed; Av = average; Harz = harzburgite; ES = early-suite; Serp = chromite-rich serpentinite; Dn = dunite; Chrm = chromitite; Opxt = orthopyroxenite; Cpxt = clinopyroxenite.

entrapped in chromite, whereas silicates become initially trapped as liquids or euhedral crystals (Talkington *et al.* 1984). Therefore, the suggestion by Gijbels *et al.* (1974), Agiorgitis & Wolf (1978), Crocket (1979) and Mitchell & Keays (1981) that the *PGE* are in solid solution in the spinel structure does not apply to the Springers Hill samples. Gijbels *et al.* (1974) have suggested that grains of *PGM* are produced by expulsion of the *PGE* from structural sites in spinel during subsolidus re-equilibration. Inclusions in chromite from the Springers Hill chromitite sample do not support this process. The occurrence of sulfide in chromite probably results because the crystallization of chromite locally reduces the FeO content of the melt, allowing sulfide to precipitate (Page 1971, Haughton *et al.* 1974).

Alteration

In order to use base- and precious-metal concentrations in whole-rock samples as petrogenetic tracers, the effects of alteration must be known. The present Fe-Ni-Cu-S assemblage represents the end product of serpentinization reactions, which yielded an assemblage of magnetite, awaruite, native metals (Cu), pentlandite and other minor phases. Such an assemblage is characteristic of serpentinized ultramafic rocks (Eckstrand 1975, Moody 1976). The pentlandite - magnetite - awaruite - native Cu assemblage is common in all environments where relict olivine and serpentine coexist, as a result of low $f(O_2)$ and low $f(S_2)$ conditions (Eckstrand 1975). The magnetite-awaruite assemblage in serpen-

tinite is evidence for a very O_2-deficient, H_2-rich environment at temperatures below 420°C (Moody 1976).

Under conditions of nonconstant volume, serpentinization is an isochemical process except for the introduction of H_2O and loss of Ca (Coleman & Keith 1971, Eckstrand 1975). Groves & Keays (1979) predicted that a system undergoing serpentinization may gain S from an external source and lose Ni from the silicate fraction into opaque phases, or from the system altogether. In terms of mobility, Fe, Ni, Co and S can move as much as 10 cm during the most active stage of serpentinization (Shiga 1987); Fe^{2+} is more mobile than Ni^{2+} because NiS has a smaller solubility product than FeS (Groves & Keays 1979). The petrographic examination of the Fe-Ni-Cu-S assemblages in samples from the Springers Hill area indicates that Fe and Ni remained essentially *in situ* in pentlandite, awaruite and magnetite, or moved a short distance (mm scale) to be incorporated into other opaque phases in serpentine. Copper was the most mobile element (mm–cm scale); in cases, it was removed from pentlandite and precipitated along fractures (Fig. 3) and grain boundaries. Hence, Fe, Ni and Cu are *in situ*, at least at the scale of a hand specimen; data on these elements should, therefore, be representative of the original composition of the whole rock prior to serpentinization.

Platinum-group elements are immobile during serpentinization (Keays & Davison 1976, Groves & Keays 1979, Oshin & Crocket 1982, Prichard & Tarkian 1988); therefore, primary magmatic abundances should survive this alteration (Oshin & Crocket 1982). Prichard & Tarkian (1988) have found, however, that the phases comprising the *PGM* assemblage will change during serpentinization; for example, hongshiite may be an alteration product of sperrylite ($PtAs_2$) (Prichard & Tarkian 1988) or cooperite (PtS) (Cabri 1981). By inference, hongshiite in the Springers Hill samples probably has a similar origin. If so, the source of Cu could be native Cu blebs and pentlandite in the early-suite clinopyroxenites. Copper remobilization in clinopyroxenite is probably related to serpentinization of the harzburgite and dunite hosting the clinopyroxenite. The preference of native Cu and Cu-*PGE* alloys for the margins of *PGM* arsenide grains (Fig. 3) strongly suggests that arsenide minerals existed prior to the introduction of Cu.

Another example of a modification in the *PGM* assemblage may result from the introduction of As. The origin of As in *PGM* is unclear; Naldrett & Cabri (1976) reported that during cooling, sulfides undergo phase transformations and the *PGE* exsolve, recrystallize, and combine with As, Te, Bi and Sb to form complex *PGM* phases. The low S–As values reported by Groves & Keays (1979) for some serpentinites (mainly talc–carbonate rocks) suggest that As was introduced by an alteration fluid. Similarly, Prichard & Tarkian (1988) argued that As could be introduced with late-magmatic fluids, or during or after low-temperature hydrous conditions suitable for chlorite formation. In the Springers Hill samples, the euhedral nature of the arsenide grains in relatively unaltered pyroxene (Figs. 2B, 3) implies that the arsenides precipitated as primary phases from a fractionating melt. Support for this was provided by Oen (1973), Lorand (1987b) and Leblanc *et al.* (1989), who proposed that the *PGE* are fractionated in an immiscible As-S-rich liquid in the early stages of crystal fractionation during mantle upwelling.

Gold may be lost during serpentinization (*e.g.*, Keays & Davison 1976), but Oshin & Crocket (1982) showed that Au may be added to harzburgite during the formation of asbestos veins. Groves & Keays (1979) proposed that the dissolution and removal of Au in an alteration environment are enhanced by high $f(O_2)$, but strongly oxidizing conditions do not appear to have prevailed in the Springers Hill area.

In conclusion, the concentrations of Fe (as total Fe), Ni, Cu and *PGE* in lithologies of the residuum and early-suite rocks in the Springers Hill area are most likely primary in origin, despite local remobilization. Solid sulfide and arsenide grains were incorporated into chromite and pyroxene as the melt evolved. Osmium–Ru–S saturation was followed by Pt–Pd–As and Fe–Ni–Cu–S saturation, respectively, all under magmatic conditions.

Petrogenetic Constraints

The concentrations of *PGE* enable constraints to be placed upon the origin of the lithologies in the Springers Hill area. The *PGE* data are presented as Pd–Ir values (Table 2) and in chondrite-normalized *PGE* plots (Fig. 5). Gold is not considered because it is more mobile than the *PGE* during serpentinization.

Origin of the Springers Hill harzburgite

Before examining the *PGE* chemistry of the Springers Hill harzburgite, it is necessary to understand the origin of these rocks. The sulfide component of the upper mantle has a low melting point (Naldrett 1973) and is largely involved in mantle melting (Garuti *et al.* 1984). This phenomenon allows the abundance of Fe–Ni–Cu–S phases to be used as an index of depletion, especially as their abundance correlates with the modal abundance of clinopyroxene and plagioclase in residual mantle material (Lorand 1988). The Springers Hill harzburgites are devoid of primary Fe–Ni–Cu–S phases, clinopyroxene and plagioclase. They have highly depleted trace-

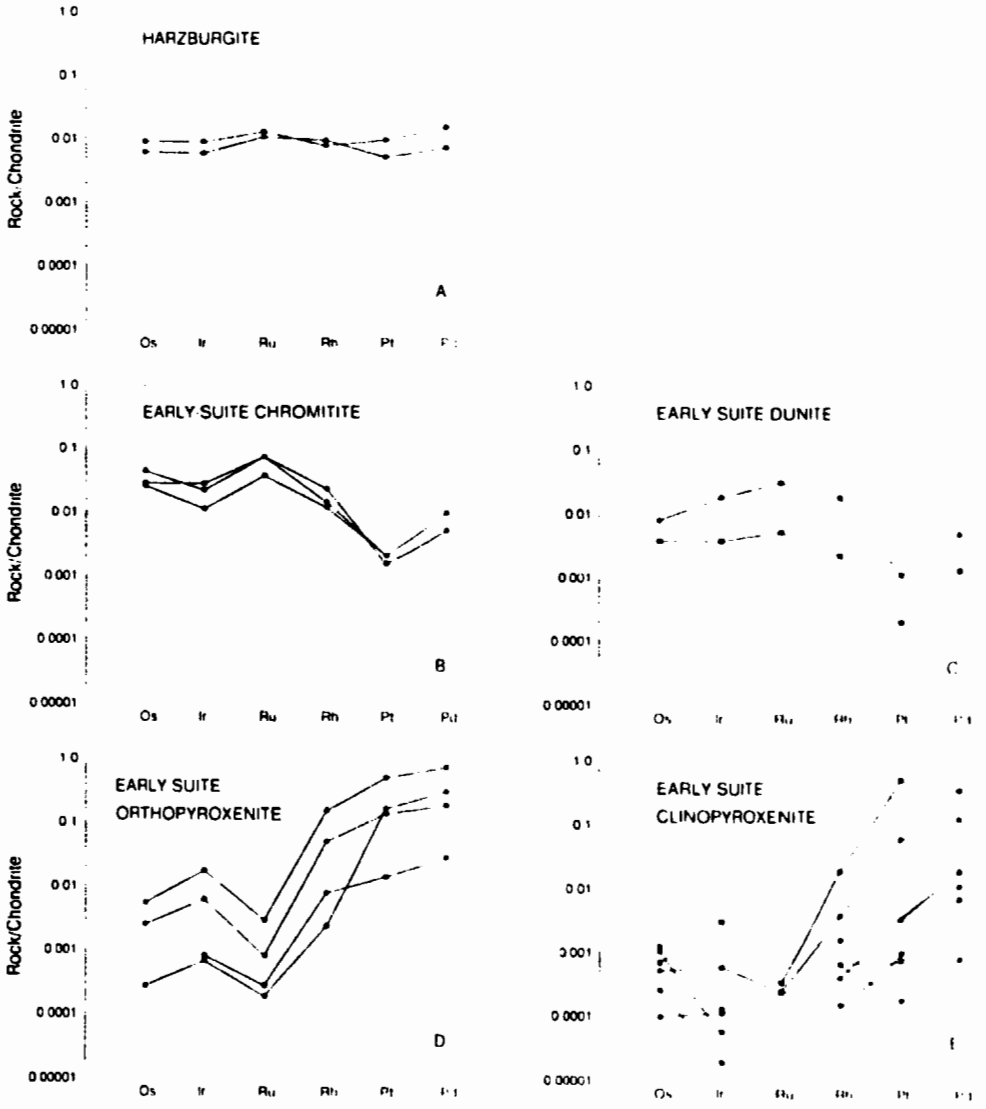

FIG. 5. Chondrite-normalized *PGE* abundances in harzburgite (A) and lithologies of the early suite (B, C, D and E) from the Springers Hill area, BIOC. All samples are represented by circles, except in C (circle: chromite rich serpentinite, square: dunite) and E (square: clinopyroxenite dyke containing xenocrysts of orthopyroxene derived from orthopyroxenite). *PGE* values used for normalization are those compiled by Naldrett & Duke (1980) for an average C1 chondrite.

and rare-earth-element characteristics, and they contain chromite associated with Mg-rich olivine and orthopyroxene. These features are all characteristic of a highly depleted mantle residuum.

It is possible to estimate the degree of partial melting required of a mantle source to yield a harzburgite residue totally barren of sulfide (Barnes *et al.* 1985). Garuti *et al.* (1984) reported an Fe-depleted, Ni- and Cu-enriched mantle sulfide component for the Baldissero and Balmuccia lherzolites of the Ivrea–Verbano mantle peridotites, western Italian Alps. These lherzolites preserve S contents of 140–320 ppm, which are representative of the S content of undepleted to partly depleted upper mantle (Garuti *et al.* 1984). For the Springers Hill harzburgites, it is assumed that the initial S content of the

mantle source was 140–320 ppm, that partial melting occurred at a depth of < 40 km (Duncan & Green 1987), and that S solubility in basic silicate melts is 0.19 wt.% (Wendlandt 1982). For these parameters, 7% to 17% partial melting is required to remove all of the mantle sulfide into the melt for, respectively, S contents between 140 and 320 ppm in the initial mantle source. Depleted mantle peridotites in the BIOC were produced by 23% partial melting of BIOC spinel lherzolite (Malpas 1978), which would leave a harzburgite residue totally devoid of any primary sulfide phase after complete extraction of melt. Basal spinel lherzolites in the BIOC have an Fe–Ni–Cu–S component of <0.005% by volume, and they grade into harzburgites totally devoid of a sulfide component (Lorand 1987a). Springers Hill harzburgites contain no petrographically visible sulfide phase, apart from that resulting from serpentinization of the silicate phases. During partial melting, the dissolution of all the mantle sulfide leaves no sulfide residue into which the *PGE* can partition. Melt has been very effectively removed from the Springers Hill harzburgites, as there is no evidence for trapped silicate or sulfide melt residing in the residuum.

The Springers Hill harzburgites contain 24–38 ppb total *PGE*. Because there is no sulfide in which the *PGE* can exist, they must be present in either chromite and silicate phases, or an intergranular phase. It has been postulated that refractory Cr-spinel and olivine in S-poor ultramafic rocks may act as a sink for Ir (Crocket 1979, Naldrett *et al.* 1979). In addition, Mitchell & Keays (1981) predicted that high-temperature Ir alloys may exist under upper-mantle *P–T* conditions in environments of low $f(S_2)$. Iridium in this form would remain as a residual phase during partial melting of the mantle (Mitchell & Keays 1981). In contrast to Ir, Pd is more volatile (Arculus & Delano 1981); therefore, during partial melting Pd fractionates from Ir, which is left in the residue (Hertogen *et al.* 1980, Mitchell & Keays 1981). Hence, highly depleted mantle peridotites have low total *PGE* contents, fractionated chondrite-normalized *PGE* patterns with negative slopes from Ir to Pd, and Pd/Ir <1. Such patterns have been reported from the Thetford Mines Ophiolite, Quebec (Oshin & Crocket 1982) and the Ronda peridotite massif, Spain (Stockman 1982), and calculated for the Vourinos Ophiolite Complex, Greece (Cocherie *et al.* 1989). The chondrite-normalized *PGE* patterns (Fig. 5A) and Pd/Ir values (1.2–1.7) of the Springers Hill harzburgites are completely inconsistent with a residual origin. In fact, the flat *PGE* patterns for Springers Hill harzburgites coincide with the chondrite-normalized *PGE* data compiled by Arculus & Delano (1981) for undepleted upper mantle (Jagoutz *et al.* 1979, Morgan & Wandless 1979, Morgan *et al.* 1980, Mitchell & Keays 1981), and yet the Springers Hill harzburgite is clearly residual in origin. In order to explain the apparent discrepancy between the *PGE* data and the residual origin for the harzburgite, it is necessary first to consider the origin and *PGE* chemistry of the early-suite lithologies.

The early suite

Lithologies of the early suite are magmatic in origin, as demonstrated earlier, and both their silicate mineralogy and *PGE* chemistry define a fractionation sequence. All of the chromitite samples (Fig. 5B) have characteristic chondrite-normalized *PGE* patterns typical of ophiolites (*e.g.*, Page *et al.* 1982, 1983, Page & Talkington 1984), but exhibit a positive slope from Pt to Pd, which appears to be a diagnostic feature of Newfoundland ophiolites (Page & Talkington 1984). The V-shaped Os–Ir–Ru patterns of the chromitites reflect the occurrence of Os-bearing laurite inclusions in chromite grains. It is important to note that a discrete Ir-bearing phase has not been found in any lithology investigated in this study.

Dunite has a nearly identical chondrite-normalized *PGE* pattern to that of serpentinite (Fig. 5C), which strongly suggests that serpentinization has not affected whole-rock *PGE* chemistry. The *PGE* patterns in Figure 5C are best explained by chromite fractionation (*cf.* Fig 5B), and the higher *PGE* content of the serpentinite is attributed to its greater abundance of chromite relative to the dunite. The low Os/Ru value of the serpentinite may argue for the presence of Os-poor or Os-free laurite in this sample. Osmium-free laurite has been observed in serpentine and chlorite interstitial to chromite grains in chromite-rich samples from the Shetland Ophiolite (Tarkian & Prichard 1987).

Chondrite-normalized *PGE* patterns for the orthopyroxenites (Fig. 5D) show an inverse correlation with respect to the chromitite and dunite patterns (Figs. 5B, 5C), which reflects the presence of Pt and Pd phases in the orthopyroxenite. Oshin & Crocket (1982), Page & Talkington (1984), Barnes *et al.* (1985) and Prichard & Tarkian (1988) have suggested that as a magma evolves, it becomes enriched in Pt and Pd relative to Ir, implying a fractionation trend. The *PGE* patterns presented in Figures 5B, 5C and 5D suggest that the orthopyroxenites precipitated from a basic melt that had previously undergone fractionation of a chromite component. The intrusive relationships, magmatic textures, fractionated *PGE* patterns, and high Pd/Ir values exhibited by the orthopyroxenites all argue against their origin as residues after partial melting. Loubet *et al.* (1976) and Loubet & Allègre (1979) proposed a residual origin for the garnet pyroxenites of Beni-Bousera, Morocco.

Chondrite-normalized *PGE* patterns are highly variable in clinopyroxenites (Fig. 5E). The clinopyroxenite richest in *PGE* has a *PGE* pattern almost identical to those of the orthopyroxenites. This clinopyroxenite intrudes an orthopyroxenite and contains orthopyroxene xenocrysts derived from the orthopyroxenite. As a result, in places, the clinopyroxenite becomes a websterite, and inherits a significant component of its *PGE* pattern from the orthopyroxene xenocrysts. Primary sulfides first appear in the clinopyroxenites, but their influence on the *PGE* patterns presently is unknown.

During fractionation in the early suite, there was a significant fluctuation in the concentration of Ir fractionating from the melt relative to Os and Ru. If an Ir-rich alloy remained in the residuum upon melt extraction (Mitchell & Keays 1981), then this could account for the V-shaped Os–Ir–Ru pattern of chromitite. However, even if this were the case, the *PGM* in chromitites should be Ir-depleted, relative to Os and Ru, in order to account for the upward V-shaped Os–Ir–Ru pattern in orthopyroxenite. This trend suggests that the relative proportions of Os, Ir and Ru present in *PGM* are very sensitive to the crystallization environment in terms of whether chromite or pyroxene is precipitating.

The complementary evolution of the *PGE* chemistry with mineralogy of the early-suite veins and dykes strongly suggests that the veins and dykes of this suite may be comagmatic and that the *PGE* patterns have not arisen through alteration. Clearly the veins and dykes are crystal fractionates and do not represent liquid compositions. The fractionation sequence olivine + orthopyroxene + clinopyroxene is typical of highly refractory melts such as boninites. The corresponding fractionation of the *PGE* to yield high Pd/Ir values in the early-suite pyroxenites also is consistent with a boninite origin for this suite, as boninites and low-Ti lavas have Pd/Ir values in the range 20–200 (data compiled by Barnes *et al.* 1988).

Modification of the Springers Hill harzburgite

The relatively unfractionated *PGE* chemistry exhibited by the otherwise highly depleted Springers Hill harzburgites is best explained in terms of the field and petrographic evidence for addition of an early-suite orthopyroxenite component to residual harzburgite. As described earlier, the addition of orthopyroxene involves either melt infiltration of orthopyroxenite into residual harzburgite, or mechanical mixing of orthopyroxenite into harzburgite by the stretching and pulling apart of orthopyroxenite veins and narrow dykes (< 1 m) hosted within residual harzburgite. These processes would increase the orthopyroxene content of depleted harzburgite. In a similar way, it is possible to produce harzburgites by adding orthopyroxene to residual or magmatic dunites.

Plotted in Figure 6 are the Pd and Ir data for the *PGE*-depleted Black Lake harzburgite (sample 1C) from the Thetford Mines Ophiolite (Oshin & Crocket 1982), the *PGE*-enriched Springers Hill harzburgite (sample L106), and the average Springers Hill

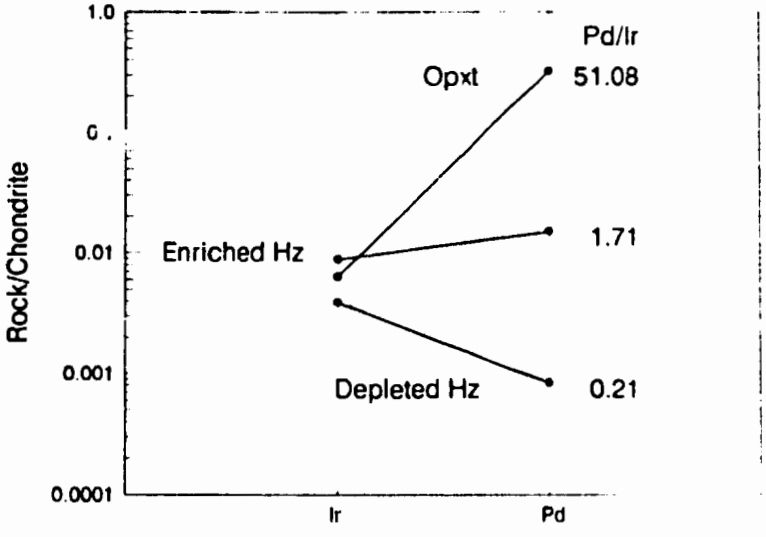

FIG. 6. Pd, Ir and Pd/Ir values for *PGE*-depleted harzburgite [sample 1C from Oshin & Crocket (1982)], *PGE*-enriched harzburgite (L106) from Springers Hill, and average early-suite orthopyroxenite composition, also from Springers Hill.

orthopyroxenite composition (Table 2). The *PGE* content of the Black Lake harzburgite is assumed to represent the *PGE* content of residual mantle. Iridium Pd slopes pivot about an essentially constant Ir value for large variations in Pd concentration (Fig. 6). Consequently, the addition of early-suite orthopyroxenite to *PGE*-depleted harzburgite will greatly alter the Pd content of the harzburgite without significantly modifying the Ir content. This trend is further supported by the differences in Pd/Ir and Pd/Pt values of the *PGE*-enriched harzburgite, compared to those of the average orthopyroxenite. Whereas Pd/Ir values for the two lithologies are vastly different, 1.7 and 51, respectively, Pd/Pt values are essentially identical, 0.86 and 0.83, respectively. The proportion of average early-suite orthopyroxenite required to change residual harzburgite compositions (sample 1C of Oshin & Crocket 1982) into Springers Hill harzburgite (sample I 106) can be calculated from simultaneous equations involving the Pd, Ir and Pd/Ir values of these three components. The *PGE* chemistry suggests that the enriched Springers Hill harzburgite (I 106) is composed of 98% residual harzburgite and 2% orthopyroxene from early-suite Springers Hill orthopyroxenite. The addition of 2% orthopyroxene to residual harzburgite is clearly inconsistent with the field and petrographic data, which suggest that up to 20 modal % orthopyroxene from orthopyroxenite is added to harzburgite. One explanation for this discrepancy appeals to the heterogeneous distribution of *PGM* in orthopyroxenite; the addition of orthopyroxene thus need not result in a proportional addition of *PGE* to the harzburgite. As an alternative, the *PGE*-enriched harzburgites may have experienced a small degree of partial melting to remove Pd relative to Ir. This is unlikely, however, because the fine, delicate, impregnated orthopyroxene in the harzburgite exhibits no evidence for corrosion resulting from partial melting. More *PGE* data from harzburgites are required in order to better understand the behavior of the *PGE* in mantle residuum in ophiolite sequences.

The question now arises as to how significant are the orthopyroxene-addition processes in terms of modifying harzburgite compositions in mantle sequences in ophiolites. In the Springers Hill area, orthopyroxenite veins and dykes are abundant, and a significant proportion of the harzburgite appears to be modified. However, the area mapped in this study is only 2 km^2. A more regional study of the BIOC mantle section is presently under way, and there is evidence for orthopyroxene impregnation in other massifs (G. Suhr, pers. comm.). A survey of the literature data on the *PGE* content of other harzburgites from ophiolites indicates that many of them preserve Pd/Ir values greater than 1, *e.g.*, Troodos Ophiolite Complex, Cyprus (Becker & Agiorgitis 1978), Thetford Mines Ophiolite, Quebec (Oshin & Crocket 1982), Vourinos Ophiolite Complex, Greece (Cocherie *et al.* 1989). Without detailed field and petrographic studies of the harzburgites from these ophiolites, it is premature to attribute the elevated Pd/Ir values to orthopyroxene addition. However, if such a process does operate in these ophiolites, then modifications of Pd/Ir values of harzburgite by orthopyroxene addition would appear to be the rule rather than the exception.

Conclusions

The main conclusions drawn from the Springers Hill area of the BIOC are summarized as follows:

1) The *PGE* are essentially immobile during serpentinization, despite modifications of *PGM* phase assemblages resulting from the addition of Cu. Consequently, chondrite-normalized *PGE* diagrams and *PGE* values are useful tools to determine the petrogenesis of ultramafic rocks.

2) Copper is locally mobilized during serpentinization, but Fe, Ni and Cu remain essentially *in situ* at the hand-specimen scale. Original Fe-Ni-Cu-S phase assemblages are affected by serpentinization.

3) The early-suite veins and dykes fractionate olivine ± chromite → orthopyroxene → clinopyroxene, which is the order of crystallization of refractory melts, *e.g.*, boninites. Fractionation of the *PGE* from a melt occurs by removal of sulfides in chromite (Os, Ru and possibly Ir) and arsenides in pyroxene (Pt and Pd). Base-metal sulfides do not seem to play a role in this fractionation.

4) Partial melting of mantle with a chondritic distribution of the *PGE* yields melt and residue with high and low Pd/Ir values, respectively. Precipitation of chromite from this melt enhances the Pd/Ir value of the residual melt. Pyroxenites with highly elevated Pd/Ir values precipitate from such a residual melt.

5) The Springers Hill harzburgites that exhibit a Pd/Ir value greater than 1 contain a component of early-suite orthopyroxenite. These harzburgites contain coexisting residual and magmatic orthopyroxenes. The residual orthopyroxene is porphyroclastic and corroded, whereas the magmatic orthopyroxene is porphyroclastic if deformed, or a delicate impregnation if undeformed.

6) Refractory pyroxenites in mantle sequences in ophiolites may be of economic interest for future mineral exploration.

Acknowledgements

Special thanks are extended to J. Lydon, who suggested this study, which forms part of the author's Ph.D. thesis under the supervision of J. Malpas. The interest shown by K. Hudson and G. Suhr led to

much invaluable discussion. K. Hudson, J. Malpas and M. Wilson are thanked for proof reading earlier versions of this manuscript. Constructive criticism by G. Himmelberg, M.L. Zientek and one anonymous reviewer greatly strengthened this manuscript. R. Martin is thanked for his editorial comments. D. Healey and S. Jackson are thanked for *PGE* analyses, as are C. Finch, P. Haring and H. Wagenbauer for fusing the *PGE* samples. C. Emerson greatly assisted with operation of the SEM. S. Dunsworth provided a very comprehensive introduction to the field area, and J. Clarke, M. Edwards and J. Saunders proved to be very able field assistants. Excellent logistical support was provided by D. and G. Mercer, Pasadena Expediting and Warehousing, and Viking Helicopters Newfoundland Ltd. This work was funded under the 1984-1989 Canada-Newfoundland Mineral Development Agreement, Geological Survey of Canada, Economic Geology and Mineralogy Division, contract number 20ST.23233-7-0402.

References

Abbey, S. (1983): Studies in "standard samples" of silicate rocks and minerals 1969-1982. *Geol. Surv. Can. Pap.* **83-15.**

Agiorgitis, G. & Wolf, R. (1978): Aspects of osmium, ruthenium and iridium contents in some Greek chromites. *Chem. Geol.* **23**, 267-272.

Andersen, T., Griffin, W.L. & O'Reilly, S.Y. (1987): Primary sulphide melt inclusions in mantle-derived megacrysts and pyroxenites. *Lithos* **20**, 279-294.

Arculus, R.J. & Delano, J.W. (1981): Siderophile element abundances in the upper mantle: evidence for a sulfide signature and equilibrium with the core. *Geochim. Cosmochim. Acta* **45**, 1331-1343.

Barnes, S.-J., Boyd, R., Korneliussen, A., Nilsson, L.-P., Often, M., Pedersen, R.B. & Robins, B. (1988): The use of mantle normalization and metal ratios in discriminating between the effects of partial melting, crystal fractionation and sulphide segregation on platinum-group elements, gold, nickel and copper: examples from Norway. *In* Geo-Platinum 87 Symp. Vol. (H.M. Prichard, P.J. Potts, J.F.W. Bowles & S.J. Cribb, eds.). Elsevier, London (113-143).

———, Naldrett, A.J. & Gorton, M.P. (1985): The origin of the fractionation of platinum-group elements in terrestrial magmas. *Chem. Geol.* **53**, 303-323.

Becker, R. & Agiorgitis, G. (1978): Iridium, osmium and palladium distribution in rocks of the Troodos Complex, Cyprus. *Chem. Erde* **37**, 302-306.

Cabri, L.J. (1981): The platinum-group minerals. *In* Platinum-Group Elements: Mineralogy, Geology, Recovery (L.J. Cabri, ed.). *Can. Inst. Min. Metall., Spec. Vol.* **23**, 83-150.

Casey, J.F., Dewey, D.L., Stroka, L.N., Karson, J.A. & Sullivan, J. (1985): Geochemical and geological evidence bearing on the origin of the Bay of Islands and Coastal Complex ophiolites of western Newfoundland. *Tectonophysics* **116**, 1-40.

———, Karson, J.A., Dewey, D., Rosencrantz, E. & Titus, M. (1983): Reconstruction of the geometry of accretion during formation of the Bay of Islands Ophiolite Complex. *Tectonics* **2**, 509-528.

Cocherie, A., Augé, T. & Meyer, G. (1989): Geochemistry of the platinum-group elements in various types of spinels from the Vourinos ophiolitic complex, Greece. *Chem. Geol.* **77**, 27-39.

Coleman, R.G. & Keith, T.E. (1971): A chemical study of serpentinization—Burro Mountain, California. *J. Petrol.* **12**, 311-328.

Constantinides, C.C., Kingston, G.A. & Fisher, P.C. (1980): The occurrence of platinum group minerals in the chromitites of the Kokkinorotsos chrome mine, Cyprus. *In* Ophiolites: Proc. Int. Ophiolite Symp. (Cyprus, 1979; A. Panayiotou, ed.). Geol. Surv. Dep., Nicosia (93-101).

Crocket, J.H. (1979): Platinum-group elements in mafic and ultramafic rocks: a survey. *Can. Mineral.* **17**, 391-402.

Dahl, R. & Watkinson, D.H. (1986): Structural control of podiform chromitite in Bay of Islands Ophiolite, Springer Hill area, Newfoundland. *Geol. Surv. Can. Pap.* **86-1B**, 757-766.

Dick, H.J.B. (1977): Evidence of partial melting in the Josephine peridotite. *Oregon Dep. Geol. Mineral Ind.* **96**, 59-62.

Duncan, R.A. & Green, D.H. (1987): The genesis of refractory melts in the formation of oceanic crust. *Contrib. Mineral. Petrol.* **96**, 326-342.

Dunsworth, S., Calon, T. & Malpas, J. (1986): Structural and magmatic controls on the internal geometry of the plutonic complex and its chromite occurrences in the Bay of Islands Ophiolite, Newfoundland. *Geol. Surv. Can. Pap.* **86-1B**, 471-482.

Eckstrand, O.R. (1975): The Dumont serpentinite: a model for control of nickeliferous opaque mineral assemblages by alteration reactions in ultramafic rocks. *Econ. Geol.* **70**, 183-201.

Edwards, S.J. (1987): Melt generation and evolution in ophiolite mantle and the development of mantle heterogeneities. *Troodos 87, Ophiolites and Oceanic Lithosphere (Nicosia, Cyprus), Abstr.* 89.

(1988a): Magmatism and deformation in the Springers Hill area of the Lewis Hills Massif, Bay of Islands Ophiolite Complex, western Newfoundland: evidence from field relationships. *Timothy Jefferson Field Research Fund Rep. (unpubl.), Geol. Soc. London.*

(1988b): Magmatic events preserved in a mantle section of the Lewis Hills Massif, Bay of Islands Ophiolite, western Newfoundland. *Geol. Assoc. Can. Mineral. Assoc. Can., Program Abstr.* **13**, A35.

CIAMICIAN, G., GORGONI, C. & SIGHINOLFI, G.P. (1984): Sulfide mineralogy and chalcophile and siderophile element abundances in the Ivrea–Verbano mantle peridotites (western Italian Alps). *Earth Planet. Sci. Lett.* **70**, 69-87.

GIBBS, R.H., MILLARD, H.T., JR., DESBOROUGH, G.A. & BARTEL, A.J. (1974): Osmium, ruthenium, iridium and uranium in silicates and chromite from the eastern Bushveld Complex, South Africa. *Geochim. Cosmochim. Acta* **38**, 319-337.

GROVES, D.I. & KEAYS, R.R. (1979): Mobilization of ore-forming elements during alteration of dunites, Mt. Keith – Betheno, Western Australia. *Can. Mineral.* **17**, 373-389.

HAUGHTON, D.R., ROEDER, P.L. & SKINNER, B.J. (1974): Solubility of sulfur in mafic magmas. *Econ. Geol.* **69**, 451-467.

HERTOGEN, J., JANSSENS, M.-J. & PALME, H. (1980): Trace elements in ocean ridge basalt glasses: implications for fractionation during mantle evolution and petrogenesis. *Geochim. Cosmochim. Acta* **44**, 2125-2143.

JACKSON, S.E., FRYER, B.J., GOSSE, W., HEALEY, D.C., LONGERICH, H.P. & STRONG, D.F. (1988): Determination of the precious metals in geological samples by ICP MS. *Geol. Assoc. Can. – Mineral. Assoc. Can., Program Abstr.* **13**, A60.

JAGOUTZ, E., PALME, H., BADDENHAUSEN, H., BLUM, K., CENDALES, M., DREIBUS, G., SPETTEL, B., LORENZ, V. & WÄNKE, H. (1979): The abundances of major, minor and trace elements in the earth's mantle as derived from primitive ultramafic nodules. *Proc. 10th Lunar Planet. Sci. Conf.*, 2031-2050.

JAQUES, A.L. & GREEN, D.H. (1980): Anhydrous melting of peridotite at 0–15 kb pressure and the genesis of tholeiitic basalts. *Contrib. Mineral. Petrol.* **73**, 287-310.

JOHAN, Z. & LE BEL, L. (1978): Origin of chromitite layers in rocks of the ophiolitic suite. *Int. Mineral. Assoc., XI Gen. Meet., Abstr.* **1**, 51-52.

KARSON, J.A. (1977): *The Geology of the Northern Lewis Hills, Western Newfoundland.* Ph.D. thesis, State Univ. New York, Albany, New York.

_____ (1979): Geology of the Lewis Hills Massif, western Newfoundland. *Geol. Surv. Can. Open File Map and Rep.* **628**.

_____ (1984): Variations in structure and petrology in the Coastal Complex, Newfoundland: anatomy of an oceanic fracture zone. *In* Ophiolites and Oceanic Lithosphere (I.G. Gass, S.J. Lippard & A.W. Shelton, eds.). *Geol. Soc. London Spec. Publ.* **13**, 131-144.

_____ & DEWEY, J.F. (1978): Coastal Complex, western Newfoundland: an Early Ordovician oceanic fracture zone. *Geol. Soc. Am. Bull.* **89**, 1037-1049.

KEAYS, R.R. & DAVISON, R.M. (1976): Palladium, iridium and gold in the ores and host rocks of nickel sulfide deposits in Western Australia. *Econ. Geol.* **71**, 1214-1228.

LEBLANC, M., GERVILLA, F. & JEDWAB, J. (1989): Noble metals segregation and fractionation in magmatic ores from Ronda and Beni Bousera lherzolite massifs (Spain, Morocco). *Mineral. Petrol.* **41**, (in press).

LORAND, J.P. (1987a): Cu-Fe-Ni-S mineral assemblages in upper-mantle peridotites from the Table Mountain and Blow-Me-Down Mountain ophiolite massifs (Bay of Islands area, Newfoundland): their relationships with fluids and silicate melts. *Lithos* **20**, 59-76.

_____ (1987b): Sur l'origine mantellaire de l'arsenic dans les roches du manteau: exemple des pyroxénites à grenat du massif lherzolitique des Beni-Bousera (Rif, Maroc). *C. R. Acad. Sci. Paris* **305**, 383-386.

_____ (1988): Fe–Ni–Cu sulfides in tectonite peridotites from the Maqsad District, Sumail Ophiolite, southern Oman: implications for the origin of the sulfide component in the oceanic upper mantle. *Tectonophysics* **151**, 57-73.

LOUBET, M. & ALLÈGRE, C.J. (1979): Trace element studies in the Alpine type peridotite of Beni-Bouchera (Morocco). *Geochem. J.* **13**, 69-75.

_____, BOUGAULT, M., SHIMIZU, N. & ALLÈGRE, C.J. (1976): Geochemical study (*REE*, Ba and partially major and transition elements analysis) of pyroxenolite layers in lherzolite type Alpine massives. *Trans. Am. Geophys. Union* **57**, 1025 (abstr.).

MALPAS, J. (1978): Magma generation in the upper mantle, field evidence from ophiolite suites, and application to the generation of oceanic lithosphere. *Phil. Trans. R. Soc. London* **A288**, 527-546.

MCADAM, R.C., SUTARNO & MOLOUGHNEY, P.E. (1973): Noble-metals-bearing sulphide concentrate PTC: its characterization and preparation for use as a standard reference material. *Canada Dep. Energy, Mines, Resources, Mines Branch, Tech. Bull.* **TB 176**.

MITCHELL, R.H. & KEAYS, R.R. (1981): Abundance and distribution of gold, palladium and iridium in some spinel and garnet lherzolites: implications for the nature and origin of precious metal-rich intergranular components in the upper mantle. *Geochim. Cosmochim. Acta* **45**, 2425-2442.

MOODY, J.B. (1976): Serpentinization: a review. *Lithos* **9**, 125-138.

MORGAN, J.W. & WANDLESS, G.A. (1979): Terrestrial upper mantle: siderophile and volatile trace element abundances. *Proc. 10th Lunar Planet. Sci. Conf.*, 855-857.

_____, _____, PETRIE, R.K. & IRVING, A.J. (1980): Earth's upper mantle: volatile element distribution and origin of siderophile element content. *Proc. 11th Lunar Planet. Sci. Conf.*, 740-742.

NALDRETT, A.J. (1973): Nickel sulfide deposits – their classification and genesis with special emphasis on deposits of volcanic association. *Can. Inst. Min. Metall. Trans.* **76**, 183-201.

_____ & CABRI, L.J. (1976): Ultramafic and related mafic rocks: their classification and genesis with special reference to the concentration of nickel sulfides and platinum-group elements. *Econ. Geol.* **71**, 1131-1158.

_____ & DUKE, J.M. (1980): Platinum metals in magmatic sulphide ores. *Science* **208**, 1417-1424.

_____, HOFFMAN, E.L., GREEN, A.H., CHOU CHEN-LIN, NALDRETT, S.R. & ALCOCK, R.A. (1979): The composition of Ni-sulfide ores, with particular reference to their content of *PGE* and Au. *Can. Mineral.* **17**, 403-415.

NICOLAS, A. & DUPUY, C. (1984): Origin of ophiolitic and oceanic lherzolites. *Tectonophysics* **110**, 177-187.

_____ & PRINZHOFER, A. (1983): Cumulative or residual origin for the transition zone in ophiolites: structural evidence. *J. Petrol.* **24**, 188-206.

OEN, I.S. (1973): A peculiar type of Cr–Ni mineralization; cordierite-chromite-niccolites ores of Málaga, Spain, and their possible origin by liquid unmixing. *Econ. Geol.* **68**, 831-842.

OSHIN, I.O. & CROCKET, J.H. (1982): Noble metals in Thetford Mines ophiolites, Quebec, Canada. I. Distribution of gold, iridium, platinum, and palladium in the ultramafic and gabbroic rocks. *Econ. Geol.* **77**, 1556-1570.

_____ & _____ (1986): Noble metals in Thetford Mines ophiolites, Quebec, Canada. II. Distribution of gold, silver, iridium, platinum, and palladium in the Lac de l'Est volcano-sedimentary section. *Econ. Geol.* **81**, 931-945.

PAGE, N.J. (1971): Comments on the role of oxygen fugacity in the formation of immiscible sulfide liquids in the H chromitite zone of the Stillwater Complex, Montana. *Econ. Geol.* **66**, 607-610.

_____, ARUSCAVAGE, P.J. & HAFFTY, J. (1983): Platinum-group elements in rocks from the Voikar Synnisky Ophiolite Complex, Polar Urals, USSR. *Miner. Deposita* **18**, 443-455.

_____, CASSARD, D. & HAFFTY, J. (1982): Palladium, platinum, rhodium, ruthenium, and iridium in chromitites from the Massif du Sud and Tiebaghi Massif, New Caledonia. *Econ. Geol.* **77**, 1571-1577.

_____ & TARKINGTON, R.W. (1984): Palladium, platinum, rhodium, ruthenium and iridium in peridotites and chromitites from the ophiolite complexes of Newfoundland. *Can. Mineral.* **22**, 137-149.

PENG ZHI-ZHONG, CHANG CHIEN-HUNG & NIE LI-LOU (1978): Discussion on new minerals of the platinum group discovered in recent years in China. *Acta Geol. Sinica (Ti Chih Hsueh Pao)* **52**, 326-336 (in Chinese, English abstr.).

PETERSON, R. & FRANCIS, D. (1977): The origin of sulfide inclusions in pyroxene megacrysts. *Am. Mineral.* **62**, 1049-1051.

PRICHARD, H.M., POTTS, P.J. & STORY, C.R. (1981): Platinum-group element minerals in the Unst chromite, Shetland Isles. *Inst. Min. Metall.* **90**, B186-B188.

_____ & TARKIAN, M. (1988): Platinum and palladium minerals from two PGE-rich localities in the Shetland Ophiolite Complex. *Can. Mineral.* **26**, 979-990.

SHARKOV, Ye. V. (1983): The petrological role of liquation in magmatic processes. *Geochem. Int.* **20**(5), 118-129.

SHIGA, Y. (1987): Behavior of iron, nickel, cobalt and sulfur during serpentinization, with reference to the Hayachine ultramafic rocks of the Kamaishi mining district, northeastern Japan. *Can. Mineral.* **25**, 611-624.

STOCKMAN, H.W. (1982): *Noble Metals in the Ronda and Josephine Peridotites*. Ph.D. thesis, Massachusetts Inst. Technology, Cambridge, Massachusetts.

SUHR, G. & CALON, T. (1987): A structural and microstructural study of mantle tectonites in the Springers Hill area (Bay of Islands Ophiolite, Newfoundland). *Geol. Surv. Can. Rep. (unpubl.).*

TARKINGTON, R.W., WATKINSON, D.H., WHITAKER, P.J. & JONES, P.C. (1983): Platinum group inclusions in chromite from the Bird River Sill, Manitoba. *Miner. Deposita* **18**, 245-255.

. . & . (1984): Platinum-group minerals and other solid inclusions in chromite of ophiolitic complexes: occurrence and petrological significance. *Tschermaks Mineral. Petrogr. Mitt.* **32**, 285-301.

Talkkari, M. & Prichard, H.M. (1987): Irarsite-hollingworthite solid-solution series and other associated Ru-, Os-, Ir-, and Rh-bearing *PGM*'s from the Shetland Ophiolite Complex. *Miner. Deposita* **22**, 178-184.

Wendlandt, R.F. (1982): Sulfide saturation of basalt and andesite melts at high pressures and temperatures. *Am. Mineral.* **67**, 877-885.

Williams, H. (1979): Appalachian Orogen in Canada. *Can. J. Earth Sci.* **16**, 792-807.

_____ & Cawood, P.A. (1989): Geology, Humber Arm Allochthon, Newfoundland. *Geol. Surv. Can., Map* **1678A**, scale 1:250 000.

Received November 8, 1989, revised manuscript accepted March 16, 1990.

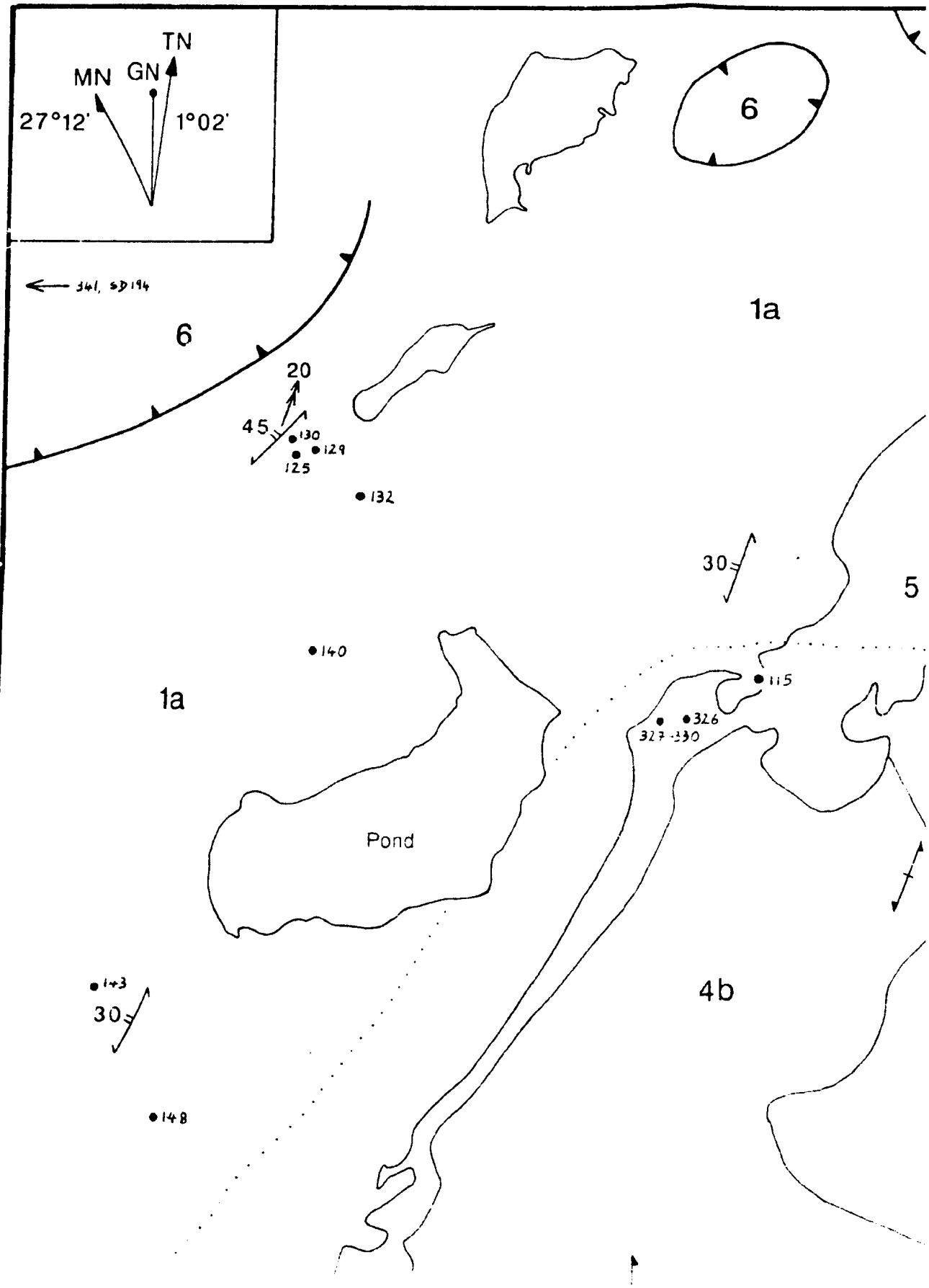
TN
MN
GN
27°12'
1°02'
341, SD 194
6
1a
20
45
130
129
125
132
30
5
140
115
326
327-330
1a
Pond
143
30
4b
148

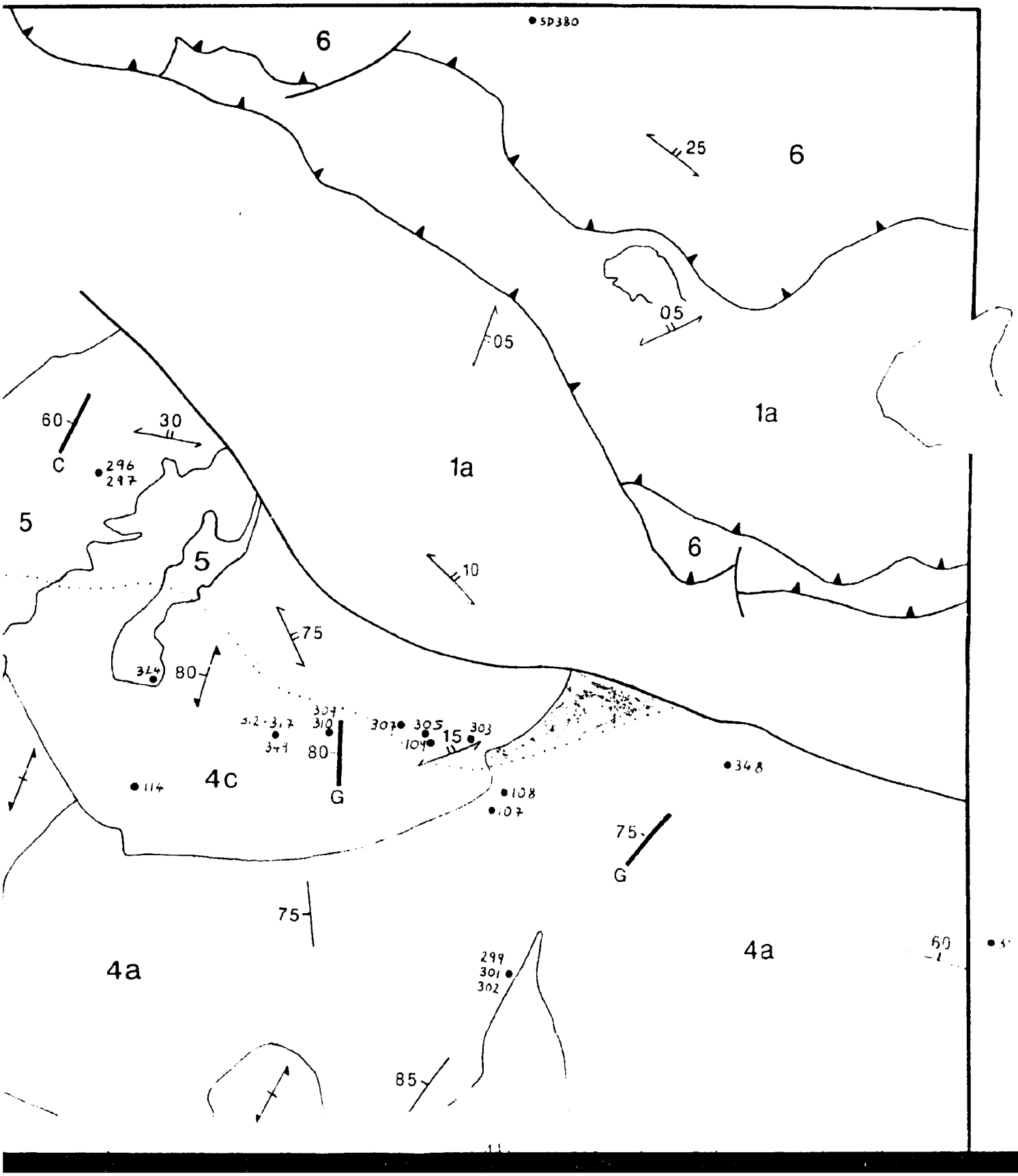
SD380
6
25
6
05
05
1a
60
30
C
296
297
1a
5
5
6
10
75
314
80
312-317
307
310
307
305
15
303
311
80
G
114
4c
348
108
107
75
G
75
4a
299
301
302
4a
60
85

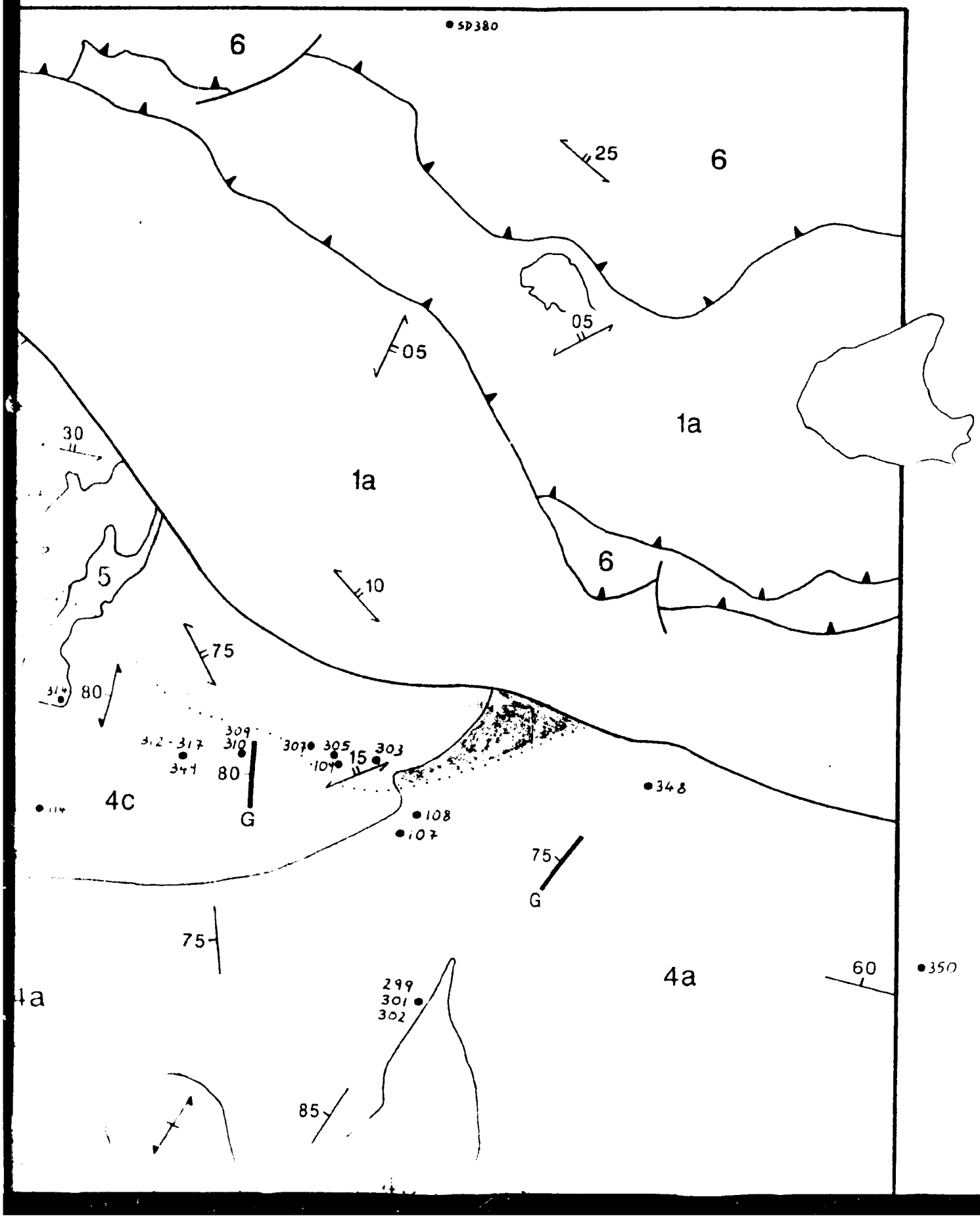
SD380
6
25
6
05
05
1a
30
1a
6
5
10
75
80
309
312 - 317
310
307
305
303
15
344
80
348
4c
G
108
107
75
G
75
4a
60
350
299
301
302
85

GEOLOGICAL MAP OF THE SPRINGERS HILL AREA

LEWIS HILLS MASSIF

BAY OF ISLANDS OPHIOLITE COMPLEX

GEOLOGY BY

STEPHEN JOHN EDWARDS

Scale 1:4000

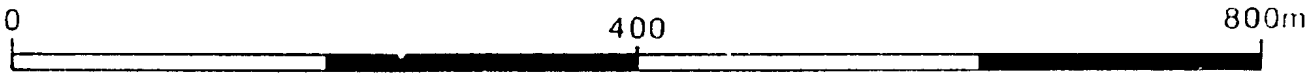

LEGEND

UNCORRELATED

6 Wehrlite and gabbro with minor amphibolite dykes

MARGINAL ZONE

5 All LALPP and HALPPG

HIGH-Al PERIDOTITES, PYROXENITES AND GABBROS (HALPPG)

4c Wehrlite, olivine clinopyroxenite and gabbro

4b Dunite, wehrlite and olivine clinopyroxenite

4a Dunite

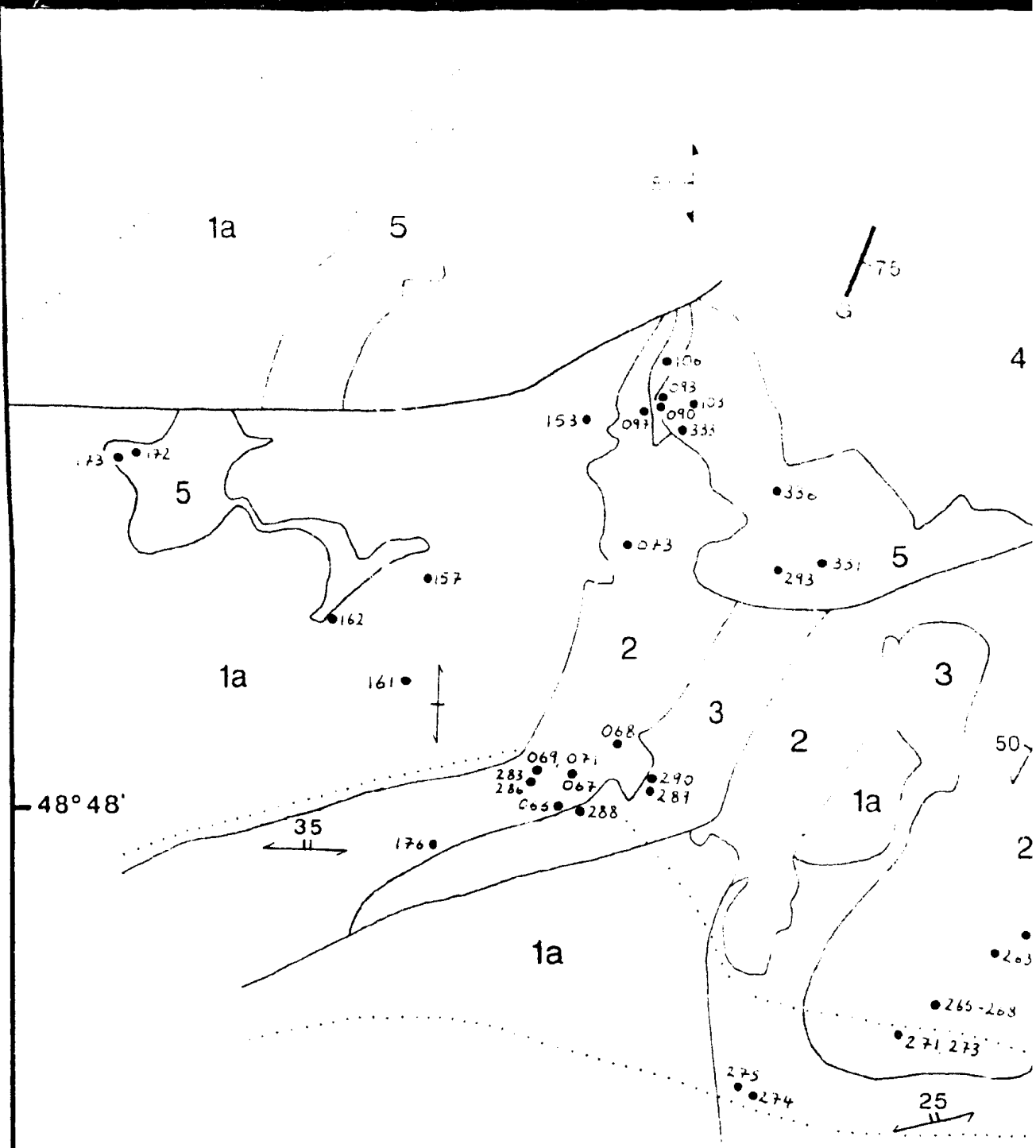
1a
5
4
5
1a
2
3
3
2
1a
2
1a
48°48'
35
25
50
LALPP: Harzburgite and
type I orthopyroxenite dominant
LALPP: Dunite
clinop

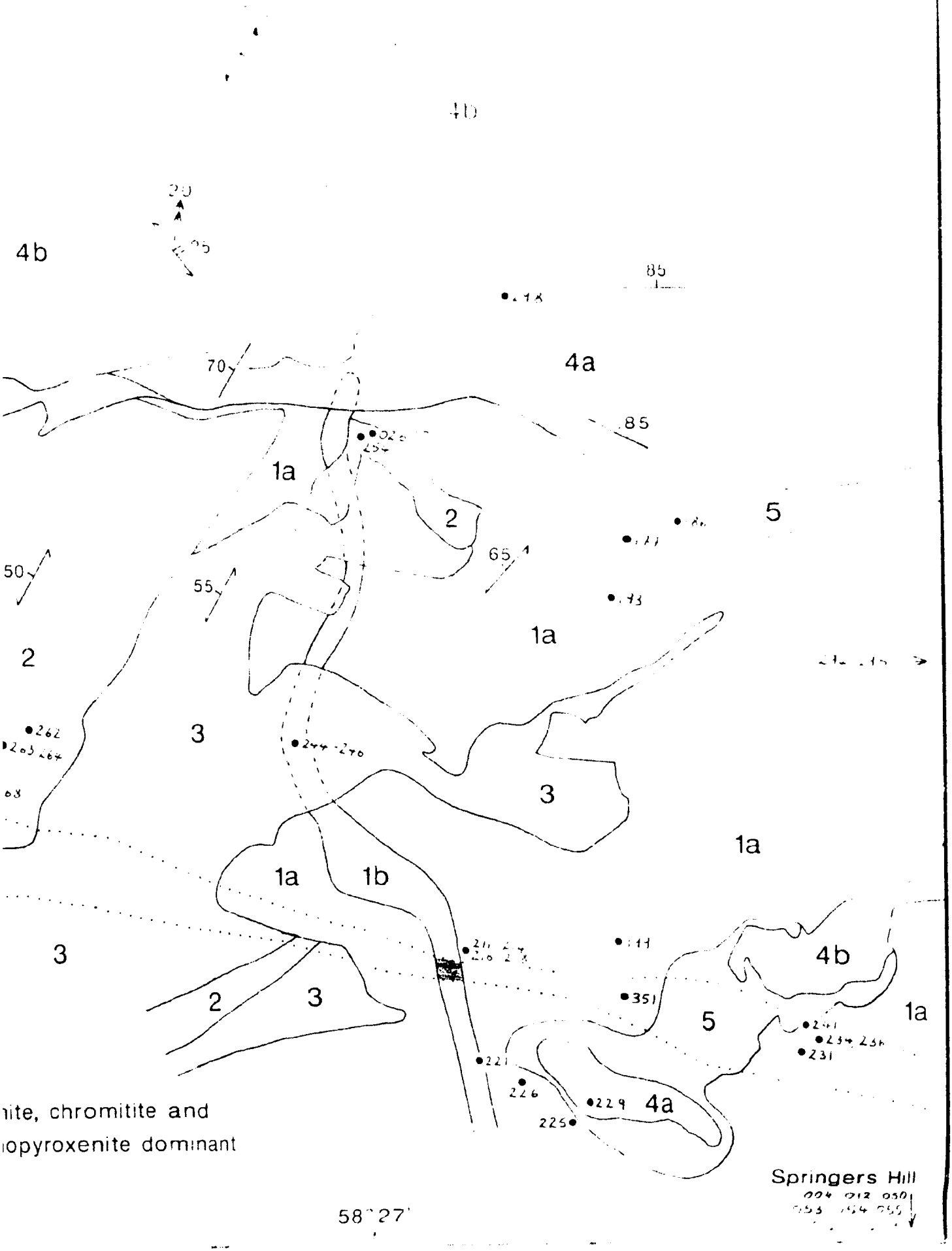

ite, chromitite and
opyroxenite dominant

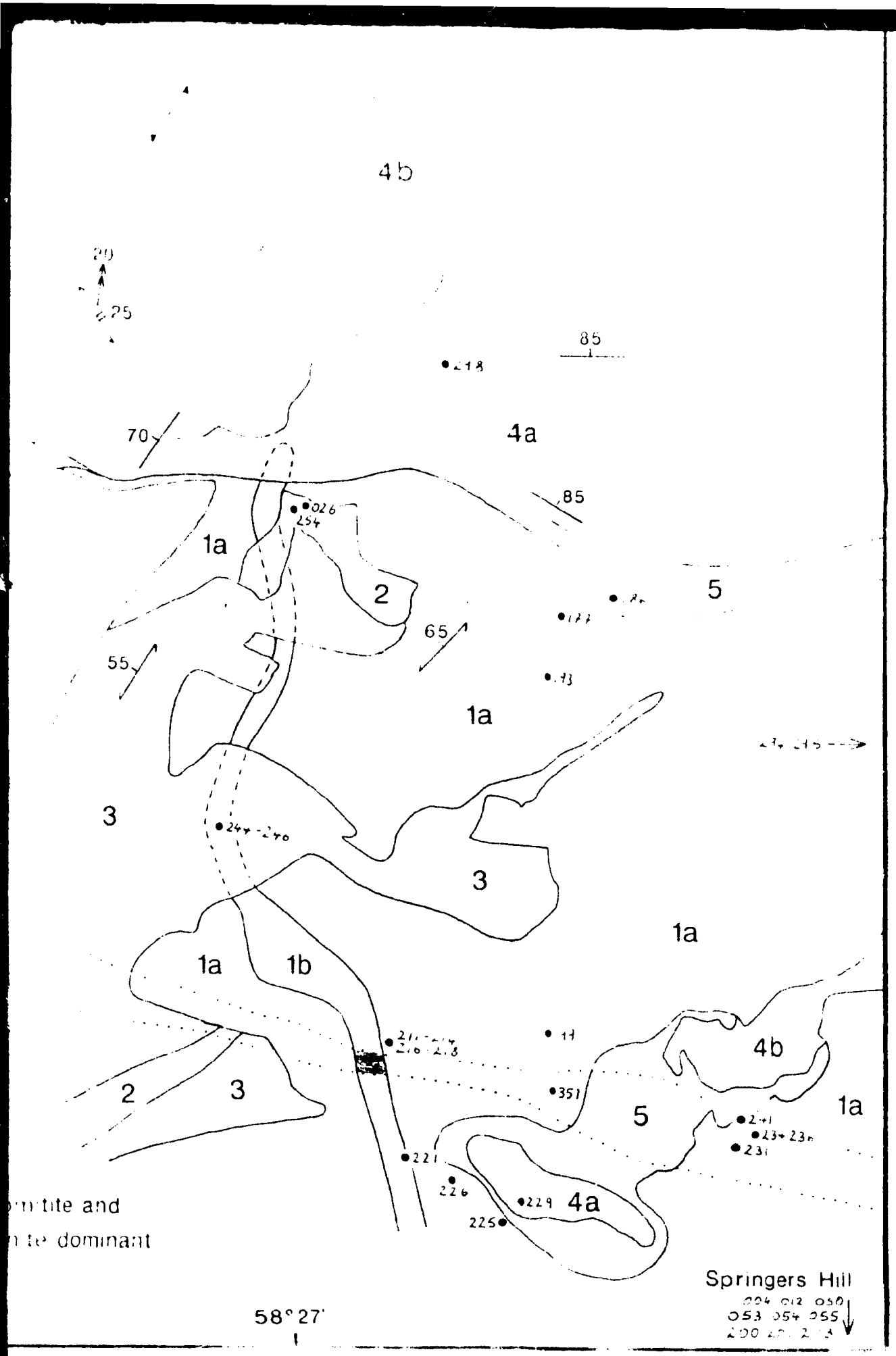

...n tite and

...te dominant

4a

3

2

1b Chromitite and associated dunite
traces of younger lithologies delineated by dashed lines

1a Harzburgite and dunite

SYMBOLS

Geological boundary (majority are gradational)

Spinel layering and banding (inclined)

Foliation — S1 of orthopyroxene in harzburgite (inclined, vertical)

S of clinopyroxene in HALPPG (inclined, vertical)

S2 (inclined)

Lineation — L2 mineral stretching (plunge)

Dyke: olivine clinopyroxenite (C), gabbro (G) (inclined)

Fault, thrust (barbs on upper slice)

Limit of D2 ductile simple shear zones; darker shading represents mylonite

Sample location

NOTES

Amphibole dunite and type II orthopyroxenite (OPXT II) of LALPP, and amphibole peridotite of HALPPG, form small bodies that are not represented on the map. These bodies mainly are confined to D2 shear zones and the marginal zone. The area records two episodes of deformation (D1 and D2). Units 1, 2 and 3 of LALPP record D1 and D2, whereas HALPPG, amphibole dunite, OPXT II, and faults and thrusts are contemporaneous with D2 and post-date D1.

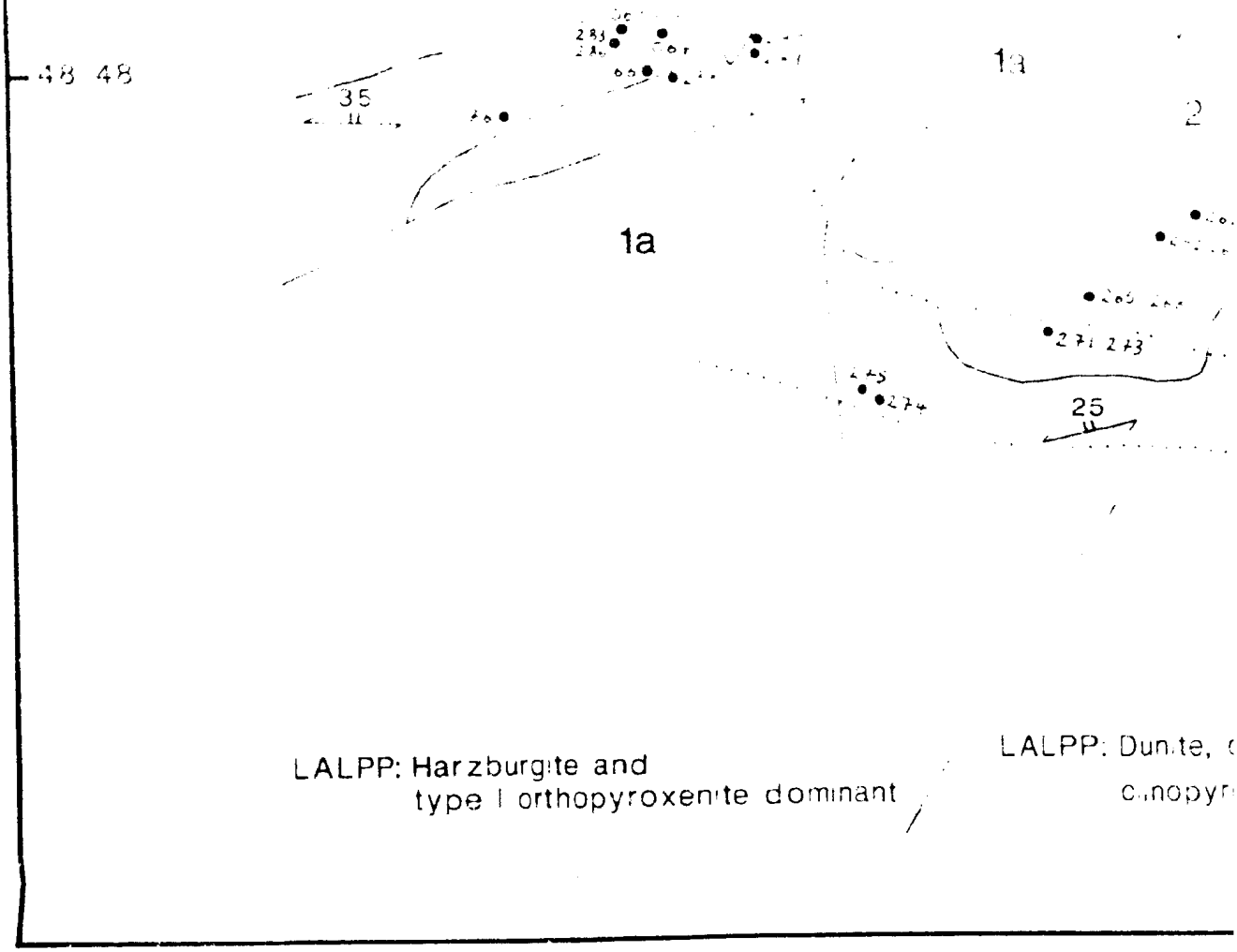
48 48
35
1a
1a
2
25
LALPP: Harzburgite and
type I orthopyroxenite dominant
LALPP: Dunite,

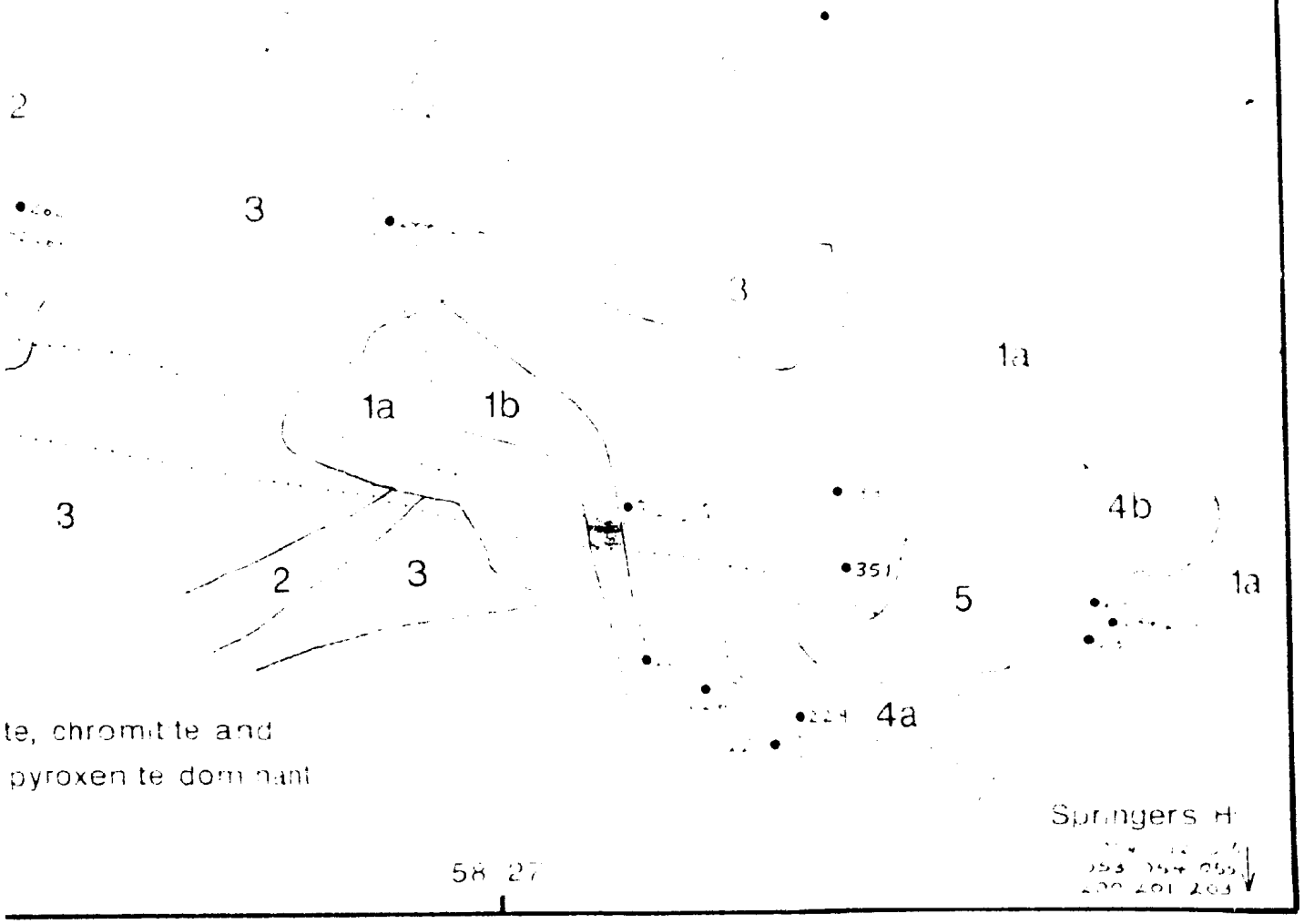
2
3
3
1a
1a
1b
3
4b
2
3
351
5
1a
4a
te, chromit te and
pyroxen te dom nant
Springers H
58 27

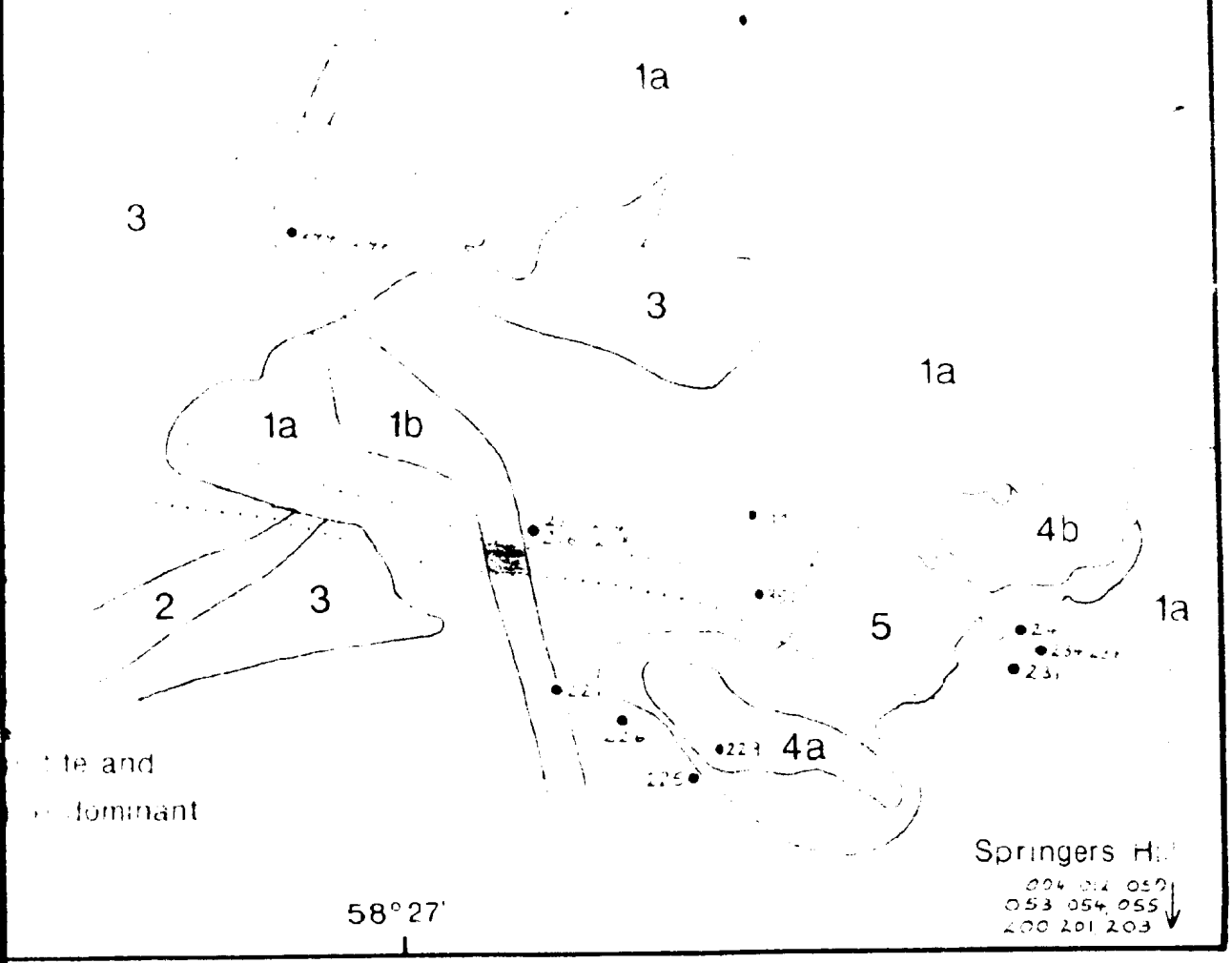
1a
3
3
1a
1a
1b
4b
2
3
5
1a
4a
te and
lominant
Springers Hi
004 052 050
053 054 055
200 201 203
58°27'

NOTES

Amphibole dunite and type 1 orthopyroxenite (OPXT 1) of LALPP and amphibole lherzolite of HALPPG form small bodies that are not represented on the map. These bodies mainly are confined to D2 shear zones and the marginal zone. The area records two episodes of deformation (D1 and D2). Units 1, 2 and 3 of LALPP record D1 and D2, whereas HALPPG, amphibole dunite, OPXT 1 and faults and thrusts are contemporaneous with D2 and post date D1.

LOCATION

Geology of the Lewis Hills Massif from Karson (1984):
Bay of Islands Ophiolite Complex (B)
Coastal Complex (C)

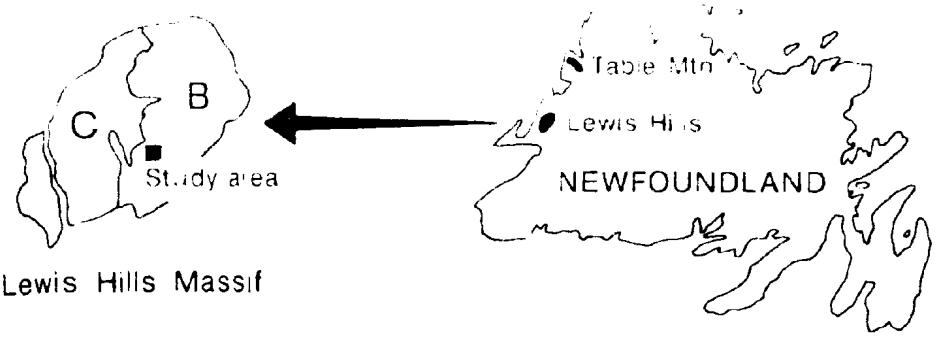

NOTICE

The quality of this microform is heavily dependent upon the quality of the original thesis submitted for microfilming. Every effort has been made to ensure the highest quality of reproduction possible.

If pages are missing, contact the university which granted the degree.

Some pages may have indistinct print especially if the original pages were typed with a poor typewriter ribbon or if the university sent us an inferior photocopy.

Reproduction in full or in part of this microform is governed by the Canadian Copyright Act, R.S.C. 1970, c. C-30, and subsequent amendments.

AVIS

La qualité de cette microforme dépend grandement de la qualité de la thèse soumise au microfilmage. Nous avons tout fait pour assurer une qualité supérieure de reproduction.

S'il manque des pages, veuillez communiquer avec l'université qui a conféré le grade.

La qualité d'impression de certaines pages peut laisser à désirer, surtout si les pages originales ont été dactylographiées à l'aide d'un ruban usé ou si l'université nous a fait parvenir une photocopie de qualité inférieure.

La reproduction, même partielle, de cette microforme est soumise à la Loi canadienne sur le droit d'auteur, SRC 1970, c. C-30, et ses amendements subséquents.

MAGMATIC AND FLUID PROCESSES IN THE UPPER MANTLE: A STUDY OF THE BAY OF ISLANDS OPHIOLITE COMPLEX, NEWFOUNDLAND

VOLUME II: Tables and Figures

©STEPHEN JOHN EDWARDS, B.Sc. (London)

A thesis submitted to the School of Graduate Studies
in partial fulfillment of the requirements for the degree of
Doctor of Philosophy

Department of Earth Sciences
Memorial University of Newfoundland
June 1991

St. John's Newfoundland

ISBN 0-315-68256-6

LIST OF TABLES

VOLUME II: Tables and Figures

TABLE 1.1. Classification of ophiolites as harzburgite ophiolite types and lherzolite ophiolite types 3

TABLE 3.1. Major and trace element and normative compositions of orthopyroxenites in ophiolitic and orogenic mantle peridotites 74

TABLE A1.1. Accuracy and precision of analyses of minerals 89

TABLE A1.2. Accuracy and precision of analyses of major elements 90

TABLE A1.3. Accuracy and precision of analyses of trace elements 90

TABLE A1.4a. Limits of detection and blank compositions of rare earth elements 91

TABLE A1.4b. Precision of rare earth elements 91

TABLE A1.4c. Accuracy and precision of analyses of rare earth elements: BCR-1 92

TABLE A1.4d. Accuracy and precision of analyses of rare earth elements: PCC-1 92

TABLE A1.5. Accuracy and precision of analyses of platinum group elements 96

TABLE A3.1. Olivine analyses 97

TABLE A3.2. Orthopyroxene analyses 107

TABLE A3.3. Clinopyroxene analyses 112

TABLE A3.4. Amphibole analyses 118

TABLE A3.5. Plagioclase analyses 122

TABLE A3.6. Spinel analyses 124

TABLE A4.1. Major and trace element analyses 138

TABLE A4.2. Rare earth element analyses 142

TABLE A4.3. Platinum group element analyses 145

LIST OF FIGURES

VOLUME II: Tables and Figures

FIGURE 1.1. Classification of ultramafic rocks 1

FIGURE 1.2. Solubilities of H_2O and CO_2 in silicate melts and of solute (melt) in H_2O- and CO_2-fluids with variation in pressure 2

FIGURE 1.3. In-situ formation of dunite 4

FIGURE 1.4. Generalized geological map of the Humber Arm Allochthon 5

FIGURE 1.5. Geological map of the Lewis Hills Massif 6

FIGURE 1.6. Composition of olivine, clinopyroxene and spinel in peridotites and pyroxenites of the Springers Hill area 7

FIGURE 2.1. Geological map of the Springers Hill area map pocket

FIGURE 2.2. Stacked sequence of thrust slices 8

FIGURE 2.3. Type I orthopyroxenite dyke pervasively intruding harzburgite 9

FIGURE 2.4. Bands of olivine and orthopyroxene defining S_1 in harzburgite 10

FIGURE 2.5. Partially recrystallized Cr-spinel in harzburgite 11

FIGURE 2.6. Impregnated orthopyroxene in harzburgite 12

FIGURE 2.7. Olivine-orthopyroxene cluster in harzburgite 13

FIGURE 2.8. Disequilibrium texture between orthopyroxene and olivine in an olivine-orthopyroxene cluster in harzburgite 14

FIGURE 2.9. Recrystallized grain of Cr-spinel in harzburgite 15

FIGURE 2.10. Grain of Ca-amphibole enclosed in coarse granular olivine in LAL dunite 16

FIGURE 2.11. Chain texture exhibited by Cr-spinel in LAL dunite 17

FIGURE 2.12. Multiple F_1 folds in a band of chromitite 18

FIGURE 2.13. LAL clinopyroxenite dyke intruding harzburgite and the centre of a type I orthopyroxenite dyke 19

FIGURE 2.14. Cumulate texture exhibited by Cr-spinel in a dunitic zone in LAL olivine clinopyroxenite 20

FIGURE 2.15. Thin bands of Cr-spinel in LAL dunite envelope around LAL olivine clinopyroxenite 21

FIGURE 2.16. Parallel intergrowth of olivine and orthopyroxene in type I orthopyroxenite 22

FIGURE 2.17. Embayment of olivine, tremolite and cummingtonite in orthopyroxene in type I orthopyroxenite 23

FIGURE 2.18. Clinopyroxene partially replaced by tremolite in type I orthopyroxenite 24

FIGURE 2.19. Tremolite and cummingtonite replacing orthopyroxene in type I orthopyroxenite 25

FIGURE 2.20. Orthopyroxene cut by shear zones in type I orthopyroxenite 26

FIGURE 2.21. Well equilibrated coarse granular texture of clinopyroxene in LAL clinopyroxenite 27

FIGURE 2.22. Irregular grain boundary of clinopyroxene in LAL clinopyroxenite 28

FIGURE 2.23. Orthopyroxene replaced by tremolite and olivine in LAL websterite 29

FIGURE 2.24. Clinopyroxene replacing orthopyroxene, and tremolite replacing ortho- and clinopyroxene in harzburgite 30

FIGURE 2.25. Web texture exhibited by type II orthopyroxenite in LAL dunite 31

FIGURE 2.26. Vein of LAL clinopyroxenite offset by narrow D_2 shear zones filled with type II orthopyroxenite ribbon mylonite 32

FIGURE 2.27. Boudin of websterite associated with ribbon mylonite of type II orthopyroxenite in D_2 shear zone 33

FIGURE 2.28. Cr-spinel hosting inclusions in web-textured type II orthopyroxenite 34

FIGURE 2.29. Monomineralic bands of orthopyroxene, olivine and Ca-amphibole in type II orthopyroxenite ribbon mylonite 35

FIGURE 2.30. Conjugate veins of type I orthopyroxenite partially pseudomorphed by amphibole dunite 36

FIGURE 2.31. Enclaves of type I orthopyroxenite in amphibole dunite 37

FIGURE 2.32. Well equilibrated mosaic equigranular texture of olivine in amphibole dunite 38

FIGURE 2.33. Sieve texture in poikiloblastic Cr-spinel in amphibole dunite 39

FIGURE 2.34. Modal layering of Al-spinel in HAL dunite 40

FIGURE 2.35. Band of fine grained Al-spinel cutting coarse grained Al-spinel in HAL dunite 41

FIGURE 2.36. Chain texture exhibited by Al-spinel in HAL dunite 42

FIGURE 2.37. Protrusion of Al-spinel associated with clinopyroxene along the grain boundary of adjacent grains of olivine in HAL dunite 43

FIGURE 2.38. Al-spinel containing inclusions in HAL wehrlite 44

FIGURE 2.39. HAL gabbro dyke grading to HAL wehrlite in a HAL gabbro-clinopyroxene dunite association 45

FIGURE 2.40. HAL wehrlite grading to HAL dunite and cut by HAL olivine clinopyroxenite 46

FIGURE 2.41. Reduction in grain size of Al-spinel from HAL dunite to HAL wehrlite 47

FIGURE 2.42. Dunitic portion of a HAL olivine clinopyroxenite dyke cutting LAL dunite 48

FIGURE 2.43. Gradational contact between LAL clinopyroxenite and HAL olivine clinopyroxenite 49

FIGURE 2.44. Interstitial clinopyroxene in a matrix of olivine in HAL wehrlite 50

FIGURE 2.45. Poikilitic clinopyroxene containing chadacrysts of olivine in HAL olivine clinopyroxenite 51

FIGURE 2.46. Xenoliths of harzburgite and LAL and HAL dunite in HAL olivine clinopyroxenite 52

FIGURE 2.47. Irregular HAL dunite xenoliths in HAL olivine clinopyroxenite 53

FIGURE 2.48. Veins of HAL olivine clinopyroxenite at the contact between HAL dunite and harzburgite 54

FIGURE 2.49. Assemblage of HAL olivine-spinel-clinopyroxene replacing harzburgite 55

FIGURE 2.50. Partially schematic phase relations for ultramafic rocks modelled by the system H_2O-Na_2O-CaO-MgO-Al_2O_3-SiO_2 with excess H_2O and Mg_2SiO_4 56

FIGURE 3.1. Frequency distribution of Mg# of olivine in LALPP 57

FIGURE 3.2. Compositional variation of orthopyroxene in LALPP 58

FIGURE 3.3. Cr# vs. Mg# of spinel in LALPP 59

FIGURE 3.4. Cr# vs. Mg# composition fields of spinel 60

FIGURE 3.5. Chondrite-normalized rare earth element abundances of LALPP 61

FIGURE 3.6. Chondrite-normalized platinum group element abundances of LALPP 65

FIGURE 3.7. Mineral/matrix equilibrium partition coefficients of rare earth elements for olivine, orthopyroxene, clinopyroxene and amphibole 69

FIGURE 3.8. CaO/Al_2O_3 vs. Mg# of harzburgites 70

FIGURE 3.9. Chondrite-normalized platinum group element abundances of a LAL clinopyroxenite dyke and associated dunite envelope and harzburgite 72

FIGURE 3.10. Estimated chondrite-normalized rare earth element abundances of magmas in equilibrium with type I orthopyroxenite and LAL clinopyroxenite 73

FIGURE 4.1. NiO vs. Mg# of olivine in HALPPG 75

FIGURE 4.2. Compositional variation of spinel in HALPPG 76

FIGURE 4.3. Compositional variation of clinopyroxene in HALPPG 77

FIGURE 4.4. $Na_2O + K_2O$-$FeO_{(total)}$-MgO (AFM) and CaO-Al_2O_3-MgO (CAM) diagrams (weight %) of whole-rock samples of HALPPG 78

FIGURE 4.5. Chondrite-normalized rare earth element abundances of HALPPG and amphibolite dykes 79

FIGURE 4.6. CAM diagram (weight %) of orthopyroxene in harzburgite and type I orthopyroxenite adjacent to HALPPG 80

FIGURE 4.7. Compositional variation of spinel in LALPP associated with HALPPG 81

FIGURE 4.8. Compositional variation of Cr-spinel in harzburgite cut by a vein of HAL olivine clinopyroxenite 82

FIGURE 4.9. Compositional variation of clinopyroxene, olivine and spinel across the contact between LAL olivine clinopyroxenite and HAL olivine clinopyroxenite 83

FIGURE 4.10. AFM and CAM diagrams (weight %) used to model the formation of HALPPG 84

FIGURE 5.1. Compositional variation of Ca-amphibole in LALPP and HALPPG 86

FIGURE 5.2. Compositional variation exhibited by a grain of spinel in amphibole dunite 87

FIGURE 5.3. Chondrite-normalized rare earth element abundances of amphibole-bearing rock types in the Springers Hill area 88

FIGURE A1.1. Precision of chondrite-normalized rare earth element abundances 93

FIGURE A1.2. Precision and accuracy of chondrite-normalized rare earth element abundances of USGS peridotite standard PCC-1 94

FIGURE A1.3. Chondrite-normalized rare earth element abundances of blanks and limits of detection in runs 182 and 024 95

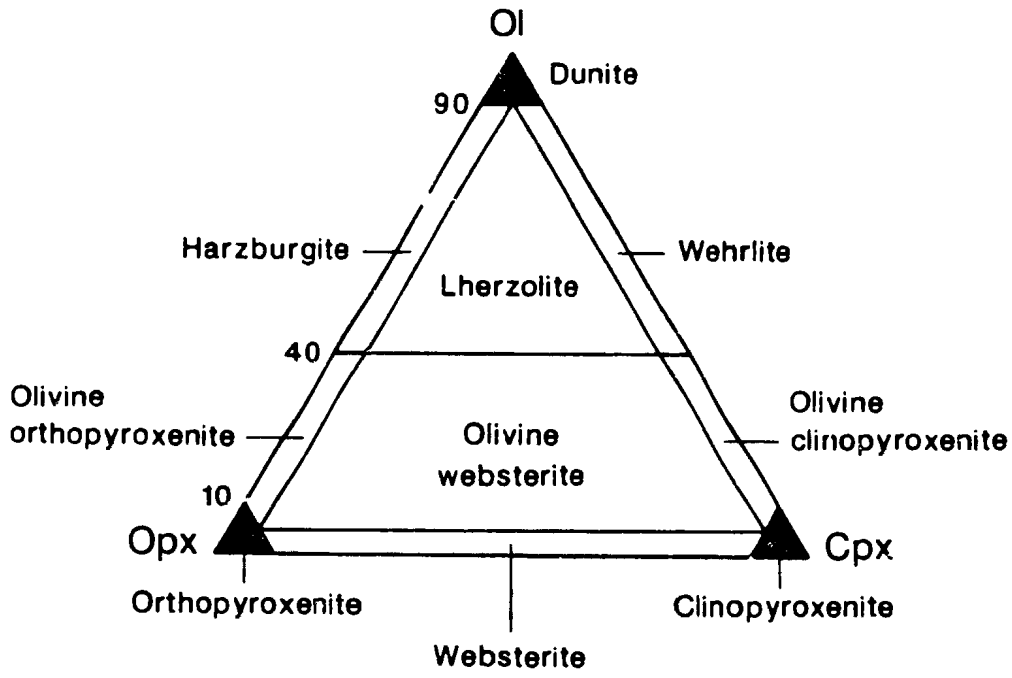

FIGURE 1.1. Classification of ultramafic rocks (Streckeisen, 1976).

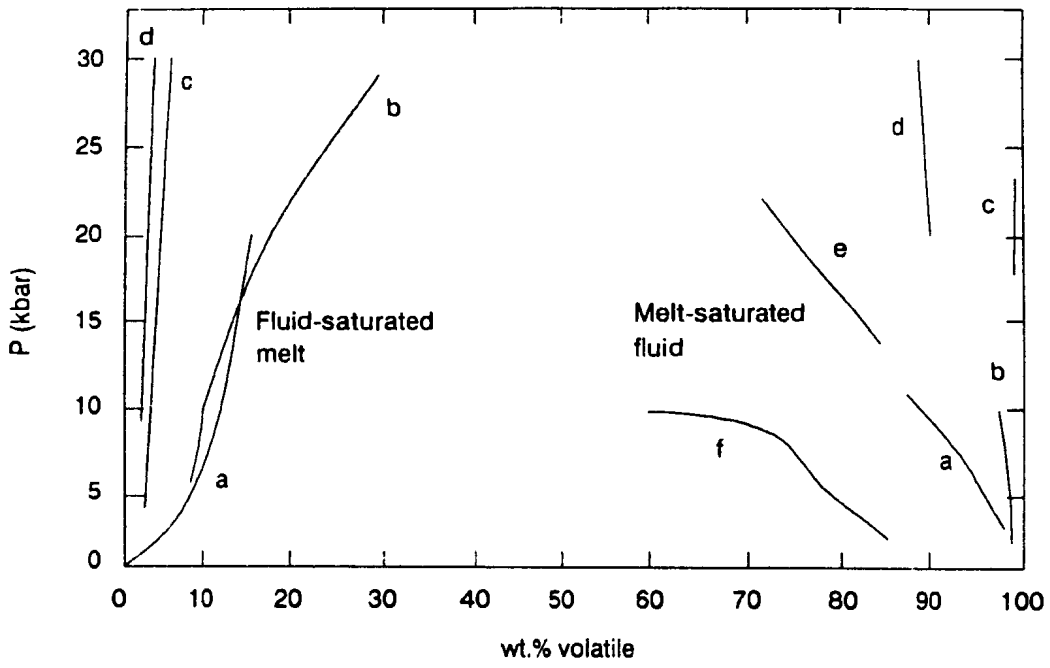

FIGURE 1.2. Solubilities of H_2O and CO_2 in silicate melts and of solute (melt) in H_2O- and CO_2-fluids with variation in pressure. Fluid-saturated melts: (a) H_2O in tholeiitic melt; (b) H_2O in diopside melt; (c) CO_2 in diopside melt; (d) CO_2 in albite melt. Melt-saturated fluids: (a) H_2O-fluid--granitic melt; (b) H_2O-CO_2-fluid--basalt melt; (c) CO_2-fluid--diopside melt; (d) H_2O-fluid--diopside melt; (e) H_2O-fluid--andesite melt; (f) H_2O-fluid--$NaAlSiO_4$ melt. Diagram from Eggler (1987).

TABLE 1.1. Classification of ophiolites as harzburgite ophiolite types (HOT) and lherzolite ophiolite types (LOT) (modified from Boudier and Nicolas, 1985; Nicolas, 1989).

	LOT	HOT
Alternative classification	high-Ti type Type I mid-ocean ridge type Liguria type W. Mediterranean type chromite-barren type	low-Ti type (1) Type III (2) supra-subduction zone type (3) Papua type (4) E. Mediterranean type (5) chromite-mineralized type (5)
Mafic crustal section	0-3 km thick	2-7 km thick
basalt	tholeiitic and alkalic, high-Ti	tholeiitic and quartz tholeiitic, low-Ti
crystallization	Ol--Plag--Cpx	Ol--Opx--Cpx--Plag
late intrusives	diabase dykes and sills	wehrlite bodies
low-T plastic deformation	very common	absent, except local shear zones
Mantle section peridotites	plagioclase lherzolite and abundant dunite within 2 km below Moho. Cr#(Sp) <60	harzburgite and abundant dunite to 10 km below Moho. Cr#(Sp) >60
podiform chromitites	uncommon to absent	always present
partial melting	low at greater depth and small volume of magma extracted	high at shallower depth and large volume of magma extracted
high-T plastic flow structures	steep foliation and moderately plunging lineation	flat foliation, locally vertical with vertical lineation
Spreading rate	incipient/slow rift	mature/fast rift
Environment	mid-ocean ridge	supra-subduction zone
Examples	Trinity, Liguria	Troodos, Papua

(1) Serri (1981), (2) Dick and Bullen (1984), (3) Pearce et al. (1984), (4) Ishiwatari (1985a), (5) Roberts (1988).

FIGURE 1.3. In-situ formation of dunite. Top: foliated plagioclase wehrlite hosting a pyroxenite vein which has a symmetrical dunite envelope that contains traces of the wehrlite; Stowbridge area, North Arm Mountain, Bay of Islands Ophiolite Complex. Bottom: dunite replacing harzburgite and veins of orthopyroxenite; Table Mountain, Bay of Islands Ophiolite Complex.

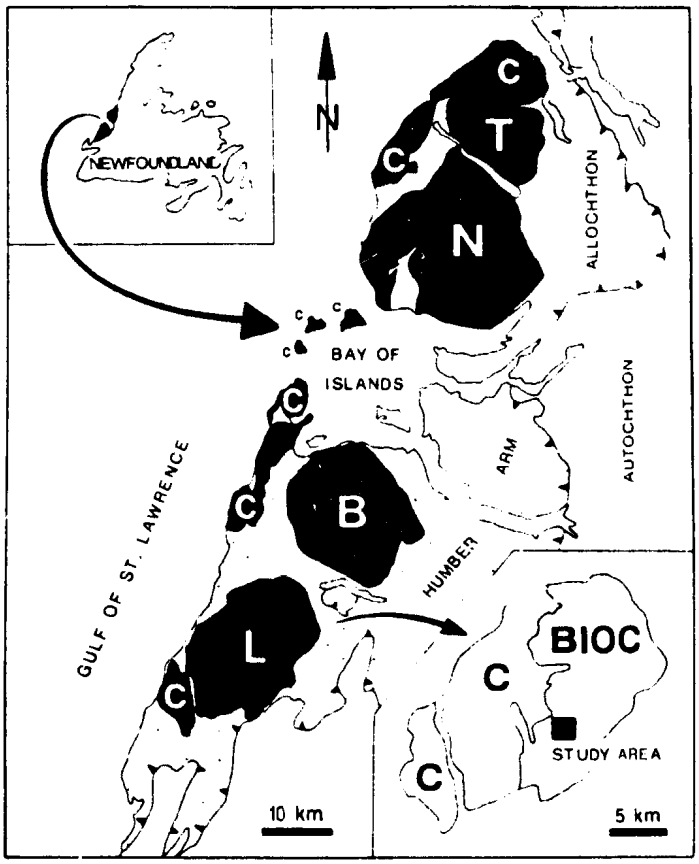

FIGURE 1.4. Generalized geological map of the Humber Arm Allochthon, western Newfoundland, Canada, after Smith (1958), Williams (1973) and Karson (1979). The Bay of Islands Ophiolite Complex (BIOC) comprises Table Mountain (T), North Arm Mountain (N), Blow Me Down Mountain (B) and Lewis Hills (L); C is the Coastal Complex; barbs on upper thrust slice.

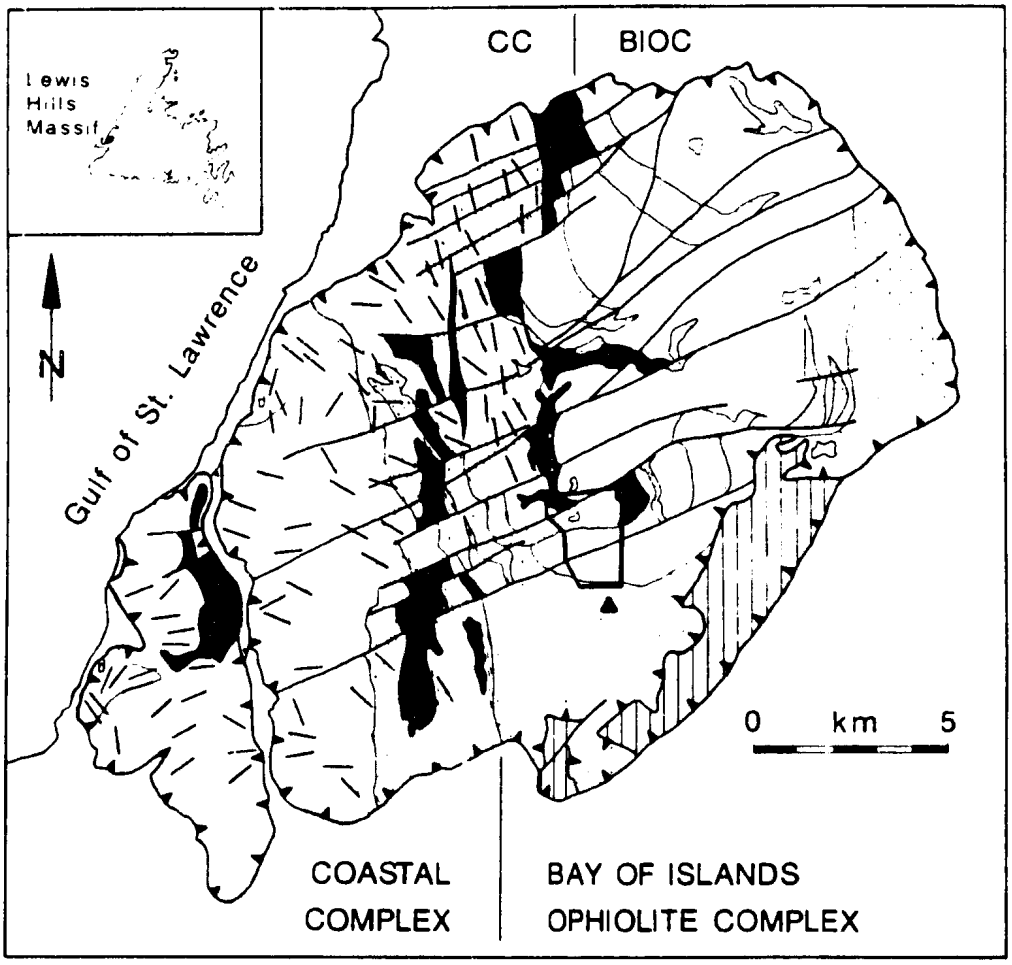

FIGURE 1.5. Geological map of the Lewis Hills Massif from Karson (1977, 1979, 1984). Bay of Islands Ophiolite Complex (BIOC): harzburgite (coarse stipple); dunite cumulates (unpatterned); variably deformed layered cumulates of dunite, wehrlite, clinopyroxenite and gabbro (dense stipple); mafic gneiss and amphibolite (metamorphic sole according to Williams and Cawood (1989)) (vertical lines which approximate orientation of foliation and mineral lineation). Coastal Complex (CC): highly deformed mafic gneiss and amphibolite of Mount Barren Assemblage (dashed lines which approximate orientation of foliation and mineral lineation); wehrlite-lherzolite crystal mush intrusions (black); gabbro and metagabbro (fine stipple); sheeted dyke complex (d); mafic dykes (short bold lines); small bodies of plagiogranite occur throughout (not shown). Faults and shear zones (thick black lines), with barbs on upper thrust slice; Springers Hill (black triangle); area of this study enclosed in thick black line.

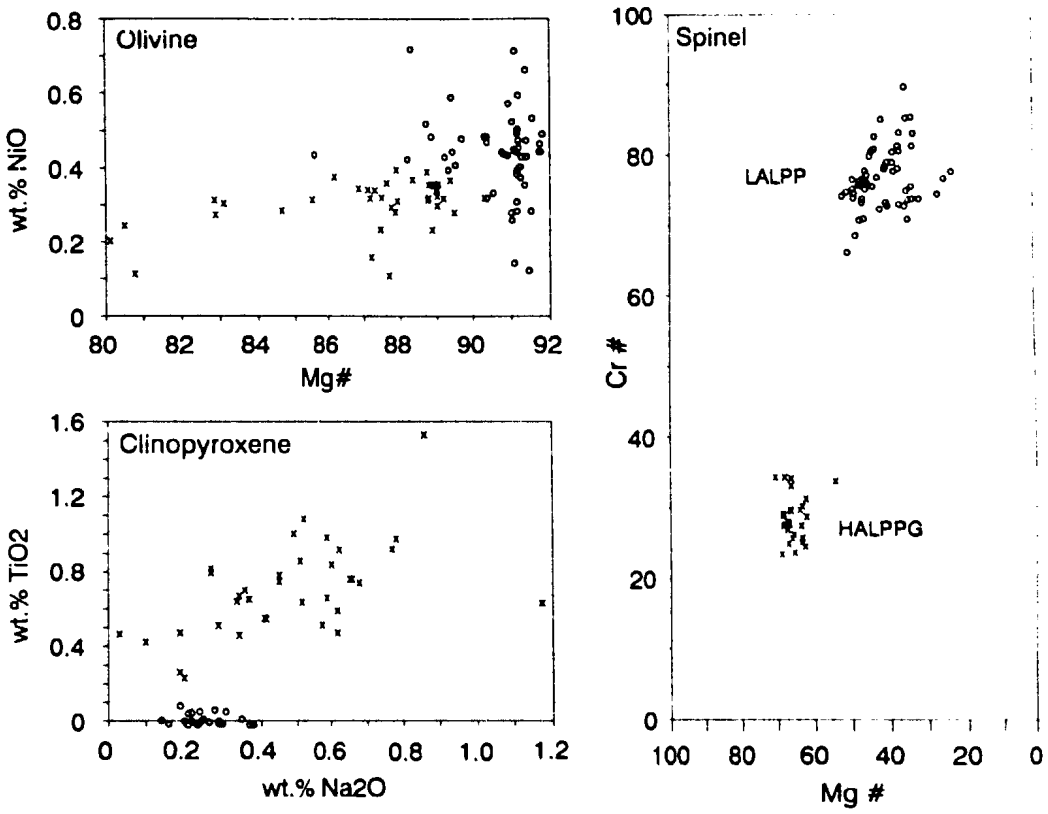

FIGURE 1.6. Composition of olivine, clinopyroxene and spinel in rocks of the Springers Hill area. Using spinel, the rocks are classified as low-Al peridotites and pyroxenites (LALPP) (o), and high-Al peridotites, pyroxenites and gabbros (HALPPG) (x).

FIGURE 2.1. Geological map of the Springers Hill area (in map pocket).

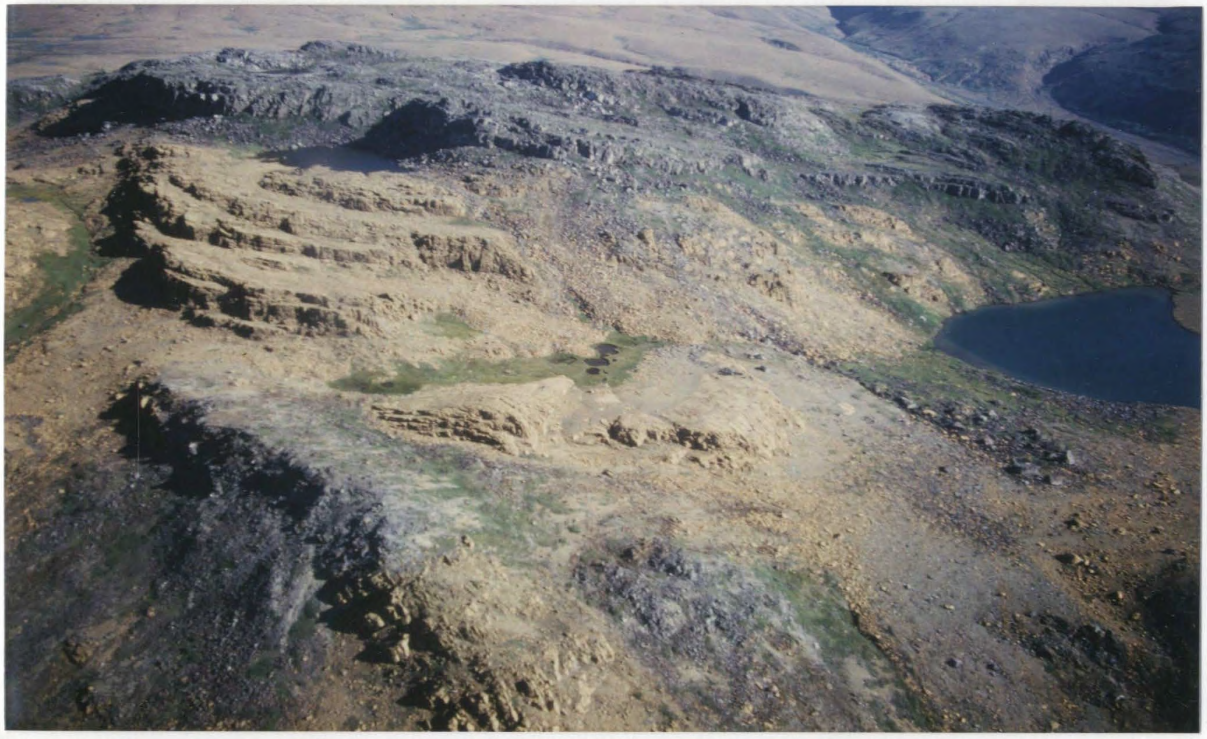

FIGURE 2.2. Stacked sequence of thrust slices of harzburgite and LAL dunite (brown), and uncorrelated wehrlite and gabbro (grey). All rocks are D_2 mylonites.

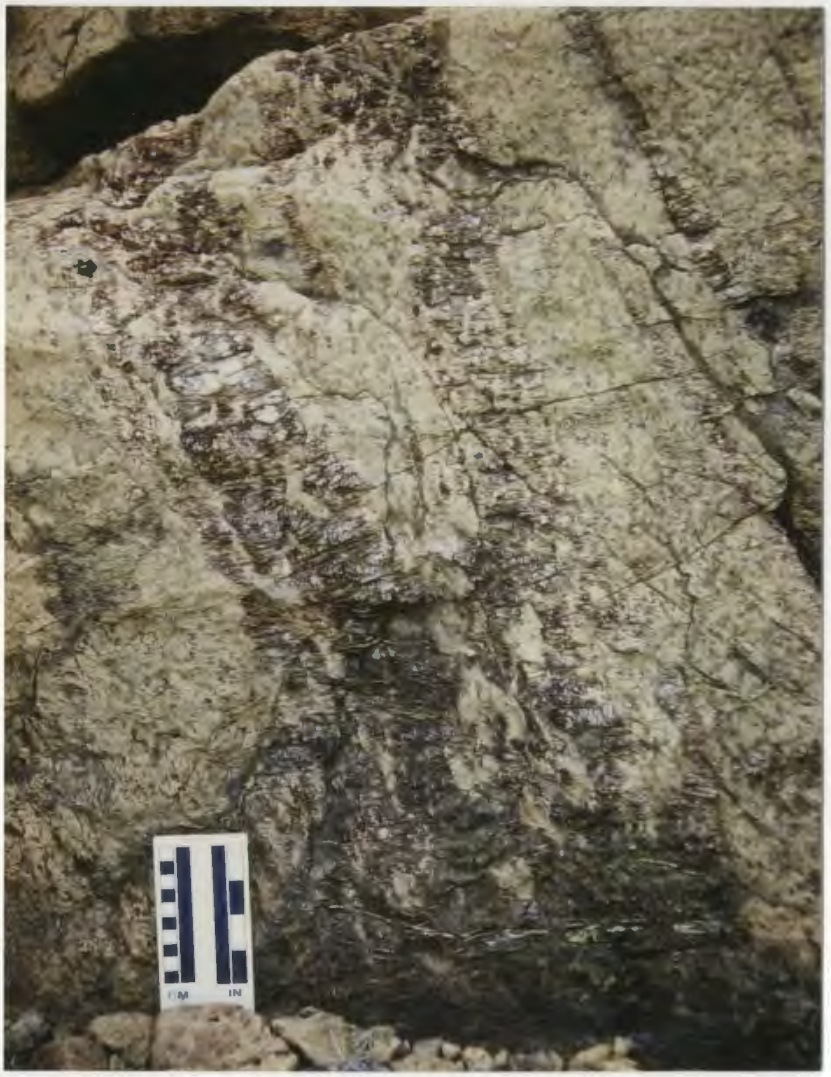

FIGURE 2.3. Type I orthopyroxenite dyke pervasively intruding harzburgite.

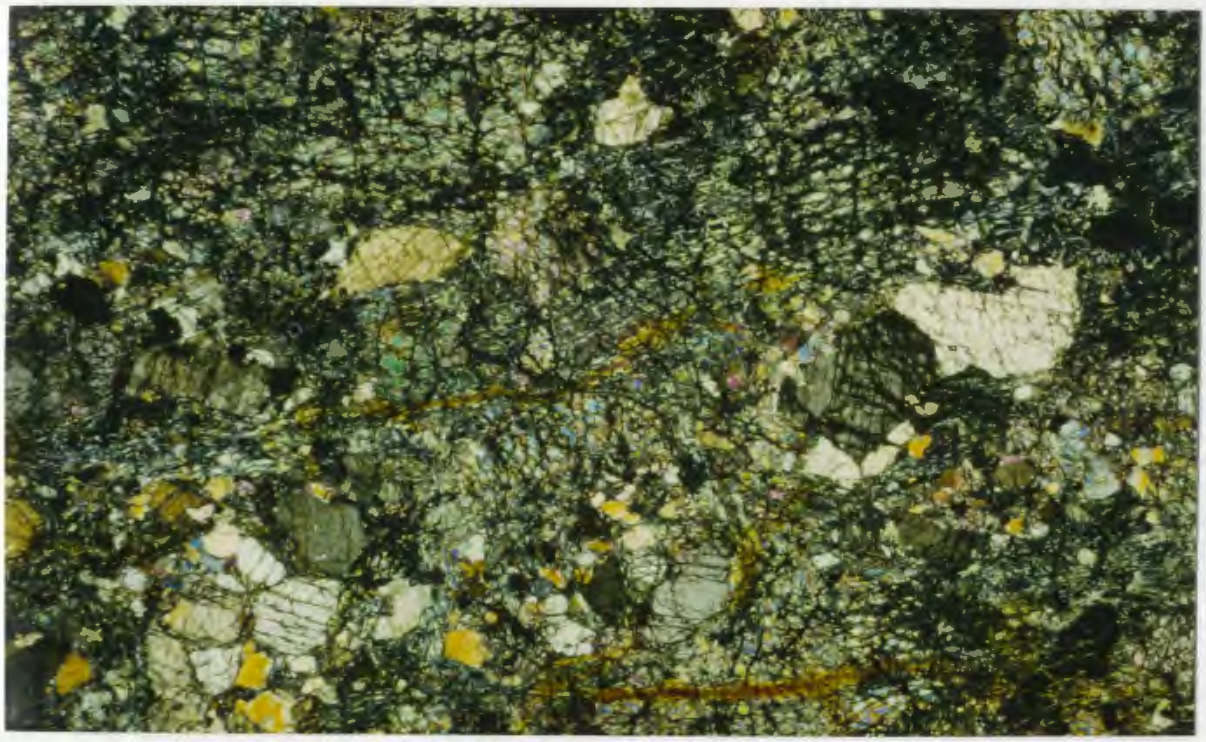

FIGURE 2.4. Bands of serpentinized coarse granular olivine and relatively unaltered porphyroclasts and neoblasts of orthopyroxene, which define S_1 in harzburgite. The foliation defined by Cr-spinel (black) is at a high angle to this banding. Harzburgite sample L106. Length of photograph 15.5 mm; crossed nicols.

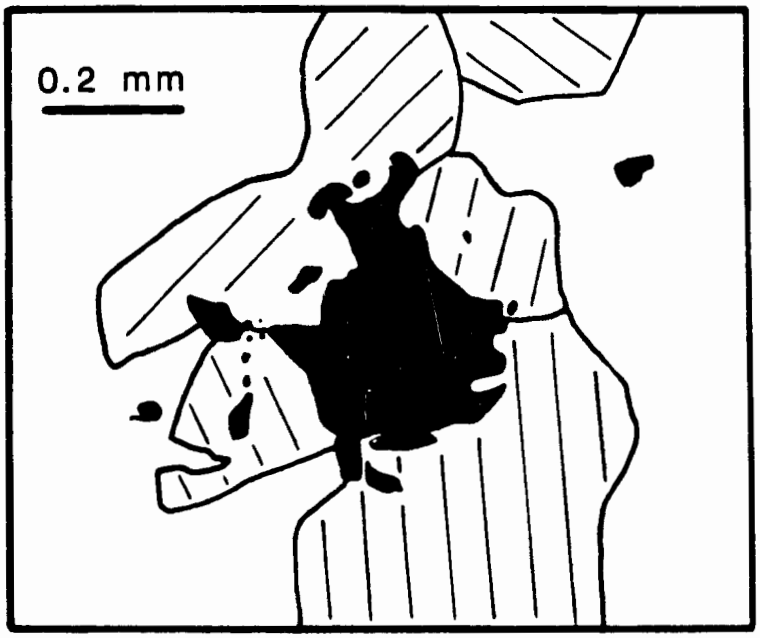

FIGURE 2.5. Partially recrystallized Cr-spinel (black) in an aggregate of porphyroclastic grains of orthopyroxene (lines defining cleavage) which have well equilibrated and embayed grain boundaries adjacent to olivine (undefined). Harzburgite sample L225. In many samples of harzburgite, similar textures of Cr-spinel are developed in olivine adjacent to orthopyroxene.

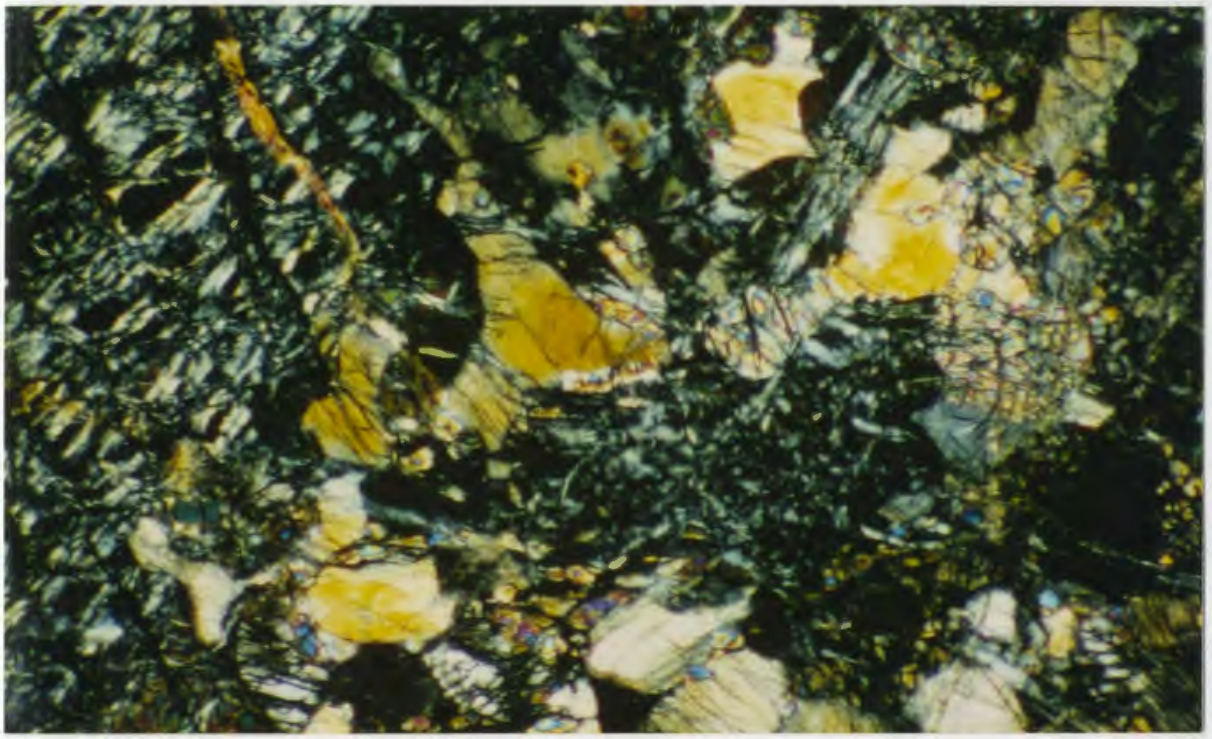

FIGURE 2.6. Impregnated orthopyroxene (yellow) in serpentinized coarse granular olivine (grey). Orthopyroxene grains are partially replaced by olivine. Harzburgite sample L106. Length of photograph 3.0 mm; crossed nicols.

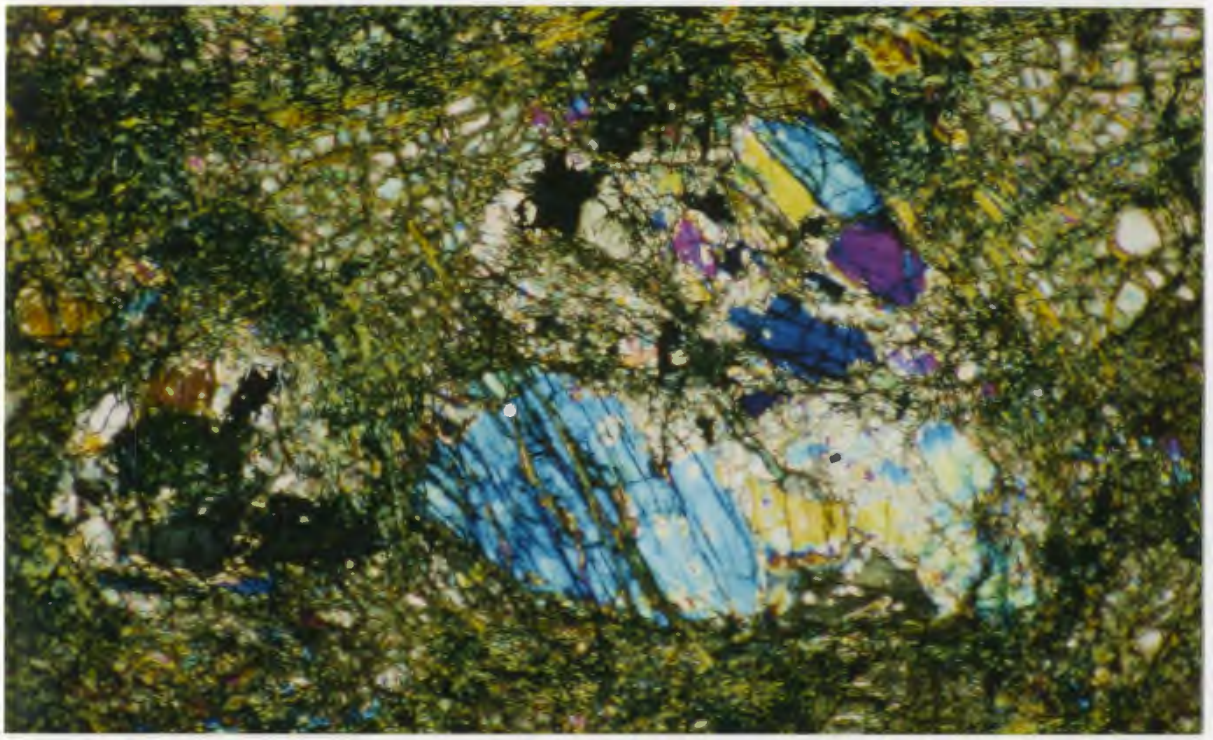

FIGURE 2.7. Olivine-orthopyroxene cluster in serpentinized coarse granular olivine. Aggregates of porphyroclasts and neoblasts of orthopyroxene are replaced by mosaic equigranular olivine. Harzburgite sample L263. Length of photograph 6.0 mm; crossed nicols.

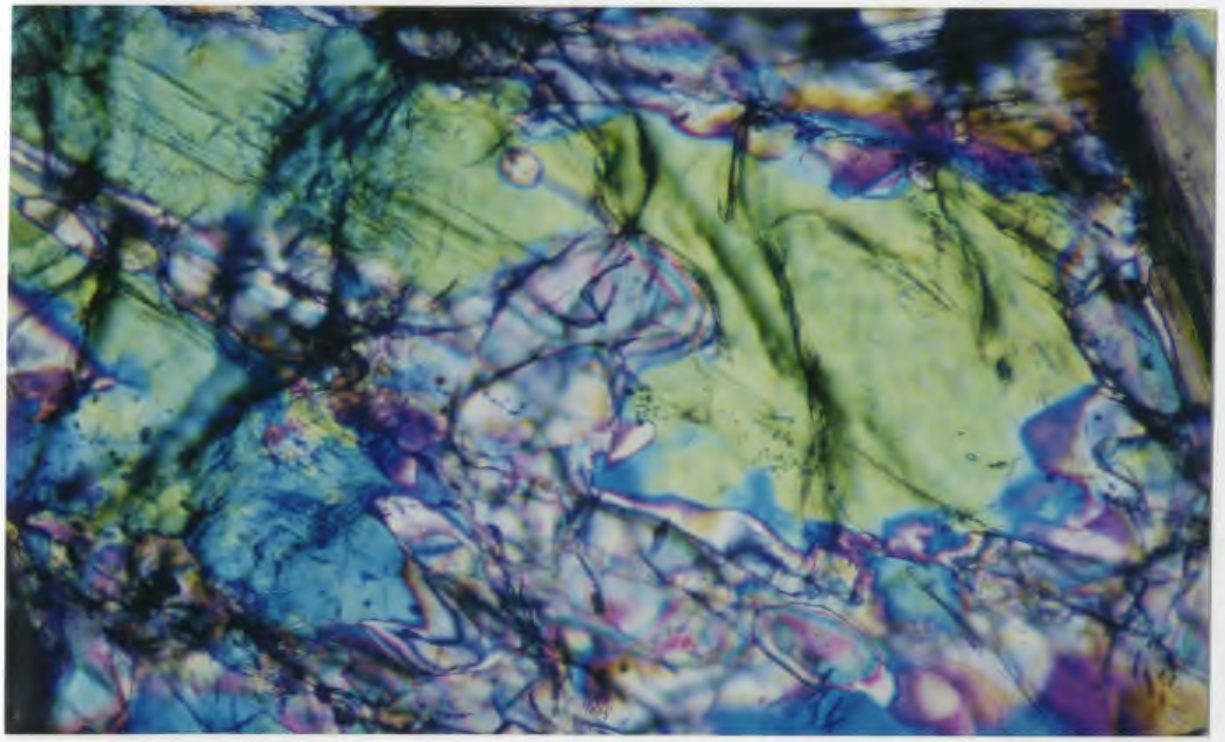

FIGURE 2.8. Disequilibrium texture between orthopyroxene (green) and olivine in an olivine-orthopyroxene cluster. Minute grains of spinel (dark spots) occur at or near the contact of olivine and orthopyroxene. Harzburgite sample L263. Length of photograph 0.55 mm; crossed nicols.

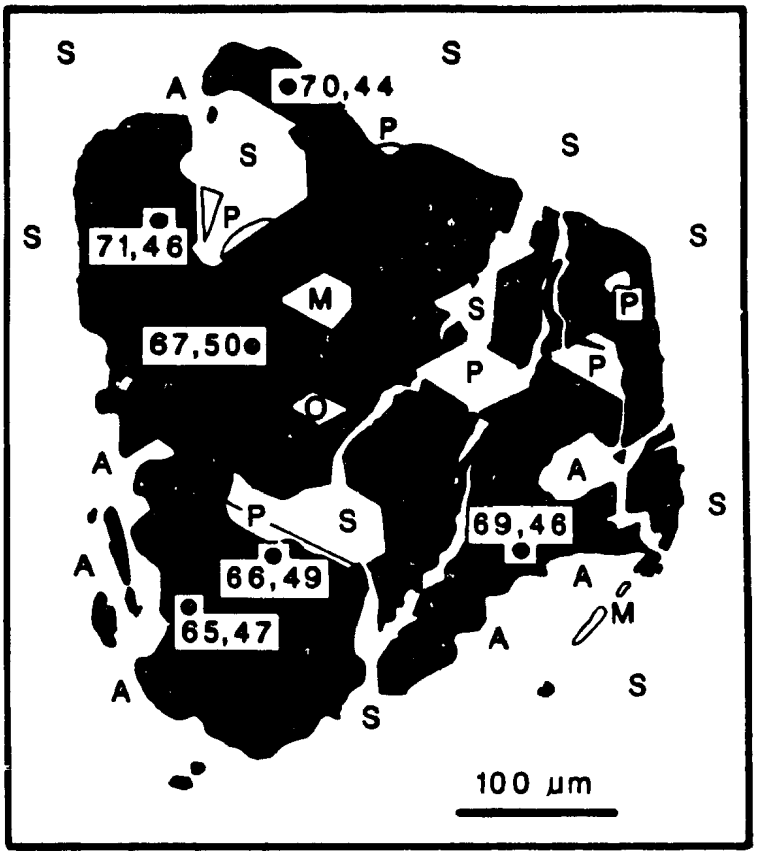

FIGURE 2.9. Recrystallized grain of Cr-spinel (black) hosting inclusions of olivine (O), serpentine (S), magnetite (M), phlogopite (P) and Ca-amphibole (A). The grain boundary of Cr-spinel is even in contact with serpentinized olivine, but highly embayed in contact with Ca-amphibole and phlogopite. Serpentinization has affected all phases. Harzburgite sample L173. (Numbers are Cr#, Mg# of points analysed in Cr-spinel).

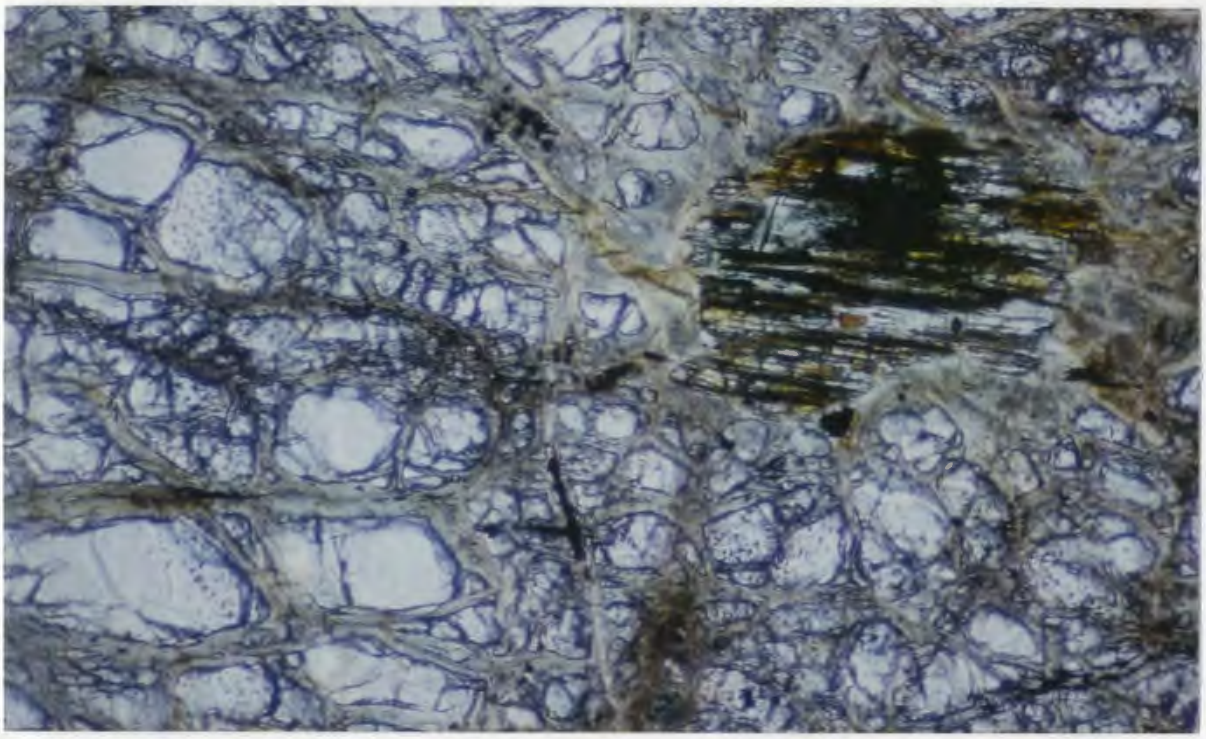

FIGURE 2.10. Grain of Ca-amphibole enclosed in serpentinized coarse granular olivine. The abundance of unidentified inclusions in olivine decreases away from Ca-amphibole. Narrow, discontinuous veins of Ca-amphibole and magnetite run parallel to trails of inclusions in the olivine (not shown). LAL dunite sample L262. Length of photograph 1.4 mm; plane-polarized light.

FIGURE 2.11. Chain texture exhibited by Cr-spinel (black) along the grain boundaries of grains of olivine (white). LAL dunite sample L162. Length of drawing 6.6 mm.

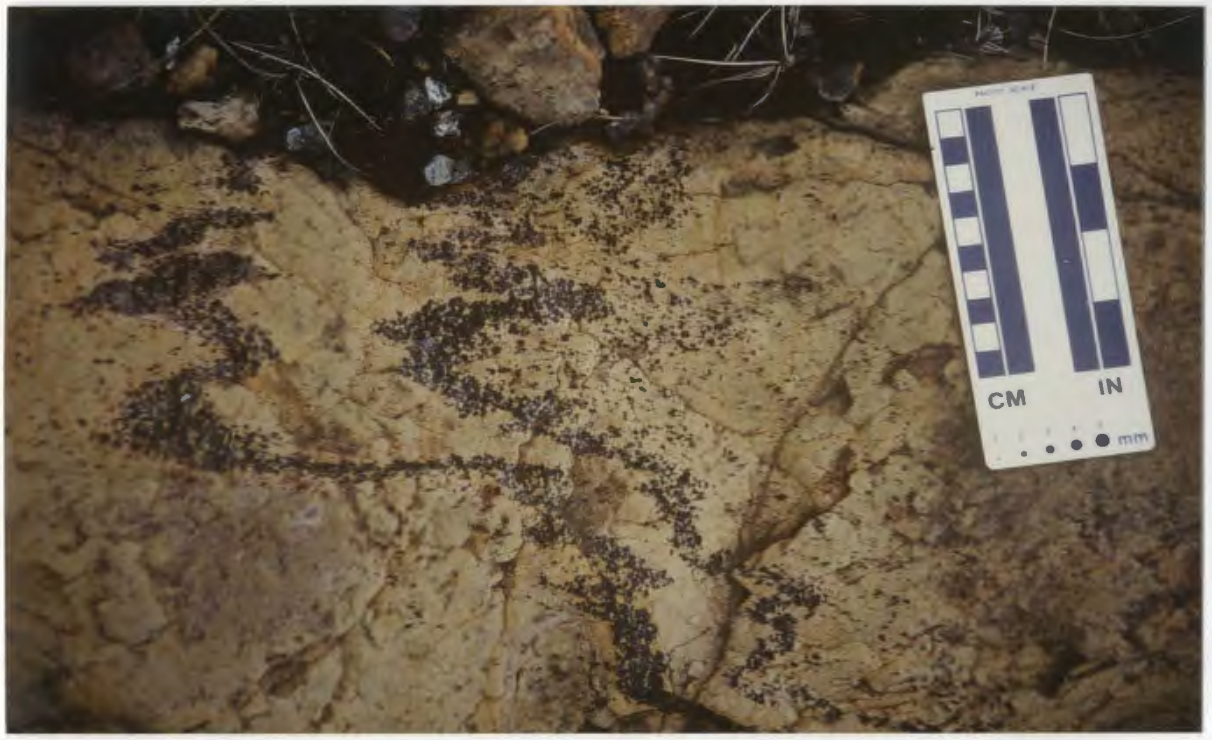

FIGURE 2.12. Multiple F_1 folds in a band of chromitite exhibiting modal layering of Cr-spinel in LAL dunite.

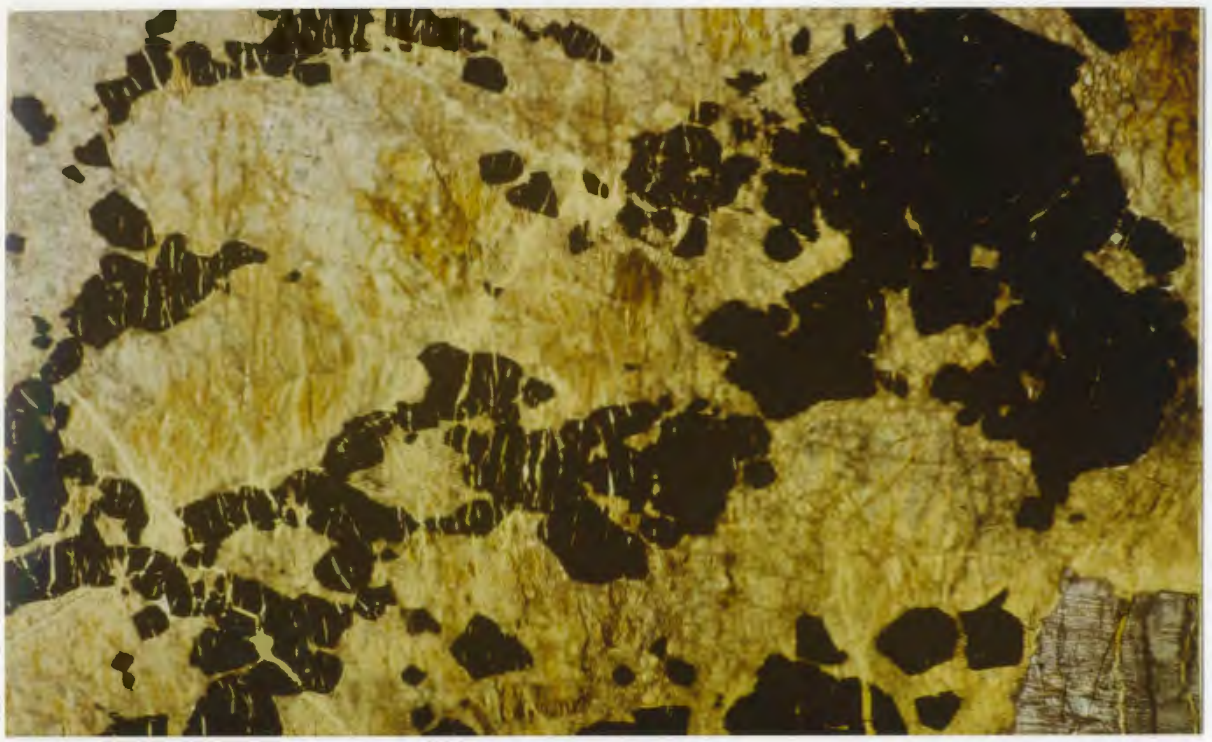

FIGURE 2.14. Cumulate texture exhibited by Cr-spinel in serpentinized olivine. Dunitic zone in LAL olivine clinopyroxenite sample L199. Length of photograph 11 mm; plane-polarized light.

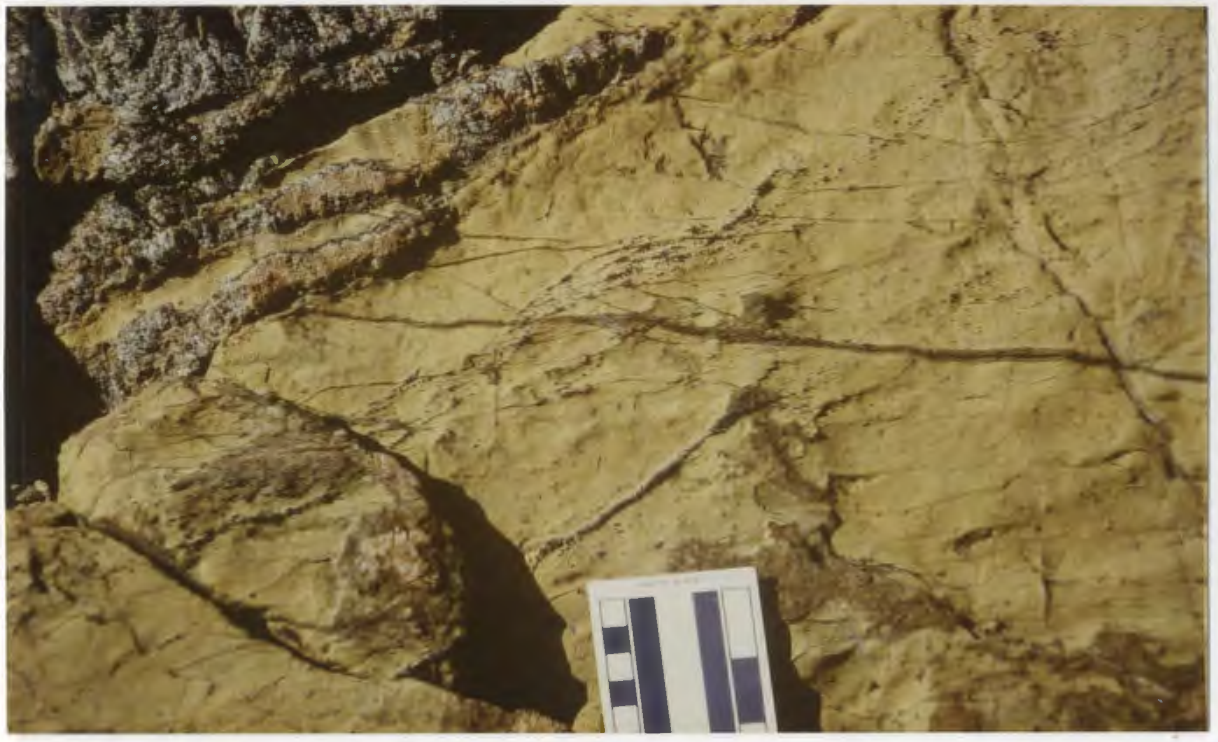

FIGURE 2.15. Thin bands of Cr-spinel in LAL dunite envelope around LAL olivine clinopyroxenite. The bands of Cr-spinel run parallel to the olivine clinopyroxenite.

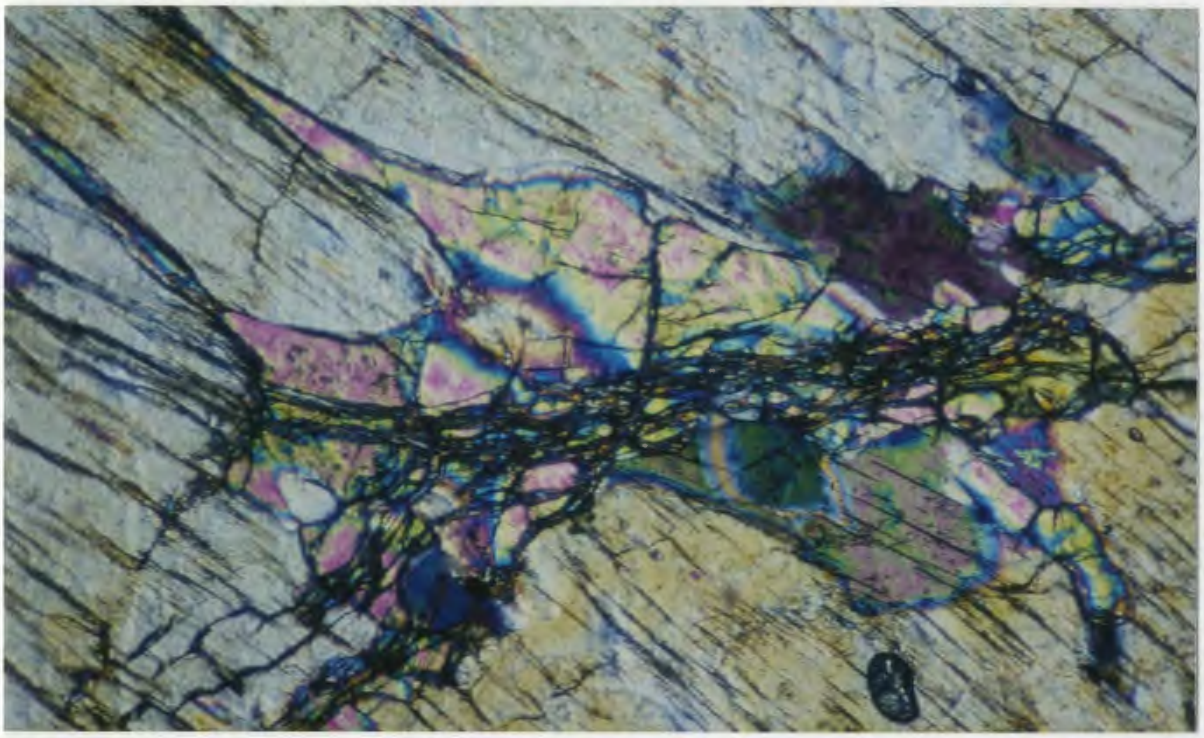

FIGURE 2.16. Parallel intergrowth of olivine (partially serpentinized) and orthopyroxene (grey). Tremolite (with cleavage and near extinction) and olivine occur along the grain boundary of adjacent grains of orthopyroxene. Type I orthopyroxenite sample L066. Length of photograph 1.3 mm; crossed nicols.

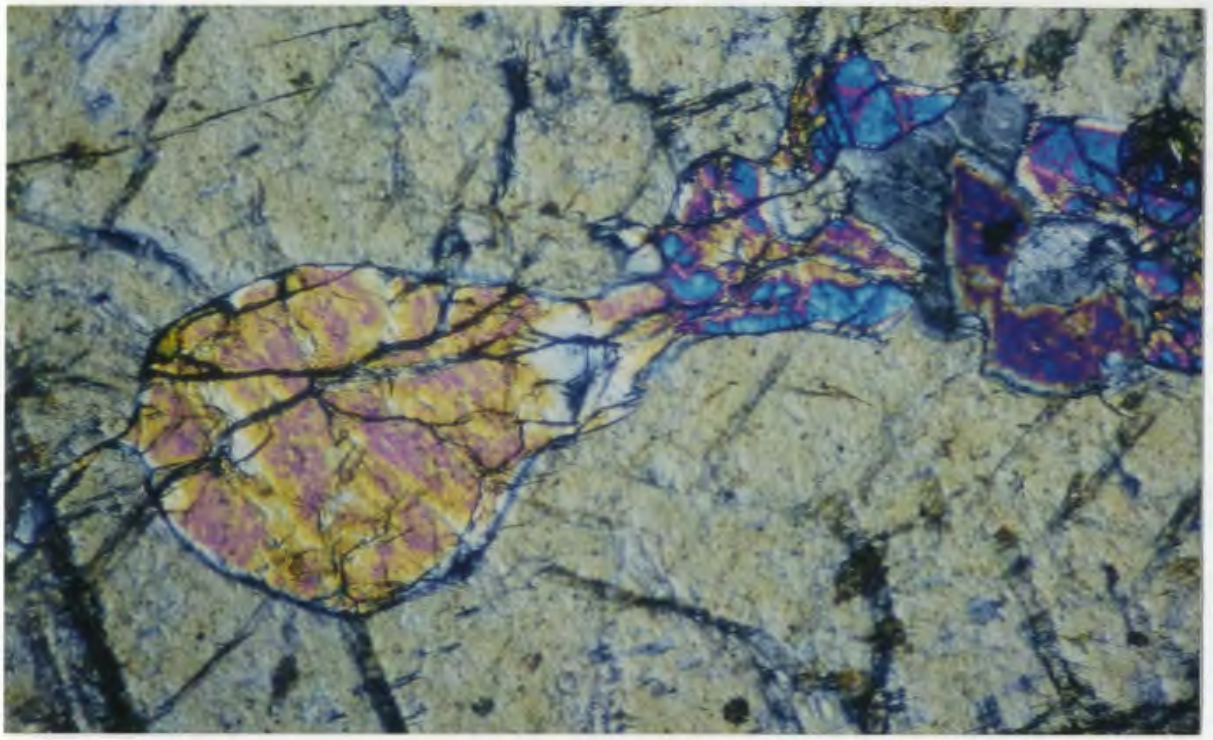

FIGURE 2.17. Embayment of olivine (orange and blue/purple), tremolite (purple near extinction) and cummingtonite (grey) in orthopyroxene. Type I orthopyroxenite sample L066. Length of photograph 1.4 mm; crossed nicols.

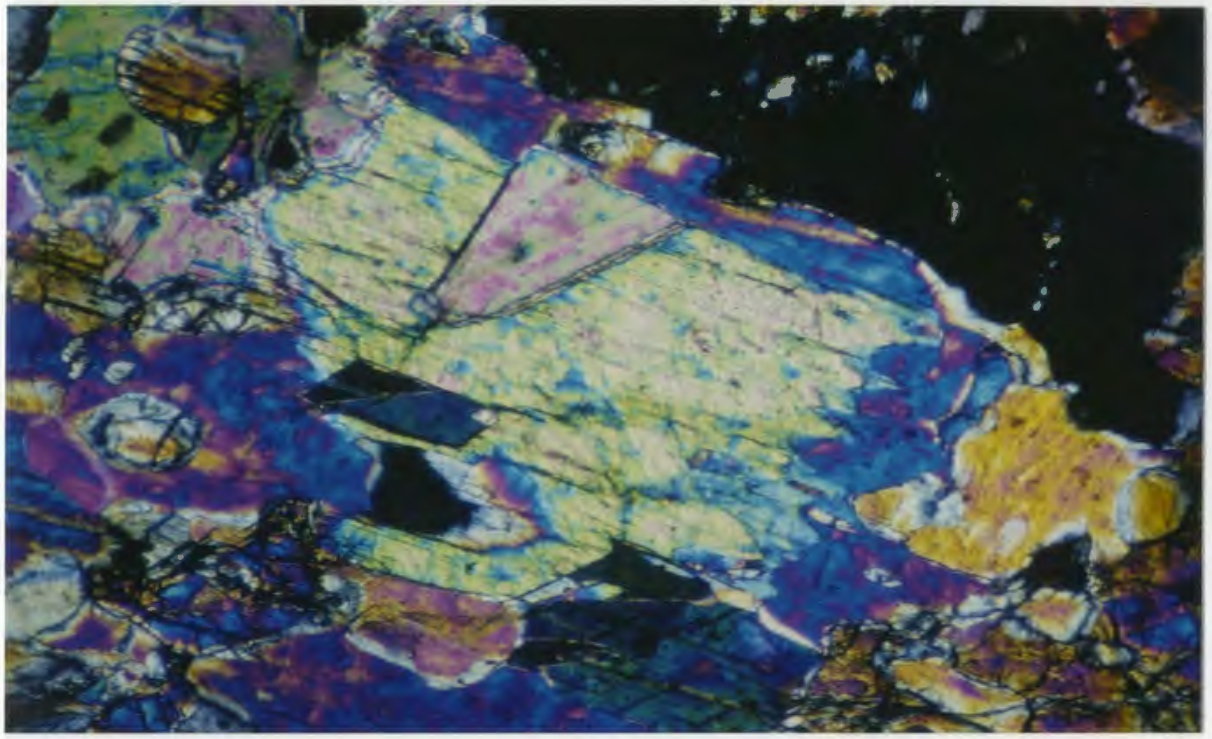

FIGURE 2.18. Clinopyroxene (green-yellow) partially replaced by tremolite (tabular grains and purple/blue grain). Tremolite contains grains of olivine and orthopyroxene. Type I orthopyroxenite sample L066. Length of photograph 1.4 mm; crossed nicols.

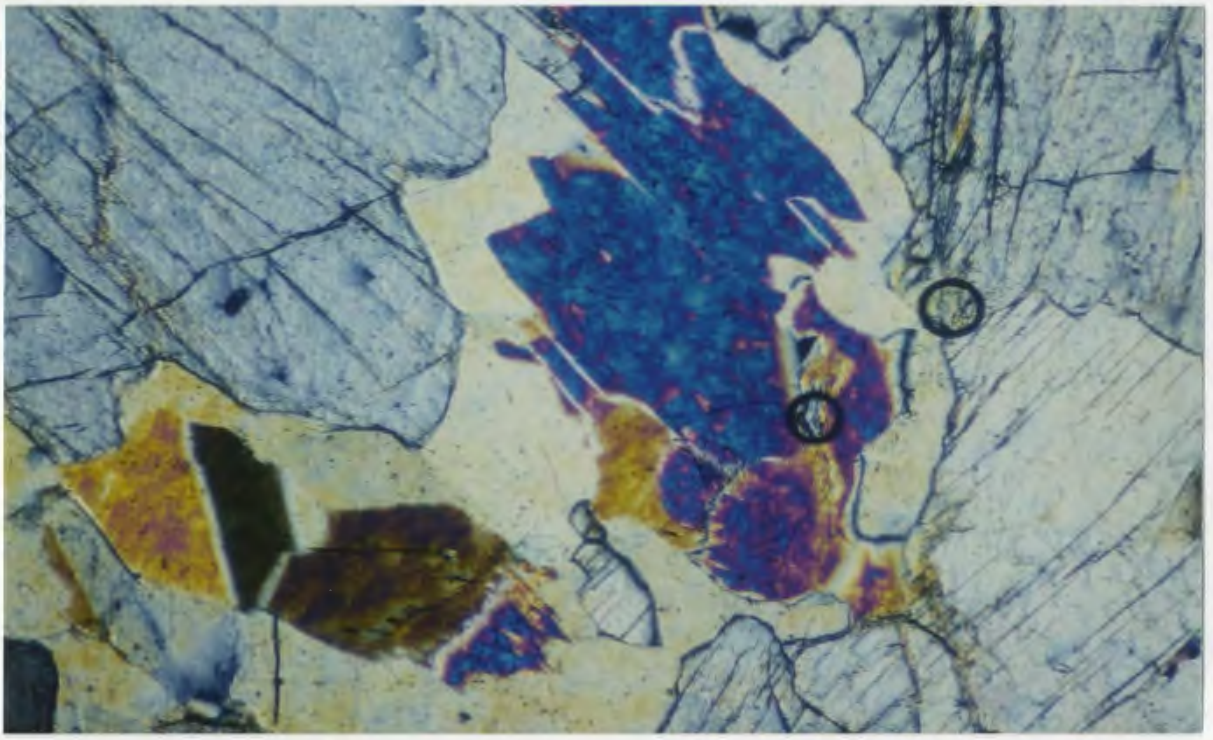

FIGURE 2.19. Tremolite (blue, purple, orange and brown) and cummingtonite (pale yellow) replacing orthopyroxene (grey). Type I orthopyroxenite sample L066. Length of photograph 1.4 mm; crossed nicols.

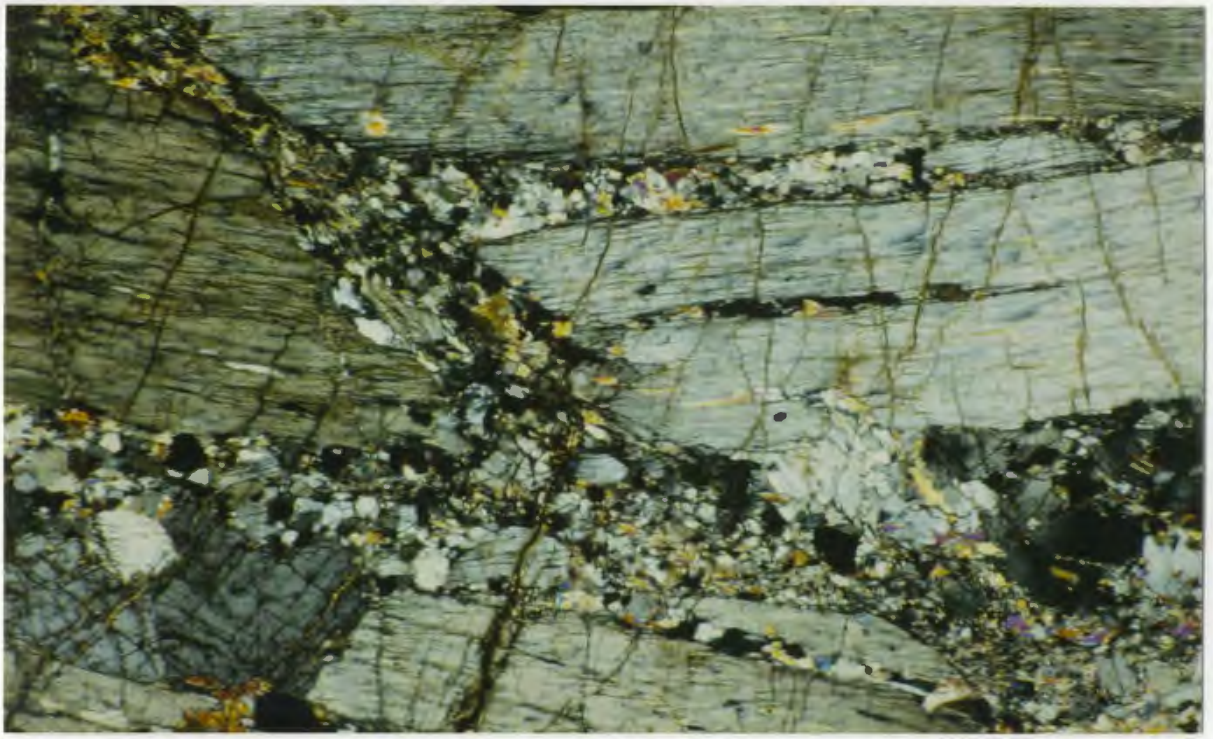

FIGURE 2.20. Orthopyroxene cut by shear zones filled with orthopyroxene, olivine and amphibole. Early shear zones (horizontal) are cut by later shear zones (diagonal). The latter are finer grained and contain higher abundances of amphibole than the former. All orthopyroxene in the photograph originally constituted a single pegmatitic grain, but deformation has produced numerous subgrains. Type I orthopyroxenite sample L067. Length of photograph 6.6 mm; crossed nicols.

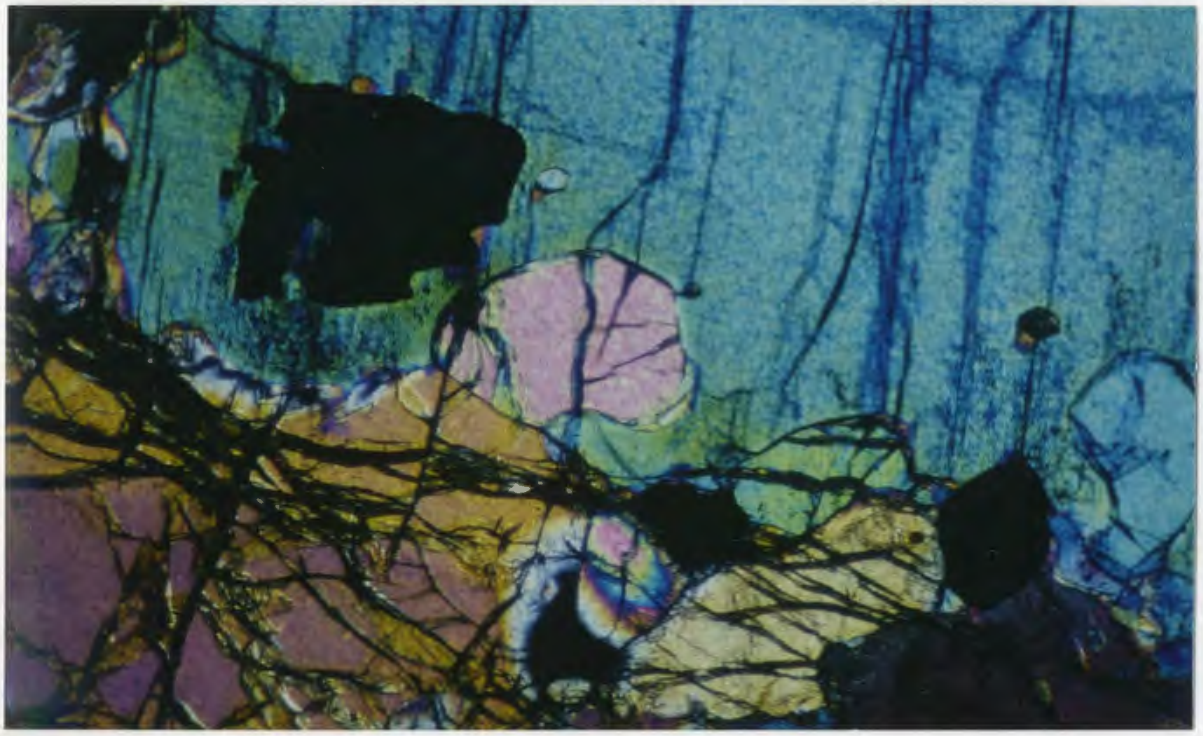

FIGURE 2.22. Irregular grain boundary of clinopyroxene (blue) in contact with Cr-spinel (black) and partially serpentinized olivine. LAL clinopyroxenite sample L026. Length of photograph 1.4 mm; crossed nicols.

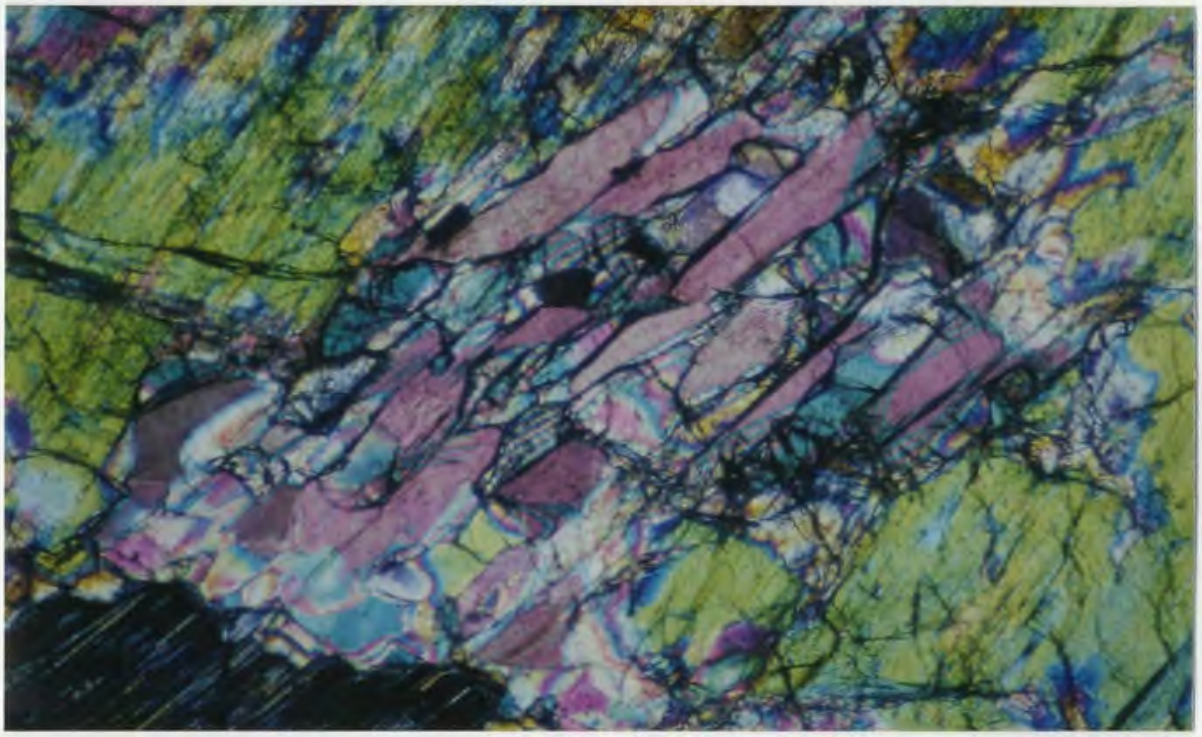

FIGURE 2.23. Orthopyroxene (yellow-green) replaced by tremolite (pink) and olivine (green). Olivine contains unidentified symplectitic inclusions. LAL websterite sample L283. Length of photograph 1.4 mm; crossed nicols.

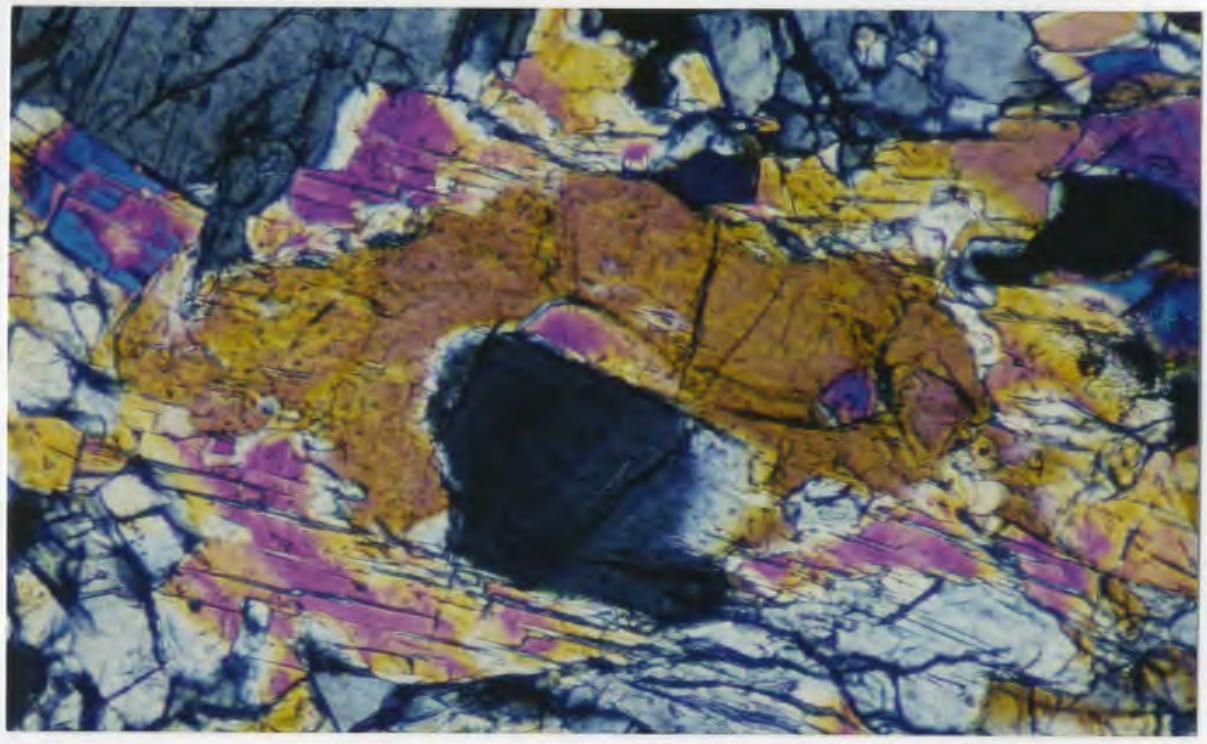

FIGURE 2.24. Clinopyroxene (deep orange) replacing orthopyroxene (grey), and tremolite (orange, purple and blue) replacing ortho- and clinopyroxene. Harzburgite sample L218. Length of photograph 0.55 mm; crossed nicols.

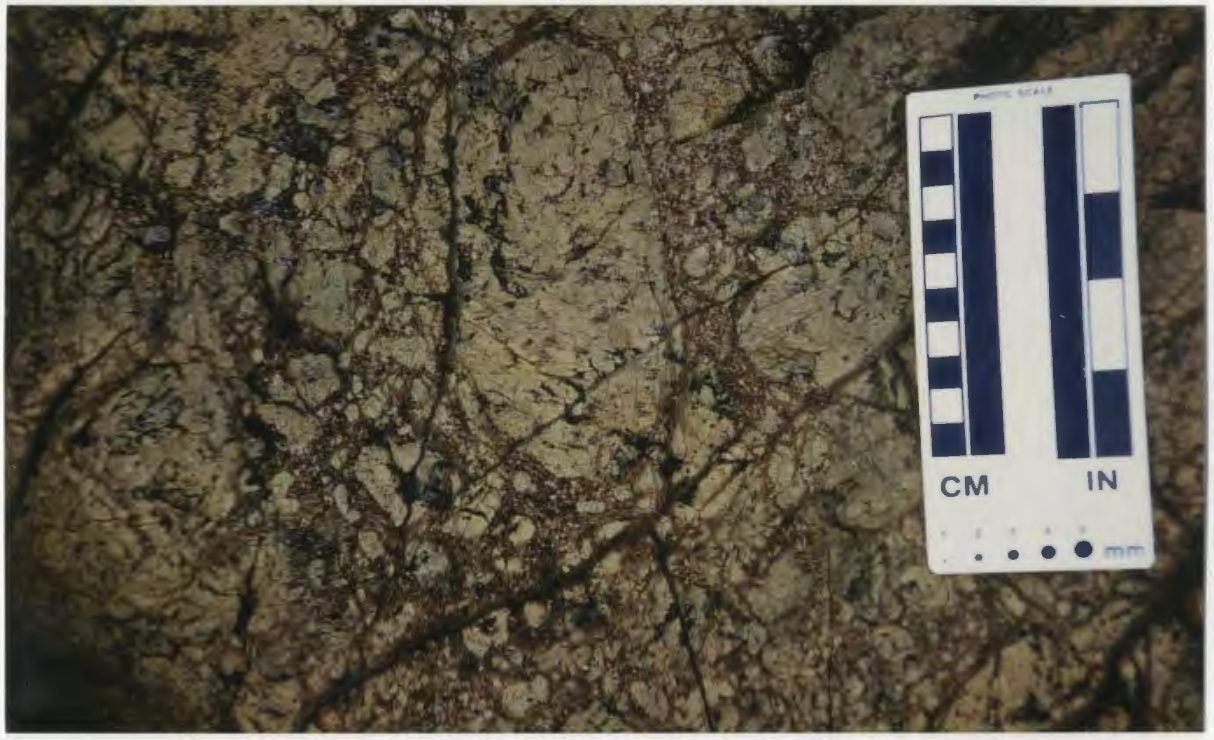

FIGURE 2.25. Web texture exhibited by type II orthopyroxenite in LAL dunite.

FIGURE 2.26. Vein of LAL clinopyroxenite offset by narrow D_2 shear zones filled with type II orthopyroxenite ribbon mylonite. Clinopyroxenite is partially replaced by the orthopyroxenite.

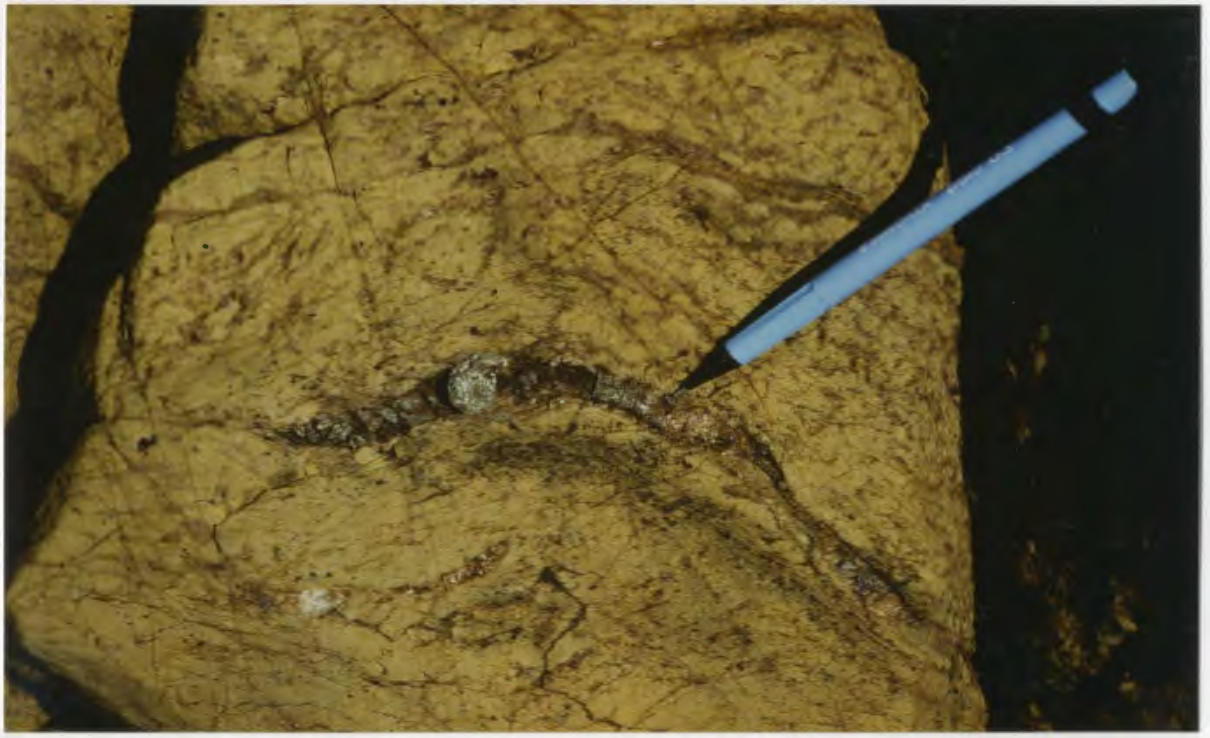

FIGURE 2.27. Boudin of websterite associated with ribbon mylonite of type II orthopyroxenite in D_2 shear zone. Clinopyroxene is green and orthopyroxene is bronze.

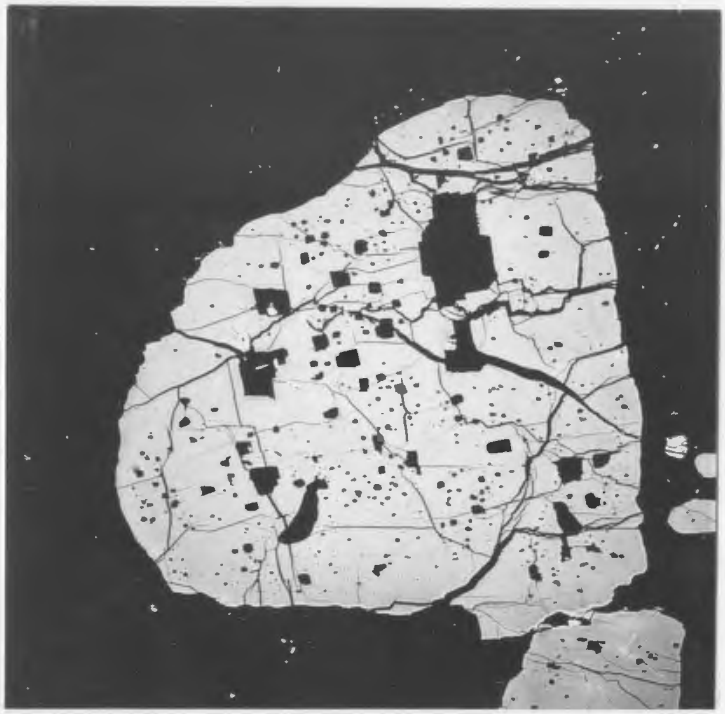

FIGURE 2.28. Cr-spinel hosting inclusions of olivine, serpentine, chlorite, ortho- and clinopyroxene(?), Ca-amphibole, Cr-cummingtonite and sulphide. Web-textured type II orthopyroxenite sample L271. Width of SEM photograph 430 μm.

FIGURE 2.29. Monomineralic bands of orthopyroxene (bottom), olivine (middle) and Ca-amphibole (top) which define S_2. Orthopyroxene is well equilibrated. Type II orthopyroxenite ribbon mylonite sample L351. Length of photograph 3.7 mm; crossed nicols.

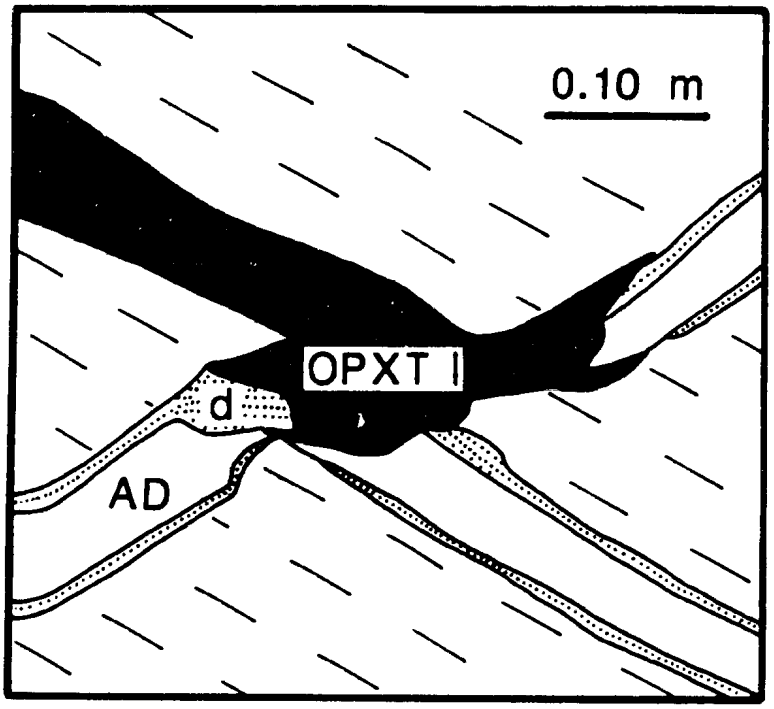

FIGURE 2.30. Conjugate vein of type I orthopyroxenite (OPXT I) partially pseudomorphed by amphibole dunite (AD). The amphibole dunite is bordered by dunite (d) which has olivine of a lower forsterite content than that in harzburgite. S_1 of harzburgite indicated by dashes.

FIGURE 2.31. Enclaves of type I orthopyroxenite (bronze) in amphibole dunite (fibrous texture) which separates orthopyroxenite from amphibole-free dunite (light brown).

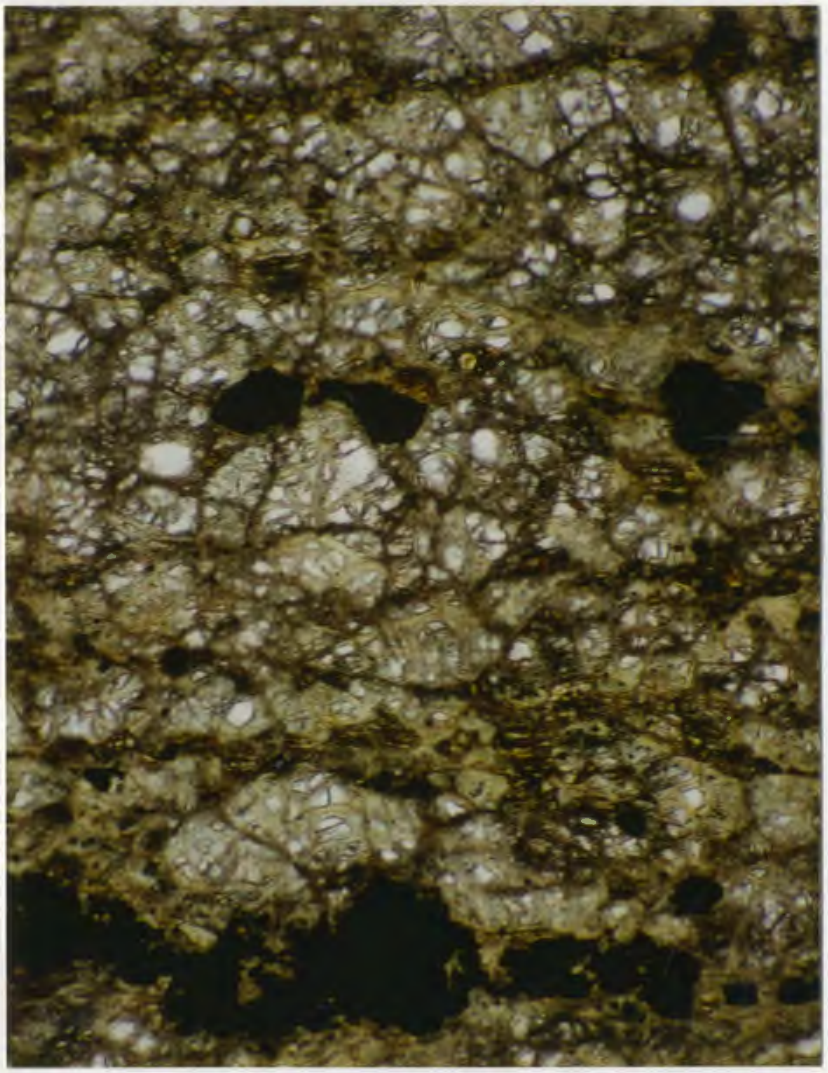

FIGURE 2.32. Well equilibrated mosaic equigranular texture of olivine (serpentinized). Ca-amphibole (dark brown) and Cr-spinel (black) both define S_2. Amphibole dunite sample L132. Length of photograph 4.3 mm; plane-polarized light.

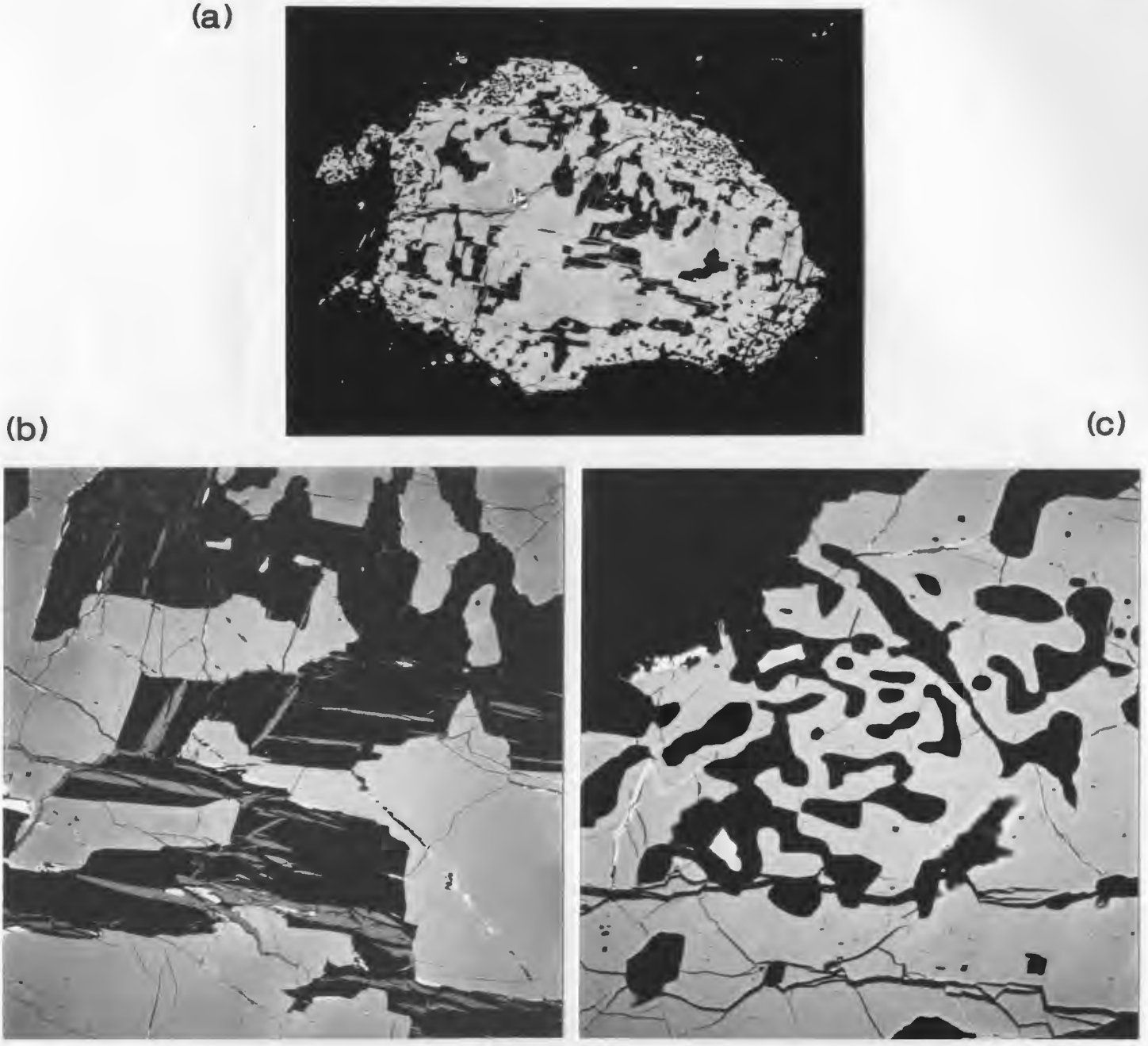

FIGURE 2.33. (a) Sieve texture in poikiloblastic Cr-spinel. Highly reflective areas are magnetite. (b) Core of the Cr-spinel, showing inclusions of phlogopite and edenitic amphibole. The fibrous lamellae in these silicates are Ca-Fe silicate. The highly reflective grains in the fracture in Cr-spinel are native Cu. (c) Margin of the Cr-spinel in contact with edenitic amphibole. The vermiform silicates are edenitic amphibole and olivine or serpentine. Amphibole dunite sample L125. Width of SEM photograph 1.6 mm (a), 350 μm (b) and 190 μm (c).

FIGURE 2.34. Modal layering of Al-spinel in HAL dunite.

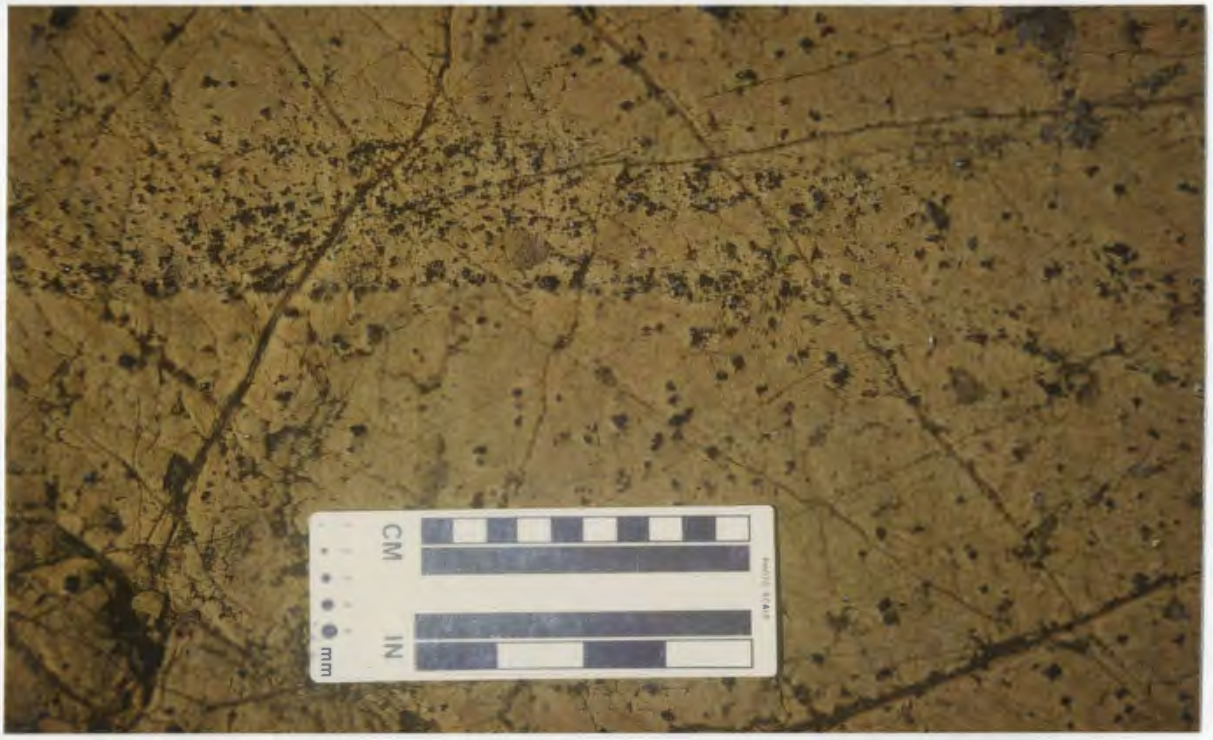

FIGURE 2.35. Band of fine grained Al-spinel cutting coarse grained Al-spinel in HAL dunite.

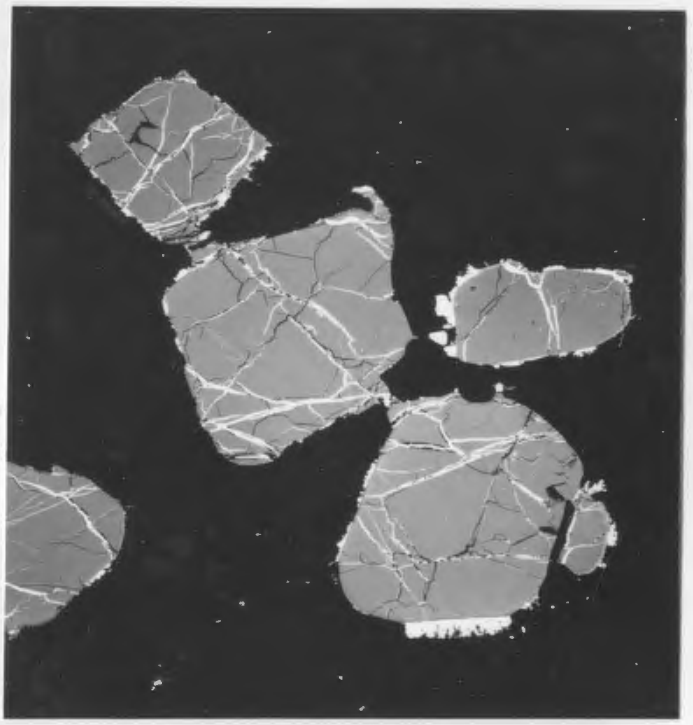

FIGURE 2.36. Chain texture exhibited by Al-spinel in serpentinized olivine. Highly reflective areas at the margins of grains of Al-spinel are magnetite and sulphide. Magnetite occurs along fractures in Al-spinel. HAL dunite sample L299. Width of SEM photograph 1.0 mm.

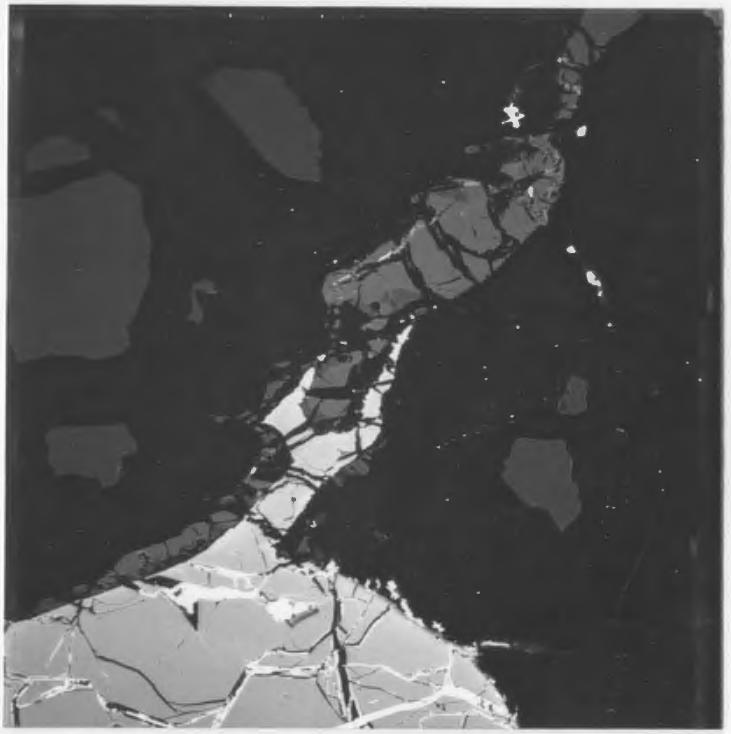

FIGURE 2.37. Protrusion of Al-spinel (light grey) associated with clinopyroxene (darker grey) along the grain boundary of adjacent grains of olivine. HAL dunite sample L350. Width of SEM photograph 370 μm.

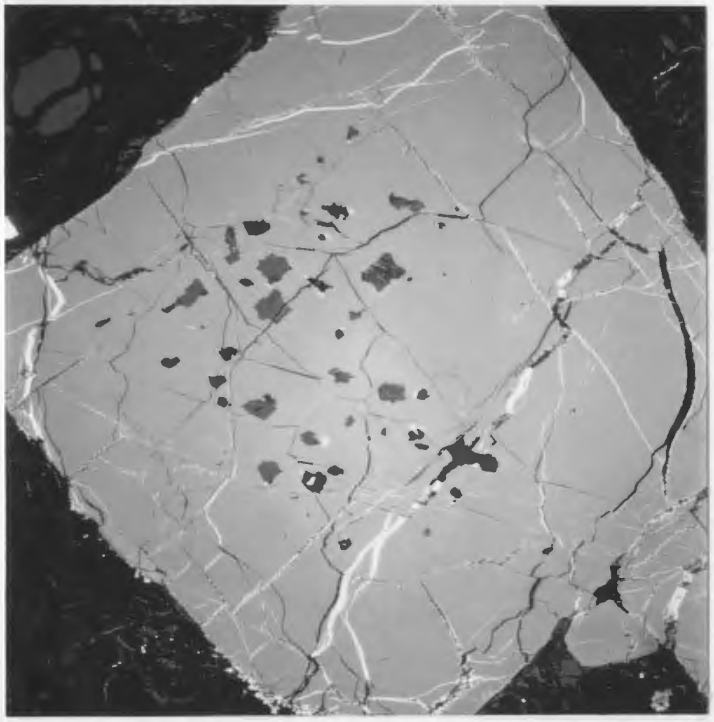

FIGURE 2.38. Al-spinel containing inclusions of olivine or serpentine, chlorite (clinochlore), tremolitic to pargasitic amphibole, phlogopite, Ca-plagioclase, orthopyroxene(?) and ilmenite. Fractures post-date inclusions. HAL wehrlite sample L301. Width of SEM photograph 1.5 mm.

FIGURE 2.39. HAL gabbro dyke (white) grading to HAL wehrlite in a HAL gabbro-clinopyroxene dunite association. The left side of the dyke has been removed by shearing.

FIGURE 2.40. HAL wehrlite (top left) grading to HAL dunite (bottom centre). Both are cut by HAL olivine clinopyroxenite (centre), which is at a high angle to the foliation in wehrlite (parallel to the length of the scale). HAL dunite lies to the right of the HAL olivine clinopyroxenite.

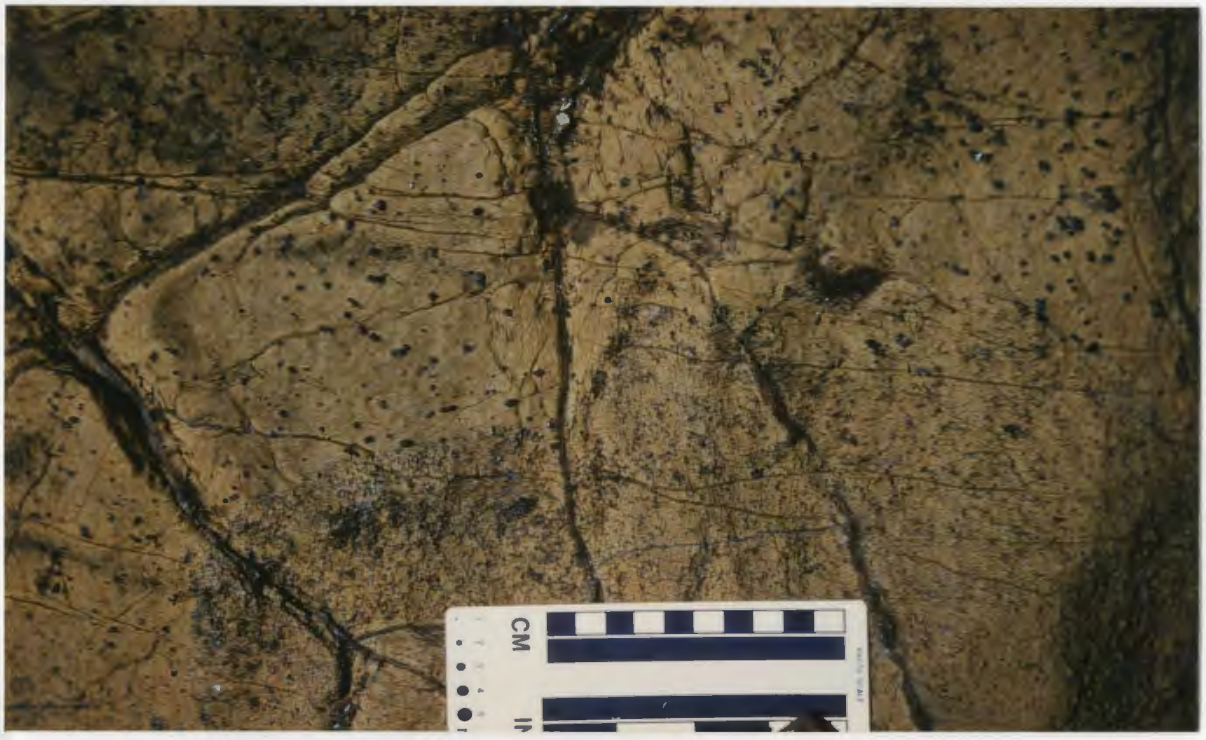

FIGURE 2.41. Reduction in grain size of Al-spinel from HAL dunite (top left) to HAL wehrlite (bottom right).

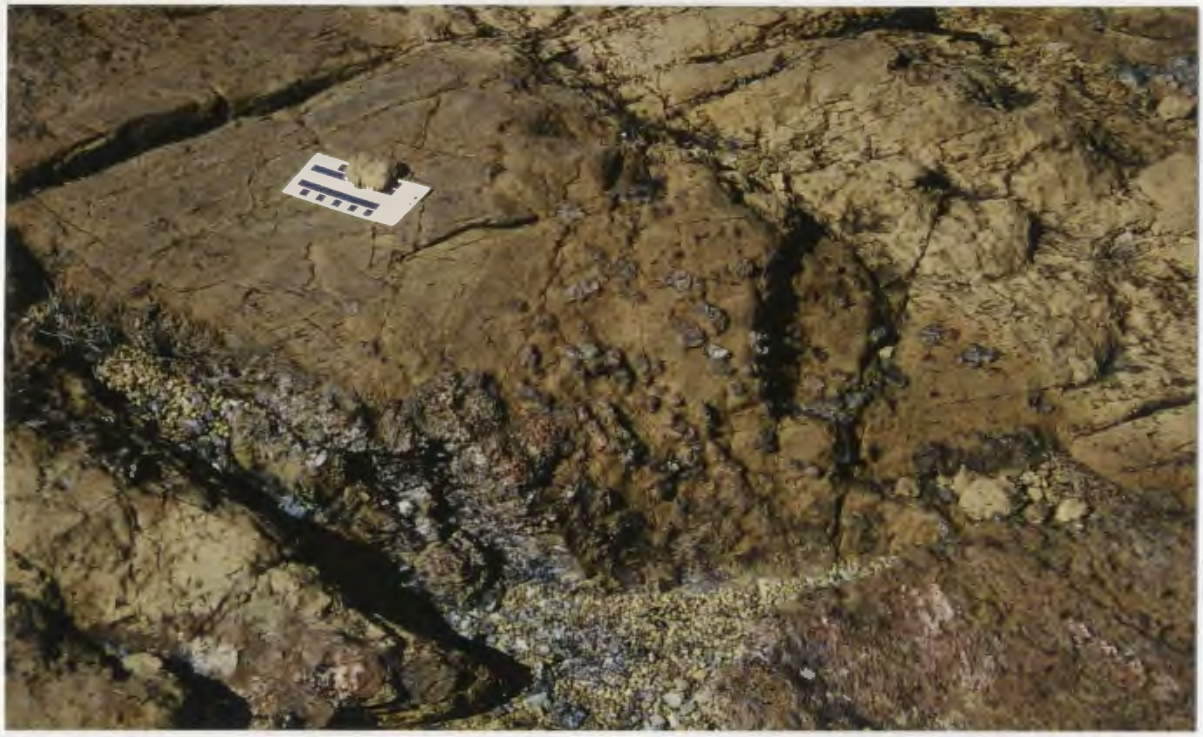

FIGURE 2.42. Dunitic portion of a HAL olivine clinopyroxenite dyke (dark brown) cutting LAL dunite (light brown). Clinopyroxene is distributed unevenly in the dyke. As the forsterite content of olivine decreases, the dunite gets darker.

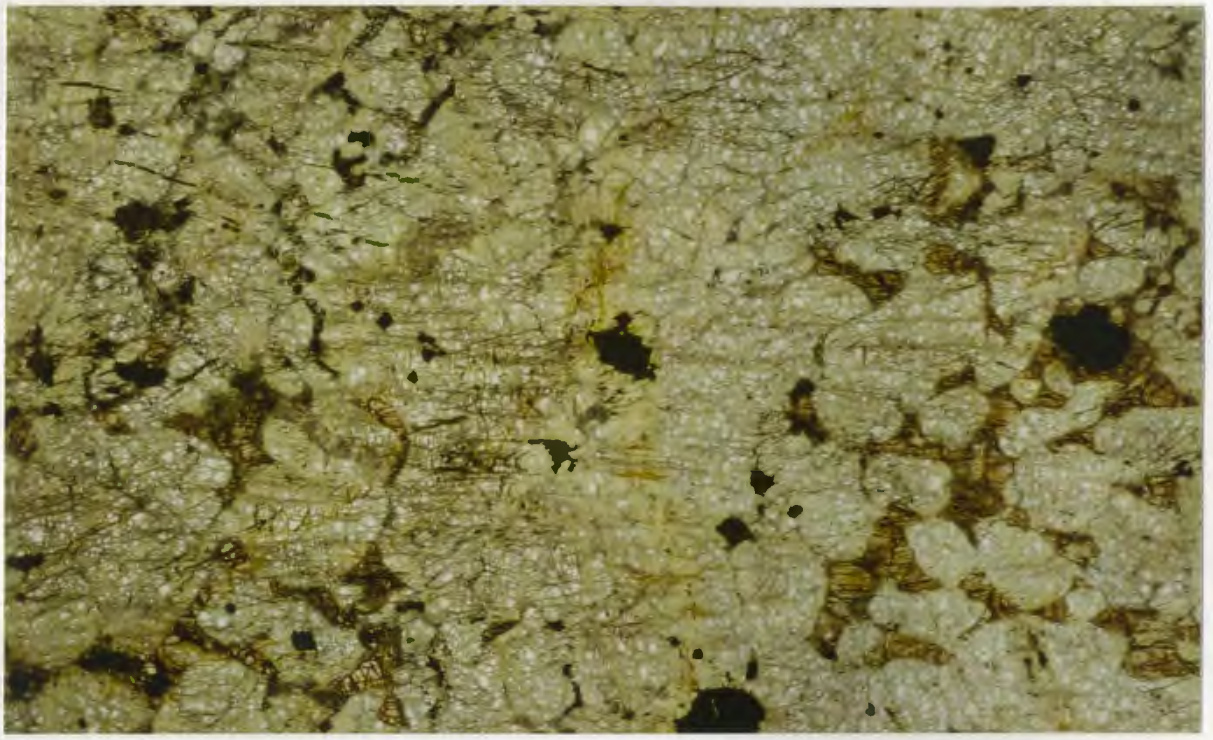

FIGURE 2.44. Interstitial clinopyroxene (brown) in a matrix of serpentinized olivine. This texture is typical of cumulates and impregnated mantle rocks. Partially altered plagioclase (top left) has the same morphology as clinopyroxene. HAL wehrlite sample L331. Length of photograph 15.5 mm; plane-polarized light.

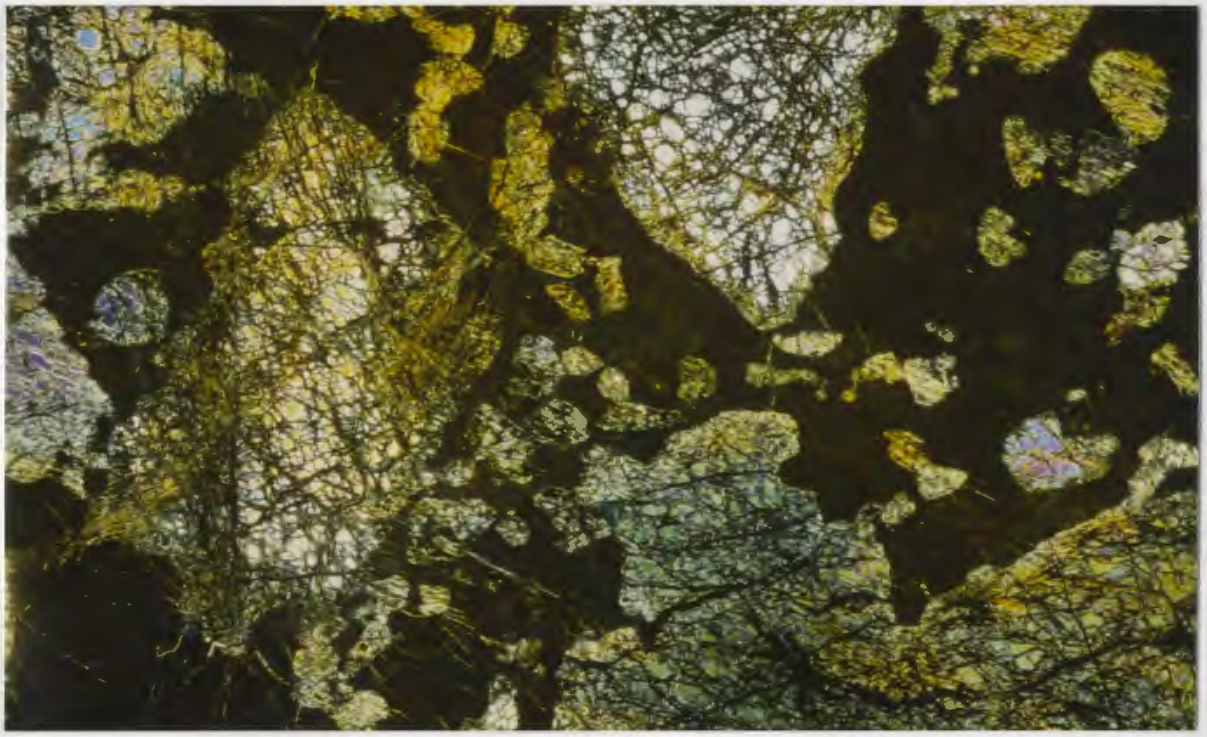

FIGURE 2.45. Large poikilitic grain of clinopyroxene (at extinction) containing chadacrysts of serpentinized olivine. HAL olivine clinopyroxenite sample L186. Length of photograph 15.5 mm; crossed nicols.

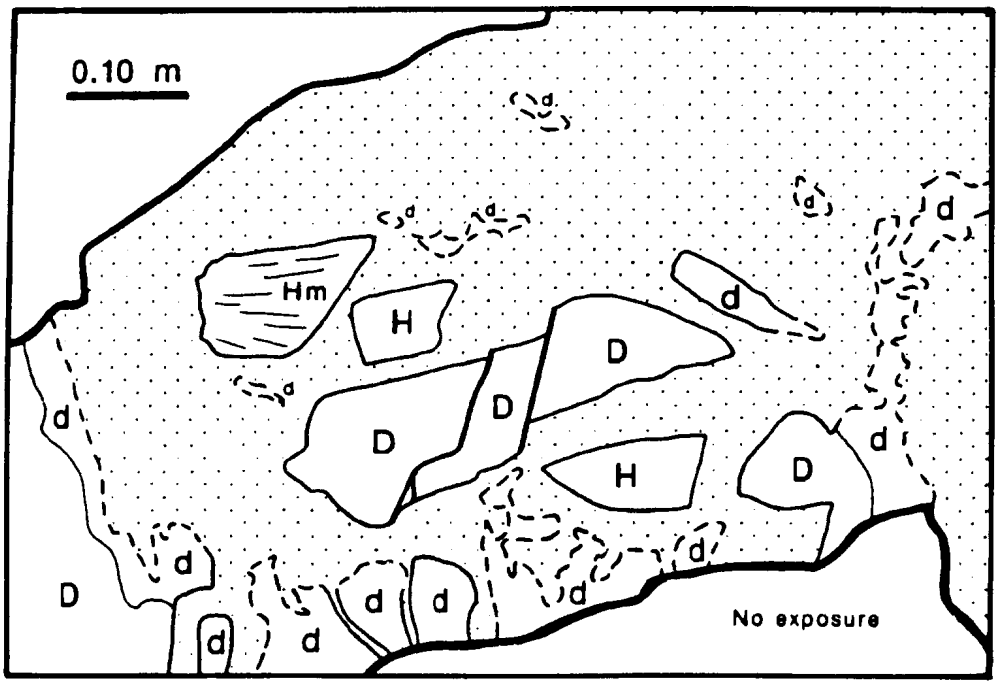

FIGURE 2.46. Xenoliths of harzburgite (H and Hm) and LAL (D) and HAL (d) dunite, in HAL olivine clinopyroxenite (stipple). Xenoliths either are angular with well defined margins (solid lines), or are irregular with gradational margins (broken lines). Irregular dunite xenoliths in some places grade from LAL to HAL as the olivine clinopyroxenite is approached. HAL dunite xenoliths often contain impregnated clinopyroxene. Offsets in the central LAL dunite xenolith are filled by HAL clinopyroxenite. The close spatial distribution of xenoliths of harzburgite (H), harzburgite mylonite (Hm) and LAL dunite (D), suggests that these xenoliths may not be in-situ.

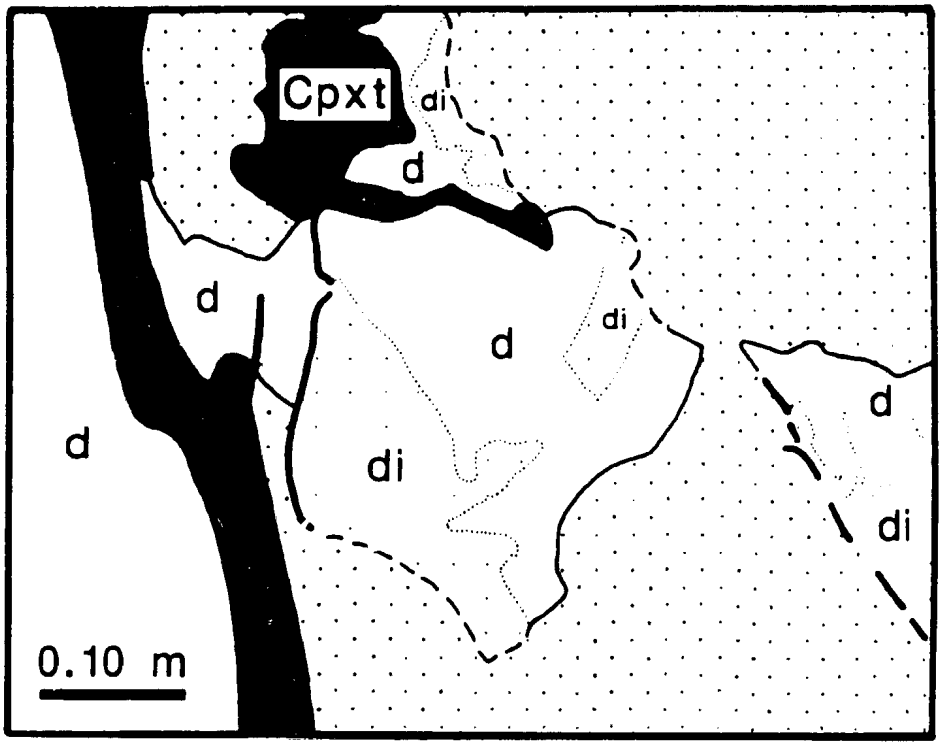

FIGURE 2.47. Irregular HAL dunite xenoliths (d) in HAL olivine clinopyroxenite (stipple). HAL clinopyroxenite (thick black lines and Cpxt) forms along the margins of dunite xenoliths. Parts of dunite xenoliths (di) contain impregnated clinopyroxene where their margins are gradational (broken lines) to olivine clinopyroxenite.

FIGURE 2.48. Veins of HAL olivine clinopyroxenite at the contact between HAL dunite (dark brown) and harzburgite (light brown with bronze speckle).

FIGURE 2.49. Assemblage of HAL olivine-spinel-clinopyroxene (centre, dark brown) replacing harzburgite (left, light brown, and right, dark brown). Note that the zone of replacement is parallel to S_1 of harzburgite as defined by orthopyroxene.

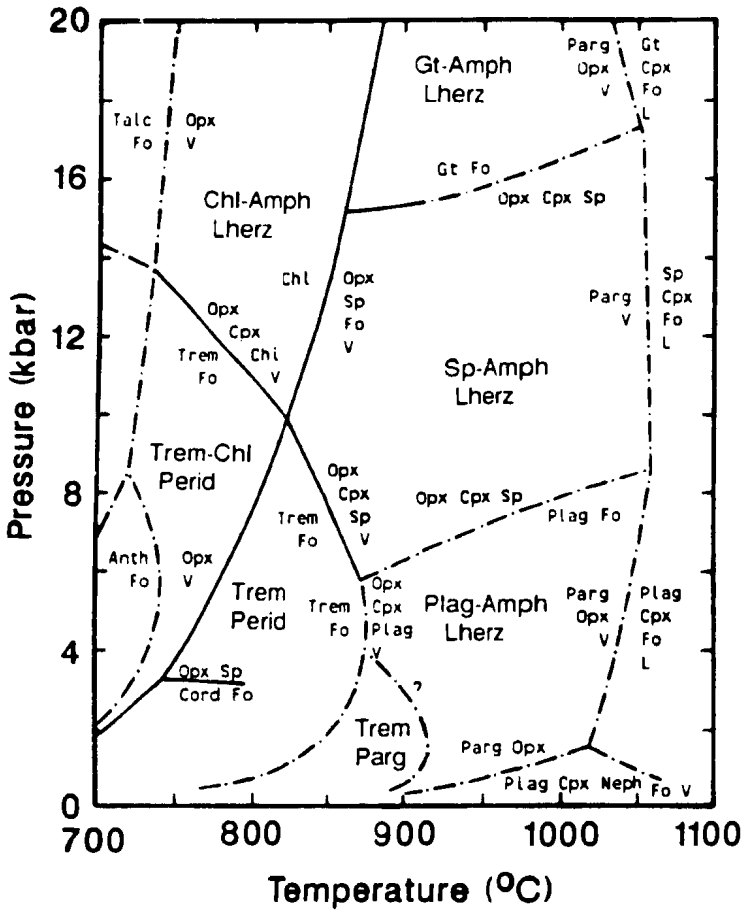

FIGURE 2.50. Partially schematic phase relations for ultramafic rocks modelled by the system H_2O-Na_2O-CaO-MgO-Al_2O_3-SiO_2 with excess H_2O and Mg_2SiO_4. Solid lines are experimentally determined. Dash-dot lines are approximated. Abbreviations: Lherz = lherzolite; Perid = peridotite; Anth = anthophyllite; Amph = pargasite-tremolite solid solutions; Chl = chlorite; Cord = cordierite; Cpx = clinopyroxene; Fo = forsterite; Gt = garnet; L = silicate magma; Neph = nepheline; Opx = orthopyroxene; Parg = pargasite; Plag = anorthitic plagioclase; Sp = spinel; Trem = tremolitic amphibole; V = aqueous vapour. Diagram from Jenkins (1983).

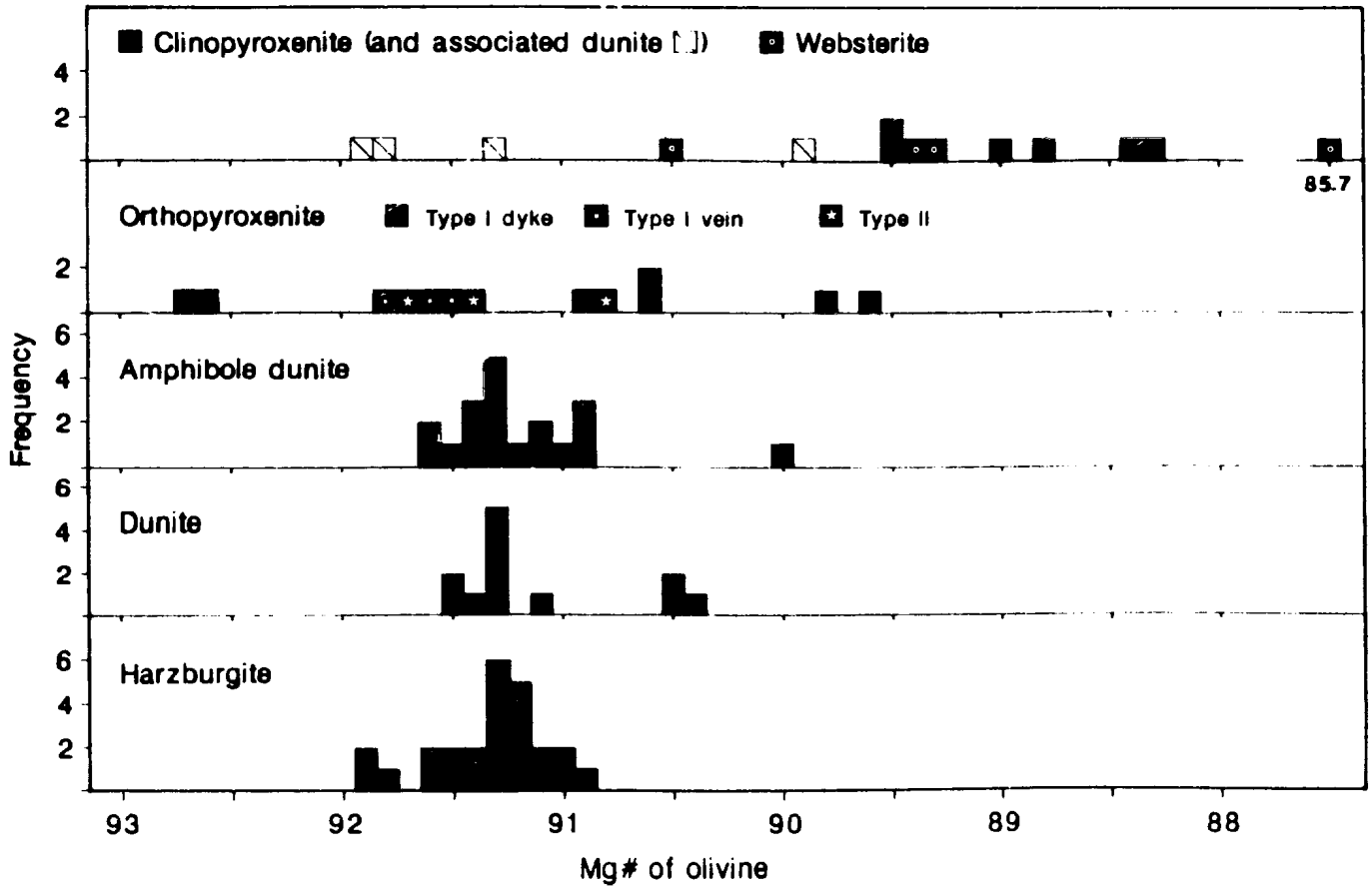

FIGURE 3.1. Frequency distribution of Mg# of olivine in LALPP.

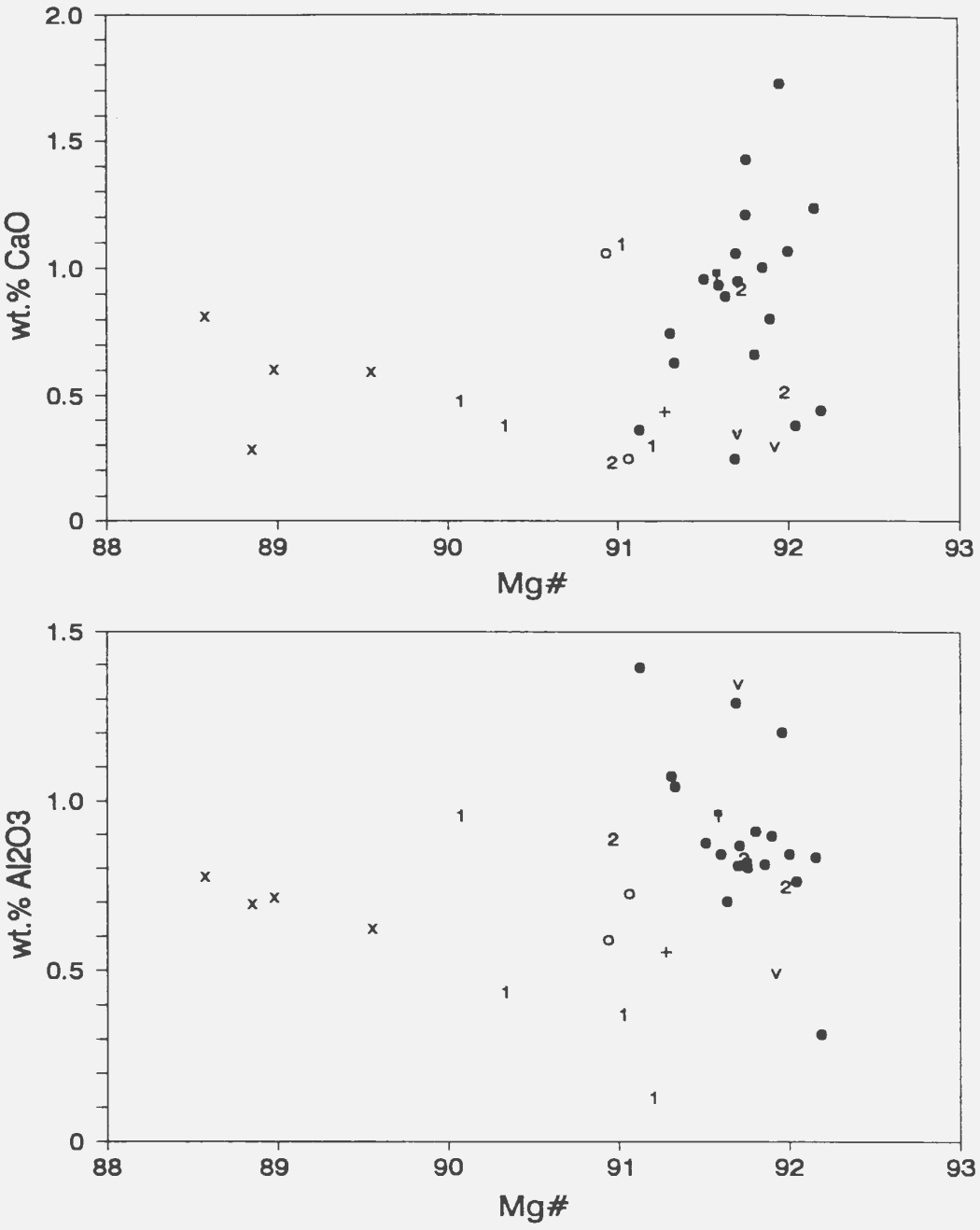

FIGURE 3.2. Compositional variation of orthopyroxene in LALPP: harzburgite (●), dunite (o), amphibole dunite (v), type I orthopyroxenite dykes (1) and vein (ī), type II orthopyroxenite (2), clinopyroxenite (x) and websterite (+).

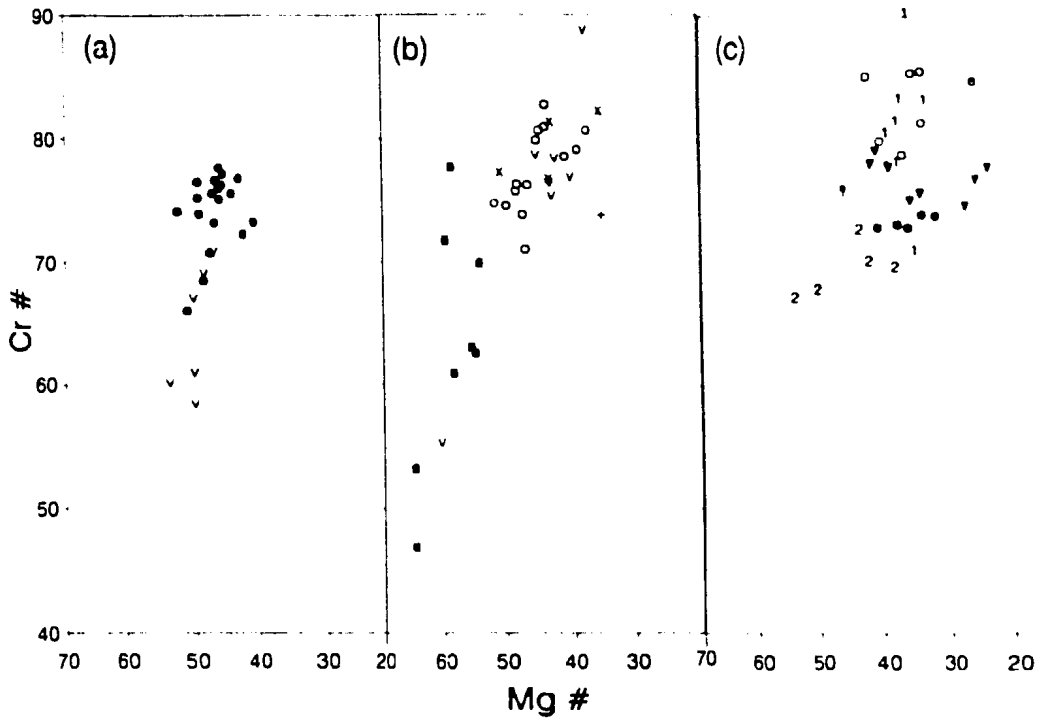

FIGURE 3.3. Cr# vs. Mg# of spinel in LALPP: **(a)** Harzburgite: no associated Ca-amphibole (●) and associated with Ca-amphibole (v). **(b)** Dunite (o), dunite associated with type I orthopyroxenite (+) and clinopyroxenite (x), chromitite (■), and amphibole dunite (v). **(c)** Type I orthopyroxenite dykes (1) and vein (!), type II orthopyroxenite (2), clinopyroxenite (o), clinopyroxenite containing xenocrysts of orthopyroxene (●), websterite (▼), and a spinel exsolution or inclusion in clinopyroxene in websterite (e).

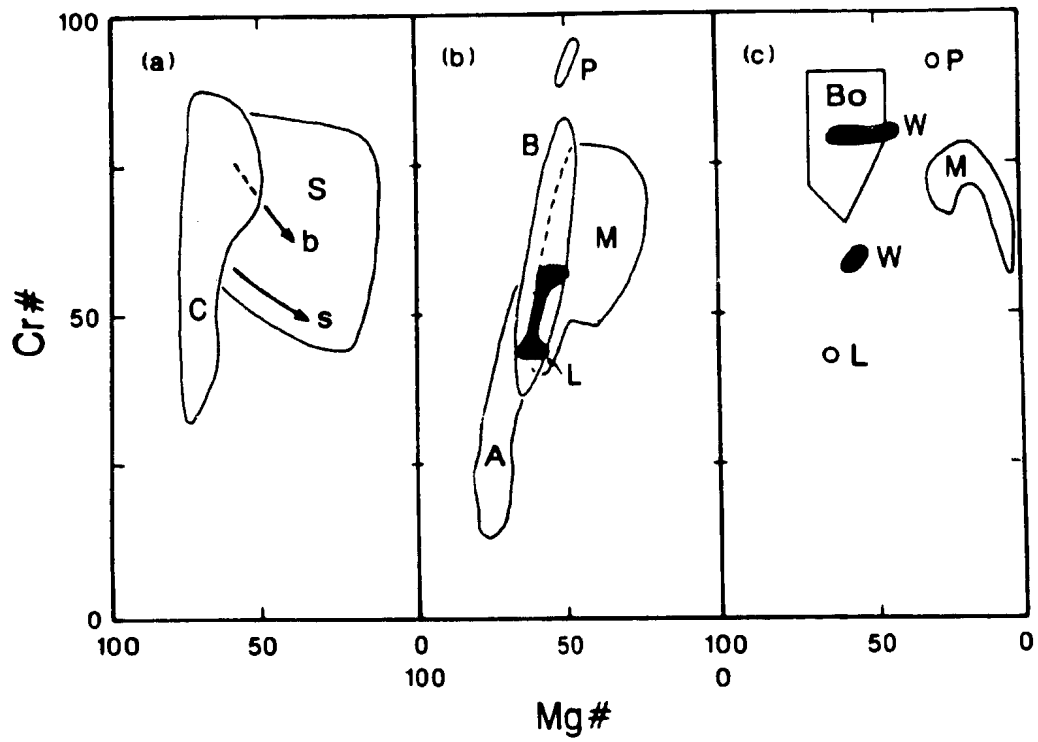

FIGURE 3.4. Cr# vs. Mg# composition fields of spinel. **(a)** Mafic-ultramafic stratiform complexes (S) (Irvine, 1967) with trends of the Bushveld (b) (De Waal, 1975) and Skaergaard (s) (Jackson, 1969); podiform deposits of ophiolite complexes (C) (Leblanc et al., 1980). **(b)** Abyssal peridotites (A) (Dick and Fisher, 1984); harzburgites and dunites of the Bay of Islands Ophiolite Complex (B) (Malpas and Strong, 1975); harzburgites of the Lewis Hills Massif (L) (Smith and Elthon, 1988) and Papuan Ultramafic Belt (P) (Jaques and Chappell, 1980); Cr-spinel harzburgites and lherzolites of the Miyamori Ophiolite Complex (M) (Ozawa, 1988). **(c)** Boninites and basaltic komatiites (Bo) (Cameron et al., 1979); orthopyroxenites of the Lewis Hills Massif (L) (Smith and Elthon, 1988) and Papuan Ultramafic Belt (P) (Jaques and Chappell, 1980); low-Al orthopyroxenites of the White Hills Peridotite (W) (Talkington and Malpas, 1984); Cr-spinel olivine clinopyroxenites of the Miyamori Ophiolite Complex (M) (Ozawa, 1988).

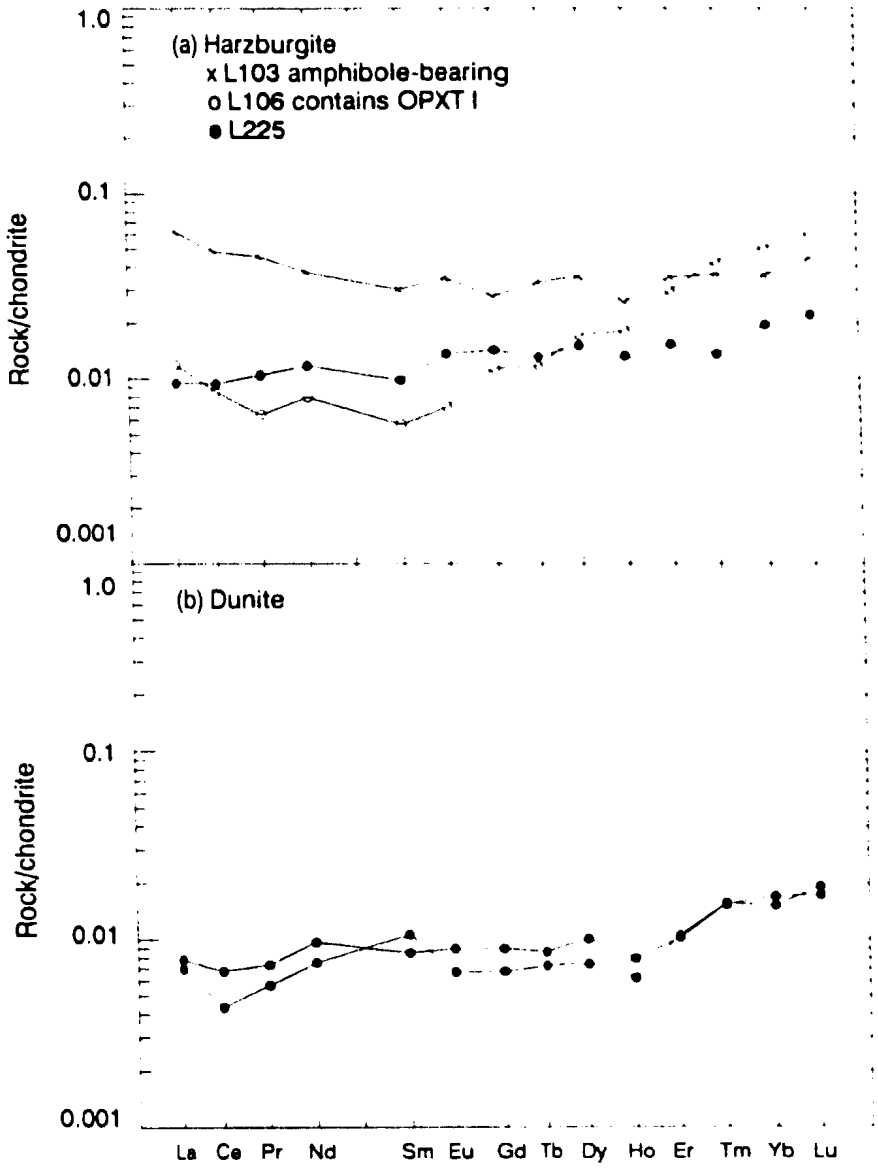

FIGURE 3.5. Chondrite-normalized rare earth element abundances of LALPP: **(a)** harzburgite samples L103, L106 and L225; **(b)** dunite samples L246 and L262. Normalization values are those of Wakita et al. (1971).

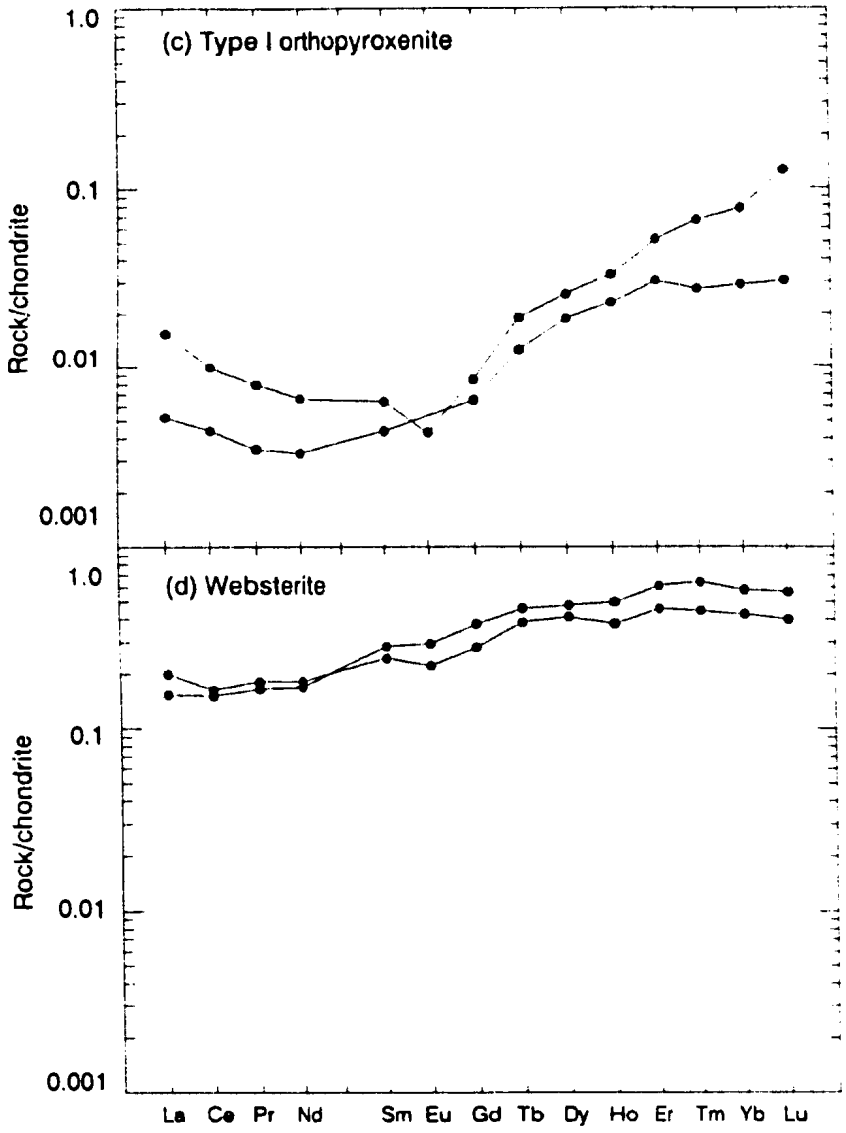

FIGURE 3.5. Chondrite-normalized rare earth element abundances of LALPP: (c) type I orthopyroxenite samples L066 and L268; (d) websterite samples L283 and L288. Normalization values are those of Wakita et al. (1971).

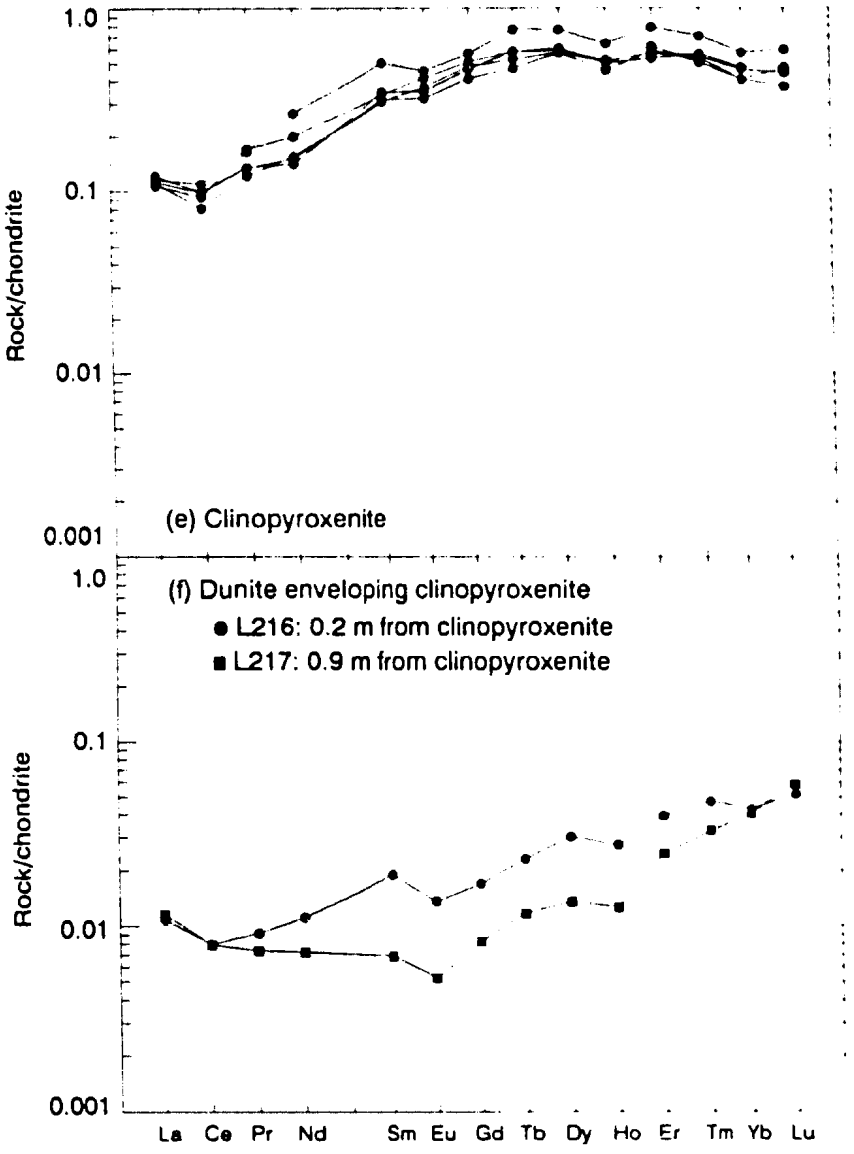

FIGURE 3.5. Chondrite-normalized rare earth element abundances of LALPP: **(e)** clinopyroxenite samples L012, L026, L213, L290 and L293; **(f)** dunite samples L216 and L217 from a dunite envelope around clinopyroxenite. Normalization values are those of Wakita et al. (1971).

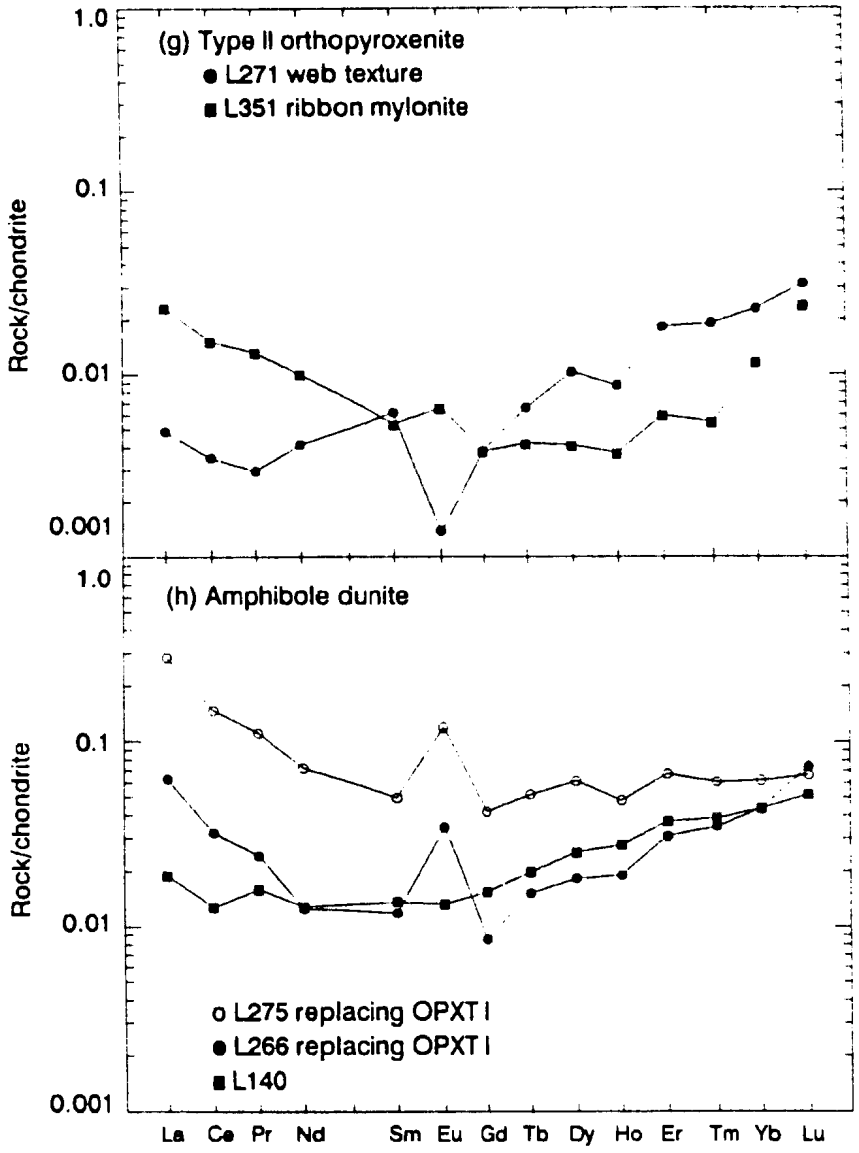

FIGURE 3.5. Chondrite-normalized rare earth element abundances of LALPP: **(g)** type II orthopyroxenite samples L271 and L351; **(h)** amphibole dunite samples L140, L266 and L275. Normalization values are those of Wakita et al. (1971).

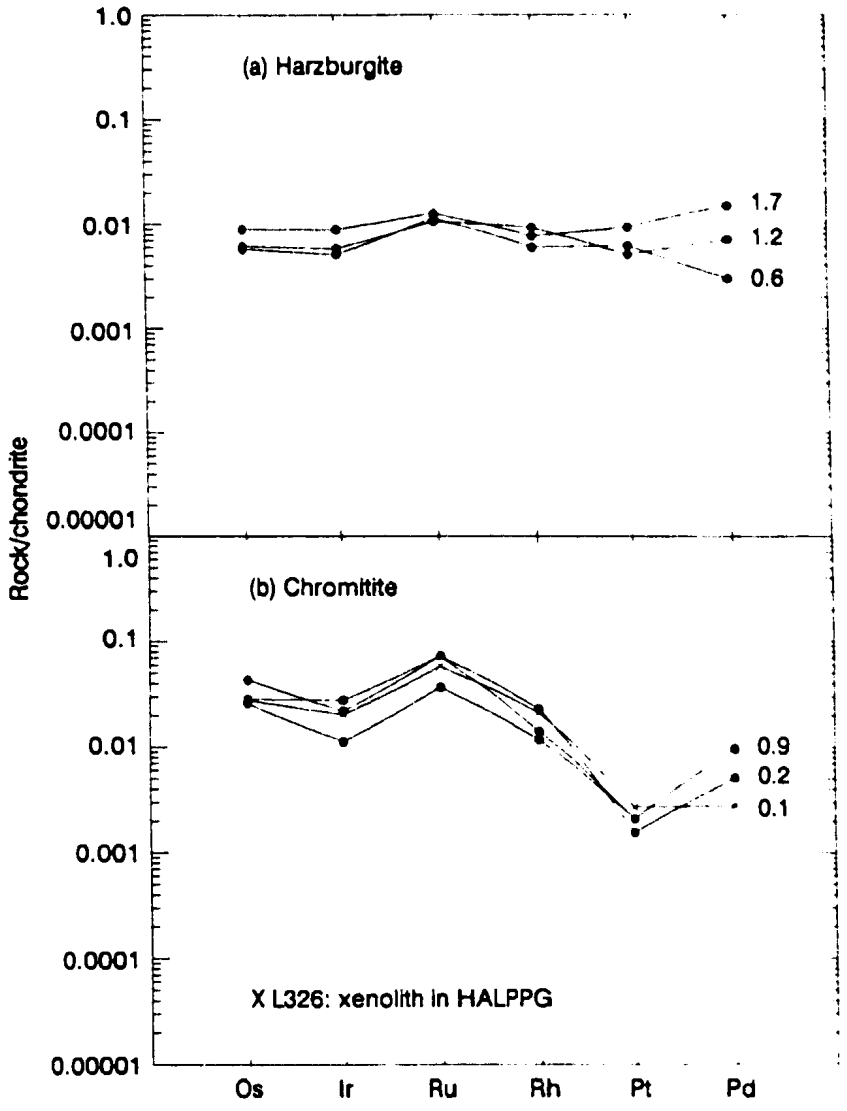

FIGURE 3.6. Chondrite-normalized platinum group element abundances of LALPP: **(a)** harzburgite samples L106, L218 and L225; **(b)** chromitite samples L203, L244, L289 and L326. Numbers to right of pattern are Pd/Ir ratios. Normalization values are those compiled by Naldrett and Duke (1980) for an average C1 chondrite.

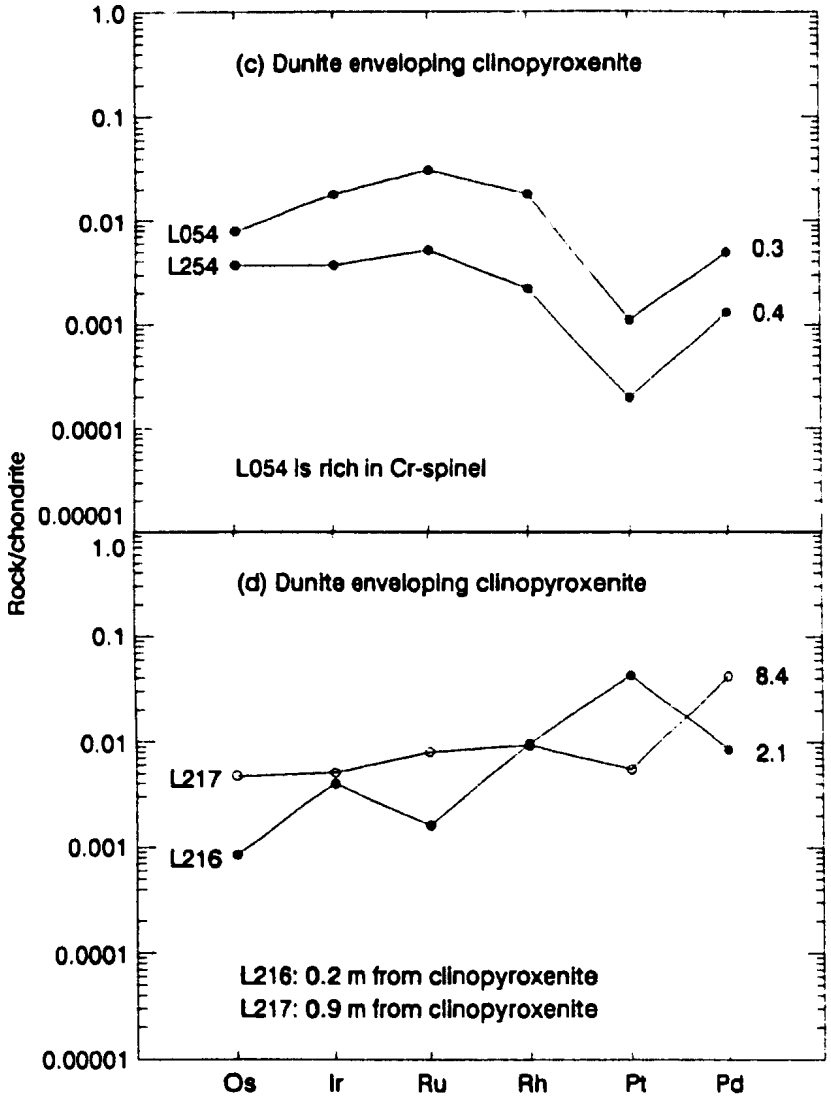

FIGURE 3.6. Chondrite-normalized platinum group element abundances of LALPP: (c) dunite samples L054 and L254 from dunite envelopes around clinopyroxenite; (d) dunite samples L216 and L217 from a dunite envelope around clinopyroxenite. Numbers to right of pattern are Pd/Ir ratios. Normalization values are those compiled by Naldrett and Duke (1980) for an average C1 chondrite.

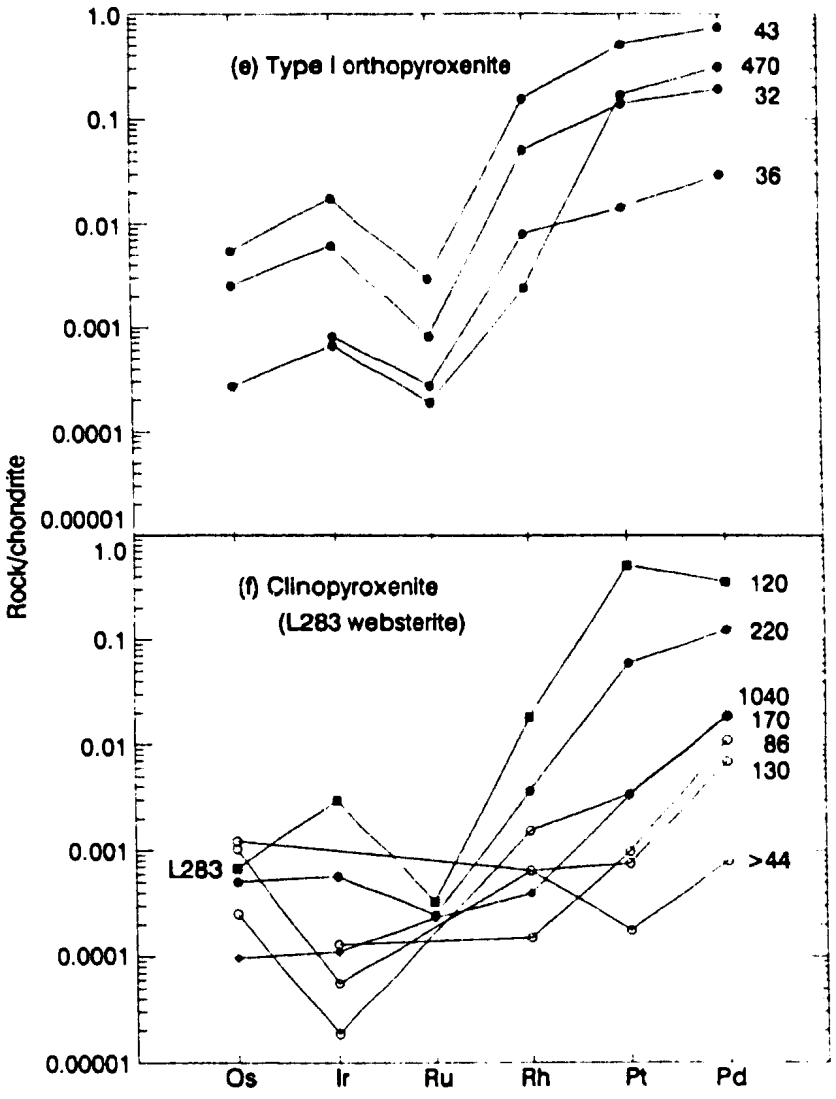

FIGURE 3.6. Chondrite-normalized platinum group element abundances of LALPP: **(e)** type I orthopyroxenite samples L068, L071, L267 and L268; **(f)** clinopyroxenite samples L026, L211, L212, L213, L214 and L293, and websterite sample L283, associated with dunite envelopes (open symbol) and with poorly developed or absent dunite envelopes (closed symbol). Numbers to right of pattern are Pd/Ir ratios. Normalization values are those compiled by Naldrett and Duke (1980) for an average C1 chondrite.

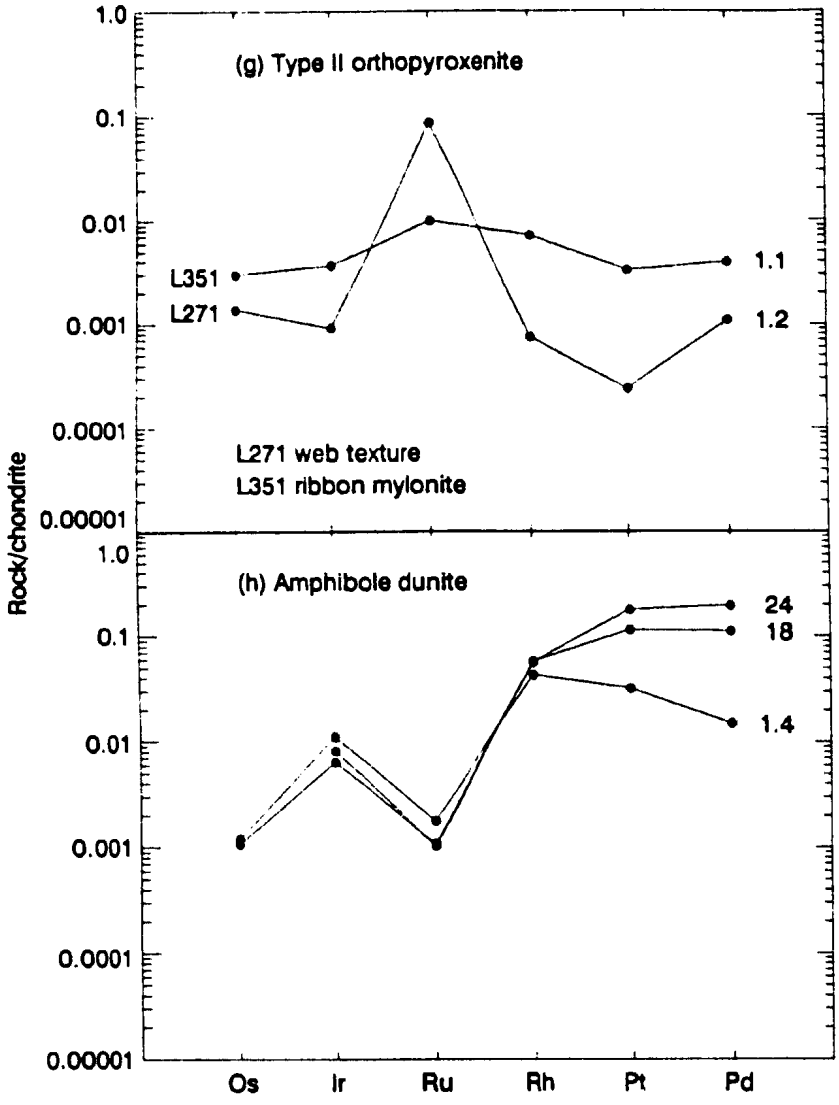

FIGURE 3.6. Chondrite-normalized platinum group element abundances of LALPP: **(g)** type II orthopyroxenite samples L271 and L351; **(h)** amphibole dunite samples L265, L266 and L275 from where type I orthopyroxenite is replaced. Numbers to right of pattern are Pd/Ir ratios. Normalization values are those compiled by Naldrett and Duke (1980) for an average C1 chondrite.

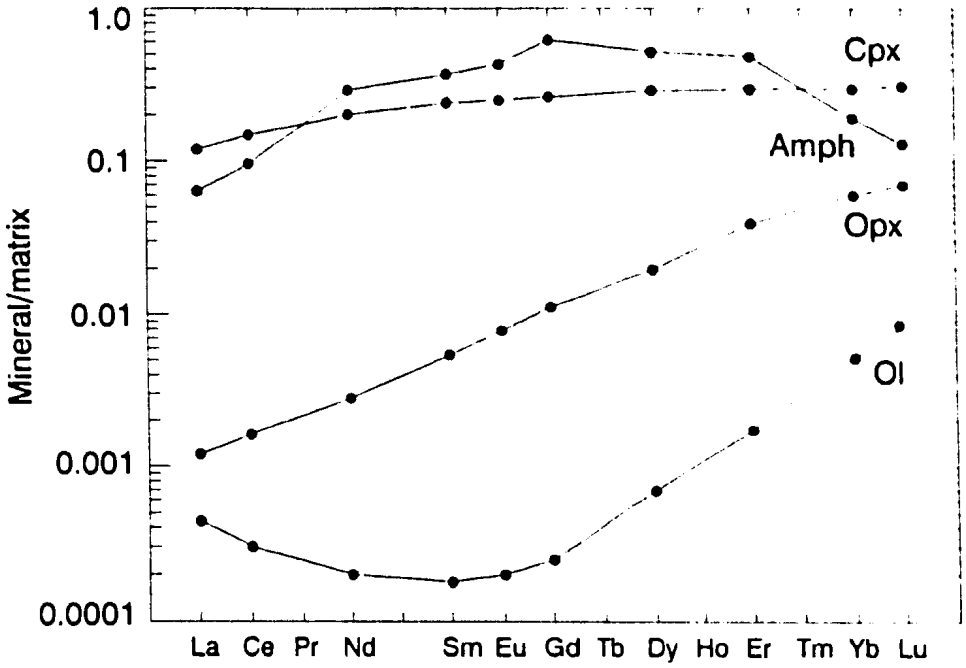

FIGURE 3.7. Mineral/matrix equilibrium partition coefficients of rare earth elements for olivine, orthopyroxene and clinopyroxene (values compiled by Prinzhofer and Allègre (1985)), and amphibole (Irving and Frey, 1984):

	Ol	Opx	Cpx	Amph
La	0.00044	0.0012	0.12	0.064
Ce	0.00030	0.00162	0.15	0.097
Nd	0.00020	0.0028	0.2	0.29
Sm	0.00018	0.0054	0.24	0.37
Eu	0.00020	0.0078	0.25	0.43
Gd	0.00025	0.0111	0.263	0.62
Dy	0.0007	0.01975	0.29	0.52
Er	0.00174	0.0392	0.294	0.48
Yb	0.00522	0.06	0.3	0.19
Lu	0.00852	0.0703	0.31	0.13

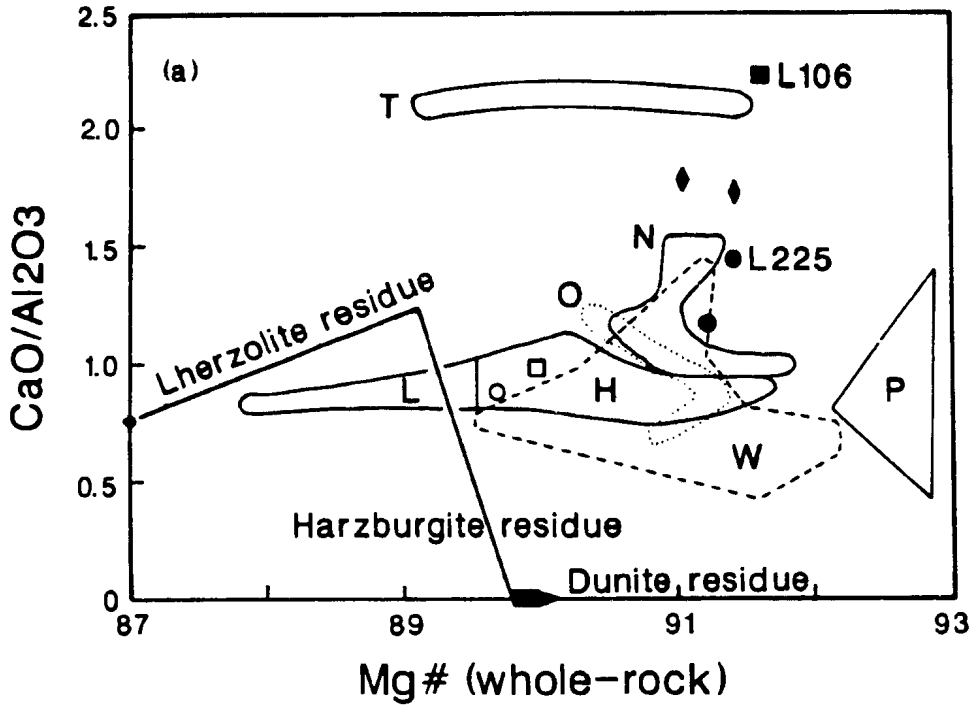

FIGURE 3.8. (a) CaO/Al_2O_3 vs. Mg# (whole-rock) of refractory harzburgites (closed circle), Ca-amphibole- and/or clinopyroxene-bearing harzburgites (solid diamond), and harzburgite containing type I orthopyroxenite (solid square) of the Springers Hill area. Fields are: harzburgites of Table Mountain (T) and North Arm Mountain (N) (Malpas, 1976), harzburgites of the Oman Ophiolite (O) (Lippard et al., 1986), harzburgites of the White Hills Peridotite (W) (Talkington, 1981), harzburgites of the Papuan Ultramafic Belt (P) (Jaques and Chappell, 1980), and harzburgites (H) and lherzolites (L) of the Ronda Peridotite (Frey et al., 1985); fertile lherzolite compositions of Maaløe and Aoki (1977) and Jagoutz et al. (1979) are open square and open circle, respectively. Trend of residue compositions from batch equilibrium partial melting of MORB pyrolite at 10 kbar from Falloon et al. (1989).

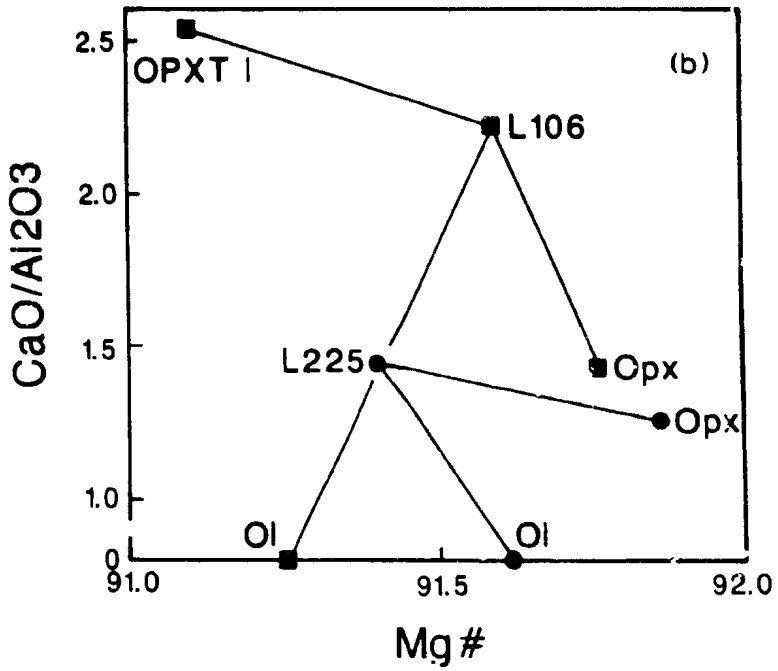

FIGURE 3.8. **(b)** CaO/Al_2O_3 vs. Mg# of harzburgite samples L106 and L225 and their constituent silicate phases.

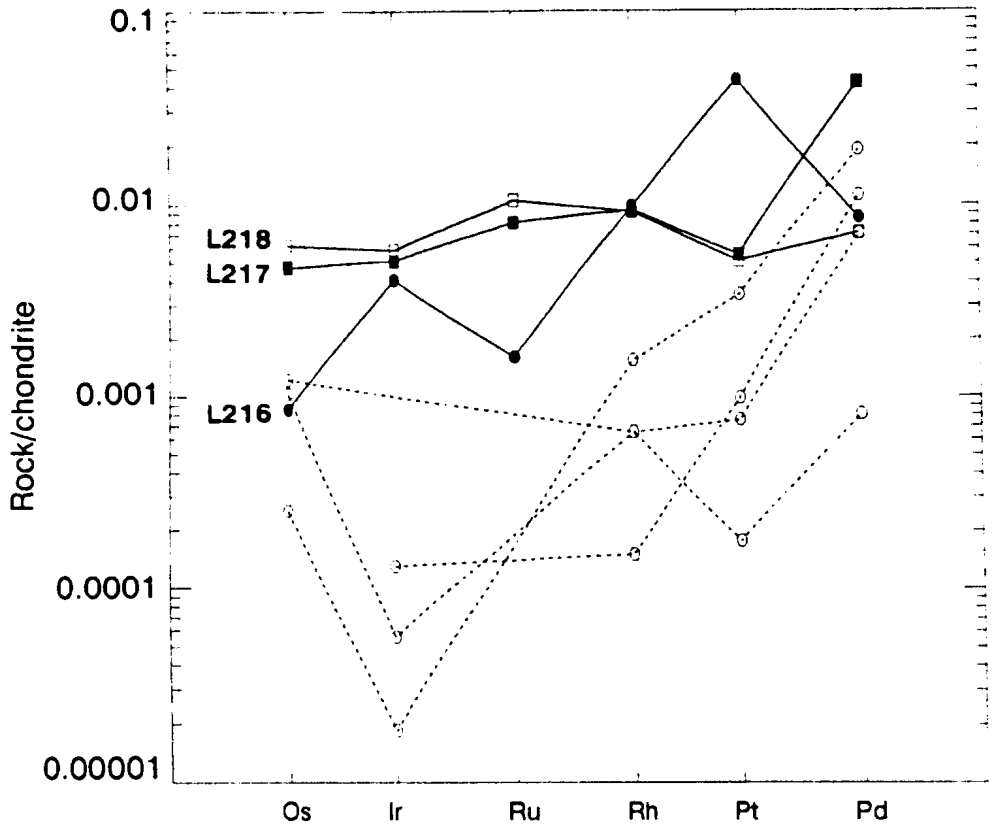

FIGURE 3.9. Chondrite-normalized platinum group element abundances of a LAL clinopyroxenite dyke and associated dunite envelope and harzburgite. Normalization values are those compiled by Naldrett and Duke (1980). All samples contain sulphide and/or native Cu.

Clinopyroxenite samples L211, L212, L213 and L214 (open circle): Pd/Ir = >44-1040, Mg#(Ol) = 88.3.

Cr-spinel-rich dunite sample L216 (closed circle): 0.2 m from clinopyroxenite, Pd/Ir = 2.1, Mg#(Ol) = 90.5.

Dunite sample L217 (closed square): 0.9 m from clinopyroxenite, Pd/Ir = 8.4, Mg#(Ol) = 91.3.

Harzburgite sample L218 (open square): 2.4 m from clinopyroxenite, Pd/Ir = 1.2, Mg#(Ol) = 91.3.

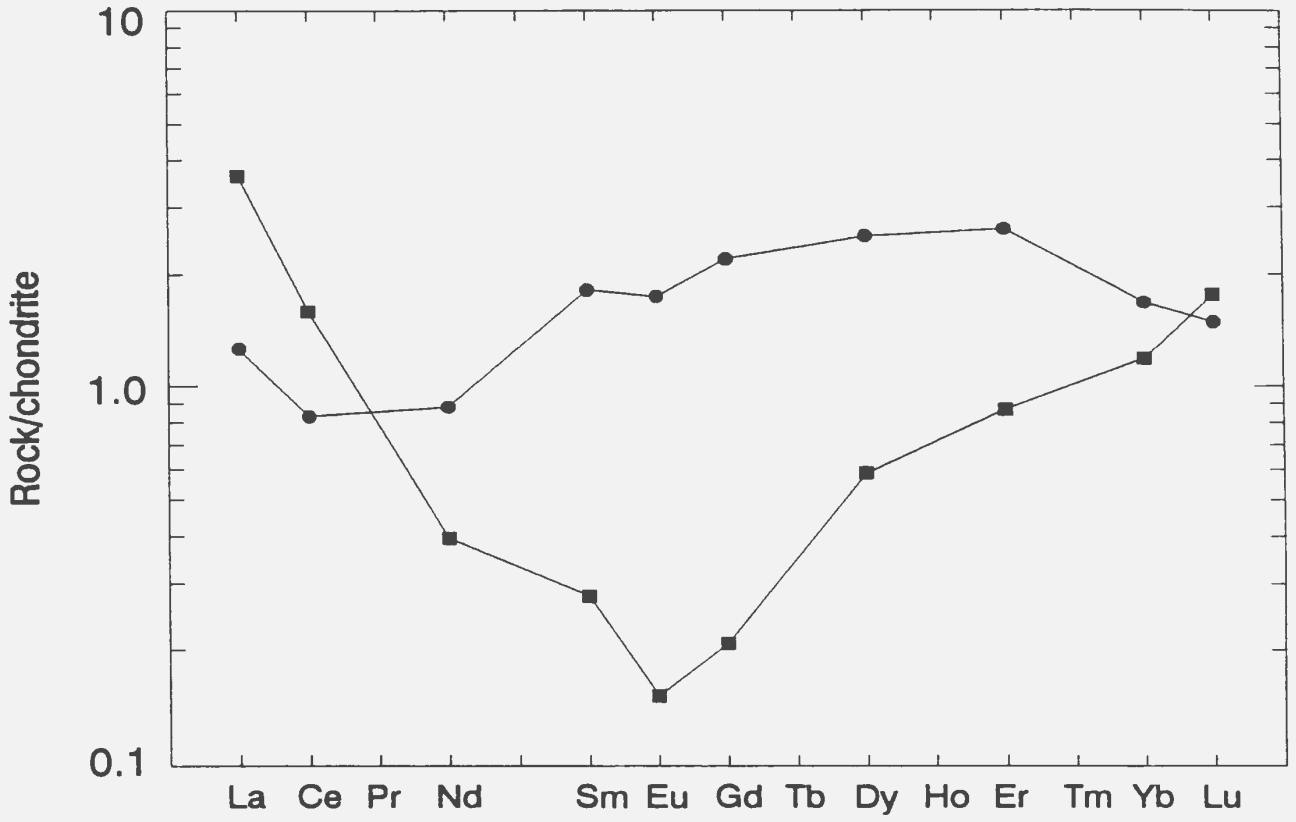

FIGURE 3.10. Estimated chondrite-normalized rare earth element abundances of magmas in equilibrium with type I orthopyroxenite sample L268 (square) and LAL clinopyroxenite sample L026 (circle). Normalization values are those of Wakita et al. (1971). Mineralogy is 95 wt.% orthopyroxene and 5 wt.% Ca-amphibole for type I orthopyroxenite sample L268, and 80 wt.% clinopyroxene and 20 wt.% olivine for clinopyroxenite sample L026 (olivine in this sample may have been overestimated due to its heterogeneous distribution). Partition coefficients are those in Figure 3.7. Equation used is E3.1.

TABLE 3.1. Major and trace element and normative compositions of orthopyroxenites in ophiolitic and orogenic mantle peridotites.

Location	SHA	O	P	T	PUB	WHP	WHP	BB
Type	LALPP					Low-Al	High-Al	
n	6	3	1	1	2	3	4	1
(wt %)								
SiO2	56 02	55 46	56 48	55 39	56 56	52 53	51 44	53 28
TiO2	bdl	bdl	0 03	0 03	0 01	0 09	0 13	0 44
Al2O3	0 66	1 67	0 91	0 83	0 19	1 64	4 38	4 07
FeO(t)	6 14	7 30	7 42	7 54	7 81	5 86	6 24	7 54
MnO	0 13	0 17	0 14	0 22	0 19	0 12	0 13	0 18
MgO	35 29	33 18	32 67	34 09	34 77	37 80	33 35	32 43
CaO	1 67	2 21	2 33	1 86	0 46	1 53	3 96	1 75
Na2O	0 07	bdl	bdl	0 04	0 01	0 35	0 17	0 31
K2O	0 01	bdl	bdl	0 00	0 00	0 03	0 14	0 00
P2O5	0 01	bdl	0 02	na	0 00	0 04	0 07	0 00
Mg#	91 1	89 0	88 7	89 0	88 8	92 0	90 5	88 5
CaO/Al2O3	2 54	1 32	2 56	2 25	2 37	0 93	0 90	0 43
(wt %)								
C								0 38
Or	0 06					0 18	0 83	
Ab	0 59			0 34	0 08	2 96	1 44	2 82
An	1 46	4 56	2 48	2 09	0 47	2 82	10 78	8 68
Ne								
Di	5 33	5 07	7 08	5 65	1 43	3 55	6 64	
Hy	81 91	81 52	86 59	80 63	91 59	58 47	51 85	70 91
Ol	10 62	8 84	3 74	11 23	6 41	31 75	28 07	16 57
Il			0 06	0 06	0 02	0 17	0 25	0 84
Ap	0 02		0 05			0 09	0 17	
(ppm)								
Sc	18	na	na	na	11	na	na	na
V	54	126	50	na	25	46	108	na
Cr	4517	4373	2350	4243	4565	4468	3822	3568
Ni	728	795	425	471	823	1544	1370	na
Cu	bdl	8	2	na	bdl	4	44	na
Zn	20	44	35	na	47	31	33	na
Rb	bdl	na	0	na	bdl	1	12	na
Sr	4	bdl	3	na	bdl	2-73	1-202	na
Y	bdl	na	na	na	bdl	3	4	na
Zr	bdl	bdl	na	na	bdl	5	7	na

SHA: Springers Hill area; O: Oman Ophiolite (Lippard et al., 1986)
P: Pindos Ophiolite (Montigny et al., 1973)
T: Troodos Ophiolite (Menzies and Allen, 1974)
PUB: Papuan Ultramafic Belt (Jaques and Chappell, 1980)
WHP: White Hills Peridotite (Talkington, 1981)
BB: Beni Bousera (Pearson, 1989)

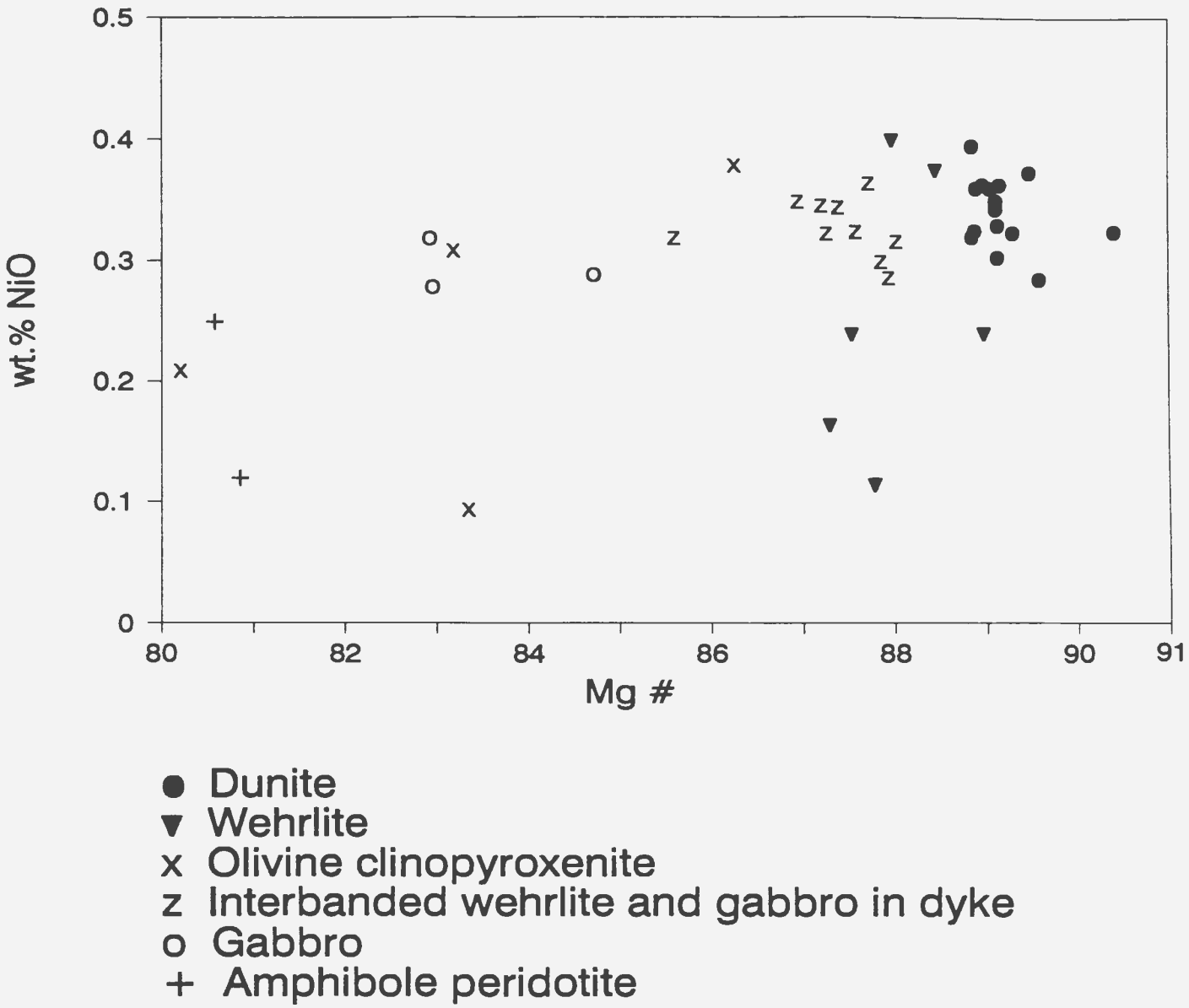

FIGURE 4.1. NiO vs. Mg# of olivine in HALPPG. Unless otherwise stated, these symbols are used throughout this chapter.

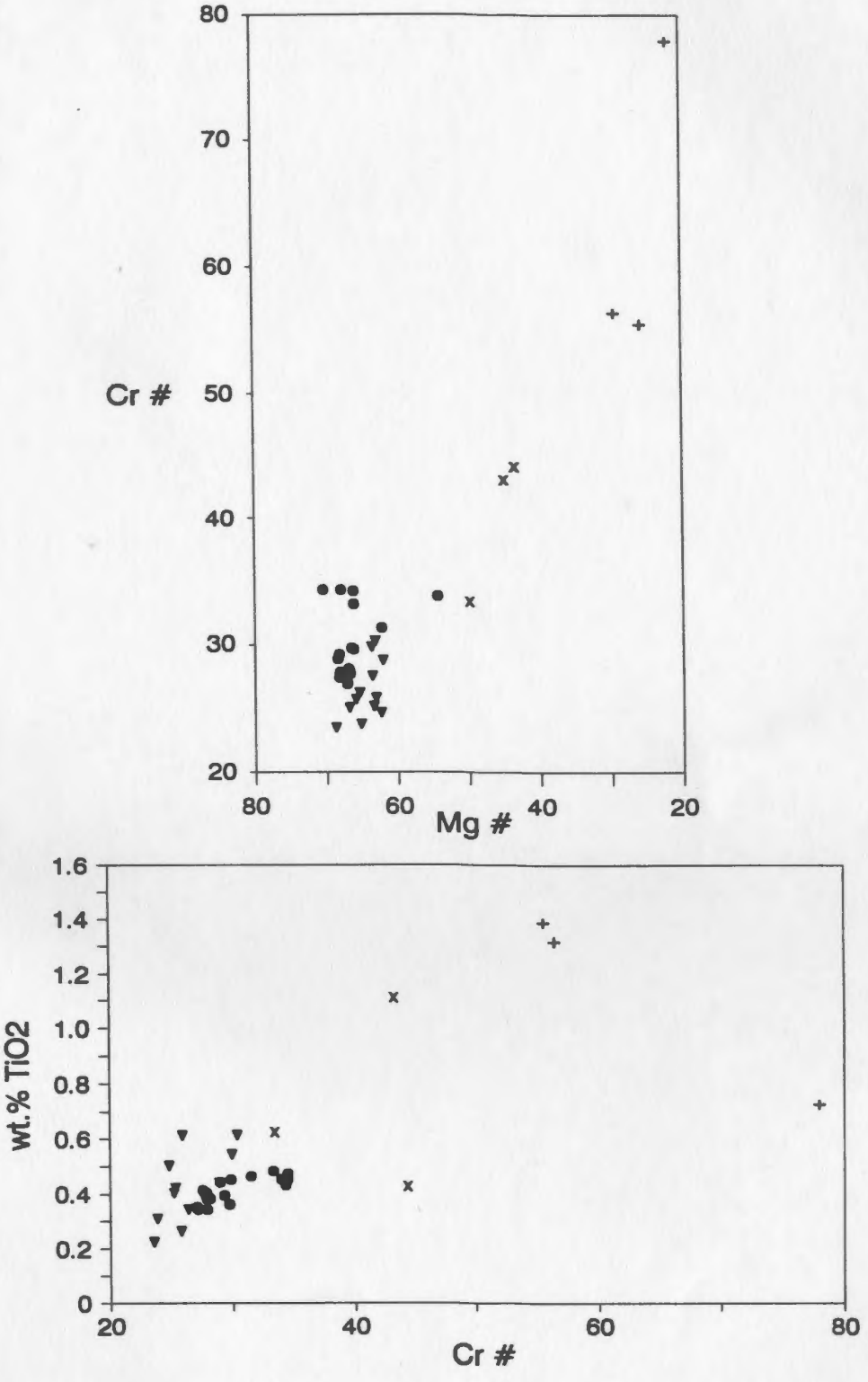

FIGURE 4.2. Compositional variation of spinel in HALPPG. Symbols as Figure 4.1.

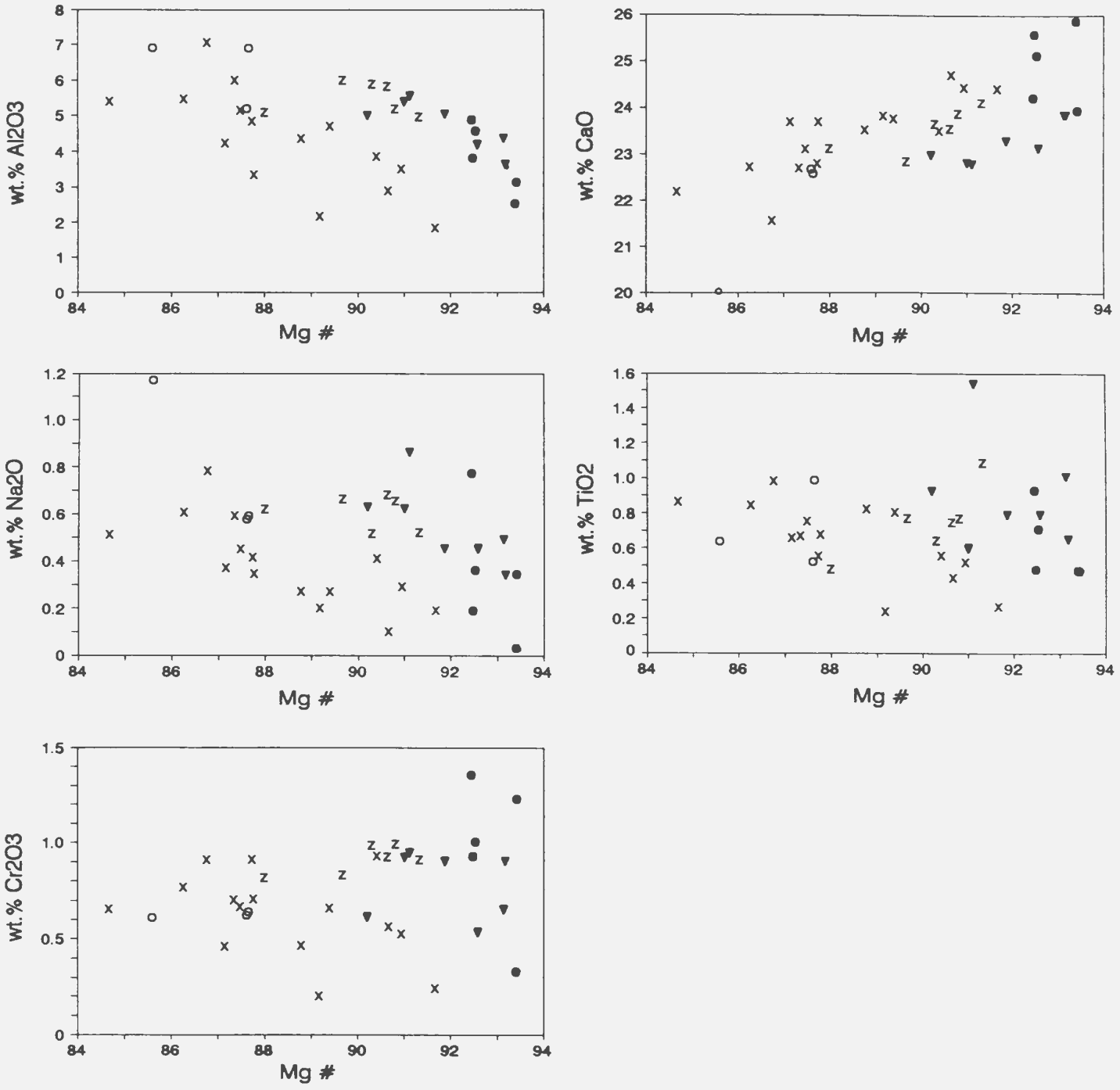

FIGURE 4.3. Compositional variation of clinopyroxene in HALPPG. Symbols as Figure 4.1.

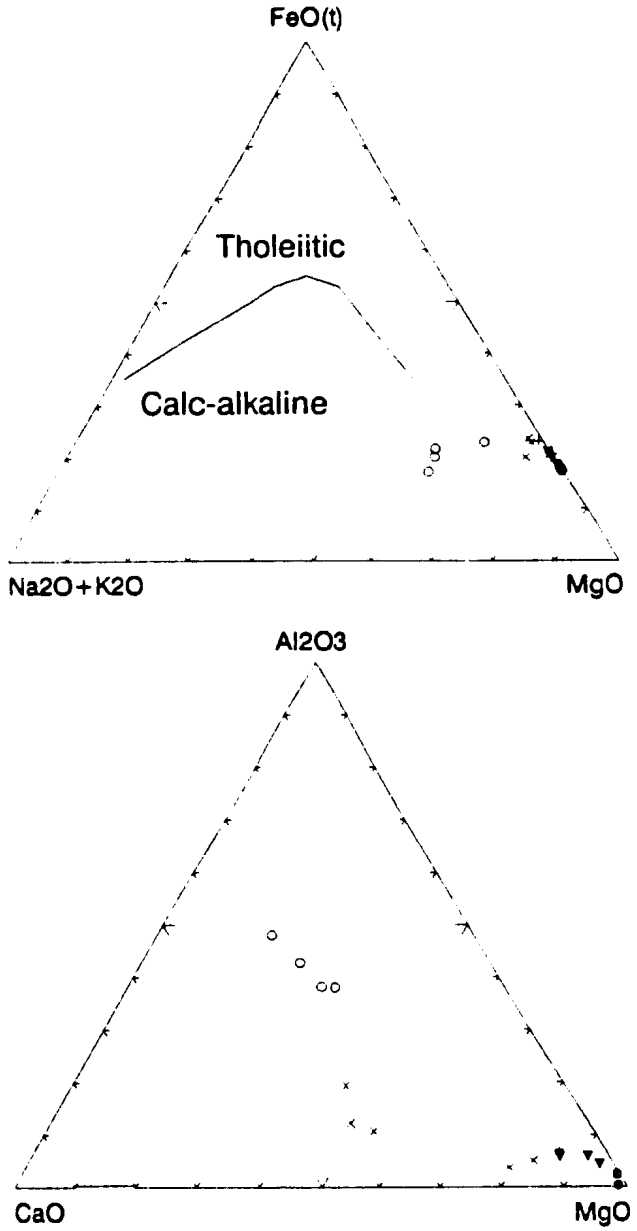

FIGURE 4.4. $Na_2O + K_2O$-$FeO_{(total)}$-MgO (AFM) and CaO-Al_2O_3-MgO (CAM) diagrams (weight %) of whole-rock samples of HALPPG. Symbols as Figure 4.1.

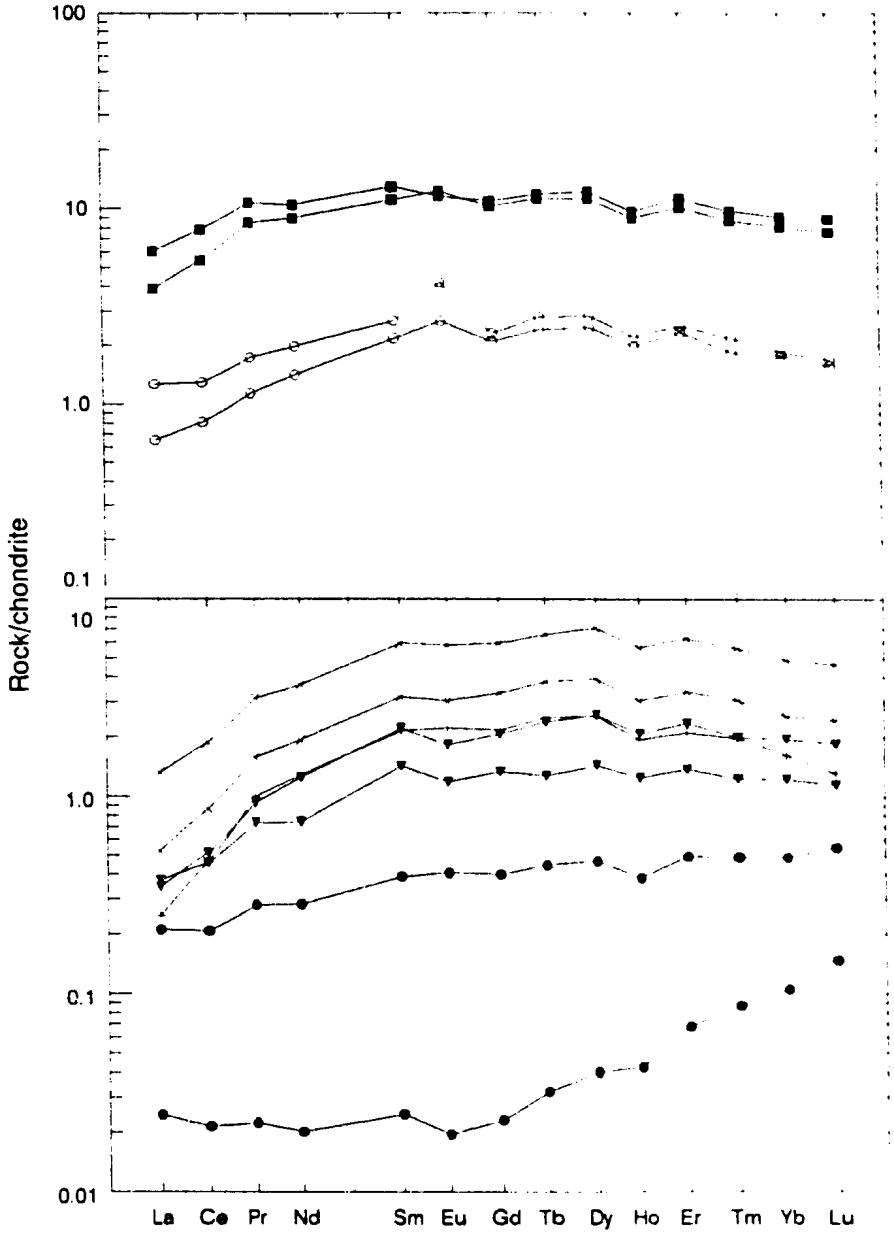

FIGURE 4.5. Chondrite-normalized rare earth element abundances of HALPPG (symbols as Figure 4.1) and amphibolite dykes (solid square). Normalization values are those of Wakita et al. (1971).

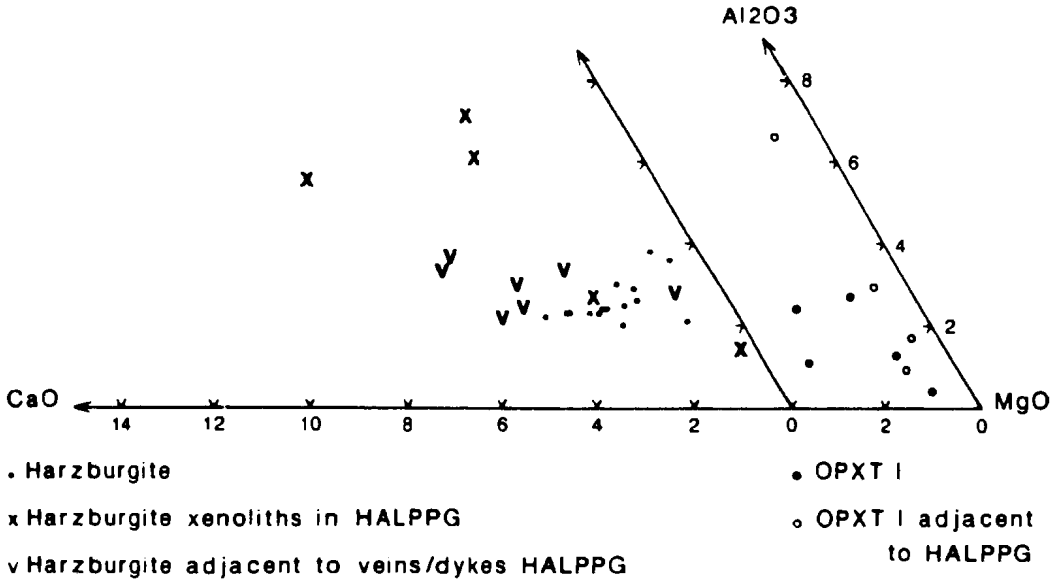

FIGURE 4.6. CAM diagram (weight %) of orthopyroxene in harzburgite and type I orthopyroxenite adjacent to HALPPG. The Mg# of orthopyroxene in contact with HALPPG is always lower than that not associated with HALPPG (this is not shown by the diagram).

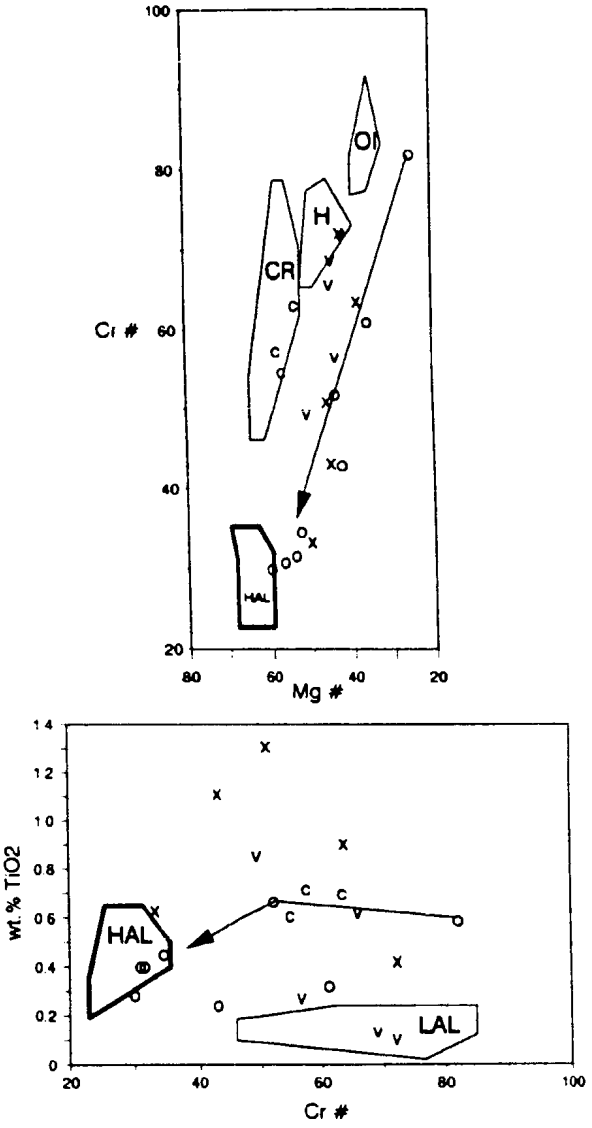

FIGURE 4.7. Compositional variation of spinel in LALPP associated with HALPPG: harzburgite xenoliths in HAL olivine clinopyroxenite (x), harzburgite adjacent to veins and dykes of HALPPG (v), chromitite xenolith in HAL olivine clinopyroxenite (c), and type I orthopyroxenite adjacent to HALPPG (o). Arrow indicates direction of compositional change over a distance of 8.5 mm on passing from type I orthopyroxenite into amphibole dunite for sample L333. Fields are from Figures 3.3 and 4.2: harzburgite (H), chromitite (CR) and type I orthopyroxenite (OI), which are the LALPP components of LAL; dunite and wehrlite of HALPPG (HAL).

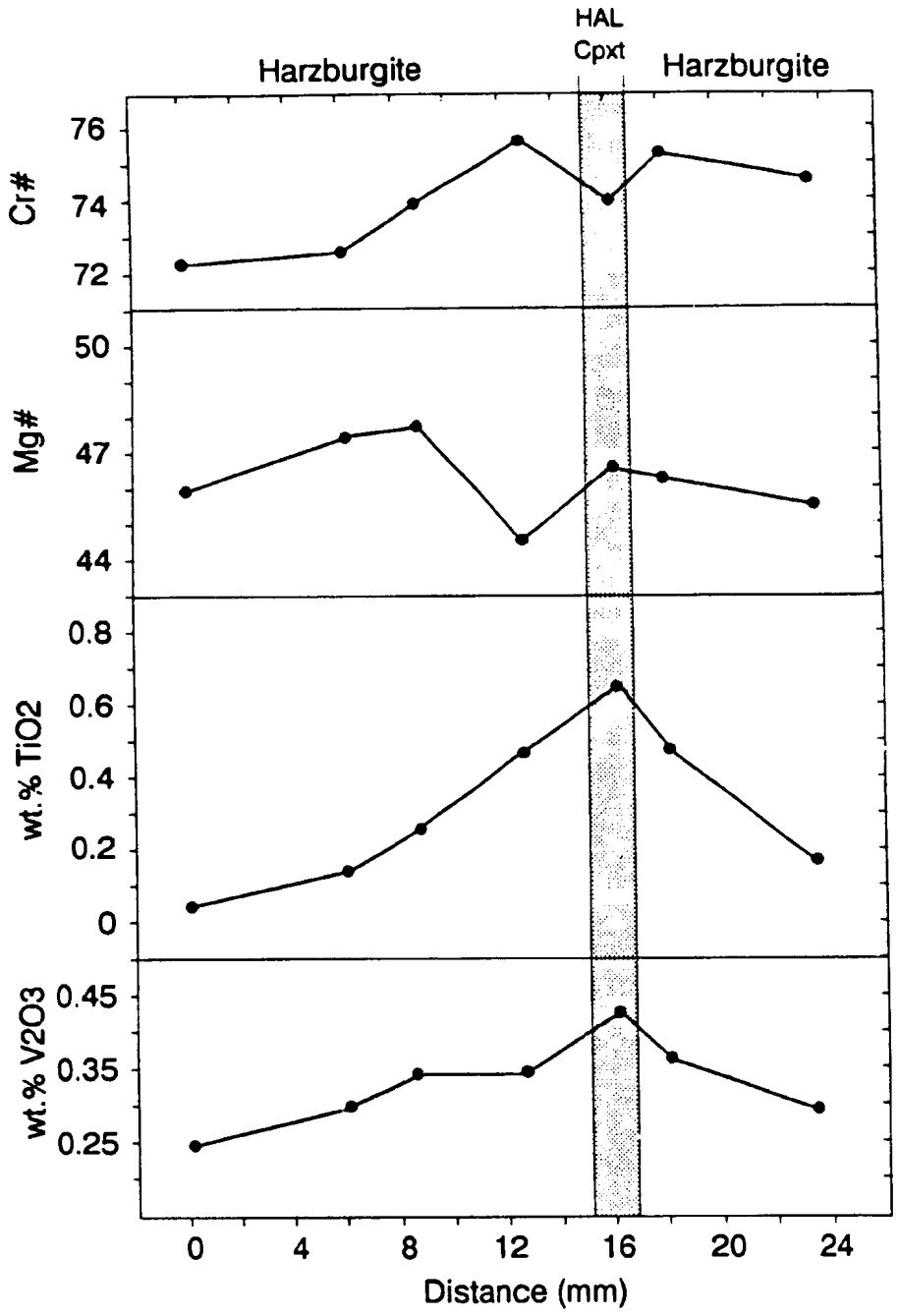

FIGURE 4.8. Compositional variation of Cr-spinel in harzburgite cut by a vein of HAL olivine clinopyroxenite.

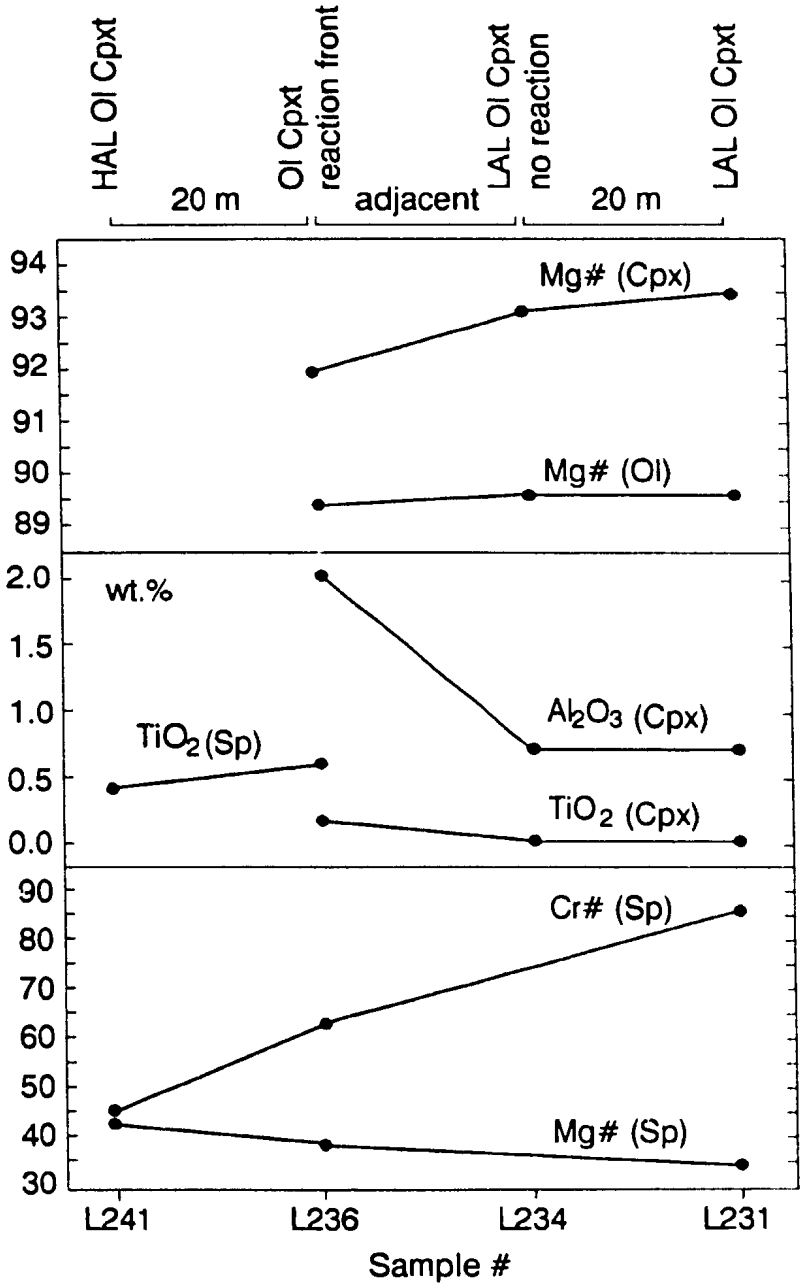

FIGURE 4.9. Compositional variation of clinopyroxene (Cpx), olivine (Ol) and spinel (Sp) across the contact between LAL olivine clinopyroxenite and HAL olivine clinopyroxenite.

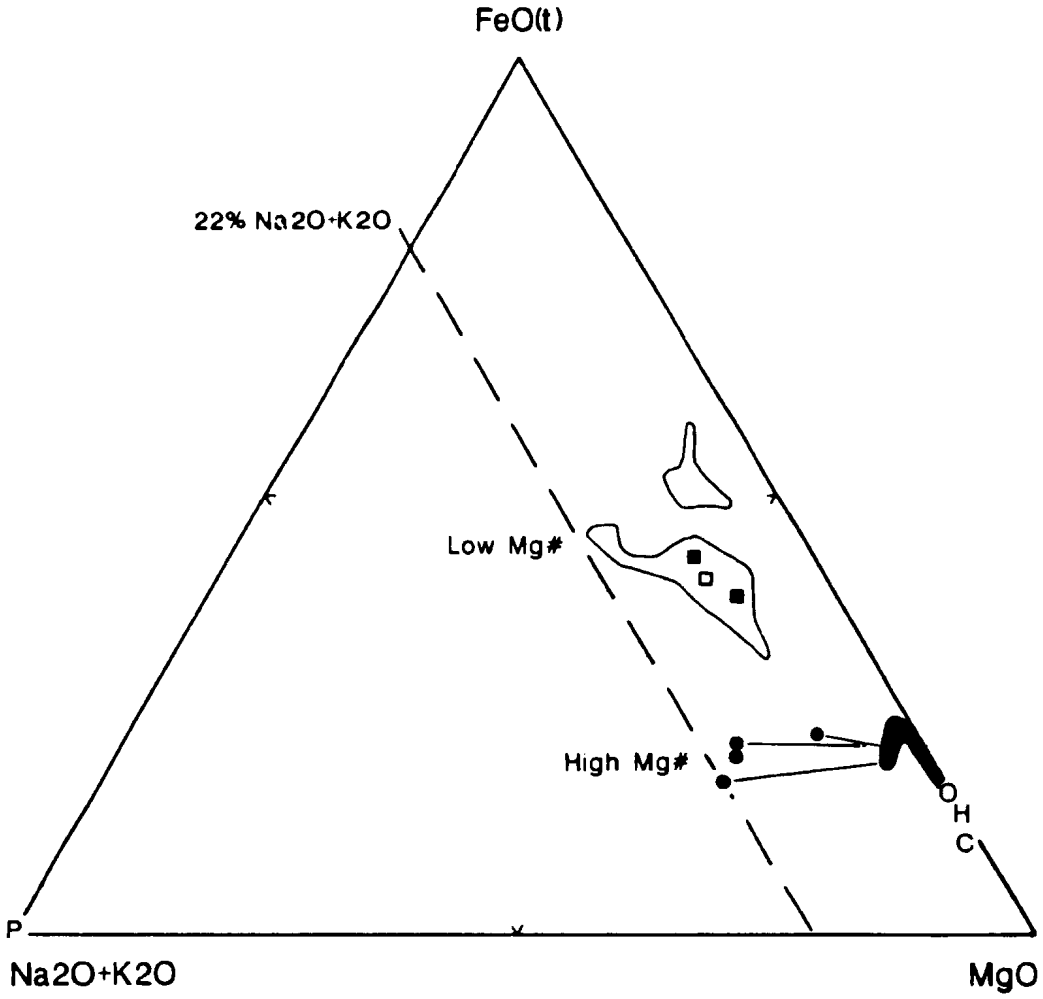

FIGURE 4.10. (a) AFM diagram (weight %) of HALPPG from Figure 4.4; tie lines connect gabbro (solid circle) and associated clinopyroxene or olivine clinopyroxenite. Composition fields: orthopyroxene in type I orthopyroxenite (O), olivine and orthopyroxene in harzburgite (H), clinopyroxene in LAL clinopyroxenite (C), amphibolite dykes (solid square), ferroan pargasite in amphibolite dykes (open square), plagioclase in amphibolite dykes (P), and diabase dykes of the Lewis Hills Depleted Suite (open field) (Casey et al., 1985; Elthon et al., 1986). Mg# reported as relatively high or low for a maximum proportion of $Na_2O + K_2O = 22$ %.

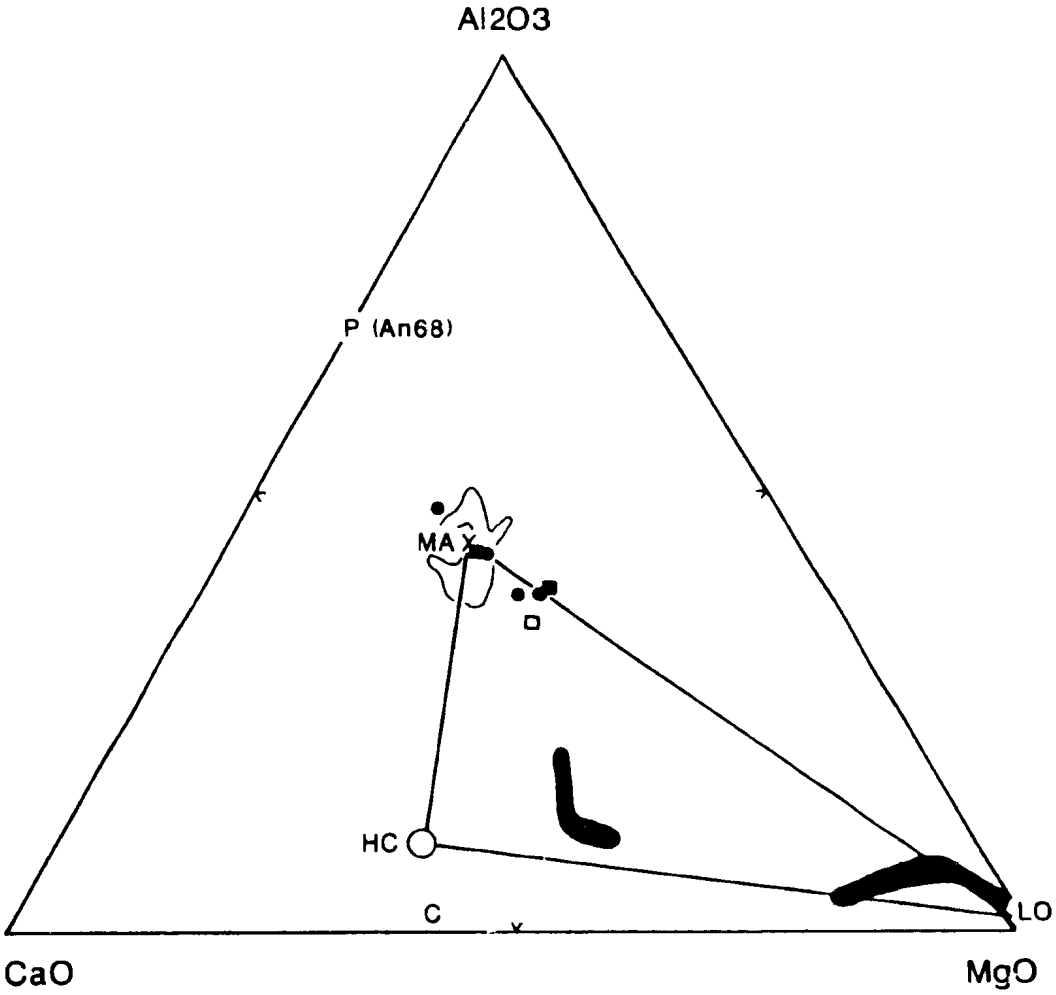

FIGURE 4.10. (b) CAM diagram (weight %) of HALPPG from Figure 4.4. Fields as for Figure 4.10a, except average composition of the Lewis Hills Depleted Suite (X). Triangle HC-MA-LO represents the three component system of 100 % unreacted olivine and orthopyroxene in harzburgite, LAL dunite and type I orthopyroxenite (LO), 100 % HAL clinopyroxenite produced by 100 % reaction of magma with LO (HC), and 100 % magma (represented by X) having experienced no reaction with LO (MA).

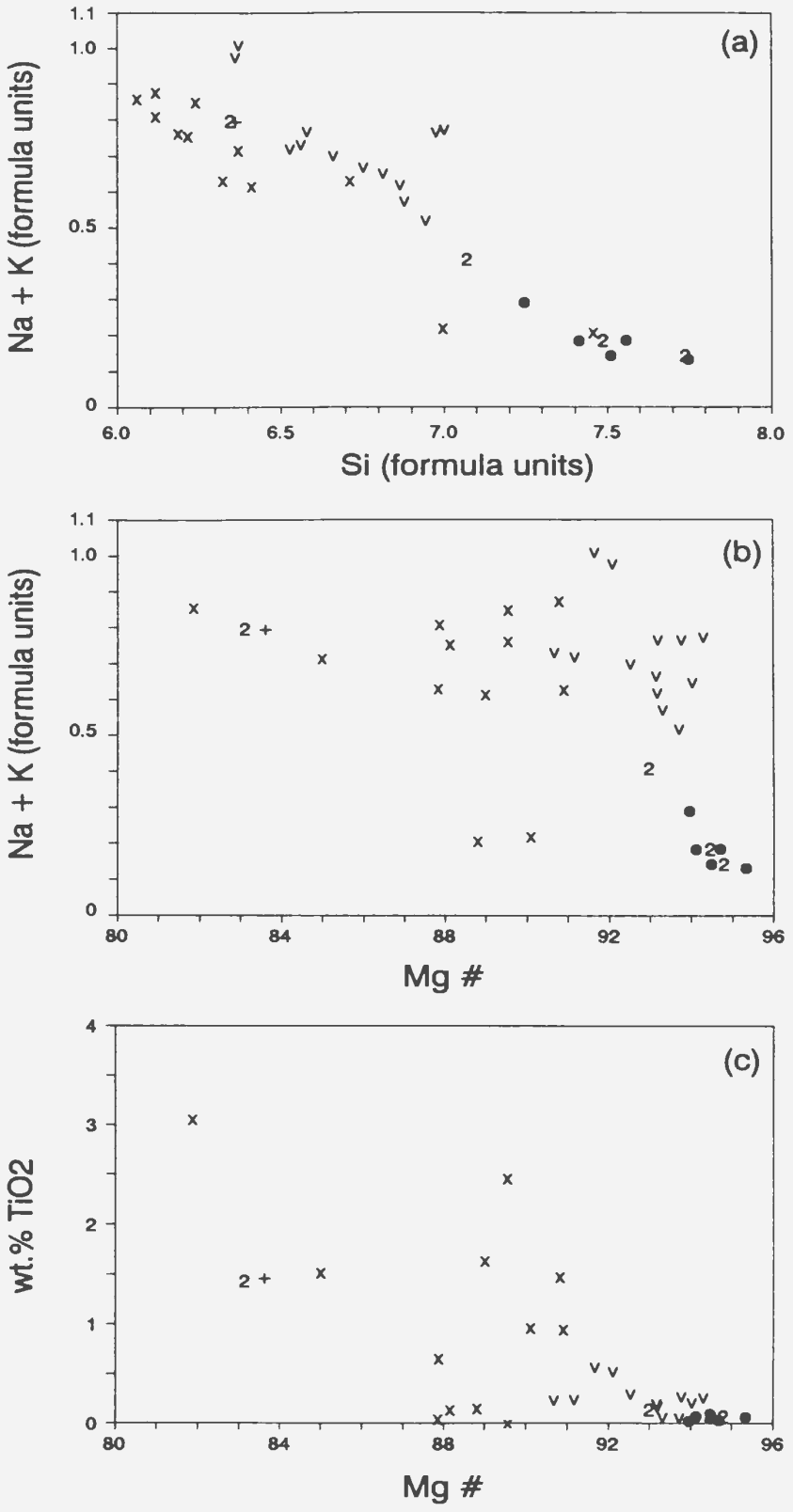

FIGURE 5.1. Compositional variation of Ca-amphibole in harzburgite (●), amphibole dunite (v) and type II orthopyroxenite (2) of LALPP, and dunite, wehrlite, olivine clinopyroxenite (x) and amphibole peridotite (+) of HALPPG. Formula units are the number of ions calculated on the basis of 23 oxygen atoms in the amphibole structure.

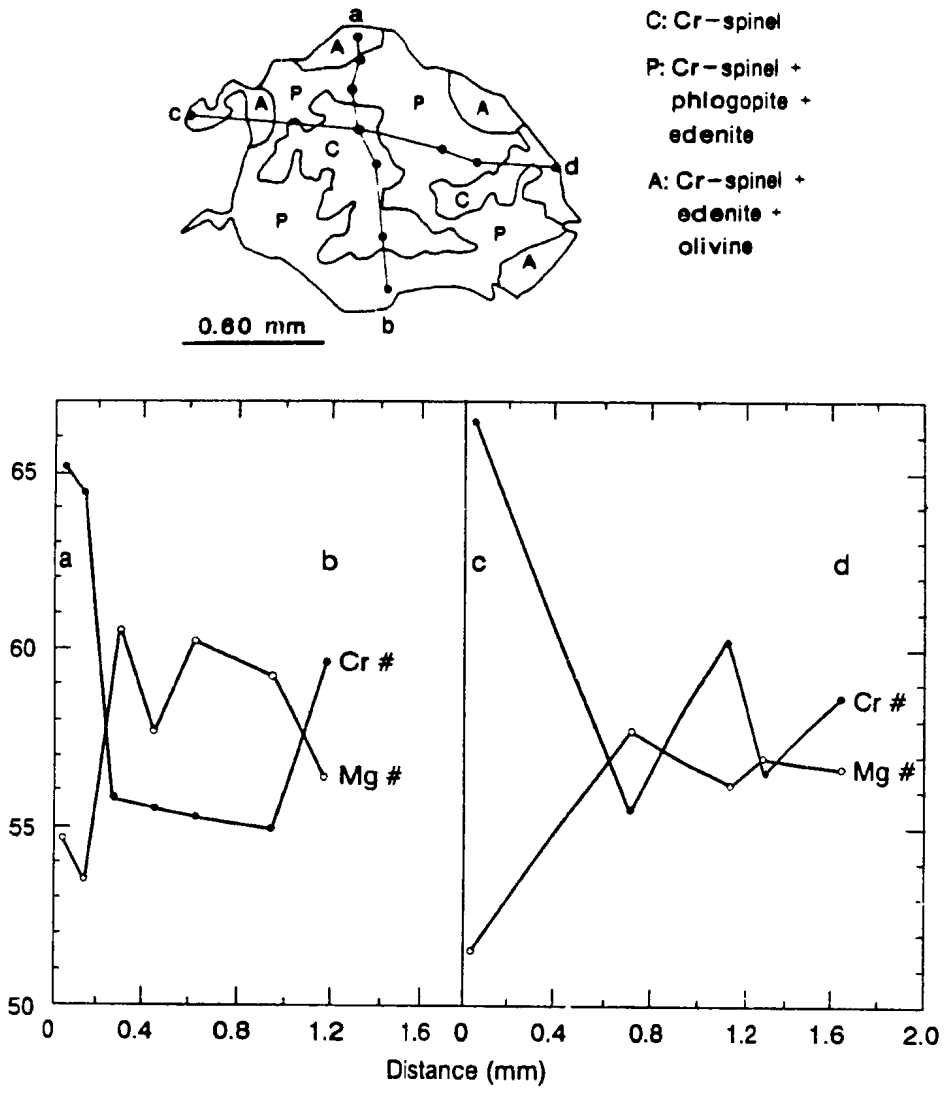

FIGURE 5.2. Compositional variation of spinel along traverses a-b and c-d in amphibole dunite sample L125. Refer to Figure 2.33 for detail of this spinel grain.

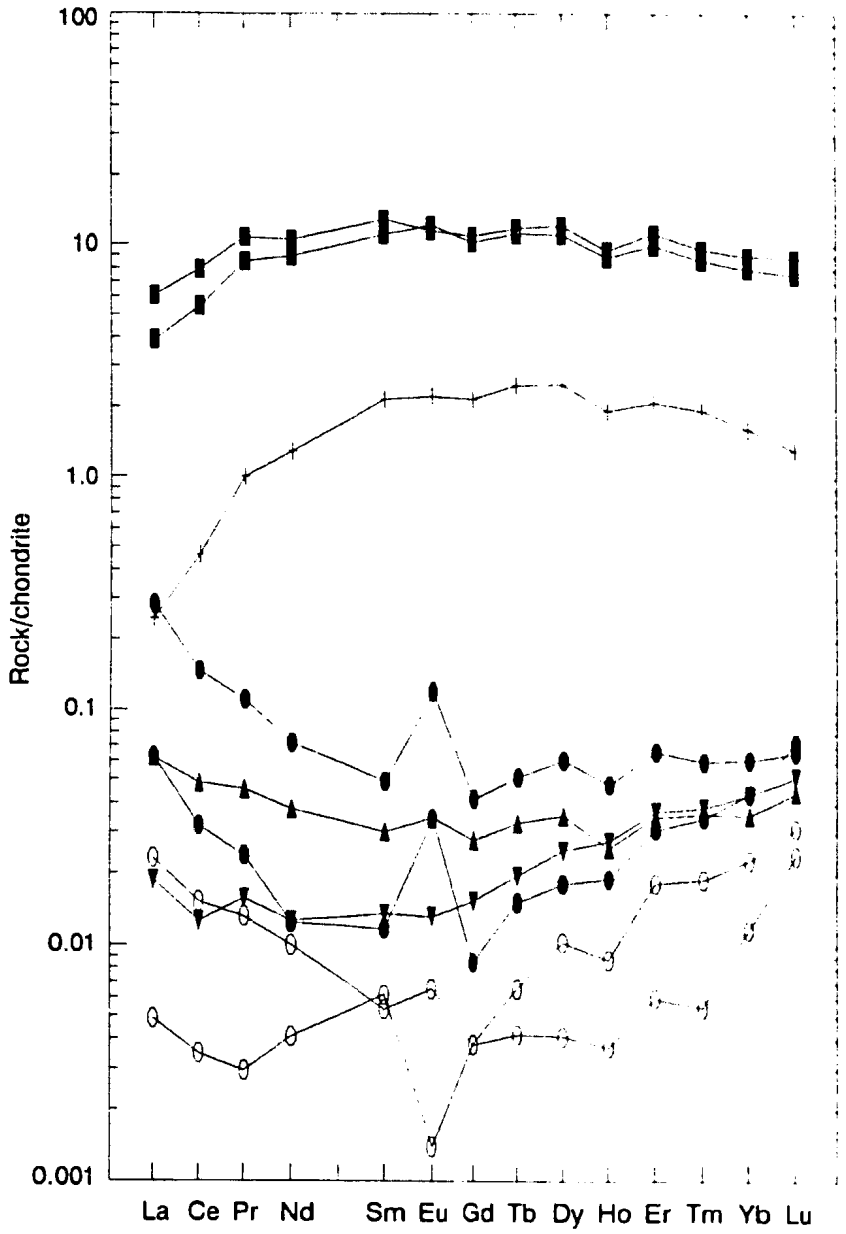

FIGURE 5.3. Chondrite-normalized rare earth element abundances of amphibole-bearing rock types in the Springers Hill area: type II orthopyroxenite (open circle), amphibole dunite replacing type I orthopyroxenite (solid circle), amphibole dunite (solid inverted triangle), and amphibole-bearing harzburgite (solid triangle) of LALPP; HAL amphibole peridotite (+); amphibolite dykes (solid square). Normalization values are those of Wakita et al. (1971).

TABLE A1.1. Accuracy and precision of analyses of minerals

	Accepted wt.%	Mean wt.%	Min wt.%	Max wt.%	SD wt.%	COV %
Olivine 174.1: Dalhousie; n=98						
SiO2	40.8	40.98	39.93	41.97	0.36	0.88
FeO	9.46	9.34	8.94	9.72	0.17	1.87
NiO	0.39	0.41	0.00	0.89	0.13	31.71
MgO	49.26	49.25	47.88	50.46	0.38	0.77
Cr-diopside: Dalhousie; n=18						
SiO2	55.12	55.15	54.62	55.76	0.37	0.67
Cr2O3	0.58	0.26	0.03	0.40	0.08	32.61
FeO	1.20	1.38	1.24	1.50	0.07	5.23
MgO	17.46	17.30	17.02	17.68	0.19	1.10
CaO	25.54	25.52	24.89	25.82	0.26	1.02
Kakanui kaersutite (KK): Dalhousie; n=50						
SiO2	40.37	40.44	38.11	41.19	0.45	1.11
TiO2	4.72	4.68	4.24	4.92	0.15	3.15
Al2O3	14.9	14.52	14.01	15.06	0.24	1.62
FeO	10.91	10.36	9.77	10.75	0.19	1.88
MgO	12.8	12.53	11.49	12.95	0.25	2.03
CaO	10.3	10.22	9.63	10.61	0.17	1.68
Na2O	2.6	2.71	2.47	3.01	0.13	4.80
K2O	2.04	1.98	1.31	2.17	0.12	6.25
Orthopyroxene grain: Dalhousie; n=3						
MnO		0.14	0.13	0.16	0.02	12.37
Spinel 53IN8: Memorial; n=25						
TiO2	1.60	1.29	1.17	1.37	0.04	3.39
V2O3	0.91	0.99	0.87	1.10	0.06	6.12
Al2O3	12.82	12.87	12.44	13.32	0.21	1.59
Cr2O3	49.31	49.11	48.42	50.16	0.43	0.87
FeO	28.15	28.00	27.23	29.10	0.40	1.43
MnO	0.32	0.26	0.18	0.32	0.03	12.37
NiO	0.06	0.08	0.04	0.12	0.02	22.71
MgO	6.12	6.04	5.81	6.23	0.11	1.88

Accepted values are those of Dalhousie University and Memorial University

TABLE A1.2. Accuracy and precision of analyses of major elements

	Accepted wt.%	Mean wt.%	Min wt.%	Max wt.%	SD wt.%	COV %
Basalt BE-N: Memorial; n=6						
SiO2	38.20	38.50	38.21	38.67	0.18	0.47
Al2O3	10.07	10.02	9.85	10.10	0.09	0.90
Fe2O3	12.84	12.84	12.69	12.96	0.11	0.86
MnO	0.20	0.19	0.19	0.19	0.00	0.00
MgO	13.15	13.14	13.04	13.27	0.07	0.53
CaO	13.87	13.91	13.84	13.96	0.05	0.36
Na2O	3.18	3.25	3.22	3.28	0.02	0.62
K2O	1.39	1.46	1.45	1.47	0.01	0.68
Basalt BCR-1: Memorial; n=1						
Fe2O3	3.59	3.49				
FeO	8.88	8.87				
P2O5	0.36	0.36				
Peridotite PCC-1: Memorial; n=2						
SiO2	41.67	41.90	41.70	42.10	0.28	0.68
Fe2O3	8.25	8.06	7.98	8.13	0.11	1.32
MnO	0.12	0.12	0.12	0.12	0.00	0.00
MgO	43.43	43.49	42.87	44.10	0.87	2.00
CaO	0.52	0.55	0.54	0.56	0.01	2.57
Peridotite PCC-1: Mines; n=6						
Al2O3	0.67	0.65	0.64	0.67	0.01	1.85

Accepted values from the compilation of Govindaraju (1989)

TABLE A1.3. Accuracy and precision of analyses of trace elements

	Accepted ppm	Mean ppm	Min ppm	Max ppm	SD ppm	COV %	LOD ppm
Basalt BCR-1: Memorial; n=3							
TiO2	22400	22900	22700	23000	0.0	0.7	200
Sc	33	32	31	33	1.2	3.7	3
V	407	424	423	425	1.0	0.2	6
Zn	130	129	127	130	1.5	1.2	9
Rb	47	48	47	49	1.0	2.1	0.9
Sr	330	338	336	339	2.3	0.7	0.8
Y	38	37	37	38	0.8	2.1	0.8
Zr	190	195	194	197	1.8	0.9	0.7
Peridotite PCC-1: Memorial; n=16							
Sc	8	7	5	10	1.6	24.1	3
V	31	31	26	34	2.1	6.7	6
Cr	2730	2873	2839	2918	21.0	0.7	5
Ni	2380	2299	2252	2343	21.0	0.9	2
Zn	42	45	42	47	1.8	3.9	9

Accepted values from the compilation of Govindaraju (1989)

TABLE A1.4a. Limits of detection and blank compositions of rare earth elements (concentrations in ppb)

Run	LOD 116	Blank 116	LOD 153	Blank 153	LOD 240	Blank 240	LOD 182	Blank 182	LOD 024	Blank 024
n		1		2		1		1		3
La	0.21	0.40	0.56	0.55	1.06	1.3	0.587	54.1	3.06	72.1
Ce	0.15	0.58	0.45	0.59	0.35	2.3	1.168	226	4.68	67.6
Pr	0.23	0.079	0.38	0.36	1.0	0.072	0.599	17.7	2.60	3.91
Nd	1.5	2.1	2.9	1.5	1.5	1.0	2.59	92.3	19.6	14.0
Sm	1.00	1.16	1.6	0.72	2.1	0.035	2.85	24.0	45.9	23.7
Eu	0.36	0.24	0.50	0.038	0.45	0.23	1.57	nd	15.5	nd
Gd	1.1	0.55	1.8	0.30	3.1	nd	4.85	20.3	17.0	nd
Tb	0.16	0.119	0.30	0.057	0.19	0.100	0.391	2.90	4.95	nd
Dy	0.40	0.80	0.84	0.34	0.86	0.125	2.45	26.6	7.43	nd
Ho	0.183	0.162	0.29	0.067	0.160	0.043	1.30	5.06	3.10	nd
Er	0.61	0.51	1.13	0.50	1.50	0.170	0.839	15.7	11.8	1.02
Tm	0.070	0.119	0.353	0.165	0.360	nd	1.43	3.22	12.4	nd
Yb	0.66	0.64	1.05	0.62	0.53	0.0076	1.54	19.4	14.1	0.056
Lu	0.062	0.193	0.33	0.043	0.190	0.39	0.488	1.65	1.40	nd

TABLE A1.4b. Precision (as COV in %) of rare earth elements

Run	116	153	240	182	024
La	26	26	26	2	2
Ce	26	26	26	2	2
Pr	31	31	31	2	2
Nd	35	35	35	3	3
Sm	23	23	23	2	2
Eu	34	34	34	4	4
Gd	40	40	40	3	3
Tb	19	19	19	3	3
Dy	21	21	21	4	4
Ho	15	15	15	3	3
Er	7	7	7	3	3
Tm	7	7	7	3	3
Yb	9	9	9	3	3
Lu	13	13	13	3	3

TABLE A1.4c. Accuracy and precision of analyses of rare earth elements

Basalt BCR-1: Memorial

	MUN ppm	Run 182 ppm	Yield %	Run 024 ppm	Yield %	Mean ppm	SD ppm	COV %
n		1		1				
La	24.9	22.4	90	24.3	98	23.4	1.3	6
Ce	53.4	45.9	86	50.1	94	48.0	3.0	6
Pr	6.9	6.26	91	6.54	95	6.40	0.19	3
Nd	28.8	24.7	86	26.4	92	25.6	1.2	5
Sm	6.59	6.03	91	6.26	95	6.14	0.17	3
Eu	1.96	1.57	80	1.67	85	1.62	0.07	4
Gd	6.64	5.36	81	5.63	85	5.49	0.19	4
Tb	1.05	0.945	90	1.01	96	0.98	0.05	5
Dy	6.42	5.87	91	6.06	94	5.97	0.14	2
Ho	1.25	1.18	95	1.22	98	1.20	0.03	2
Er	3.67	3.53	96	3.49	95	3.51	0.03	1
Tm	0.59	0.490	83	0.509	86	0.500	0.013	3
Yb	3.37	3.19	95	3.19	95	3.192	0.004	0.1
Lu	0.497	0.494	99	0.477	96	0.486	0.012	2

MUN are the Memorial University accepted values

TABLE A1.4d. Accuracy and precision of analyses of rare earth elements

Peridotite PCC-1: Memorial

	Accepted ppb	Min ppb	Max ppb	Run 116 ppb	Run 153 ppb	Run 240 ppb	Run 024 ppb	Mean ppb	SD ppb	COV %
n				1	1	1	1			
La	43	32	55	150	160	150		150	6	4
Ce	88	66	120	37	44	49		43	6	14
Pr	11	7	15	5.3	5.8	5.8		5.6	0.3	5
Nd	49	33	80	20	23	23		22	2	8
Sm	6.5	5.4	8.5	3.8	5.1	2.6		3.8	1.3	33
Eu	6.2	0.96	29	0.75	0.64	0.65		0.68	0.06	9
Gd	8.1	3.4	14	4.1	5.6	3.8		4.5	1.0	21
Tb	1.7	1.2	3	0.50	1.11	2.0		1.2	0.8	64
Dy	8.7	6.5	10	7.4	8.1	4.8		6.8	1.7	26
Ho	2.7	1.3	4	1.49	2.1	1.26		1.6	0.4	27
Er	8.4	4.7	12	4.9	8.4	5.4		6.2	1.9	31
Tm	2.6	0.77	4	1.11	1.54	1.79		1.48	0.34	23
Yb	25	7.5	31	9.8	10.8	15.5	32.9	12.0	3.0	25
Lu	5.3	1.6	8.5	1.78	2.4	5.0	6.23	3.1	1.7	56

Accepted, minimum and maximum values are from the compilation of Frey (1984)

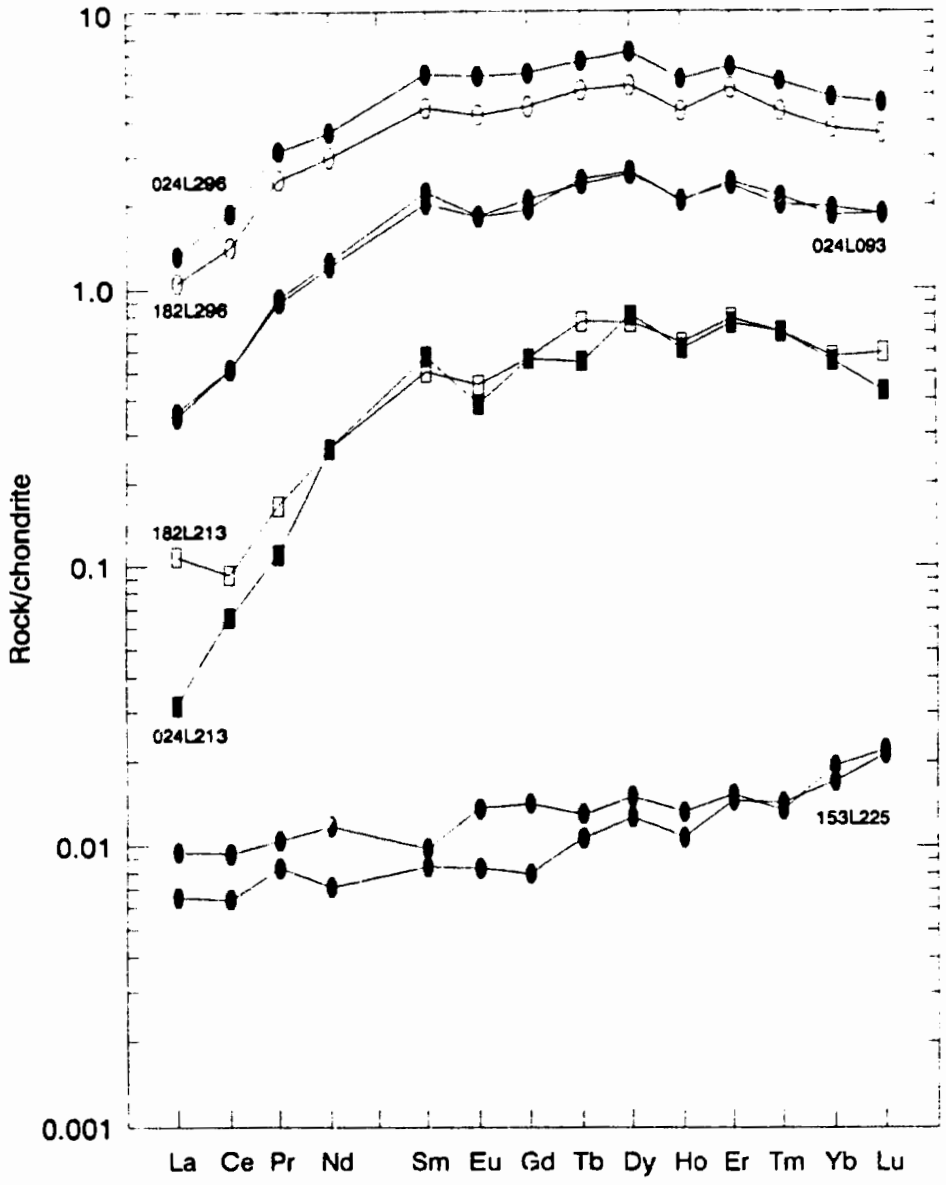

FIGURE A1.1. Precision of chondrite-normalized rare earth element abundances of representative analyses from runs 153 and 024, and between runs 182 and 024. Each point represents a single determination. Normalization values are those of Wakita et al. (1971).

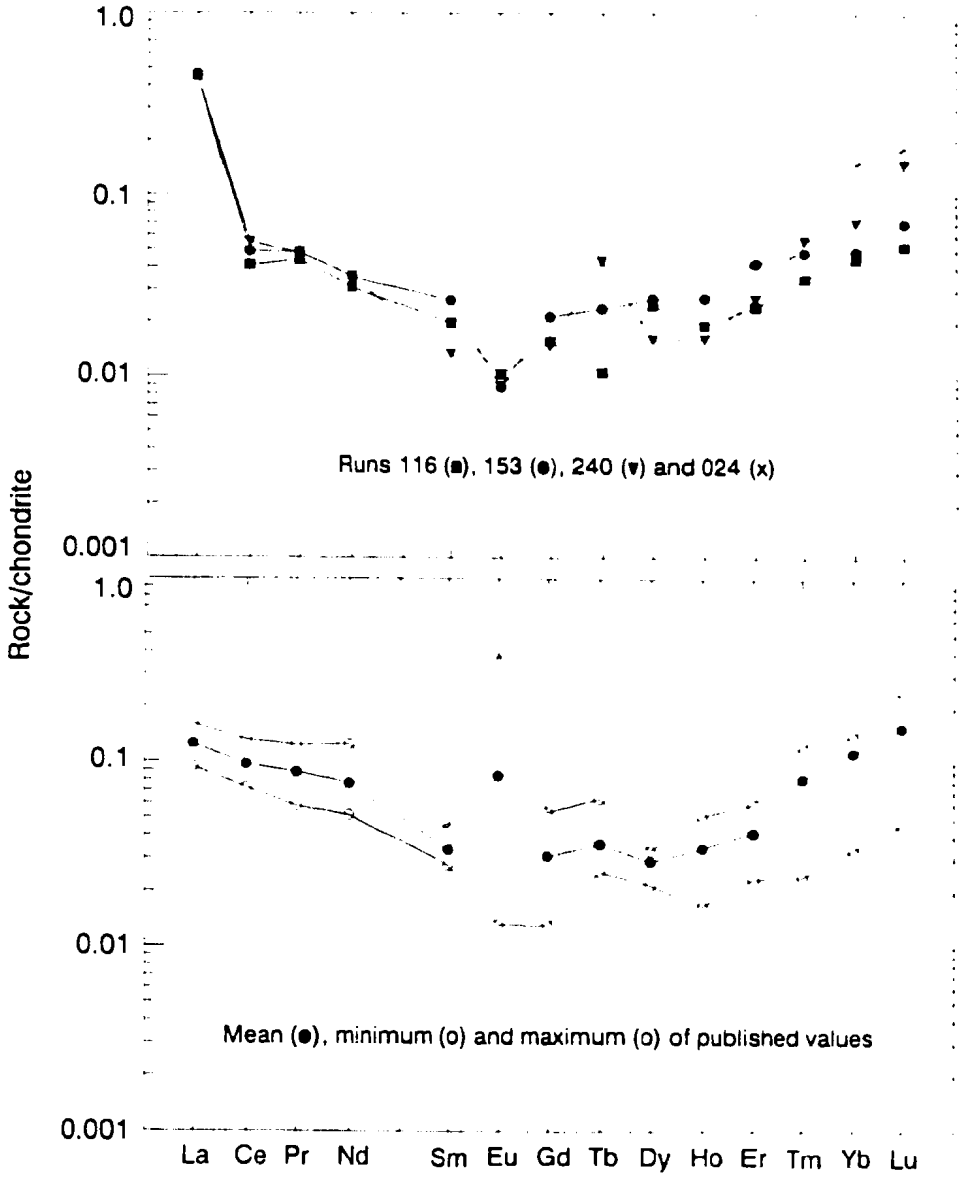

FIGURE A1.2. Precision and accuracy of chondrite-normalized rare earth element abundances of USGS peridotite standard PCC-1. Each point in runs 116, 153, 240 and 024 represents a single determination. The mean, minimum and maximum of published values are from the compilation of Frey (1984). Normalization values are those of Wakita et al. (1971).

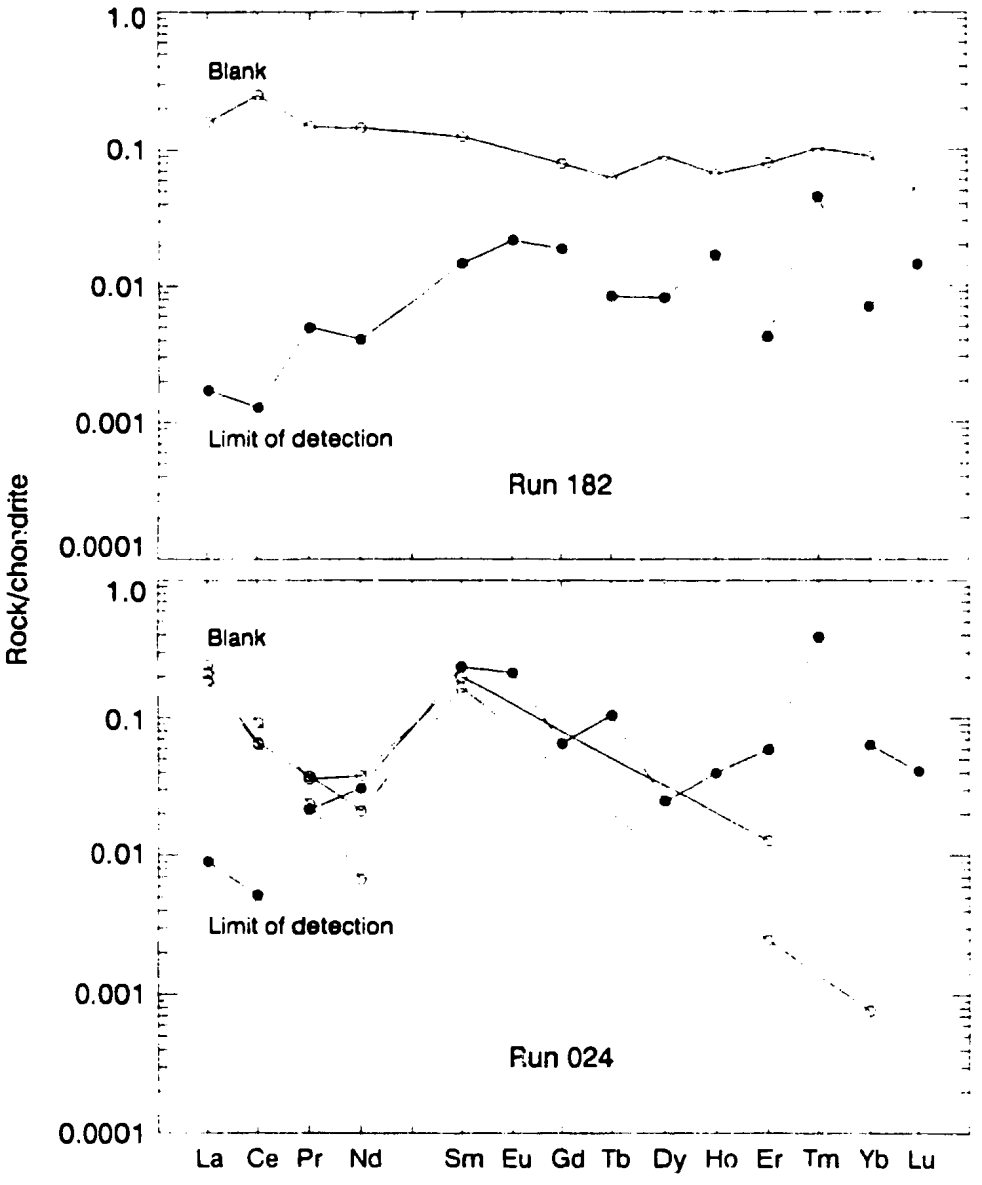

FIGURE A1.3. Chondrite-normalized rare earth element abundances of blanks and limits of detection in runs 182 and 024. Normalization values are those of Wakita et al. (1971).

TABLE A1.5. Accuracy and precision of analyses of platinum group elements

PTC-1: Memorial; n=5

	Accepted ppb	MUN ppb	Mean ppb	Min ppb	Max ppb	SD ppb	COV %	LOD ppb
Ru	650	440	418	346	503	67	16.0	0.08
Rh	620	609	605	582	626	16	2.7	0.02
Pd	12700	11405	11402	10392	11813	577	5.1	0.13
Re		67	72	55	90	15	20.4	0.04
Os	240	192	139	54	218	66	47.3	0.31
Ir	170	164	170	153	184	11	6.7	0.01
Pt	3000	2699	2609	2165	3250	416	15.9	0.05
Pd/Ir	75	70	67					

Accepted values from McAdam et al. (1973); MUN are accepted values from Memorial University

TABLE A3 1 Olivine analyses (oxides in wt %, number of ions on basis of 4 O)

Rock	H	H	H	H	H	H	H	H	H	H	H	H	H	H	H
Sample	L097	L097	L106	L106	L106	L153	L153	L157	L157	L157	L157	L157	L157	L193	L193
Location	1–Ol	4–Ol	3–Ol	3–Ol	3–Ol	1–Ol	1–Ol	1–Ol	1–Ol	3–Ol	5–Ol	5–Ol	6–Ol	2–Ol	3–Ol
Type	LALPP	LALPP	LALPP	LALPP	LALPP	LALPP	LALPP	LALPP	LALPP	LALPP	LALPP	LALPP	LALPP	LALPP	LALPP
SiO2	40.49	40 59	41.26	41.41	41 40	41 53	40 70	41 37	40 26	40.86	41 29	41 01	41 00	41 38	41 03
TiO2	0.02	0.02	0.00	0.01	0 01	0 00	0 00	0.02	0.02	0 00	0 01	0.03	0 00	0 00	0 00
Al2O3	0.01	0.00	0.00	0.00	0.00	0 03	0 01	0 05	0 00	0 00	0 00	0 01	0 00	0 04	0 03
Cr2O3	0.05	0.00	0.04	0 00	0.00	0 00	0 02	0 00	0 09	0 00	0 00	0 00	0 00	0 00	0 00
FeO	8.58	8.77	8.41	8.48	8 56	8 61	8 45	8 62	8 61	8 56	8 72	8 26	8 64	8 42	8 54
MnO	0.02	0.06	0 11	0.15	0.13	0 03	0 00	0 08	0.17	0 05	0 13	0 07	0 11	0 05	0 03
NiO	0.46	0 44	0.41	0 46	0 15	0 44	0 39	na	0 72	0 45	0 58	0 67	0 27	0 50	0 53
MgO	49 70	49 34	49 81	49.99	49 64	48 95	49 46	50 12	50 02	49 97	49 73	49.73	49 79	49 37	49 23
CaO	0.00	0 00	0.00	0.00	0 00	0 00	0.00	0 00	0 00	0 00	0.00	0 00	0 00	0 00	0 00
Na2O	0.00	0.01	0.01	0 03	0 03	0 00	0 01	0 03	0 04	0.02	0.00	0 02	0 02	0 00	0 01
K2O	0.00	0.00	0 00	0 00	0 00	0 00	0.00	0.00	0 00	0 00	0 00	0 00	0 00	0 00	0 00
Total	99 30	99.23	100.05	100.53	99 92	99 59	99 03	100 29	99.93	99 91	100.46	99 79	99 81	99 76	99 40
Si	0.995	0.999	1.005	1.004	1.008	1.015	1.002	1.005	0.987	0.998	1.003	1.002	1 001	1 010	1 006
Ti	0.000	0.000	0.000	0.000	0.000	0.000	0.000	0.000	0 000	0 000	0.000	0.001	0.000	0 000	0 000
Al	0.000	0.000	0 000	0.000	0.000	0.001	0 000	0 001	0.000	0 000	0 000	0 000	0 000	0 001	0 001
Cr	0.001	0.000	0 001	0.000	0 000	0 000	0.000	0.000	0.002	0 000	0 000	0 000	0.000	0 000	0 000
Fe2+	0.176	0.180	0.171	0.172	0.174	0.176	0.174	0.175	0.176	0 175	0.177	0 169	0.176	0 172	0 175
Mn	0.000	0.001	0.002	0.003	0 003	0 001	0 000	0 002	0 004	0.001	0 003	0 001	0 002	0 001	0 001
Ni	0.009	0.009	0.008	0.009	0.003	0.009	0 008	0.000	0 014	0.009	0 011	0 013	0 005	0.010	0 010
Mg	1.821	1.810	1.808	1.807	1.802	1 783	1 814	1 815	1.828	1 819	1.802	1 811	1 813	1.796	1 800
Ca	0.000	0.000	0.000	0.000	0.000	0.000	0.000	0 000	0.000	0.000	0 000	0 000	0 000	0 000	0 000
Na	0.000	0.001	0.000	0.001	0.001	0 000	0 000	0 001	0.002	0 001	0 000	0.001	0 001	0 000	0 000
K	0.000	0.000	0.000	0.000	0.000	0.000	0 000	0.000	0.000	0.000	0 000	0.000	0 000	0 000	0.000
Total	3.004	3.001	2.995	2.996	2.992	2 985	2 998	2 999	3.013	3.003	2.996	2 998	2 999	2 990	2 994
Mg#	91 2	90.9	91 3	91.3	91 2	91 0	91 3	91 2	91 2	91 2	91 0	91 5	91 1	91 3	91 1

Rock	H	H	H	H	H	H	H	H	H	H	D	D	D	D	D
Sample	L218	L218	L225	L225	L225	L225	L226	L226	L2e4	L336	L055	L055	L055	L143	L143
Location	2-Ol	2-Ol	2-Ol	4-Ol	5-Ol	6-Ol	1-Ol	4-Ol	1-Ol	1-Ol	4-Ol	6-Ol	7-Ol	1-Ol	2-Ol
Type	LALPP	LALPP	LALPP	LALPP	LALPP	LALPP	LALPP	LALPP	LALPP	LALPP	LALPP	LALPP	LALPP	LALPP	LALPP
SiO2	41.27	41.00	41.00	40.99	41.10	41.14	41.04	40.74	41.35	41.18	40.88	41.19	41 34	41 45	41 16
TiO2	0.01	0.01	0.00	0.00	0.00	0.00	0.01	0.01	0.03	0.00	0.00	0.00	0 00	0.04	0 00
Al2O3	0 00	0.00	0.02	0.03	0.01	0.03	0.00	0.00	0.00	0.01	0.03	0.04	0.03	0 01	0.00
Cr2O3	0.02	0.02	0.00	0.00	0.00	0.00	0.00	0.01	0.02	0.00	0.00	0.03	0.05	0 00	0 04
FeO	8.41	8.39	7.95	8.28	8 36	7.83	7.91	8.15	8.14	8.39	9 68	8.39	7.91	8.49	8 48
MnO	0.00	0.17	0.02	0.01	0 02	0.03	0.14	0.15	0.15	0.00	0.04	0.00	0 02	0 20	0 21
NiO	0 60	0.40	0.45	0.48	0 44	0 50	0.45	0.13	0.29	0.44	0 31	0 38	0 40	0 32	0 51
MgO	49.44	49 23	50 13	49.90	49.61	49 99	50.03	49.54	49.93	49.92	48.08	49.23	50 06	49 71	49 75
CaO	0.00	0.00	0.00	0.00	0.00	0.00	0.00	0.00	0 00	0.00	0.00	0 00	0 00	0 00	0 00
Na2O	0.04	0.03	0.01	0.00	0.01	0.00	0.01	0.02	0 02	0.01	0.00	0.00	0 01	0.05	0.03
K2O	0.00	0.00	0.00	0.00	0 00	0.00	0.00	0.00	0 00	0.00	0.00	0.00	0 00	0 00	0 00
Total	99.79	99.24	99.58	99 68	99.53	99.45	99.59	98.73	99 91	90 93	99 02	99.27	99 82	100 25	100 18
Si	1.008	1.007	1.001	1 001	1.005	1.005	1.002	1.003	1.006	1.003	1.010	1.010	1.006	1 007	1 002
Ti	0 000	0 000	0 000	0 000	0.000	0 000	0 000	0 000	0.000	0 000	0.000	0.000	0.000	0 001	0 000
Al	0.000	0.000	0.001	0.001	0.000	0 001	0.000	0 000	0.000	0 000	0 001	0.001	0 001	0 000	0 000
Cr	0.000	0.000	0.000	0 000	0 000	0.000	0.000	0.000	0.000	0.000	0.000	0.001	0.001	0 000	0 001
Fe2+	0 172	0.172	0 162	0 169	0.171	0 160	0 162	0 168	0 166	0.171	0 200	0.172	0 161	0 172	0 173
Mn	0.000	0 004	0.000	0 000	0 000	0 001	0 003	0 003	0.003	0.000	0 001	0.000	0 000	0 004	0 004
Ni	0 012	0 008	0 009	0 009	0 009	0 010	0 009	0.003	0 006	0 009	0 006	0 007	0.008	0 006	0 010
Mg	1.799	1 802	1 825	1 817	1 809	1 818	1 821	1 819	1 811	1 813	1 771	1 799	1 816	1 800	1 806
Ca	0 000	0.000	0 000	0 000	0.000	0 000	0 000	0 000	0 000	0 000	0 000	0 000	0 000	0 000	0 000
Na	0 002	0 001	0 000	0 000	0 000	0 000	0 000	0 001	0 001	0 000	0 000	0 000	0 000	0 002	0 001
K	0 000	0 000	0 000	0 000	0 000	0 000	0 000	0 000	0 000	0 000	0 000	0 000	0 000	0 000	0 000
Total	2 993	2 994	2 999	2 998	2 995	2 995	2 998	2 997	2 993	2 997	2 989	2 990	2 993	2 993	2 998
Mg#	91 3	91 3	91 8	91 5	91 4	91 9	91 9	91 6	91 6	91 4	89 9	91 3	91 9	91 3	91 3

Rock	D	D	D	D	D	D	D	D	D	D	D	AD	AD	AD	AD
Sample	L162	L193	L199	L216	L216	L217	L246	L254	L262	L262	L262	L125	L125	L129	L129
Location	5-Ol	1-Ol	5-Ol	1-Ol	5-Ol	1-Ol	2-Ol	1-Ol	1-Ol	2-Ol	3-Ol	1-Ol	1-Ol	2-Ol	5-Ol
Type	LALPP	LALPP	LALPP	LALPP	LALPP	LALPP	LALPP	LALPP	LALPP	LALPP	LALPP	LALPP	LALPP	LALPP	LALPP
SiO2	40.47	40.90	40.74	40.30	40.63	41.28	40.94	41.19	41.10	41.14	41.17	40.66	40.77	40.88	40.57
TiO2	0.00	0.01	0.00	0.00	0.00	0.02	0.00	0.03	0.00	0.00	0.00	0.00	0.00	0.00	0.00
Al2O3	0.02	0.03	0.00	0.02	0.03	0.00	0.00	0.01	0.02	0.02	0.03	0.00	0.00	0.04	0.03
Cr2O3	0.00	0.00	0.00	0.00	0.00	0.05	0.00	0.06	0.00	0.00	0.00	0.16	0.00	0.00	0.00
FeO	8.64	8.38	8.06	9.39	9.26	8.45	8.43	9.20	8.46	8.35	8.32	8.55	8.56	8.38	8.45
MnO	0.00	0.00	0.05	0.03	0.05	0.21	0.11	0.18	0.02	0.01	0.02	0.05	0.13	0.03	0.00
NiO	0.29	0.48	0.53	0.49	0.48	0.41	0.29	0.49	0.38	0.36	0.44	0.22	0.40	0.47	0.47
MgO	49.72	49.31	50.34	49.56	49.33	50.01	49.41	48.94	50.15	50.19	50.29	50.17	49.42	49.90	49.93
CaO	0.00	0.00	0.00	0.00	0.00	0.00	0.00	0.00	0.00	0.00	0.00	0.00	0.00	0.00	0.00
Na2O	0.00	0.00	0.00	0.01	0.01	0.02	0.02	0.05	0.00	0.00	0.00	0.00	0.00	0.00	0.00
K2O	0.00	0.00	0.00	0.00	0.00	0.00	0.00	0.00	0.00	0.00	0.00	0.00	0.00	0.00	0.00
Total	99.13	99.11	99.70	99.80	99.77	100.45	99.20	100.15	100.13	100.06	100.26	99.81	99.28	99.69	99.45
Si	0.996	1.005	0.995	0.990	0.997	1.002	1.005	1.006	1.000	1.001	1.000	0.994	1.002	0.999	0.995
Ti	0.000	0.000	0.000	0.000	0.000	0.000	0.000	0.001	0.000	0.000	0.000	0.000	0.000	0.000	0.000
Al	0.000	0.001	0.000	0.001	0.001	0.000	0.000	0.000	0.001	0.001	0.001	0.000	0.000	0.001	0.001
Cr	0.000	0.000	0.000	0.000	0.000	0.001	0.000	0.001	0.000	0.000	0.000	0.003	0.000	0.000	0.000
Fe2+	0.178	0.172	0.165	0.193	0.190	0.172	0.173	0.188	0.172	0.170	0.169	0.175	0.176	0.171	0.173
Mn	0.000	0.000	0.001	0.001	0.001	0.004	0.002	0.004	0.000	0.000	0.000	0.001	0.003	0.001	0.000
Ni	0.006	0.009	0.010	0.010	0.009	0.008	0.006	0.010	0.007	0.007	0.009	0.004	0.008	0.009	0.009
Mg	1.824	1.806	1.833	1.815	1.805	1.810	1.808	1.782	1.819	1.820	1.821	1.828	1.810	1.819	1.826
Ca	0.000	0.000	0.000	0.000	0.000	0.000	0.000	0.000	0.000	0.000	0.000	0.000	0.000	0.000	0.000
Na	0.000	0.000	0.000	0.000	0.000	0.001	0.001	0.002	0.000	0.000	0.000	0.000	0.000	0.000	0.000
K	0.000	0.000	0.000	0.000	0.000	0.000	0.000	0.000	0.000	0.000	0.000	0.000	0.000	0.000	0.000
Total	3.004	2.994	3.005	3.010	3.003	2.998	2.995	2.994	3.000	2.999	3.000	3.005	2.998	3.000	3.004
Mg#	91.1	91.3	91.8	90.4	90.5	91.3	91.3	90.5	91.4	91.5	91.5	91.3	91.1	91.4	91.3

Rock	AD	AD	AD	AD	AD	AD	AD	AD	AD	AD	AD	Ol	Ol	Ol	Ol
Sample	L132	L140	L140	L148	L148	L148	L172	L172	L275	L336	L336	L068	L073	L073	L153
Location	2-Ol	1-Ol	4-Ol	6-Ol	7-Ol	8-Ol	2-Ol-1	2-Ol-2	2-Ol	2-Ol	3-Ol	5-Ol	1-Ol	2-Ol-B	4-Ol
Type	LALPP	LALPP	LALPP	LALPP	LALPP	LALPP	LALPP	LALPP	LALPP	LALPP	LALPP	LALPP	LALPP	LALPP	LALPP
SiO2	40.83	40.45	40.45	40.58	40.60	41.25	40.76	40.70	40.39	41.20	41.33	40.37	41.38	40.32	41.03
TiO2	0.02	0.00	0.00	0.00	0.00	0.00	0.00	0.00	0.00	0.00	0.00	0.00	0.02	0.00	0.00
Al2O3	0.00	0.02	0.01	0.03	0.02	0.03	0.03	0.04	0.02	0.02	0.03	0.01	0.01	0.00	0.01
Cr2O3	0.01	0.03	0.00	0.00	0.00	0.02	0.00	0.00	0.02	0.00	0.00	0.00	0.33	0.05	0.00
FeO	8.69	8.41	8.47	8.52	8.78	8.77	8.54	8.24	9.77	8.17	8.24	9.93	7.15	9.15	8.10
MnO	0.16	0.00	0.00	0.05	0.03	0.06	0.02	0.04	0.06	0.01	0.04	0.02	0.14	0.22	0.00
NiO	0.08	0.30	0.32	0.37	0.32	0.36	0.49	0.47	0.25	0.39	0.38	0.49	0.25	0.34	0.54
MgO	50.18	49.65	49.96	49.39	49.06	49.07	50.25	50.32	49.18	49.70	50.00	48.94	50.69	49.69	49.87
CaO	0.00	0.00	0.00	0.00	0.00	0.00	0.00	0.00	0.00	0.00	0.00	0.00	0.00	0.00	0.00
Na2O	0.02	0.00	0.00	0.01	0.01	0.01	0.00	0.00	0.03	0.00	0.00	0.00	0.00	0.02	0.00
K2O	0.00	0.00	0.00	0.00	0.00	0.00	0.00	0.00	0.00	0.00	0.00	0.00	0.00	0.00	0.00
Total	99.98	98.86	99.21	98.90	98.83	99.57	100.08	99.81	99.70	99.47	100.00	99.74	99.97	99.79	99.55
Si	0.998	0.997	0.994	1.000	1.002	1.010	0.994	0.994	0.994	1.007	1.005	0.994	1.001	0.990	1.003
Ti	0.000	0.000	0.000	0.000	0.000	0.000	0.000	0.000	0.000	0.000	0.000	0.000	0.000	0.000	0.000
Al	0.000	0.000	0.000	0.001	0.000	0.001	0.001	0.001	0.000	0.000	0.001	0.000	0.000	0.000	0.000
Cr	0.000	0.001	0.000	0.000	0.000	0.000	0.000	0.000	0.000	0.000	0.000	0.000	0.006	0.001	0.000
Fe2+	0.177	0.173	0.174	0.176	0.181	0.180	0.174	0.168	0.201	0.167	0.168	0.205	0.145	0.188	0.166
Mn	0.003	0.000	0.000	0.001	0.001	0.001	0.000	0.001	0.001	0.000	0.001	0.000	0.003	0.005	0.000
Ni	0.002	0.006	0.006	0.007	0.006	0.007	0.010	0.009	0.005	0.008	0.007	0.010	0.005	0.007	0.011
Mg	1.825	1.825	1.831	1.815	1.806	1.791	1.827	1.832	1.804	1.811	1.813	1.797	1.829	1.819	1.817
Ca	0.000	0.000	0.000	0.000	0.000	0.000	0.000	0.000	0.000	0.000	0.000	0.000	0.000	0.000	0.000
Na	0.001	0.000	0.000	0.000	0.001	0.000	0.000	0.000	0.001	0.000	0.000	0.000	0.000	0.001	0.000
K	0.000	0.000	0.000	0.000	0.000	0.000	0.000	0.000	0.000	0.000	0.000	0.000	0.000	0.000	0.000
Total	3.004	3.002	3.006	3.000	2.998	2.990	3.006	3.005	3.007	2.993	2.994	3.006	2.989	3.010	2.997
Mg#	91.1	91.3	91.3	91.2	90.9	90.9	91.3	91.6	90.0	91.6	91.5	89.8	92.7	90.6	91.6

Rock	OI	OI	OI	OI	OII	OII	OII	C	C	C	C	C	WB	WB	WB
Sample	L153	L153	L268	L286	L271	L271	L351	L004	L199	L213	L213	L231	L069	L283	L283
Location	5–OI	8–OI	2–OI	1–OI	1–OI	1–OI	3–OI	4–OI	2–OI	1–OI	2–OI	3–OI	1–OI	1–OI	1–OI
Type	LALPP	LALPP	LALPP	LALPP	LALPP	LALPP	LALPP	LALPP	LALPP	LALPP	LALPP	LALPP	LALPP	LALPP	LALPP
SiO2	41.41	40.73	40.77	41.00	41.37	41.29	41.34	40.11	40.32	40.86	40.71	40.98	41.43	40.59	40.74
TiO2	0.00	0.00	0.00	0.00	0.00	0.00	0.02	0.00	0.00	0.03	0.00	0.00	0.03	0.00	0.00
Al2O3	0.04	0.01	0.00	0.01	0.03	0.04	0.01	0.03	0.02	0.01	0.02	0.04	0.00	0.01	0.02
Cr2O3	0.00	0.00	0.00	0.02	0.01	0.01	0.00	0.01	0.00	0.05	0.06	0.00	0.02	0.00	0.00
FeO	7.98	8.24	10.05	8.90	8.11	8.44	8.91	10.68	10.85	11.25	11.24	10.19	9.33	10.21	10.31
MnO	0.05	0.00	0.03	0.02	0.07	0.09	0.12	0.06	0.00	0.21	0.27	0.06	0.13	0.07	0.04
NiO	0.47	0.44	0.42	0.45	0.48	0.41	0.60	0.49	0.53	0.73	0.43	0.60	0.33	0.40	0.44
MgO	50.38	49.71	48.60	49.69	50.13	50.12	49.14	48.27	48.37	48.06	47.62	48.74	49.70	48.36	48.38
CaO	0.00	0.00	0.00	0.00	0.00	0.00	0.00	0.00	0.00	0.00	0.00	0.00	0.00	0.00	0.00
Na2O	0.01	0.00	0.00	0.00	0.01	0.00	0.04	0.01	0.01	0.05	0.05	0.00	0.00	0.00	0.00
K2O	0.00	0.00	0.00	0.00	0.00	0.00	0.00	0.00	0.00	0.00	0.00	0.00	0.00	0.00	0.00
Total	100.33	99.12	99.86	100.07	100.21	100.40	100.15	99.64	100.09	101.23	100.40	100.61	100.96	99.64	99.91
Si	1.003	1.001	1.002	1.000	1.004	1.002	1.008	0.993	0.994	0.998	1.002	1.001	1.003	1.001	1.002
Ti	0.000	0.000	0.000	0.000	0.000	0.000	0.000	0.000	0.000	0.000	0.000	0.000	0.001	0.000	0.000
Al	0.001	0.000	0.000	0.000	0.001	0.001	0.000	0.001	0.001	0.000	0.001	0.001	0.000	0.000	0.001
Cr	0.000	0.000	0.000	0.000	0.000	0.000	0.000	0.000	0.000	0.001	0.001	0.000	0.000	0.000	0.000
Fe2+	0.162	0.169	0.207	0.182	0.165	0.171	0.182	0.221	0.224	0.230	0.231	0.208	0.189	0.210	0.212
Mn	0.001	0.000	0.001	0.000	0.001	0.002	0.002	0.001	0.000	0.004	0.006	0.001	0.003	0.001	0.001
Ni	0.009	0.009	0.008	0.009	0.009	0.008	0.012	0.010	0.010	0.014	0.009	0.012	0.006	0.008	0.009
Mg	1.820	1.821	1.781	1.808	1.814	1.813	1.787	1.781	1.777	1.751	1.747	1.775	1.794	1.778	1.774
Ca	0.000	0.000	0.000	0.000	0.000	0.000	0.000	0.000	0.000	0.000	0.000	0.000	0.000	0.000	0.000
Na	0.000	0.000	0.000	0.000	0.000	0.000	0.002	0.000	0.000	0.002	0.002	0.000	0.000	0.000	0.000
K	0.000	0.000	0.000	0.000	0.000	0.000	0.000	0.000	0.000	0.000	0.000	0.000	0.000	0.000	0.000
Total	2.996	2.999	2.998	2.999	2.995	2.997	2.992	3.007	3.006	3.002	2.998	2.998	2.996	2.999	2.998
Mg#	91.8	91.5	89.6	90.9	91.7	91.4	90.8	89.0	88.8	88.4	88.3	89.5	90.5	89.4	89.3

Rock	WB	W	W	D	D	D	D	D	D	D	D	D	D	D
Sample	L288	L201	L201	L229	L229	L229	L298	L299	L299	L299	L299	L302	L302	L305
Location	1-Ol	2-Ol	3-Ol	1-Ol	2-Ol	3-Ol	3-Ol	1-Ol	2-Ol	3-Ol-1	3-Ol-2	2-Ol	3-Ol	1-Ol
Type	LALPP	LALPP	LALPP	HALPPG	HALPPG	HALPPG	HALPPG	HALPPG	HALPPG	HALPPG	HALPPG	HALPPG	HALPPG	HALPPG
SiO2	39.77	41.30	41.21	40.41	40.82	41.09	41.11	40.95	40.88	40.84	40.73	40.70	40.97	40.92
TiO2	0.00	0.00	0.00	0.00	0.01	0.00	0.00	0.00	0.00	0.00	0.02	0.00	0.00	0.01
Al2O3	0.01	0.00	0.01	0.02	0.02	0.02	0.02	0.05	0.02	0.03	0.02	0.00	0.03	0.05
Cr2O3	0.00	0.00	0.00	0.00	0.00	0.00	0.00	0.00	0.00	0.00	0.01	0.00	0.14	0.00
FeO	13.55	8.39	8.19	10.73	10.38	10.46	10.50	10.65	10.63	10.12	10.42	10.47	10.02	10.67
MnO	0.12	0.12	0.12	0.05	0.02	0.01	0.08	0.04	0.07	0.08	0.07	0.07	0.03	0.08
NiO	0.44	0.54	0.18	0.32	0.32	0.30	0.33	0.36	0.33	0.37	0.36	0.35	0.29	0.40
MgO	45.51	49.88	50.05	47.95	48.55	48.11	48.27	47.77	47.63	48.23	47.98	48.01	48.31	47.63
CaO	0.00	0.01	0.00	0.01	0.00	0.01	0.10	0.17	0.19	0.15	0.19	0.03	0.00	0.00
Na2O	0.00	0.01	0.00	0.00	0.00	0.00	0.01	0.01	0.02	0.00	0.01	0.00	0.00	0.01
K2O	0.00	0.00	0.00	0.00	0.00	0.00	0.00	0.00	0.00	0.00	0.00	0.00	0.00	0.00
Total	99.40	100.23	99.75	99.49	100.12	100.01	100.42	100.01	99.76	99.83	99.81	99.63	99.76	99.75
Si	0.999	1.004	1.004	1.000	1.002	1.009	1.008	1.007	1.008	1.005	1.004	1.004	1.007	1.009
Ti	0.000	0.000	0.000	0.000	0.000	0.000	0.000	0.000	0.000	0.000	0.000	0.000	0.000	0.000
Al	0.000	0.000	0.000	0.000	0.001	0.000	0.001	0.001	0.001	0.001	0.001	0.000	0.001	0.001
Cr	0.000	0.000	0.000	0.000	0.000	0.000	0.000	0.000	0.000	0.000	0.000	0.000	0.003	0.000
Fe2+	0.285	0.171	0.167	0.222	0.213	0.215	0.215	0.219	0.219	0.208	0.215	0.216	0.206	0.220
Mn	0.003	0.002	0.002	0.001	0.000	0.000	0.002	0.001	0.001	0.002	0.001	0.001	0.001	0.002
Ni	0.009	0.011	0.004	0.006	0.006	0.006	0.006	0.007	0.006	0.007	0.007	0.007	0.006	0.008
Mg	1.705	1.808	1.818	1.769	1.776	1.761	1.761	1.752	1.751	1.768	1.762	1.766	1.770	1.751
Ca	0.000	0.000	0.000	0.000	0.000	0.000	0.003	0.005	0.005	0.004	0.005	0.001	0.000	0.000
Na	0.000	0.000	0.000	0.000	0.000	0.000	0.000	0.000	0.001	0.000	0.000	0.000	0.000	0.000
K	0.000	0.000	0.000	0.000	0.000	0.000	0.000	0.000	0.000	0.000	0.000	0.000	0.000	0.000
Total	3.001	2.996	2.996	3.000	2.998	2.991	2.994	2.992	2.992	2.995	2.996	2.996	2.992	2.991
Mg#	85.7	91.4	91.6	88.8	89.3	89.1	89.1	88.9	88.9	89.5	89.1	89.1	89.6	88.8

Rock	D	W	W	W	W	W	W	C	C	C	C	WG	WG	WG	WG
Sample	L350	L109	L114	L301	L301	L316	L317	L296	L303	L310	L315	L309A	L309A	L309A	L309B
Location	1-Ol	2-Ol	1-Ol	1-Ol	5-Ol	1-Ol	1-Ol	3-Ol	2-Ol	2-Ol	3-Ol	1-Ol	3-Ol	5-Ol	2-Ol
Type	HALPPG	HALPPG	HALPPG	HALPPG	HALPPG	HALPPG	HALPPG	HALPPG	HALPPG	HALPPG	HALPPG	HALPPG	HALPPG	HALPPG	HALPPG
SiO2	41.12	40.54	40.32	40.23	40.22	40.75	40.72	39.43	39.31	40.05	39.52	40.50	40.10	40.28	40.57
TiO2	0.04	0.03	0.02	0.03	0.02	0.00	0.01	0.00	0.04	0.02	0.03	0.00	0.01	0.00	0.02
Al2O3	0.00	0.00	0.00	0.01	0.00	0.00	0.03	0.01	0.00	0.00	0.00	0.03	0.03	0.01	0.03
Cr2O3	0.01	0.01	0.02	0.00	0.00	0.03	0.01	0.00	0.00	0.01	0.02	0.01	0.00	0.00	0.01
FeO	9.37	11.20	11.73	12.32	12.18	10.58	11.65	15.92	17.96	12.92	15.81	12.40	12.28	11.71	11.94
MnO	0.19	0.19	0.20	0.21	0.22	0.20	0.06	0.09	0.33	0.17	0.29	0.09	0.09	0.12	0.10
NiO	0.33	0.38	0.12	0.17	0.24	0.24	0.40	0.31	0.21	0.38	0.10	0.35	0.35	0.29	0.37
MgO	49.53	48.06	47.27	47.47	48.01	47.93	47.83	44.19	40.84	45.51	44.41	47.39	47.75	47.94	47.84
CaO	0.16	0.00	0.01	0.00	0.00	0.00	0.00	0.00	0.00	0.00	0.00	0.00	0.00	0.00	0.00
Na2O	0.02	0.04	0.03	0.03	0.02	0.07	0.01	0.01	0.03	0.04	0.05	0.02	0.01	0.02	0.00
K2O	0.00	0.00	0.00	0.00	0.00	0.00	0.00	0.00	0.00	0.00	0.00	0.00	0.00	0.00	0.00
Total	100.74	100.42	99.70	100.45	100.90	99.80	100.71	99.95	98.72	99.10	100.20	100.79	100.61	100.38	100.86
Si	0.999	0.997	1.000	0.994	0.989	1.005	1.000	0.996	1.014	1.006	0.995	0.997	0.990	0.993	0.996
Ti	0.001	0.000	0.000	0.001	0.000	0.000	0.000	0.000	0.001	0.000	0.000	0.000	0.000	0.000	0.000
Al	0.000	0.000	0.000	0.000	0.000	0.000	0.001	0.000	0.000	0.000	0.000	0.001	0.001	0.000	0.001
Cr	0.000	0.000	0.000	0.000	0.000	0.001	0.000	0.000	0.000	0.000	0.000	0.000	0.000	0.000	0.000
Fe2+	0.190	0.230	0.243	0.254	0.251	0.218	0.239	0.336	0.387	0.271	0.333	0.255	0.253	0.242	0.245
Mn	0.004	0.004	0.004	0.004	0.005	0.004	0.001	0.002	0.007	0.004	0.006	0.002	0.002	0.003	0.002
Ni	0.006	0.007	0.002	0.003	0.005	0.005	0.008	0.006	0.004	0.008	0.002	0.007	0.007	0.006	0.007
Mg	1.794	1.762	1.748	1.748	1.760	1.761	1.750	1.664	1.571	1.704	1.667	1.739	1.757	1.762	1.751
Ca	0.004	0.000	0.000	0.000	0.000	0.000	0.000	0.000	0.000	0.000	0.000	0.000	0.000	0.000	0.000
Na	0.001	0.002	0.001	0.001	0.001	0.003	0.000	0.000	0.002	0.002	0.002	0.001	0.000	0.001	0.000
K	0.000	0.000	0.000	0.000	0.000	0.000	0.000	0.000	0.000	0.000	0.000	0.000	0.000	0.000	0.000
Total	3.000	3.003	3.000	3.006	3.011	2.997	3.000	3.004	2.986	2.995	3.006	3.003	3.010	3.007	3.003
Mg#	90.4	88.4	87.8	87.3	87.5	89.0	88.0	83.2	80.2	86.3	83.4	87.2	87.4	87.9	87.7

Rock	WG	WG	WG	WG	WG	WG	G	G	G	H	H	H	D	H
Sample	L309C	L309C	L309C	L309C	L314	L314	L294	L295	L295	L177	L177	L177	L221	L221
Location	2-Ol	4-Ol	5-Ol	7-Ol	2-Ol	3-Ol	1-Ol	3-Ol	6-Ol	2-Ol	2-Ol	7-Ol	3-Ol	5-Ol
Type	HALPPG	HALPPG	HALPPG	HALPPG	HALPPG	HALPPG	HALPPG	HALPPG	HALPPG	LALPP	LALPP	LALPP	HALPPG	LALPP
SiO2	39.76	40.20	40.78	40.31	40.54	39.80	39.27	39.75	40.00	40.60	40.42	40.34	40.28	40.44
TiO2	0.00	0.00	0.00	0.00	0.00	0.00	0.00	0.00	0.00	0.00	0.00	0.00	0.00	0.00
Al2O3	0.04	0.04	0.03	0.04	0.02	0.04	0.05	0.03	0.00	0.02	0.01	0.00	0.02	0.02
Cr2O3	0.01	0.00	0.02	0.00	0.01	0.01	0.04	0.00	0.01	0.00	0.00	0.00	0.00	0.00
FeO	12.67	11.74	11.59	12.29	11.94	13.77	16.14	15.82	14.47	10.38	10.68	11.13	12.16	11.36
MnO	0.13	0.02	0.08	0.11	0.11	0.13	0.14	0.13	0.04	0.04	0.01	0.10	0.04	0.00
NiO	0.35	0.30	0.32	0.32	0.33	0.32	0.32	0.28	0.29	0.54	0.45	0.32	0.31	0.29
MgO	47.35	47.62	47.77	47.20	47.24	45.93	44.00	43.23	45.00	48.50	48.48	48.24	46.63	47.69
CaO	0.00	0.00	0.00	0.00	0.00	0.00	0.00	0.00	0.00	0.00	0.00	0.00	0.00	0.02
Na2O	0.02	0.02	0.00	0.02	0.02	0.00	0.03	0.00	0.00	0.00	0.00	0.02	0.00	0.00
K2O	0.00	0.00	0.00	0.00	0.00	0.00	0.00	0.00	0.00	0.00	0.00	0.00	0.00	0.00
Total	100.35	99.94	100.59	100.28	100.20	100.00	99.98	99.24	99.81	100.07	100.05	100.13	99.45	99.81
Si	0.987	0.995	1.002	0.997	1.002	0.995	0.993	1.009	1.003	0.998	0.995	0.995	1.003	1.000
Ti	0.000	0.000	0.000	0.000	0.000	0.000	0.000	0.000	0.000	0.000	0.000	0.000	0.000	0.000
Al	0.001	0.001	0.001	0.001	0.001	0.001	0.001	0.001	0.000	0.000	0.000	0.000	0.001	0.000
Cr	0.000	0.000	0.000	0.000	0.000	0.000	0.001	0.000	0.000	0.000	0.000	0.000	0.000	0.000
Fe2+	0.263	0.243	0.238	0.254	0.247	0.288	0.341	0.336	0.304	0.213	0.220	0.229	0.253	0.235
Mn	0.003	0.000	0.002	0.002	0.002	0.003	0.003	0.003	0.001	0.001	0.000	0.002	0.001	0.000
Ni	0.007	0.006	0.006	0.006	0.006	0.006	0.007	0.006	0.006	0.011	0.009	0.006	0.006	0.006
Mg	1.751	1.758	1.749	1.741	1.740	1.711	1.659	1.636	1.683	1.778	1.780	1.773	1.732	1.758
Ca	0.000	0.000	0.000	0.000	0.000	0.000	0.000	0.000	0.000	0.000	0.000	0.000	0.000	0.001
Na	0.001	0.001	0.000	0.001	0.001	0.000	0.001	0.000	0.000	0.000	0.000	0.001	0.000	0.000
K	0.000	0.000	0.000	0.000	0.000	0.000	0.000	0.000	0.000	0.000	0.000	0.000	0.000	0.000
Total	3.013	3.005	2.998	3.003	2.998	3.005	3.006	2.990	2.997	3.001	3.004	3.006	2.996	3.000
Mg#	86.9	87.9	88.0	87.3	87.6	85.6	82.9	83.0	84.7	89.3	89.0	88.5	87.2	88.2

Rock	H	H	H	AP	AP	Ol	H-X	H-X	H-X	H-X	H-X	H-X	H-X	C	D-X
Sample	L221	L221	L221	L274	L274	L274	L327	L327	L327	L327	L327	L328	L328	L328	L329
Location	6-Ol	8-Ol	10-Ol	2-Ol	3-Ol	4-Ol	1-Ol	2-Ol	3-Ol	3-Ol	3-Ol	2-Ol	4-Ol	7-Ol	1-Ol
Type	LALPP	LALPP	LALPP	HALPPG	HALPPG	LALPP	LALPP	LALPP	LALPP	LALPP	LALPP	LALPP	LALPP	HALPPG	LALPP
SiO2	40.40	40.59	40.62	39.28	39.38	40.32	40.50	40.72	40.58	40.19	41.07	40.06	40.16	39.77	40.25
TiO2	0.01	0.00	0.00	0.03	0.03	0.03	0.00	0.00	0.00	0.00	0.00	0.00	0.00	0.00	0.01
Al2O3	0.00	0.01	0.00	0.00	0.00	0.01	0.03	0.03	0.01	0.03	0.00	0.02	0.02	0.03	0.03
Cr2O3	0.00	0.00	0.00	0.04	0.03	0.02	0.01	0.00	0.01	0.00	0.01	0.00	0.00	0.00	0.00
FeO	11.37	9.55	9.97	17.80	17.98	12.55	13.52	11.91	10.34	10.07	9.82	13.72	13.91	15.31	13.54
MnO	0.08	0.01	0.05	0.33	0.34	0.25	0.07	0.06	0.01	0.03	0.03	0.05	0.11	0.08	0.11
NiO	0.38	0.45	0.44	0.12	0.25	0.27	0.34	0.46	0.49	0.30	0.48	0.34	0.38	0.36	0.32
MgO	47.65	49.10	49.17	42.17	41.86	46.67	46.26	47.27	48.64	48.01	49.15	46.04	45.36	43.98	45.63
CaO	0.00	0.00	0.00	0.01	0.00	0.00	0.00	0.00	0.00	0.00	0.00	0.00	0.00	0.00	0.00
Na2O	0.00	0.00	0.01	0.05	0.02	0.02	0.00	0.00	0.01	0.00	0.00	0.00	0.01	0.00	0.00
K2O	0.00	0.00	0.00	0.00	0.00	0.00	0.00	0.00	0.00	0.00	0.00	0.00	0.00	0.00	0.00
Total	99.88	99.71	100.25	99.83	99.89	100.12	100.73	100.45	100.08	98.65	100.56	100.22	99.94	99.52	99.87
Si	0.999	0.998	0.995	1.002	1.005	1.000	1.002	1.003	0.997	1.000	1.001	0.998	1.004	1.005	1.005
Ti	0.000	0.000	0.000	0.000	0.001	0.000	0.000	0.000	0.000	0.000	0.000	0.000	0.000	0.000	0.000
Al	0.000	0.000	0.000	0.000	0.000	0.000	0.001	0.001	0.000	0.001	0.000	0.000	0.001	0.001	0.001
Cr	0.000	0.000	0.000	0.001	0.001	0.000	0.000	0.000	0.000	0.000	0.000	0.000	0.000	0.000	0.000
Fe2+	0.235	0.196	0.204	0.380	0.384	0.260	0.280	0.245	0.212	0.210	0.200	0.286	0.291	0.324	0.283
Mn	0.002	0.000	0.001	0.007	0.007	0.005	0.002	0.001	0.000	0.001	0.001	0.001	0.002	0.001	0.002
Ni	0.008	0.009	0.009	0.002	0.005	0.005	0.007	0.009	0.010	0.006	0.009	0.007	0.008	0.007	0.006
Mg	1.757	1.799	1.796	1.603	1.592	1.726	1.706	1.736	1.782	1.781	1.787	1.710	1.690	1.657	1.698
Ca	0.000	0.000	0.000	0.000	0.000	0.000	0.000	0.000	0.000	0.000	0.000	0.000	0.000	0.000	0.000
Na	0.000	0.000	0.000	0.002	0.001	0.001	0.000	0.000	0.000	0.000	0.000	0.000	0.000	0.000	0.000
K	0.000	0.000	0.000	0.000	0.000	0.000	0.000	0.000	0.000	0.000	0.000	0.000	0.000	0.000	0.000
Total	3.001	3.002	3.005	2.999	2.995	2.999	2.997	2.996	3.003	2.999	2.998	3.002	2.996	2.995	2.995
Mg#	88.2	90.2	89.8	80.9	80.6	86.9	85.9	87.6	89.3	89.5	89.9	85.7	85.3	83.7	85.7

Rock	C	W	Ol	Ol	C	C	C
Sample	L329	L333	L333	L333	L348	L234	L236
Location	3-Ol	1-Ol	6-Ol	9-Ol	3-Ol	1-Ol	1-Ol
Type	HALPPG	HALPPG	LALPP	LALPP	HALPPG		
SiO2	39 91	40 14	40.76	40.88	41.07	40 62	40 52
TiO2	0 00	0 02	0 04	0 04	0 04	0 04	0 01
Al2O3	0.02	0 01	0 01	0 00	0.00	0 00	0 02
Cr2O3	0 00	0.05	0 00	0.07	0 07	0.10	0.00
FeO	14 27	12 33	10 40	10.37	12 08	10 10	10 25
MnO	0 07	0 27	0 24	0.19	0.19	0 23	0 05
NiO	0 32	0 15	0 34	0 29	0 43	0.45	0 42
MgO	45 48	46 99	48 67	49 12	47.31	48 43	48 34
CaO	0 00	0 00	0 00	0 00	0.00	0 00	0 00
Na2O	0 00	0 06	0 07	0.04	0 05	0 03	0 00
K2O	0 00	0 00	0 00	0 00	0.00	0.00	0 00
Total	100 06	100 02	100 51	101.00	101 24	100 00	99 61
Si	0 998	0 996	0 998	0 996	1.005	0 999	1 000
Ti	0 000	0 000	0 001	0 001	0 001	0.001	0 000
Al	0 001	0 000	0 000	0 000	0 000	0 000	0 001
Cr	0 000	0 001	0 000	0 001	0 001	0 002	0 000
Fe2+	0 298	0 256	0 213	0 211	0 247	0 208	0 212
Mn	0 001	0 006	0 005	0 004	0 004	0 005	0 001
Ni	0 006	0 003	0 007	0 006	0 008	0 009	0 008
Mg	1 696	1 739	1 776	1 783	1 726	1 776	1 778
Ca	0 000	0 000	0 000	0 000	0 000	0 000	0 000
Na	0 000	0 003	0 003	0 002	0.002	0 001	0 000
K	0 000	0 000	0 000	0 000	0 000	0 000	0 000
Total	3 001	3 004	3 003	3 004	2 995	3 000	3 000
Mg#	85 0	87 2	89 3	89 4	87 5	89 5	89 4

TABLE A3 2 Orthopyroxene analyses (oxides in wt %, number of ions on basis of 6 O)

Rock	H	H	H	H	H	H	H	H	H	H	H	H	H	H	H
Sample	L106	L106	L106	L106	L106	L153	L157	L157	L157	L157	L157	L157	L193	L218	L218
Location	1-Opx	1-Opx-1	1-Opx-2	3-Opx core	3-Opx rim	1-Opx	1-Opx core	1-Opx rim	1-Opx	3-Opx	5-Opx	6-Opx	2-Opx	2-Opx core	2-Opx rim
Type	LALPP	LALPP	LALPP	LALPP	LALPP	LALPP	LALPP	LALPP	LALPP	LALPP	LALPP	LALPP	LALPP	LALPP	LALPP
SiO2	58 34	57.47	57.75	57 49	57 83	57 81	56 78	57 75	57 60	57 24	57.54	57 21	57 85	57 63	57 51
TiO2	0.00	0 00	0 03	0.01	0 02	0 00	0 00	0.06	0 01	0 04	0 03	0 03	0 00	0 02	0.02
Al2O3	0 32	0.83	0.88	0 81	0.91	0 88	1 40	0 82	1.21	1 30	1.08	1 05	0 92	0.71	0 69
Cr2O3	0 41	0.44	0.47	0.39	0 43	0 42	0.53	0.30	0 11	0 47	0.39	0 35	na	0 35	0 36
FeO	5 27	5 42	5 50	5 41	5 73	5 67	6 01	5.60	5.34	5 62	5 77	5.80	5 38	5 55	5 67
MnO	0 18	0.12	0 15	0 16	0 12	0 04	0 20	0 19	0.08	0.21	0.18	0.19	0 04	0.20	0 19
NiO	0.00	0 11	0.00	0 00	0.00	0 16	0 03	0.00	0 09	0.09	0.08	0 10	0 22	0 00	0.00
MgO	34 90	33 81	34.13	33 81	34 52	34 29	34 63	34 93	34 25	34 76	34 01	34.27	33.79	34 08	33 88
CaO	0 45	1 22	0 96	1 43	0 59	0 96	0 37	0 24	1 73	0 26	0 75	0 64	0 67	0 90	1 04
Na2O	0 02	0 02	0 02	0 03	0.02	0 00	0.02	0.03	0 00	0 02	0 03	0 02	0 00	0 02	0 03
K2O	0 00	0 00	0 00	0 00	0 00	0.00	0 00	0.00	0 00	0 00	0 00	0 00	0 00	0.00	0 00
Total	99 88	99 41	99 88	99 54	100 15	100 24	99 97	99 92	100.42	99 99	99.86	99.63	98 86	99 44	99 36
Si	2.002	1.989	1 988	1.988	1 985	1 985	1 959	1.985	1 975	1.969	1 983	1 977	2 005	1 993	1 992
Ti	0.000	0 000	0.001	0.000	0 000	0 000	0 000	0.002	0.000	0 001	0.001	0 001	0.000	0 000	0 000
Al	0 013	0 034	0.036	0.033	0 037	0 036	0 057	0 033	0.049	0 053	0.044	0 043	0.037	0 029	0 028
Cr	0 011	0 012	0.013	0 011	0.012	0.011	0.014	0.008	0.003	0 013	0.011	0.009	0.000	0 010	0 010
Fe2+	0 151	0.157	0.158	0 157	0 164	0 163	0.173	0.161	0.153	0 162	0.166	0.168	0.156	0 160	0.164
Mn	0.005	0.004	0.004	0 005	0 003	0 001	0 006	0.006	0.002	0.006	0 005	0 006	0 001	0 006	0.005
Ni	0 000	0.003	0.000	0.000	0 000	0 004	0 001	0.000	0.002	0 002	0.002	0.003	0.006	0 000	0 000
Mg	1.786	1.744	1.752	1 743	1 766	1.755	1.781	1 789	1 751	1 782	1 747	1.766	1 746	1 757	1 750
Ca	0.016	0.045	0.035	0.053	0 022	0 035	0.014	0 009	0 064	0.009	0 028	0.024	0 025	0 033	0 038
Na	0 001	0 001	0.001	0 002	0.001	0.000	0.001	0 002	0 000	0 001	0.002	0.001	0 000	0 001	0.002
K	0.000	0 000	0.000	0 000	0 000	0 000	0.000	0.000	0.000	0.000	0 000	0 000	0.000	0 000	0 000
Total	3.986	3.989	3.988	3 991	3 991	3 991	4.006	3.994	3 999	3.998	3.990	3 997	3 976	3.988	3.990
En	91 42	89.63	90.05	89.27	90 47	89 85	90 49	91.33	88 99	91 25	90 01	90 24	90 62	90 0.	89 63
Fs	7.74	8 05	8 14	8 02	8 43	8 34	8 81	8 21	7.78	8 27	8 56	8 56	8 09	8 22	8 41
Wo	0 84	2 32	1.81	2.71	1 10	1 81	0 69	0 45	3 23	0 48	1 43	1 20	1 29	1 70	1 97
Mg#	92 2	91 8	91 7	91 8	91 5	91 5	91 1	91 7	92 0	91 7	91 3	91 3	91 8	91 6	91 4
Cr#	46.2	26 1	26 5	24 6	24 1	24 0	20 3	19 7	5 7	19 6	19 5	18 1		24 9	25 8

Rock	H	H	H	H	H	H	H	H	H	H	H	H	D	D	AD
Sample	L225	L225	L225	L225	L225	L225	L225	L226	L264	L264	L336	L336	L216	L216	L129
Location	2-Opx core	2-Opx rim	6-Opx-1 core	6-Opx-1 rim	6-Opx-2 core	6-Opx-2 rim	6-Opx-2 rim	1-Opx	1-Opx core	1-Opx rim	4-Opx	5-Opx	2-Opx	4-Opx	5-Opx
Type	LALPP	LALPP	LALPP	LALPP	LALPP	LALPP	LALPP	LALPP	LALPP	LALPP	LALPP	LALPP	LALPP	LALPP	LALPP
SiO2	57.37	57.82	57.34	57.25	57.18	58.20	57.90	57.28	57.92	58.12	57.09	57.41	57.64	56.83	57.48
TiO2	0.00	0.00	0.00	0.00	0.01	0.00	0.00	0.00	0.01	0.01	0.00	0.00	0.00	0.00	0.08
Al2O3	0.82	0.49	0.85	0.85	0.82	0.76	0.46	0.84	0.77	0.45	0.90	0.85	0.73	0.60	1.35
Cr2O3	na	na	na	na	na	na	na	0.53	0.38	0.18	0.47	0.42	0.31	0.26	0.48
FeO	5.47	5.51	5.33	5.42	5.38	4.94	5.09	5.15	5.40	5.74	5.39	5.60	6.11	6.02	5.60
MnO	0.02	0.01	0.05	0.01	0.03	0.04	0.00	0.18	0.16	0.18	0.00	0.08	0.03	0.07	0.19
NiO	0.13	0.16	0.17	0.00	0.21	0.18	0.13	0.00	0.00	0.00	0.14	0.10	0.12	0.15	0.04
MgO	33.88	34.96	34.37	34.08	34.02	34.90	35.30	33.95	35.04	35.01	34.33	34.26	34.92	33.90	34.69
CaO	1.06	0.19	1.07	1.10	1.01	0.58	0.21	1.24	0.39	0.32	0.81	0.94	0.25	1.07	0.35
Na2O	0.03	0.00	0.02	0.02	0.04	0.00	0.00	0.03	0.03	0.01	0.01	0.01	0.00	0.01	0.02
K2O	0.00	0.00	0.00	0.00	0.00	0.00	0.00	0.00	0.00	0.00	0.00	0.00	0.00	0.00	0.00
Total	98.78	99.14	99.18	98.73	98.67	99.60	99.09	99.20	100.07	100.02	99.14	99.66	100.11	98.90	100.26
Si	1.995	1.999	1.986	1.991	1.991	1.999	1.999	1.985	1.986	1.995	1.980	1.983	1.982	1.983	1.971
Ti	0.000	0.000	0.000	0.000	0.000	0.000	0.000	0.000	0.000	0.000	0.000	0.000	0.000	0.000	0.002
Al	0.033	0.020	0.035	0.035	0.034	0.031	0.019	0.034	0.031	0.018	0.037	0.035	0.030	0.025	0.055
Cr	0.000	0.000	0.000	0.000	0.000	0.000	0.000	0.015	0.010	0.005	0.013	0.011	0.008	0.007	0.013
Fe2+	0.159	0.159	0.154	0.158	0.157	0.142	0.147	0.149	0.155	0.165	0.156	0.162	0.176	0.176	0.160
Mn	0.000	0.000	0.001	0.000	0.001	0.001	0.000	0.005	0.005	0.005	0.000	0.002	0.001	0.002	0.005
Ni	0.004	0.004	0.005	0.000	0.006	0.005	0.004	0.000	0.000	0.000	0.004	0.003	0.003	0.004	0.001
Mg	1.756	1.802	1.775	1.767	1.766	1.787	1.816	1.754	1.791	1.792	1.775	1.764	1.790	1.764	1.773
Ca	0.040	0.007	0.040	0.041	0.038	0.021	0.008	0.046	0.014	0.012	0.030	0.035	0.009	0.040	0.013
Na	0.002	0.000	0.001	0.001	0.002	0.000	0.000	0.002	0.002	0.001	0.000	0.000	0.000	0.000	0.001
K	0.000	0.000	0.000	0.000	0.000	0.000	0.000	0.000	0.000	0.000	0.000	0.000	0.000	0.000	0.000
Total	3.990	3.991	3.997	3.992	3.993	3.986	3.992	3.991	3.994	3.993	3.995	3.994	3.999	4.001	3.994
En	89.84	91.55	90.15	89.89	90.09	91.63	92.15	89.98	91.38	91.04	90.49	89.97	90.64	89.11	91.10
Fs	8.13	8.09	7.84	8.02	7.99	7.28	7.45	7.66	7.90	8.37	7.98	8.25	8.89	8.88	8.24
Wo	2.03	0.36	2.02	2.09	1.92	1.09	0.39	2.36	0.72	0.59	1.53	1.77	0.47	2.01	0.66
Mg#	91.7	91.9	92.0	91.8	91.9	92.6	92.5	92.2	92.0	91.6	91.9	91.6	91.1	90.9	91.7
Cr#								29.7	24.6	21.2	25.7	24.7	21.9	22.4	19.3

Rock	AD	OI	OI	OI	OI	OI	OI	OI	OI	OI	OII	OII	OII	OII	OII
Sample	L172	L068	L068	L068	L073	L073	L073	L073	L153	L268	L271	L271	L271	L271	L271
Location	1-Opx	2-Opx	6-Opx	6-Opx	2-Opx	2-Opx	2-Opx	2-Opx-A	5-Opx	2-Opx	1-Opx	1-Opx	1-Opx	1-Opx	1-Opx
		core	rim	rim	core	rim	rim				core	rim	rim	rim	
Type	LALPP	LALPP	LALPP	LALPP	LALPP	LALPP	LALPP	LALPP	LALPP	LALPP	LALPP	LALPP	LALPP	LALPP	LALPP
SiO2	58 04	57.55	57 42	58 44	58.07	57 84	58.47	57.74	57.73	57 48	58.34	56 74	56 73	58 04	58 03
TiO2	0 00	0.01	0 01	0.00	0.02	0 02	0 01	0.03	0 01	0 00	0.01	0 03	0.00	0.02	0 00
Al2O3	0 50	0 96	0.96	0 34	0 38	0 34	0 10	0.13	0 96	0 44	0 75	0 53	0 44	0 63	0 55
Cr2O3	0 20	0.34	0.33	0.10	0 28	0 31	0.09	0.14	0 41	0 19	0 12	0 12	0 11	0 12	0 08
FeO	5 52	6.62	6.75	6.79	6.02	6 14	6.30	6.05	5 64	6 45	5.42	5.84	5.57	5 86	5 52
MnO	0 06	0 00	0 04	0.05	0 18	0 23	0 21	0.15	0 06	0.00	0 12	0 11	0 10	0 05	0 09
NiO	0 18	0.12	0 11	0.08	0 04	0 00	0 13	0 00	0.15	0.14	0.19	0.16	0.16	0 13	0 17
MgO	35 25	33.71	34.02	34.38	34 27	33 99	34 92	35 20	34.43	33 84	34 85	34 79	36 33	35 27	35 02
CaO	0 30	0 48	0 40	0.21	1.10	1 32	0 26	0 30	0 97	0 38	0 52	0 29	0.03	0 30	0 22
Na2O	0 00	0 00	0.00	0 00	0 07	0 04	0 03	0 00	0 00	0 00	0.04	0 02	0 01	0 03	0 00
K2O	0.00	0.00	0 00	0.00	0.00	0 00	0.00	0 00	0 00	0.00	0 00	0 00	0 00	0 00	0 00
Total	100.05	99.79	100.03	100 39	100 40	100 22	100 50	99.74	100 35	98 92	100.34	98.63	99 48	100 42	99 68
Si	1.991	1.989	1.982	2.005	1 994	1 993	2.003	1 992	1 980	2 001	1.995	1 960	1 963	1 986	1 996
Ti	0 000	0 000	0.000	0 000	0 001	0 001	0 000	0 001	0 000	0.000	0.000	0.001	0 000	0 000	0 000
Al	0 020	0.039	0 039	0.014	0 015	0 014	0 004	0 005	0 039	0 018	0 030	0 022	0 018	0 025	0 022
Cr	0 005	0.009	0.009	0.003	0 007	0 008	0.002	0.004	0.011	0.005	0 003	0 003	0 003	0 003	0 002
Fe2+	0 158	0.191	0 195	0 195	0.173	0.177	0.180	0 175	0.162	0.188	0.155	0.170	0.161	0 168	0.159
Mn	0 002	0 000	0 001	0.001	0 005	0 007	0.006	0.004	0.002	0.000	0.003	0.003	0 003	0 001	0 003
Ni	0 005	0.003	0 003	0 002	0 001	0 000	0 004	0 000	0 004	0 004	0.005	0.004	0 004	0 003	0.005
Mg	1 803	1 737	1.750	1.759	1.754	1 746	1.784	1 810	1 761	1 756	1.776	1 810	1 874	1 799	1 796
Ca	0.011	0.018	0.015	0 008	0 040	0 049	0 009	0 011	0 036	0 014	0 019	0 011	0.001	0 011	0.008
Na	0 000	0.000	0.000	0.000	0.004	0.003	0 002	0 000	0.000	0.000	0 002	0.001	0 001	0 002	0 000
K	0 000	0.000	0 000	0.000	0.000	0.000	0 000	0 000	0 000	0 000	0 000	0 000	0.000	0 000	0 000
Total	3 996	3.987	3 994	3.987	3 996	3.997	3 994	4 003	3.994	3.987	3 989	4.007	4 027	4 000	3 991
En	91 41	89.25	89.31	89.67	89.16	88 56	90 39	90.70	89 92	89 69	91.09	90.90	92 03	90 98	91 50
Fs	8 03	9.83	9.93	9.93	8.79	8 97	9 14	8.75	8 26	9 59	7 94	8.56	7 92	8 47	8 09
Wo	0.56	0.91	0.75	0.39	2.05	2 46	0 47	0 56	1 82	0 72	0 97	0 54	0 05	0 55	0 41
Mg#	91 9	90 1	90 0	90 0	91 0	90 8	90 8	91 2	91 6	90 3	92 0	91 4	92 1	91 5	91 9
Cr#	21 2	19.2	18.7	16 5	33.0	37 6	37.6	41 9	22 3	22 5	9 3	13 2	14 4	11 4	8 9

Rock	Oll	Oll	Oll	C	C	C	C	WB	W	H	H	H	H	H
Sample	L271	L271	L351	L199	L213	L213	L213	L06	L201	L177	L177	L177	L177	L221
Location	2-Opx core	2-Opx rim	1-Opx	2-Opx	1-Opx	2-Opx	4-Opx	1-Opx	3-Opx	2-Opx	3-Opx	4-Opx	5-Opx	7-Opx core
Type	LALPP	LALPP	ALPP	LALPP	LALPP	LALPP	LALPP	LALPP	LALPP	LALPP	LALPP	LALPP	LALPP	LALPP
SiO2	57.85	58.45	58.18	56.88	57.21	57.42	57.27	58.19	57.69	56.70	57.53	57.71	57.59	56.79
TiO2	0.00	0.01	0.03	0.00	0.03	0.05	0.00	0.03	0.04	0.04	0.00	0.00	0.01	0.00
Al2O3	0.83	0.51	0.89	0.63	0.78	0.72	0.70	0.56	0.61	1.31	1.00	1.06	1.21	1.20
Cr2O3	0.19	0.10	0.21	0.28	0.28	0.35	0.31	0.22	0.32	0.41	0.42	0.44	0.50	na
FeO	5.48	5.66	6.08	7.01	7.53	7.34	7.49	5.93	5.61	6.70	6.30	6.27	6.77	6.45
MnO	0.05	0.09	0.19	0.05	0.25	0.24	0.22	0.13	0.20	0.05	0.06	0.04	0.01	0.03
NiO	0.18	0.16	0.04	0.16	0.00	0.04	0.13	0.14	0.17	0.13	0.15	0.16	0.11	0.13
MgO	34.10	34.68	34.35	33.71	32.76	33.26	33.47	34.82	34.79	32.59	34.30	33.11	33.26	32.27
CaO	0.92	0.27	0.24	0.60	0.82	0.61	0.29	0.44	0.35	1.90	0.36	1.48	1.08	1.97
Na2O	0.03	0.02	0.02	0.00	0.03	0.05	0.03	0.01	0.05	0.04	0.00	0.01	0.01	0.03
K2O	0.00	0.00	0.00	0.00	0.00	0.00	0.00	0.00	0.00	0.00	0.00	0.00	0.00	0.00
Total	99.62	99.95	100.21	99.30	99.68	100.07	99.90	100.46	99.81	99.86	100.12	100.26	100.52	98.87
Si	1.995	2.005	1.995	1.983	1.991	1.989	1.987	1.992	1.987	1.970	1.981	1.988	1.981	1.987
Ti	0.000	0.000	0.001	0.000	0.001	0.001	0.000	0.001	0.001	0.001	0.000	0.000	0.000	0.000
Al	0.034	0.021	0.036	0.026	0.032	0.029	0.029	0.023	0.025	0.054	0.041	0.043	0.049	0.049
Cr	0.005	0.003	0.006	0.008	0.008	0.009	0.009	0.006	0.009	0.011	0.011	0.012	0.013	0.000
Fe2+	0.158	0.162	0.174	0.204	0.219	0.213	0.217	0.170	0.161	0.195	0.181	0.181	0.195	0.189
Mn	0.001	0.003	0.006	0.001	0.007	0.007	0.006	0.004	0.006	0.001	0.002	0.001	0.000	0.001
Ni	0.005	0.004	0.001	0.004	0.000	0.001	0.004	0.004	0.005	0.004	0.004	0.004	0.003	0.004
Mg	1.753	1.774	1.756	1.752	1.700	1.717	1.731	1.777	1.787	1.688	1.760	1.700	1.706	1.683
Ca	0.034	0.010	0.009	0.022	0.031	0.023	0.011	0.016	0.013	0.071	0.013	0.055	0.040	0.074
Na	0.002	0.001	0.001	0.000	0.002	0.003	0.002	0.001	0.003	0.002	0.000	0.001	0.000	0.002
K	0.000	0.000	0.000	0.000	0.000	0.000	0.000	0.000	0.000	0.000	0.000	0.000	0.000	0.000
Total	3.987	3.983	3.984	4.000	3.989	3.992	3.995	3.993	3.997	3.997	3.993	3.985	3.987	3.989
En	90.13	91.14	90.57	88.55	87.19	87.95	88.36	90.53	91.11	86.42	90.04	87.85	87.91	86.50
Fs	8.12	8.34	8.99	10.32	11.24	10.89	11.09	8.65	8.23	9.97	9.28	9.33	10.04	9.70
Wo	1.75	0.52	0.45	1.13	1.57	1.16	0.55	0.82	0.66	3.61	0.68	2.82	2.05	3.80
Mg#	91.7	91.6	91.0	89.6	88.6	89.0	88.9	91.3	91.7	89.7	90.7	90.4	89.8	89.9
Cr#	13.3	11.6	13.4	23.0	19.4	24.3	22.9	20.5	25.9	17.4	22.0	21.9	21.5	

Rock	H	H	H	Ol	Ol	H-X	H-X	H-X	H-X	H-X	Ol	Ol	Ol
Sample	L221	L221	L221	L274	L274	L327	L327	L328	L328	L328	L333	L333	L348
Location	7-Opx rim	8-Opx	9-Opx	4-Opx core	4-Opx rim	3-Opx-1	3-Opx-2	1-Opx	1-Opx	5-Opx	6-Opx	7-Opx	1-Opx
Type	LALPP	LALPP	LALPP	LALPP	LALPP	LALPP	LALPP	LALPP	LALPP	LALPP	LALPP	LALPP	LALPP
SiO2	57.83	57.12	57.19	56.67	56.81	57.02	57.89	56.85	55.58	55.26	57.70	58.07	56.05
TiO2	0.00	0.00	0.00	0.05	0.05	0.01	0.00	0.09	0.22	0.11	0.08	0.06	0.07
Al2O3	0.49	0.80	0.89	0.99	0.48	0.94	0.48	2.13	2.54	1.94	0.61	0.32	2.38
Cr2O3	na	0.38	na	0.32	0.11	0.36	0.09	0.38	0.48	0.35	0.08	0.25	0.32
FeO	6.65	6.27	6.28	8.07	8.02	6.82	7.25	8.28	8.29	8.21	7.29	6.71	7.95
MnO	0.07	0.04	0.01	0.26	0.29	0.09	0.05	0.13	0.10	0.09	0.29	0.22	0.21
NiO	0.15	0.13	0.16	0.00	0.00	0.17	0.16	0.13	0.09	0.12	0.04	0.09	0.00
MgO	34.34	33.26	33.41	33.26	33.10	33.18	34.29	31.49	31.40	30.18	34.54	34.71	33.21
CaO	0.26	1.74	1.53	0.28	0.20	0.94	0.13	1.25	1.11	2.52	0.20	0.40	0.34
Na2O	0.00	0.05	0.02	0.03	0.03	0.00	0.00	0.03	0.00	0.04	0.05	0.05	0.05
K2O	0.00	0.00	0.00	0.00	0.00	0.00	0.00	0.00	0.00	0.00	0.00	0.00	0.00
Total	99.79	99.76	99.49	99.91	99.07	99.53	100.34	100.57	99.79	98.82	100.88	100.88	100.58
Si	1.997	1.982	1.986	1.972	1.991	1.983	1.994	1.963	1.943	1.958	1.980	1.989	1.938
Ti	0.000	0.000	0.000	0.001	0.001	0.000	0.000	0.002	0.006	0.003	0.002	0.002	0.002
Al	0.020	0.033	0.037	0.040	0.020	0.038	0.019	0.087	0.104	0.081	0.025	0.013	0.097
Cr	0.000	0.010	0.000	0.009	0.003	0.010	0.002	0.011	0.013	0.010	0.002	0.007	0.009
Fe2+	0.192	0.182	0.182	0.235	0.235	0.198	0.209	0.240	0.242	0.243	0.209	0.192	0.230
Mn	0.002	0.001	0.000	0.008	0.009	0.003	0.001	0.004	0.003	0.003	0.008	0.006	0.006
Ni	0.004	0.003	0.004	0.000	0.000	0.005	0.004	0.004	0.003	0.003	0.001	0.002	0.000
Mg	1.768	1.720	1.729	1.725	1.729	1.720	1.760	1.627	1.636	1.595	1.767	1.772	1.712
Ca	0.010	0.064	0.057	0.010	0.007	0.035	0.005	0.046	0.042	0.096	0.007	0.015	0.013
Na	0.000	0.003	0.001	0.002	0.002	0.000	0.000	0.002	0.000	0.003	0.003	0.003	0.003
K	0.000	0.000	0.000	0.000	0.000	0.000	0.000	0.000	0.000	0.000	0.000	0.000	0.000
Total	3.993	3.999	3.997	4.003	3.997	3.993	3.995	3.987	3.992	3.995	4.006	4.001	4.009
En	89.76	87.48	87.85	87.55	87.71	88.05	89.18	85.04	85.21	82.47	89.08	89.55	87.59
Fs	9.75	9.24	9.26	11.92	11.92	10.16	10.58	12.54	12.62	12.58	10.55	9.71	11.76
Wo	0.49	3.28	2.90	0.53	0.37	1.79	0.24	2.42	2.17	4.95	0.37	0.74	0.64
Mg#	90.2	90.4	90.5	88.0	88.0	89.7	89.4	87.2	87.1	86.8	89.4	90.2	88.2
Cr#		24.3		17.7	13.3	20.6	11.2	10.8	11.2	10.8	8.1	34.4	8.3

TABLE A3.3. Clinopyroxene analyses (oxides in wt %, number of ions on basis of 6 O)

Rock	H	D	D	D	D	D	OI	C	C	C	C	C	C	C	C
Sample	L157	L162	L216	L216	L254	L254	L073	L004	L004	L004	L213	L213	L231	L231	L231
Location	4-Cpx	1-Cpx	3-Cpx	6-Cpx	2-Cpx	3-Cpx	2-Cpx-A	1-Cpx	2-Cpx	3-Cpx	1-Cpx	3-Cpx-B	1-Cpx	3-Cpx	4-Cpx
Type	LALPP	LALPP	LALPP	LALPP	LALPP	LALPP	LALPP	LALPP	LALPP	LALPP	LALPP	LALPP	LALPP	LALPP	LALPP
SiO2	54 73	54 51	54 36	54 14	54 88	55.17	54 68	54.00	54.36	54 35	54 80	54 94	54.60	54 30	54 71
TiO2	0.03	0 00	0 00	0 02	0 07	0 07	0.02	0 01	0.03	0 00	0.06	0.02	0 01	0 01	0.02
Al2O3	0.97	0 84	0 65	0 65	0.69	0.86	0.21	0.46	0.46	0.50	0 81	0.81	0 48	0.69	0 70
Cr2O3	0.62	1 65	0 69	0 58	0.65	0 67	0.33	0.55	0.52	0.42	0.57	0.64	0.80	0.69	0 69
FeO	1 59	1 52	1 70	1 34	1.84	1.77	1.83	1.87	2 15	2 19	2.30	2.34	2 08	2 57	1 93
MnO	0 11	0 04	0 00	0.00	0 11	0.06	0 12	0.00	0.04	0.07	0.04	0.00	0.00	0.00	0.02
NiO	0 13	0 00	0.11	0 13	0.00	0 01	0.00	0 13	0.17	0 15	0 12	0 07	0 07	0.05	0.11
MgO	17 62	17 40	17 42	18 17	17.01	17.23	17 80	17 28	17 14	17 21	17.36	17.30	17.90	17 81	17 55
CaO	24 45	24 36	24 27	23 36	25 06	25.53	25.04	24 91	2 · 79	24 84	24 45	24 60	23 41	23 13	23.78
Na2O	0 15	0 39	0 25	0 30	0 32	0 23	0 23	0 24	0.28	0 22	0 22	0 21	0 17	0 31	0.28
K2O	0 00	0.00	0 00	0 00	0 00	0 02	0 00	0 00	0.00	0.00	0 00	0.00	0 00	0 00	0 00
Total	100.38	100 69	99 44	99 19	100 63	101 58	100 26	99 44	99.92	99 93	100 73	100 93	99 52	99 55	99 78
Si	1 977	1 988	1 984	1 978	1 984	1 976	1 984	1 978	1 982	1 982	1 979	1 980	1 989	1 981	1 988
Ti	0 001	0 000	0 000	0 001	0 002	0 002	0 001	0 000	0 001	0 000	0 002	0 001	0 000	0 000	0 000
Al	0 041	0.036	0 028	0 028	0 029	0 036	0 009	0 020	0 020	0 021	0 034	0 034	0 021	0 030	0 030
Cr	0 018	0 047	0 020	0 017	0 019	0 019	0 009	0 016	0 015	0 012	0 016	0 018	0 023	0 020	0 020
Fe2+	0 048	0 046	0 052	0 056	0 056	0 053	0 056	0 057	0 065	0 067	0 069	0 071	0 063	0 078	0 059
Mn	0 003	0 001	0 000	0 000	0 003	0 002	0 004	0 000	0 001	0 002	0 001	0 000	0 000	0 000	0 001
Ni	0 004	0 000	0 003	0 004	0 000	0 000	0 000	0 004	0 005	0 004	0 003	0 002	0 002	0 001	0 003
Mg	0 949	0 936	0 948	0 990	0 917	0 920	0 963	0 943	0 932	0 935	0 935	0 930	0 972	0 969	0 951
Ca	0 946	0 942	0 949	0 915	0 970	0 979	0 973	0 978	0 968	0 970	0 946	0 950	0 914	0 904	0 926
Na	0 011	0 027	0 017	0 021	0 022	0 016	0 016	0 017	0 018	0 016	0 015	0 015	0 012	0 022	0 019
K	0 000	0 000	0 000	0 000	0 000	0 000	0 000	0 000	0 000	0 000	0 000	0 000	0 000	0 000	0 000
Total	3 998	4 004	4 001	4 009	4 002	4 003	4 014	4 013	4 008	4 009	4 002	4 000	3 995	4 005	3 996
En	48 83	48 65	48 64	50 48	47 18	47 12	48 34	47 89	47 40	47 43	47 93	47 67	49 88	49 64	49 13
Fs	2 46	2 38	2 66	2 87	2 86	2 71	2 79	2 90	3 33	3 38	3 56	3 62	3 25	4 02	3 03
Wo	48 70	48 97	48 70	46 65	49 96	50 17	48 87	49 41	49 27	49 19	48 51	48 72	46 88	46 34	47 84
Mg#	95 2	95 3	94 8	94 6	94 3	94 6	94 5	94 3	93 4	93 4	93 1	92 9	93 9	92 5	94 2
Cr#	30 0	58 9	41 6	37 4	38 7	34 3	51 3	44 8	42 1	36 3	32 1	34 8	52 6	40 0	39 6

Rock	C	C	C	WB	WB	WB	WB	W	W	W	D	D	D	W
Sample	L231	L231	L231	L069	L283	L283	L283	L201	L201	L201	L302	L305	L350	L109
Location	5-Cpx	5-Cpx core	5-Cpx rim	3-Cpx	3-Cpx-1 rim	3-Cpx-2 core	3-Cpx-2 rim	3-Cpx	4-Cpx	4-Cpx	5-Cpx	2-Cpx	2-Cpx	3-Cpx core
Type	LALPP	LALPP	LALPP	LALPP	LALPP	LALPP	LALPP	LALPP	LALPP	LALPP	HALPPG	HALPPG	HALPPG	HALPPG
SiO2	54.61	54.42	54.56	54.86	55.89	55.66	55.25	54.51	55.06	54.58	52.63	52.17	50.21	49.57
TiO2	0.01	0.02	0.01	0.00	0.02	0.03	0.03	0.07	0.10	0.08	0.49	0.48	0.94	1.55
Al2O3	0.69	0.83	0.65	0.43	0.30	0.50	0.35	0.63	0.45	0.67	2.59	3.20	4.95	5.61
Cr2O3	0.63	0.65	0.62	0.63	0.58	0.42	0.55	0.60	0.52	0.89	0.34	1.24	1.37	0.96
FeO	2.10	2.20	1.93	1.87	1.69	1.94	1.68	1.80	1.61	1.67	2.05	2.07	2.24	2.69
MnO	0.00	0.00	0.00	0.00	0.00	0.00	0.10	0.08	0.08	0.19	0.00	0.07	0.08	0.18
NiO	0.11	0.12	0.08	0.00	0.01	0.00	0.07	0.01	0.01	0.08	0.09	0.00	0.00	0.00
MgO	17.31	17.48	17.47	17.21	17.44	17.64	17.61	17.45	17.66	17.53	16.28	16.54	15.41	15.52
CaO	24.22	24.01	24.44	24.56	24.32	24.54	24.36	24.93	24.41	24.81	25.91	24.00	24.27	22.82
Na2O	0.30	0.25	0.26	0.38	0.39	0.36	0.35	0.25	0.20	0.29	0.04	0.36	0.78	0.87
K2O	0.00	0.00	0.00	0.00	0.00	0.00	0.00	0.00	0.00	0.00	0.00	0.00	0.00	0.00
Total	99.98	99.98	100.00	99.94	100.64	101.09	100.34	100.33	100.10	100.79	100.41	100.10	100.24	99.76
Si	1.985	1.978	1.982	1.993	2.009	1.996	1.997	1.976	1.993	1.971	1.916	1.901	1.838	1.821
Ti	0.000	0.000	0.000	0.000	0.001	0.001	0.001	0.002	0.003	0.002	0.013	0.013	0.026	0.043
Al	0.030	0.036	0.028	0.018	0.013	0.021	0.015	0.027	0.019	0.029	0.111	0.137	0.214	0.243
Cr	0.018	0.019	0.018	0.018	0.016	0.012	0.016	0.017	0.015	0.025	0.010	0.036	0.040	0.028
Fe2+	0.064	0.067	0.059	0.057	0.051	0.058	0.051	0.055	0.049	0.050	0.062	0.063	0.069	0.083
Mn	0.000	0.000	0.000	0.000	0.000	0.000	0.003	0.002	0.002	0.006	0.000	0.002	0.002	0.006
Ni	0.003	0.004	0.002	0.000	0.000	0.000	0.002	0.000	0.000	0.002	0.003	0.000	0.000	0.000
Mg	0.938	0.947	0.946	0.932	0.935	0.943	0.949	0.943	0.953	0.944	0.884	0.898	0.841	0.850
Ca	0.943	0.935	0.951	0.956	0.937	0.943	0.943	0.968	0.947	0.960	1.010	0.937	0.952	0.898
Na	0.021	0.018	0.018	0.027	0.027	0.025	0.024	0.018	0.014	0.020	0.003	0.025	0.055	0.062
K	0.000	0.000	0.000	0.000	0.000	0.000	0.000	0.000	0.000	0.000	0.000	0.000	0.000	0.000
Total	4.002	4.003	4.004	4.002	3.989	3.999	3.999	4.009	3.994	4.010	4.012	4.012	4.037	4.032
En	48.22	48.59	48.37	47.92	48.62	48.51	48.84	47.97	48.91	48.29	45.17	47.32	45.18	46.43
Fs	3.28	3.43	3.00	2.92	2.64	2.99	2.61	2.78	2.50	2.58	3.18	3.32	3.68	4.51
Wo	48.49	47.98	48.63	49.15	48.73	48.50	48.55	49.25	48.59	49.12	51.65	49.35	51.13	49.06
Mg#	93.6	93.4	94.2	94.3	94.8	94.2	94.9	94.5	95.1	94.9	93.4	93.4	92.5	91.1
Cr#	38.0	34.4	39.0	49.6	56.5	36.0	51.3	39.0	43.7	47.1	8.1	20.7	15.6	10.3

Rock	W	W	W	W	W	W	W	C	C	C	C	C	C	C	C
Sample	L109	L301	L301	L315	L316	L317	L317	L296	L296	L296	L303	L310	L315	L349	L349
Location	3-Cpx rim	3-Cpx	4-Cpx	4-Cpx	2-Cpx	1-Cpx	2-Cpx	1-Cpx	2-Cpx	3-Cpx	1-Cpx	1-Cpx	1-Cpx	1-Cpx	2-Cpx
Type	HALPPG	HALPPG	HALPPG	HALPPG	HALPPG	HALPPG	HALPPG	HALPPG	HALPPG	HALPPG	HALPPG	HALPPG	HALPPG	HALPPG	HALPPG
SiO2	49 08	51 10	50.80	50.76	50 77	50.77	51 98	50 92	53 01	51 28	51.13	52 61	49.99	51.02	49.20
TiO2	1 73	0 80	1 02	0 94	0 61	0 80	0 66	0.68	0 25	0.82	0 57	0 28	0.88	0.77	1.00
Al2O3	6.58	4 24	4 43	5.04	5.43	5 10	3.70	6.06	2.23	4 76	4 90	1.90	5.44	5 21	7.13
Cr2O3	1.03	0 54	0 66	0 62	0 93	0 91	0.91	0.71	0.21	0.67	0.92	0.25	0 66	0 68	0.92
FeO	2.61	2 43	2 19	3.12	2.71	2 49	2.14	3.83	3.56	3 27	3.85	2.72	4.78	3.73	3 98
MnO	0.12	0 13	0.06	0.16	0.17	0 00	0.00	0.00	0 00	0.02	0.16	0.16	0.13	0.15	0.14
NiO	0.01	0 00	0.00	0.00	0.04	0 11	0.09	0.09	0 13	0 07	0.00	0 00	0.00	0 00	0.03
MgO	15 59	17 02	16.72	16.14	15 42	15.82	16 45	14 85	16 48	15 47	15 45	16 83	14 84	14 64	14 65
CaO	21 41	23 18	23 89	23 02	22 85	23 33	23.90	22 73	23 85	23 79	22 83	24 45	22.23	23.13	21 60
Na2O	1 09	0 46	0 50	0 64	0 63	0 46	0.35	0 60	0 21	0.28	0 43	0 20	0.52	0 46	0 79
K2O	0 00	0 00	0.00	0 00	0 00	0.00	0 00	0.00	0 00	0 00	0.00	0 00	0 00	0.00	0.00
Total	99 22	99 89	100 27	100.41	99 56	99 79	100.18	100 47	99 93	100.41	100.21	99.40	99.47	99.77	99.42
Si	1 805	1 866	1 851	1 850	1 861	1 857	1 891	1 854	1 939	1 869	1 869	1 934	1 848	1 872	1 813
Ti	0 048	0 022	0 028	0 026	0 017	0 022	0 018	0 019	0 007	0 022	0 016	0 008	0.024	0 021	0 028
Al	0 285	0 182	0 190	0.216	0 235	0 220	0 159	0 260	0 096	0 204	0.211	0.082	0 237	0.225	0 310
Cr	0 030	0 016	0 019	0 018	0 027	0 026	0.026	0 020	0 006	0 019	0.027	0 007	0 019	0 020	0 027
Fe2+	0 080	0 074	0 067	0 095	0 083	0 076	0 085	0 117	0.109	0 100	0.118	0 084	0.148	0 114	0 123
Mn	0 004	0 004	0 002	0 005	0 005	0 000	0 000	0 000	0 000	0 000	0 005	0 005	0 004	0 005	0 004
Ni	0 000	0 000	0 000	0 000	0 001	0 003	0 003	0 003	0 004	0 002	0 000	0 000	0 000	0 000	0 001
Mg	0 855	0 926	0 908	0 877	0 843	0 863	0 892	0 806	0 899	0 840	0 842	0 922	0 818	0 801	0 805
Ca	0 844	0 907	0 933	0 899	0 897	0 914	0 932	0 887	0 935	0 929	0 894	0 963	0 881	0 910	0 853
Na	0 078	0 033	0 035	0 045	0 045	0 033	0 025	0 042	0 015	0 020	0 030	0 014	0 037	0 033	0 056
K	0 000	0 000	0 000	0 000	0 000	0 000	0 000	0 000	0 000	0 000	0 000	0 000	0 000	0 000	0 000
Total	4 028	4 030	4 034	4 030	4 014	4 014	4 011	4 008	4 010	4 007	4 011	4 020	4 017	4 000	4 019
En	48 07	48 58	47 61	46 87	46 22	46 55	47 23	44 55	46 27	44 96	45 42	46 84	44 30	43 88	45 20
Fs	4 51	3 88	3 50	5 08	4 56	4 11	3 45	6 45	5 61	5 33	6 34	4 25	8 01	6 27	6 89
Wo	47 43	47 54	48 89	48 05	49 22	49 34	49 32	49 01	48 12	49 71	48 24	48 91	47 69	49 84	47 91
Mg#	91 4	92 6	93 2	90 2	91 0	91 9	93 2	87 4	89 2	89 4	87 7	91 7	84 7	87 5	88 6
Cr#	9 5	7 9	9 1	7 6	10 3	10 7	14 2	7 3	5 9	8 6	11 2	8 1	7 6	8 0	8 0

Rock	C	WG	WG	WG	WG	WG	WG	G	G	G	C	C	D	D
Sample	L349	L309A	L309B	L309C	L309C	L314	L314	L294	L294	L295	L115	L177	L221	L221
Location	3-Cpx	3-Cpx	1-Cpx	1-Cpx	5-Cpx	3-Cpx	6-Cpx	2-Cpx	4-Cpx	1-Cpx	1-Cpx	9-Cpx	1-Cpx	4-Cpx
Type	HALPPG	HALPPG	HALPPG	HALPPG	HALPPG	HALPPG	HALPPG	HALPPG	HALPPG	HALPPG	HALPPG	HALPPG	HALPPG	core HALPPG
SiO2	51.49	50.09	50.65	50.33	50.82	50.08	50.95	50.13	49.77	50.19	54.91	52.35	51.52	50.72
TiO2	0.69	0.78	0.76	0.66	1.10	0.78	0.49	0.54	0.65	1.00	0.08	0.57	0.49	0.72
Al2O3	3.40	5.25	5.86	5.93	5.02	6.04	5.16	5.26	6.96	6.96	1.00	3.91	3.89	4.63
Cr2O3	0.72	1.00	0.93	1.00	0.92	0.84	0.83	0.63	0.62	0.65	0.52	0.94	0.94	1.01
FeO	3.86	2.70	2.75	2.81	2.61	3.02	3.57	3.83	4.51	3.51	1.61	2.93	2.27	2.19
MnO	0.21	0.05	0.00	0.03	0.06	0.00	0.01	0.11	0.07	0.01	0.08	0.01	0.00	0.00
NiO	0.02	0.13	0.14	0.17	0.10	0.07	0.06	0.15	0.12	0.11	0.09	0.10	0.10	0.07
MgO	15.54	14.98	14.93	14.66	15.42	14.72	14.69	15.20	15.05	14.00	17.71	15.52	15.68	15.25
CaO	23.72	23.91	23.58	23.68	24.15	22.87	23.14	22.70	20.06	22.61	24.44	23.54	25.62	25.17
Na2O	0.36	0.67	0.69	0.53	0.53	0.67	0.63	0.59	1.18	0.60	0.24	0.42	0.20	0.37
K2O	0.00	0.00	0.00	0.00	0.00	0.00	0.00	0.00	0.00	0.00	0.00	0.00	0.00	0.00
Total	99.99	99.54	100.30	99.78	100.73	99.09	99.52	99.11	98.99	99.64	100.68	100.29	100.70	100.13
Si	1.893	1.846	1.847	1.846	1.849	1.847	1.875	1.856	1.837	1.840	1.977	1.905	1.876	1.857
Ti	0.019	0.022	0.021	0.018	0.030	0.022	0.014	0.015	0.018	0.028	0.002	0.016	0.013	0.020
Al	0.147	0.228	0.252	0.256	0.215	0.263	0.224	0.229	0.303	0.301	0.042	0.168	0.167	0.200
Cr	0.021	0.029	0.027	0.029	0.026	0.024	0.024	0.018	0.018	0.019	0.015	0.027	0.027	0.029
Fe2+	0.119	0.083	0.084	0.086	0.079	0.093	0.110	0.118	0.139	0.108	0.048	0.089	0.089	0.067
Mn	0.007	0.01	0.000	0.001	0.002	0.000	0.000	0.003	0.002	0.000	0.002	0.000	0.000	0.000
Ni	0.001	0.004	0.004	0.005	0.003	0.002	0.002	0.004	0.004	0.003	0.003	0.003	0.003	0.002
Mg	0.851	0.823	0.812	0.802	0.836	0.809	0.806	0.839	0.823	0.765	0.951	0.842	0.851	0.832
Ca	0.934	0.944	0.921	0.931	0.941	0.904	0.912	0.901	0.793	0.888	0.943	0.918	1.000	0.987
Na	0.025	0.048	0.049	0.037	0.037	0.048	0.045	0.042	0.084	0.043	0.017	0.030	0.014	0.026
K	0.000	0.000	0.000	0.000	0.000	0.000	0.000	0.000	0.000	0.000	0.000	0.000	0.000	0.000
Total	4.017	4.028	4.017	4.012	4.019	4.012	4.010	4.026	4.027	3.994	4.000	3.997	4.021	4.022
En	44.72	44.47	44.68	44.09	45.03	44.81	44.08	45.15	47.04	43.45	48.95	45.54	44.34	44.12
Fs	6.22	4.50	4.62	4.73	4.28	5.16	6.01	6.38	7.91	6.11	2.50	4.82	3.60	3.55
Wo	49.06	51.03	50.70	51.18	50.69	50.03	49.91	48.48	45.06	50.44	48.55	49.64	52.06	52.33
Mg#	87.8	90.8	90.6	90.3	91.3	89.7	88.0	87.6	85.6	87.7	95.1	90.4	92.5	92.5
Cr#	12.4	11.3	9.7	10.1	10.9	8.5	9.7	7.4	5.6	5.9	25.9	13.9	13.9	12.8

Rock	D	C	C	C	C	C	C	W	W	W	C	C	C	C	C
Sample	L221	L327	L328	L328	L328	L329	L329	L333	L333	L333	L348	L348	L348	L234	L236
Location	4-Cpx	1-Cpx	6-Cpx	6-Cpx	8-Cpx	2-Cpx	4-Cpx	2-Cpx	3-Cpx	3-Cpx	1-Cpx	1-Cpx	2-Cpx	2-Cpx	3-Cpx
	rim		core	rim					core	rim	core	rim			core
Type	HALPPG	HALPPG	HALPPG	HALPPG	HALPPG	HALPPG	HALPPG	HALPPG	HALPPG	HALPPG	HALPPG	HALPPG	HALPPG		
SiO2	51 24	50 95	50 32	50.78	51.44	52 30	52 27	54 09	54 12	53 51	53.96	54 64	53 34	54 97	53 52
TiO2	0.64	0.84	0.86	0.65	0.67	0 53	0.44	0.20	0.14	0 22	0.15	0.10	0.16	0 03	0 16
Al2O3	3.68	4 41	5.53	5.29	4 29	3 57	2.94	0.81	0.65	0 96	1 71	1 26	2 32	0 73	2 04
Cr2O3	0 93	0 48	0.78	0 77	0.47	0 54	0.57	0.30	0.29	0.40	0.61	0.55	0 77	0 55	0 84
FeO	2.37	3.51	4.15	3.44	3.98	2 82	2.90	2.23	2 25	2.33	2.47	2 41	2 39	2 30	2 62
MnO	0.00	0 05	0.00	0 00	0.00	0 00	0.00	0.14	0.15	0.21	0.13	0.16	0 16	0.21	0 00
NiO	0.12	0 11	0 09	0.00	0.00	0 07	0.06	0 00	0.00	0 00	0.01	0 00	0 00	0 12	0 12
MgO	15.79	15 58	14 65	15 36	15.17	15 90	15.83	17 36	17.53	17 23	16 52	17 26	16 45	17 42	16 95
CaO	25 32	23 55	22 75	22 95	23.72	24.47	24 75	24 86	24 80	25.20	24.72	24 51	24 71	23 92	23 34
Na2O	0 29	0 28	0 61	0 42	0 38	0 30	0 11	0.13	0.13	0.13	0.14	0 15	0 19	0 26	0 36
K2O	0.00	0 00	0.00	0.00	0 00	0 00	0.00	0 00	0.00	0.00	0.00	0.00	0 00	0.00	0 00
Total	100.38	99.73	99.73	99.86	100.12	100.48	99.87	100.10	100 06	100.19	100.41	101 04	100 49	100 51	99.95
Si	1.874	1 872	1 853	1.859	1.885	1 902	1.915	1 968	1 971	1 952	1 959	1 968	1.937	1 987	1 949
Ti	0.018	0.023	0.024	0.023	0 018	0 014	0 012	0 005	0.004	0 006	0 004	0 003	0 004	0 001	0 004
Al	0.159	0 191	0.240	0.228	0 185	0 153	0 127	0 035	0.028	0 041	0 073	0 053	0 099	0 031	0 088
Cr	0.027	0 014	0 023	0 022	0 014	0 015	0 017	0 009	0 008	0 012	0 018	0 016	0 022	0 016	0 024
Fe2+	0 072	0 108	0 128	0 105	0.122	0 086	0 089	0 068	0 069	0 071	0 075	0 073	0 073	0 070	0 080
Mn	0 000	0 001	0 000	0 000	0 000	0 000	0 000	0 004	0 005	0 006	0 004	0 005	0 005	0 006	0 000
Ni	0 004	0 003	0 003	0 000	0 000	0 002	0 002	0 000	0 000	0 000	0 000	0 000	0 000	0 003	0 003
Mg	0 861	0 853	0 804	0 838	0 829	0 862	0 865	0 942	0 952	0 937	0 894	0 927	0 880	0 939	0 920
Ca	0 992	0 927	0 897	0 900	0 931	0 953	0 971	0 969	0 967	0 965	0 961	0 946	0 961	0 926	0 910
Na	0 021	0 020	0 044	0 030	0 027	0 021	0 008	0 009	0 009	0 009	0 010	0 010	0 013	0 018	0 025
K	0 000	0 000	0 000	0 000	0 000	0 000	0 000	0 000	0 000	0 000	0 000	0 000	0 000	0 000	0 000
Total	4 026	4 013	4 014	4 007	4 011	4 009	4 005	4 009	4 012	4 020	3 997	4 000	4 005	3 998	4 004
En	44 71	45 20	43 96	45 47	44 03	45 34	44 92	47 59	47 88	47 01	46 30	47 64	46 27	48 52	48 16
Fs	3 76	5 70	6 99	5 71	6 48	4 50	4 62	3 43	3 45	3.57	3 88	3 73	3 77	3 59	4 18
Wo	51 53	49 10	49 05	48 82	48 48	50 16	50 47	48 98	48 68	49 42	49 81	48 62	49 96	47 88	47 66
Mg#	92 2	88 8	86 3	88 8	87 2	91 0	90 7	93 3	93 3	92 9	92 3	92 7	92 5	93 1	92 3
Cr#	14 5	6 7	8 6	8 9	6 8	9 1	11 6	19 9	23 0	21 8	19 4	22 7	18 2	33 6	21 6

Rock	C
Sample	L236
Location	2–Cpx
	rim
Type	
SiO2	54.13
TiO2	0.11
Al2O3	1.41
Cr2O3	0.43
FeO	2.51
MnO	0.00
NiO	0.10
MgO	17.05
CaO	24.16
Na2O	0.24
K2O	0.00
Total	100.14
Si	1.967
Ti	0.003
Al	0.060
Cr	0.012
Fe2+	0.076
Mn	0.000
Ni	0.003
Mg	0.924
Ca	0.941
Na	0.017
K	0.000
Total	4.003
En	47.60
Fs	3.93
Wo	48.48
Mg#	92.4
Cr#	16.9

TABLE A3.4. Amphibole analyses (oxides in wt %, number of ions on basis of 23 O)

Rock	H	H	H	H	H	D	AD	AD	AD	AD	AD	AD	AD	AD	AD
Sample	L157	L157	L157	L218	L218	L216	L125	L125	L125	L125	L129	L129	L132	L132	L148
Location	2-Amph	3-Amph	5-Amph	1-Amph	1-Amph	2-Amph	1-Amph	1-Amph	1-Amph	1-Amph	3-Amph	4-Amph	1-Amph	3-Amph	2-Amph
Type	LALPP	LALPP	LALPP	LALPP	LALPP	LALPP	LALPP	LALPP	LALPP	LALPP	LALPP	LALPP	LALPP	LALPP	LALPP
SiO2	54 31	53 26	51 66	54 14	56 47	55.18	46 58	47 99	49 04	48 92	49 20	48 82	50 05	50 08	44 30
TiO2	0 10	0 09	0 04	0.05	0.08	0 04	0 18	0 21	0.19	0 22	0 07	0 07	0 28	0.27	0 53
Al2O3	4.10	5.06	7.16	3 88	2 29	3.00	10 75	9 64	8 91	9.11	8.73	8 17	7 04	6.82	11.57
Cr2O3	1 11	1 26	0.65	0 77	0 57	0.94	2.47	2 24	1 65	2.04	2.06	1 87	1 70	1 80	2 06
FeO	2 27	2 37	2.33	2.16	1.98	2 07	2.56	2 61	2 67	2 32	2 58	2.38	2 50	2 29	2 88
MnO	0 07	0.09	0.04	0 03	0.00	0.00	0.05	0.08	0 17	0.06	0 00	0 00	0.07	0.10	0 00
NiO	0 02	0.25	0.00	0.00	0 00	0.15	0.39	0 12	0.16	0.23	0.14	0 21	0 50	0.48	0 12
MgO	21 90	21.35	20.36	21.71	22.72	22.53	19 69	20 01	20.54	20.56	20.24	19 94	21.12	21.30	18 88
CaO	12 93	12 50	12.85	12.88	12 92	12 76	12 01	12 02	12 00	12 40	12 64	12 71	12 36	11 99	12 86
Na2O	0 55	0 71	1 05	0 70	0 51	0 64	2 74	2 41	2.24	2 42	2 03	1 80	2 84	2 85	3 45
K2O	0 00	0 00	0 05	0 00	0.00	0 00	0 11	0 08	0 08	0 00	0.14	0 15	0 02	0 03	0 11
Total	97 34	96 92	96 19	96 32	97 54	97 29	97 49	97 39	97 65	98.28	97.85	96 09	98 46	97.99	96 76
Si	7 511	7 414	7 247	7 556	7 747	7.621	6 582	6 754	6 866	6 813	6 882	6 944	6 977	7 002	6 363
Ti	0 010	0 009	0 004	0 005	0 008	0 004	0 019	0 022	0.020	0 023	0 008	0 007	0 029	0 028	0 057
Al	0 667	0 830	1.184	0 638	0 370	0 488	1 790	1 599	1 470	1 495	1 440	1 369	1 157	1 123	1 958
Cr	0 121	0 139	0 072	0 085	0 062	0 102	0 275	0 249	0 183	0 225	0 228	0 210	0 187	0 199	0 234
Fe2+	0 263	0 276	0 273	0 252	0 227	0 239	0 302	0 307	0 313	0 270	0 302	0 282	0 291	0 267	0 346
Mn	0 008	0 011	0 005	0 004	0 000	0 000	0 005	0 010	0 020	0 007	0 000	0 000	0 008	0 012	0 000
Ni	0 002	0 027	0 000	0 000	0 000	0 017	0 044	0 014	0 018	0 026	0 016	0 023	0 055	0 054	0 014
Mg	4 514	4 429	4 258	4 517	4 647	4 638	4 147	4 199	4 287	4 268	4 221	4 227	4 388	4 440	4 042
Ca	1 915	1 863	1 931	1 926	1 899	1 887	1 818	1 813	1 800	1 850	1 894	1 936	1 846	1 795	1 979
Na	0 147	0 190	0 286	0 189	0 136	0 170	0 751	0 656	0 608	0 653	0 550	0 496	0 768	0 773	0 961
K	0 000	0 000	0 009	0 000	0 000	0 000	0 020	0 014	0 014	0 000	0 026	0 026	0 003	0 004	0 020
Total	15 158	15 188	15 268	15 172	15 096	15 166	15 752	15 636	15 599	15 631	15 564	15 521	15 708	15 697	15 974
Mg#	94 5	94 1	94 0	94 7	95 3	95 1	93 2	93 2	93 2	94 0	93 3	93 7	93 8	94 3	92 1
Cr#	15 4	14 3	5 7	11 7	14 3	17 3	13 3	13 5	11 1	13 1	13 7	13 3	13 9	15 1	10 7

Rock	AD	AD	AD	AD	OI	OI	OI	OI	OII	OII	OII	OII	C	WB	WB
Sample	L148	L275	L275	L336	L068	L068	L068	L068	L271	L351	L351	L351	L213	L069	L069
Location	4-Amph	4-Amph	5-Amph	3-Amph	1-Amph	3-Amph	4-Amph	6-Amph	1-Amph	1-Amph	2-Amph	4-Amph	1-Amph	1-Amph	2-Amph
Type	LALPP	LALPP	LALPP	LALPP	LALPP	LALPP	LALPP	LALPP	LALPP	LALPP	LALPP	LALPP	LALPP	LALPP	LALPP
SiO2	44 24	46 27	46 13	47.18	52 69	55 67	56.12	55 50	43 96	50.80	54 03	56 35	53 47	54 69	56.55
TiO2	0.58	0.25	0 24	0 31	0 11	0.05	0 02	0 06	1 43	0.14	0 09	0 08	0 14	0 04	0 08
Al2O3	11 60	12.33	11 83	10 95	5 20	3.06	2.30	3.36	12.13	8.19	4 29	2.63	4 70	3.33	1 54
Cr2O3	1 82	1.38	1 40	1 52	1 47	0 62	0.51	0 67	1.61	1.05	0.86	0 44	1.28	0 81	0.47
FeO	3.01	3 27	3.47	2 80	2 52	2 31	2.19	2.46	6.10	2.75	2.30	2 20	2.86	2 20	2 11
MnO	0.00	0 02	0.00	0 00	0 00	0 00	0.00	0 00	0.16	0 11	0.07	0 14	0.04	0.06	0.07
NiO	0.14	0.07	0.07	0.12	0 13	0.16	0.15	0.12	0.05	0.00	0.01	0 07	0 00	0 07	0.14
MgO	18.60	18.96	18.96	19.52	21.13	22.58	22.63	22.26	16.88	20.48	22.02	22 44	21.04	22 48	23.08
CaO	12.84	12.17	11.85	12.03	12.43	12.43	12 67	12.55	11.85	12.45	12 82	12 65	12 90	12.70	12 59
Na2O	3.55	2.59	2.61	2.54	1.08	0 62	0.48	0.71	2.75	1 52	0.70	0 54	1 00	1 12	0 58
K2O	0 12	0.09	0.09	0.06	0.02	0 00	0.00	0.00	0.16	0 00	0 00	0 00	0.00	0 00	0.00
Total	96 50	97.38	96.62	97.02	96.75	97.48	97 03	97.70	97.08	97 48	97.15	97.52	97.43	97.49	97.21
Si	6.373	6.529	6.562	6.661	7.366	7.658	7.746	7.630	6.346	7.070	7.487	7 737	7.428	7.558	7.793
Ti	0.063	0.026	0.026	0.032	0 011	0.005	0.002	0.006	0.155	0.015	0.009	0 008	0.015	0 004	0.008
Al	1.970	2.050	1.984	1.822	0 856	0.496	0.373	0.545	2.064	1 343	0.700	0 426	0.770	0 542	0.250
Cr	0.207	0.153	0.157	0.170	0.162	0.067	0.055	0.073	0.184	0.116	0.094	0 048	0.141	0 089	0.051
Fe2+	0.363	0.385	0.412	0.331	0.294	0.265	0.252	0 283	0.736	0 320	0.266	0.252	0.332	0 254	0 243
Mn	0 000	0.002	0.000	0.000	0 000	0.000	0.000	0.000	0 020	0 012	0 008	0 016	0.005	0.007	0.008
Ni	0.016	0.008	0.007	0.014	0.014	0 018	0.016	0.014	0.006	0.000	0.001	0 007	0 000	0 008	0 016
Mg	3.995	3 988	4 020	4 109	4 403	4 631	4.656	4.562	3.633	4 248	4.548	4 593	4 357	4 631	4.742
Ca	1.982	1.839	1.806	1 820	1 861	1 832	1 873	1.848	1.833	1 856	1 903	1 861	1 920	1 880	1.859
Na	0 992	0.707	0.719	0.694	0 291	0 164	0.128	0 189	0.770	0 410	0.187	0 144	0 269	0 300	0 155
K	0 022	0.016	0.016	0.010	0.003	0 000	0.000	0 000	0.029	0 000	0.000	0 000	0 000	0.000	0 000
Total	15.982	15.705	15.709	15.662	15.261	15 137	15.102	15.150	15.775	15 391	15 201	15.091	15 237	15.273	15.125
Mg#	91.7	91.2	90.7	92.6	93.7	94.6	94.9	94 2	83.1	93.0	94 5	94 8	92 9	94 8	95 1
Cr#	9.5	7.0	7.3	8 5	16 0	11 9	12 9	11.8	8 2	7.9	11 9	10.1	15 4	14 0	17 0

Rock	WB	D	W	W	W	W	W	W	C	C	C	C	AP
Sample	L069	L305	L109	L109	L301	L301	L315	L316	L296	L296	L310	L177	L274
Location	3-Amph	5-Amph	1-Amph	1-Amph	1-Amph	2-Amph	4-Amph	3-Amph	2-Amph	4-Amph	1-Amph	9-Amph	2-Amph
Type	LALPP	HALPPG	HALPPG	HALPPG	HALPPG	HALPPG	HALPPG	HALPPG	HALPPG	HALPPG	HALPPG	HALPPG	HALPPG
SiO2	53.26	44.05	43.25	43.17	43.91	44.84	48.95	42.99	41.96	53.91	45.29	44.67	43.87
TiO2	0.11	0.01	0.66	2.47	0.15	0.06	0.97	1.48	3.07	0.16	1.64	1.52	1.46
Al2O3	4.53	16.24	16.70	13.56	16.04	15.86	6.08	14.62	14.32	5.34	12.68	13.50	12.13
Cr2O3	1.31	0.00	0.13	1.59	0.08	0.00	0.59	1.77	1.22	0.01	1.13	0.99	1.47
FeO	2.67	3.66	4.23	3.59	4.22	4.32	3.10	3.18	6.05	4.68	3.90	5.16	5.86
MnO	0.08	0.00	0.14	0.14	0.12	0.10	0.13	0.00	0.00	0.05	0.12	0.00	0.15
NiO	0.00	0.00	0.00	0.09	0.00	0.00	0.00	0.00	0.10	0.09	0.00	0.13	0.04
MgO	21.66	17.63	17.22	17.29	17.63	17.55	15.86	17.66	15.35	20.83	17.74	16.47	16.79
CaO	12.63	12.30	12.38	12.09	12.52	12.27	21.44	12.50	12.10	12.07	12.77	12.30	11.80
Na2O	1.54	3.11	2.87	2.52	2.76	2.32	0.80	3.02	2.84	0.79	2.25	2.28	2.75
K2O	0.00	0.00	0.14	0.36	0.00	0.00	0.00	0.14	0.34	0.00	0.00	0.49	0.14
Total	97.79	96.99	97.72	96.85	97.42	97.31	97.92	97.43	97.34	97.91	97.52	97.47	96.44
Si	7.385	6.240	6.117	6.187	6.216	6.325	6.997	6.118	6.060	7.458	6.411	6.370	6.363
Ti	0.011	0.001	0.070	0.266	0.015	0.006	0.104	0.158	0.333	0.017	0.175	0.163	0.159
Al	0.740	2.711	2.784	2.290	2.675	2.636	1.024	2.452	2.438	0.870	2.116	2.269	2.073
Cr	0.144	0.000	0.015	0.180	0.009	0.000	0.067	0.199	0.139	0.001	0.126	0.112	0.169
Fe2+	0.310	0.434	0.500	0.430	0.500	0.510	0.371	0.378	0.730	0.541	0.462	0.615	0.710
Mn	0.009	0.000	0.017	0.016	0.014	0.012	0.016	0.000	0.000	0.005	0.014	0.000	0.018
Ni	0.000	0.000	0.000	0.010	0.000	0.000	0.000	0.000	0.012	0.010	0.000	0.015	0.004
Mg	4.478	3.724	3.630	3.694	3.719	3.691	3.380	3.747	3.304	4.295	3.744	3.493	3.630
Ca	1.876	1.866	1.876	1.856	1.899	1.855	3.284	1.906	1.872	1.789	1.937	1.879	1.833
Na	0.414	0.853	0.787	0.700	0.758	0.635	0.222	0.853	0.796	0.211	0.618	0.630	0.773
K	0.000	0.000	0.025	0.066	0.000	0.000	0.000	0.025	0.063	0.000	0.000	0.089	0.026
Total	15.368	15.830	15.820	15.695	15.805	15.668	15.464	15.837	15.748	15.196	15.602	15.036	15.757
Mg#	93.5	89.6	87.9	89.6	88.2	87.9	90.1	90.8	81.9	88.8	89.0	85.0	83.6
Cr#	16.2	0.0	0.5	7.3	0.3	0.0	6.1	7.5	5.4	0.1	5.6	4.7	7.5

Rock	W	AD	AMPT	AMPT
Sample	L333	L333	L341B	L341B
Location	2-Amph	8-Amph	1-Amph	1-Amph
Type	HALPPG	LALPP	UC	UC
SiO2	47.16	49.95	42.01	41.45
TiO2	0.95	0.27	3.31	3.27
Al2O3	9.53	8.20	13.23	13.26
Cr2O3	1.53	1.10	0.28	0.34
FeO	3.36	3.13	11.03	10.84
MnO	0.12	0.15	0.22	0.23
NiO	0.00	0.04	0.16	0.00
MgO	18.89	20.43	12.87	13.00
CaO	12.95	12.28	11.90	11.68
Na2O	2.29	1.79	3.02	2.79
K2O	0.00	0.00	0.24	0.26
Total	96.78	97.33	98.27	97.10
Si	6.713	6.996	6.144	6.125
Ti	0.102	0.028	0.364	0.363
Al	1.599	1.353	2.280	2.308
Cr	0.172	0.122	0.032	0.040
Fe2+	0.400	0.367	1.349	1.339
Mn	0.014	0.018	0.027	0.028
Ni	0.000	0.005	0.019	0.000
Mg	4.009	4.266	2.806	2.864
Ca	1.975	1.842	1.865	1.849
Na	0.632	0.486	0.856	0.798
K	0.000	0.000	0.045	0.048
Total	15.616	15.482	15.787	15.762
Mg#	90.9	92.1	67.5	68.1
Cr#	9.7	8.3	1.4	1.7

TABLE A3.5. Plagioclase analyses (oxides in wt.%, number of ions on basis of 32 O)

Rock	WG	WG	WG	WG	WG	WG	WG	WG	WG	WG	WG	WG	WG	WG	G
Sample	L309B	L309B	L309C	L309C	L309C	L314	L314	L314	L314	L314	L314	L314	L314	L314	L294
Location	3-Plag	5-Plag	3-Plag	4-Plag	6-Plag	1-Plag	2-Plag	4-Plag	5-Plag core	5-Plag rim	6-Plag-1	6-Plag-2	7-Plag core	7-Plag rim	3-Plag
Type	HALPPG	HALPPG	HALPPG	HALPPG	HALPPG	HALPPG	HALPPG	HALPPG	HALPPG	HALPPG	HALPPG	HALPPG	HALPPG	HALPPG	HALPPG
SiO2	50.75	49.46	50.02	49.69	50.65	50.64	50.86	50.43	50.36	50.72	49.70	50.16	50.38	49.70	50.63
TiO2	0.00	0.00	0.00	0.28	0.01	0.00	0.00	0.00	0.00	0.00	0.00	0.00	0.01	0.00	0.00
Al2O3	31.84	32.69	31.97	32.04	31.81	31.58	31.10	31.59	31.43	31.33	31.99	31.31	31.28	31.67	31.41
Cr2O3	0.00	0.00	0.00	0.00	0.00	0.00	0.00	0.00	0.00	0.00	0.00	0.00	0.00	0.00	0.00
FeO	0.13	0.15	0.16	0.13	0.10	0.06	0.19	0.11	0.09	0.12	0.10	0.08	0.06	0.09	0.12
MnO	0.00	0.00	0.00	0.00	0.00	0.00	0.00	0.00	0.00	0.00	0.00	0.00	0.00	0.00	0.00
NiO	0.05	0.04	0.04	0.05	0.09	0.07	0.07	0.04	0.03	0.07	0.05	0.04	0.02	0.03	0.12
MgO	0.00	0.00	0.00	0.00	0.00	0.00	0.00	0.00	0.00	0.00	0.00	0.00	0.00	0.00	0.00
CaO	14.74	15.48	14.77	15.08	14.65	14.22	14.24	14.38	14.54	14.29	14.92	14.52	14.73	15.02	14.53
Na2O	3.08	2.78	3.09	3.03	3.31	3.50	3.39	3.29	3.43	3.33	3.01	3.34	3.45	3.14	3.63
K2O	0.00	0.00	0.00	0.00	0.00	0.00	0.00	0.04	0.01	0.00	0.00	0.00	0.00	0.00	0.00
Total	100.57	100.61	100.05	100.28	100.62	100.06	99.84	99.83	99.93	99.86	99.77	99.44	99.92	99.64	100.43
Si	9.191	8.984	9.117	9.051	9.177	9.215	9.276	9.199	9.192	9.247	9.089	9.196	9.199	9.108	9.202
Ti	0.000	0.000	0.000	0.038	0.001	0.000	0.000	0.000	0.000	0.000	0.000	0.000	0.001	0.000	0.000
Al	6.795	7.000	6.869	6.878	6.793	6.774	6.685	6.791	6.762	6.732	6.895	6.765	6.731	6.840	6.729
Cr	0.000	0.001	0.000	0.000	0.000	0.000	0.000	0.000	0.000	0.000	0.000	0.000	0.000	0.000	0.000
Fe2+	0.020	0.023	0.024	0.020	0.015	0.009	0.028	0.017	0.014	0.018	0.015	0.011	0.009	0.014	0.018
Mn	0.000	0.000	0.000	0.000	0.000	0.000	0.000	0.000	0.000	0.000	0.000	0.000	0.000	0.000	0.000
Ni	0.007	0.006	0.005	0.007	0.013	0.010	0.010	0.006	0.005	0.010	0.007	0.005	0.002	0.004	0.017
Mg	0.000	0.000	0.000	0.000	0.000	0.000	0.000	0.000	0.000	0.000	0.000	0.000	0.000	0.000	0.000
Ca	2.859	3.014	2.884	2.942	2.845	2.773	2.783	2.811	2.843	2.791	2.924	2.851	2.881	2.948	2.830
Na	1.080	0.978	1.093	1.070	1.164	1.235	1.197	1.164	1.215	1.175	1.067	1.187	1.220	1.114	1.278
K	0.000	0.000	0.000	0.000	0.000	0.000	0.000	0.000	0.009	0.002	0.000	0.000	0.000	0.000	0.000
Total	19.951	20.005	19.994	20.007	20.007	20.015	19.980	19.987	20.039	19.976	19.997	20.015	20.044	20.029	20.073
An	72.59	75.50	72.51	73.33	70.96	69.18	69.92	70.72	69.91	70.33	73.26	70.60	70.26	72.58	68.90
Ab	27.41	24.50	27.49	26.67	29.04	30.82	30.08	29.28	29.88	29.61	26.74	29.40	29.74	27.42	31.10
Or	0.00	0.00	0.00	0.00	0.00	0.00	0.00	0.00	0.21	0.06	0.00	0.00	0.00	0.00	0.00

Rock	G	G	G	G	AMPT
Sample	L295	L295	L295	L295	L341B
Location	2-Plag	6-Plag core	6-Plag rim	6-Plag	1-Plag
Type	HALPPG	HALPPG	HALPPG	HALPPG	UC
SiO2	52.02	50.43	50.34	51.02	50.99
TiO2	0.00	0.00	0.00	0.15	0.02
Al2O3	31.90	32.08	32.06	31.49	31.01
Cr2O3	0.00	0.00	0.00	0.00	0.01
FeO	0.09	0.13	0.10	0.10	0.25
MnO	0.00	0.00	0.00	0.00	0.06
NiO	0.06	0.05	0.06	0.03	0.00
MgO	0.00	0.00	0.01	0.00	0.03
CaO	13.78	14.33	14.47	13.87	13.98
Na2O	3.81	3.40	3.51	3.80	3.64
K2O	0.00	0.00	0.00	0.00	0.00
Total	101.66	100.43	100.54	100.43	99.99
Si	9.299	9.150	9.131	9.247	9.289
Ti	0.000	0.000	0.000	0.020	0.003
Al	6.721	6.860	6.854	6.726	6.658
Cr	0.000	0.000	0.000	0.000	0.001
Fe2+	0.013	0.020	0.015	0.014	0.038
Mn	0.000	0.000	0.000	0.000	0.010
Ni	0.009	0.007	0.009	0.004	0.000
Mg	0.000	0.000	0.003	0.000	0.007
Ca	2.639	2.785	2.813	2.693	2.729
Na	1.320	1.197	1.233	1.334	1.285
K	0.000	0.000	0.000	0.000	0.000
Total	20.001	20.019	20.058	20.037	20.021
An	66.65	69.94	69.52	66.88	68.00
Ab	33.35	30.06	30.48	33.12	32.00
Or	0.00	0.00	0.00	0.00	0.00

TABLE A3.6. Spinel analyses (oxides in wt.%, number of ions on basis of 32 O)

Rock	H	H	H	H	H	H	H	H	H	H	H	H	H	H	H
Sample	L097	L103	L103	L103	L106	L106	L106	L106	L106	L106	L106	L106	L153	L173	L173
Location	7-Sp	1-Sp*	1-Sp	4-Sp	1-Sp	1-Sp	1-Sp	4-Sp	5-Sp	6-Sp	7-Sp	8-Sp	2-Sp	1-Sp*	1-Sp*
Type	LALPP	LALPP	LALPP	LALPP	core LALPP	rim LALPP	rim LALPP	LALPP	LALPP	LALPP	LALPP	LALPP	LALPP	LALPP	LALPP
TiO2	0.05	0.18	0.11	0.09	0.12	0.16	0 14	0.12	0.11	0.11	0.15	0.17	0.13	0.12	0.13
V2O3	0.26	0 19	0.19	0.24	0.24	0.27	0.25	0.25	0.28	0.25	0.27	0.26	0 22	0 19	0.20
Al2O3	11.16	19.33	12.58	12.47	11.32	11.79	12.49	11.80	13.07	13.24	12.15	11.60	11 66	14 39	20 52
Cr2O3	55.01	45.28	51 79	56 63	55.47	55.51	54.93	54.89	55.65	54.38	55.41	55.22	56.42	52.53	46 50
FeO	23.08	24 04	26 57	21 86	20.72	22 44	21 67	23 14	20 70	21 12	21.39	23 69	21.76	21 54	20 57
MnO	0 34	0.26	0 33	0.28	0.28	0 26	0 25	0 29	0.29	0.26	0.27	0.30	0.31	0.29	0 18
NiO	0 08	0 04	0 00	0 04	0 07	0 04	0 05	0 08	0 02	0 06	0 05	0 05	0 04	0.04	0.09
MgO	9 36	10 57	8 16	9.45	9.83	9 84	9 73	8 86	10 09	9 48	10 05	9 42	9 21	9 52	11 40
Total	99 33	99 86	99 72	101 06	98.05	100 30	99.49	99 42	100 20	98 87	99 73	100.71	99 74	98 61	99 59
Ti	0 010	0 030	0 022	0 017	0 024	0 031	0 027	0.024	0 021	0 022	0 029	0 033	0 025	0 023	0 024
V	0.055	0 038	0 040	0 051	0.052	0 056	0 053	0 054	0 059	0 053	0 056	0 055	0 047	0 039	0 041
Al	3 487	5.757	3 923	3 820	3.568	3 633	3 868	3 691	4 004	4 117	3.753	3 575	3 630	4 462	6 070
Cr	11 537	9 048	10 838	11 634	11 726	11 473	11 413	11 514	11 438	11 345	11 479	11 412	11 784	10 928	9 228
Fe3+	0 901	1 097	1 155	0 460	0 605	0 776	0 612	0 694	0 456	0 441	0 653	0 893	0 488	0 524	0 613
Fe2+	4 218	3 983	4 728	4 290	4 028	4 130	4 151	4 440	4 045	4 220	4 034	4 286	4 319	4 216	3 705
Mn	0 075	0 055	0 073	0 061	0 063	0 057	0 055	0 064	0 063	0 057	0 059	0 066	0 068	0 064	0 038
Ni	0 017	0 008	0 000	0 008	0 015	0 008	0 010	0 017	0 004	0 013	0 010	0 010	0 008	0 008	0 018
Mg	3 699	3 984	3 221	3 659	3 919	3 836	3 811	3 503	3 909	3 732	3 925	3 671	3 629	3 735	4 264
Total	24 000	24 000	24 000	24 000	24 000	24 000	24 000	24 000	24 000	24 000	24 000	24 000	24 000	24 000	24 000
Mg#	46 7	50 0	40 5	46 0	49 3	48 2	47 9	44 1	49 2	48 9	49 3	46 1	45 7	47 0	53 5
Cr#	76 8	61 1	73 4	75 3	76 7	75 9	74 7	75 7	74 1	73 4	75 4	76 1	76 4	71 0	60 3

Rock	H	H	H	H	H	H	H	H	H	H	H	H	H	H	H
Sample	L173	L173	L173	L173	L173	L173	L173	L173	L218	L225	L225	L225	L225	L226	L263
Location	2-Sp*	2-Sp*	3-Sp*	3-Sp*	3-Sp*	3-Sp*	3-Sp*	3-Sp*	3-Sp	7-Sp	8-Sp	9-Sp	9-Sp	2-Sp	1-Sp
Type	LALPP	LALPP	LALPP	LALPP	LALPP	LALPP	LALPP	LALPP	LALPP	LALPP	LALPP	core LALPP	rim LALPP	LALPP	LALPP
TiO2	0.13	0.11	0.08	0.11	0.11	0.07	0.08	0.09	na	0.14	0.14	0.16	0.14	0.20	0.11
V2O3	0.20	0.25	0.21	0.20	0.21	0.15	0.26	0.23	na	0.17	0.19	0.24	0.21	0.20	0.24
Al2O3	15.18	22.11	17.66	14.96	14.27	16.48	17.33	15.58	16.04	12.17	10.66	11.36	11.38	13.00	13.58
Cr2O3	50.92	46.57	49.78	52.98	52.02	50.35	51.15	51.63	52.33	56.73	55.83	57.66	57.52	55.66	53.32
FeO	21.57	20.98	21.49	22.38	22.14	21.22	21.58	22.02	23.25	19.86	22.36	21.45	21.68	19.89	22.41
MnO	0.32	0.14	0.21	0.31	0.33	0.24	0.32	0.16	na	0.29	0.34	0.29	0.27	0.27	0.27
NiO	0.02	0.06	0.03	0.04	0.06	0.05	0.02	0.07	na	0.01	0.03	0.08	0.00	0.05	0.07
MgO	9.86	10.81	9.83	8.96	9.20	10.31	10.19	9.50	10.36	9.50	9.18	9.23	9.36	10.79	8.44
Total	98.19	101.03	99.29	99.92	98.35	98.86	100.92	99.27	101.97	98.87	98.72	100.45	100.55	100.26	98.43
Ti	0.025	0.020	0.015	0.021	0.022	0.013	0.015	0.017	0.000	0.028	0.028	0.031	0.027	0.038	0.022
V	0.043	0.050	0.044	0.041	0.045	0.030	0.053	0.048	0.000	0.036	0.040	0.050	0.044	0.042	0.050
Al	4.697	6.449	5.358	4.593	4.449	5.025	5.178	4.781	4.768	3.806	3.365	3.519	3.519	3.963	4.267
Cr	10.568	9.112	10.132	10.914	10.876	10.301	10.255	10.626	10.435	11.900	11.817	11.986	11.933	11.424	11.236
Fe3+	0.642	0.348	0.435	0.410	0.587	0.617	0.484	0.512	0.797	0.202	0.722	0.383	0.449	0.494	0.404
Fe2+	4.094	3.993	4.191	4.466	4.309	3.976	4.092	4.283	4.106	4.205	4.283	4.334	4.308	3.808	4.591
Mn	0.070	0.029	0.045	0.068	0.073	0.052	0.068	0.035	0.000	0.064	0.076	0.064	0.059	0.058	0.060
Ni	0.004	0.012	0.006	0.008	0.013	0.010	0.004	0.014	0.000	0.002	0.006	0.017	0.000	0.010	0.015
Mg	3.857	3.986	3.773	3.479	3.627	3.975	3.852	3.685	3.894	3.756	3.662	3.617	3.660	4.162	3.355
Total	24.000	24.000	24.000	24.000	24.000	24.000	24.000	24.000	24.000	24.000	24.000	24.000	24.000	24.000	24.000
Mg#	48.5	50.0	47.4	43.8	45.7	50.0	48.5	46.3	48.7	47.2	46.1	45.5	45.9	52.2	42.2
Cr#	69.2	58.6	65.4	70.4	71.0	67.2	66.4	69.0	68.6	75.8	77.8	77.3	77.2	74.2	72.5

Rock	H	H	H	D	D	D	D	D	D	D	D	D	D	D	D
Sample	L263	L263	L336	L050A	L053	L055	L143	L162	L162	L176	L199	L216	L216	L216	L217
Location	2-Sp	3-Sp	6-Sp	2-Sp	5-Sp	3-Sp	3-Sp	1-Sp	2-Sp	3-Sp	6-Sp	3-Sp	8-Sp	9-Sp	2-Sp-1
Type	LALPP	LALPP	LALPP	LALPP	LALPP	LALPP	LALPP	LALPP	LALPP	LALPP	LALPP	LALPP	LALFP	LALPP	LALPP
TiO2	0.19	0.19	0.17	0.14	0.17	0.13	na	0.22	0.24	0.22	na	na	na	na	na
V2O3	0.19	0.23	0.20	0.26	0.16	0.26	na	0.16	0.11	0.35	na	na	na	na	na
Al2O3	14.43	16.86	11.23	8.16	11.25	11.46	12.28	12.17	10.93	12.33	8.41	9.22	9.16	9.20	9.89
Cr2O3	52.43	49.24	56.08	56.79	57.32	56.79	54.16	51.51	52.89	51.87	55.04	56.90	57.38	57.53	56.13
FeO	22.66	22.83	22.75	27.06	21.22	23.40	23.61	24.83	25.37	28.60	25.82	23.55	26.20	23.95	24.91
MnO	0.23	0.28	0.27	0.38	0.28	0.28	na	0.26	0.29	0.34	na	na	na	na	na
NiO	0.09	0.05	0.05	0.06	0.04	0.05	na	0.04	0.03	0.08	na	na	na	na	na
MgO	9.82	10.73	8.59	6.81	10.25	8.74	10.11	9.45	9.63	6.99	8.34	8.77	7.37	8.88	7.62
Total	100.02	100.40	99.33	99.65	100.69	101.09	100.17	98.63	99.48	100.76	97.62	100.44	100.10	99.56	98.55
Ti	0.037	0.036	0.034	0.028	0.033	0.025	0.000	0.043	0.047	0.043	0.000	0.000	0.000	0.000	0.000
V	0.039	0.046	0.042	0.056	0.033	0.054	0.000	0.034	0.023	0.073	0.000	0.000	0.000	0.000	0.000
Al	4.408	5.046	3.532	2.603	3.453	3.539	3.772	3.807	3.406	3.846	2.719	2.892	2.908	2.904	3.172
Cr	10.744	9.889	11.830	12.248	11.807	11.768	11.155	10.805	11.053	10.854	11.942	12.391	12.227	12.184	12.072
Fe3+	0.736	0.947	0.529	1.015	0.642	0.589	1.073	1.268	1.424	1.139	1.339	0.717	0.865	0.911	0.757
Fe2+	4.175	3.904	4.548	5.157	3.982	4.539	4.072	4.241	4.184	5.191	4.587	4.523	5.040	4.454	4.909
Mn	0.050	0.059	0.060	0.087	0.061	0.061	0.000	0.058	0.064	0.075	0.000	0.000	0.000	0.000	0.000
Ni	0.019	0.010	0.011	0.013	0.008	0.010	0.000	0.008	0.006	0.017	0.000	0.000	0.000	0.000	0.000
Mg	3.793	4.063	3.415	2.771	3.982	3.415	3.928	3.736	3.793	2.760	3.413	3.477	2.980	3.546	3.091
Total	24.000	24.000	24.000	24.000	24.000	24.000	24.000	24.000	24.000	24.000	24.000	24.000	24.000	24.000	24.000
Mg#	47.6	51.0	42.9	35.0	50.0	42.9	49.1	46.8	47.5	34.7	42.7	43.5	37.0	44.3	38.6
Cr#	70.9	66.2	77.0	82.4	77.4	76.9	74.7	73.9	76.4	73.8	81.5	81.1	80.8	80.8	79.2

Rock	D	D	D	D	D	D	D	D	CR	CR	CR	CR	CR	CR	CR
Sample	L217	L217	L226	L226	L246	L254	L262	L262	L130	L130	L161	L203	L245	L289	L289
Location	2-Sp-2	3-Sp	3-Sp core	3-Sp rim	1-Sp	4-Sp	6-Sp	7-Sp	1-Sp	4-Sp	Sp	Sp	7-Sp	2-Sp	4-Sp core
Type	LALPP	LALPP	LALPP	LALPP	LALPP	LALPP	LALPP	LALPP	LALPP	LALPP	LALPP	LALPP	LALPP	LALPP	LALPP
TiO2	na	na	0.16	0.27	0.17	na	0.19	0.23	0.13	0.21	0.17	0.23	0.13	0.12	0.16
V2O3	na	na	0.20	0.20	0.19	na	0.24	0.24	0.19	0.19	0.19	0.11	0.15	0.17	0.17
Al2O3	10.54	11.61	12.13	11.65	11.92	8.03	9.52	13.93	19.44	19.16	14.72	10.89	13.72	25.06	29.70
Cr2O3	57.79	55.99	53.92	54.68	55.87	57.88	56.83	51.12	48.73	48.92	51.22	56.94	52.11	42.61	39.26
FeO	24.19	23.55	22.77	21.47	23.18	26.55	23.38	23.81	19.33	20.19	20.71	19.99	19.46	17.43	16.82
MnO	na	na	0.38	0.30	0.23	na	0.31	0.25	0.23	0.25	0.09	0.20	0.15	0.18	0.21
NiO	na	na	0.10	0.06	0.03	na	0.07	0.00	0.02	0.02	0.04	0.14	0.11	0.12	0.09
MgO	8.21	9.46	10.40	9.91	9.88	8.77	8.91	9.50	11.56	11.83	11.01	12.05	12.15	14.34	14.76
Total	100.73	100.62	100.05	98.53	101.46	101.22	99.44	99.07	99.62	100.76	98.15	100.54	97.97	100.02	101.16
Ti	0.000	0.000	0.031	0.053	0.033	0.000	0.038	0.045	0.024	0.039	0.033	0.044	0.025	0.021	0.026
V	0.000	0.000	0.042	0.043	0.039	0.000	0.052	0.050	0.038	0.037	0.039	0.022	0.031	0.033	0.032
Al	3.292	3.580	3.723	3.647	3.631	2.509	3.005	4.307	5.770	5.627	4.528	3.309	4.209	7.114	8.187
Cr	12.105	11.579	11.103	11.484	11.421	12.136	12.031	10.605	9.703	9.639	10.569	11.609	10.727	8.113	7.260
Fe3+	0.603	0.840	1.069	0.719	0.844	1.355	0.836	0.949	0.441	0.620	0.798	0.972	0.984	0.696	0.466
Fe2+	4.756	4.312	3.891	4.050	4.168	4.534	4.398	4.275	3.630	3.587	3.721	3.339	3.253	2.815	2.824
Mn	0.000	0.000	0.083	0.067	0.050	0.000	0.069	0.055	0.048	0.052	0.020	0.043	0.033	0.036	0.041
Ni	0.000	0.000	0.021	0.013	0.006	0.000	0.015	0.000	0.004	0.004	0.008	0.029	0.023	0.023	0.017
Mg	3.244	3.688	4.036	3.924	3.809	3.466	3.555	3.714	4.341	4.395	4.284	4.633	4.717	5.147	5.146
Total	24.000	24.000	24.000	24.000	24.000	24.000	24.000	24.000	24.000	24.000	24.000	24.000	24.000	24.000	24.000
Mg#	40.6	46.1	50.9	49.2	47.7	43.3	44.7	46.5	54.5	55.1	53.5	58.1	59.2	64.6	64.6
Cr#	78.6	76.4	74.9	75.9	75.9	82.9	80.0	71.1	62.7	63.1	70.0	77.8	71.8	53.3	47.0

Rock	CR	AD	AD	AD	AD	AD	AD	AD	AD	AD	AD	AD	AD	AD	AD
Sample	L289	L125	L125	L125	L125	L125	L125	L125	L125	L125	L125	L125	L140	L140	L148
Location	4-Sp rim	1-Sp	1-Sp	1-Sp	1-Sp	1-Sp	1-Sp	1-Sp	1-Sp	1-Sp	1-Sp	1-Sp	3-Sp core	3-Sp rim	1-Sp core
Type	LALPP	LALPP	LALPP	LALPP	LALPP	LALPP	LALPP	LALPP	LALPP	LALPP	LALPP	LALPP	LALPP	LALPP	LALPP
TiO2	0 11	0.11	0 09	0.11	0 12	0.15	0.14	0 10	0 13	0 16	0.13	0.11	0 20	0.19	0 31
V2O3	0.17	0 11	0.15	0.22	0.19	0.20	0.20	0.21	0 22	0.19	0.14	0.19	0.11	0.12	0 09
Al2O3	20.75	17.33	17.94	18.73	23.74	23.54	24.15	24.53	21.50	20.62	23.11	21.70	4.91	4.86	10.08
Cr2O3	48.48	51.20	49.83	50.43	44.88	43.98	44.68	44.77	47.37	48.50	45.14	46.07	58.42	56.91	54.84
FeO	18.61	20.46	19.98	19.81	17.58	20.02	17.45	18.61	18.70	20.21	18.67	20.59	27.99	29.15	25.84
MnO	0 22	0 29	0 26	0 31	0.25	0.25	0 28	0 23	0.29	0 25	0 25	0 21	0 41	0 37	0 39
NiO	0.10	0.08	0 07	0.07	0 06	0 11	0.11	0 07	0.08	0 09	0.11	0 05	0 08	0.07	0 09
MgO	12 60	10 86	11 54	11 42	13.27	12 68	13 15	13 14	12 17	12 04	12.35	12.38	7 17	6 67	8 42
Total	101 03	100.42	99.86	101 11	100 08	100.93	100.15	101 65	100.43	100 05	99 88	101.30	99.29	98.34	100.06
Ti	0.020	0.021	0.017	0.020	0 022	0.027	0 025	0.018	0.024	0.030	0.024	0.020	0 041	0 040	0.061
V	0 034	0 023	0 031	0.044	0 037	0 040	0 038	0 041	0.044	0 037	0.027	0.037	0.024	0.027	0 019
Al	6 012	5 177	5 347	5 513	6 822	6.744	6 929	6 941	6 260	6 047	6.707	6 254	1 601	1.606	3 165
Cr	9 424	10 263	9 962	9 956	8 650	8.452	8.601	8 500	9.255	9.147	8.791	8 909	12 783	12.607	11 547
Fe3+	0 490	0 495	0 626	0 446	0 448	0 710	0 382	0 483	0 393	0 709	0 427	0 760	1 510	1 681	1 146
Fe2+	3 336	3 844	3 599	3 690	3 136	3 360	3 172	3 254	3 470	3 495	3 418	3 452	4 967	5 150	4 610
Mn	0 045	0 061	0 055	0 065	0 051	0 051	0 057	0 046	0 060	0 052	0 051	0 043	0 097	0 087	0 089
Ni	0 020	0 012	0 014	0 014	0 012	0 021	0 021	0 013	0 012	0 018	0 022	0 010	0 018	0 016	0 019
Mg	4 619	4 103	4 349	4 251	4 823	4 595	4 775	4 704	4 482	4 465	4 533	4 516	2 960	2 788	3 343
Total	24 000	24 000	24 000	24 000	24 000	24 000	24 000	24 000	24 000	24 000	24 000	24 000	24 000	24 000	24 000
Mg#	58 1	51 6	54 7	53 5	60 6	57 8	60 1	59 1	56 4	56 1	57.0	56 7	37 3	35 1	42 0
Cr#	61 1	66 5	65 1	64 4	55 9	55 6	55 4	55 0	59 7	60 2	56 7	58 8	88 9	88 7	78 5

Rock	AD	AD	AD	AD	AD	OI	OI	OI	OI	OI	OI	OI	OI	OI	OI
Sample	L148	L148	L148	L275	L336	L066	L066	L066	L066	L073	L153	L176	L268	L268	L268
Location	1-Sp rim	2-Sp	3-Sp	6-Sp	7-Sp	2-Sp	3-Sp	4-Sp	5-Sp	1-Sp	9-Sp	2-Sp	3-Sp	4-Sp core	4-Sp rim
Type	LALPP	LALPP	LALPP	LALPP	LALPP	LALPP	LALPP	LALPP	LALPP	LALPP	LALPP	LALPP	LALPP	LALPP	LALPP
TiO2	0.42	0.36	0.37	0.23	0.18	na	na	na	na	na	0.12	0.13	0.20	0.18	0.18
V2O3	0.09	0.09	0.09	0.29	0.19	na	na	na	na	na	0.22	0.33	0.30	0.35	0.34
Al2O3	12.15	10.85	9.97	11.14	12.25	7.28	8.34	9.76	8.88	4.63	12.01	14.05	10.26	7.69	7.25
Cr2O3	51.76	52.89	55.24	55.63	56.30	54.58	55.03	52.55	55.16	61.63	56.25	51.55	54.07	57.28	57.24
FeO	26.94	27.10	25.38	24.19	22.43	29.75	28.45	29.29	27.09	27.12	22.49	27.55	27.02	27.42	27.82
MnO	0.48	0.27	0.38	0.29	0.36	na	na	na	na	na	0.29	0.32	0.32	0.33	0.37
NiO	0.07	0.07	0.09	0.03	0.03	na	na	na	na	na	0.08	0.09	0.08	0.06	0.05
MgO	8.61	8.70	9.06	7.96	8.62	7.17	7.34	7.37	7.64	6.88	9.23	7.08	7.69	6.46	5.90
Total	100.82	100.32	100.57	99.75	100.35	98.78	99.16	98.96	98.76	100.25	100.67	101.09	96.92	99.76	99.14
Ti	0.083	0.071	0.073	0.046	0.035	0.000	0.000	0.000	0.000	0.000	0.023	0.025	0.040	0.037	0.037
V	0.019	0.019	0.019	0.063	0.039	0.000	0.000	0.000	0.000	0.000	0.046	0.068	0.064	0.076	0.075
Al	3.740	3.379	3.103	3.508	3.801	2.358	2.678	3.118	2.849	1.503	3.701	4.338	3.239	2.482	2.369
Cr	10.686	11.046	11.532	11.744	11.717	11.862	11.857	11.264	11.880	13.424	11.632	10.677	11.448	12.402	12.538
Fe3+	1.389	1.416	1.201	0.594	0.372	1.780	1.465	1.618	1.271	1.073	0.574	0.866	1.169	0.967	0.944
Fe2+	4.495	4.570	4.403	4.807	4.585	5.060	5.018	5.023	4.899	5.175	4.345	5.170	4.882	5.313	5.502
Mn	0.107	0.060	0.084	0.065	0.079	0.000	0.000	0.000	0.000	0.000	0.063	0.070	0.072	0.076	0.086
Ni	0.015	0.015	0.019	0.006	0.006	0.000	0.000	0.000	0.000	0.000	0.017	0.019	0.017	0.013	0.011
Mg	3.467	3.426	3.566	3.168	3.384	2.940	2.982	2.977	3.101	2.825	3.598	2.767	3.069	2.635	2.436
Total	24.000	24.000	24.000	24.000	24.000	24.000	24.000	24.000	24.000	24.000	24.000	24.000	24.000	24.000	24.000
Mg#	43.5	42.8	44.7	39.7	42.6	36.7	37.3	37.2	38.8	35.3	45.3	34.9	38.6	33.2	30.7
Cr#	74.1	76.6	78.8	77.0	75.5	83.4	81.6	78.3	80.7	89.9	75.9	71.1	77.9	83.3	84.1

Rock	Oll	Oll	Oll	Oll	Oll	C	C	C	C	C	C	C	C	C	C
Sample	L271	L271	L351	L351	L351	L004	L004	L004	L004	L026	L026	L053	L055	L213	L213
Location	3-Sp	5-Sp	4-Sp	5-Sp	7-Sp	5-Sp core	5-Sp rim	6-Sp core	6-Sp rim	1-Sp	1-Sp	1-Sp	1-Sp	5-Sp	6-Sp
Type	LALPP	LALPP	LALPP	LALPP	LALPP	LALPP	LALPP	LALPP	LALPP	LALPP	LALPP	LALPP	LALPP	LALPP	LALPP
TiO2	0.14	0.08	0.07	0.13	0.12	0.16	0.16	0.15	0.15	na	na	0.16	0.18	na	na
V2O3	0.16	0.16	0.10	0.24	0.20	0.28	0.28	0.26	0.26	na	na	0.23	0.30	na	na
Al2O3	16.64	16.16	15.24	13.62	15.00	13.00	12.43	13.00	11.73	8.66	6.71	9.40	10.03	12.65	11.99
Cr2O3	50.78	50.86	52.28	54.22	52.68	52.38	53.21	53.00	55.05	56.92	57.72	56.15	55.90	53.60	51.06
FeO	21.76	22.06	23.44	22.28	22.95	27.28	26.93	26.51	25.84	26.58	26.47	25.96	25.88	28.63	28.82
MnO	0.30	0.28	0.31	0.27	0.30	0.38	0.37	0.38	0.40	na	na	0.34	0.33	na	na
NiO	0.06	0.06	0.07	0.05	0.04	0.09	0.07	0.09	0.07	na	na	0.07	0.05	na	na
MgO	11.33	10.29	7.55	8.66	8.44	7.19	6.28	7.52	7.35	6.52	8.15	7.84	7.20	6.42	6.66
Total	101.17	99.95	99.04	99.47	99.74	100.73	99.71	100.90	100.86	98.69	99.04	100.14	99.86	101.30	98.54
Ti	0.026	0.015	0.014	0.025	0.023	0.031	0.032	0.029	0.029	0.000	0.000	0.032	0.036	0.000	0.000
V	0.033	0.033	0.021	0.052	0.043	0.058	0.060	0.054	0.054	0.000	0.000	0.049	0.064	0.000	0.000
Al	4.936	4.888	4.758	4.231	4.630	4.042	3.937	4.027	3.659	2.911	2.160	2.971	3.184	3.942	3.832
Cr	10.102	10.318	10.951	11.304	10.908	10.920	11.306	11.013	11.526	12.391	12.471	11.902	11.908	11.202	10.942
Fe3+	0.878	0.729	0.243	0.362	0.373	0.917	0.633	0.847	0.702	0.798	1.369	1.015	0.772	0.856	1.226
Fe2+	3.701	4.006	4.950	4.550	4.653	5.102	5.419	4.980	5.021	5.324	4.680	4.807	5.059	5.472	5.308
Mn	0.063	0.060	0.069	0.060	0.066	0.084	0.083	0.084	0.091	0.000	0.000	0.076	0.074	0.000	0.000
Ni	0.012	0.012	0.015	0.010	0.008	0.019	0.015	0.019	0.015	0.000	0.000	0.015	0.011	0.000	0.000
Mg	4.251	3.937	2.981	3.405	3.296	2.826	2.514	2.947	2.903	2.676	3.320	3.134	2.892	2.528	2.692
Total	24.000	24.000	24.000	24.000	24.000	24.000	24.000	24.000	24.000	24.000	24.000	24.000	24.000	24.000	24.000
Mg#	53.5	49.6	37.8	42.8	41.5	35.6	31.7	37.2	36.6	33.5	41.5	39.5	36.4	31.6	33.6
Cr#	67.2	67.9	69.7	72.8	70.2	73.0	74.2	73.2	75.9	81.5	85.2	80.0	78.9	74.0	74.1

Rock	C	C	C	WB	WB	WB	WB	WB	WB	WB	WB	WB	WB	WB	WB
Sample	L213	L231	L231	L069	L283	L283	L283	L283	L283	L283	L283	L283	L288	L288	L288
Location	7-Sp	1-Sp	6-Sp	Sp	2-Sp	2-Sp	3-Sp	3-Sp	5-Sp	5-Sp	6-Sp	2-Sp	3-Sp	4-Sp	5-Sp
Type	LALPP	LALPP	LALPP	LALPP	core LALPP	rim LALPP	core LALPP	rim LALPP	core LALPP	rim LALPP	LALPP	LALPP	LALPP	LALPP	LALPP
TiO2	na	na	na	0.14	0.12	0.14	0.17	0.11	0.11	0.14	0.13	0.16	0.20	0.16	0.11
V2O3	na	na	na	0.25	0.30	0.26	0.28	0.23	0.30	0.29	0.22	0.31	0.29	0.26	0.23
Al2O3	13.05	6.62	6.46	10.45	11.64	10.31	9.69	6.77	10.44	10.11	6.84	10.21	9.79	11.57	11.14
Cr2O3	52.53	58.25	57.43	55.84	52.59	54.21	55.06	59.69	54.79	55.35	57.10	50.76	51.37	51.04	51.96
FeO	26.36	26.67	27.73	24.64	27.82	28.07	26.52	24.87	26.41	26.83	29.25	31.50	32.65	30.71	29.57
MnO	na	na	na	0.35	0.45	0.38	0.38	0.38	0.38	0.43	0.45	0.49	0.44	0.42	0.39
NiO	na	na	na	0.06	0.09	0.14	0.09	0.04	0.09	0.11	0.06	0.44	0.07	0.06	0.11
MgO	8.16	6.74	6.44	8.17	6.99	7.16	8.00	7.16	7.61	7.48	4.76	4.72	4.41	5.22	6.70
Total	100.09	98.28	98.07	99.90	99.99	100.66	100.18	99.25	100.12	100.74	98.81	98.59	99.22	99.44	100.21
Ti	0.000	0.000	0.000	0.028	0.024	0.028	0.034	0.022	0.022	0.028	0.027	0.033	0.041	0.032	0.022
V	0.000	0.000	0.000	0.054	0.063	0.055	0.059	0.050	0.063	0.061	0.049	0.068	0.063	0.056	0.049
Al	4.050	2.171	2.130	3.288	3.667	3.243	3.053	2.196	3.290	3.174	2.264	3.330	3.189	3.711	3.518
Cr	10.939	12.822	12.699	11.786	11.116	11.443	11.636	12.979	11.581	11.663	12.677	11.111	11.224	10.981	11.003
Fe3+	1.011	1.006	1.171	0.816	1.106	1.204	1.185	0.731	1.022	1.046	0.956	1.425	1.441	1.187	1.387
Fe2+	4.795	5.204	5.314	4.685	5.114	5.063	4.744	4.988	4.882	4.934	5.913	5.869	6.103	5.802	5.234
Mn	0.000	0.000	0.000	0.079	0.103	0.085	0.085	0.090	0.087	0.098	0.108	0.116	0.104	0.098	0.090
Ni	0.000	0.000	0.000	0.013	0.019	0.030	0.019	0.009	0.019	0.023	0.013	0.099	0.015	0.013	0.023
Mg	3.205	2.796	2.686	3.252	2.788	2.850	3.186	2.936	3.033	2.973	1.993	1.949	1.819	2.119	2.675
Total	24.000	24.000	24.000	24.000	24.000	24.000	24.000	24.000	24.000	24.000	24.000	24.000	24.000	24.000	24.000
Mg#	40.1	35.0	33.6	41.0	35.3	36.0	40.2	37.0	38.3	37.6	25.2	24.9	23.0	26.8	33.8
Cr#	73.0	85.5	85.6	78.2	75.2	77.9	79.2	85.5	77.9	78.6	84.8	76.9	77.9	74.7	75.8

Rock	D	D	D	D	D	D	D	D	D	D	D	D	D	D
Sample	L108	L108	L108	L108	L108	L298	L298	L298	L298	L299	L299	L299	L299	L299
Location	2-Sp	3-Sp	3-Sp	4-Sp	5-Sp	1-Sp	1-Sp	2-Sp	4-Sp	3-Sp	3-Sp	5-Sp	6-Sp	6-Sp
Type	HALPPG	core HALPPG	rim HALPPG	HALPPG	HALPPG	core HALPPG	rim HALPPG	HALPPG	HALPPG	core HALPPG	rim HALPPG	HALPPG	core HALPPG	rim HALPPG
TiO2	0.47	0 35	0.32	0.46	0.45	0.48	0.39	0.46	0.49	0.39	0.37	0.36	0.40	0.43
V2O3	0.17	0.18	0 16	0.16	0 18	0.15	0.18	0.19	0.20	0.18	0.19	0.19	0 16	0.17
Al2O3	36 12	39 75	40.21	37 63	39.37	35.88	36 98	30 88	36.72	39.67	39.59	40.53	39 10	40.10
Cr2O3	24.74	22.98	22.79	23.89	23.95	28.17	26 67	23 67	27.35	23 20	22.92	22.44	24 22	22.96
FeO	22 82	18 89	18.94	20.26	18.37	17.40	18 86	31 56	19.45	19.59	20 07	19 75	18 93	19 55
MnO	0.20	0 21	0 21	0 22	0 18	0 19	0 13	0 24	0 22	0 15	0 16	0 18	0 13	0 17
NiO	0.26	0 20	0.19	0 20	0 21	0.23	0 23	0.29	0 21	0 21	0.20	0 21	0 20	0.16
MgO	14 38	15 99	16 30	15.47	16.13	16.45	16 33	12.19	15 57	15.82	15 61	15.95	16.13	15 97
Total	99 16	98 55	99 12	98 28	98 84	98.95	99.77	99.47	100.21	99.20	99 11	99 61	99.27	99 51
Ti	0 082	0 060	0 054	0 080	0 077	0 083	0.067	0 083	0 084	0 067	0 063	0 061	0 068	0 073
V	0 032	0 033	0 029	0 030	0 033	0 028	0 033	0 036	0 037	0 033	0 035	0 034	0 029	0 031
Al	9 870	10 667	10 706	10 228	10 550	9 716	9 913	8 682	9 868	10 606	10 608	10 760	10 452	10 671
Cr	4 535	4 137	4 070	4 356	4 306	5 117	4 796	4 465	4 931	4 161	4 120	3 996	4 343	4 098
Fe3+	1 399	1 043	1 086	1 227	0 958	0 974	1 125	2 652	0 997	1 067	1 111	1 087	1 039	1 055
Fe2+	3 025	2 554	2 492	2 681	2 535	2 389	2 462	3 645	2 712	2 650	2 705	2 633	2 551	2 637
Mn	0 039	0 041	0 040	0 043	0 035	0 037	0 025	0 048	0 042	0 029	0 031	0 034	0 025	0 033
Ni	0 048	0 037	0 035	0 037	0 038	0 043	0 042	0 056	0 039	0 038	0 037	0 038	0 036	0 029
Mg	4 969	5 429	5 488	5 319	5 469	5 634	5 537	4 334	5 291	5 350	5 291	5 355	5 455	5 375
Total	24 000	24 000	24 000	24 000	24 000	24 000	24 000	24.000	24 000	24 000	24 000	24 000	24 000	24 000
Mg#	62 2	68 0	68 8	66 5	68 3	70 4	69 2	54 3	66 1	66 9	66 2	67 0	68 1	67 1
Cr#	31 5	27 9	27 5	29 9	29 0	34 5	32 6	34 0	33 3	28 2	28 0	27 1	29 4	27 7

Rock	D	D	D	D	D	D	D	D	D	D	W	W	W	W	W
Sample	L299	L299	L299	L299	L302	L302	L350	L350	L350	L350	L109	L109	L109	L109	L109
Location	E-Sp	F-Sp	G-Sp	G-Sp	5-Sp	5-Sp	3-Sp	3-Sp	4-Sp	4-Sp	1-Sp	2-Sp	3-Sp	3-Sp	5-Sp
Type	HALPPG	HALPPG	core HALPPG	rim HALPPG	core HALPPG	rim HALPPG	core HALPPG	rim HALPPG	core HALPPG	rim HALPPG	HALPPG	HALPPG	core HALPPG	rim HALPPG	HALPPG
TiO2	0.42	0.41	0.35	0.55	0.37	0.36	0.46	0.54	0.44	0.59	0.27	0.41	0.62	0.40	0.35
V2O3	0.19	0.20	0.16	0.21	0.21	0.21	0.18	0.18	0.21	0.19	0.24	0.21	0.19	0.16	0.23
Al2O3	40.69	30.85	40.08	38.69	39.26	38.27	36.99	33.84	36.24	32.82	43.26	43.55	38.71	42.48	42.75
Cr2O3	23.08	22.95	22.28	22.56	24.80	24.20	29.02	29.54	28.28	27.01	22.45	21.86	25.21	22.92	22.84
FeO	18.62	19.34	19.80	21.50	20.20	22.80	17.90	21.93	19.67	25.23	17.17	16.77	19.11	17.15	16.74
MnO	0.18	0.13	0.12	0.18	0.23	0.23	0.22	0.24	0.16	0.18	0.18	0.19	0.21	0.18	0.17
NiO	0.18	0.20	0.20	0.21	0.26	0.27	0.24	0.18	0.23	0.32	0.16	0.20	0.23	0.16	0.17
MgO	16.28	15.73	15.84	15.50	15.80	14.77	16.14	14.84	15.62	13.82	15.74	16.00	14.79	15.78	15.51
Total	99.64	98.82	98.83	99.40	101.13	101.21	101.16	101.31	100.87	100.17	99.47	99.19	99.07	99.24	98.76
Ti	0.071	0.070	0.060	0.094	0.062	0.061	0.078	0.093	0.075	0.104	0.045	0.069	0.107	0.068	0.059
V	0.034	0.036	0.029	0.038	0.038	0.039	0.033	0.034	0.039	0.036	0.043	0.038	0.035	0.029	0.042
Al	10.776	10.687	10.728	10.380	10.361	10.189	9.829	9.150	9.704	9.035	11.410	11.481	10.471	11.254	11.378
Cr	4.100	4.129	4.000	4.060	4.390	4.322	5.173	5.359	5.080	4.988	3.973	3.866	4.575	4.073	4.077
Fe3+	0.947	1.007	1.123	1.333	1.086	1.329	0.809	1.271	1.027	1.733	0.483	0.477	0.705	0.509	0.386
Fe2+	2.552	2.673	2.638	2.760	2.696	2.695	2.566	2.936	2.709	3.196	2.731	2.660	2.963	2.715	2.775
Mn	0.034	0.025	0.023	0.035	0.044	0.045	0.043	0.048	0.031	0.036	0.034	0.036	0.041	0.034	0.033
Ni	0.033	0.037	0.037	0.038	0.046	0.048	0.044	0.034	0.043	0.059	0.029	0.036	0.042	0.029	0.031
Mg	5.452	5.336	5.362	5.261	5.276	4.973	5.424	5.076	5.291	4.813	5.252	5.337	5.061	5.289	5.221
Total	24.000	24.000	24.000	24.000	24.000	24.000	24.000	24.000	24.000	24.000	24.000	24.000	24.000	24.000	24.000
Mg#	68.1	66.6	67.0	65.6	66.2	62.4	67.9	63.4	66.1	60.1	65.8	66.7	63.1	66.1	65.3
Cr#	27.6	27.9	27.2	28.1	29.8	29.8	34.5	36.9	34.4	35.6	25.8	25.2	30.4	26.6	26.4

Rock	W	W	W	W	W	W	W	W	W	W	W	W	W	C
Sample	L109	L114	L114	L114	L114	L301	L301	L301	L301	L316	L316	L316	L316	L241
Location	6-Sp	1-Sp	1-Sp	2-Sp	3-Sp	6-Sp	6-Sp	7-Sp	7-Sp	1-Sp	1-Sp	2-Sp	2-Sp	1-Sp
		core	rim			core	rim	core	rim	core	rim	core	rim	
Type	HALPPG	HALPPG	HALPPG	HALPPG	HALPPG	HALPPG	HALPPG	HALPPG	HALPPG	HALPPG	HALPPG	HALPPG	HALPPG	HALPPG
TiO2	0.23	0 51	0.45	0.43	0.62	0 32	0.21	0.45	0.25	0.39	0.29	0.55	0.43	0.43
V2O3	0.14	0 21	0.22	0.20	0.21	0.21	0.16	0.19	0.16	0.18	0.17	0.22	0.21	0.26
Al2O3	45.26	42 27	38.52	42 00	41.17	45.40	47.16	40.99	44.61	42.40	42.77	40.42	41.73	29 00
Cr2O3	20.84	20.77	23.36	21.22	21.51	21.23	19.59	24.84	21.47	24.17	24.02	25.78	21.38	34.37
FeO	15 98	19.90	21 79	19.20	20.08	17 83	17 59	19 49	18.54	16 62	16.79	17.49	18.15	24 92
MnO	0.16	0.21	0.22	0.18	0.18	0.24	0 14	0 20	0.21	0.21	0.12	0.16	0 22	0.23
NiO	0.20	0 21	0.15	0.19	0.25	0.23	0.16	0.16	0 24	0.19	0.17	0.20	0.24	0.10
MgO	16.61	14 75	13.41	14 91	14 92	15 92	16.07	14 89	15.76	15.05	15.24	15.15	16.21	9 41
Total	99.42	98 83	98.12	98.34	98.94	101 39	101 09	101.21	101.26	99.22	99.57	99.97	98.57	98.71
Ti	0 038	0 087	0 079	0 074	0 106	0 052	0 035	0.076	0 042	0 066	0 049	0.094	0 073	0 081
V	0 025	0 038	0 041	0 037	0 038	0 038	0 028	0.035	0.029	0 033	0 031	0.040	0.038	0.052
Al	11 795	11 305	10 589	11 277	11 032	11 702	12.096	10.811	11 548	11 294	11.333	10.774	11.103	8 454
Cr	3 644	3 726	4 308	3.822	3 867	3 671	3.371	4.396	3 730	4 319	4 270	4 610	3 817	6 723
Fe3+	0 460	0 757	0 904	0.717	0 851	0 486	0 434	0 607	0.609	0.222	0 269	0.390	0 896	0.610
Fe2+	2 496	3 019	3 346	2 940	2 967	2 775	2 767	3 040	2 797	2 920	2 888	2 918	2 531	4 544
Mn	0 030	0 040	0 043	0 035	0 035	0 045	0 026	0 039	0 040	0 040	0 023	0 031	0 042	0 048
Ni	0 036	0 038	0 028	0 035	0 046	0 041	0 029	0 029	0 043	0 035	0 031	0 036	0 044	0 020
Mg	5 477	4 989	4 662	5 064	5 058	5 191	5 213	4 967	5 162	5 072	5 108	5 108	5 456	3 469
Total	24 000	24 000	24 000	24 000	24 000	24 000	24.000	24 000	24 000	24 000	24 000	24 000	24 000	24 000
Mg#	68 7	62 3	58 2	63 3	63 0	65 2	65 3	62.0	64 9	63 5	63 9	63 6	68 3	43 3
Cr#	23 6	24 8	28 9	25 3	26.3	23 9	21 8	28 9	24 4	27 7	27 4	30 0	25 6	44 3

Rock	H	H	H	H	H	H	C	H	H	H	D	D	H	H	AP
Sample	L115	L115	L115	L115	L115	L115	L115	L177	L177	L177	L221	L221	L221	L221	L274
Location	1-Sp	2-Sp	3-Sp	4-Sp	6-Sp	8-Sp	9-Sp	1-Sp	6-Sp	11-Sp	2-Sp	11-Sp	7-Sp	12-Sp	5-Sp
Type	LALPP	LALPP	LALPP	LALPP	LALPP	LALPP	HALPPG	LALPP	LALPP	LALPP	HALPPG	HALPPG	LALPP	LALPP	HALPPG
TiO2	0.06	0.16	0.27	0.48	0.48	0.18	0.66	0.86	0.62	0.28	0.55	0.55	0.11	0.14	1.39
V2O3	0.25	0.31	0.35	0.35	0.37	0.30	0.43	0.24	0.24	0.28	0.15	0.18	0.14	0.16	0.30
Al2O3	13.81	13.54	12.78	11.65	11.97	12.42	12.57	26.09	16.61	22.40	38.82	37.46	13.60	15.22	20.20
Cr2O3	54.11	54.05	54.21	54.47	54.68	54.67	53.40	38.17	47.78	43.75	23.96	24.49	52.30	50.23	37.70
FeO	21.64	21.80	22.39	22.98	21.67	21.82	21.92	22.96	24.12	23.21	24.21	25.30	23.41	23.58	35.76
MnO	0.31	0.33	0.33	0.32	0.29	0.31	0.33	0.38	0.23	0.34	0.22	0.23	0.26	0.30	0.32
NiO	0.07	0.07	0.05	0.06	0.07	0.07	0.13	0.12	0.09	0.04	0.15	0.17	0.08	0.04	0.12
MgO	9.34	9.72	9.83	9.02	9.38	9.17	9.52	11.17	9.29	9.20	14.32	13.83	8.33	8.96	5.51
Total	99.59	99.98	100.21	99.33	98.91	98.95	98.96	99.99	98.90	99.49	102.38	102.21	98.22	98.63	101.30
Ti	0.012	0.031	0.053	0.096	0.096	0.036	0.131	0.158	0.122	0.053	0.093	0.094	0.022	0.027	0.269
V	0.052	0.065	0.073	0.074	0.079	0.064	0.091	0.048	0.049	0.056	0.026	0.032	0.030	0.034	0.062
Al	4.264	4.158	3.926	3.645	3.745	3.883	3.916	7.528	5.094	6.679	10.250	9.979	4.283	4.720	6.118
Cr	11.204	11.133	11.168	11.430	11.477	11.465	11.161	7.389	9.829	8.751	4.243	4.377	11.045	10.445	7.661
Fe3+	0.456	0.581	0.727	0.659	0.508	0.516	0.569	0.719	0.784	0.408	1.294	1.424	0.599	0.747	1.621
Fe2+	4.283	4.169	4.152	4.442	4.303	4.324	4.277	3.982	4.463	4.502	3.242	3.358	4.630	4.441	6.066
Mn	0.069	0.073	0.073	0.072	0.065	0.070	0.074	0.078	0.050	0.072	0.041	0.043	0.058	0.066	0.069
Ni	0.015	0.015	0.010	0.013	0.015	0.015	0.028	0.023	0.004	0.008	0.027	0.031	0.017	0.008	0.024
Mg	3.645	3.775	3.818	3.569	3.713	3.628	3.753	4.075	3.604	3.470	4.783	4.662	3.317	3.512	2.109
Total	24.000	24.000	24.000	24.000	24.000	24.000	24.000	24.000	24.000	24.000	24.000	24.000	24.000	24.000	24.000
Mg#	46.0	47.5	47.9	44.6	46.3	45.6	46.7	50.6	44.7	43.5	59.6	58.1	41.7	44.2	25.8
Cr#	72.4	72.8	74.0	75.8	75.4	74.7	74.0	49.5	65.9	56.7	29.3	30.5	72.1	68.9	55.6

Rock	AP	AP	OI	H-X	H-X	H-X	C	C	CR-X	CR-X	CR-X	OI	AD	AD	AD
Sample	L274	L274	L274	L327	L327	L328	L328	L330	L326	L326	L326	L333	L333	L333	L333
Location	6-Sp	7-Sp	8-Sp	4-Sp	5-Sp	3-Sp	9-Sp	1-Sp	3-Sp	3-Sp	4-Sp	10-Sp	11-Sp	12-Sp	13-Sp
Type	HALPPG	HALPPG	LALPP	LALPP	LALPP	LALPP	HALPPG	HALPPG	LALPP	LALPP	LALPP	LALPP	LALPP	LALPP	LALPP
TiO2	0 73	1 32	0 33	0 42	0 91	1 31	0 63	1 12	0 70	0 72	0 61	0 59	0 67	0 29	0 40
V2O3	0 19	0 25	0 22	0 24	0 28	0 32	0 28	0 41	0 19	0 21	0 21	0 19	0 29	0 13	0 26
Al2O3	9 73	20 12	18 97	13 24	17 37	23 26	36 72	28 30	18 43	21 90	23 60	8 19	24 13	38 43	39 03
Cr2O3	51 35	38 94	44 61	51 56	45 50	36 21	27 58	32 18	47 38	44 16	42 64	56 00	38 96	24 61	27 04
FeO	32 48	31 96	26 66	26 19	27 96	27 28	24 69	26 95	21 94	20 66	19 81	30 03	26 70	22 94	20 65
MnO	0 36	0 30	0 42	0 29	0 31	0 38	0 23	0 24	0 23	0 08	0 18	0 43	0 27	0 29	0 29
NiO	0 07	0 11	0 02	0 07	0 09	0 10	0 16	0 11	0 18	0 11	0 05	0 07	0 07	0 03	0 07
MgO	4 27	6 17	7 30	8 88	8 01	9 93	11 63	9 96	11 49	12 94	12 49	4 84	9 56	14 21	12 53
Total	99 17	99 18	98 53	100 67	100 42	98 79	101 91	99 26	100 54	100 77	99 58	100 35	100 66	100 92	100 27
Ti	0 152	0 260	0 064	0 083	0 176	0 249	0 110	0 206	0 132	0 133	0 113	0 122	0 125	0 049	0 070
V	0 042	0 053	0 046	0 049	0 059	0 064	0 051	0 080	0 038	0 041	0 042	0 041	0 058	0 024	0 048
Al	3 175	6 188	5 857	4 069	5 283	6 904	9 979	8 200	5 450	6 311	6 844	2 655	7 048	10 284	10 603
Cr	11 245	8 035	9 240	10 634	9 283	7 209	5 028	6 254	9 398	8 537	8 296	12 175	7 633	4 418	4 927
Fe3+	1 234	1 205	0 728	1 081	1 023	1 326	0 722	1 054	0 851	0 846	0 592	0 883	1 010	1 177	0 282
Fe2+	6 289	5 770	5 114	4 632	5 010	4 420	4 039	4 486	3 753	3 379	3 485	6 023	4 524	3 180	3 698
Mn	0 083	0 065	0 094	0 063	0 067	0 080	0 044	0 049	0 048	0 016	0 037	0 101	0 056	0 055	0 056
Ni	0 015	0 023	0 004	0 014	0 018	0 020	0 029	0 021	0 036	0 021	0 010	0 015	0 014	0 005	0 013
Mg	1 765	2 401	2 852	3 374	3 081	3 729	3 997	3 649	4 295	4 716	4 581	1 983	3 532	4 809	4 303
Total	24 000	24 000	24 000	24 000	24 000	24 000	24 000	24 000	24 000	24 000	24 000	24 000	24 000	24 000	24 000
Mg#	21 9	29 4	35 8	42 1	38 1	45 8	49 7	44 9	53 4	58 3	56 8	24 8	43 8	60 2	53 8
Cr#	78 0	56 5	61 2	72 3	63 7	51 1	33 5	43 3	63 3	57 5	54 8	82 1	52 0	30 0	31 7

Rock	AD	AD	OI	OI	OI	C	C
Sample	L333	L333	L348	L348	L348	L236	L236
Location	14-Sp	14-Sp	4-Sp	5-Sp	6-Sp	5-Sp	7-Sp
Type	LALPP	LALPP	LALPP	LALPP	LALPP		
TiO2	0.40	0.45	0.25	0.13	0.25	0.45	0.76
V2O3	0.21	0.26	0.11	0.15	0.18	0.23	0.24
Al2O3	39.12	38.34	29.11	41.08	29.63	18.14	19.04
Cr2O3	26.15	28.90	32.80	25.91	37.19	47.34	44.61
FeO	19.72	21.90	28.78	19.90	20.50	26.85	26.80
MnO	0.17	0.25	0.25	0.19	0.16	0.27	0.34
NiO	0.10	0.03	0.12	0.03	0.13	0.11	0.12
MgO	13.17	12.10	9.36	14.14	12.00	6.84	9.45
Total	99.05	100.23	100.77	101.53	100.03	100.23	101.34
Ti	0.071	0.080	0.045	0.022	0.045	0.089	0.144
V	0.039	0.049	0.022	0.026	0.034	0.047	0.048
Al	10.682	9.998	8.331	10.857	8.388	5.560	5.648
Cr	4.789	5.334	6.298	4.594	7.061	9.733	8.878
Fe3+	0.349	0.460	1.259	0.479	0.427	0.483	1.138
Fe2+	3.472	3.814	4.584	3.253	3.691	5.356	4.504
Mn	0.033	0.049	0.051	0.036	0.032	0.059	0.072
Ni	0.018	0.006	0.023	0.005	0.025	0.023	0.024
Mg	4.547	4.211	3.387	4.728	4.296	2.651	3.545
Total	24.000	24.000	24.000	24.000	24.000	24.000	24.000
Mg#	56.7	52.5	42.5	59.2	53.8	33.1	44.0
Cr#	31.0	34.8	43.1	29.7	45.7	63.6	61.1

TABLE A4.1. Major and trace element analyses (oxides in wt.%, trace elements in ppm)

Rock	H	H	H	H	H	D	D	D	D	D	AD	AD	AD	AD	AD
Sample	L097	L103	L106	L218	L225	L216	L217	L246	L254	L262	L132	L140	L172	L200	L265
Type	LALPP	LALPP	LALPP	LALPP	LALPP	LALPP	LALPP	LALPP	LALPP	LALPP	LALPP	LALPP	LALPP	LALPP	LALPP
SiO2	37.30	35.20	40.00	38.80	38.30	38.80	35.80	na	33.40	39.60	35.80	37.00	38.40	35.10	na
TiO2	na	bdl	bdl	bdl	bdl	bdl	bdl	na	bdl	na	na	na	na	na	bdl
Al2O3	0.24	0.23	0.36	0.19	0.18	0.39	0.12	0.29	0.21	0.11	0.23	0.06	na	0.21	na
Fe2O3	3.44	3.02	2.41	3.37	4.13	2.79	2.97	na	4.42	4.18	4.09	3.61	3.99	3.58	na
FeO	4.04	4.35	4.43	4.01	3.02	4.63	4.65	na	3.28	3.91	3.30	3.94	3.23	3.55	na
MnO	0.11	0.11	0.12	0.11	0.10	0.12	0.10	na	0.11	0.11	0.10	0.11	0.10	0.10	na
MgO	41.75	42.25	40.55	40.21	40.23	39.49	42.56	na	40.28	41.30	40.77	42.69	39.48	41.54	na
CaO	0.28	0.40	0.80	0.34	0.26	0.88	0.14	na	0.24	0.14	0.64	0.44	0.41	0.36	na
Na2O	0.02	0.02	0.02	0.02	0.02	0.02	0.01	na	0.01	0.01	0.04	0.01	0.05	0.03	na
K2O	0.00	0.00	0.00	0.00	0.00	0.00	0.00	na	0.00	0.00	0.00	0.00	0.01	0.01	na
P2O5	0.00	0.00	0.00	0.00	0.01	0.00	0.00	na	0.00	0.00	0.01	0.00	0.00	0.00	na
LOI	12.96	14.51	11.00	12.88	13.93	10.70	12.84	na	16.32	10.39	15.14	11.90	14.17	15.00	na
Total	100.14	100.09	99.89	99.93	100.18	97.82	99.19		98.27	99.75	100.12	99.76	99.84	99.48	
FeO(t)	7.14	7.07	6.60	7.04	6.74	7.14	7.32	na	7.26	7.67	6.98	7.19	6.82	6.77	na
Mg#	91.2	91.4	91.6	91.1	91.4	90.8	91.2		90.8	90.6	91.2	91.4	91.2	91.6	
Cr#			44.2	51.0		77.3	61.0		72.1						
CaO/Al2O3	1.17	1.74	2.22	1.79	1.44	2.26	1.17		1.14	1.27	2.78	7.33		1.71	
Sc	na	na	6	4	na	bdl	bdl	na	bdl	na	na	na	na	na	16
V	na	na	28	12	na	63	bdl	na	15	na	na	na	na	na	57
Cr	na	na	2910	2013	na	13539	1914	na	5536	na	na	na	na	na	9959
Ni	na	na	1908	1992	na	2289	2211	na	2186	na	na	na	na	na	1081
Cu	na	na	bdl	bdl	na	bdl	bdl	na	bdl	na	na	na	na	na	bdl
Zn	na	na	24	26	na	37	26	na	25	na	na	na	na	na	36
Rb	na	bdl	bdl	bdl	bdl	bdl	bdl	na	bdl	bdl	bdl	bdl	bdl	bdl	bdl
Sr	na	8	2	bdl	4	1	bdl	na	15	bdl	11	2	3	2	7
Y	na	bdl	bdl	bdl	bdl	bdl	bdl	na	bdl	bdl	bdl	bdl	bdl	bdl	bdl
Zr	na	bdl	bdl	bdl	bdl	bdl	bdl	na	bdl	bdl	bdl	bdl	bdl	bdl	bdl

Rock	AD	AD	OI	OI	OI	OI	OI	OI	OI	OII	OII	C	C	C	C
Sample	L266	L275	L066	L067	L068	L071	L073	L267	L268	L271	L351	L004	L012	L026	L211
Type	LALPP	LALPP	LALPP	LALPP	LALPP	LALPP	LALPP	LALPP	LALPP	LALPP	LALPP	LALPP	LALPP	LALPP	LALPP
SiO2	39.20	38.60	54.10	53..0	53.70	53.00	54.80	53.30	54.90	40.70	na	48.70	50.20	53.20	na
TiO2	bdl	bdl	na	na	bdl	bdl	na	bdl	bdl	na	na	na	na	bdl	bdl
Al2O3	1.24	1.88	0.60	na	1.00	0.48	0.39	0.70	0.64	0.29	0.66	0.76	0.82	0.67	na
Fe2O3	4.52	3.44	0.62	1.18	1.37	0.35	1.19	0.98	1.06	3.50	na	1.15	1.10	0.29	na
FeO	2.70	4.21	4.73	5.24	4.81	5.50	4.76	5.47	5.18	3.42	na	3.42	3.20	3.43	na
MnO	0.11	0.13	0.13	0.15	0.14	0.11	0.10	0.11	0.15	0.11	na	0.11	0.11	0.11	na
MgO	36.45	38.10	33.95	33.95	33.65	35.26	34.85	33.98	32.25	39.52	na	27.35	24.30	21.41	na
CaO	1.16	1.10	2.80	1.80	1.70	1.30	1.54	1.24	1.08	0.34	na	14.60	17.55	19.94	na
Na2O	0.11	0.14	0.08	0.12	0.12	0.07	0.04	0.06	0.06	0.14	na	0.17	0.21	0.16	na
K2O	0.00	0.01	0.01	0.03	0.02	0.02	0.01	0.01	0.01	0.00	na	0.00	0.00	0.00	na
P2O5	0.05	0.00	0.03	0.01	0.01	0.01	0.00	0.00	0.00	0.05	na	0.01	0.01	0.02	na
LOI	13.02	12.23	1.94	3.76	3.77	3.08	1.42	3.06	2.87	12.45	na	3.44	2.20	1.38	na
Total	98.56	97.84	98.99	99.34	100.29	99.18	99.10	98.91	98.20	100.52		99.71	99.70	100.61	
Fe0(t)	6.77	7.31	5.29	6.30	6.04	5.81	5.83	6.35	6.13	6.57	na	4.45	4.19	3.69	na
Mg#	90.6	90.3	92.0	90.6	90.8	91.5	91.4	90.5	90.4	91.5		91.6	91.2	91.2	
Cr#	30.8	20.9			31.2	44.7		39.6	42.4					32.4	
CaO/Al2O3	0.94	0.59	4.67		1.70	2.71	3.95	1.77	1.69	1.17		19.21	21.40	29.76	
Sc	23	18	na	na	20	15	na	17	19	na	na	na	na	42	37
V	40	32	na	na	69	42	na	52	52	na	na	na	na	94	97
Cr	5635	5057	na	na	4631	3952	na	4686	4799	na	na	na	na	3275	4781
Ni	943	948	na	na	721	775	na	711	703	na	na	na	na	744	948
Cu	bdl	bdl	na	na	bdl	bdl	na	bdl	bdl	na	na	na	na	313	176
Zn	26	29	na	na	20	17	na	23	21	na	na	na	na	bdl	bdl
Rb	bdl	bdl	1	na	1	1	na	bdl	bdl	bdl	na	bdl	na	bdl	bdl
Sr	13	12	4	na	4	6	na	3	2	bdl	na	6	na	19	5
Y	bdl	1	bdl	na	bdl	bdl	na	bdl	bdl	bdl	na	bdl	na	bdl	bdl
Zr	1	2	bdl	na	bdl	bdl	na	bdl	bdl	bdl	na	bdl	na	bdl	bdl

Rock	C	C	C	C	C	C	WB	WB	W	D	D	D	W	W	W
Sample	L212	L213	L214	L231	L290	L293	L283	L288	L201	L107	L302	L324	L093	L307	L316
Type	LALPP	LALPP	LALPP	LALPP	LALPP	LALPP	LALPP	LALPP	LALPP	HALPPG	HALPPG	HALPPG	HALPPG	HALPPG	HALPPG
SiO2	52.40	54.60	48.00	50.70	53.80	50.50	53.70	53.60	35.90	33.40	34.20	35.00	39.10	38.00	36.90
TiO2	bdl	bdl	bdl	na	na	bdl	bdl	na	na	na	bdl	bdl	0.15	0.04	0.08
Al2O3	0.89	0.91	0.61	0.58	0.75	0.75	0.67	0.96	0.19	1.07	1.27	0.18	na	1.86	2.47
Fe2O3	0.35	0.45	0.97	0.93	0.40	0.47	1.14	0.45	4.32	3.41	4.42	3.34	4.29	3.50	2.75
FeO	3.37	2.78	4.70	2.81	3.41	2.76	2.41	2.82	2.82	5.77	4.58	5.73	4.61	5.02	5.69
MnO	0.11	0.11	0.12	0.11	0.11	0.09	0.11	0.11	0.10	0.14	0.12	0.14	0.14	0.13	0.14
MgO	21.96	20.00	27.87	23.18	22.14	21.74	23.58	20.20	40.46	42.05	39.60	40.27	32.09	39.12	36.47
CaO	19.90	20.15	12.78	17.45	17.42	19.68	15.12	19.88	0.58	0.20	0.32	0.48	6.34	0.98	3.22
Na2O	0.17	0.18	0.12	0.19	0.21	0.09	0.28	0.27	0.03	0.02	0.01	0.02	0.13	0.09	0.11
K2O	0.00	0.00	0.00	0.00	0.00	0.00	0.01	0.00	0.00	0.00	0.00	0.00	0.00	0.00	0.00
P2O5	0.00	0.00	0.00	0.00	0.04	0.00	0.01	0.00	0.01	0.00	0.01	0.00	0.00	0.00	0.00
LOI	0.92	0.71	2.82	2.71	1.33	2.80	1.11	1.25	14.91	13.22	14.19	12.75	9.41	11.78	10.70
Total	100.07	99.89	97.99	98.66	99.61	98.88	98.17	99.54	99.32	99.28	99.72	97.91	96.26	100.52	98.53
Fe0(t)	3.68	3.18	5.57	3.65	3.77	3.18	3.44	3.22	6.71	8.84	8.56	8.74	8.47	8.17	8.16
Mg#	91.4	91.8	89.9	91.9	91.3	92.4	92.4	91.8	91.5	89.5	89.2	89.2	87.1	89.5	88.8
Cr#	31.2	32.0	32.2			23.7	41.0				24.9	53.9		17.4	11.4
CaO/Al2O3	22.36	22.14	20.95	30.09	23.23	26.24	22.57	20.71	3.05	0.19	0.25	2.67		0.53	1.30
Sc	40	39	29	na	na	47	27	na	na	na	bdl	bdl	28	4	13
V	106	104	72	na	na	106	68	na	na	na	25	15	116	33	54
Cr	4125	4359	2953	na	na	2373	4747	na	na	na	4289	2145	4083	3998	3229
Ni	794	558	1354	na	na	560	493	na	na	na	2115	2029	1281	2088	1870
Cu	132	na	125	na	na	na	na	na	na	na	bdl	bdl	424	na	3
Zn	bdl	bdl	bdl	na	na	bdl	bdl	na	na	na	35	35	29	31	26
Rb	bdl	bdl	bdl	bdl	bdl	bdl	bdl	bdl	bdl	na	bdl	bdl	bdl	bdl	bdl
Sr	2	2	2	11	11	2	53	64	bdl	na	16	8	14	9	11
Y	1	2	bdl	bdl	bdl	2	1	1	bdl	na	bdl	bdl	3	bdl	2
Zr	bdl	bdl	bdl	bdl	bdl	bdl	2	2	bdl	na	bdl	bdl	4	1	3

Rock	W	W	C	C	C	C	C	C	G	G	G	G	AP	AMPT	AMPT
Sample	L317	L331	L186	L241	L296	L297	L312	L328	L090	L294	L295	L313	L273	SD194	SD380
Type	HALPPG	HALPPG	HALPPG	HALPPG	HALPPG	HALPPG	HALPPG	HALPPG	HALPPG	HALPPG	HALPPG	HALPPG	HALPPG	UC	UC
SiO2	36.90	35.80	38.30	40.10	46.70	47.60	45.00	na	47.30	44.10	42.10	46.70	36.70	43.60	43.40
TiO2	na	0.03	0.10	0.12	0.45	0.44	0.36	0.25	0.21	0.18	0.22	0.20	0.36	1.40	1.20
Al2O3	2.52	2.48	2.06	1.46	4.34	5.15	8.31	na	19.10	15.87	15.56	21.33	2.87	14.70	16.80
Fe2O3	2.84	3.55	5.13	5.12	1.44	0.78	0.98	na	0.13	0.48	1.34	0.28	5.75	1.10	1.03
FeO	5.87	6.28	4.35	3.34	5.55	5.54	4.12	na	3.72	4.57	2.97	2.06	5.27	8.44	8.08
MnO	0.13	0.14	0.14	0.13	0.13	0.13	0.10	na	0.07	0.09	0.07	0.06	0.15	0.14	0.14
MgO	36.91	38.11	33.39	31.05	21.80	20.64	19.03	na	11.40	13.92	12.69	8.23	34.64	12.69	9.50
CaO	3.30	1.42	4.92	6.54	14.42	16.42	15.45	na	14.10	11.84	12.48	14.85	2.88	10.24	12.74
Na2O	0.11	0.11	0.11	0.11	0.60	0.57	1.02	na	1.55	3.96	3.92	2.75	0.32	2.21	1.83
K2O	0.00	0.01	0.00	0.00	0.01	0.01	0.08	na	0.09	0.28	0.09	0.17	0.05	0.17	0.55
P2O5	0.00	0.00	0.00	0.00	0.01	0.00	0.00	na	0.09	0.00	0.00	0.00	0.00	0.01	0.01
LOI	10.46	10.78	11.56	10.13	3.80	2.15	5.12	na	2.02	4.10	8.20	3.33	11.33	3.60	3.77
Total	99.04	98.71	100.06	98.10	99.25	99.43	99.57		99.78	99.39	99.64	99.96	99.96	98.50	99.05
FeO(t)	8.43	9.47	8.97	7.95	6.85	6.24	5.00	na	3.84	5.00	4.18	2.31	10.44	9.43	9.01
Mg#	88.6	87.8	86.9	87.4	85.0	85.5	87.2		84.1	83.2	84.4	86.4	85.5	70.6	65.3
Cr#		12.3	11.0	9.0	5.8		3.7		0.3	0.6	0.7	0.7			
CaO/Al2O3	1.31	0.57	2.39	4.48	3.32	3.19	1.86		0.74	0.75	0.80	0.70	1.00	0.70	0.76
Sc	na	5	18	28	61	na	53	29	34	32	27	30	na	na	na
V	na	37	77	97	257	na	182	129	109	105	88	90	na	na	na
Cr	na	3583	2595	1475	2723	na	3228	1703	605	1029	1057	1488	na	na	na
Ni	na	1376	1294	1274	657	na	724	1275	242	385	509	326	na	na	na
Cu	na	bdl	237	193	18	na	22	na	27	58	33	21	na	na	na
Zn	na	36	29	24	19	na	11	34	bdl	13	9	bdl	na	na	na
Rb	bdl	bdl	bdl	bdl	bdl	na	6	bdl	2	14	4	3	bdl	na	na
Sr	13	13	25	9	37	na	294	11	321	864	740	721	18	na	na
Y	2	bdl	2	3	13	na	10	5	7	4	5	4	4	na	na
Zr	3	1	4	3	14	na	22	7	16	34	33	30	3	na	na

TABLE A4 2 Rare earth element analyses (concentrations in ppb)

Rock	H	H	H	D	D	D	D	AD	AD	AD	OI	OI	OII	OII	C
Sample	L103	L106	L225	L216	L217	L246	L262	L140	L266	L275	L066	L268	L271	L351	L012
Type	LALPP	LALPP	LALPP	LALPP	LALPP	LALPP	LALPP	LALPP	LALPP	LALPP	LALPP	LALPP	LALPP	LALPP	LALPP
Run	116	116	153	116	116	153	153	153	240	153	153	240	153	240	182
La	21	4 1	3 2	3 7	3.9	2.7	2.4	6 4	21	96	1 8	5.4	1 7	7 9	(38 5)
Ce	44	7 8	8 5	7 2	7.2	6 1	4 0	11 5	29	130	4 1	9 2	3 2	14	(89 8)
Pr	5 5	0 78	1 3	1 1	0 89	0 89	0 69	1 9	2 9	13	(0 43)	(1 0)	(0 36)	1 6	(16 3)
Nd	24	5 1	7 5	7 1	4 6	6 2	4 8	8 1	8 0	46	(2 2)	4 3	(2 6)	6 4	(96 2)
Sm	5 9	(1 11)	(1 9)	3 7	(1 3)	(1 7)	(2 1)	2 6	(2 3)	9 7	(0 87)	(1 28)	(1 21)	(1 04)	(61 7)
Eu	2 5	0 51	1 0	1 0	(0 38)	0 66	(0 49)	1 0	2 5	8 7	nd	(0 32)	(0 10)	(0 48)	23 4
Gd	7 2	2 9	3 7	4 4	2 1	2 3	(1 8)	4 0	(2 2)	11	(1 7)	(2 3)	(1 0)	(1 0)	107
Tb	1 55	0 55	0 61	1 08	0.55	0 40	(0 34)	0 93	0 71	2 4	0 60	0 92	(0 31)	(0 20)	21 9
Dy	10 6	5 2	4 5	9 1	4 0	3 0	2 2	7 6	5 5	18	5 8	7 9	3 1	1 23	171
Ho	2 0	1 40	1 03	2 1	0 98	0 62	0 49	2 1	1 48	3 8	1 85	2 6	0 68	0 29	35 5
Er	7 1	5 9	3 06	7 9	4 9	2 04	2 11	7 4	6 2	13 3	6 3	10 6	3 65	(1 19)	116
Tm	1 16	1 36	0 43	1 51	1 06	0 49	0 50	1 24	1 11	1 94	0 90	2 17	0 61	(0 174)	17 1
Yb	7 9	11 1	4 3	9 4	9 0	3 7	3 3	9 6	9 7	13 6	6 6	17 5	5 0	2 58	101
Lu	1 52	2 05	0 75	1 76	2 00	0 59	0 65	1 77	2 5	2 25	1 07	4 4	1 07	0 82	15 0
Yb*	15 1	(13 4)						33 6		29 9	17 7	35 4	17 6		
Lu*	2 36	2 94						7 98		7 14	1 17	3 86	4 39		

Rock	C	C	C	C	WB	WB	D	D	W	W	C	C	G	G	AP
Sample	L026	L213	L290	L293	L283	L288	L302	L305	L093	L317	L296	L328	L294	L313	L273
Type	LALPP	LALPP	LALPP	LALPP	LALPP	LALPP	HALPPG	HALPPG	HALPPG	HALPPG	HALPPG	HALPPG	HALPPG	HALPPG	HALPPG
Run	182	182	182	182	182	182	116	182	024	024	024	182	024	024	024
La	(41.2)	(36.7)	(39.4)	(38.0)	(63.8)	(49.4)	8.3	(71.2)	(117.3)	(126.9)	449	(179)	(222)	431	(83.7)
Ce	(90.9)	(84.9)	(99.9)	(74.0)	(139.4)	(129.7)	19	(188)	467	416	1700	784	734	1179	422
Pr	(16.3)	(19.9)	(20.6)	(14.79)	(20.6)	(18.9)	2.7	(33.8)	112.3	88.6	379	191	138.0	210	120.5
Nd	(90.2)	(170)	(127)	(99.3)	(110)	(102)	13	(180)	800	473	2340	1230	903	1260	822
Sm	(67.8)	98.2	(65.4)	(59.8)	(44.9)	(51.9)	4.8	(76.1)	432	279	1152	618	425	522	420
Eu	25.5	32.9	30.0	26.8	15.3	20.2	1.4	29.7	133	86	424	221	195	306	162
Gd	120	147	132	125	68.8	92.2	6.0	104	540	347	1540	867	546	600	565
Tb	27.2	35.9	27.0	24.6	17.1	20.3	1.50	21.0	112	60.0	310	178	113	132	118
Dy	175	229	182	172	117	135	12.1	141	780	434	2140	1180	740	850	760
Ho	40.5	49.8	38.8	39.7	27.7	36.6	3.3	30.0	162	97.2	442	237	155	171	151
Er	124	157	106	113	86.2	116	13.6	98.8	471	276	1260	678	467	504	424
Tm	16.0	22.4	17.9	16.9	13.4	19.3	2.79	15.7	64.0	39.4	179	97.6	59.0	69.6	62.9
Yb	89.1	125	105	89.7	88.4	120	23.1	107	430	270	1070	562	389	405	356
Lu	12.7	20.1	16.1	15.8	12.8	18.1	5.0	18.7	63.1	39.1	158	82.7	53.4	57.8	44.7
Yb*							53.9								
Lu*							12.9								

Rock	AMPT	AMPT
Sample	SD194	SD380
Type	UC	UC
Run	182	182
La	2050	1330
Ce	7100	4930
Pr	1299	1023
Nd	6700	5710
Sm	2510	2170
Eu	850	900
Gd	2850	2690
Tb	559	529
Dy	3670	3360
Ho	748	697
Er	2240	2010
Tm	309	277
Yb	1980	1750
Lu	300	256
Yb*		
Lu*		

TABLE A4 3. Platinum group element analyses (concentrations in ppb)

Rock	H	H	H	D	D	D	D	CR	CR	CR	CR-X	AD	AD	AD
Sample	L106	L218	L225	L054	L216	L217	L254	L203	L244	L289	L326	L265	L266	L275
Type	LALPP	LALPP	LALPP	LALPP	LALPP	LALPP	LALPP	LALPP	LALPP	LALPP	LALPP	LALPP	LALPP	LALPP
Ru	8 75	7.23	7.90	20.98	1.11	5.56	3.56	50 66	50 41	25.60	40 35	0 74	0 71	1 22
Rh	1 53	1.84	1.19	3 59	1.96	1.88	0.44	4 62	2 83	2 35	4.26	11.59	11.32	8 68
Pd	8 16	3 87	1.63	2.67	4 83	23 06	0 71	2.79	0 00	5 31	1 52	60 72	106 01	8.06
Re	0 39	0.05	bdl	0.00	0.00	0.01	bdl	0 06	0 00	0 00	bdl	0 09	bdl	0.38
Os	4 61	3 16	2 96	4 04	0 44	2 44	1.90	14 61	22 41	13 31	14.29	0 55	bdl	0 62
Ir	4 76	3 13	2.76	9 60	2.20	2.76	2 00	15 05	11.91	6 05	10.99	3 45	4 40	5 97
Pt	9 54	5.19	6.31	1.13	44.27	5 58	0.20	1 58	2 13	2 13	2 73	117 09	182.33	33 01
Sum PGE	37.74	24.47	22 75	42 01	54 61	41 29	8 81	89 37	89.69	54 75	74 14	194.23	304 77	57 94
Pd/Ir	1 71	1 24	0 59	0 28	2.10	8 36	0 36	0.19		0 88	0.14	17.60	24.09	1 35

Rock	OI	OI	OI	OI	OII	OII	C	C	C	C	C	C	WB
Sample	L068	L071	L267	L268	L271	L351	L026	L211	L212	L213	L214	L293	L283
Type	LALPP	LALPP	LALPP	LALPP	LALPP	LALPP	LALPP	LALPP	LALPP	LALPP	LALPP	LALPP	LALPP
Ru	0.13	0.19	0 56	2 02	58 99	6 84	0 17	bdl	bdl	bdl	bdl	0.16	0.23
Rh	0.48	1.60	10 12	30 92	0 15	1.42	0.74	0 31	0 13	0.13	0.03	0 08	3 73
Pd	170 38	15 92	104 74	405 68	0 59	2.11	67 98	10 38	0.44	3 83	6 05	10 16	193.71
Re	0.00	16 43	0 30	0 00	0 07	0 06	0 00	0 94	0.54	1 05	13.28	0 00	0 05
Os	0.14	bdl	1 29	2 79	0 71	1 54	0.26	0.13	0 63	0 53	bdl	0.05	0.35
Ir	0.36	0.44	3 32	9 51	0.49	1 98	0 31	0 01	bdl	0 03	0 07	0 06	1 62
Pt	170 85	14.58	141 70	517 20	0 24	3 34	61 24	3 47	0.18	0 77	1 00	3.41	520 53
Sum PGE	342 34	49 16	262 03	968 12	61 24	17 29	130.70	15 24	1 92	6 34	20.43	13.92	720.22
Pd/Ir	473.28	36.18	31 55	42 66	1.20	1 07	219.29	1038.00		127 67	86 43	169.33	119 57

MAGMATIC AND FLUID PROCESSES IN THE UPPER MANTLE: A STUDY OF THE BAY OF ISLANDS OPHIOLITE COMPLEX, NEWFOUNDLAND

VOLUME I: Text

©STEPHEN JOHN EDWARDS, B.Sc. (London)

A thesis submitted to the School of Graduate Studies
in partial fulfillment of the requirements for the degree of
Doctor of Philosophy

Department of Earth Sciences
Memorial University of Newfoundland
June 1991

St. John's Newfoundland